Measurements and Analysis of the Microwave Dielectric Properties of Human and Animal Tissues

Andrew James Gorton
Department of Physics and Astronomy
University of Glasgow

Presented for the degree of Doctor of Philosophy
to the University of Glasgow
September 1996

© Andrew Gorton 1996

ProQuest Number: 13833356

All rights reserved

INFORMATION TO ALL USERS
The quality of this reproduction is dependent upon the quality of the copy submitted.

In the unlikely event that the author did not send a complete manuscript
and there are missing pages, these will be noted. Also, if material had to be removed,
a note will indicate the deletion.

ProQuest 13833356

Published by ProQuest LLC (2019). Copyright of the Dissertation is held by the Author.

All rights reserved.
This work is protected against unauthorized copying under Title 17, United States Code
Microform Edition © ProQuest LLC.

ProQuest LLC.
789 East Eisenhower Parkway
P.O. Box 1346
Ann Arbor, MI 48106 – 1346

Thesis
10643
Copy 1

GLASGOW
UNIVERSITY
LIBRARY

Declaration.

This thesis has been composed by the undersigned. It has not been accepted in any previous application for a degree. The work of which it is a record has been done by myself, unless indicated otherwise in the text. I further state that no part of this has already been or is being concurrently submitted for any such degree or qualification at any other university.

Andrew James Gorton.

Acknowledgements

This work was carried out whilst I was a student in the Department of Physics and Astronomy, University of Glasgow, and in receipt of a research studentship grant as part of the Robertson Trust award for the development of microwave thermography.

I should like to offer my thanks to the following people for their help in completing this thesis:

Dr D.V. Land, my supervisor and the initiator of this research, who constructed the experimental probes used in this study, and sent us to several conferences in pleasant locations.

Alan and Gavin of the Royal Infirmary Mortuary, Robert and Patricia of the Western Infirmary Mortuary, and Dr. Owen of the Western Infirmary Department of Pathology, who so helpfully provided the specimens of human tissue.

John Stewart Butchers, of Byres Road, who provided much of the animal tissues at generously low cost.

Gavin Hamilton, my lab colleague, with whom I worked and suffered in close tandem throughout the long hours of sample preparation and measurement, and also Margaret Duffy (née Kelso), who kept us all amused.

Alan Seath and all the technical staff associated with the microwave group.

Dr. H. Ward, my cheerful secondary supervisor.

My mum and dad, to whom special thanks are due, for tolerating my often ill temper, and helping to keep my car running.

All the other friends who have kept me going over the last few years.

Table of Contents.

Abstract.

Microwave thermography, tomography and hyperthermia are potentially useful clinical techniques that are currently at the development stage. They may ultimately assist in the early detection and treatment of breast cancer and other conditions causing a local temperature or tissue permittivity anomaly in the body. Accurate complex permittivity values for human tissues are needed for computer modelling to fulfil the potential of these techniques.

A novel open-ended co-axial probe measurement system operating at room temperature was used to investigate the complex permittivity of many animal and human tissues at a frequency of 3 GHz. The probe was calibrated using a bilinear transform method based on an equivalent circuit model of the probe aperture. A quarter-wave choke at the probe aperture provided an area of high impedance around the open-end. This minimised the effects of surface currents, and thus greatly improved measurement repeatability and general probe performance in comparison with ordinary co-axial probes.

Mixture equations were used to analyse the measured permittivity values in terms of the permittivities of the other major component materials of biological tissue. By considering all the sources contributing to the microwave permittivity, the amount of bound water in tissues was estimated, and an approximate value for its average relaxation frequency evaluated using an extrapolation technique. Further measurements on partially dehydrated tissue samples extended the range of tissue water content investigated, and permitted better extrapolation of the bound water relaxation frequency. These values were in close agreement with the estimates of previous researchers.

To verify the validity of this method, aqueous gelatine solutions were used as simple tissue phantoms. Since the solutions contained comparatively few distinct components, it was possible to use mixture equations again to extrapolate the permittivity of water bound to the gelatine polymer molecules. The method gave highly consistent estimates for the bound water relaxation frequency using either or both of the real and imaginary parts of the measured solution permittivity.

Summary.

The original work herein presented mainly concerns the measurement and interpretation of the values of the dielectric complex permittivity of human and animal biological tissues, at frequencies corresponding to part of the microwave band of the electromagnetic spectrum. This research has been carried out as part of a project to improve microwave radiometer measurement technique and interpretation for clinical microwave thermography.

If such a technique is to be useful for detecting thermal anomalies in the human body at depths of up to several centimetres below the skin, then it is essential that a general model of the expected complex permittivity of the tissue in the region of the anomaly be formed. It is also important to be aware of the values of the thermal conductivity of these tissues, and how the thermal conductivity and dielectric permittivity are related within biological tissues. Only through knowledge of these quantities can a microwave thermographic scan be used to successfully reconstruct a subcutaneous temperature profile.

A specially designed, and suitably calibrated, open-ended co-axial probe was used in this study to measure the complex permittivity of small volumes of a wide variety of human and animal tissues. The measurements were made *in-vitro,* at a frequency of 3 GHz, which is the central operating frequency of the Glasgow thermography system. After dielectric measurement, the water content of the tissue samples was measured by dehydration. In collaboration with a colleague, the thermal conductivity of many of these samples was also measured so that the relationship between the thermal and dielectric properties of tissues may be investigated.

It is usually accepted that the complex permittivity of biological tissues is mainly dependent on the water content of the tissue. Water composes ~60% of the mass of the average human male and ~55% of the mass of the average human female. As water has a considerably higher permittivity and thermal conductivity than other constituents of human tissue, it may be expected to provide the dominant mechanism for both of these parameters.

To fully investigate the role of water in determining the permittivity of tissues, tissue specimens across the whole range of water content, from fats, often <10% water, to intestinal tissue, >90% water, were examined. The tissue samples were dried in an oven after dielectric measurement to find their water content.

Initial permittivity measurements were made on commercially obtained animal tissues. The expected similarity in the properties of corresponding human and animal tissue enabled selection for permittivity measurement of suitable samples of human tissue, which were taken mainly from the subjects of post-mortem examinations. Animal and human tissues were compared, and it was noted that both displayed a similar linear relationship between the real and imaginary parts of their complex permittivity.

Water does not exist within tissue in a free pure liquid state. Rather, the molecules are thought to be distributed between the free state, and many states of molecular binding, through hydrogen bonding to large macromolecules such as proteins in the tissue. This bonding can restrict the rotational mobility of water molecules, and thus alter their dielectric behaviour. In addition, the tissue water also contains a variety of dissolved ions, usually represented by 0.15M (physiological) saline. The level of binding and ionic profile in a tissue type will contribute largely to the level of electromagnetic attenuation in that tissue type.

Mixture equations describe the permittivity of materials composed of two evenly distributed substances in terms of the volume fraction of each component. Tissues can be approximated as a mixture of water, with a high permittivity, and protein, which has a low permittivity at 3 GHz. By considering the difference between the measured tissue permittivity values and the values predicted by mixture equations, a first estimate as to the amount of bound water in the tissues which does not contribute significantly to the net dielectric constant was made.

There is a general gap in tissue water contents between ~30% and 70%. By subjecting tissue samples to *partial dehydration*, artificial tissues with water contents in this range were created. The partial dehydration method involved evaporating a proportion of the tissue water from a sample by gentle heating in an oven at temperatures well below 100°C. This process alters the proportion of bound water in the dehydrated tissues, so

permittivity measurements on these samples were used to support the values estimated for the bound water content of undehydrated tissues.

To model the form of the behaviour of water in biological tissue, the permittivity of semi-solid aqueous gelatine solutions was measured. These can be regarded as a simplified tissue phantom, as they contain only two substances, water and gelatine, an animal protein. Some of the water in these solutions is hydrogen bonded to the protein polymer molecules in a similar manner to the water binding in tissues.
Using mixture equations, a new technique for investigating the state of bound water in protein solutions was employed. Taking the permittivity results of gelatine solutions of many concentrations, the *effective* permittivity of the water fraction in the solutions was calculated. The effective permittivity of the water fraction is dependent on gelatine concentration, as a greater fraction of water may be bound when there is a greater gelatine concentration. Extrapolating the behaviour of the effective water permittivity to very high gelatine concentration therefore gave an estimate of the permittivity of the bound water in the gelatine solutions.
The same technique was then applied to the high water content biological tissue permittivity measurements. However, as the range of water contents for biological tissues was so limited, the extrapolation process was very prone to uncertainty, and gave mutually inconsistent results for the dielectric constant and loss factor of the bound water. By using the permittivity data from partial dehydration samples, the range of water content was extended. The behaviour of the effective permittivity of the tissue water was more reliably extrapolated, and led to conclusions about the dielectric properties of bound water in tissues which were fairly consistent with the conclusions of previous researchers in the field.

This thesis is divided into three distinct sections. The first section is introductory and comprises chapters 1 to 3. In it, the need for accurate and comprehensive knowledge of the complex permittivity of tissues for analysis of radiometric data is established, and combined thermal and dielectric modelling is briefly discussed. Then the relaxation equations which are used to parameterise the dielectric behaviour of pure substances are presented, followed by a review of the mixture equations commonly used to predict the

permittivity of two-phase materials. Finally, the dielectric behaviour of water, saline, and tissue-simulating water / polymer solutions at microwave frequencies are discussed in some detail.

Chapters 4 and 5 form the second section, in which the choice and design of the co-axial permittivity measuring probe used in this study are explained, and the probe performance is compared to that of earlier designs. Several methods for calibration of co-axial probes are considered, their applicability to the current case is established, and the inherent calibration and measurement errors are evaluated.

In the third section, the measured biological tissue permittivity data are presented and compared with previously measured data where available. The major tissue types investigated included fats from many regions of the body, skeletal, cardiac and smooth muscle tissues, and liver and kidney tissues. Limited measurements were made on small specimens of skin, blood and pancreatic, splenetic, uterine and brain tissues. Similarity between animal and human tissues, and between human tissues of similar water content is discussed. Analysis by mixture equations of permittivity measurements on tissues and gelatine tissue phantom materials with many different water concentrations is used to evaluate the applicability of mixture equations to biological tissue, and to estimate the dielectric properties of bound water.

At this stage it is useful to define the dielectric terminology which is used extensively in this study. There appears to be considerable inconsistency in the current usage of the terms describing dielectric behaviour. Here, the definitions used are taken from Von Hippel (1954), and concur with those used by the American Institute of Physics (Link and Herrmann, 1972).

The intrinsic property of a material which describes its ability to store electrical energy is its *relative dielectric constant*, ε'. The term *constant* refers to the independence of ε' on field strength. Part of the electrical energy put into a dielectric is dissipated, and is therefore not recoverable from storage. The intrinsic property which measures dissipation is the *relative loss factor*, ε''. The *relative permittivity* ε_r of the material in an alternating electric field is given by;

$$\varepsilon_r = \varepsilon' - j\varepsilon''$$

where $j = \sqrt{-1}$. As this is a complex quantity, ε_r is often referred to as the *complex relative permittivity*.

All these parameters are *relative* values, as they are all measured relative to the *permittivity of free space*, ε_0, which is equal to 8.854×10^{-12} Fm^{-1}. The *absolute* permittivity of a material is equal to $\varepsilon\varepsilon_0$, and so, by association, the *absolute* dielectric constant and *absolute* loss factor of the material are equal to $\varepsilon'\varepsilon_0$ and $\varepsilon''\varepsilon_0$ respectively. However, in this study, all the measured values are quoted as relative permittivities, relative dielectric constants and relative loss factors. Therefore, the word *relative* will be usually dropped, except in cases where otherwise made clear, without risking confusion. In conclusion then, the complex parameter ε_r will generally be referred to as the *permittivity*; the real part of the permittivity will be referred to as the *dielectric constant*, and the imaginary part will be referred to as the *loss factor*.

Chapter 1. Microwave Radiometry of the Human Body.

1.1. Introduction.

In this chapter the fundamental aspects of microwave radiometry, and the need for accurate tissue permittivity data are presented. Similar requirements are also established for microwave hyperthermia and tomographic techniques. The relationship between the temperature and permittivity of body tissue and the microwave radiometer signal is then investigated.

By combining the spectral intensity of thermal radiation from a black-body material with the *equation of transfer*, an expression for the intensity of microwave radiation inside body tissues is found. The microwave signal detected by a radiometer antenna is dependent on the intensity of microwave radiation in the medium under investigation and the geometry dependent spatial response pattern of the antenna to incident radiation. Microwave radiometry antenna response functions are then considered, and a simplified model is used to show how approximate equations for antenna signals can be obtained. A brief review of the common methods used to evaluate real antenna response patterns is then presented, with emphasis on the problems encountered in near-field measurement. Radiometer and antenna design are described, and recent modifications considered, with respect to minimising unwanted signal from sources other than the tissue region of interest, and improving spatial resolution.

As it is found that the radiation intensity profile is dependent on the local temperature profile, the merits of using the popular bioheat equations to assist the prediction of local microwave temperatures in the body are discussed. Finally, simplified thermal modelling of the human body is used to find a suitable expression for the form of the major temperature variations in simple tissue volumes, illustrative of the measurement conditions of microwave thermography.

1.2. Practical Microwave Radiometry.

Microwave thermography is the name given to a method of estimating the effective internal temperature of the human body, by measuring the intensity of thermal radiation, naturally emitted from the body, at microwave frequencies. Microwave radiation will

penetrate to the order of several centimetres into body tissues, and so radiation emitted from points at medically useful distances under the skin surface will reach the skin where it may be detected.

As many medical conditions are characterised by an increase in body temperature around the area affected, microwave thermography is a potentially useful clinical technique for the detection of such conditions as cause a localised temperature increase situated inside the body. Examples of such temperature changes are the inflamed tissue of joints affected by arthritis, and the 'hot-spots' associated with many breast cancers.

A microwave scan may be taken passively, non-invasively, and in an environment without strict temperature controls, as the features detected lie at sufficient depths within the body not to be too seriously affected by moderate alterations in ambient or skin temperatures.

Typical equipment used for basic body temperature measurements is shown in fig. 1.a. Similar apparatus to this has been used in various clinical studies by the Glasgow and other research groups (e.g. Kelso, 1995, Fraser et al 1987, Abdul-Razzak et al, 1987, Barrett et al, 1980). To measure the microwave signal incident on the skin from tissue within the body, the procedure is simply to place the end of the antenna in contact with the skin. Radiation couples with the antenna, which is a dielectrically loaded waveguide section, and a signal is transmitted to a radiometer receiver which measures the radiation signal. The radiometer output is presented as a degrees Celsius equivalent temperature, which is often recorded and displayed by computer as colour-coded temperature patterns.

1.2.1. Fundamentals of Operation.

Any mass, with temperature above absolute zero, emits electromagnetic radiation as a consequence of the thermal agitation of its constituent particles. At microwave frequencies it is found that the spectral intensity of emissions is a linear function of temperature in a given medium.

The broad spectrum of microwave signals picked up by the antenna are processed by a Dicke - type radiometer, which ignores radiation outside the bandwidth of interest, and amplifies the desired frequency components. As the microwave signal from the antenna is of very low intensity, being the result of thermal 'noise' in the human body, it is

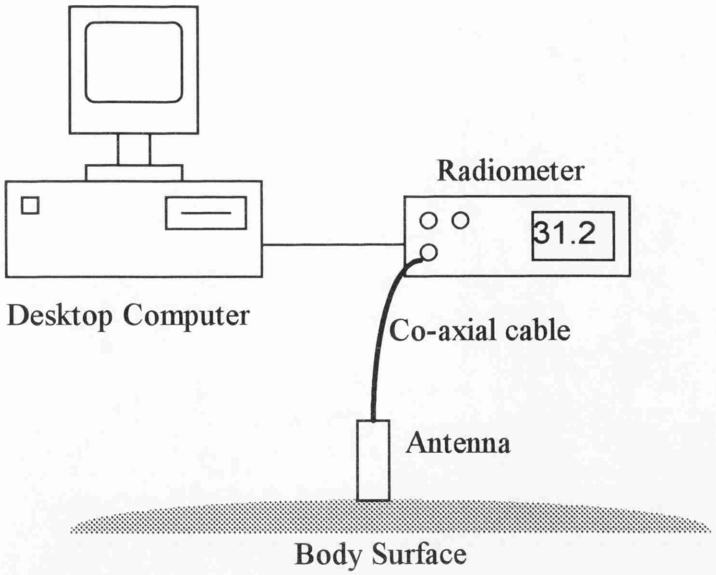

Figure 1.a. Clinical radiometer apparatus for body temperature measurement. The equipment consists of a dielectrically loaded waveguide antenna connected to the radiometer, which amplifies the thermal microwave signal, and displays the effective microwave temperature on a digital display. A personal computer displays and records the measured data.

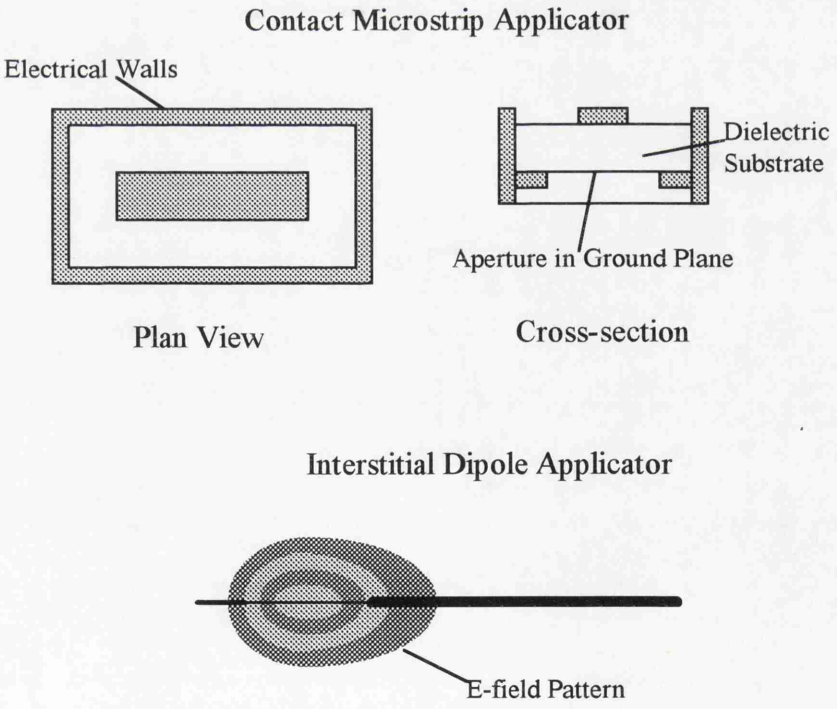

Figure 1.b. Schematic diagrams of common applicator types for microwave hyperthermia treatment.

essential to ensure, by suitable radiometer design, that as little as possible excess noise is added to the signal by the radiometer detection and amplification circuits. The resulting signal is interpreted in terms of an 'effective microwave temperature,' which is a weighted mean of the temperature distribution at all points in the volume viewed by the antenna.

Thorough knowledge of the antenna response function is essential for evaluation of the temperature of the tissue under investigation. This response function is also dependent on the dielectric permittivity of the tissue, the value of which determines both the radiation penetration depth into the tissue, and the spatial resolution of the radiometer. It is to the measurement and values of the dielectric permittivity of body tissues that the majority of work presented herein is dedicated.

1.3. Hyperthermia and Tomography.

Two areas of research closely associated with microwave thermography are microwave hyperthermia and microwave tomography. Whereas thermography relies on the detection of naturally emitted radiation from the body, both the hyperthermia and tomography techniques 'actively' illuminate parts of the body with higher intensity microwave radiation from a generator. The behaviour of body tissues to artificially applied radiation is identical to the behaviour to natural thermal radiation, so the principles involved in equipment design and tissue modelling in these techniques are the same as those employed for microwave thermography.

Microwave hyperthermia is a method of preferentially destroying tumour cells by concentrated microwave irradiation of the affected region. This heats the tumour to temperatures between 42 to 45 °C, sufficient to destroy preferentially the malignant cells whilst not damaging excessively the normal surrounding tissues.

Radiation is commonly delivered to the tumour using a contact 'microstrip' applicator, dielectrically loaded waveguide, or invasive 'interstitial' antennae (fig. 1.b). It is necessary to restrict the heated volume as closely as possible to that of the tumour itself, or healthy surrounding tissue will be at risk of destruction. Therefore these antennae are designed to have a response function with a heavily localised distribution which can be centred on the tumour (e.g. Johnson et al, 1995).

Knowledge of the dielectric permittivity of tissue, as well as its thermal behaviour, is vital to calculation of the microwave energy dose rate which must be supplied to the applicator to maintain the correct temperature in the tumour.

Tomography is a technique already in clinical use at X-ray wavelengths as a medical imaging method. Radiation of the chosen wavelength is applied to one side of the tissue region under investigation. It propagates through the region, is attenuated and scattered by the irregularities and absorption of the tissue, and the resulting radiation distribution is detected at the other side of the region by an antenna array. The amplitude, and in microwave tomography, also the phase, of the radiation reaching each point opposite the emitter is used to reconstruct the three-dimensional density, or for microwaves, complex permittivity distribution in the viewed volume, even for strongly inhomogeneous regions. Microwave tomography systems are also still at an experimental stage of research, but are a potentially useful medical tool. This technique may be utilised not only for locating cancers, but also for tissue thermometry to monitor hyperthermia treatment, on account of the variation in tissue permittivity with temperature (Broquetas et al, 1989).
To fulfil the potential of microwave hyperthermia and tomography, it is essential to establish the values and ranges of the permittivity of both healthy and tumour tissue.

1.4. Black-body Thermal Radiation.

An object which absorbs all the radiation incident upon it is known as a 'black-body.' By the *Principle of Detailed Balance* (Reif, 1965), the power radiated by a black-body in thermal equilibrium in any frequency bandwidth must be equal to the power absorbed in that bandwidth. This holds over any particular element of the black-body, and for any direction of polarisation. Thus, the perfectly absorbing black-body is also a perfect emitter of radiation.

The intensity of radiation emitted by a black-body in the frequency range $\nu \rightarrow \nu + d\nu$ is given, as a function of absolute temperature, T, by the Planck function:

$$B_\nu(T)d\nu = \frac{2h\nu^3}{c^2(e^{\frac{h\nu}{kT}} - 1)}d\nu \qquad (1.4.1)$$

where $B_\nu(T)dv$ is the power emitted per unit surface area, into unit solid angle in the frequency range dv, h is Planck's constant, c is the velocity of light, and k is Boltzmann's constant.

It is important to distinguish between *total intensity* and *spectral intensity*. The total intensity of radiation refers to radiation emitted over all frequencies, and may be evaluated for a black-body by integration of eqn. 1.4.1. Total intensity has dimensions $Js^{-1}m^{-2}$. Spectral intensity refers to the radiation emitted in a small frequency band dv, and so has dimensions Jm^{-2}. As microwave radiometers operate in a narrow frequency band, it is the spectral intensity of the body that is of interest. Hereafter, the *spectral intensity* is referred to as the *intensity* without risk of confusion.

The intensity distribution (1.4.1) is plotted as a function of ν for T = 300K (approximately that of the human body) in fig. 1.c. Peak intensity occurs at a frequency of $\sim 3.1 \times 10^{13}$ Hz, in the infra-red spectral region, and has a magnitude $\sim 10^8$ times that of the intensity at the frequencies used for microwave thermography. However, the fact that the microwave intensity is so low is not of importance in thermography, as the microwave thermal signal from the environment and measurement equipment is similarly reduced.

At 3 GHz, and a temperature of 300K, the exponent $h\nu/kT$ is very small: .

$$h\nu/kT \approx 4.8 \times 10^{-4} \quad \Rightarrow \quad (e^{\frac{h\nu}{kT}} - 1) \approx h\nu/kT \tag{1.4.2}$$

Thus the Planck function (eqn. 1.4.1) may be approximated by the Rayleigh-Jeans function for this situation, and the intensity expressed as:

$$B_\nu(T) = \frac{2kT\nu^2}{c^2} \tag{1.4.3}$$

showing the intensity to be a linear function of temperature.

Although no real material behaves as a perfect black-body at all temperatures and over the entire frequency range, it is shown, in the following sections, that the Rayleigh-Jeans law has an important place in evaluating the intensity of the microwave signal from the human body.

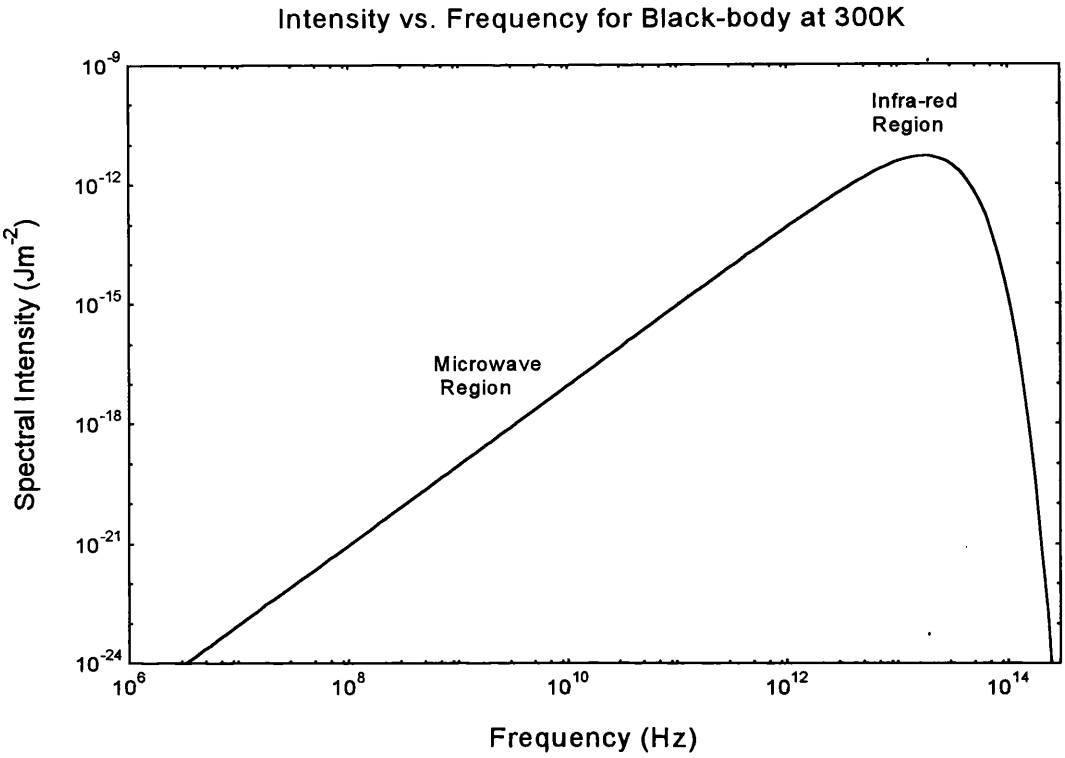

Figure 1.c. Black-body spectrum for material at a temperature of 300K, approximately equal to that of the human body. Microwave radiation has intensity only 10^{-8} times the peak infra-red intensity.

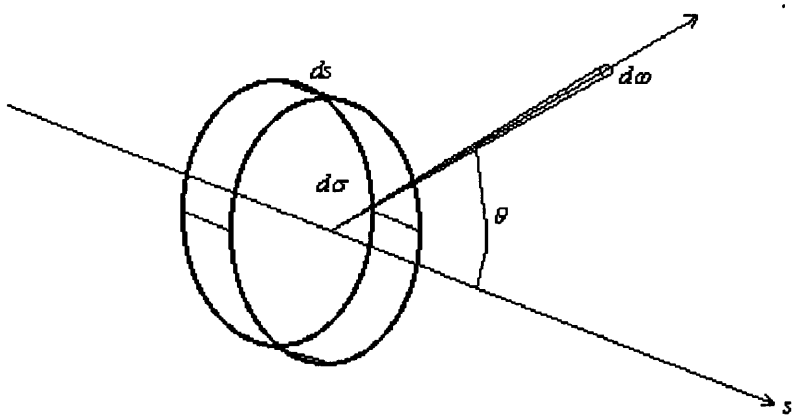

Figure 1.d. Small cylindrical volume element lying parallel to the *s*-axis in a radiation field, with an element of solid angle $d\omega$ subtended from its centre.

1.5. Equation of Radiative Transfer.

The following treatment uses the formalism of Chandrasekhar (1950) in his book 'Radiative Transfer' for radio astronomy. The problem of interpreting radio emissions from the layered atmospheres of stars or planets is analogous to that encountered in interpreting the microwave signal emanating from a human body.

In a radiation field, the radiative power dP_ν in a frequency band $d\nu$, transported across area $d\sigma$, confined to an element of solid angle $d\omega$, is related to the intensity I_ν by:

$$dP_\nu = I_\nu \cos\theta d\omega d\sigma d\nu \qquad (1.5.1)$$

where θ is the angle between the direction considered and the outward normal to the surface $d\sigma$. The radiation intensity I_ν may be a function of position, and of direction at the position.

Consider a small cylindrical element of cross-sectional area $d\sigma$ and length ds aligned parallel to the s -direction in a material supporting a radiation field (fig. 1.d). This material is characterised by a mass absorption co-efficient κ_ν, a mass emission co-efficient j_ν, and density ρ. The s co-ordinate may be described in terms of the Cartesian co-ordinates x, y, z and the direction cosines l, m and n by:

$$s = lx + my + nz \qquad (1.5.2)$$

Radiation of intensity I_ν per unit bandwidth, per unit area incident normal to this element will be transmitted normal to the element at an intensity $I_\nu + dI_\nu$, where the increment dI_ν is found by combining the absorbed and emitted radiation across the element. Absorption of the incident radiation over a distance ds will reduce the original intensity by an amount $dI_{\nu(abs)}$, given by:

$$dI_{\nu(abs)} = -\kappa_\nu \rho I_\nu ds \qquad (1.5.3)$$

Therefore the power absorbed by the cylindrical element in the frequency interval $\nu \rightarrow \nu + d\nu$ confined to the element of solid angle $d\omega$ is:

$$\kappa_\nu \rho I_\nu ds d\nu d\sigma d\omega \qquad (1.5.4)$$

The emission co-efficient is defined such that an element of mass dm emits radiation in the frequency interval $\nu \rightarrow \nu + d\nu$, confined to the solid angle element $d\omega$, at a power given by:

$$j_\nu dm d\omega d\nu = j_\nu ds d\sigma d\omega d\nu \tag{1.5.5}$$

The difference in radiant power in the frequency interval $\nu \rightarrow \nu + d\nu$ crossing the two faces of the cylinder normally, confined to the solid angle element $d\omega$, is:

$$\frac{dI_\nu}{ds} ds d\nu d\sigma d\omega \tag{1.5.6}$$

Combining eqns. 1.5.4, 1.5.5 and 1.5.6, yields:

$$\frac{dI_\nu}{ds} ds d\nu d\sigma d\omega = j_\nu \rho ds d\nu d\sigma d\omega - \kappa_\nu \rho I_\nu ds d\nu d\sigma d\omega \tag{1.5.7}$$

$$\Rightarrow \frac{dI_\nu}{ds} = j_\nu \rho - \kappa_\nu \rho I_\nu \tag{1.5.8}$$

This equation (1.5.8) is known as the 'Equation of Transfer.'

The *Source Function*, $\Im_\nu$, is defined as the ratio of the emission to absorption co-efficients:

$$\Im_\nu = \frac{j_\nu}{\kappa_\nu} \tag{1.5.9}$$

and allows the equation of transfer to be written:

$$-\frac{1}{\kappa_\nu \rho} \frac{dI_\nu}{ds} = I_\nu - \Im_\nu \tag{1.5.10}$$

1.5.2. Intensity Profile in Body Tissue Regions.

The equation of transfer is now applied to a model of the human body, and solutions found to express the microwave radiation intensity as a function of position. For a more rigorous discussion of the solutions to the equation of transfer, the reader is referred to Chandrasekhar (1950, 1939).

The equation of transfer is generally an *integro-differential* equation, as the emission co-efficient, and therefore the source function, is often functionally dependent on the intensity at a point. In a medium, bounded on the s-axis at the point a, the formal solution to eqn. 1.5.10 is:

$$I_\nu(s) = I_\nu(a) e^{-\tau(s,a)} + \int_a^s \Im_\nu(s') e^{-\tau(s,s')} \kappa_\nu \rho ds' \tag{1.5.11}$$

where $\tau(s,s') = \int_{s'}^{s} \kappa_\nu \rho ds$ is the *optical thickness* of the material between points s' and s.

The optical thickness is equivalent to the power attenuation constant of electromagnetic radiation: $$\kappa_\nu \rho = 2\alpha \quad (1.5.12)$$

where α is the plane wave electric field attenuation constant, a parameter related to the complex permittivity $\varepsilon_r = (\varepsilon' - j\varepsilon'')$ by:

$$\alpha = \omega k / c \quad \text{where} \quad k = \mathrm{Im}\sqrt{\varepsilon_r} \quad (1.5.13)$$

Thus the intensity in a particular direction at a point in a medium results from *the sum of the emissions, reduced by their corresponding absorption factors, from all anterior points, and an expression representing the intensity incident upon the medium at its anterior boundary.*

Kirchoff's radiation law (Chandrasekhar, 1939) states that "The ratio j_ν / κ_ν of the emission to the absorption co-efficients of any body in thermodynamic equilibrium is equal to the specific intensity, B_ν, of the ν-radiation emitted by a black-body of the same temperature." The human body is not in perfect thermodynamic equilibrium, but as the temperature gradient within the body is small, and the absorption co-efficient generally high, a temperature, T, may be ascribed to each point, P, inside the body, such that the properties of the tissue around P are identical. In such circumstances the body is said to be in *local thermodynamic equilibrium.* Thus Kirchoff's law may be applied, and the source function for microwave radiation in the human body may be given as the Rayleigh-Jeans function: $$\Im_\nu = \frac{2kT\nu^2}{c^2} \quad (1.5.14)$$

Thus, for a single semi-infinite medium bounded at $s = 0$, the intensity at the surface is:

$$I_\nu(0) = \tfrac{2k\nu^2}{c^2} \int_0^\infty 2\alpha T(s) e^{-2\alpha s} ds \quad (1.5.15)$$

Brown (1989) considered a simple, yet realistic, model of certain regions of the human body, shown in fig. 1.e. Body tissue is stratified in parallel planes of different tissue types. A cross-section through the abdomen or a large limb may have this form. In the x-y plane the physical properties of the tissue are invariant for a given value of z co-ordinate. Under such circumstances, the plane-wave approximation may be applied to

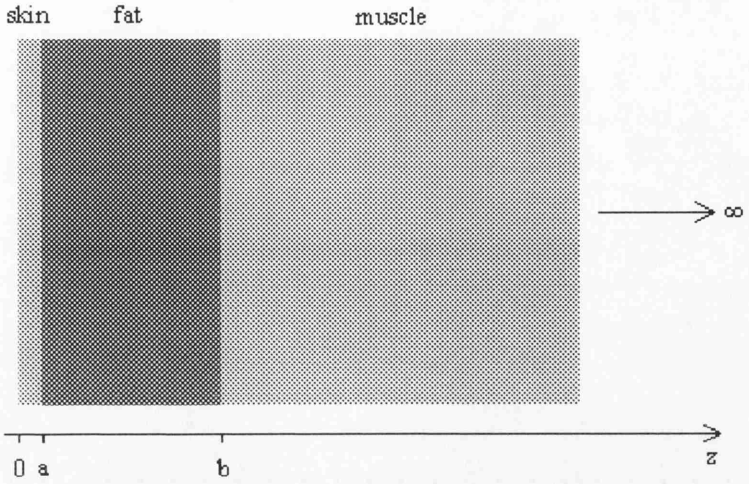

Figure 1.e. Section of body tissue considered in eqn. 1.5.16, viewed perpendicular to the supposed axis of plane-wave radiation propagation towards skin surface.

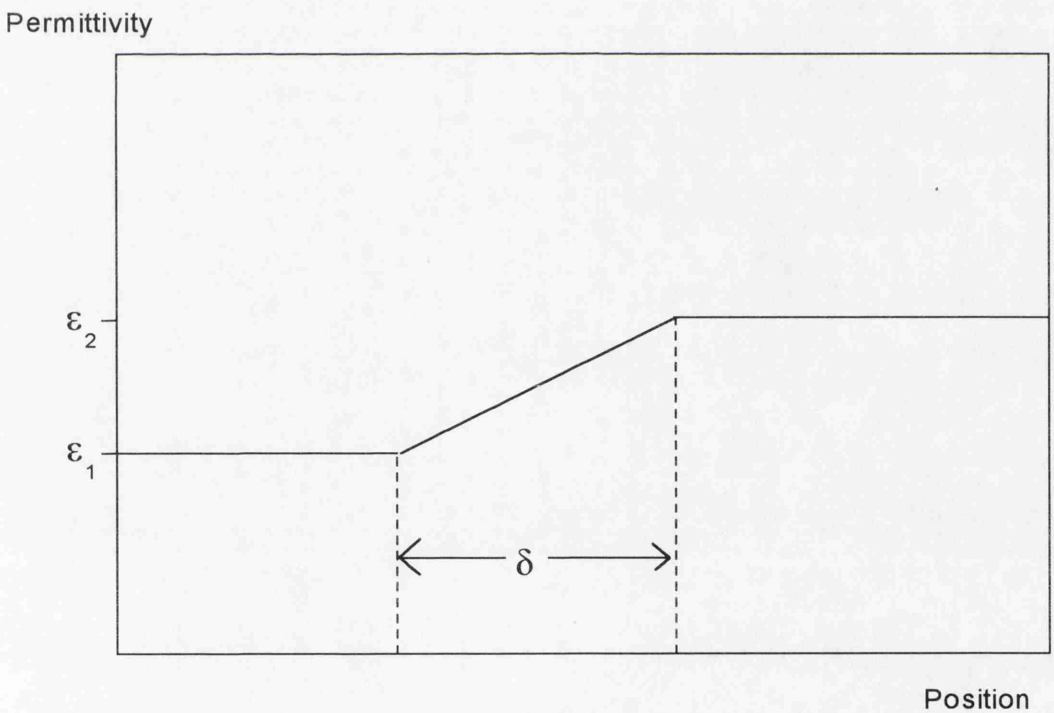

Figure 1.f. Schematic diagram of a transition between two media, in which the permittivity undergoes a gradual change, rather than an abrupt discontinuity. This is likely to be a better approximation of the tissue boundaries in the human body.

the radiation field in the tissue volume, as the radiation intensity at a given value of z is independent of the x and y co-ordinates.

Using eqns. 1.5.12, 1.5.13 and 1.5.14 in eqn. 1.5.11, the intensity at the skin surface may be given:

$$I_\nu(0) = 2k\nu^2\left[\frac{1}{c_s^2}\int_0^a 2\alpha_s T(z)e^{-2\alpha_s z}dz + \frac{e^{-2\alpha_s a}}{c_f^2}\int_a^b 2\alpha_f T(z)e^{-2\alpha_f(z-a)}dz + \frac{e^{-2(\alpha_s a+\alpha_f(b-a))}}{c_m^2}\int_b^\infty 2\alpha_m T(z)e^{-2\alpha_m z}dz\right]$$

(1.5.16), where the subscripts s, f and m refer to skin, fat and muscle respectively. This approximation ignores the reflection of radiation at tissue layer boundaries. Taking typical permittivity values for the three tissue types from the data presented in chapter 6, the power reflection co-efficients, R_{i-j}, at each boundary may be evaluated, and incorporated with eqn. 1.5.16 to give a better approximation of the signal intensity at the skin surface.

$$\varepsilon_{muscle} = 50 - j18,\ \varepsilon_{fat} = 15 - j3,\ \varepsilon_{skin} = 35 - j11,\ \text{gives:}$$

$$R_{muscle-fat} = 0.08;\ R_{fat-skin} = 0.04 \qquad (1.5.17)$$

These reflection co-efficients are themselves slightly unrealistic as real dielectric boundaries in the human body are unlikely to be sudden discontinuities, but spread over a few millimetres. Wilheit (1978) considers the reflection at non-abrupt boundaries between two media of permittivities ε_1 and ε_2 as shown in fig. 1.f. If the transition distance, δ, is long, i.e. $\delta >> \lambda$, then the reflection is zero, and if $\delta << \lambda$, the reflection is the same as that for an abrupt boundary. In the human body, 3 GHz radiation has a wavelength of ~1.5cm to 4cm, and tissue boundaries are spread over only several millimetres. Thus reflection co-efficients will be comparable to those obtained by straightforward Fresnel equations.

1.6. Antennae for Microwave Thermography.

The thermal radiation power per unit bandwidth received by an antenna is given by:

$$W_\nu = \tfrac{1}{2}\int_V I_\nu(\underline{r})P_n(\underline{r})d\tau \qquad (1.6.1)$$

where $I_\nu(\underline{r})$ is the intensity of radiation of frequency ν emitted by the volume element $d\tau$ at position $(\underline{r})$, the form of which has been discussed above, and $P_n(\underline{r})$ is the normalised power response pattern of the antenna as a function of position $(\underline{r})$. The factor of $\frac{1}{2}$

occurs because any antenna only responds to one radiation polarisation component. As the incident radiation is incoherent and unpolarised, half the total incident power is lost. It is therefore essential for radiometric temperature retrieval that the antenna spatial response is known. The form of this function is dependent on many parameters; the antenna geometry, the loading dielectric of the antenna, and the dielectric properties and geometry of the investigated volume.

In this section, the observed behaviour of the antennae used in the Glasgow radiometer is considered, with reference to finding an approximate response function, which can be used in eqn. 1.6.1 in conjunction with the radiation intensity function (eqn. 1.5.15). Sections 1.7 and 1.8 discuss the techniques employed for more rigorous evaluation of antenna response functions.

The Glasgow antenna (fig. 1.g) is a cylindrical waveguide section of length 5.2cm and diameter 2.5cm, loaded with a proprietary dielectric powder of relative permittivity $\varepsilon = 12 - 0.008i$. This dielectric is approximately matched to the overall effective permittivity of tissue near the skin surface. Although the permittivity of skin is significantly higher than this value, the skin layer is sufficiently thin that the effect of subcutaneous fat is more important. The dielectric also contributes very little noise to the received signal because of its low absorption, and reduces the required antenna diameter for detection of 3 GHz radiation from that of a hollow guide by a factor of $\sqrt{12}$. This also improves the transverse spatial response by the same factor.

Only one mode of radiation transmission in the antenna is measured. Over the whole range of radiometer operating frequency (3 - 3.5 GHz), only the transverse electric TE_{11} mode of radiation will propagate freely in the antenna. The transverse magnetic TM_{01} mode may propagate at frequencies above ~3.2 GHz, but this contributes little to the received signal, because the coupling between antenna and this mode is weak at the fin-line transition to co-axial cable. A quarter-wave choke at the waveguide to co-axial cable junction provides a high impedance area between the inner and outer conductors of the cable across the end of one fin.

The power dissipation density in the field of an antenna radiating into a medium is expressed:

$$P(\underline{r}) = \tfrac{1}{2}\sigma|\underline{E}(\underline{r})|^2 \qquad (1.6.2)$$

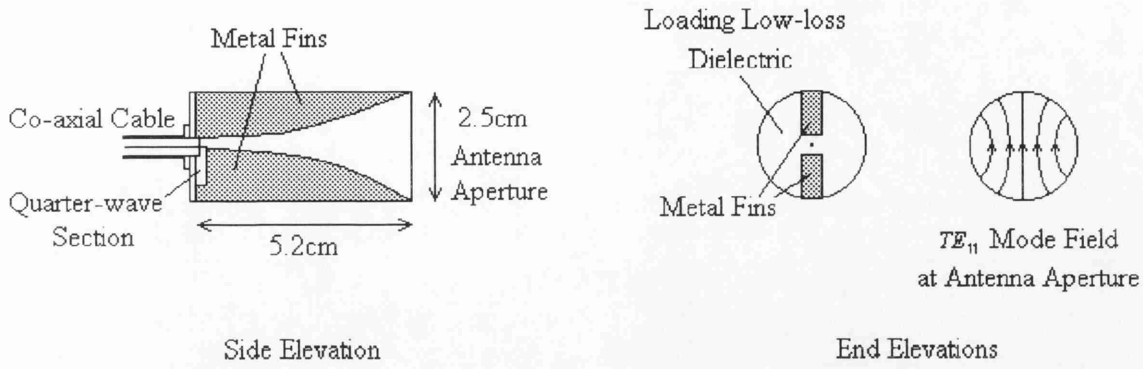

Figure 1.g. Cross-sectional views of the radiometer antenna used at Glasgow. The metal fins make a quasi parallel-plate transmission line region and the quarter-wave section gives a high impedance at the co-axial cable junction. The antenna is loaded with a low-loss dielectric with $\varepsilon_r \approx 12$ to reduce the required antenna size for wave propagation.

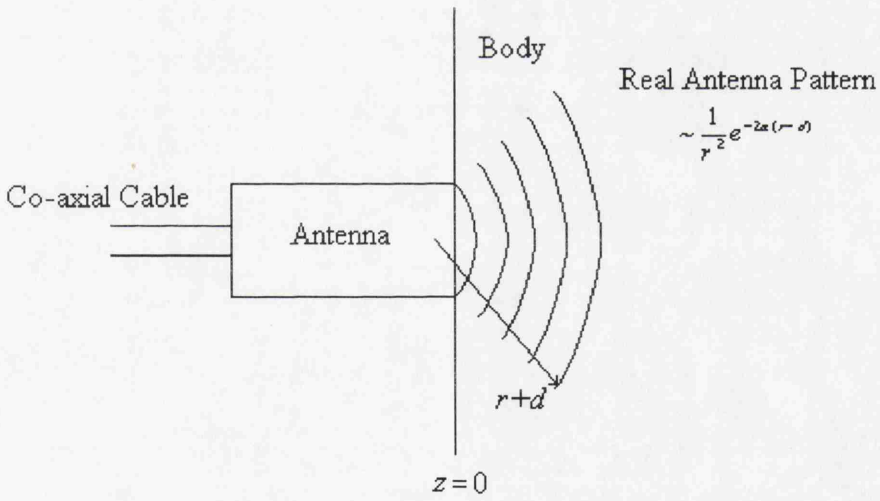

Figure 1.h. Representation of wavefronts from a real antenna radiating into a body. The factor d is a correction factor dependent on position, which allows for the fact the centre of spherical wave expansion is actually inside the antenna, not on the boundary at the aperture.

where σ is the conductivity of the medium representing all loss mechanisms, and $|\underline{E}(\underline{r})|^2$ is the magnitude of the square of the electric field at position $\underline{r}$. By the antenna reciprocity theorem (Slater, 1942), the receiving power pattern of an antenna is the same as its power dissipation pattern when operating in active mode. Therefore, the receiving power response function is proportional to eqn. 1.6.2.

$$P_n(\underline{r}) = A|\underline{E}(\underline{r})|^2 \tag{1.6.3}$$

where A is a constant of proportionality.

The antenna response function is normalised such that: $\int_v P_n(\underline{r})d\tau = 1.$ (1.6.4)

An ideal antenna produces a pattern of plane wavefronts over the area of the aperture of the antenna. In a lossy medium the plane wave electric field amplitude $|\underline{E}(\underline{r})|$ decays $\propto e^{-\alpha z}$. In this case the power response function is given by the axial response, multiplied by the normalised lowest order Bessel function $P_n'(x,y)$ describing the distribution of field over the area of the aperture in the *x-y* plane:

$$P_n(\underline{r}) = P_n'(x,y)2\alpha e^{-2\alpha z} \tag{1.6.5}$$

where α is the field attenuation constant of the viewed medium.

For an ideal antenna the viewed volume is a cylinder of the diameter of the antenna, so in cylindrical polar co-ordinates, the power received per unit bandwidth is given by:

$$W_v = \tfrac{1}{2}\int_0^{\infty}\int_0^{2\pi}\int_0^{\text{antenna radius}} I_v(\underline{r})P_n'(x,y)2\alpha e^{-2\alpha z} r\,dr\,d\theta\,dz \tag{1.6.6}$$

However, a real antenna produces a more complicated field distribution (fig. 1.h). At large distances from the antenna (far-field region), the wavefronts are quasi-spherical, giving a $1/r^2$ dependence to the power response function. In the region near the aperture (near-field region), higher order terms in $1/r$ are dominant in the $\underline{E}$ and $\underline{H}$ fields, due to fringing of the wavefronts around the conducting surface of the antenna. In lossy media, these fields contribute to signal loss through the in-phase current term. Signal loss in the near-field may account for 20% to 50% of the total signal in practical thermography situations (Land, 1995)

Thus, the response function is a complex function of position and of the dielectric constant of the viewed material, tending, when r is large, to be proportional to

$\frac{1}{r^2}e^{-2\alpha(r-d)}$, where $d(r,\theta,\phi)$ is a correction function allowing for the distance to the centre of expansion of the spherical waves. (see fig. 1.h)

The permittivity of the viewed medium affects the response function in several ways. It not only defines the attenuation constant, α, but also affects the extent of the near-field fringing, and the shape of the volume of viewed material, through the change of the wavelength in the dielectric. A good match between the permittivity of the antenna loading dielectric and the material of the viewed volume restricts wavefront fringing around the aperture (Land, 1995), and as a consequence, changes the shape of the volume of viewed material. The viewed volume takes the form of a cone, whose vertex is the centre of spherical wave expansion, the position of which is determined by the local permittivity of the material in the near-field region. Since the permittivity of tissue varies with position, refraction effects, acting on the wavefronts at the periphery of the viewed volume, will alter the direction of propagation of these wavefronts. Thus the effective position of the vertex of wave expansion will also be dependent on position, $\underline{r}$. The near-field fringing effects of the antenna may be minimised by attaching a large, conducting ground plane to the aperture (Decreton et al, 1974). But in practice this is unwieldy, and gives variable electrical contact between the antenna aperture and the body under investigation.

Evaluating the response function clearly requires tissue modelling and numerical computation. There is one notable simplification which assists in evaluating the far-field contribution to the overall signal (Brown, 1989). The real and ideal antenna axial responses are shown in fig. 1.i; in the far-field, the $1/r^2$ term may be incorporated into the exponential decay term, giving an effective attenuation constant α_e, such that $\alpha_e > \alpha$. Thus the real antenna response is approximated by an ideal antenna radiating into a medium of slightly higher loss:

$$P_n(r) \propto 2\alpha e^{-2\alpha_e z} \qquad (1.6.7)$$

Experiment has shown (Mimi, 1990) that for a TE_{11} mode cylindrical antenna, α_e varies from 1.05α to 1.4α depending on the permittivity of the medium under investigation. However, despite the success of this method, it is usually necessary to measure or compute numerically the real antenna response function, especially in the near-field region.

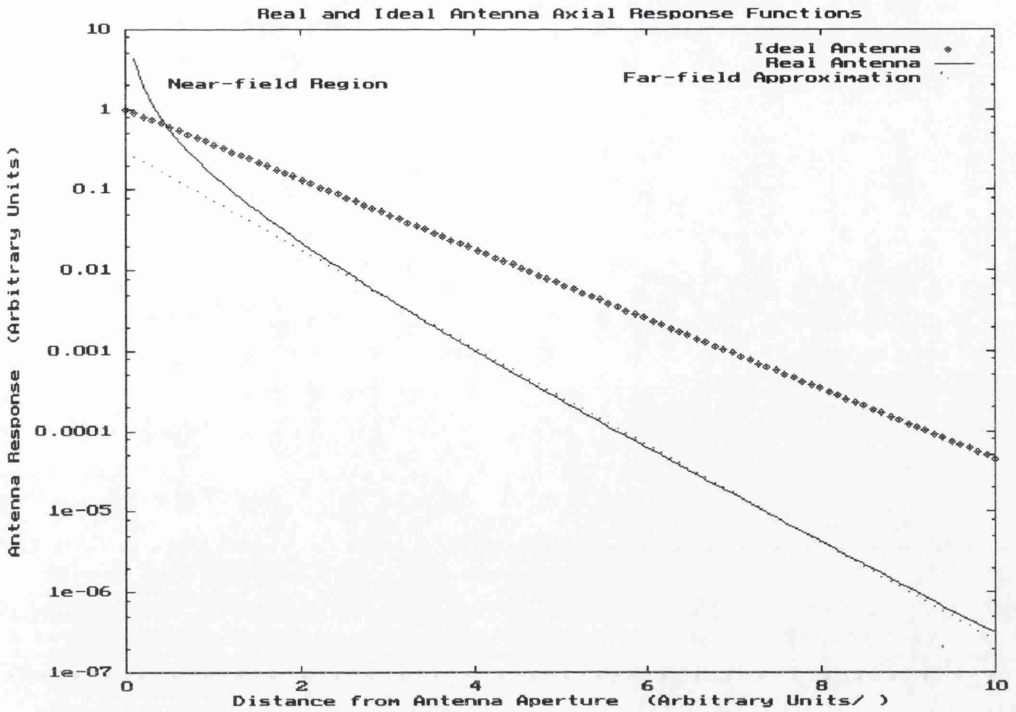

Figure 1.i. Schematic comparison between ideal and real antenna response functions, showing that in the far-field region, the real response can be approximated by an ideal exponential response with slightly larger attenuation constant.

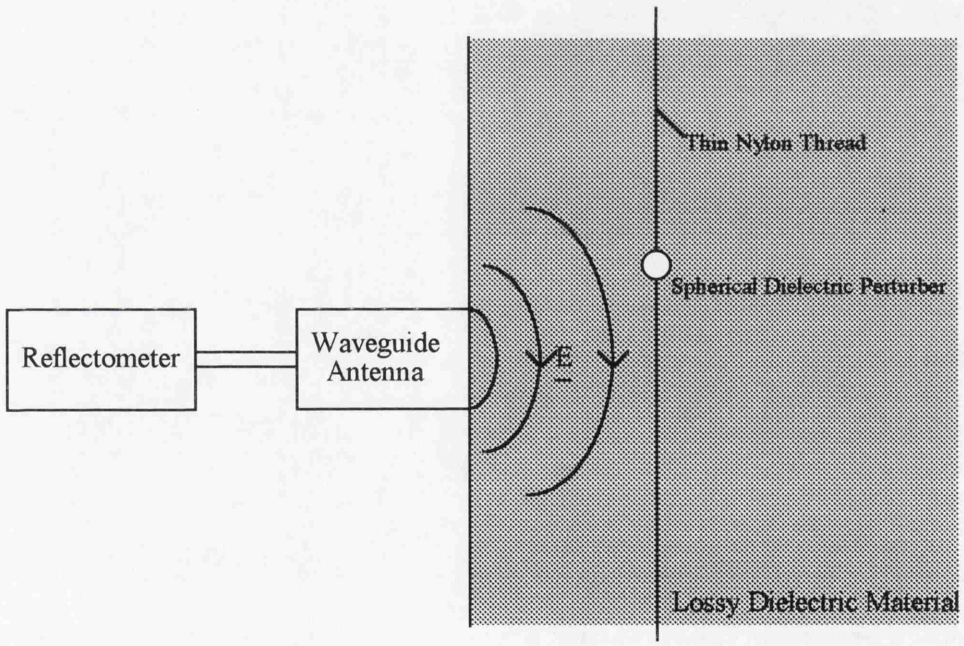

Figure 1.j Schematic diagram of non-resonant perturbation method of measuring antenna spatial response. Fields propagating into a lossy tissue phantom from the test antenna are perturbed by small dielectric volumes of known geometry, and the resulting change in reflection co-efficient from the antenna measured. From this the antenna field can be calculated.

1.7. Real Antenna Spatial Response Functions.

For practical purposes, the antenna response function may be evaluated by direct measurement, or by mathematical modelling techniques. Mathematical modelling has recently become a more realistic method, as computing power becomes inexpensive and accessible, but direct measurement in tissue simulating media is still popular for its reliability, and to provide 'real' results with which to compare computed patterns.
The antenna response function is measured in active mode, radiating into a tissue phantom, as the active fields will be identical in structure to the passive response fields, by the reciprocity theorem (Slater, 1942).
The most satisfactory measurement method is the non-resonant perturbation technique (Land, 1984, 1988, 1992) as shown in fig. 1.j. The test antenna is supplied, via a waveguide coupled to the antenna port, with a microwave signal which radiates into a liquid tissue phantom. A directional coupling element is used to view the signal reflected from the test antenna. The amplitude and phase of this signal are measured. Field perturbing objects of known dimensions and permittivity are introduced to the viewed region of the phantom medium, and the change in field reflection co-efficient is measured.
Applying the field form of the reciprocity relationship over the stationary boundaries of the system yields exact expressions for the change in reflection co-efficient produced at the antenna port by the presence of a perturber at a particular position (Land, 1984). For a non-magnetic dielectric perturber, the change in reflection co-efficient, $\Delta\Gamma$, is given by:

$$\Delta\Gamma = \int_{v} j\omega(\varepsilon_p - \varepsilon_m)\frac{\mathbf{E}_1 \cdot \mathbf{E}_2}{4W_i}dV \qquad (1.7.1)$$

where ε_p and ε_m are the complex permittivities of the perturber and phantom material respectively, W_i is the power incident from the test antenna upon the viewed volume, and $\mathbf{E}_1$ and $\mathbf{E}_2$ are respectively the electric fields before and after the introduction of the perturbing object.
Dielectric perturbers are generally used to interact only with the electric field, and conducting perturbers can be used to investigate magnetic field distribution.
Non-resonant perturbation has several advantages over other field pattern measurement methods. Firstly, if measurements are made using spherical dielectric perturbers, then

they are field polarisation independent; secondly, the suspending structure of the perturber (e.g. nylon thread) can have negligible interaction with the field, even at near-field positions; and thirdly, an absolute, rather than just a relative, measurement of antenna response is yielded.

Suitable choice of perturber shape allows specific characteristics of the field pattern to be investigated; for example, thin perturbing rods are used to determine the directionality of field components, and thin sheet perturbers can be used in near plane-wave regions (Land, 1992)

This technique is particularly useful for establishing near-field effects. In realistic body simulations it is found that layering of the dielectric structure immediately in front of the antenna aperture has a significant effect. Figure 1.k shows an example of this, by comparing the response at a fixed depth of simulated muscle tissue for different thickness of simulated fat. The central response falls steadily for increasing low-permittivity layer, and is far lower than the response for a single region of higher loss, higher permittivity muscle. The width of the response also increases with increasing low-permittivity layer, showing that a reduction in plane-wave attenuation constant in the near-field is more than compensated for by the increased fringing effects caused.

1.8. Antenna Response Modelling.

Antenna modelling is of significant interest in this study, as the similar modelling of the admittance of open-ended co-axial probes is essential to calibrate the probes used to make the permittivity measurements which form the basis of this research. The particular case of modelling co-axial probes is discussed thoroughly in chapter 5. Here, discussion is limited to a brief overview of the common techniques used to model the near-fields of waveguide antennae as used in microwave radiometry studies.

The technique of modal-matching has been extensively used to find the near-field distribution in lossy dielectric media. Cheever et al (1987) modelled and measured the $1/e$ penetration depth of 3 - 5 GHz radiation from a rectangular TE_{10} mode waveguide. The aperture is modelled as a junction between the supply waveguide, corresponding to the antenna, and a much larger waveguide containing the dielectric medium. At the open end, the field in the dielectric is expressed as a superposition of normal modes in the

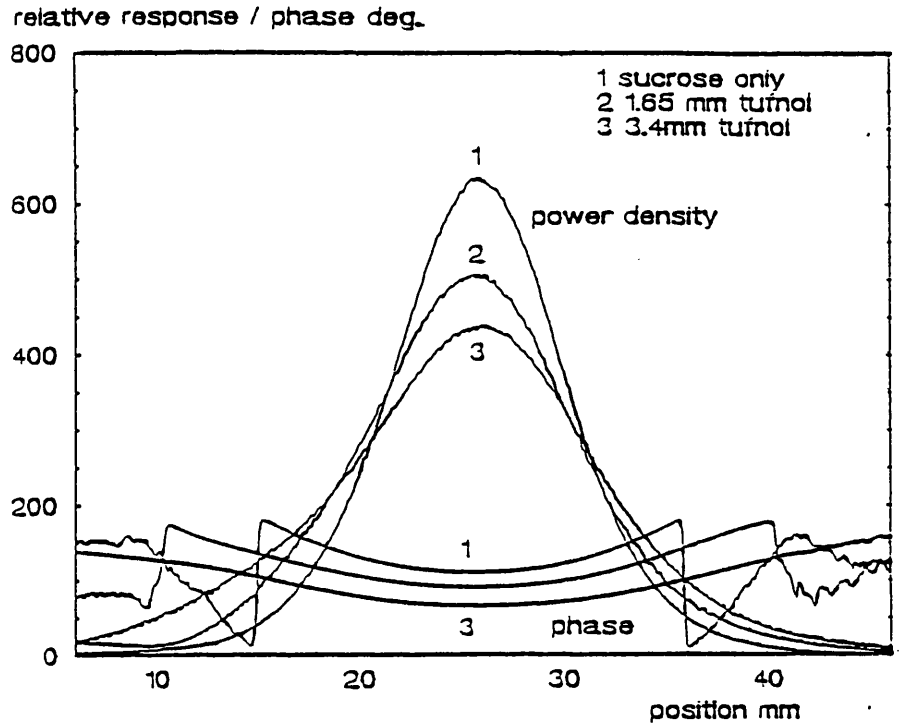

Figure 1.k. Graph showing the variation with lateral position in the relative magnitude and phase of a microwave signal at a depth of ~1cm into a sucrose solution tissue phantom. The waveguide antenna aperture which irradiates the volume is centred at a lateral position of 25mm. Fat simulating tufnol sheets can be placed between the aperture and the sucrose, which reduces the response magnitude, despite the tufnol being of lower permittivity than the sucrose which it displaces. Reproduced from Land, 1995.

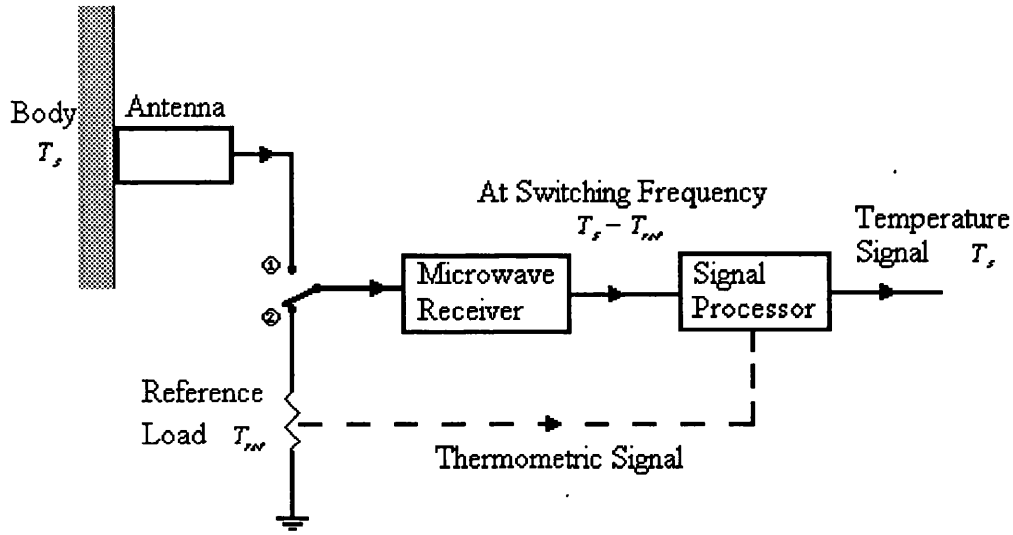

Figure 1.l. Schematic diagram of Dicke-type radiometer. When switch is in position 1 the received signal is proportional to $T_s + T_n$, and in position 2 the signal is proportional to $T_{ref} + T_n$. At the switching frequency, the output varies as the difference $T_s - T_{ref}$ between the two signals.

larger waveguide. This model makes the assumption that the field at the aperture corresponds only to the TE_{10} mode of the smaller guide. In fact there exist at the aperture incident and reflected TE_{10} modes, and also significant higher evanescent mode fields.
At the University of Lille Hyperfrequency Group, Mamouni et al (1991) used a similar modal technique which accounts for these fields. Radiometric tests based on predicting the observed microwave temperature increase associated with 'hot-spots' in semi-infinite lossy media (Bocquet et al, 1993) have shown sufficiently good agreement with measured values for this model to be incorporated with medical radiometry applications.

Modal methods are limited to the study of plane stratified media boundaries, and cannot be easily extended to allow for heterogeneous tissue structures. Purely computational methods must be used to account for varying geometry of tissue and applicator, as it is necessary to solve Maxwell's equations with complex boundary conditions. Computer models based on the Finite Difference Time Domain (FDTD) algorithm, introduced by Yee (1966), are most commonly applied (Taylor et al 1995, Chive et al 1995).
To implement this algorithm, the volume under investigation, including the radiation source, is divided into a square grid or lattice (3-D). Each lattice cell is specified by the dielectric parameters of complex permittivity, and each lattice point has its own associated set of $\underline{E}$ and $\underline{H}$ field components. An electromagnetic field source is excited in the volume at the appropriate co-ordinates to start the simulation. Finite difference approximations of Maxwell's time dependent equations are then time-stepped over all the lattice points to simulate the propagation of the field. The antenna pattern may be evaluated when once steady state is attained. A comprehensive study on this method in a radiological environment is presented by Lau et al (1986).
Increased computer power will allow a larger volume of tissue, divided into finer lattice cells, to be modelled, thus reducing error.

Other numerical methods of waveguide antenna modelling include the Method of Moments (Livesay & Chen, 1974) and Finite Element analysis (Lynch & Paulsen, 1985). The Moment method is impractical as it involves the solution of integral equations at each lattice point, via the inversion of large matrices, which consumes huge computer resources. Finite Element analysis requires more computing power than the FDTD

method, but has the advantages that heterogeneous tissue properties and irregular boundary conditions are accounted for fundamentally within the formulation, and elements of varying shapes and sizes may be chosen within a model.

It is intended that the complex permittivity data on biological tissue presented in chapter 6 of this study will provide raw data to be used in subsequent computer modelling of the antenna response functions of thermography antennae. This will assist in determination of the subcutaneous temperature distribution measured by microwave thermographic scanning.

1.9. Radiometer Design.

One important requirement of microwave thermography research is to produce a radiometry system which is useful in a clinical environment, for monitoring the temperature of subcutaneous tissue. An 'ideal' clinical radiometer system would possess the following qualities: (1) usefully small spatial resolution. (2) usefully large penetration depth into tissue. (3) adequately sensitive temperature resolution. (4) fast response time.

Spatial resolution and penetration depth are dependent on the frequency of radiation considered, and on the design of the receiving antenna. Unfortunately, an improvement in spatial resolution by increasing measurement frequency produces a corresponding reduction in penetration depth. An optimum combination must be chosen, which may vary for different applications. The necessity for a fast response time is a purely clinical requirement - data collection from a patient must be performed in a restricted time period. However, it is a characteristic of radiometers that a fast response time conflicts with good temperature resolution. It is found that clinical and physical considerations lead to design compromises in practical radiometers.
In general, for useful clinical operation, a radiometer should have spatial resolution ~1cm, penetration depth ~several cm, temperature resolution ~0.1K, and temperature stability ~0.3K. As human body temperature is 310K, the temperature resolution must be ~0.03%, and stability ~0.1% at worst. It is with these requirements in mind that the operating frequency and electrical design of thermographic radiometers are chosen.

1.9.1. Choice of Measurement Frequency.

For a real antenna, the maximum detectable noise power in the Rayleigh-Jeans limit at temperature T, is given by: $W = kTB$ (1.9.1)

where B is the measurement bandwidth. The frequency independence of this quantity is a result of cancellation of the frequency dependence of the black-body radiation intensity (eqn. 1.4.3) with the effective antenna area (see Brown, 1989). A large bandwidth may be desirable, as this gives a large signal, but in practice, problems such as antenna impedance matching restrict the obtainable measurement bandwidth.

The central frequency of this bandwidth must be selected to give the best compromise between spatial resolution and penetration depth. Simple geometrical optics gives the lateral spatial resolution of a radiation detecting device as approximately half the wavelength of the radiation in the medium in question. If the complex perimittivity of a medium, ε_r, is given by $\varepsilon_r = \varepsilon' - j\varepsilon''$, then:

$$\text{Spatial Resolution} \cong \frac{\lambda_o}{2\sqrt{\varepsilon'}} \tag{1.9.2}$$

Decreasing wavelength improves the spatial resolution of the radiometer.

The amplitude attenuation constant, α, of radiation in tissue was given in section 1.5 as:

$$\alpha = \frac{\omega \,\mathrm{Im}\sqrt{\varepsilon_r}}{c} \tag{1.9.3}$$

The plane wave power penetration depth is the depth of tissue required to attenuate an incident plane wave to $1/e$ of its original intensity, and is given by the inverse of the power attenuation constant 2α. In practice, because antennae do not have plane-wave response functions, the effective power penetration depth will always be less than $1/2\alpha$.

From eqn. 1.9.3:
$$\alpha = \frac{2\pi}{\lambda_o}\sqrt{\frac{\varepsilon'\mu_r}{2}}\left[\left(1+\left(\frac{\varepsilon''}{\varepsilon'}\right)^2\right)^{\frac{1}{2}} - 1\right]^{\frac{1}{2}} \tag{1.9.4}$$

For biological tissues, the ratio $\varepsilon''/\varepsilon'$ is generally ≤ 0.3. When $\varepsilon''/\varepsilon'$ is <1, eqn. 1.9.4 may be approximated as:
$$\alpha = \frac{\pi\sqrt{\varepsilon'}}{\lambda_o}\left(\frac{\varepsilon''}{\varepsilon'}\right) \tag{1.9.5}$$

The quantity $\varepsilon''/\varepsilon'$ is called the 'loss tangent,' $\tan\delta$, of the material; if the permittivity is given by $|\varepsilon|e^{-i\delta}$, the loss angle δ is given by $\delta = \tan^{-1}\left(\varepsilon''/\varepsilon'\right)$.

Hence, for optimised radiometer performance, a microwave frequency must be chosen which minimises the quantities in eqns. 1.9.2 and 1.9.5. This is achieved by minimising the product of these expressions, which is proportional to the loss tangent. Therefore, the optimal frequency depends on the material under investigation.

Flesh tissue of the human body is mainly composed of electrolytic water (~75% by mass), with an ionic profile that may be accurately approximated by 0.15**M** saline solution. The loss factor of saline is composed of two terms, one caused by *ionic* conductivity of the dissolved ions, and one effective *relaxation* conductivity caused by absorption by polar water molecules. At a frequency of ~3 GHz the ionic effect, which decreases with frequency, and the molecular effect, which passes through a maximum value at ~25 GHz, combine to give a local minimum value of the loss factor and therefore the loss tangent. Thus 3 GHz is an optimal frequency in the microwave range. The loss factor of saline is shown in fig. 3.c, and is discussed in more detail in subsequent chapters. Although much of the saline in biological tissue exits in bound and semi-bound states, it can be assumed that the minimum loss tangent of human tissue will approximately correspond to that of physiological saline.

At 3 GHz frequency, the permittivity of human tissue is such that the power penetration depth is ~6mm (muscle) to ~5cm (fat), and the spatial resolution ranges from ~0.7cm (muscle) to ~2cm (fat).

1.9.2. The Dicke Radiometer.

The radiometer used in clinical studies at Glasgow is a Dicke - type comparison radiometer (Land 1987) shown schematically in fig. 1.1. All radiometers have a temperature resolution given by the Gabor relationship:

$$\Delta T = \frac{Q(T_s + T_n)}{\sqrt{Bt}} \qquad (1.9.6)$$

where Q is the radiometer constant for the receiver, T_s is the source temperature, T_n is the radiometer effective noise temperature, B is the radiometer bandwidth, and t is the radiometer response time. For Dicke - type radiometers, Q is typically ~ 4.6 - 6.6 (Land,

1983), T_s is ~310K (human body), and B is determined by the amplifier bandwidth and also by the antenna impedance matching range, which will only allow good power transmission into the antenna over a narrow frequency range.

At 310K, thermal microwave radiation is of very low intensity, with randomly fluctuating amplitude and phase. It is therefore necessary to amplify the microwave signal before detection. A simple total power amplifier cannot be used, as its gain, G, is highly dependent on amplifier temperature. The output signal, R, of a total power radiometer is given by:

$$R = G(T_s + T_n) \tag{1.9.7}$$

A small change, δG in the gain, causes a change in the output of magnitude

$$\delta R = \delta G(T_s + T_n) \tag{1.9.8}$$

Thus if T_s and T_n are both around 300K, a 1% change in G gives a change in output reading of 6K, which is far larger than any local temperature variation in the human body. Additionally, the radiometer noise temperature is prone to variation which can not be distinguished from source temperature variation.

These problems can be overcome by the Dicke radiometer, which switches its input between the antenna source, and a matched resistance load at an accurately known temperature, measured by a semiconducting temperature sensor. This system produces an output, R, at the switching frequency that is proportional to the temperature difference between the source and the reference load.

$$R = G(T_s + T_n) - G(T_{ref} + T_n) = G(T_s - T_{ref}) \tag{1.9.9}$$

The signal is now independent of the radiometer noise temperature, T_n, and by setting the reference temperature close to the source temperature, the difference $(T_s - T_{ref})$ is small, so the effect of receiver gain fluctuations is reduced.

A practical system constructed from FET microwave amplifiers and low-loss circuit components may have an effective noise temperature of ~300K, and predetection bandwidth of ~500MHz at 3GHz. Thus, from eqn. 1.9.6, a temperature resolution of 0.1K may be attained with a response time of ~2 seconds.

Commonly used radiometer input circuits also compensate for the partial reflection of the 'true' microwave signal at the antenna aperture, by directing the noise from the reference source towards the antenna via a circulator when the Dicke switch is on the antenna. As the reference source is at a similar temperature to the antenna, approximately the same amount of reference noise signal is reflected back into the antenna as is lost from the true

signal. Similar performance can be obtained with self-balancing radiometers, as proposed by Ludecke (1978) and others, which adjust the reference temperature to be exactly equal to the source temperature, eliminating the effect of antenna reflections. However, this improvement is at the expense of increased response time.

1.10. Design Refinements for Microwave Thermography Radiometers.

A microwave radiometer may sense the 'effective temperature' of a body, that is, a temperature representing a weighted sum of the temperature at each point anterior to the antenna. If measurement is made at a single frequency, information about the internal temperature distribution can be obtained only with the use of a thermal model of the viewed tissue, and *a-priori* information about the viewed volume.

1.10.1. Multi-spectral Radiometers.

The need for *a-priori* information may be reduced by multi-spectral radiometers which take effective temperature readings over several distinct frequency bands. As radiation penetration depth is dependent on frequency, emissions at different frequencies relate to the effective temperature over different depths of tissue. Radiometric data taken at different frequencies can assist in the reconstruction of a subcutaneous temperature profile, but it is still necessary to make certain assumptions concerning the tissue volume under investigation.

Two approaches to these assumptions may be taken. The first is to assume the shape of the temperature profile in the body is already known; this reduces the temperature reconstruction to a process which estimates only the actual values of the parameters which describe the shape.

This approach is utilised by the University of Lille Hyperfrequency group. Preliminary experiments using a dual frequency (1.5 and 3 GHz) radiometer have deduced the 'visibility threshold' of thermal anomalies as a function of their depth (Bocquet et al, 1986). Figure 1.m shows a schematic representation of these experiments. The antenna is placed in contact with a thermostated, thin-walled cylinder filled with water at a known temperature T. A small cylinder of diameter D, filled with water at a temperature $T+\Delta T$, is introduced to the system, at an axial distance z from the antenna.

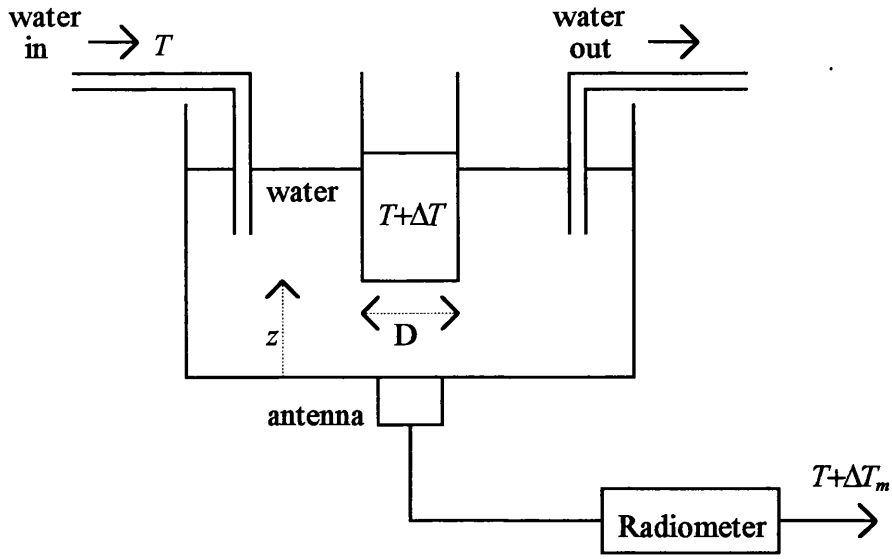

Figure 1.m. Schematic diagram of dual frequency radiometer experiments conducted by the University of Lille. An anomalous 'hot-spot' is introduced to a temperature controlled water bath and the change in effective microwave temperature measured at several frequencies. Lateral movement of the antenna can be used to estimate the diameter of the anomaly.

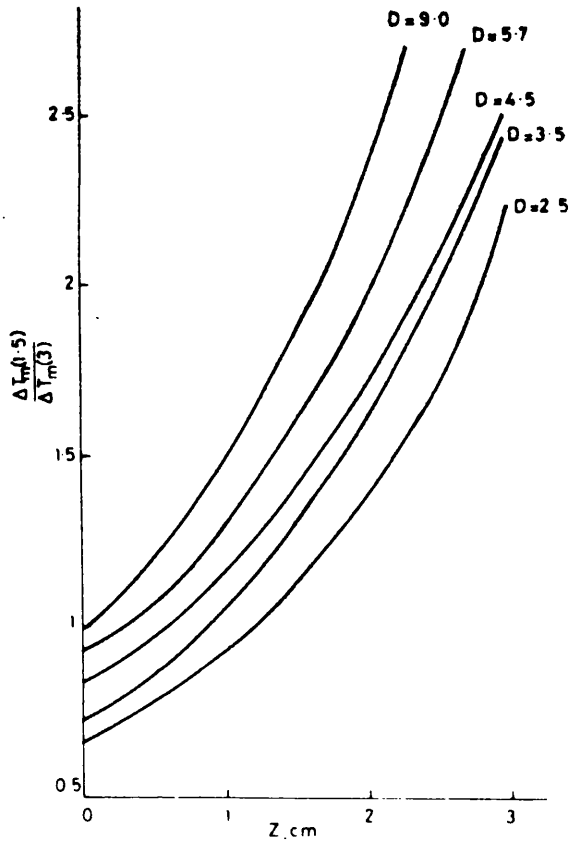

Figure 1.n. Sample calibration chart for estimation of the position of thermal anomalies in a medium of otherwise uniform temperature. Measured values of $\Delta T_{m(1.5GHz)}$ and $\Delta T_{m(3GHz)}$, and an estimation of the anomaly diameter, D, by lateral threshold visibility give an approximate value of the immersion depth, z. Reproduced from Bocquet et al, 1986.

At each measurement frequency, the observed effective temperature increase ΔT_m, created by the presence of the small hotter cylinder is measured. Threshold visibility is attained when ΔT_m is greater than the radiometer temperature resolution, in this case 0.1°C. The diameter of the anomaly can be estimated by scanning the probe in a direction perpendicular to its axis to find the lateral threshold visibility points.

Plots of the ratio $\Delta T_{m(1.5\text{GHz})} / \Delta T_{m(3\text{GHz})}$ against immersion depth, z, measured for several different anomaly diameter values, D, define a calibration chart from which the depth of subsequent unknown thermal anomalies can be estimated from measured values of $\Delta T_{m(1.5\text{GHz})} / \Delta T_{m(3\text{GHz})}$, as shown in fig. 1.n. Thus an overall estimate of the position of the anomaly is obtained.

By this method, a temperature change can only be measured with reference to some other known, or in a clinical case, 'normal', temperature. A thermal anomaly in the human body can only be resolved if there is a surrounding unaffected area, over which the same assumptions about the axial temperature profile may be made. As lateral resolution is still of the order of 1cm, there is still some error involved in estimating the size and position of the 'hot-spot.'

In an alternative approach adopted by Bardati et al (1989) and Caorsi et al (1993), the temperature retrieval from multi-spectral radiometer data is modelled as the solution of an inverse problem based on a Fredholm Integral of the first kind. This method is dependent on prior knowledge of the permittivity of the viewed volume at all measurement frequencies. It is found that solutions to the integral are severely ill-conditioned, so large variations may arise from only small departures between data sets. Bardati et al (1993) investigated the capability of this method for imaging an homogeneous cylindrical liquid phantom, of radius 60mm, with an off-centre 'hot-spot' of radius 5mm. Measuring at 4 discrete frequencies, and at 17 equiangular positions, a minimum temperature resolution of 1.5°C to 5°C (depending on noise propagation estimates) was calculated for image formation of the hot-spot. It is unlikely that thermal anomalies in the human body will be of sufficient magnitude to be detected by this method at this stage. Tests on the human forearm using this technique (Bardati, 1989) have as yet yielded unrealistic temperature distributions.

1.10.2 Correlation Thermography.

In an effort to improve spatial resolution, multi-probe correlation radiometers have been designed by Enel et al (1984), Mamouni (1983), and their performance modelled and measured by Mamouni (1988 ,1991) and Newton (1986). Correlation radiometers combine the signals from two or more receiving antennae in contact with the body by means of an analogue microwave multiplier, connected via a delay line, and followed by an integrator. The signal recombination process defines an artificial antenna with an effective response function which is dependent on only the volume of material which is shared by each antenna (see fig. 1.o). As the shared volume is small, correlation radiometers are sensitive to the relative position of thermal structures, which may be located by positioning of the antenna array, or by adjusting the delay time on one of the antennae. Correlation radiometry is also sensitive to thermal gradients in the shared volume, rather than to the absolute temperature. It can be shown (Mamouni, 1983) that the correlated output is zero if the viewed medium is of uniform temperature. Since the temperature gradients in the human body are small, the correlated output will be always be small, so considerable problems are encountered with the consequent small signal / noise ratio.

1.10.3. Deconvolution and Weiner Filtering.

To further improve resolution, the radiometric data can be processed by deconvolution and Weiner filtering. The 2-dimensional data, ΔT_m, result from the convolution of the 2-dimensional temperature distribution, with the sum of the response functions corresponding to each point. Deconvolution of these data by Fourier Transform directly yields the true temperature distribution. It has been shown (Bocquet, 1995) that this method is not badly susceptible to errors in the response function caused by misjudgement of the underlying tissue permittivity. However, as with Bardati's integral temperature retrieval method, blurring of ΔT_m by radiometer noise produces great error in the deconvolved ΔT. This problem is partially alleviated by Weiner Filtering of the data, (minimisation of the quadratic error between the true temperature and its estimate), which increases the signal to noise ratio (Bocquet et al 1993b).

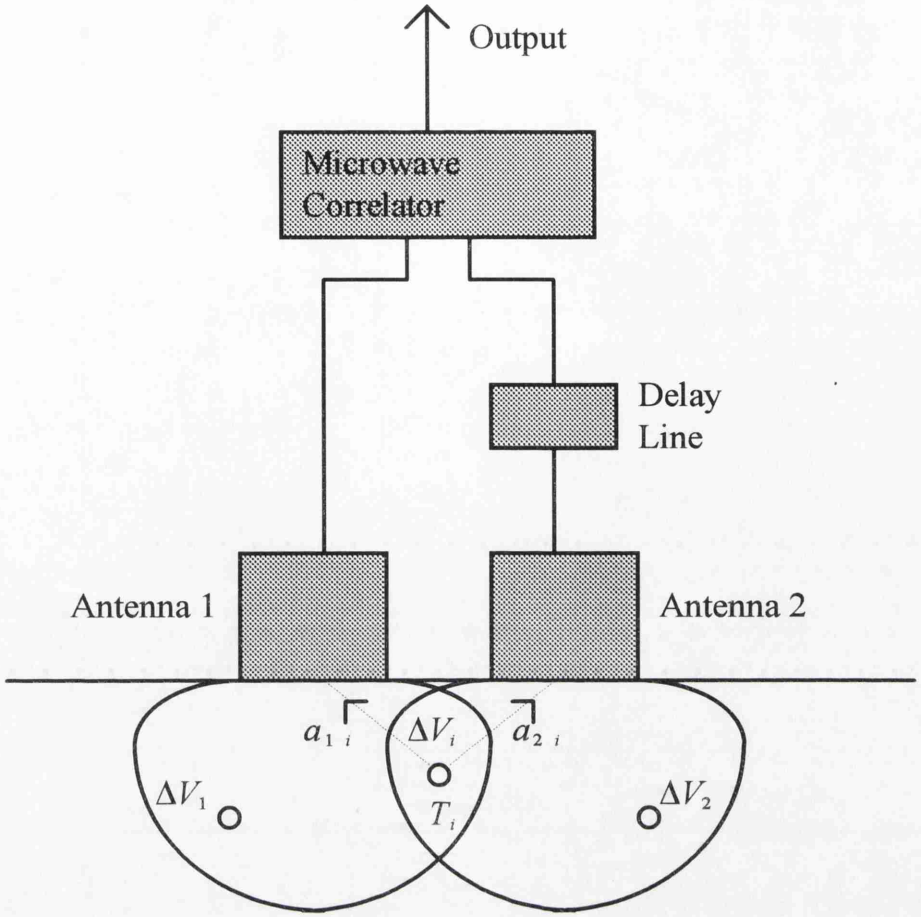

Figure 1.o. Schematic diagram of correlation radiometer. The output from one of the antennae is pulsed so that the overall output signal from the correlator is proportional only to the signal emanating from the subvolumes ΔV_i which are coupled to both antennae. Signals from subvolumes ΔV_1 and ΔV_2 which couple only to one antenna do not contribute to the correlated output signal.

Tissue Type	Thermal Conductivity ($m^{-1}K^{-1}$)	Reference
Water	0.61	Touloukan et al, 1970
0.15**M** NaCl Solution (aq.)	0.60	Hamilton, 1996
Skeletal Muscle	0.44 0.50	Hatfield, 1953 Hamilton, 1996
Kidney	0.53	Hamilton, 1996
Liver	0.51 0.49	Valvano et al, 1985 Hamilton, 1996
Fat	0.22 0.23	Lipkin and Hardy, 1954 Hamilton, 1996
Bone	0.8	Kirkland, 1967

Table 1.a. List of measured average thermal conductivity values for some tissues and tissue simulating materials.

of features

These processes enable shape and temperature retrieval from radiometric data neither whose classical thermal image nor image threshold can resolve, although a great deal of raw data must be discarded in the process. Resolution is such that two cylindrical thermal objects of diameter 20mm located at 5mm depth, and separated by 1mm in a tissue phantom have been resolved, albeit with 700 sets of probe position data.

The reliability of multi-spectral radiometry, and all the image recombination methods described above, can be improved by accurate knowledge of tissue permittivity.

1.11. Tissue Thermal Modelling.

As microwave thermography measures the temperature of a body, it is temperature which is the driving parameter determining the intensity of microwave signal that may be detected. So far, the other physical properties of body tissue and the detection system that affect the signal have been discussed.
Clinically, however, a certain amount of information, dependent on the sophistication of the detection system, about the characteristic local temperatures expected of a healthy individual must be known, before the presence of an 'anomaly' can be deduced. Furthermore, the resolvability of an anomaly is affected by the extent of thermal conduction of the observable phenomenon away from its source, by means of blood flow and tissue thermal conductivity. Thermal modelling of the body is clearly of considerable importance to the interpretation of radiometric data.

1.11.1. Bioheat Equations.

Pennes (1948) proposed the standard bioheat transfer equation, based on the Fourier heat transfer equation. It was assumed that arterial blood enters the capillaries in an element of tissue with temperature T_{art}, undergoes instantaneous thermal equilibration, and leaves the element into a vein at the local tissue temperature T. Thus the rate of change of stored energy in the volume element is given by:

$$\rho_t c_t \frac{dT}{dt} = k_t \nabla^2 T - w_b c_b (T - T_{art}) + Q \qquad (1.11.1)$$

where ρ_t, c_t, and k_t are the tissue density, specific heat and thermal conductivity respectively, w_b and c_b are the blood perfusion and specific heat, and Q is the heat generated in the element by metabolic activity. The first term on the right-hand side of eqn. 1.11.1 represents the energy transfer rate by conduction and the second term represents the heat supplied by blood flow.

There are a number of simplifications inherent in this equation. Heat exchange between blood and tissue in all blood vessels except capillaries is neglected, as is heat exchange between adjacent arteries and veins running counter-currently in opposite directions. Thus the local arterial temperature is always taken to be equal to the body core temperature. In addition, the directionality of blood flow is ignored, and the equation implies that two different temperatures, T, and T_{art}, may exist simultaneously at the same point in space.

By measuring blood velocity, arterial diameter, and the interaction factor between blood and tissue, Green (1950) found that thermal equilibrium in blood occurs in the secondary and tertiary branches, and not in the capillaries. Green was not however able to allow for counter-current heat exchange between arteries and adjacent veins, which may further lower the distance blood may travel before reaching thermal equilibrium. Weinbaum and Jiji (1984a,b 1985) have proposed that the primary heat exchange mechanism is counter-current exchange, and so introduced an effective tissue conductivity tensor, k_{eff}, to represent convection by small to medium sized blood vessels:

$$\rho_t c_t \frac{dT}{dt} = k_{eff} \nabla^2 T + Q \qquad (1.11.3)$$

Evaluation of k_{eff} is dependent on many other local vascular parameters and is therefore prone to error. Wissler (1987) questioned the validity of eqn. 1.11.3, as the model overlooks the need for a heat source / sink term, as is present in the original Pennes equation. The Weinbaum and Jiji equation describes the effect of perfusion as an increase in effective conductivity, and so this formulation cannot describe the observed rewarming effect of increased blood flow in cold tissue. It is concluded that despite its conceptual irregularities, the Pennes model is still sufficient for basic thermal modelling, although a comprehensive bioheat equation would contain elements of both the Pennes formulation, and that of Weinbaum and Jiji.

1.11.2. Elementary Theoretical Temperature Profile in Body Tissues.

To estimate the variation of tissue temperature with distance into the body, the solution to the steady-state Pennes bioheat equation in a semi-infinite, homogeneous layer of tissue is presented. The solution can be used in radiometric modelling. If the layer is bounded at $z = 0$, the bioheat equation becomes:

$$\frac{d^2T}{dz^2} = \beta^2(T - T_{art}) - \frac{Q}{k_t} \tag{1.11.4}$$

where $\beta = \sqrt{\frac{w_b c_b}{k_t}}$. With the restriction that $T \neq \infty$ as $z \to \infty$, this has general solution:

$$T(z) = Ae^{-\beta z} + T_a' \tag{1.11.5}$$

where A is a constant, and $T_a' = T_{art} + \frac{Q}{w_b c_b}$, i.e. the body core temperature. It is found that the core temperature is usually reached at a maximum depth of ~5cm into the body, so any region with a thickness of over 10cm may be regarded as being 'semi-infinite.'

At the tissue boundary, $z = 0$, heat is usually lost to the environment, in a manner approximately described by the Newtonian cooling equation:

$$k_t \left.\frac{dT}{dz}\right|_{z=0} = H(T_{surface} - T_{ambient}) \tag{1.11.6}$$

The cooling co-efficient H is defined by a combination of cooling mechanisms; radiation, convection and evaporation ($H = h_{rad} + h_{con} + h_{eva}$). For the average human body, H has an estimated overall value of approximately $1 Wm^{-2}K^{-1}$ (Brown, 1989).
Applying the heat flux continuity eqn. 1.11.6 to the general solution eqn. 1.11.5. yields an expression for the temperature profile:

$$T(z) = \frac{(T_{ambient} - T_a')}{(1 + \frac{\beta k_t}{H})} e^{-\beta z} + T_a' \tag{1.11.7}$$

For the more realistic case of a plane-stratified tissue structure, the bioheat equation may be solved in a similar manner, using the heat flux boundary condition at the tissue-type boundaries.

1.11.3. Computer Thermal Modelling.

Thermal computer models may be implemented in a similar fashion to electrical tissue modelling discussed in section 1.8. Finite Difference or Finite Element techniques can be

used, with each cell specified by a thermal conductivity and a perfusion rate. The Pennes bioheat equation is stepped over all the lattice points, until a steady-state temperature distribution is reached. Such an approach was used by Harness (1994), to provide comparison data for the analysis of microwave thermographic images. Since the thermal and electrical problems can be solved using the same mesh, a combined thermal and microwave computer model is possible, which should completely define the antenna microwave signal.

The combined permittivity and thermal conductivity measurements made as part of this study will be analysed in a subsequent publication (Hamilton, 1996), providing a more quantitative estimate of the connection between these parameters and tissue water content. This relation can then be incorporated into more accurate combined computer simulations for analysis of radiometric data.

1.11.4 Combined Thermal and Microwave Modelling.

Brown (1989) has shown that combining temperature profiles, obtained from simple thermal modelling, such as eqn. 1.11.7, with the equations previously derived for the signal power input to a microwave antenna, allows the effective microwave temperature to be expressed in terms of the ambient, surface and core temperatures, and the microwave and thermal conductivities. For the case of a perfect antenna in contact with a single semi-infinite tissue region, the effective microwave temperature is given by:

$$T_{mw} = \int_0^\infty 2\alpha T(z) e^{-2\alpha z} dz \qquad (1.11.8)$$

Incorporating $T(z)$ as given by eqn. 1.11.7 yields:

$$T_{mw} = \frac{(T_{surface} - T_a')}{(1+\frac{\beta}{2\alpha})} + T_a' \qquad (1.11.9)$$

The surface temperature is found from the continuity of heat flux equation:

$$T_{surface} = \frac{(T_{ambient} - T_a')}{(1+\frac{\beta k_t}{H})} + T_a' \qquad (1.11.10)$$

As T_{mw}, $T_{surface}$, $T_{ambient}$, and T_a' can all be measured, two expressions are generated, dependent on three unknowns; w_b, the blood perfusion, k_t, the tissue thermal conductivity, and α, the microwave penetration depth.

It has already been suggested that α is dependent on the water content of the tissue, as saline water composes ~75% of tissue mass, and has a high loss factor. Since water also has a high thermal conductivity, it is reasonable to assume that k_t is also strongly dependent on tissue water content. Table 1.a lists typical values of thermal conductivity and water contents for selected tissues, and shows that this assumption is borne out in practise. Therefore there exists a general relation between the thermal and microwave conductivities of soft body tissues. One of the three unknown variables in eqn. 1.11.10 may therefore be eliminated, making it possible to estimate the effective arterial blood perfusion in the viewed tissue.

Kelso (1995) has used this concept to estimate the water content and perfusion of human limbs and breast from thermometric measurements, and has found favourable comparison with similar 2-dimensional finite difference computer modelling. Therefore the single region model is still considered to be a useful technique, given the present knowledge of tissue properties.

Chapter 2. The Dielectric Behaviour of Pure and Heterogeneous Materials.

2.1. Introduction.

In this chapter, the polarisation response of homogeneous materials to an applied electric field is considered, leading to the formulation of dispersion equations to describe the dielectric behaviour of substances relaxing under an alternating applied field. Four of the dispersion equations most commonly used to parameterise biological tissues, tissue-simulating materials, and the equipment calibration liquids mentioned in chapter 4, are presented, and their differences discussed.

As biological tissues are heterogeneous mixtures, mainly of water and protein, a selection of equations which relate the dielectric permittivity of a mixture to that of its constituents is introduced. A brief discussion of the theory behind each mixture equation is given, and their ranges of validity when applied to simple liquid mixtures, and to tissue, are considered both theoretically and experimentally.

2.2. Polarisation and the Complex Permittivity.

When a medium is subjected to a static electric field, the material may respond in two fundamental ways. Firstly, charges of opposite sign on an atom or molecule may become displaced with respect to each other by an amount proportional to the electric field strength. This gives each atom or molecule in the medium a dipole moment, leading to a dielectric polarisation **P**. Secondly, charges in the medium may move freely in the medium under the influence of the field, leading to a static conductivity. Both types of response are observed in biological materials.

The permittivity and conductivity of a material are respectively the charge density and current density induced in the material by an applied electric field of unit amplitude. In a linear, isotropic and homogeneous material, these parameters are defined using Maxwell's equations by;

$$\mathbf{D} = \varepsilon_0 \mathbf{E} + \mathbf{P} = \varepsilon_0 \varepsilon_{r(static)} \mathbf{E} \quad (\text{as } \mathbf{P} = \varepsilon_0 (\varepsilon_{r(static)} - 1)\mathbf{E})$$

$$\mathbf{j} = \sigma_s \mathbf{E} \qquad (2.2.1)$$

where ε_0 is the permittivity of free space, **E** is the electric field, **D** is the electric displacement and **j** is the current density in a medium with static permittivity ε_s and

static conductivity σ_s. The modifying term 'static' denotes that these parameters refer to the behaviour of the material under a static electric field. Comprehensive discussions on the theory of the permittivity and conductivity of dielectrics can be found in Bleaney and Bleaney, 1976, and Ramo, Whinnery and Van Duzer, 1994.

The macroscopic electric dipole moment of a material is the vector sum of the individual dipole moments of the constituents of the material. It is possible to distinguish between three mechanisms which can contribute to the dielectric polarisation in a material. Each atom, ion or non-polar molecule in the material has zero dipole moment in zero field, but acquires a dipole moment when a field is applied. Such moments are known as 'induced dipoles.' In polar substances, such as water, the polar molecules have permanent dipole moments, which are randomly orientated in the absence of an electric field. In the presence of an electric field, molecular orientations for which the dipole moment is parallel to the field have a lower energy, and so are statistically more favourable, giving a resultant dipole moment in the direction of the field. These two former mechanisms are collectively known as 'dipolar polarisation' mechanisms. Space-charge polarisation is a third process, caused by free charges, usually at interfaces in the material. Biological materials contain permanent dipoles, and so potentially possess all three types of polarisability.

The dipolar polarisation of a material may itself be due to several mechanisms: electronic polarisation, caused by the displacement of atomic electrons relative to their nucleus; atomic polarisation, caused by relative displacements of atoms within the same molecule; and orientational polarisation, caused by the tendency of polar molecules to align their permanent dipole moment with the field, and which is opposed by thermal agitation, intermolecular binding and collisions with neighbouring molecules.

As dielectric polarisation in a material is caused by the physical displacement of charge, it therefore takes time to develop when once an electric field is applied. When the external field is removed, the polarisation of the medium decays exponentially with time, at a rate usually characterised by the *relaxation time*, τ, which is the time in which the polarisation drops to $1/e$ of its original value under the static field. If an alternating field is applied, the response of the medium gives rise to a polarisation which lags behind the field, and which develops and relaxes at about the same rate as the field alternates.

For alternating electric fields of microwave frequencies, electronic and atomic polarisation effects are unimportant, as they occur only at much higher frequencies. The

dominant dielectric relaxation process is that of orientational polarisation. An important dielectric, water, has a permittivity of about 80 at radio to microwave frequencies, but an optical refractive index of only 1.3, not $\sqrt{80}$. Hence it may be concluded that the electronic contribution to the permittivity is only approximately 1.7, and the rest is due to the orientational polarisability of the water molecule.

Polar molecules, or molecular groups, rotate under the influence of the alternating microwave field. If the polar molecules are large, or if the frequency of the applied field is great, then the molecules do not rotate sufficiently quickly to maintain equilibrium with the field. The polarisation loses phase with the electric field, resulting in thermal dissipation of the field energy.

A complex representation of the permittivity is needed to represent lossy material of this type;

$$\varepsilon_r = \varepsilon' - j\varepsilon'' \qquad (2.2.2)$$

where ε' is the dielectric constant and ε'' is the loss factor. The loss factor may be composed of contributions to the conductivity arising from both dielectric relaxation and ionic conductivity;

$$\varepsilon'' = \frac{\sigma}{\omega\varepsilon_0} = \frac{\sigma_{dispersion}}{\omega\varepsilon_0} + \frac{\sigma_{ionic}}{\omega\varepsilon_0} \qquad (2.2.3)$$

The combined conductivity $\sigma = \sigma_{dispersion} + \sigma_{ionic}$ is often referred to as the *effective conductivity*. When discussing the complex permittivity of tissue, it may often be more instructive to refer to the conductivity rather than the loss factor, as the conductivity is a more empirical parameter. For a simple material, with no ionic conductivity, the polarisation of the material will relax towards the steady state as a first order process characterised by the relaxation time τ.

2.3. Debye Dispersion Equation.

Debye (1929) derived the form of a generalised equation for the dielectric constant of a material with orientational polarisability, in the region where the dielectric polarisation is 'relaxing,' shown graphically in fig. 2.a. When the frequency of the applied field is much greater than the reciprocal of the alignment time, the permittivity tends to a frequency independent value ε_∞ representing the electronic and atomic polarisation. For much lower frequencies it tends to a constant value ε_s, the 'static,' or low frequency, permittivity. It is, strictly, misleading to regard ε_s and ε_∞ as the 'static' and 'infinite' frequency limits, as there may be other dispersion regions, at other frequencies,

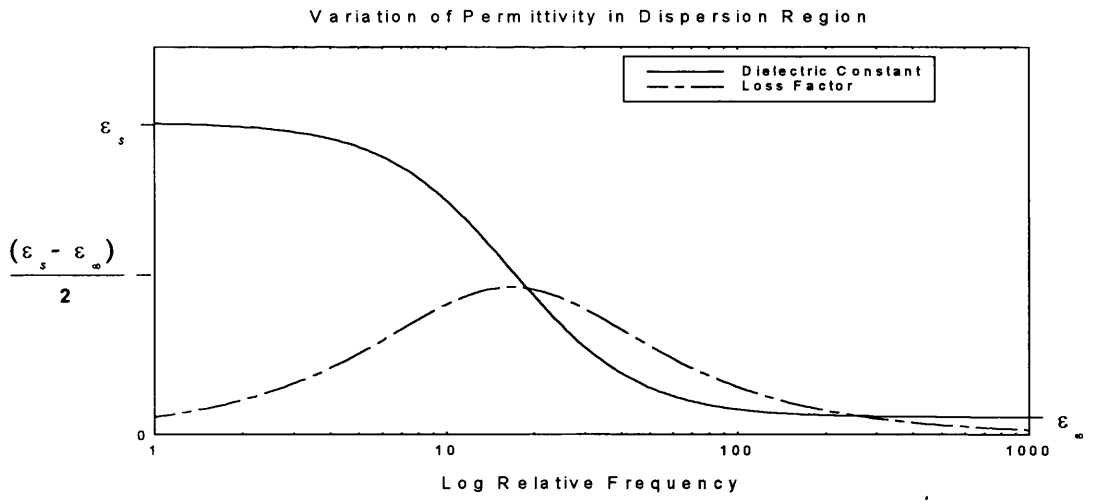

Figure 2.a. Behaviour of the components of the permittivity of a material subjected to an electrical signal with period similar to the orientational relaxation time of the constituent molecules.

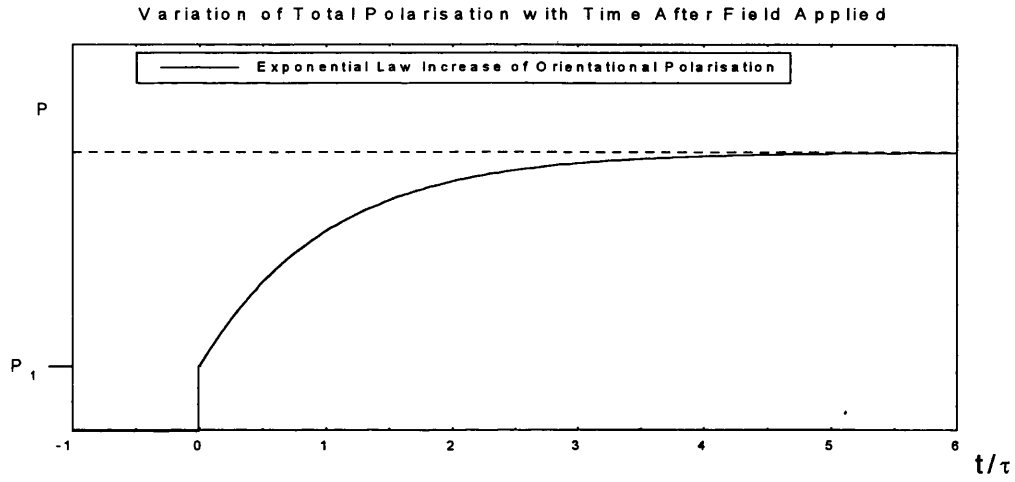

Figure 2.b(i). Increase in polarisation of a material subjected to a constant electric field at time t = 0. Electronic polarisation effects occur almost immediately, with orientational polarisation increasing with time following an exponential law.

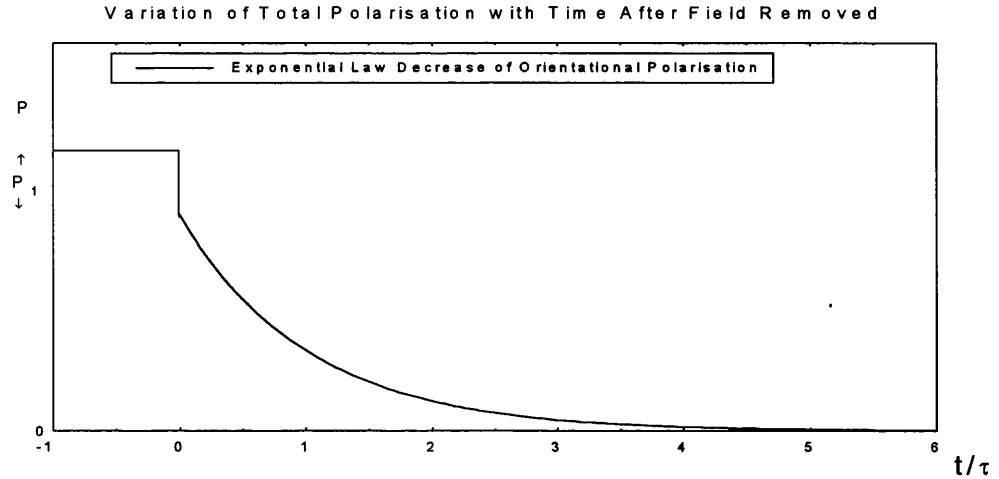

Figure 2.b(ii). Decrease in polarisation of a material when a constant electric field is removed at time t = 0.

associated with the other polarisation processes, which effect the ultimate limits of the permittivity.

Consider a field E applied to a dielectric material with both orientational and electronic polarisability, given by P_2 and P_1 respectively. The electronic polarisation will be established very quickly, instantaneously compared with the time intervals of interest here, but the remaining dipolar polarisation, P_2, takes time to reach its equilibrium value. If it is assumed P_2 increases at a rate proportional to its departure from equilibrium value, then

$$\frac{dP_2}{dt} = \frac{P - P_1 - P_2}{\tau} \tag{2.3.1}$$

where P is the equilibrium value of the *total* polarisation, and τ is the macroscopic relaxation time. If the field is applied at time t=0, then the solution for P_2 is given by

$$P_2 = (P - P_1)\left[1 - \exp\left(\frac{-t}{\tau}\right)\right] \tag{2.3.2}$$

so that P_2 approaches its equilibrium value according to an exponential law. Similarly, if the polarisation P is already established in a steady field E, which is removed at time t=0, P_1 falls immediately to zero, and the rate of change of P_2 is given by

$$\frac{dP_2}{dt} = -\frac{P_2}{\tau}$$

yielding

$$P_2 = (P - P_1)\exp\left(-\frac{t}{\tau}\right) \tag{2.3.3}$$

This behaviour is shown graphically in fig. 2.b.

Now consider an applied field with alternating angular frequency ω. This can be represented by

$$E = E_0 \exp(j\omega t) \tag{2.3.4}$$

The polarisability P can be expressed in terms of the applied field E and relative permittivity ε_r: at low frequency, the relative permittivity is equal to the 'static' permittivity ε_s.

$$P = \varepsilon_0[\varepsilon_s - 1]E \tag{2.3.5}$$

The high frequency permittivity limit ε_∞ is defined in terms of P_1 and E

$$P_1 = \varepsilon_0[\varepsilon_\infty - 1]E \tag{2.3.6}$$

As before, the rate of change of P_2 is proportional to its departure from equilibrium

$$\frac{dP_2}{dt} = \frac{P - P_1 - P_2}{\tau}$$

$$\Rightarrow \frac{dP_2}{dt} = \frac{\varepsilon_0}{\tau}(\varepsilon_s - \varepsilon_\infty)E_0 \exp(j\omega t) - \frac{P_2}{\tau} \tag{2.3.7}$$

In steady state a solution is expected of the form

$$P_2 = A\exp(j\omega t) \tag{2.3.8}$$

Substituting this expression back into the differential equation (2.3.7) gives

$$P_2 = \frac{\varepsilon_0(\varepsilon_s - \varepsilon_\infty)E}{1+j\omega\tau} \tag{2.3.9}$$

The total polarisability P is equal to the sum of P_1 and P_2

$$P_1 + P_2 = \varepsilon_0(\varepsilon_\infty - 1)E + \frac{\varepsilon_0(\varepsilon_s - \varepsilon_\infty)E}{1+j\omega\tau} \quad = \quad \varepsilon_0[\varepsilon_r(\omega) - 1]E \tag{2.3.10}$$

and so the relative permittivity of the material is, as a function of frequency, equal to

$$\varepsilon_r(\omega) = \varepsilon' - j\varepsilon'' = \varepsilon_\infty + \frac{\varepsilon_s - \varepsilon_\infty}{1+j\omega\tau} \tag{2.3.11}$$

This equation is commonly known as the Debye dispersion equation.

Separating eqn. 2.3.11 into real and imaginary parts gives

$$\varepsilon' = \varepsilon_\infty + \frac{\varepsilon_s - \varepsilon_\infty}{1+(\omega\tau)^2} \quad \text{and} \quad \varepsilon'' = \frac{(\varepsilon_s - \varepsilon_\infty)\omega\tau}{1+(\omega\tau)^2} \tag{2.3.12}$$

It is common to express these parameters in terms of a characteristic relaxation frequency, or wavelength, rather than a relaxation time, where $\tau = 1/2\pi f_c = \lambda_c/2\pi c$.

2.4. Distribution of Relaxation Times.

In a real material, which may be a mixture of different substances, a solution, or just a material with a non-linear relaxation process, a distribution of relaxation times is expected. This is characterised by a broader dispersion curve and lower maximum loss than is predicted by the Debye relationship (see fig. 2.c). The Cole-Cole equation is an empirical equation which parameterises dispersion data whilst allowing for a symmetrical distribution of relaxation times characterised by α ,about a central mean value τ.

$$\varepsilon_r = \varepsilon_\infty + \frac{\varepsilon_s - \varepsilon_\infty}{1+(j\omega\tau)^{1-\alpha}} \qquad 0 \le \alpha \le 1 \tag{2.4.1}$$

The Cole-Davidson equation allows for an asymmetrical distribution of relaxation times. It is mainly used for viscous fluids, such as glycerol, but rarely for biological substances, or their components, which are composed mainly of water, a non-viscous liquid.

$$\varepsilon_r = \varepsilon_\infty + \frac{\varepsilon_s - \varepsilon_\infty}{(1+j\omega\tau)^{1-\alpha}} \tag{2.4.2}$$

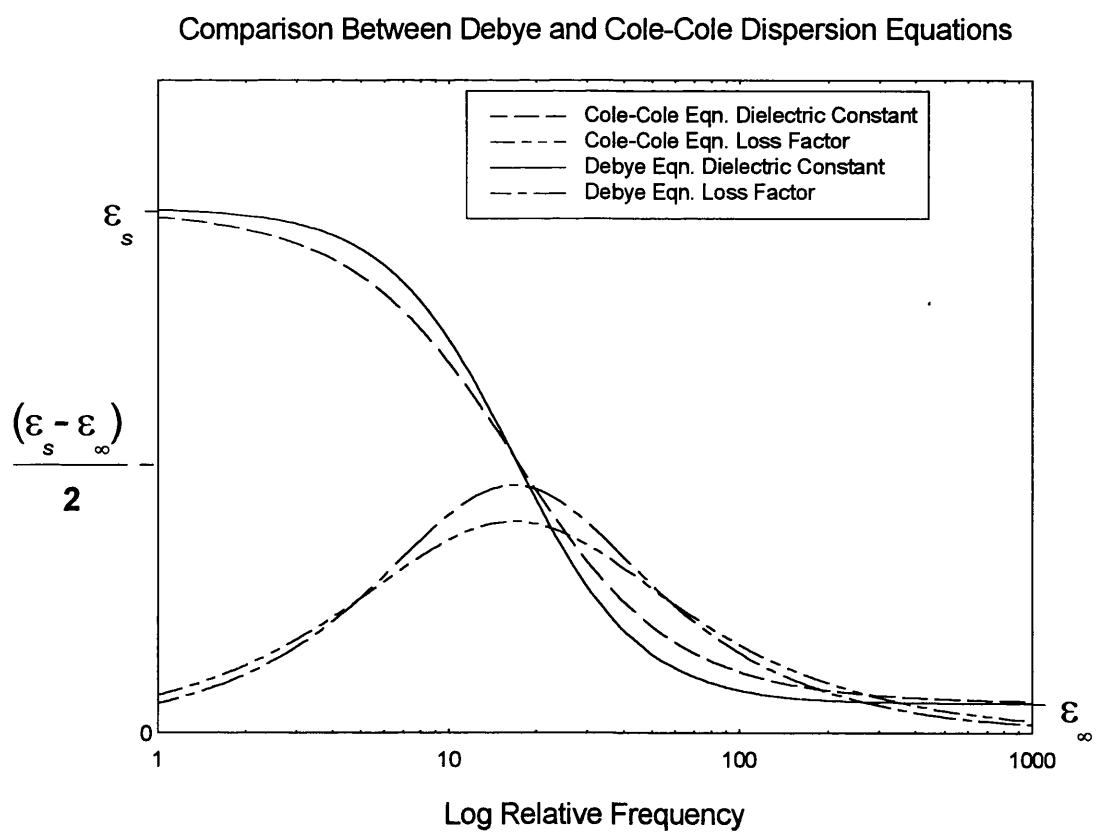

Figure 2.c. Comparison between Debye dispersion equation representing a single relaxation time in a material, and Cole-Cole dispersion equation representing a distribution of relaxation times characterised by α, equal here to 0.1. Note frequency spread of dispersion, and lower maximum loss for Cole-Cole eqn.

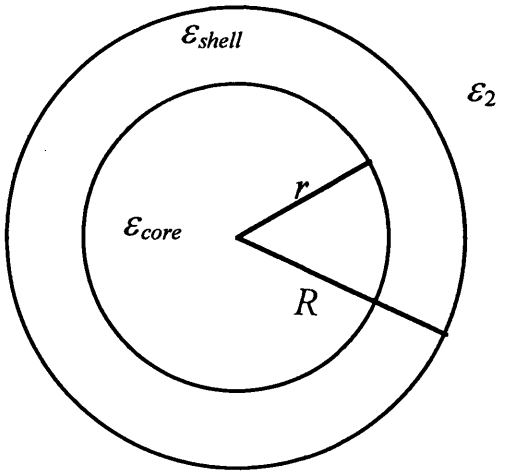

Figure 2.d. Shell covered sphere with overall permittivity ε_{sphere} given by eqn. 2.8.5.

Measurements have shown that the microwave dispersions of certain substances, such as ethylene glycol, are characterised by two independent Debye processes. For such substances, a multicomponent Debye equation is often the best way to parameterise the dielectric behaviour.

$$\varepsilon_r = \varepsilon_\infty + \frac{\varepsilon_s - \varepsilon_H}{1 + j\omega\tau_1} + \frac{\varepsilon_H - \varepsilon_\infty}{1 + j\omega\tau_2} \qquad (2.4.3)$$

where τ_1 and τ_2 are the relaxation times of the two processes, and ε_H is an intermediate permittivity limit. Multicomponent Debye dispersions have been use by Stoy et al (1982) to account for the behaviour of membrane - bound tissue structures at megahertz frequencies. At these frequencies, however, the tissue permittivity is determined mainly by cell membranes rather than water content within the tissue. In the microwave frequency range, where the effect of water dominates the tissue permittivity, the simple Debye and Cole-Cole dispersion equations are usually those used to model the dielectric behaviour of the components of biological tissue.

2.5. Dielectric Mixtures.

In the study of biological materials, it is found that tissues are heterogeneous substances, which cannot therefore be described dielectrically, in a particular frequency range, by one single dispersion equation of the forms already described (eqns. 2.3.11 and 2.4.1-3). Rather, they must be considered as a combination of two or more individual substances, each with its own distinct dielectric behaviour. In the case of biological materials, the two major constituent materials are water (containing dissolved ions) and proteins. When estimating the permittivity of an heterogeneous mixture of two substances at microwave frequencies, the permittivity of each constituent substance may first be found by examination of its dipolar relaxation dispersion. Then, the overall permittivity of the mixture may be estimated, using a suitable *mixture equation* to combine the individual values.

There exist a large number of mixture equations relating the bulk properties of two phase materials, consisting of one phase of particles distributed in various manners in the second continuous phase, to the properties of the two constituent phases themselves. In general, each mixture equation was originally derived specifically to solve a problem of particular interest to the proposer, and so each equation assumes a certain geometry of

particle distribution, and may have been derived to model one of many bulk transport co-efficients of the material.

Mixture equations have been derived individually for the electrical permittivity and conductivity, the magnetic permeability, and the thermal conductivity and diffusivity. Each mixture equation is, however, governed by the *principle of generalised conductivity*, and so each can be regarded as being equally applicable to all other transport co-efficients, provided the mixture characteristics and geometry are suitable. The principle of generalised conductivity is a thermodynamic argument which is justified by the fact that the behaviour of the flux vectors and thermodynamical forces of all bulk transport properties of materials are of the same form at boundaries between two media. This is due to the formal coincidence of the differential equations of stationary heat flow, electric current, electric and magnetic induction and diffusion streams. Lewin (1947) showed that this principle is valid for mixture formulae representing either the static or the complex permittivity of a disperse system, providing the wavelength of the applied electric field is large in comparison to the dimensions of the disperse particles.

Thorough reviews of this principle, and of the history and theory behind many mixture equations can be found in Dukhin (1971), Van Beek (1965) and Campbell (1990). Here, only those simple mixture equations most commonly applied to biological systems are introduced.

It is important to note that despite referring to mixture materials as being heterogeneous, bulk transport mixture equations relate to macroscopic bulk properties, and so are valid only when applied to a volume of mixture material which is sufficiently large that the volume may be characterised by a single definite value of the transport co-efficient of interest. A macroscopic E-field is the average field over a volume containing a large number of dispersed particles, and so the disperse mixture system must be regarded as isotropic, homogeneous, and represented by a single dielectric constant ε_{mix}, such that

$$\overline{\mathbf{D}} = \varepsilon_{mix}\varepsilon_0\overline{\mathbf{E}} \qquad (2.5.1)$$

where $\overline{\mathbf{E}}$ and $\overline{\mathbf{D}}$ are the average intensity and induction of the applied field.

2.6. Limits on Mixture Permittivity.

A first approximation to the maximum and minimum limits of the permittivity of a mixture may be obtained by a method based on capacitance theory. Weiner (1912)

considered a mixture to consist of a collection of fibres, lying either parallel or perpendicular to the plates of a capacitor. When the fibres lie perpendicular to the plates, the mixture permittivity is maximised as a straight line between the permittivity values, ε_1 and ε_2, of the two component materials.

$$\varepsilon_{max} = v_1\varepsilon_1 + (1-v_1)\varepsilon_2 \qquad (2.6.1)$$

where v_1 is the volume fraction of material 1 in the mixture. When the fibres lie parallel to the plates, the mixture permittivity is minimised.

$$\frac{1}{\varepsilon_{min}} = \frac{v_1}{\varepsilon_1} + \frac{(1-v_1)}{\varepsilon_2} \qquad (2.6.2)$$

Hashin and Shtrikman (1961) derived more restrictive limits, originally for the magnetic permeability of a mixture, by maximising and minimising the free energy of the mixture.

When $\varepsilon_2 > \varepsilon_1$,

$$\frac{\varepsilon_{max} - \varepsilon_2}{\varepsilon_{max} + 2\varepsilon_2} = \frac{\varepsilon_1 - \varepsilon_2}{\varepsilon_1 + 2\varepsilon_2} v_1$$

and

$$\frac{\varepsilon_{min} - \varepsilon_1}{\varepsilon_{min} + 2\varepsilon_1} = \frac{\varepsilon_2 - \varepsilon_1}{\varepsilon_2 + 2\varepsilon_1}(1-v_1) \qquad (2.6.3)$$

The Hashin and Shtrikman bounds always lie within the Weiner bounds, and are the best possible bounds for the dielectric constant of a two phase material if no structural information apart from the volume fractions is available. These limiting values do not require any assumptions about the geometry of the mixture system, only that sufficient volume of the mixture is considered that the mixture may be regarded as isotropic and quasi-homogeneous.

2.7. Maxwell's Mixture Equation.

Maxwell (1881) proposed the first mixture equation, to calculate the conductivity of a dilute suspension of spherical particles. When a small volume of spheres of medium 1 are suspended in medium 2, the permittivity of the mixture is given by;

$$\frac{\varepsilon_{mix} - \varepsilon_2}{\varepsilon_{mix} + 2\varepsilon_2} = \frac{\varepsilon_1 - \varepsilon_2}{\varepsilon_1 + 2\varepsilon_2} v_1 \qquad (2.7.1)$$

In deriving this equation, Maxwell first solved Laplace's equation to determine the electric field around a single suspended particle, then calculated an equivalent conductivity for a larger sphere that contained many such particles. Mutual polarisation of the suspended particles is not taken into consideration in the derivation, and so this

equation is only strictly valid when the concentration of the suspension is sufficiently dilute that the suspended particles do not interact. The limiting volume fraction is usually assumed to be $v_1 \approx 0.2$.

The similarity of form between Maxwell's mixture equation and the bounding limits of Hashin and Shtrikman (eqns. 2.6.3) is significant. The permittivity of a mixture, where $\varepsilon_1 > \varepsilon_2$, is bounded above by the permittivity of a suspension of spherical particles of medium 2 in a continuous medium 1, and is bounded below by the permittivity of a suspension of particles of medium 1 in a continuous medium 2.

2.8. Extensions of Maxwell's Mixture Equation.

Wagner (1914) took Maxwell's original equation, which referred only to static permittivity, and extended the analysis to show its validity for materials with complex permittivities under alternating fields, which is the case in this research. Other researchers have considered alternative suspended particle geometries in the Maxwell-Wagner theory. Fricke (1924) allowed the suspended particles to be prolate or oblate spheroids, by introducing a form factor, γ, which is a function of the generalised conductivity (in this case permittivity) of the two phases, and of the axial ratio a/b of the suspended spheroids.

$$\frac{\varepsilon_{mix} - \varepsilon_2}{\varepsilon_{mix} + \gamma\varepsilon_2} = \frac{\varepsilon_1 - \varepsilon_2}{\varepsilon_1 + \gamma\varepsilon_2} v_1 \qquad (2.8.1)$$

where the form factor is $$\gamma = -\frac{\varepsilon_2(1-\beta) - \varepsilon_1}{\varepsilon_2 - \varepsilon_1(1+\beta)}, \qquad (2.8.2)$$

$$\beta = \left[\frac{2}{(\varepsilon_1 + 2\varepsilon_2) - (3M/2)(\varepsilon_2 - \varepsilon_1)}\right]\left[\frac{\varepsilon_2 - \varepsilon_1}{3}\right] \qquad (2.8.3)$$

and, for oblate spheroids,

$$M(a<b) = \frac{\cos(\phi)(\phi - \tfrac{1}{2}\sin(2\phi))}{\sin^3(\phi)} \qquad \cos(\phi) = a/b \qquad (2.8.4)$$

The value of the form factor γ is 1 for cylindrical particles oriented normal to the field, and reduces to 2 for spheres. Velick and Gorin (1940) further extended the theory to cover suspended ellipsoids, with three differing principal axes.

A final variation on the simple Maxwell-Wagner theory that may have a useful application in the analysis of biological materials is the case of a shell covered sphere, as

shown in fig. 2.d. This may be a more realistic simulation of the cellular structure found in tissue. Maxwell showed that the equivalent permittivity, ε_{sphere}, of a sphere of radius R, consisting of an inner core sphere of radius r and permittivity ε_{core}, surrounded by a shell of thickness d and permittivity ε_{shell}, may be given by

$$\frac{\varepsilon_{sphere} - \varepsilon_{shell}}{\varepsilon_{sphere} + 2\varepsilon_{shell}} = \left(\frac{r}{R}\right)^3 \frac{\varepsilon_{core} - \varepsilon_{shell}}{\varepsilon_{core} + 2\varepsilon_{shell}} \tag{2.8.5}$$

The permittivity of a suspension of such spheres may be calculated using two successive applications of the Maxwell-Wagner theory. First, by using eqn. 2.8.2 to evaluate the effective permittivity of the composite spheres, then using eqn. 2.7.1 to evaluate the overall permittivity of the suspension. Again, this only strictly applies to dilute suspensions with non-interacting particles. A more complete analysis requires consideration of the higher order field terms from nearby particles.

2.9. Mixture Equations for Concentrated Systems.

In concentrated disperse systems, mutual polarisation between suspended particles limits the range of applicability of equations based on the Maxwell-Wagner theory. When the space distribution of suspended particles is strictly ordered in the system, mutual polarisation may quite easily be accounted for. However, in real disperse systems, the particles are distributed randomly in space. One way of overcoming this problem is to use the self-consistent theory (SCS), in which it is assumed that each particle is surrounded by the composite material with permittivity ε_{mix}, rather than by the continuum medium of permittivity ε_2. This is also referred to as the effective medium theory (EMT) (Bergman, 1978).

Bruggeman's equation (1935) applies to spherical suspensions, and is obtained through an integral method, increasing the volume fraction of the suspended medium from 0 to v_1 by successive addition of infinitesimal quantities of the disperse phase.

Let, at a given concentration v_1' of the disperse phase 1, the mixture permittivity be equal to ε_{mix}. Then let an increase in concentration $\delta v_1'$ cause a variation in ε_{mix} of $\delta\varepsilon_{mix}$. Maxwell's equation (2.7.1) can be used to relate the new mixture permittivity

$\varepsilon_{mix} + \delta\varepsilon_{mix}$, to the old mixture permittivity ε_{mix}, the suspended phase permittivity ε_1, and the increased volume fraction $\frac{\delta v_1'}{(1-v_1')}$. This gives

$$\frac{(2\varepsilon_{mix}+\varepsilon_1)\delta\varepsilon_{mix}}{(3\varepsilon_{mix}+\delta\varepsilon_{mix})(\varepsilon_1-\varepsilon_{mix})} = \frac{\delta v_1'}{(1-v_1')}$$

which, for small $\delta\varepsilon_{mix}$,

$$\approx \frac{(2\varepsilon_{mix}+\varepsilon_1)\delta\varepsilon_{mix}}{3\varepsilon_{mix}(\varepsilon_1-\varepsilon_{mix})} = \frac{\delta v_1'}{(1-v_1')} \qquad (2.9.1)$$

Integrating this expression from the continuum permittivity ε_2 to ε_{mix}, and from 0 to v_1 yields

$$\left(\frac{\varepsilon_2}{\varepsilon_{mix}}\right)^{\frac{1}{3}}\left(\frac{\varepsilon_1-\varepsilon_{mix}}{\varepsilon_1-\varepsilon_2}\right) = (1-v_1') \qquad (2.9.2)$$

This equation is known as Bruggeman's equation, and was, like Maxwell's equation, first derived for static permittivities only. Hanai (1968) not only demonstrated its validity for complex permittivities, but later showed that, like the Maxwell equation, the theory could be extended, by successive application, to predict the permittivity of suspensions of shell-covered spheres.

2.10. Other Mixture Equations

2.10.1. Polder and Van Santen's Equation.

A general equation for the permittivity of a random suspension of ellipsoidal particles was derived by Polder and Van Santen (1946).

$$\varepsilon_{mix} = \varepsilon_2 + \frac{(\varepsilon_1-\varepsilon_2)v_1}{3}\sum_{1,2,3}\frac{\bar{\varepsilon}}{\left[\bar{\varepsilon}+A_i(\varepsilon_1-\bar{\varepsilon})\right]} \qquad (2.10.1)$$

In this equation, the A_i represent depolarisation form factors (c.f. Fricke's eqn. 2.8.1), dependent on the semi-axes of the ellipsoids, and $\bar{\varepsilon}$ is a non-specific factor representing the medium immediately surrounding each suspended particle ($\varepsilon_{mix} \le \bar{\varepsilon} \le \varepsilon_2$).

Biological tissues are complex materials, whose behaviour is not fully understood at microwave frequencies, and so it is not feasible to utilise Polder and Van Santen's equation in this form. However, the limiting cases of this equation for spherical particles yields two simple and useful mixture equations.

When the suspension is concentrated, $\bar{\varepsilon} \approx \varepsilon_{mix}$, yielding Bottcher's (1945) equation

$$\frac{\varepsilon_{mix}-\varepsilon_2}{3\varepsilon_{mix}} = \frac{\varepsilon_1-\varepsilon_2}{2\varepsilon_{mix}+\varepsilon_1}v_1 \qquad (2.10.2)$$

In fact, Bottcher's equation was derived from a self-consistent scheme approach before Polder and Van Santen showed it to be a result of their general equation.
Boned and Peyrelasse (1983) also showed that by taking the low concentration limit of eqn. 2.10.1 and adding successive permittivity increments, after the fashion of Bruggeman, a cubic equation for the permittivity of high concentration ellipsoidal suspensions can be obtained.

2.10.2. Looyenga's and Lichteneker's Formulae.

Campbell (1990) also considered the application of Lichteneker's (1929) and Looyenga's (1965) mixture equations to the permittivity of biological tissue. Both of these equations are simple in form, and are supported by certain experimental evidence, but are also considered to be fundamentally flawed. Lichteneker's logarithmic law is expressed

$$\log \varepsilon_{mix} = v_1 \log \varepsilon_1 + (1 - v_1) \log \varepsilon_2 \qquad (2.10.3)$$

Looyenga's equation draws the conclusion that the cube roots of permittivity are additive in a disperse system

$$\varepsilon_{mix}^{\frac{1}{3}} = v_1 \varepsilon_1^{\frac{1}{3}} + (1 - v_1) \varepsilon_2^{\frac{1}{3}} \qquad (2.10.4)$$

Dukhin (1971) points out that Looyenga's equation had previously been derived by Landau, and in a more rigorous manner. Furthermore, Landau noted that the validity of the equation is limited to the case where the permittivities of both components of the mixture are similar i.e. $|\varepsilon_2 - \varepsilon_1| << \varepsilon_{mix}$. It is additionally pointed out that both of these equations are flawed in their initial assumptions by requiring, at different stages, the disperse system to be both random and ordered simultaneously.

2.11. Mixture Equations and Space Charge Polarisation.

It was stated in section 2.2 that biological materials may be subject to both dipolar and space charge polarisation effects, when subjected to an electric field. Dipolar dispersions in pure materials are modelled by the Debye-type dispersion equations previously discussed. Space charge polarisation effects occur in composite materials, and may be classified as interfacial polarisation, and counterion diffusion polarisation effects. Interfacial polarisation is more important at high frequencies in biological systems, and is

a consequence of non-uniform distribution of free electronic charges across the interfaces between phases in composite materials.

In general, heterogeneous media exhibit frequency-dependent dielectric and conductive properties that differ from those of the constituentt materials, on account of interfacial polarisation. This can be illustrated by considering a simple two-layered composite material placed between the electrodes of a capaciitor, as shown in fig. 2.e. The model effectively represents two capacitors in series. If, for simplicity, the conductivity σ_2 is negligible, and the dielectric constants ε_1' and ε_2', and also σ_1, are frequency independent, then the two complex capacitances are given by

$$C_1 = \frac{A\varepsilon_0(\varepsilon_1' - j\sigma_1/\omega\varepsilon_0)}{d_1} \text{ and } C_2 = \frac{A\varepsilon_0\varepsilon_2'}{d_2} \qquad (2.11.1)$$

The total effective capacitance, C_{tot}, is given, in terms of the effective permittivity ε_{tot}, by

$$\frac{1}{C_{tot}} = \frac{1}{C_1} + \frac{1}{C_2} = \frac{d}{A\varepsilon_0\varepsilon_{tot}}$$

so

$$C_{tot} = \frac{A\varepsilon_0\varepsilon_2'(\varepsilon_1' - j\sigma_1/\omega\varepsilon_0)}{d_2(\varepsilon_1' - j\sigma_1/\omega\varepsilon_0) + d_1\varepsilon_2'} = \frac{A\varepsilon_0\varepsilon_{tot}}{d} \qquad (2.11.2)$$

Therefore the limiting low and high frequency permittivities are given by

$$\varepsilon_{tot}(\omega \to 0) = \frac{\varepsilon_2' d}{d_2} = \varepsilon_s \quad \text{and} \quad \varepsilon_{tot}(\omega \to \infty) = \frac{\varepsilon_1'\varepsilon_2' d}{d_2\varepsilon_1' + d_1\varepsilon_2'} = \varepsilon_\infty \qquad (2.11.3)$$

It can be shown that at intermediate frequencies

$$\varepsilon_{tot} = \varepsilon_\infty + \frac{(\varepsilon_s - \varepsilon_\infty)(-d_2 j\sigma_1/\omega\varepsilon_0)}{(\varepsilon_1' d_2 + \varepsilon_2' d_1 - d_2 j\sigma_1/\omega\varepsilon_0)} = \varepsilon_\infty + \frac{\varepsilon_s - \varepsilon_\infty}{1 + j\omega\tau} \qquad (2.11.4)$$

and so the two-layer system exhibits a dielectric dispersion with relaxation time given by

$$\tau = \frac{(\varepsilon_1' d_2 + \varepsilon_2' d_1)\varepsilon_0}{\sigma_1 d_2} \qquad (2.11.5)$$

In suspension mixtures the situation is more complicated, but mixture equations not only predict interfacial dispersions, but can be manipulated to parameterise the dispersions according to Deybe-type dispersion equations (Pauly and Schwan, 1959). The Maxwell theory predicts a small dispersion in biological tissues at frequencies of a few hundred MHz, because of the dissimilar electrical properties of protein and aqueous electrolyte. A conductivity increase of several hundredths of a Sieman per metre is predicted (Foster and Schwan, 1989), at a relaxation frequency of ~300 kHz. Therefore at microwave frequencies, the effect of interfacial dispersion in biological tissue is negligible.

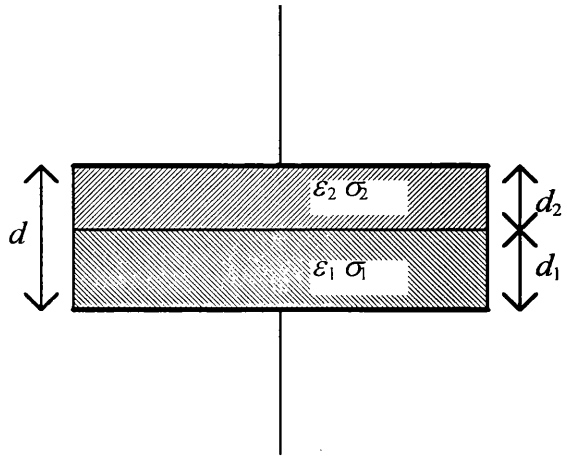

Figure 2.e. Two-layer heterogeneous capacitative system.

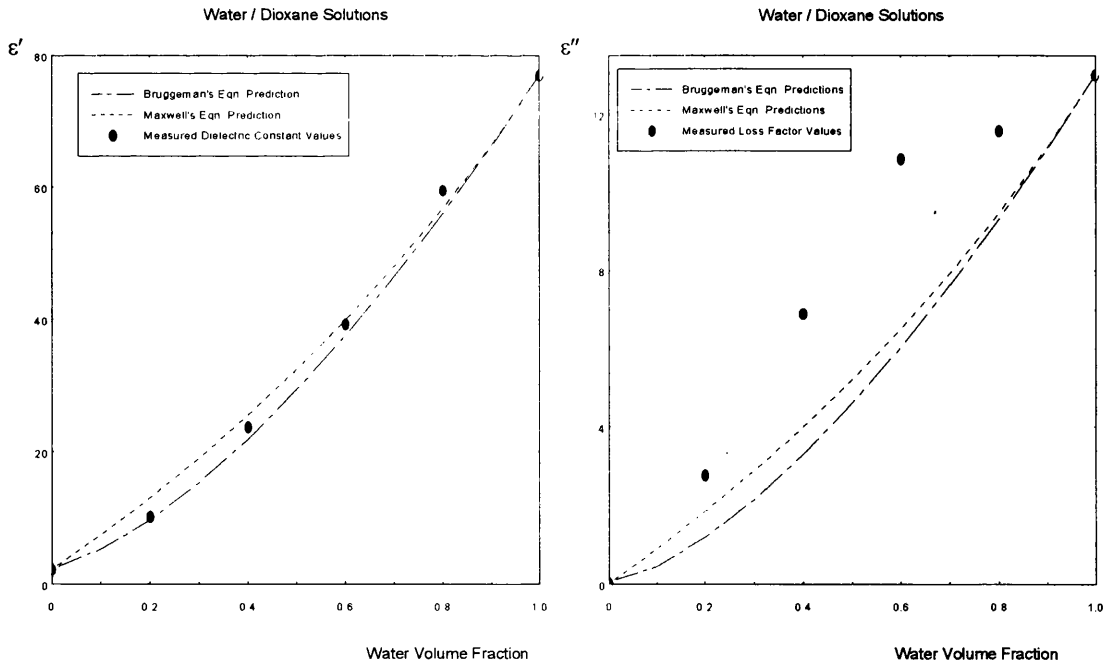

Figure 2.f. Measured dielectric constant and loss factor vs. water content for water / dioxane solutions, also showing mixture equation predictions.

2.12. Mixture Equation Symmetry.

A mixture equation is said to be symmetric if, by interchanging v_1 with $(1-v_1)$, and ε_2 with ε_1, the overall predicted permittivity is unchanged. Symmetric equations therefore suggest that a suspension of protein spheres, of volume fraction 0.3, in water, has the same dielectric behaviour as a suspension of water spheres, of volume fraction 0.7, in protein. Symmetrical mixture equations run contrary to the Maxwell-Wagner theory, which is still the basis for most other mixture equations, and have been shown by Clausse (1983), both theoretically and experimentally, to be inconsistent. The formulae of Lichteneker, Looyenga and Bottcher all fall into this category, as of course do Weiner's limit equations. Hale (1976) does however argue that Bottcher's equation is an appropriate approximation for a solid conglomerate of particles of two different materials.

2.13. Experimental Verification of Mixture Equations for Related Problems.

Using his own rendering of Maxwell's equation (3.8.1), Fricke (1925a,b) compared the predictions of mixture theory with the measured electrical conductivity of cream suspensions in milk, and of red corpuscles in canine blood. Fricke assumed that cream particles were spherical, and that the axial ratio of red corpuscles was $1/4.25$. Measuring at frequencies of up to 200 kHz, , the formula was verified, to within ~0.5%, for volume fractions of up to 62% for cream, and up to 80% for blood. Velick and Gorin (1940) later verified the predictions at volume fractions of up to 50% for suspensions of duck blood in saline. Much later, Fricke (1955) also estimated the thickness of cell walls, using the multi-layer extension of the Maxwell-Wagner theory.

Such correlation is encouraging, if not rather unexpected, as the original Maxwell equation is only strictly valid for dilute suspensions. It has been suggested by Lewin (1947) that in the case of non-conducting suspensions (e.g. cream, which is essentially butterfat), the term 'dilute' is applicable up to the stage where neighbouring spheres begin to touch. With equally sized spheres this happens at a volume fraction of about 50%. In practice, however, the spheres will not be all of equal size, allowing a greater packing ratio. This hypothesis was supported by Lewin's measurements on powder mixtures, which also agreed with his own formula at up to 75% volume fraction.

Hanai et al, (1975) made extensive study of the permittivity of water / oil emulsions at frequencies up to 3 MHz, finding that his complex rendering of Bruggeman's equation predicts the high frequency limiting values of the mixture permittivity more reliably than does the Maxwell-Wagner theory. Good agreement was observed at up to 80% volume fraction, not only for water / oil emulsions, but also for spherical glass bead suspensions, and suspensions of dog blood cells. Bruggeman himself measured the static permittivity of mixtures of water, alcohol and paraffin oil to demonstrate the validity of the incremental effective medium theory used to formulate his equation.

2.14. Mixture Equations Applied to Mixtures of Interacting Substances.

Mixture equations are most successful at predicting the permittivity of mixtures of two substances which, when mixed, do not interact with each other. Hanai's studies of suspensions of minute glass beads in oil are an example of this. It is supposed in the formulation of mixture equations, that the two phases will not chemically interact when mixed. If, when two materials are mixed, the separate phases affect the way the molecules or components of each phase are bonded, mixture equations may fail to directly predict the permittivity of the combined mixture.

Such failures are common with mixtures of polar substances such as water, which form dipole bonds with other molecular species. To illustrate this problem, the results of permittivity measurements on aqueous solutions of 1,4-dioxane, methanol, propan-2-ol and ethylene glycol are presented. All the permittivity measurements were made at room temperature, using the co-axial probe technique described in chapters 4 and 5, operating at 3 GHz. This frequency is close to the orientational relaxation frequencies of water (~17GHz), methanol (~2.8GHz), and ethylene glycol (~1.1GHz) (from Jordan et al, 1979). It is not intended here to quantitatively analyse the bonding behaviour of these solutions; only to qualitatively investigate why mixture equations may fail to predict the correct permittivity of the solutions.

None of these solutions can be considered to be a mixture of two non-interacting species. The polar molecules of the alcohols can form hydrogen bonds with the water molecules, even the non-polar dioxane molecule is known to be efficient at breaking the structure of dipole-correlating hydrogen bonds in water (Hasted, 1973). Thus an aqueous solution of any of these solutions may contain molecules in states varying from

those of pure water to those of the pure solute, with a number of cross-species hydrogen bonded states in between. This may affect the macroscopic dielectric constant and loss factor of the solution.

Figures 2.f to 2.j show the results of these measurements, together with the predictions of the Maxwell and Bruggeman mixture equations, based on the known permittivities of the pure liquids, which are presented in chapter 4. From fig. 2.f, it can be seen that the dielectric constant of the water / dioxane solution is quite well predicted by the mixture equations. The maximum deviation between theoretical and experimental values is only around 2.5 relative units, about 1.5 times the experimental error. On the other hand, the loss factor differs by up to 4.5 units, which is over 40% of the measured value, and many times greater than the experimental error. Similar behaviour of dielectric constant and loss factor is also shown in the water / methanol and water / glycol solutions.

The effect is most evident in the permittivity of water/propanol solutions. Deviation between the prediction of mixture equations and the measured loss factor of the solution can be of a factor of up to two, but the maximum deviation between theory and experiment for the dielectric constant is only around ~9%.

From these results it can be seen that this type of intermolecular bonding in aqueous solutions can have a pronounced effect on the loss factor of a solution, without affecting the dielectric constant by a sufficient amount to be measurable by current techniques. It must be supposed that there are cross-species bonded states in these mixtures which have a high loss factor at this frequency.

If similar interactions were to occur between the component phases in tissues, mixture equations would not be an appropriate method to analyse tissue permittivity values. In biological tissues, the two phases, water and protein, do in fact interact, forming hydrogen bonds which bind a small fraction of the water to protein molecules. However, there is a fundamental difference between this and the aqueous solutions considered above. At microwave frequencies, the protein in the tissue is a purely passive phase. That is to say, when hydrogen bonds are formed between the large protein polymer molecules and water molecules, the dielectric behaviour of the protein itself is unchanged. Proteins have orientational relaxation frequencies many orders of magnitude below 3 GHz, due to their mass, which may be up to several million a.m.u., and so are not affected by the bonding. This means that the 3 GHz permittivity of the protein fraction of a tissue is essentially unchanged from its value as a pure substance.

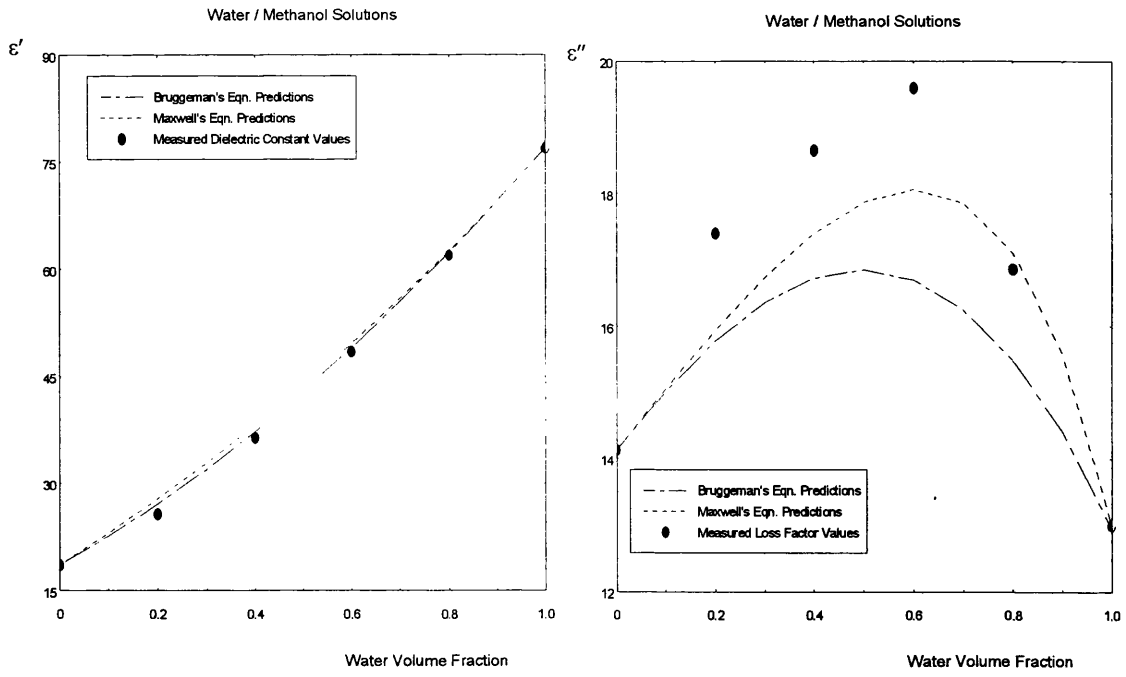

Figure 2.g. Measured dielectric constant and loss factor vs. water content for water / methanol solutions, also showing mixture equation predictions.

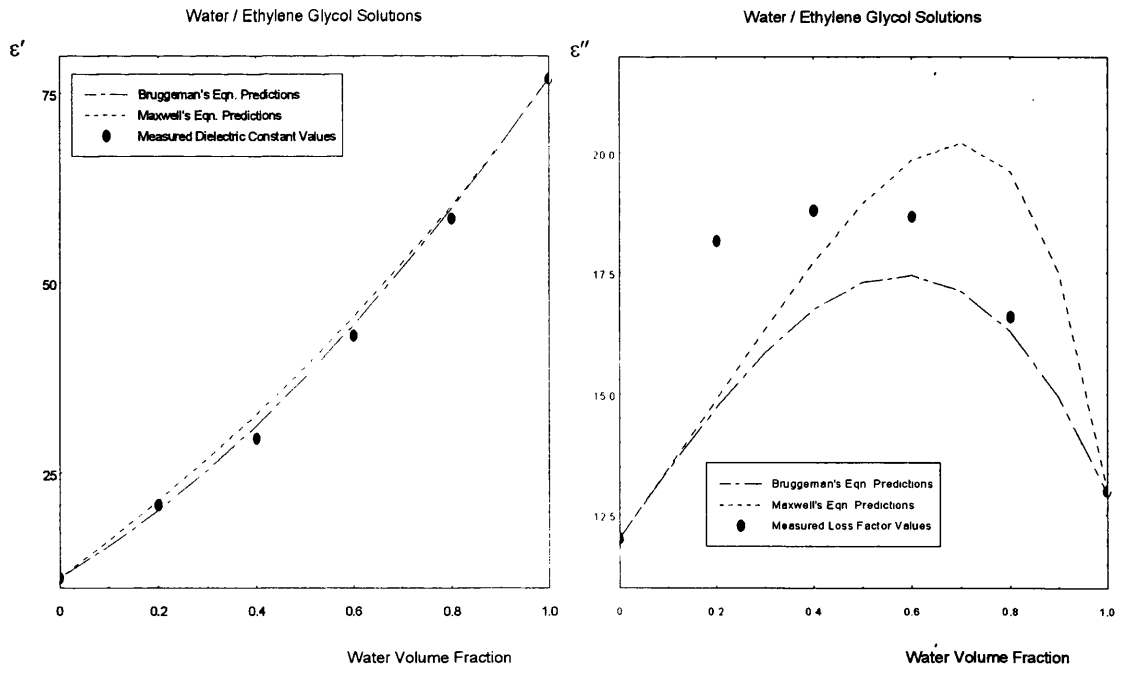

Figure 2.h. Measured dielectric constant and loss factor vs. water content for water / ethylene glycol solutions, also showing mixture equation predictions.

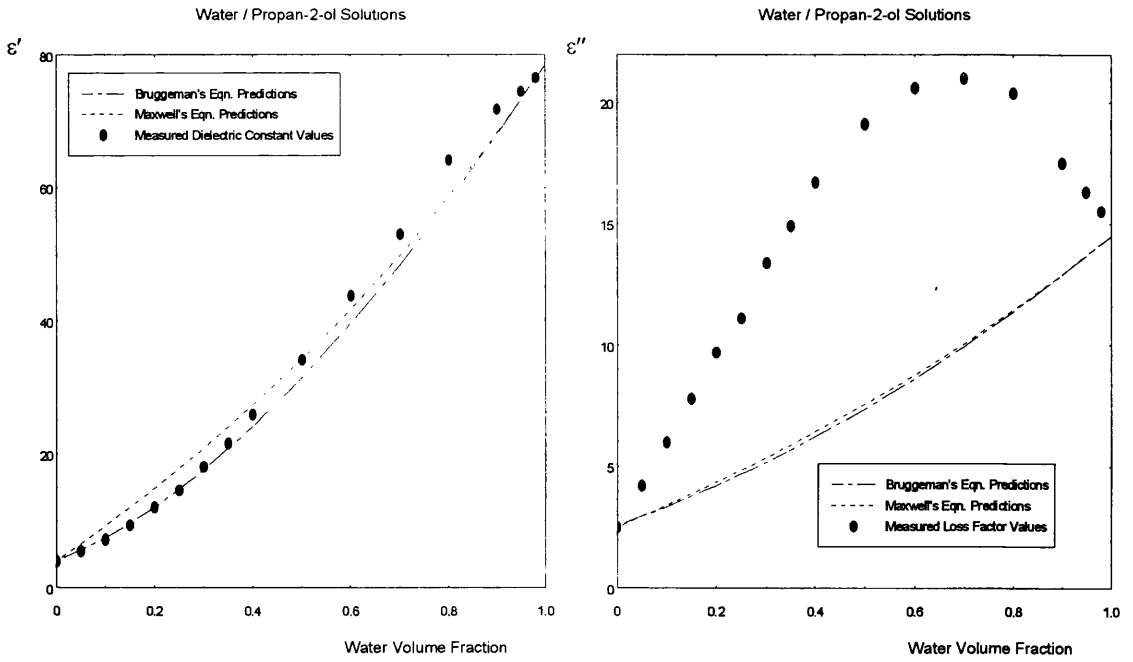

Figure 2.i. Measured dielectric constant and loss factor vs. water content for water / propanol solutions, also showing mixture equation predictions.

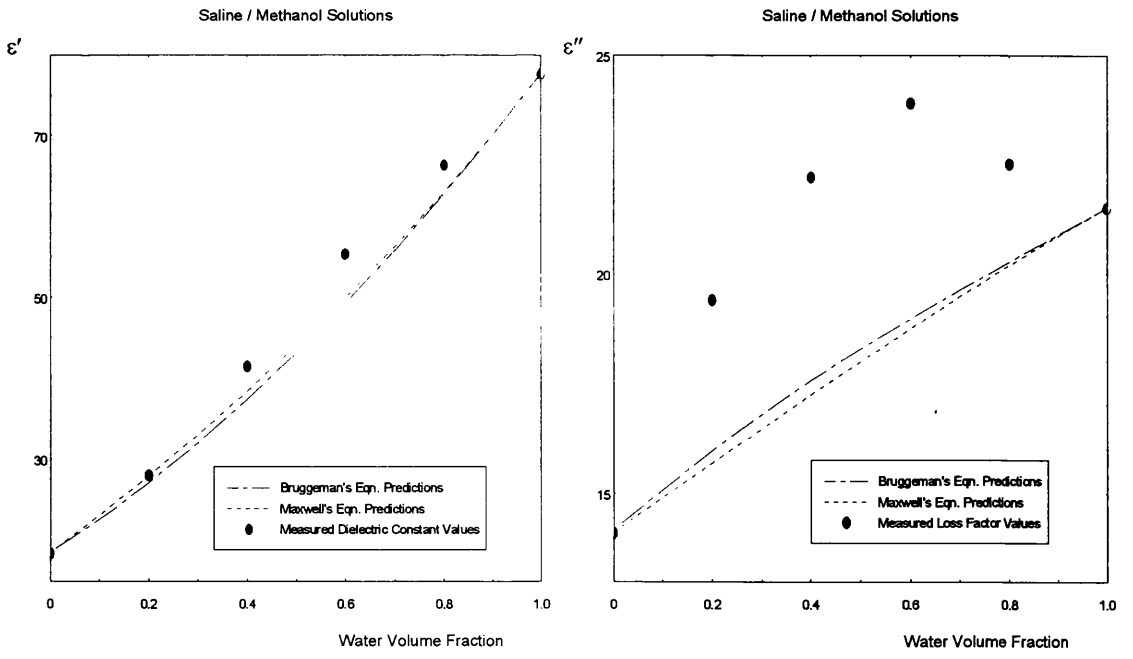

Figure 2.j. Measured dielectric constant and loss factor vs. water content for saline / methanol solutions, also showing mixture equation predictions.

The protein/water mixture is therefore a simpler substance than the aqueous solutions considered above. Dielectrically, it contains protein, unbound free water and bound water. The binding does alter the net permittivity of the water fraction in the mixture, but this is by the more simple process of reducing the relaxation frequency of the bound water molecules, and not by forming new cross-species states with unknown dielectric behaviour.

When analysing the permittivity of biological tissues, it is therefore not expected that the mixture equation should precisely predict the permittivity of the tissue. Rather, the analysis is based on assessing the *difference* between the predicted and measured permittivity values. This difference can be used to interpret to what extent the water is bound to the protein. An example of how mixture equations can be used in this way can be found in section 3.12.

2.15. Applicability of Mixture Equations to Biological Tissue.

The mixture equations presented in sections 2.6 to 2.11 are those which will be used in subsequent chapters to help to analyse the permittivity of biological tissue, and tissue simulating materials. All of these equations are of a simple form, and do not require detailed knowledge of the geometry of the suspended system, as, in general, they assume that the suspended particles are spherical.

Figure 2.k shows a comparison between selected measured tissue permittivity data, and the predictions of several mixture equations for a suspension of protein (assumed here to have permittivity $\varepsilon_r = 2.5 - j0.2$), in physiological electrolyte ($\varepsilon_r = 75 - j22$).

It can be seen that the complex permittivities predicted by each equation do not differ by a great deal in comparison to the spread of data points. Indeed, data spread is as large as the predicted permittivity difference between Fricke's equations for suspended spheres, and for suspended long cylinders. Some tissue data have loss factor values which lie outside the Hashin and Shtrikman upper limits, so an important effect clearly is being overlooked. As all other mixture equations give predictions which lie within the Hashin and Shtrikman limits, it is not sensible to consider the application of these more sophisticated formulae, until gross effects are explained. Simple mixture equations must be used only as an approximate guideline for predicting the dielectric behaviour of tissue,

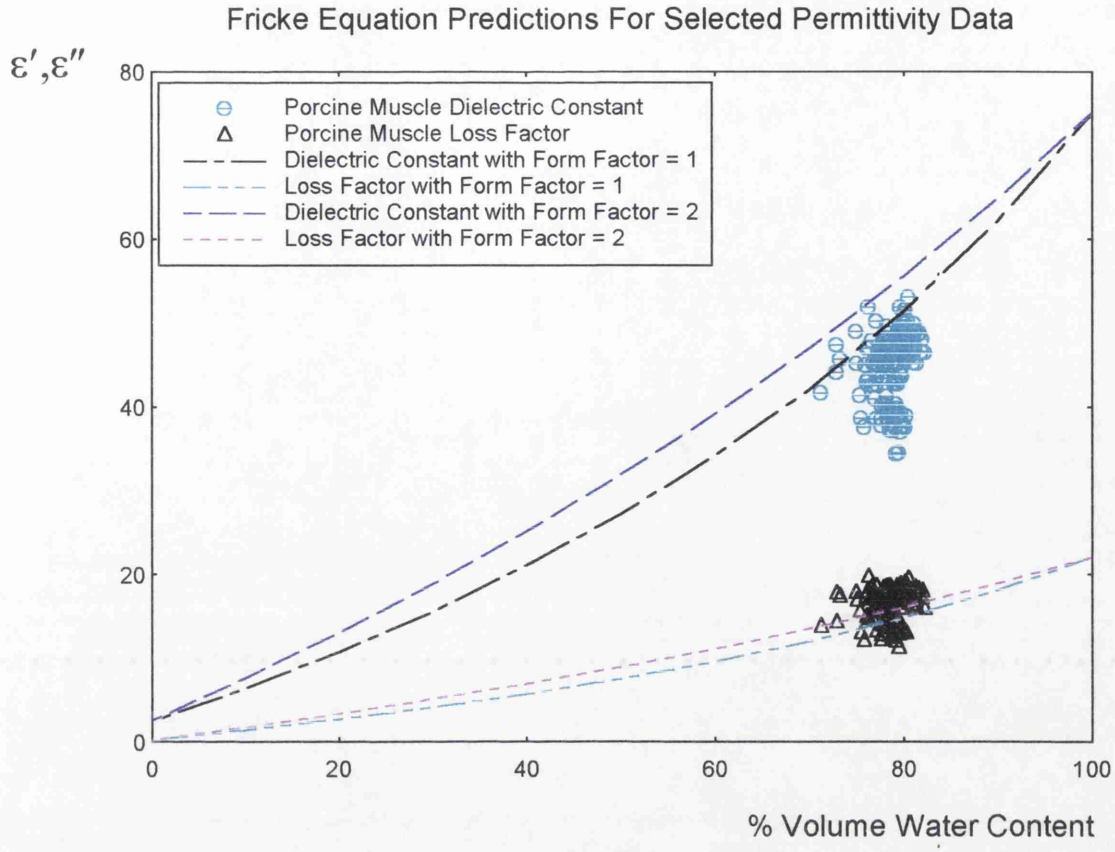

Figure 2.k. Comparison between the permittivity predictions of the Fricke equation with form factor = 2 (Maxwell equation), and with form factor = 1, with selected animal muscle permittivity data. The equation with form factor equal to 2 is also the upper Hashin/Shtrikman limit for such a mixture. Tissue is assumed to be a suspension of protein in saline. Data spread is larger than the difference between the predictions at all water content values, and loss factor is often higher than upper limit.

and not as an exact reproduction of this behaviour. The introduction of extraneous theoretical variables by using complex mixture equations may even cloud the main issue. Most other researchers in similar fields have also so far concentrated on simple mixture equations such as Maxwell and Bruggeman's equations for tissue modelling (see Foster and Schwan, 1989). To make analytical use of some of the many more sophisticated mixture equations, it is essential not only that the distribution of relaxation times in tissue water is known, but also that dielectric measuring techniques yield data of much greater accuracy than is, at this stage, available.

On account of the corroborative evidence which supports the Maxwell and Bruggeman formulae, much research into the high frequency dielectric behaviour of biological tissues has been analysed using these equations. Maxwell's equation (and Fricke's extension) has been used extensively by the University of Pennsylvania Bioengineering Department, under Foster and Schwan, to parameterise tissue data over the whole range of water content (Smith and Foster, 1985), and also to predict the proportion of bound water not contributing to conduction at microwave frequencies (Foster et al 1979,1980, Schepps and Foster 1980). Steel and Sheppard's (1985) analysis of rabbit brain tissue was also analysed using the Maxwell-Fricke equations, and provided estimates of bound water consistent with Foster's measurements, and low frequency measurements on protein solutions (Bull and Breese, 1969). Foster et al (1984) utilised both Maxwell and Bruggeman formulae to investigate bound water in tissue simulating polymer solutions. More detailed discussion of this important paper, and also of the properties of bound water in biological tissue, follows in chapter 3.

Chapter 3. Microwave Dielectric Properties of Tissues and Their Components.

3.1. Introduction.

Before interpretation of measured microwave tissue permittivity data can be made, it is essential that the dielectric behaviour of biological tissue, and of the major constituent materials of tissue, are known and understood, at and below the measurement frequency. In section 3.2, the structure of the constituent materials of biological tissues are briefly discussed, with particular reference to those factors, such as ionic conductivity and water binding, which affect the tissue microwave permittivity. The previously reported dielectric behaviour at frequencies up to the microwave region of the major soft tissues is then introduced, and reasons given for the observed phenomena.

Water is the most important single substance in determining the microwave permittivity of biological tissues. Tissues are composed mainly of aqueous electrolytic solutions, divisible into two types; *extracellular* and *intracellular* electrolyte. The ionic profile of extracellular electrolyte can be closely approximated by aqueous 0.15**M** NaCl solutions, often referred to as *physiological saline*. Detailed reviews of the microwave dispersion parameters of water, and subsequently, of saline solution, are therefore presented. It was particularly important accurately to know the permittivity of these materials in this study, as water and saline were also used as calibration materials for dielectric measurements.

A solution with ionic profile similar to that of intracellular electrolyte was then made, and its permittivity measured. It is shown that, at 3 GHz, the permittivity of this solution is sufficiently close to that of 0.15**M** saline, that physiological saline is an acceptable phantom for all types of tissue electrolyte.

The properties of water that is motionally restricted by binding to protein macromolecules is then dicussed. A short review is given of the research published to date, concerning evaluation of both the amount of bound water in tissues and liquid protein solutions, and the characteristic relaxation times observed in this bound water. Lastly, the details of a previous study are summarised, which shows the effectiveness of mixture equations as a tool for evaluating the properties of bound water in tissue-simulating solutions.

3.2. Tissue Structure and Cell Physiology.

3.2.1. Water.

Water is the major component material of biological tissues, and is also the major contributer to the microwave dielectric permittivity of tissues. It constitutes 50% to 70% of the total body weight of the average adult male, and 45% to 65% of the total body weight of the average adult female. It is convenient to compartmentalise the body water content into distinct groups, although this is not a strictly correct concept, as water molecules are able to move within the body. According to this idea there are two basic kinds of water in the body: *intracellular* water, which exists within tissue cells, and *extracellular* water, in which the cells are suspended. Extracellular water itself is compartmentalised into *plasma* and *interstitial* (or intercellular) water.

All tissue is made up of cells, whose functions are specialised for each different tissue type. Cells are usually made up of a central nucleus, surrounded by a mass of protoplasm, and bounded by a mainly lipid membrane. The protoplasm contains proteins, sugars, lipids, dissolved salts and nucleic acids (DNA, RNA). These cellular molecules are suspended in intracellular water, which comprises about 67% of the total water mass in the body. Interstitial water, which suspends the cells themselves, constitutes 25% of the total water mass, and plasma, the remaining 8%. Although the proportions of each water type are accurately maintained by the body, individual water molecules may, with time, transfer between water types by osmosis.

Different tissue types however, contain differing proportions of these fluids. Figure 3.a shows schematically the approximate quantities of intracellular and extracellular materials in several animal tissue types. Over 80% of the water in skeletal muscle tissue is of the intracellular type, whereas for tendon, a connective tissue containing few cells, over 50% of the tissue water is extracellular.

In general, the active tissues of the body contain more water than inactive ones; for example, white matter of the brain, with the fibrous neuron connections contains around 70% water, whereas the grey matter, which is the functional part of the brain made up of neuron cell bodies, contains around 84% water (Biology Data Book, 1972)

Water occurs in the cells in two forms, *free* and *bound*, although as water molecules are continually moving, partition between the two forms is indefinite. Free water is able to move as a liquid in the cell. Bound water is loosely attached to protein molecules by

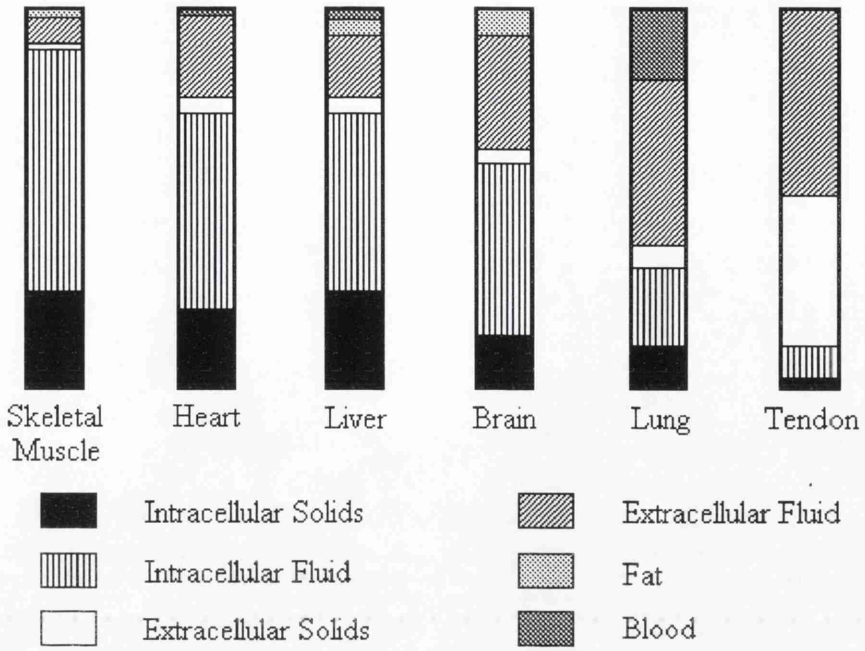

Figure 3.a. Schematic representation of the materials in selected animal tissues. Adapted from Lowry, 1943.

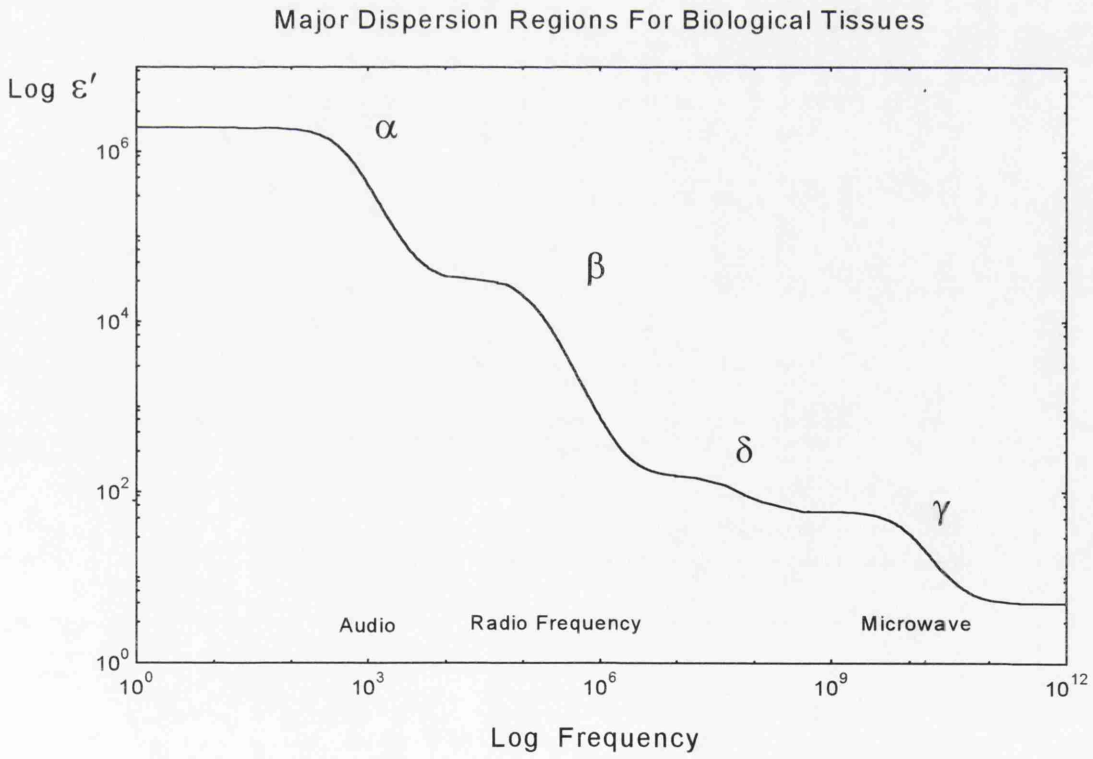

Figure 3.b. Schematic illustration of the major dispersion regions typically found in soft biological tissues.

hydrogen bonding caused by dipole attraction. Water bound to protein molecules forms part of the structure of protoplasm. The amount of bound water in a tissue is hard to define. Physiologically, free water is water which is available for metabolic processes, whereas bound water is not. Dielectrically, at microwave frequencies, free water responds to alternating fields in the same way as pure liquid water, whereas bound water has an increased relaxation time, due to hydrogen bonding with the protein. It is likely that only a small fraction of the total water in the tissue is bound sufficiently strongly as to be unavailable for action as a solvent in which metabolic reactants may dissolve (Giese, 1973). There may however, be many states of water binding in tissues between the fully *free* and *bound* states. The dielectric properties of bound water are considered in detail in section 3.11.

3.2.2. Proteins.

The majority of the non-water material in tissues is either protein or lipid. Skeletal muscle is around 75% water by mass; around 20% is protein, 2% is lipid, and 1% is salts, which are dissolved in the tissue water.

Proteins are polymer molecules responsible for the structure of the cell. There are many different types of protein molecule in the body, ranging in molecular weight from around 6000 to several million a.m.u. (Giese, 1973). Because of their size, protein molecules are often refered to as *macromolecules.*

Protein molecules are made up of chains of different amino acids, of which there are 20 types in the body, connected by their respective amino and carboxyl groups forming peptide links. The bonds occur in such a way as to give protein molecules a characteristic helical shape. Because of the water binding properties and interlinking bonds, the presence of only a very small percentage of protein in an aqueous solution can make a solid gel. This property of proteins is utilised in chapter 8, where gelatine solutions are used to model the dielectric behaviour of bound water is a tissue-like protein substance.

3.2.3. Lipids.

Lipids are fats and fat-like substances, found mainly in the cells of adipose (fatty) tissue, and in the membranes of other tissue types. Most lipids are esters of fatty acids, and have an average molecular weight of around 700 a.m.u. They are insoluble in water, but form a cell bounding layer which is semipermeable to the ions and molecules of the surrounding electrolyte fluids.

3.2.4. Salts.

All three types of electrolyte in the body, intracellular, intercellular and plasma, contain many species of dissolved salts, whose presence is essential to the functions of life. Tables 3.a to 3.c show typical values of the ionic profiles of each of the three fluids. Ionic concentrations in the tables are expressed in terms of the *milliequivalent weight* (mEq), which, for a given ion, is given by:

$$\text{mEq} = \frac{\text{Gram Molar Weight}}{\text{Valence} \times 1000} \qquad (3.2.1)$$

For instance, the milliequivalent weight of the sodium ion is $\frac{23}{1 \times 1000} = 23mg$.

Because of the prevalence of Na^+ and Cl^- ions in intercellular and plasma fluids, it is common to treat all extracellular fluid as 0.15M sodium chloride solution. Intracellular fluid contains few sodium and chloride ions, and instead has many K^+ (potassium) and HPO_4^{--} (hydrogen phosphate) ions. Maintenance of the balance betwen the ionic profiles of intracellular and extracellular fluids by osmotic pressure is vital to cell function.

3.3. The Dielectric Behaviour of High Water-Content Biological Tissue.

Pure liquid materials usually have a permittivity which varies with frequency in three distinct regions. The dielectric constant is high at low frequencies, then drops, in stages, over regions of absorption associated with molecular rotation at microwave frequencies, molecular vibration in the infra-red, and finally electronic transitions at visible and higher frequencies. Associated with each drop in dielectric constant is a frequency peak in the loss factor.

INTRACELLULAR FLUID			
Cations	Concentration (mEq/l)	Anions	Concentration (mEq/l)
K^+	160	Cl^-	3
Ca^{++}	2	HPO_4^{--}	100
Na^+	10	HCO_3^-	10
Mg^{++}	26	SO_4^{--}	20
		Proteins	65
Total = 198mEq/l		Total = 198mEq/l	

Table 3.a. Electrolyte ion profile of intracellular fluid of the human body. Adapted from Brooks and Brooks, 1980.

EXTRACELLULAR PLASMA			
Cations	Concentration (mEq/l)	Anions	Concentration (mEq/l)
K^+	4	Cl^-	101
Ca^{++}	5	HPO_4^{--}	2
Na^+	142	HCO_3^-	27
Mg^{++}	2	SO_4^{--}	1
		Organic acids	6
		Proteins	16
Total = 153mEq/l		Total = 153mEq/l	

Table 3.b. Electrolyte ion profile of extracellular plasma fluid of the human body. Adapted from Brooks and Brooks, 1980.

INTERSTITIAL FLUID			
Cations	Concentration (mEq/l)	Anions	Concentration (mEq/l)
K^+	4	Cl^-	114
Ca^{++}	5	HPO_4^{--}	2
Na^+	145	HCO_3^-	31
Mg^{++}	2	SO_4^{--}	1
		Organic acids	7
		Proteins	1
Total = 156mEq/l		Total = 156mEq/l	

Table 3.c. Electrolyte ion profile of extracellular intercellular fluid of the human body. Adapted from Brooks and Brooks, 1980.

Free liquid water, for example, displays a rotational absorption at a wavelength of approximately 1.8cm (at 20°C), and vibrational absorption at wavelengths of 2.77μm, 2.90μm and 6.10μm. Liquid water also exhibits intermolecular absorption at longer infra-red wavelengths which significantly affects the permittivity. Most soft biological tissue, however, despite being composed mainly of water, exhibits three major permittivity dispersions at frequencies below the infra-red vibrational region.
A schematic diagram (fig. 3.b) shows that the tissue dispersions, known as the alpha, beta and gamma dispersions, lie in the kilohertz, hundreds of kilohertz and gigahertz ranges respectively.

At low frequencies the dielectric constant of tissues is very high, generally of the order of 10^6 relative units. The conductivity, on the other hand, is very low, being around 0.15 S/m. Cell walls are poorly conducting at audio frequencies and below, and so only the material outside the cells (ie. extracellular electrolyte) can contribute to conduction. Observed soft-tissue conductivities to direct current are consistent with those expected from a substance comprising 15% extracellular electrolyte, and a non-conducting remainder. Alpha dispersion is thought to be caused by counterion diffusion, with possible contribution from cellular membrane impedance variation. However, the conductivity increase of approximately 0.01 S/m over this dispersion is negligible even compared to that of the extracellular electrolyte, and so is of limited significance.
The beta dispersion is associated with the relaxation of cellular membranes. Dipolar relaxation of large protein molecules may also arise at similar frequencies. Typically, the dielectric constant of soft-tissue falls by several thousand at a frequency around 500 kHz. The conductivity increase is approximately double the d.c. conductivity, rising by about 0.4 S/m. Above ~10MHz cell membranes offer little or no barrier to current flow, and tissues can thus be regarded as being electrically similar to suspensions of non-conducting proteins, and other solids, in an electrolytic solution.
Gamma dispersion is caused by dipolar relaxation of water molecules in tissue electrolyte. The dispersion cannot be characterised by a single dispersion equation: at high microwave frequencies, the dielectric constant tends to limiting value similar to that of pure water, as may be expected from a material 80% of which is water, whereas at low frequencies, cellular structure and the beta dispersion raises the dielectric constant above that expected from simple mixture theory. There are, additionally, three

significant conduction processes contributing to the overall conductivity in the gamma dispersion region. Firstly there is the ionic conductivity of dissolved ions in tissue electrolyte; secondly there is the dipolar conductivity of free water in the electrolyte, and thirdly there is the dipolar conductivity of bound water in the electrolyte. Water molecules temporarily bonded to protein molecules have a reduced average relaxation frequency, reported as ranging from below 1GHz to over 5GHz (Steel and Sheppard 1985, Clegg et al 1984). At 3GHz the conductivity arising from each of these sources may be of similar magnitude in high water content tissue.
Over the whole gamma dispersion the dielectric constant of most soft tissues falls by approximately 50 to a value of around 4, and the conductivity increases by around 70 S/m. Above about 20 GHz, only the free 'bulk' water contributes significantly to the conductivity, and so interpretation of dielectric data becomes more simple

3.3.1. Delta Dispersion.

One minor dispersion, often known as the delta dispersion, is typically observed between 0.1 and 3 GHz in soft tissues, in addition to the three major dispersion regions. Between these two frequencies, a fall in dielectric constant of around 15, with an associated conductivity increase from 0.4 to 0.5 S/m is usually measured. The delta dispersion region straddles the frequency range lying in between the beta and gamma dispersion regions, and is difficult to interpret due to the lack of a single dominant relaxation process. It is thought to be caused by dipolar relaxation of the most tightly bound water molecules, rotational relaxation of polar side chains on protein macromolecules, possible counterion diffusion, or some combination of each of these mechanisms.

3.4. Low Water Content Tissues.

The dielectric behaviour of fat tissue is significantly different from that of high water content tissues discussed above. This behaviour is of great interest to the microwave thermographer, as most of the body regions to which thermography might be usefully applied, the female breast in particular, are covered by a considerable volume of fat tissue, through which emitted radiation from the region under investigation must travel before detection.

Fatty tissues constitute approximately 20% of the body mass of the average adult human, and contain less than 30% water by mass. Water in fatty tissue is almost exclusively extracellular, and the cells are filled largely with lipid. Fat therefore has a more simple structure than high water content tissue. Because of this, it can be assumed that modelling the dielectric behaviour of fat tissue as a mixture of lipid cells and extracellular water, should provide a good approximation as to the true permittivity and conductivity of these tissue regions.

Fat displays a large alpha dispersion up to radio frequencies, and a much smaller beta dispersion than high water content tissues. The conductivity of fat at low frequencies has been found (Smith and Foster 1985) to be rather higher than that of high water content tissues, a fact explained by the larger extracellular water fraction of fat.

As there is little or no protein at all in fat tissue, and much of the lipid is shielded by cell walls from contact with water, it is unlikely that there is sufficient bound water in fatty tissue to complicate the microwave dispersion of fats. Campbell (1990) measured the dielectric constant and loss factor of breast fat tissue at 3.2 GHz, finding both parameters to lie within the Hashin and Shtrikman limits. Smith and Foster also showed that the (1 GHz) permittivity of fat tissue was in general agreement with Maxwell-Fricke mixture theory, taking the tissue to be a simple mixture of extracellular water, and the non-water fraction of lipid.

3.5. Tumour Tissue.

Tumour tissues are usually characterised by a high water content, which is often around 80%. This may differ significantly from the water content of the surrounding soft tissue, and give rise to local high permittivity regions in otherwise low permittivity tissue. Campbell (1990) showed that tumour affected tissues from the outer female breast were clearly distinguishable from unaffected fatty tissue by dielectric measurement at 3 GHz. It was also shown, however, that it was not possible to differentiate between benign and malignant tumours by this method.

The difference in permittivity between tumour and fat tissues in the breast region may even allow tumour detection by non-invasive *in-vivo* dielectric measurement of the breast. Ni et al (1993) constructed a breast phantom consisting of skin and fat simulating layers, into which tumour phantoms of several sizes were implanted. A high

field penetration, 0.5 GHz current sheet resonator, with accurately known field distribution, was placed in contact with the skin to make permittivity measurements of the phantom at various points on its surface. The measured permittivity was calculated from the change in resonant frequency and Q-factor of the resonator. A significant fall in resonant frequency and Q-factor change indicated the presence of a high permittivity perturber beneath the surface. Tumours as small as 1cm in diameter could be reliably located at a depth of up to 1cm beneath the phantom surface. Encouraging clinical evaluation of this technique is currently underway.

As mentioned in chapter 1, breast tumours are also readily detectable by microwave thermography, as a local tissue temperature increase is often associated with a tumour. This is due to the creation of a knot of small blood vessels around a tumour, which greatly increases the local blood perfusion.

Homburger and Fishman (1953) suggested that the high water content of tumours may be due to an increase in protein hydration. Cell membrane breakdown by necrosis in tumours has been observed to lead to increased low frequency conductivity. Although these factors may alter the microwave permittivity of tumour tissue as compared to healthy high water content tissue, it is not yet clear whether the differences are sufficient to be resolveable by dielectric measurement.

3.6. Ionic Conductivity of Tissue Electrolytes.

At frequencies well below the dipolar (gamma) dispersion of tissue water, the conductivity of most high water content biological tissues is around 0.5 S/m. This conductivity is mainly due to ionic conductivity of the tissue electrolyte, which is an ionically similar solution to 0.15**M** saline, and which constitutes around 80% of the mass of most soft tissues. According to the CRC Handbook (1974), the conductivity of 0.15**M** saline is 1.44 S/m at 20°C. The tissue conductivity is therefore of considerably lower magnitude than may be expected of a mixture of 80% 0.15**M** saline with a non-conducting remainder.

This is due to restriction of the ionic conductivity of the tissue electrolyte by the presence of other materials in tissue, particularly the dissolved proteins found mainly in intracellular water. Dissolved proteins in aqueous solutions have the effect of binding the water molecules to form a semi-solid gel, thus reducing the mobility of the bound

water molecules. The mobility of the ions in such solutions is also reduced near protein molecules, lowering the conductivity of the solution.

In most real biological tissues, it is not possible to separate the three fluid types, to examine to what extent the ionic conductivity of each fluid is restricted in each tissue. However, ionic conductivity reduction has also been observed in artificial aqueous solutions containing salts and proteins (Bull and Breese, 1969), in polyethylene oxide solutions also containing salts (Foster et al , 1984), and in the study of blood. Blood is unique amongst tissues in that the extracellular water can be separated from the cells, by centrifugation. Pauly and Schwan (1966) measured the conductivity of blood plasma and red blood cells at frequencies high enough to penetrate the cell membrane, but well below the gamma dispersion. Plasma contained around 7% by mass protein, and had a conductivity of around 1.25 S/m, only a little below the value expected of such a mixture. The red cells, which are approximately two thirds water, and one third protein by mass, had a conductivity of around 0.5 S/m, rather than the value of around 0.9 S/m expected for such a substance. The high protein concentration in red blood cells was thought to be responsible for this reduction in conductivity.

Blood contains no intercellular water, but as intercellular water contains very little dissolved protein (~1%), it is expected that the conductivity of intercellular electrolyte is very similar to that of 0.15**M** saline. This explains the high conductivity of fat tissue at low frequencies. Fat tissues contain only around 20% water, but almost all of this is intercellular water, which has a high conductivity. Other soft tissues, such as skeletal muscle, contain much more water in total, but usually only around 15% extracellular water. Because cell membranes do not permit low frequency current flow, the intracellular water in most soft tissues can not conduct at low frequencies, which leaves only the extracellular water in these tissues free to conduct.

3.7. Microwave Permittivity of Water.

Measurement of the radio and microwave frequency dielectric permittivity of pure water has been of great interest to many researchers, especially in the field of radio communications. As a consequence there is a large amount of measurement data available. The orientational polarisation dispersion resonance in water is centred on a frequency of approximately 20 GHz at room temperature. Almost all researchers have

attempted to fit their observed results to the parameters of a standard relaxation equation, usually the Debye or Cole-Cole equations of the form

$$\varepsilon_r = \varepsilon_\infty + \frac{\varepsilon_s - \varepsilon_\infty}{1+(j\omega\tau)^{(1-\alpha)}} \qquad (3.7.1)$$

where $\alpha = 0$ for the Debye approximation.

It is intended here to give a brief summary of those results, one parameter at a time, and to assess which results are the most thorough and comprehensive. The data fall into two categories: those data which are the results of specific measurement of the parameter ε_s or ε_∞; and those values which are inferred from measured values of the complex permittivity of water in the microwave region. Relaxation time figures, however, can only be obtained from measured permittivity values. Comprehensive reviews of the measurement of the microwave permittivity of water have been published by Hasted in his book 'Aqueous Dielectrics' (1973) and also in 'Water: A Comprehensive Treatise' (1972).

3.7.1. Permittivity Measurements of Water in the Microwave Region.

To evaluate accurately the dispersion parameters of a material, it is necessary to measure the permittivity at a large number of frequencies. Several researchers however (Collie et al 1948, Cook 1952, Saxton, 1949) have, as a part of their investigations, made permittivity measurements at a frequency of exactly 3 GHz, the frequency of interest to this study, and the data thus obtained are shown in table 3.d.

Absolute values of the permittivities published by each author tended to differ from each other only by an amount consistent with the error on the quoted permittivities, which usually ranged from ± 1 to ± 3%. For instance, the published dispersion parameters of a wide range of authors (Collie et al, Cook, Hasted and el-Sabeh 1953, Saxton, 1952, Grant et al, 1957, Haggis et al, 1952) all yield 3 GHz permittivities at 20°C with real parts in the range 77.5 ± 0.5 and loss factors in the range 13.4 ± 0.4. Permittivity results from these sources only deviate by more than the experimental error at temperatures around 0°C.

Where available, characteristic relaxation times deduced by each author from measurements at all frequencies are shown in table 3.e. At temperatures below ~30°C there is deviation of up to ~10% between the quoted relaxation times. Much of this

Reference	Temperature (°C)	Dielectric Constant	Loss Factor
Collie et al (1948)	0	79.7	24.7
	10	78.1	17.5
	20	77.4	13.1
	30	76.8	9.8
	40	72.6	7.5
Cook (1952)	0	80.2	24.0
	10	79.4	17.5
	20	77.7	13.0
	30	75.3	9.9
	40	72.6	7.6
Saxton (1947)	0	78.8	26.1
	10	79.1	19.0
	20	77.4	13.8
	30	75.6	10.0
	40	72.2	7.5

Table 3.d. Results of permittivity measurement of water at 3 GHz.

Author	0°C	10°C	20°C	30°C	40°C	50°C	60°C
Saxton, 1952	18.7	13.6	10.1	7.5	5.9	--	--
Collie, 1947	17.7	12.7	9.55	7.4	5.9	4.8	4.0
Grant, 1957	17.7	12.6	9.2	7.2	5.8	4.7	3.9
Cook, 1952 (approximate)	18	13	9.5	7.5	6	--	--

Table 3.e. Characteristic relaxation times in picoseconds of water at various temperatures.

Temperature °C	ε_∞
0	4.35
10	4.32
20	4.28
30	4.23
40	4.17
50	4.11
60	4.05

Table 3.f. High frequency limiting permittivity of water as a function of temperature, according to calculations by Hill, 1963.

deviation may be attributed to the values of ε_s and ε_∞ chosen by each author, and also to the choice of Debye or Cole-Cole equation to parameterise the data. It will be noted that the data of Grant et al lie consistently below the others'. This is at least partially accounted for by the fact that Grant used a Cole-Cole equation with a relaxation time distribution parameter α equal to 0.02, rather than a Debye equation, to fit the data.

3.7.2. Low Frequency Permittivity Limit ε_s.

There have been many measurements of the low frequency (or in this case 'static') dielectric constant of water, and all are in close agreement. Malmberg and Maryott's (1956) measurements of ε_s from 0 to 100°C and at frequencies between 3 and 96 kHz are the accepted modern standards. The best fit to their data is given by the equation

$$\varepsilon_s = 87.74 - 0.40008T + 9.398 \times 10^{-4} T^2 - 1.410 \times 10^{-6} T^3 \qquad (3.7.2)$$

where T is the temperature in degrees centigrade. A maximum uncertainty of $\pm$ 0.05 units was claimed for this data fit.

Static permittivity values can also be inferred from microwave data. The values of ε_s calculated by Grant et al (1957), Saxton, (1949) and Collie et al (1948) differ from each other and from the measurements of Malmberg and Maryott by a maximum of only 0.46 units over the temperature range 0 to 50°C. This small inconsistency in inferred values of ε_s may arise mainly from the early uncertainty of similar magnitude in the value of ε_∞. In this study, the expression of Malmberg and Maryott was used for the static dielectric constant.

3.7.3. The High Frequency Permittivity Limit ε_∞.

All early values of the high frequency permittivity limit, before the appearance of submillimetre measurements, were inferred from microwave data, and can differ from those values accepted today by up to 25%. It must be noted that this error does not seriously invalidate or prejudice those original measurements, as the overall complex permittivity is not strongly affected by error in the variable ε_∞. The fact that ε_∞ differs from the square of the optical refractive index ($n^2 = 1.79$) is due to the existence of dispersion regions in the infra-red.

Saxton (1947) and Collie et al (1948) both found that a temperature invariant value for ε_∞ of 5.5 provided the best fit of their measured permittivity data to the parameters of a Debye equation. Subsequent improved measurements on both pure water and aqueous solutions by Saxton and Lane (1949,1952a), suggested that a value of 4.9 was more realistic.

Concurrently, independent measurements by Cook (1952) also showed that a value of 5.0 provided the best overall fit to a Debye equation. However, a value of $\varepsilon_\infty = 4.0$ was found to optimise the fit of the data to a Cole-Cole equation. Grant et al (1957) used a Cole-Cole representation to parameterise their data, concluding that ε_∞ was ~ 4.5, and was temperature invariant.

By allowing ε_∞ to vary in such a way as to reproduce the observed temperature variation of ε_s and the dipole moment of the water molecule (μ~1.83D), Hill (1963) calculated empirical values for ε_∞, as shown in table 3.f. At 20°C, the average measurement temperature for the data in this work, the value of ε_∞ is approximately 4.3. Calculations performed by Hasted (1973), based on regression analysis of collected microwave data fitted to a Cole-Cole equation concluded that at 20°C, ε_∞ is approximately equal to 4.2. In this study, a value for ε_∞ of 4.3 was used in equations to calculate the permittivity of pure water for probe calibration purposes.

3.7.4. Overall Parameters of Dispersion Equations for Water.

To the degree of precision required for calibration of equipment for measuring the permittivity of biological tissues, the permittivity of water in the room to body temperature range (15 to 40°C) may be adequately described by a simple Debye dispersion equation. The Debye dispersion parameters used for this purpose by the Glasgow Microwave Group have been evaluated by averaging the measured values of collected microwave data, selected according to their measurement precision, and the validity of assumptions concerning the high frequency permittivity limit.

In terms of a characteristic relaxation frequency f_c, the Debye equation can be given as

$$\varepsilon_r = \varepsilon_\infty + \frac{\varepsilon_s - \varepsilon_\infty}{1 + j\left(f/f_c\right)} \qquad (3.7.3)$$

The equations used for the temperature dependence of the dispersion parameters $\varepsilon_s, \varepsilon_\infty$ and f_c were as follows:

$$\varepsilon_s = 87.74 - 0.40008T + 9.398 \times 10^{-4} T^2 - 1.41 \times 10^{-6} T^3 \quad \text{(Malmberg and Maryott)}$$

$$\varepsilon_\infty = 4.3 \quad \text{(Submillimetre value)} \qquad (3.7.4)$$

$$f_c(GHz) = 7.99 + 0.375T + 0.00205T^2$$

where T is the temperature in degrees Celsius.

The mean equation for the characteristic relaxation frequency of water was interpolated from the permittivity results presented by Collie et al (1948), Cook (1952), and Saxton (1952). Although it is now thought that ε_∞ varies with temperature, this value may be assumed to be constant in the room temperature region (15 to 40°C) without incurring any significant error in the overall permittivity value.

The approximate expressions quoted above for the dispersion parameters $\varepsilon_s, \varepsilon_\infty$ and f_r give the complex permittivity of water at temperatures from 0 to 60°C as shown in table 3.g.

The uncertainty in these permittivity values is estimated to be equal to the uncertainty in the measured values of which these are an approximation. Therefore the error on the real part of the permittivity is approximately ± 2%, and on the imaginary part approximately ± 3%.

Using a constraint procedure based on regression analysis of collected microwave data, Hasted (1972,73) presented calculated best-fit parameters for the permittivity of water as expressed by both Debye and Cole-Cole equations. Raw data was taken from many sources, including those mentioned above, together with more recent values for the limiting permittivities ε_∞ and ε_s. It was found that there is a better than 99% certainty that the spread of relaxation times is real, and that a Cole-Cole equation is therefore the most suitable representation of the microwave dispersion of water. The calculated Cole-Cole parameters for temperatures up to 60°C, together with their resultant permittivities, are reproduced in table 3.h.

At the time of publishing, the statistical confidence limits on the calculated best-fit dispersion parameters in table 3.h were not available, but the data imply that a temperature independent relaxation spread parameter α equal to 0.012 should be used for consistent calculations.

Temperature °C	ε'	ε''
0	77.4	27.5
10	79.2	18.8
20	77.7	13.5
30	75.2	10.1
40	72.2	7.8
50	69.2	6.1
60	66.1	4.9

Table 3.g. Dielectric permittivity of water as predicted by equations 3.7.4.

Temperature ℃	ε_s	ε_∞	$\tau(ps)$	α	ε'	ε''
0	88.3	4.46	17.9	0.014	79.1	25.4
10	84.1	4.10	12.6	0.014	79.3	18.1
20	80.4	4.23	9.3	0.013	77.7	13.1
30	76.8	4.20	7.2	0.012	75.2	9.9
40	73.2	4.16	5.8	0.009	72.2	7.6
50	70.0	4.13	4.8	0.013	69.3	6.1
60	66.6	4.21	3.9	0.011	66.2	4.7

Table 3.h. Cole-Cole parameters for water calculated from measured data.

Ion	Dielectric Decrement δ_+, δ_- (±1)	Relaxation Decrement $\delta\tau_+, \delta\tau_-(ps)$ (±0.1ps)
H^+	-17	+0.2
Li^+	-11	-0.15
Na^+	-8	-0.2
K^+	-8	-0.2
Rb^+	-7	-0.25
Mg^{++}	-24	-0.2
Ba^{++}	-22	-0.45
F^-	-5	-0.2
Cl^-	-3	-0.2
I^-	-7	-0.75
OH^-	-13	-0.1
SO_4^{--}	-7	-0.55

Table 3.i. Decrements for the dielectric constant and relaxation time for ions dissolved in water. From Hasted, 1973.

It can be seen that the values obtained from our Debye relation approximation agree very closely with those obtained from the Cole-Cole parameters deduced by Hasted (1973) in table 3.h. Except at 0°C, the permittivity values given by the two methods lie within the estimated error boundaries on each reading. The consistently higher imaginary part, as evaluated by the Debye method, may be simply due to the dispersion approximations of the Glasgow method mainly being based on later permittivity measurements by Saxton, which found a consistently higher relaxation time and lower ε_∞ than previous measurements.

3.8. Permittivity of Saline Solution.

Water in the human body is not present in a pure form, but as a solute containing, in varying amounts, many species of dissolved ions. The ionic profile of water from different cellular regions is shown in tables 3.a to 3.c. Extracellular fluid can usually be approximated by a 0.15 **M** NaCl solution (physiological saline). Conventionally, the permittivity of low-concentration electrolytic solutions is expressed by a modified Debye equation thus

$$\varepsilon_r = \left[\varepsilon_\infty + \frac{\varepsilon_s - \varepsilon_\infty}{1 + j\omega\tau}\right] + j\frac{\sigma_i}{\omega\varepsilon_0} \qquad (3.8.1)$$

where σ_i represents the *ionic* conductivity of the solution. Dissolved salts have a considerable effect on the dielectric properties of the water solvent. In an ionic solution, the ions orient the water molecules around them, reducing the ability of the water molecules to orient in an applied field. The permittivity expression therefore consists of one term representing the dielectric behaviour of the water solvent, albeit slightly altered by the presence of dissolved ions, and another term representing the action of the ions themselves. Most researchers have been content to use a simple Debye type equation for the water solvent term, rather than the more complex Cole-Cole equation, because the effect of the ionic conductivity far outweighs any possible increase in accuracy of the permittivity of the water solvent that might be achieved by a more complex representation.

The ionic conductivity is assumed to be frequency independent, and takes the low frequency value at all frequencies. At high frequencies water molecules can not be forced to oscillate significantly, so the tendency for ions to impede the oscillation is unimportant. Therefore the high frequency permittivity limit ε_∞ is independent of

salinity, and takes the same value as for pure water. The static dielectric constant and relaxation time of an ionic solution are functions of temperature and the concentration of the solution.

Stogryn (1971) presented equations, based on the work of previous authors, which describe the variation of these factors for sodium chloride solution. In these equations, N represents the *normality* of the solution, which for exclusively monovalent ionic solutions is equivalent to the molarity. For $0 \le T \le 40°C$ and $0 \le N \le 3$

$$\varepsilon_s(T,N) = \varepsilon_s(T,0) \times (1.000 - 0.2551N + 0.05151N^2 - 6.889 \times 10^{-3} N^3) \qquad (3.8.2)$$

$$\tau(T,N) = \tau(T,0) \times (1.463 \times 10^{-3} NT + 1.000 - 0.04896N - 0.02967N^2 + 5.664 \times 10^{-3} N^3)$$

$$\varepsilon_\infty = 4.9$$

Here, $\varepsilon_s(T,0)$ is the static dielectric constant of pure water according to Malmberg and Maryott (eqn. 3.7.2), and $\tau(T,0)$ is the relaxation time of pure water according to Grant et al (1957), which can be approximated by the following polynomial function

$$\tau(ps) = 17.7 - 0.600T + 0.0103T^2 - 6.49 \times 10^{-5} T^3 \qquad (3.8.3)$$

An expression for the ionic conductivity of NaCl solution was also derived by Stogryn, which gave a conductivity of 1.36 S/m at 20°C

Using these parameters in the Debye dispersion equation, the Stogryn formulae are found fairly accurately to predict the real part of the permittivity, but consistently to underestimate the loss factor, at least for low ionic concentrations, by as much as 1.5 units.

There are several reasons for this underestimation. Firstly, the relaxation times calculated by Grant et al (1957) for pure water are rather lower than those published by other authors. At 20°C Grant quotes a value of τ equal to $9.2ps$, whereas Collie gives $9.55ps$, and Saxton gives $10.1ps$. At frequencies lower than the resonance frequency, choosing a lower value of τ reduces the magnitude of the simple Debye loss factor. The discrepancy partly arises because the relaxation times given by Grant were calculated to fit a Cole-Cole dispersion relation (eqn 2.4.1), with a value of α equal to 0.02. By using Cole-Cole parameters in a Debye equation, Stogryn contributes to underestimation of the imaginary part, as the factor $j\omega\tau$ is not raised to the power (1-α) in the Debye equation. Substitution of Saxton's Debye equation values for the relaxation time of water into Stogryn's formulae increases the estimated loss factor of pure water from 12.8 to 13.6. This new value is similar to that originally calculated by Saxton. Alternatively, using

Grant's figures in a Cole-Cole equation as originally intended, gives a value of 13.0 for the loss factor, which is still higher than Stogryn's estimation.

In addition, the net relaxation time quoted by Stogryn only closely agrees with the published data from which it is deduced at concentrations greater than ~1**M**. At lower concentrations the net relaxation time, as calculated by Stogryn's formula does not reproduce the values measured by the original researchers.

Many researchers also find that Stogryn underestimates the ionic conductivity component. At 20°C the Stogryn formula for the ionic conductivity gives a value of 1.36 S/m, and so contributes 8.2 units to the net loss factor. Smith and Scott (1990) published alternative formulae for calculating the ionic conductivity of low normality saline solutions at room temperatures. These formulae give a value of 1.41 S/m for the ionic conductivity of 0.15**M** saline at 20°C, an increase of ~4% over Stogryn's formulae. According to the CRC Handbook, the ionic conductivity of 0.15**M** NaCl can be approximated at low temperatures by the linear expression

$\sigma_i(T,0.15) = 0.806 + 0.0317T$, which gives the conductivity at 20°C as 1.44 S/m.

Saxton and Lane (1952b) published data on 0 to 3N saline solutions, also based on a Debye equation, with additional ionic conductance loss. The temperature dependence of the measured dispersion parameters may be interpolated to give

$$\begin{aligned} \varepsilon_\infty &= 4.9 \\ \varepsilon_s(T,0.15) &= 84.3 - 0.348T \\ \tau(T,0.15) &= 18.1 - 0.529T + 0.00557T^2 \\ \sigma_i(T,0.15) &= 0.0314T + 0.905 \end{aligned} \qquad (3.8.4)$$

These parameters give the 3 GHz relative permittivity of 0.15**M** saline at 20°C as being equal to 75.0 - *j*22.1, with an ionic conductivity of 1.53 S/m contributing 9.2 units to the net loss factor. This overall permittivity value is in agreement with the experimental permittivity value of 75.0 - *j*22.2, specifically measured at 3GHz for 0.15**M** concentration in the Glasgow group, by Land (1993). Misra and Staebell (1990) also reported that Saxton's formulae gave good overall results at low saline concentrations. The proportion of the loss factor due to ionic conductivity is, however, considerably higher than is expected from all other data sources. According to the CRC Handbook expression, the ionic conductivity of 0.15**M** NaCl gives the ionic contribution to the loss

factor as 8.6, rather lower than that of Saxton, but higher than those of Smith and Scott, and Stogryn.

Taking into account all these data, it was decided that, to the degree of accuracy required, the permittivity of 0.15**M** physiological saline at 20°C could be taken as being equal to 75 - *j*22, the value measured by the Glasgow group, and by Saxton. The ionic contribution to the loss factor was assumed to take the CRC Handbook value of 8.6. This leaves 75 - *j*13.4 as the contribution from Debye dispersion, which is a value broadly consistent with interpolations from measured data, and with the value obtained by applying Stogryn's normality corrections (eqns. 3.8.2) to the averaged Debye dispersion parameters for pure water, presented in the previous section (eqns. 3.7.4). Figure 3.c shows the variation of the loss factor of 0.15**M** saline with frequency in the microwave region. It can be seen that at a frequency of approximately 3 GHz, the loss factor reaches a local minimum value. The combination of penetration depth and spatial resolution, so important to microwave thermography, will therefore be optimised at this frequency (Land, 1987). Lower loss factors are only found at frequencies above $\sim 5 \times 10^{10}$Hz, at which frequencies the wavelength and penetration of microwaves into the body will only be several millimetres, which is not a medically useful distance.

3.8.1. Dielectric Decrements.

The static dielectric constant of salt solutions with low concentrations, *c*, can be approximated by a linear relationship $\varepsilon_s = \varepsilon_{sw} + 2\bar{\delta}c$, where ε_{sw} is the static dielectric constant of pure water, and $\bar{\delta}$ is the *mean dielectric decrement* for the particular combination of ions in the solution. For a solution in which the positive / negative ion ratio is equal to 1, the mean dielectric decrement is the mean value of the decrements associated with each ion species $\bar{\delta} = \frac{\delta_+ + \delta_-}{2}$. Table 3.i contains estimated values of the dielectric decrements of many common ions, as first presented by Hasted et al (1948). However, these values are lower than those suggested by the data of other workers. It can be seen that for NaCl, the mean dielectric decrement is equal to -5.5, and so the reduction in static dielectric constant effected by dissolving 0.15mol/l NaCl in pure water is, according to this method, only 1.65. All other researchers report an initial

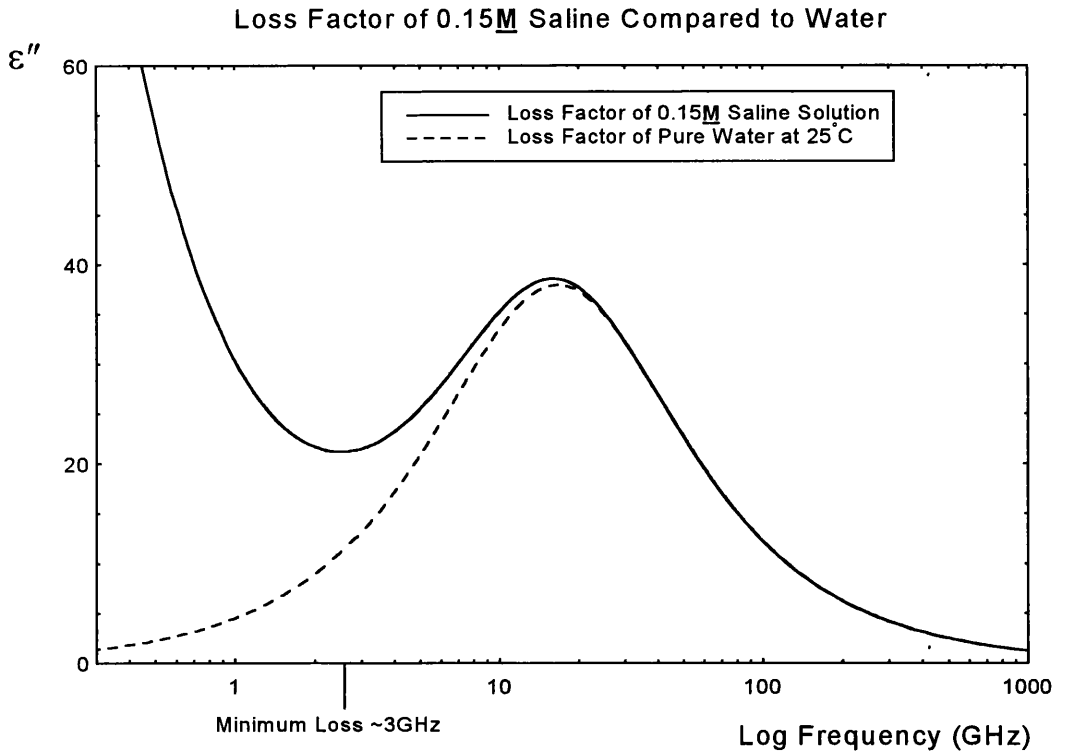

Figure 3.c. Variation of the loss factor of physiological saline in the microwave region compared to that of water. Minimum loss at ~ 3 GHz gives optimum combination of penetration depth and spatial resolution.

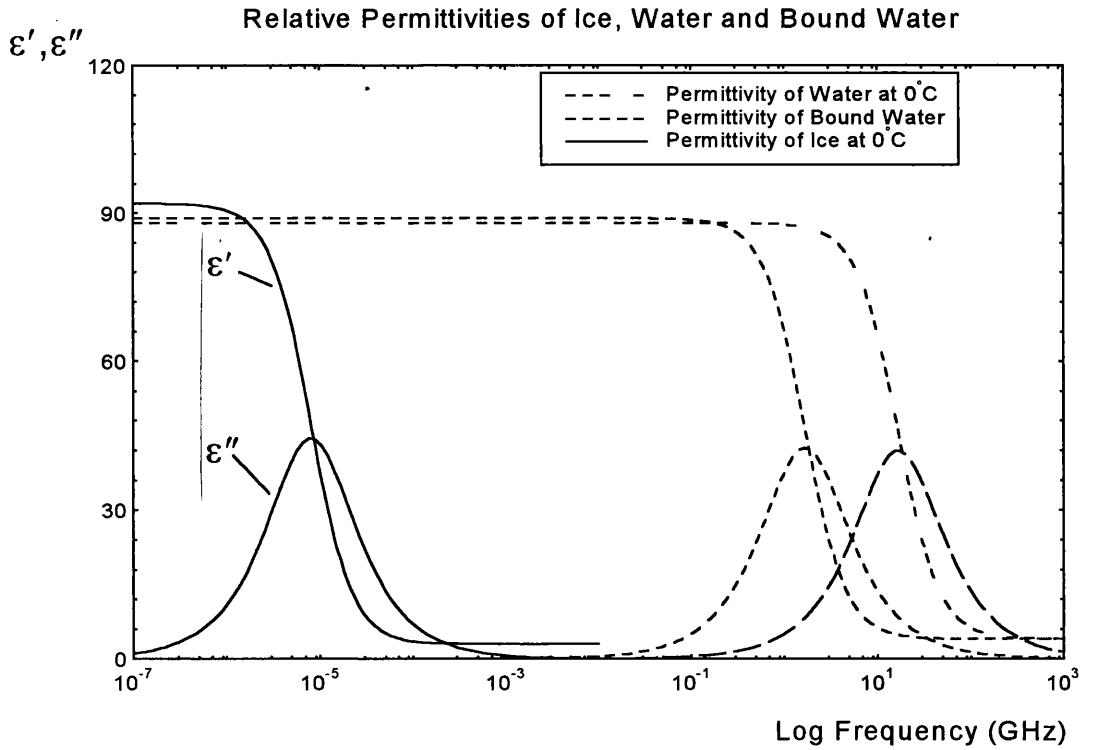

Figure 3.d. Schematic variation with frequency of the dielectric constant and loss factor of ice, typical bound water, and free water over the orientational polarisation dispersion region. Adapted from Schwan, 1965.

fall in ε_s, from the pure water value, of approximately 2.5 for the same concentration of saline.

Similarly, the reduction in relaxation time may be expressed by a relaxation decrement $\delta\tau$ such that $\tau_s = \tau_w + 2\overline{\delta\tau}$. Relaxation decrements for common ions are also presented in table 3.i, although these data seem also to be lower in magnitude than those evaluated by other researchers. Haggis et al (1952) reported alternative values of $\overline{\delta}_{NaCl} = -8$ and $\overline{\delta\tau}_{NaCl} = -0.5ps$ for 0 to 2 **M** NaCl at 20°C. These values are in better agreement with the data of Hasted and el-Sabeh, and Saxton and Lane.

Comparisons of dielectric decrements of different ions may be useful when comparing the properties of different electrolytic solutions.

3.9. Approximating the Ionic Profile of Water in Body Tissue.

The dielectric permittivity at 3 GHz of 0.15**M** saline solution, which is similar to the extracellular fluids in the human body, has been established above. Two processes are responsible for the overall permittivity of 0.15**M** saline solution at 3 GHz; the dipolar relaxation of water, and ionic conductivity of the dissolved salt. It has been shown that the permittivity component from the water is very similar to that of pure water, although the salt has the effect of slightly lowering both the dielectric constant and loss factor of the water at 3 GHz. The ionic conductivity of a free solution of 0.15**M** saline gives rise to an effective loss factor at 3 GHz which can be accounted for by assuming that the ionic conductivity is unchanged at this high frequency from its low frequency (d.c.) value. It is in fact found that when in a tissue, rather than as a free solution, the ionic conductivity of physiological saline is reduced, due to restriction of ionic mobility by other materials, such as dissolved proteins. Also, the dipolar relaxation of some of the water is altered by bonding to proteins when in real tissues, so 0.15**M** saline is only a realistic phantom for the free (unbound) extracellular water in tissues.

However, 0.15**M** saline is ionically only similar to the *extracellular* fluid of the body. Extracellular fluids comprise only one third of the total body water content. The rest is *intracellular* fluid, which has a quite different ionic profile. Tables 3.a to 3.c show the ionic profile of the fluids in the human body, which are further discussed in section 3.2. The dominant ions in intracellular fluid are the potassium (K^+) and hydrogen phosphate

(HPO_4^{--}) ions. In previous research it has been assumed that all body water can be approximated by 0.15**M** saline, although it was realised that the level of ionic conductivity restriction in extracellular fluid differs from that in intracellular fluid due to the differing protein concentrations. Here measurements are presented made on an intracellular fluid phantom which show that the permittivity component due to the dipolar relaxation of free intracellular water is very similar to that observed for 0.15**M** saline.

Based on the milliequivalent weights in table 3.a, a solution of 0.1**M** K_2HPO_4 was used for the intracellular fluid phantom. This contains 200 mEq/l of K^+ ions and also of HPO_4^{--} ions. In real intracellular fluid there are 160 mEq/l of K^+ ions, so only 25% of the cation concentration is misrepresented in the phantom. The HPO_4^{--} ion constitutes around 50% of the anion concentration in the real fluid. When the concentration of the similar SO_4^{--} anion is also considered, it is clear that the only major omission from this approximate phantom is the effect of proteins in the liquid. But proteins also have the effect of binding to water molecules, drastically altering their 3 GHz permittivity, and so were omitted from the test phantom, to be considered separately, in terms of water binding.

Using the dielectric probe measurement technique, described in chapter 5 of this study, the permittivity of 0.15**M** saline was compared with that of the 0.1**M** K_2HPO_4 (anhydrous) intracellular fluid phantom. Measured at 19°C, at a frequency of 3 GHz, the permittivity of 0.15**M** NaCl was found to be equal to 75.4 - *j*22.8, and that of 0.1**M** K_2HPO_4 was equal to 74.8 - *j*23.9. The dielectric constants of these solutions are very similar, differing by less than 1%, and the loss factors are also comparable, lying within the range of experimental error of each other.

It may be possible to account for most of the difference in loss factor between these two electrolytic solutions, by considering the values of their d.c. conductivity. The CRC Handbook (1974) gives the conductivity of 0.15**M** NaCl at 20°C as 1.44S/m, and the conductivity of 0.1**M** K_2HPO_4 at 20°C as 1.585S/m. At 3 GHz, ionic conductivity therefore contributes 8.6 units to the loss factor of 0.15**M** saline, and 9.5 units to the loss factor of 0.1**M** K_2HPO_4. This extra ionic conductivity almost precisely accounts for the higher measured loss factor of 0.1**M** K_2HPO_4. The permittivities of these two solutions

were measured over the range of operation of the dielectric probe from 2 to 4 GHz, and consistently showed the loss factor to be around 1 unit higher for 0.1M K_2HPO_4 than for physiological saline. However, this frequency range is insufficient to estimate the dispersion parameters for either solution, and so no absolutely definite conclusions concerning the contributions from Debye relaxation or ionic conductivity could be obtained.

These observations do however suggest that the permittivity component from dipolar relaxation of water is very similar in both of these solutions. It was therefore decided that, to a good first approximation, the free water in all body electrolytes could be treated as being equivalent to the free water in 0.15M NaCl.

This means that tissues can be dielectrically modelled , using mixture equations, as mixtures of proteins, both dissolved and undissolved, in a majority substance of 0.15M saline solution. Consequently, any deviation in the dielectric constant of a tissue from its expected value can be attributed to water molecules binding to protein molecules, and any deviation in the loss factor of that tissue from its expected value can be attributed to the effects of water binding, and also to ionic conductivity restriction due to proteins dissolved in the tissue electrolyte.

3.10. Permittivity of Protein and Lipid.

Protein and lipids constitute the great majority of the non-water fraction in soft biological tissues. If tissue permittivity data is to be analysed, it is necessary to know the permittivity of the proteins and lipids which are considered to be suspended in the physiological electrolyte. Estimated values of the permittivity of proteins at 3 GHz have ranged from 2 to around 5 relative units. Foster et al (1984) considered the high frequency limit of the protein-bound water composite to be approximately $4 - j0$, suggesting that the permittivity of the protein was around $3 - j0$. Campbell (1990) was able to measure the permittivity of pure protein and lipid from dehydrated tissue samples, using the resonant cavity method. The average value for pure protein was $2.5 - j0.2$, and for pure lipid, $2.7 - j0.2$. These are the values which will be used in this study.

3.11. The Effects of Bound Water in Tissues.

Although composed mainly of water, soft biological tissues are of a solid or semi-solid structure. This is mainly the result of hydrogen bonding of water molecules to long-chain protein molecules in the tissue. Such bonding restricts the translational and rotational motion of bonded water molecules, and therefore increases the characteristic relaxation time of the bonded water molecules at microwave frequencies. Water which is involved in hydrogen bonding with other molecular species in tissues is known as *bound water* or, sometimes ambiguously, *water of hydration.* Water which is not involved in extra hydrogen bonding is referred to as *free* or *unbound* water. The degree to which the bound water is rotationally restricted depends on the availability and character of the other molecules with which the water molecules are linked.

In ice, water molecules are often regarded as being hydrogen bonded to the maximum extent. At a temperature of 0°C, the Debye resonance in liquid water, due to orientational polarisation, is centred around a frequency of approximately 9 GHz. The Debye dispersion parameters have respective values of $\varepsilon_{s(water)} = 88.3, \varepsilon_{\infty(water)} = 4.3$ and $\tau_{(water)} = 18ps$. For ice, at the same temperature of 0°C, the frequency range of the equivalent dispersion is drastically altered. The high and low frequency limits on the permittivity of ice are remarkably unchanged from the liquid values at $\varepsilon_{s(ice)} = 92$ and $\varepsilon_{\infty(ice)} = 3.$. However, the relaxation time, τ_{ice}, is increased to $20\mu s$. This reduces the relaxation frequency of this dispersion to approximately 10 kHz (see fig. 3.d).

The structure of bound water in biological tissues appears to intermediate between that of ice and free water. It has been reported by Schwan (1965) and Risman (1988) that the parameters ε_s and ε_∞ of bound water in biological tissues are close to the values for free water and ice. Extra hydrogen bonding in water seems only to affect significantly the relaxation time of the water, and not the other dispersion parameters.

Were the bound water molecules in biological tissues to be as strongly hydrogen bonded as those in solid ice, they would not contribute at all to dispersion in the microwave region. Thus the microwave dielectric constant and loss factor of tissue would both be of lower magnitude than those of a solution containing a non-interacting liquid mixed with free tissue electrolyte to similar proportions as found in biological tissue.

Measurements on real tissues, including those presented herein, show that rather than being reduced, the loss factor of tissue electrolyte at 3 GHz is increased above the value expected if the water in the tissue electrolyte were unbound. This suggests that the increase in relaxation time due to binding is sufficiently small that the dipolar relaxation frequency of the bound water is still in the microwave region. Assuming the dispersion parameters ε_s and ε_∞ remain constant, it can be shown that, at 20°C, an increase in the dipolar relaxation time of water from $10ps$ to up to $270ps$ results in an increase in the loss factor of the water (see fig. 3.e). Above this value of relaxation time, the high frequency tail of the bound water dispersion has a lower magnitude than the low frequency tail of the free water dispersion.

It is misleading to regard the water in tissue electrolyte as being separable into 'bound' and 'unbound' fractions. Measurements suggest that a broad distribution of relaxation times exists. There may be several reasons for this: firstly, the protein-water bonds at different bonding locations on protein molecules may be of a variety of strengths, and secondly, there is evidence which indicates that water molecules close to protein molecules, but not directly bonded to the protein, are nevertheless motionally restricted to some extent.

A simple first estimate as to the amount of tissue water which is bound to protein molecules may be obtained thus. Consider one repeat unit (monomer) in a section of a glycine based polypeptide molecule, surrounded by water, as shown in fig. 3.f. This is the simplest protein polymer, with no side chains. Hydrogen bonds may be formed between hydrogen atoms and either oxygen, nitrogen or fluorine atoms, provided the hydrogen atom is itself (polar) covalently bonded to one of the three latter atomic species. Therefore, two, or possibly three (see fig. 3.f), water molecules at most may be directly bonded on to each repeat unit length of the protein. The mass of the repeat unit is 57amu, and that of a water molecule is 18amu, so, as a first approximation, 1 gram of protein may hydrogen bond with ~0.6 grams of water.

Table 3.j displays measured values of the water of hydration associated with some real dry biological polymer substances. This shows that the measured values are at least of the same order of magnitude as the amount estimated above, although no simple relation exists between water uptake of proteins at any arbitrary humidity, and what can be regarded as water binding. At very high humidity, the water uptake is very much

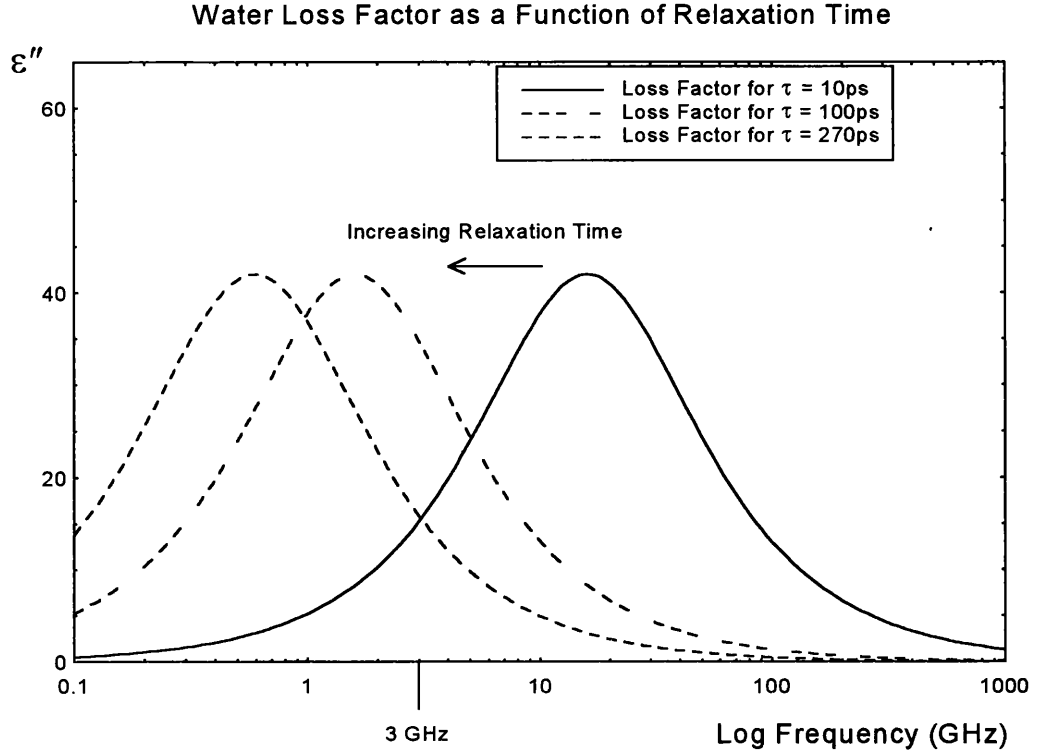

Figure 3.e. Comparison of water loss factor for a variety of relaxation times, assuming that ε_s and ε_∞ remain constant. Note that at 3 GHz an increase in loss factor is obtained for all bound water relaxation times up to 270ps.

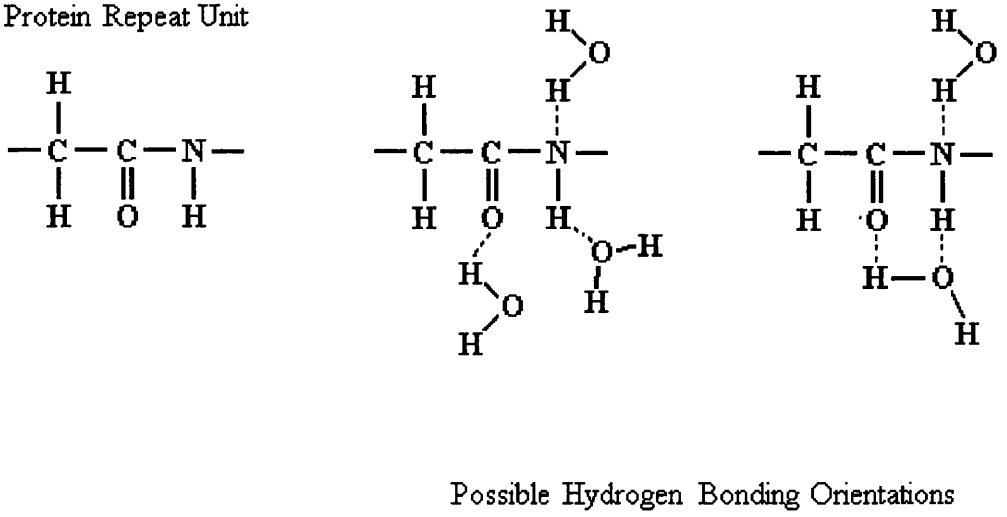

Figure 3.f. Schematic diagram of a simplified approximation of water bonding to glycine monomer.

Molecular Type	Water Uptake at 90% Relative Humidity (g water / g solid)	Non-freezing Water (g water / g solid)
Polypeptides		
p-Alanine	0.13	0.14
p-Glycine	0.2	0.23
p-Glutamate	0.7	0.75
p-Lysine	0.35	0.32
Globular Proteins	0.3 - 0.4	0.3 - 0.5
Fibrous Proteins	0.4	0.3 - 0.5
DNA	0.6 - 0.9	0.6
Membranes	0.25	0.25
Lipids	0.25 - 0.3	0.28
Cells		
Muscle	0.45	0.8
Stratum Corneum	0.4	0.37

Table 3.j. Representative estimates of hydration water associated with some biological molecular species. Adapted from Cooke and Kuntz, 1974.

greater. However, the data in column 3 of table 3.j refer to the amounts of water associated with the macromolecules that will not freeze, and indicate that around 0.3 to 0.5 grams of water per gram of biological polymer is considerably affected in its physical properties. Using these data, Cooke and Kuntz (1974) estimate that, for proteins consisting mainly of simple amino acid monomers as considered above, approximately 2 moles of water are bound to each mole of amino acid. The bonding geometry of bound water in real proteins is not so simple as is shown in fig. 3.f, as the characteristic helical conformation of proteins is partially stabilised by hydrogen bonds on amino acid units.

Cooke and Kuntz proposed that tissue water be categorised as (i). *bulk* water, the majority component, which is essentially free, (ii). motionally restricted *bound* water, which lies close to macromolecules and has an increased relaxation time, and (iii). *irrotationally bound* water, which constitutes only a small fraction of the total, and is semi-permanently site-bound to the macromolecule for periods of the order of microseconds. This is shown schematically in fig. 3.g. Water molecules may alternate between free and bound states by Brownian motion. NMR measurements on a 20% protein solution suggested that 90% of the water solvent was bulk water, 10% bound water, and ~0.1% irrotationally bound water, so approximately 0.5g water is bound per gram protein.

An extension of this concept was suggested by Spirdonov (1982), with regard to calibrating UHF water content meters. Water absorbed by porous or powdered solids was regarded as binding to the solid in layers. As the distance from the solid surface increased, each successive molecular layer was considered to be characterised by a lower relaxation time than the previous layer, until the free water parameters were reached (see fig. 3.h). At this point the water ceases to be held to the surface, and begins to flow like a bulk liquid. To apply this model, the binding energy of each layer must be known, so that the complex permittivity of the moist substance can be found by integration over all the layers. At this stage, such an involved procedure cannot be applied to biological systems, as there is far too little information known about the state and distribution of water binding in tissues.

A great deal of research has been published on the measurement of the amount of motionally restricted water associated with aqueous solutions of biological polymers. A

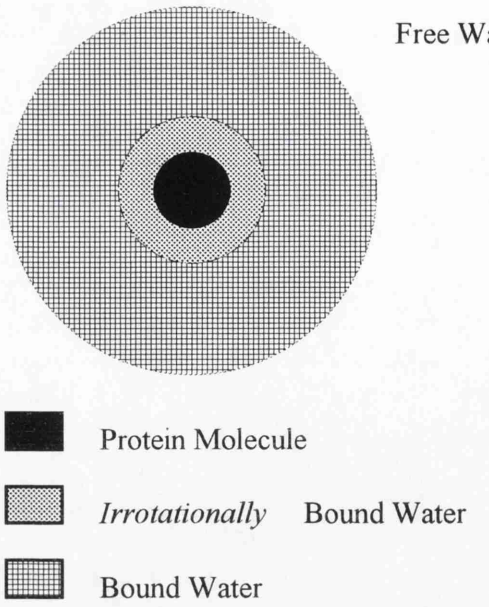

Figure 3.g. Cross-sectional schematic diagram of protein molecule showing Cooke and Kuntz' categorisation of water in biological tissue.

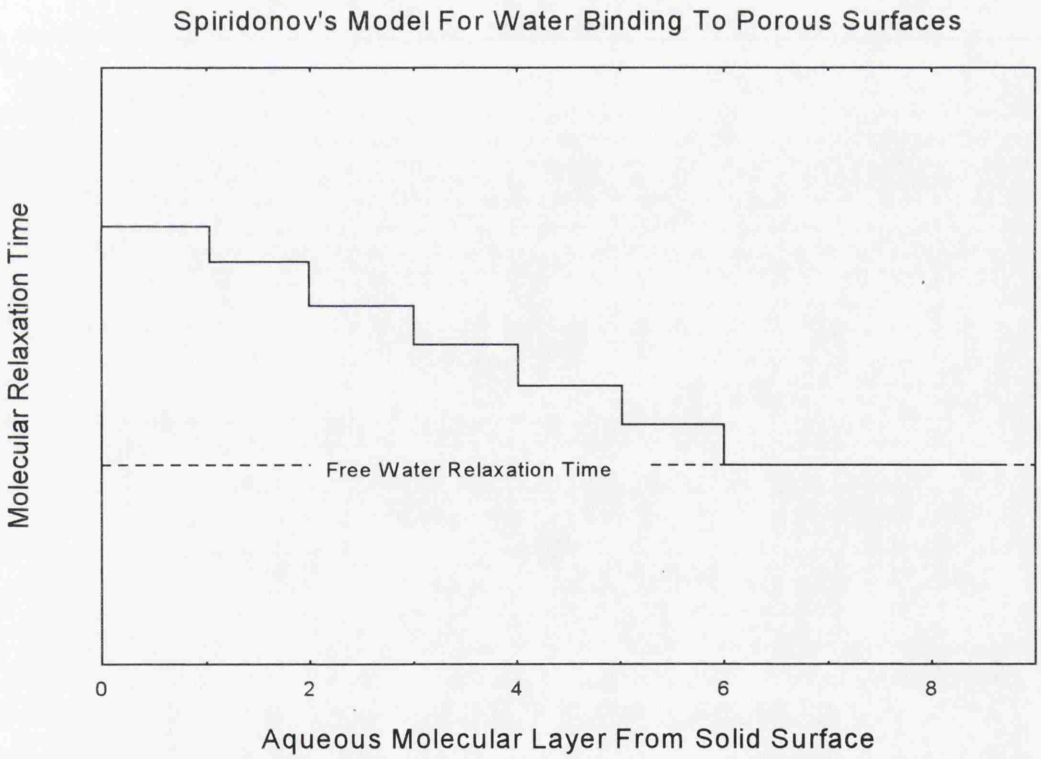

Figure 3.h. Diagram showing Spiridonov's model for the relaxation time of water which is bound or partially bound to a solid surface. Each molecular layer around the solid is supposed to be characterised by its own relaxation time, decreasing with increasing distance from the surface until the free water parameter is reached. If the discrete relaxation times and the number of molecules in each state are known, then the overall permittivity can be estimated.

variety of methods have been used, including low-frequency conductivity measurements (Bull and Breese 1969), analysis of dielectric behaviour over frequencies between the β and γ dispersions (Schwan 1965), and investigation of the amount of unfrozen water in otherwise frozen solutions (Kuntz 1971). By using a solution of a single protein species rather than real tissue, the dielectric behaviour is made more predictable, and the number of extraneous variables is reduced, thus simplifying the analysis of dielectric data.

On account of the differing measurement techniques, and the difficulty, due in part to relaxation of protein polar side chains, in resolving precisely those effects caused only by bound water, it is not always evident whether individual results refer to the same types of bound water, or volumes with differing properties.

It is clear, however, that there is general agreement, from the earliest measurements by Buchanan et al (1952) on simple proteins, to those on DNA solutions by Foster et al (1984), that approximately 0.5 grams of water per gram dissolved polymer can be regarded as being 'bound' to biological polymers. The relaxation frequency of this bound water has been estimated as ranging from below 1 GHz to around 5 GHz, and so is important to consider in the analysis of tissue permittivity. It is notable that mixture equation analysis in many of these studies showed that the dielectric properties of protein solutions were essentially independent of the length of the polymer chain, despite the wide variation in axial ratios of the protein molecules investigated. This suggests that mixture equations may also be applied to real tissue data, for which the shape, size and mass of the protein molecules is unknown, without affecting the validity of conclusions. Some protein molecules in the human body are much larger than those considered here, having molecular masses of many millions.

An involved discussion on the effects of dissolved ions in protein solutions by Eagland (1972) suggests that although certain ionic species are found to either inhibit or increase hydrogen bonding with proteins, the levels of bound water in water/protein solutions which contain dissolved salts will be very similar to those in simple water/protein solutions containing no salts.

The amounts of bound water measured on real biological tissue are broadly consistent with those of protein solutions. Foster et al (1980) studied the permittivity of barnacle muscle tissue, concluding that ~5% of the water was bound, and relaxed at a low GHz frequency. Clegg et al (1984) measured the permittivity of cysts of the crustacean

Artemia, which is a tissue that can be reversibly hydrated and dehydrated by the addition or removal of water, and found that the bound water had a relaxation time of between 2 and 7 GHz. On human tissues the bound water fraction is very similar to that of protein solutions: Schepps (1981) estimated the bound water fraction of muscle, brain and liver to be approximately 0.4, 0.5 and 0.58 grams per gram dry weight respectively; Steel and Sheppard (1985) concur with Schepps, finding that 0.5g water/g solid is bound in human brain, with a relaxation frequency below 5 GHz. Grant (1984) showed that less than 2% of the water in blood is bound, and Smith and Foster (1985) estimated that only a very small amount of water in fatty tissue is bound.

Dielectric measurement of bound water are usually analysed using either a multi-component dispersion equation, or by the use of mixture theory. A study which compares the two methods, and the dielectric information they yield, is discussed in the following section. Many of the important features of the behaviour of bound water in polymer systems are also presented.

3.12. Dielectric Permittivity of Bound Water in Polymer Solutions.

An illuminating study of the relaxation properties of water in aqueous polymer solutions has been carried out by Kaatze et al (1978a,b), and latterly by Foster et al (1984). The water soluble polymer polyethylene oxide (PEO) was chosen for most of the measurements. PEO is commercially available in several different polymer chain lengths, and has a simple monomer basis (see fig. 3.i), the direct hydrogen bonding properties of which are more easy to estimate than those of biological proteins.

Kaatze measured the dielectric permittivity, between 0.4 and 40 GHz, of PEO solutions with concentrations up to 12 moles of monomer per litre, and polymer chain lengths from 75 to 13600 monomer units. The results for a chain length of 850 monomer units are reproduced in fig. 3.j. As the polymer concentration increases, the real part of the permittivity decreases, and the overall relaxation frequency is reduced. It may be noted, even at this stage, that despite the reduction in the maximum loss, caused by the lower number density of water molecules in solutions of greater polymer concentration, the net effect at 3 GHz of the water binding is an increase in dielectric loss. The data were analysed using a multi-component Cole-Cole type equation of the form

PEO Polymer Repeat Unit

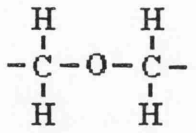

Figure 3.i. Schematic diagram of the monomer basis of polyethylene oxide.

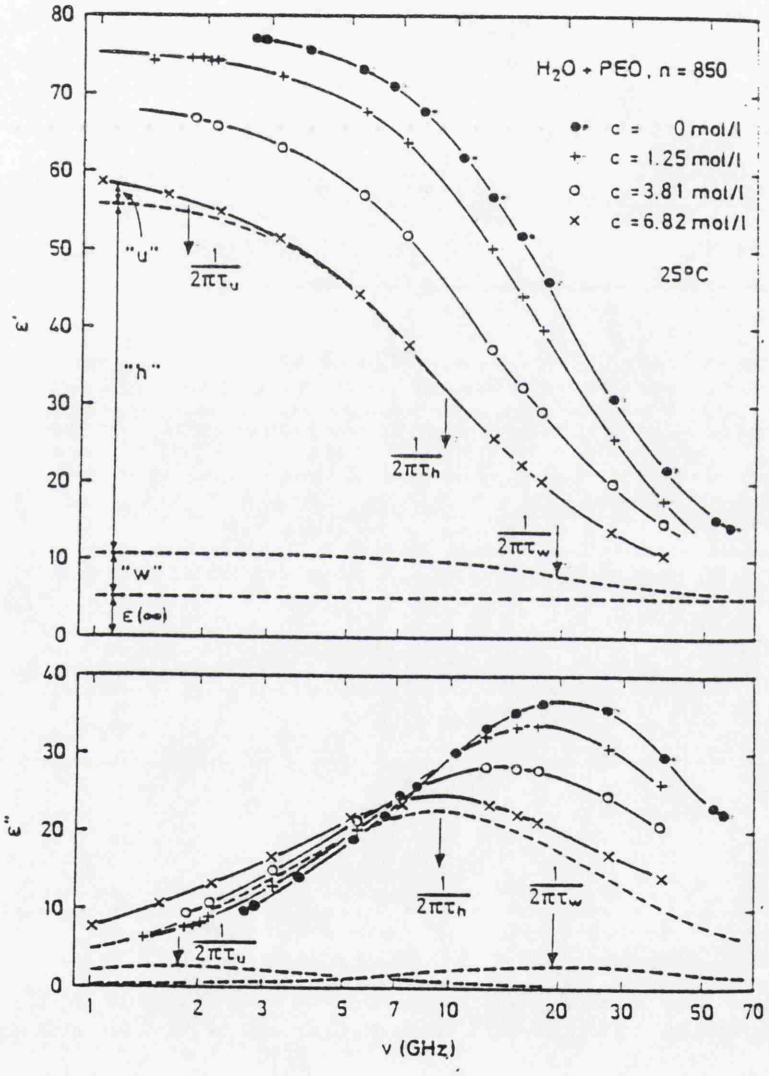

Figure 3.j. Plots of dielectric constant and loss factor of aqueous PEO solutions vs. frequency. The dashed lines give the superdivision of the overall values into different terms representing the contribution from each of the terms in equation 3.12.1. Note that the largest contribution is due to bound water. Reproduced from Kaatze et al, 1978a.

$$\varepsilon' - j\varepsilon'' = \varepsilon_\infty + \frac{\varepsilon_m - \varepsilon_\infty}{c_w}\left[\frac{Z_h c}{1+(j\omega\tau_h)^{(1-h)}} + \frac{c_w - Z_h c}{1+(j\omega\tau_w)^{(1-h_w)}}\right] + \frac{\varepsilon_s - \varepsilon_m}{1+j\omega\tau_u} \qquad (3.12.1)$$

The first relaxation term on the right-hand side of eqn. 3.12.1 represents the dielectric relaxation of the hydration water, distributed about a mean relaxation time τ_h. In doing so, Z_h is the number of affected water molecules per monomer unit, and c is the monomer concentration. The second term refers to the unaffected free water, with molarity $c_w - Z_h c$ ($c_w = 55.5$, the molarity of pure liquid water), which is assumed to relax with the same reorientation time, $\tau_w = 8.25ps$ (at 25°C), as pure water. The combination of both types of solvent water to the permittivity at frequencies well below 1 GHz is ε_m: ε_s is the limiting value of the total permittivity at low frequency and ε_∞ is the limiting value at high frequency. As the polymer solute molecules may also contribute a small amount to the permittivity, especially at low frequency, the final term represents a Debye relaxation for the polymer, characterised by τ_u. Equation 3.12.1 was fitted to the experimental data using a non-linear least-squares routine, which yielded values for all the dielectric parameters.

Amongst the many conclusions drawn from this work were two of particular interest here. Firstly it was found that approximately 5.5 hydration water molecules could be associated with each EO monomer group. Chemical considerations (Franks, 1973) suggest that because the EO group can accept two protons in forming hydrogen bonds, a hydration number of 2 is expected. Finding more than double this number is consistent with the supposition that the polymer bonding affects not only those water molecules directly adjacent to the bonding site, but also those in a more distant layer.

The relaxation time of the hydration water was found to be, on average, 18.6*ps*, which reduces the relaxation frequency at 25°C from 20 GHz to under 10 GHz.

Secondly, the dielectric parameters had no discernible dependence on the polymer length used. This was most notable for the parameter ε_m, as the measured values could be compared to those predicted by mixture equations for suspended particles ranging from spherical to elongated cylindrical in shape. Across the range of polymer chain lengths, and at all concentrations, the measured data showed agreement with the mixture equation for spherical molecules rather than cylindrical. Extra measurements on suspensions of polyvinylalcohol and polyvinylpyrrolidone also displayed the same behaviour. This finding was striking, as it was supposed that the macromolecules would

adopt elongated shapes in aqueous solution. It is interesting to note that, when making low frequency (1 kHz) conductivity measurements on protein suspensions, Bull and Breese (1969) noted the apparent independence of conductivity on particular shape. Kaatze suggested that this may be due to each segment of the flexible chain polymer molecule behaving as an individual sphere in the solution.

In addition to these findings, Kaatze also performed similar calculations on water / dioxane mixtures. Despite being the cyclic ethylene oxide dimer, the hydration water reorientation times were found to differ considerably from those of the PEO polymer solutions, suggesting that some unknown property (possibly geometrical) of polymer molecules is important in determining the dielectric behaviour of their aqueous solutions.

Foster (1984) presents an alternative analysis of Kaatze's measurements, using the Maxwell and Bruggeman mixture equations rather than fitting the data to a multi-component dispersion relation. In addition to the original dielectric dispersion data, measurements of several other transport properties of PEO solutions, including thermal conductivity and self-diffusivity. Graphs representing those values are presented in fig. 3.k.

The variation of thermal conductivity with PEO concentration is found to be (very) approximately described by the mixture equations, whereas the water self-diffusion co-efficient, which is more dependent on the bulk mobility of the water solvent molecules, shows a marked decrease from predicted values. It is notable that tissue thermal conductivity is also found to display this characteristic behaviour as a function of water content (Hamilton, 1996)

In the limit of low PEO volume fractions, it was found that the measured water self-diffusion co-efficient corresponded to an effective volume fraction of PEO approximately 2.4 times the true value. This extra volume must be associated with those water molecules that are bound to the PEO, and are therefore unable to contribute to self-diffusion. An average hydration number of 3.1 water molecules per EO monomer group is suggested by this figure. Once the PEO volume fraction is over ~40%, no free water molecules remain, and so fewer are associated with each monomer group.

To analyse Kaatze's data, a first order expansion of the Maxwell-Fricke equation was used:

$$\sigma = \frac{(2\pi f^2 / f_c)(\varepsilon_s - \varepsilon_\infty)\varepsilon_0}{1+(f/f_c)^2}\left[\frac{1-p'}{1+(p'/2)}\right] + \sigma_p\left[\frac{3}{2+p'}\right]^2$$

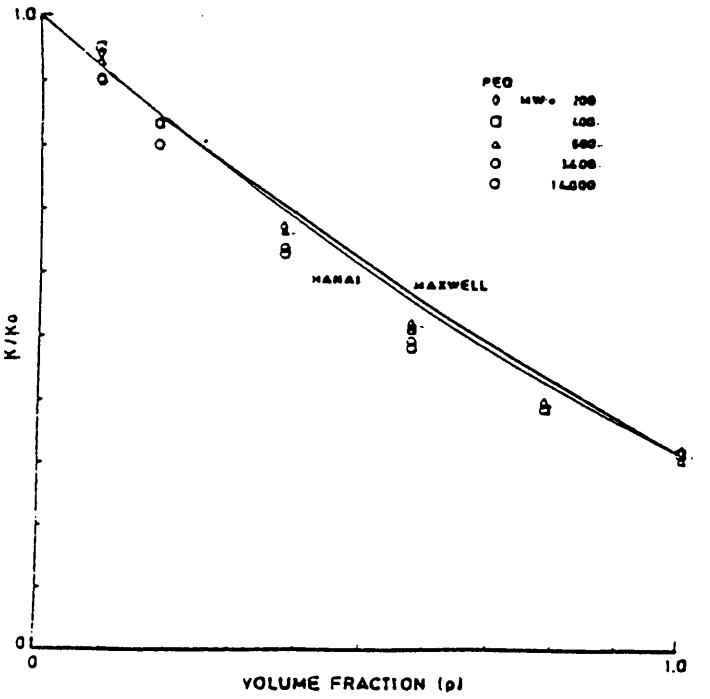

Figure 3.k(i). Thermal conductivity of PEO solutions, divided by that of pure water K_0, vs. polymer volume fraction. Also shown are the predictions of the Maxwell and Hanai (Bruggeman) mixture equations. Reproduced from Foster et al, 1984.

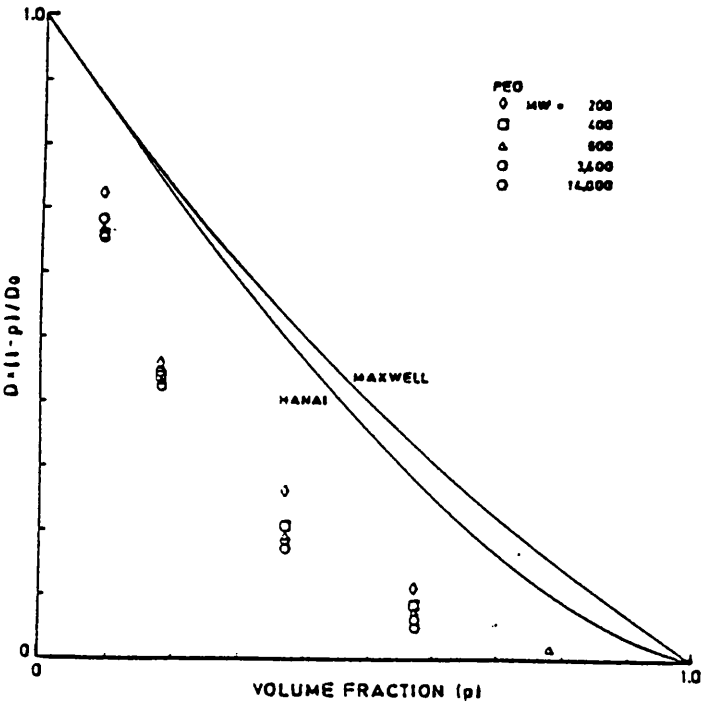

Figure 3.k(ii). Normalised water self-diffusion co-efficient of PEO solutions vs. polymer volume fraction. Reproduced from Foster et al, 1984.

and $$\varepsilon = \left[\frac{\varepsilon_s - \varepsilon_\infty}{1+(f/f_c)^2} + \varepsilon_\infty\right]\left[\frac{1-p'}{1+(p'/2)}\right] + \varepsilon_p\left[\frac{3}{2+p'}\right]^2 p' \qquad (3.12.2)$$

Here, ε_s and ε_∞ are the low and high frequency permittivity limits, p' is the effective volume fraction of PEO polymer, f_c is the relaxation frequency of free water, the Fricke shape factor γ is taken as 2, and σ_p and ε_p are the conductivity and permittivity of the polymer respectively. In equations 3.12.2, the first terms on the right-hand side represent the contributions of the free water, and the last terms represent the effects of the polymer.

At sufficiently high frequencies, the increase in conductivity with frequency should be dominated by the dielectric relaxation of the free water. A plot of conductivity against x, where $x = \left[(2\pi f^2 / f_c)\varepsilon_0\right] / \left[1+(f/f_c)^2\right]$, should, at high frequencies, tend to a linear function with slope $\left[(\varepsilon_s - \varepsilon_\infty)(1-p')\right]/(1+p'/2)$. The results of this analysis on a 25% volume fraction PEO solution are reproduced in fig. 3.1. An effective volume fraction of 0.6 is estimated, corresponding to 3.0 water molecules per EO group, or 1.2 grams per gram of polymer. The relaxation frequency of this bound water is taken to be the frequency at which the conductivity of the slowly relaxing fraction is half its limiting value, and is found to be between 4 and 5 GHz.

These conclusions differ from Kaatze's own analysis, suggesting that the original estimated hydration number of 5.5, and relaxation frequency of 10 GHz are rather high. Foster draws the reader's attention to the dangers of over-interpreting dielectric data with dispersion equations. However, it is nevertheless confirmed that water bonding on this polymer affects more molecules than chemical considerations suggest can directly bond to the polymer. It has been proposed that the very fact that this polymer is water soluble may be due to it fitting into the water 'lattice' unusually well. Similar bonding properties were observed on emulsified solutions of insoluble oils by Epstein et al (1983), which appear to contradict this particular hypothesis.

3.13. Summary.

In conclusion to this chapter, the significant elements are summarised as follows:

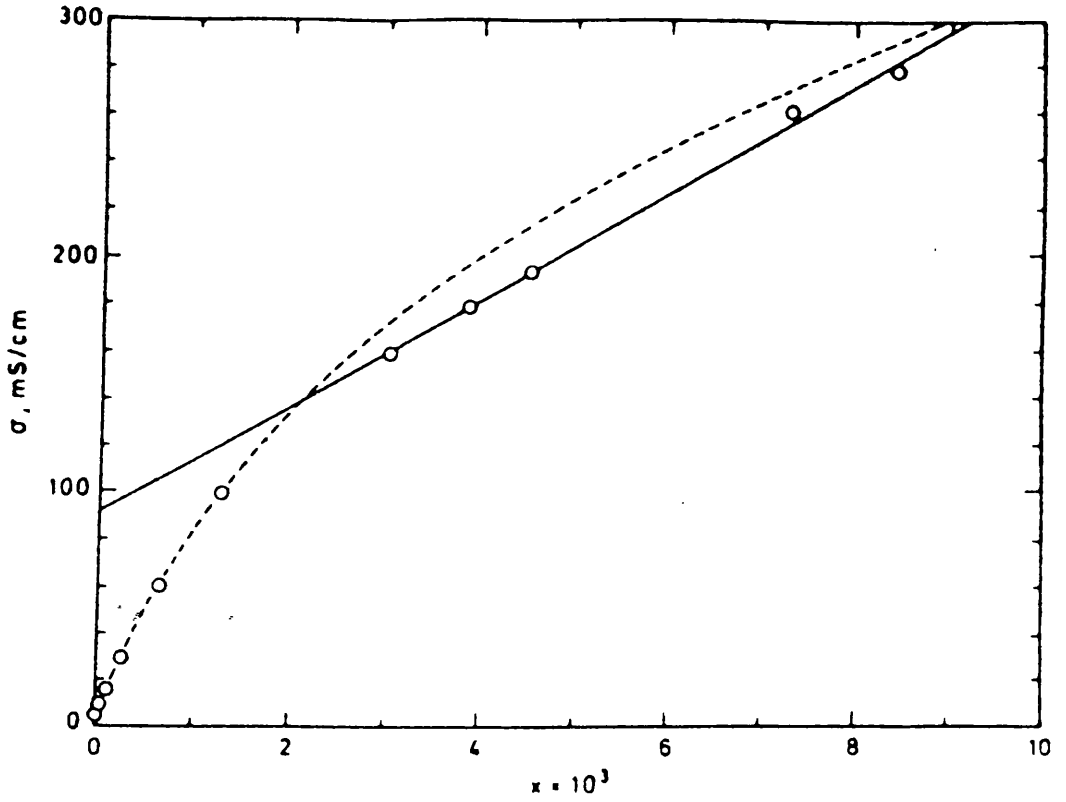

Figure 3.1. Plot of effective conductivity against the factor x, given in the text, for an aqueous PEO solution, with polymer volume fraction equal to 0.25, and molecular weight equal to 37400. A linear fit to the data above 12 GHz gives a slope of 0.227mS/cm and an intercept of 91mS/cm. This suggests an effective volume fraction of 0.6, and a relaxation frequency for the bound water (taken to be the frequency at which the conductivity of the bound fraction is half of its limiting value of 91mS/cm) of ~ 4 - 5 GHz. Reproduced from Foster et al, 1984.

The microwave permittivity of biological tissues is primarily determined by the amount of water in the tissue, and by the low frequency conductivity of the tissue, which is due mainly to ions dissolved in the tissue water.

In the liquid state, water has a 3 GHz permittivity of approximately 77.7 - *j*13.5 at 20°C. All other main constituents of tissues, such as protein and lipid, have a permittivity of around 2 at 3 GHz, as these large molecules have very much lower relaxation frequencies than water.

The water in tissues can be divided broadly into three types; intracellular, intercellular and plasma electrolytes. Although each contains a different profile of dissolved ions, the permittivity of simulated solutions of all three fluids was found to be sufficiently similar that, for the purposes of dielectric modelling, each can be mimicked by a 0.15**M** saline solution, which at 20°C, has a 3 GHz permittivity of approximately 75 - *j*22.

In biological tissue, around 10% of the water component is affected by molecular binding onto large protein molecules, forming a semi-solid gel. This binding reduces the relaxation frequency of the affected molecules, so reducing the 3 GHz permittivity of the tissue water fraction as a whole. Also, the gel restricts the mobility of the ions dissolved in the electrolyte, thus reducing the conductivity contribution from the ions below the value expected for a free ionic solution.

Comparison between the measured dielectric constant of the tissue, and the value predicted by mixture equation, gives a difference which is due to the presence of bound water in the tissue. With sufficient data, measurement of this difference allows an estimate of the amount of bound water in the tissue to be made.

Chapter 4. Measuring the Complex Permittivity of Biological Tissue.

4.1. Introduction.

Many researchers have made dielectric measurement of human and animal tissue using a variety of methods. In this chapter, those methods are reviewed, with particular attention to the theoretical and practical considerations which led to the selection of the open-ended co-axial probe technique for this work. The apparatus required to make permittivity measurements is considered, and details of the equipment used in this particular study are discussed. An improved experimental co-axial probe design, as used in this work, is presented, and its performance compared with that of a simple probe such as has been used in previous studies.

Prior to making permittivity measurements on sample materials, the co-axial probe had to be calibrated and checked for accuracy across the permittivity range expected of biological tissues, by making measurements on liquids of known permittivity. Choice of these calibration liquids is discussed, and the physical parameters of the dielectric dispersion equations used to calculate the 'known' permittivities are presented.

4.2. Techniques for Measuring the Permittivity of Biological Tissue.

When choosing a technique for the measurement of the complex permittivity of human and animal tissues at 3 GHz, the following major criteria were considered.

- Human tissue samples available from surgery are usually very small, with volumes often less than $1\,cm^3$. Also, some samples tend to be quite inhomogeneous in shape and formation, even over a small distance. It was therefore necessary that the measurement technique used could be applied to small tissue volumes, in the cubic millimetre range.

- Since it was intended to make a very large number of dielectric measurements, it was essential that both the measurement process and the computation required to obtain the dielectric information from raw data had to be fairly simple and rapid.

- As it was desired to make water content measurement on every dielectrically

investigated sample, the measurement procedure had to not damage or degrade the tissue sample prior to drying.

- Working in collaboration with a colleague, the thermal conductivity and dielectric permittivity of tissue samples was to be compared, as part of a program of combined thermal and dielectric tissue modelling. Therefore the dielectric permittivity measurement had to not render a sample useless for subsequent thermal measurement, and should, if possible, measure over approximately the same volume of tissue.

4.2.1. Waveguide Techniques for Measuring Complex Permittivity.

The complex permittivity of a material at a given frequency can be measured using a waveguide in several configurations. Most simply, if a waveguide is terminated (preferably on a ground plane), by a semi-infinite sample of test material, then the relative permittivity of the test material can be calculated from the reflection co-efficient of an incident wave reflected back along the guide from the open end. This configuration is discussed by Decreton and Gardiol (1974), and is shown in fig. 4.a.
Other similar methods involve measuring the reflection co-efficient from a sample of material placed within the guide. This sample may be a plug, across the whole width of the guide, or a symmetrical perturber, placed centrally inside the guide (see Marcuvitz, 1951 p.217).
It may be noted that the open-ended guide configuration is the 'active mode' equivalent of the waveguide antenna arrangement, used passively to measure the intensity of emitted microwave radiation in a microwave radiometer, as mentioned in chapter 1. As the field distribution at the open end takes the same form in active and passive modes, the discussion of the difficulties in modelling the radiometer antenna pattern in section 1.6 also applies to this permittivity measurement technique. The spreading of the external fields within the test material makes accurate calculation of its permittivity from reflection co-efficient data a computationally intensive problem.
A problem more fundamental to all waveguide techniques of measuring complex permittivity at 3 GHz is one of dimensions. Each waveguide has a characteristic 'cut-off' wavelength, dependent on the guide dimensions, above which length radiation will not propagate along the line. Propagation even of the lowest TE_{01} mode oscillation in a

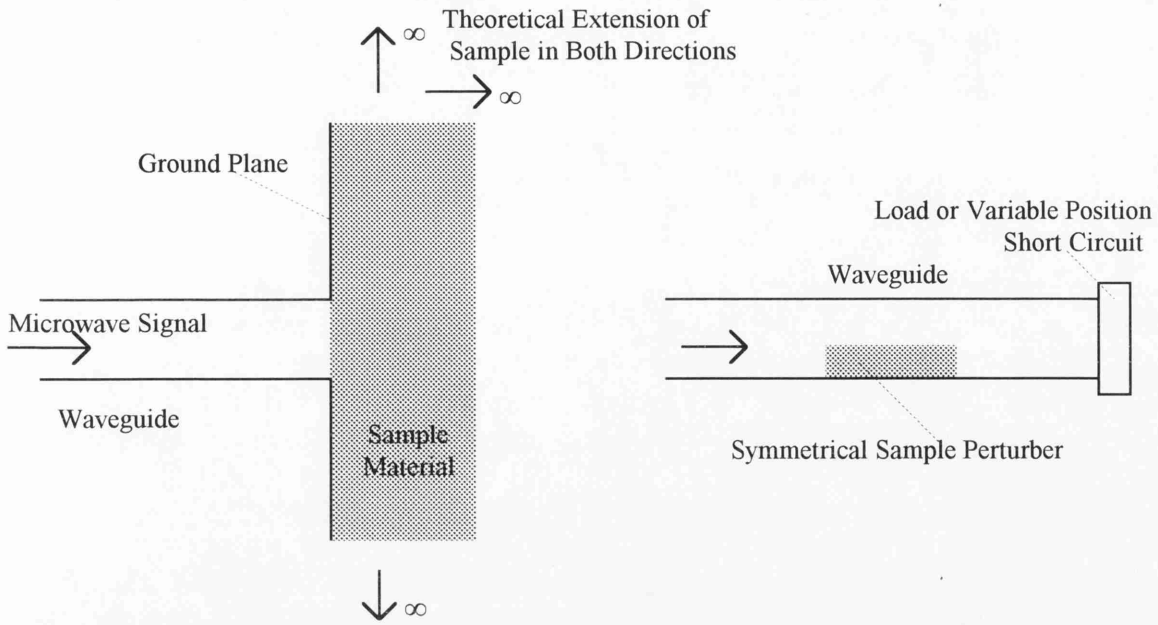

Figure 4.a. Cross-sectional views of two common waveguide configurations for measuring the permittivity of lossy materials.

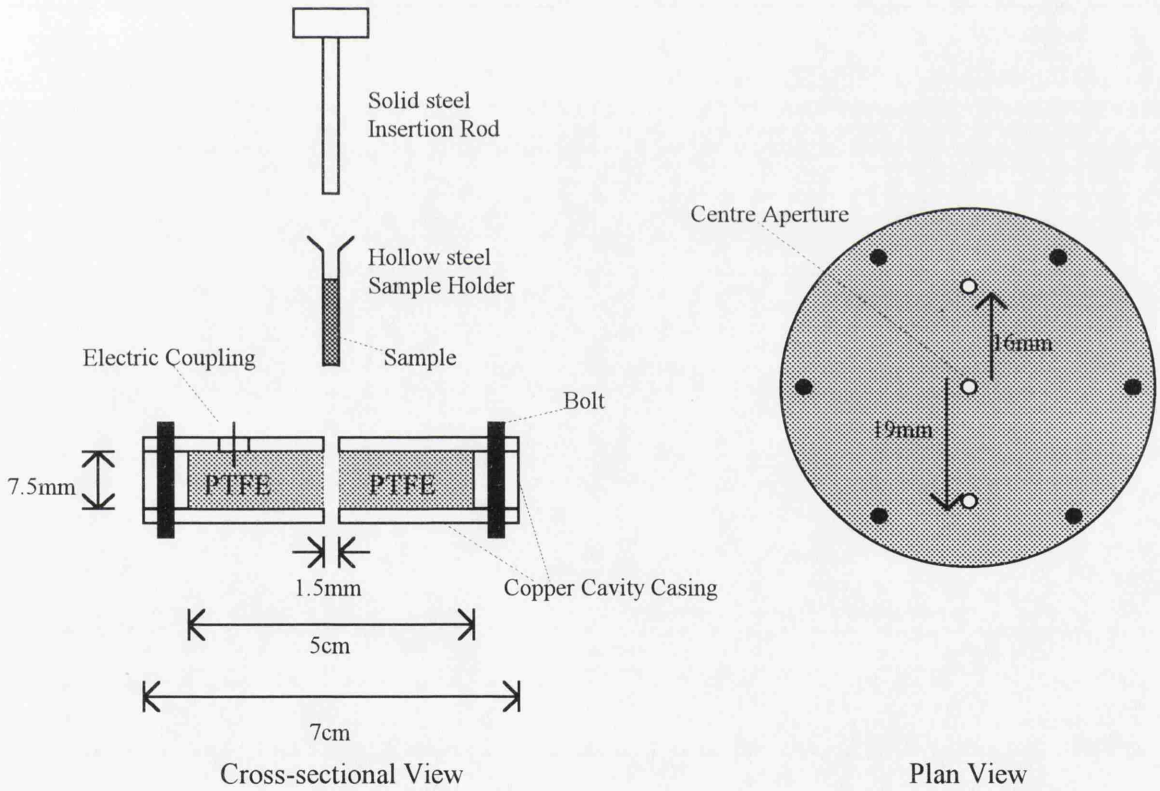

Figure 4.b. The resonant cavity method previously used in the group to measure the permittivity of tissue samples. Only one of the three measurement apertures visible in the plan view is shown in the cross-sectional view. Samples were inserted into the apertures from a correctly sized hollow sample holder.

rectangular guide requires that the guide width, a, satisfies the equation $a > \frac{\lambda_0}{2\sqrt{\varepsilon_g \mu_g}}$, where ε_g and μ_g, are the relative permittivity and permeability respectively of the medium which fills the waveguide. So, for an air-filled guide, at a measurement frequency of 3 GHz, the guide width must be at least 5cm. Loading the guide with a low loss dielectric material will reduce the minimum required width by a factor of $\sqrt{\varepsilon_g}$, but even with a high permittivity loading material, the guide will still need to be ~1cm in width or diameter. In addition to this, the field pattern from such a waveguide extends several centimetres into the test material. To contain even the majority of this external field, the terminating sample has to have a volume of several cubic centimetres, and be sufficiently planar as to form a good electrical contact across the entire end of the guide. It is inconceivable that many tissue samples from surgery will be of such large dimensions and homogeneity.

4.2.2. Resonant Cavity Perturbation.

Previous research into the dielectric properties of tissue, carried out at the University of Glasgow, has used the resonant cavity perturbation technique to make permittivity measurements (Campbell, 1990). A dielectrically loaded cylindrical resonant cavity is perturbed by the insertion of a small cylindrical sample of the tissue to be investigated (see fig. 4.b). When this material is introduced to the cavity, the resonant frequency of the cavity, and the shape of the resonance curve are altered. By measuring the change in resonant frequency, and the quality factor Q_L, associated with broadening of the resonance curve, the complex permittivity of the perturbing material may be evaluated. This technique was successfully used by Campbell to measure the permittivity of over one hundred samples of human tissue, mainly from the female breast. Samples of tissue, cut to shape, were inserted into the cavity from a holder, by a steel inserting rod (fig. 4b.). There was a number of disadvantages associated with this technique.

- Cavity cleanliness: Between each sample measurement, the cavity aperture and sample holder had to be cleaned, and dried with alcohol. Before the next measurement the cleanliness and dryness of the cavity had to be checked by a measurement of Q_L,

which decreased if the cavity was contaminated. Occasionally, when a semi-liquid fatty sample had been measured, sample leakage along the upper and lower plates of the cavity deteriorated the quality factor to the extent that the whole cavity had to be dismantled, thoroughly cleaned, reassembled, and recalibrated.

- Sample Preparation: Before dielectric measurement, each tissue sample had to be cut and moulded into a suitable shape for insertion. The process of cutting and pushing can cause fluid loss, especially from high water content tissues. This can cause the complex permittivity to be underestimated. Compression of the sample in the sample holder and aperture could also give misleading results. For some harder samples, such as tumours, the aperture can only be filled by cutting the sample into many small pieces before loading in the sample holder. This risked the possibility of leaving air pockets within the sample, which may have affected the estimated dielectric properties. Also, the necessity to cut long, thin, homogeneous samples meant that this method was inefficient in tissue - only a few measurable samples may be usually prepared from even quite a large original tissue sample.

- Measurement Problems: Even with a resonant cavity of 5cm internal diameter, and an aperture diameter of 1.5mm, Campbell found that high permittivity samples, loaded centrally, could perturb the cavity Q-factor to such an extent, that good measurement of the resonance was not possible. Thus, a number of apertures had to be drilled in the cavity, at a variety of distances from the centre (fig. 4.b), where the electric field is smaller than at the centre. In an aperture away from the centre, the perturbing effect of a high permittivity sample was sufficiently small to be measurable. This meant that three separate aperture calibrations had to be made, and checked regularly. Also, with constant use, the apertures in the cavity were found to expand slightly, and so had to be examined frequently under a travelling microscope to check if their shape had changed.

4.2.3 Co-axial Line Reflection Methods for Measuring Dielectric Permittivity.

By far the largest amount of research into the permittivity of biological substances at microwave frequencies has been carried out using co-axial line measurement techniques. In principle, co-axial line techniques are similar to waveguide techniques. The co-axial

line is either terminated, or symmetrically obstructed by the sample material. An input signal of the desired frequency is applied to the line, and is partially reflected at the boundaries of the terminating material. The effect of different terminating materials on the magnitude and phase of the reflected wave is measured by examining the profile of the resulting standing wave pattern. Unlike waveguides, however, the dominant lowest transverse mode in a co-axial line is not subject to a 'cut-off' wavelength dependent on line dimensions. Higher order modes are subject to a cut-off wavelength given by $\lambda_c \approx \frac{2(b-a)}{n}$ where b and a are the outer and inner co-axial conductor radii respectively, and n is the mode order. Therefore co-axial lines which only propagate the *TEM* mode, and which have dimensions consistent with clinical tissue sample dimensions can easily be constructed and used for permittivity measurements.

A review by Stuchly and Stuchly (1980a) characterised twelve co-axial line measurement configurations which can be used to measure the permittivity of biological samples. These are shown schematically in fig. 4.c. Those configurations marked (a) to (h) require the sample to be of a specific and definite shape. In the case of tissue samples from surgery, this will only be achievable by careful cutting or moulding of the sample. As one of the criteria for choosing the measurement technique is that samples must still be fit for further thermal measurement after the dielectric measurement, it is clear that configurations (a) to (h) are unsuitable for our purposes.

Of the remaining configurations, (i) and (k) place the least constraints on sample geometry, requiring only that the sample have good electrical contact with the co-axial probe across the whole plane of the open end of the probe. In theory, the samples need to be infinite in extent, so that all the field from the open end, both radiated and induction, lies completely within the sample. However, for the practical dimensions of co-axial lines used at 3 GHz, the fields are negligible at distances more than a few millimetres from the open end, and so tissue samples need only have dimensions of a few millimetres.

Considerable research has been carried out using open ended co-axial lines to measure the permittivity of materials in the microwave region, and there exist several simple modelling methods which relate the reflection co-efficient of a terminated line with the dielectric permittivity of the terminating medium. Therefore a small diameter open-ended co-axial line, possibly with a slightly extended central conductor was chosen as the

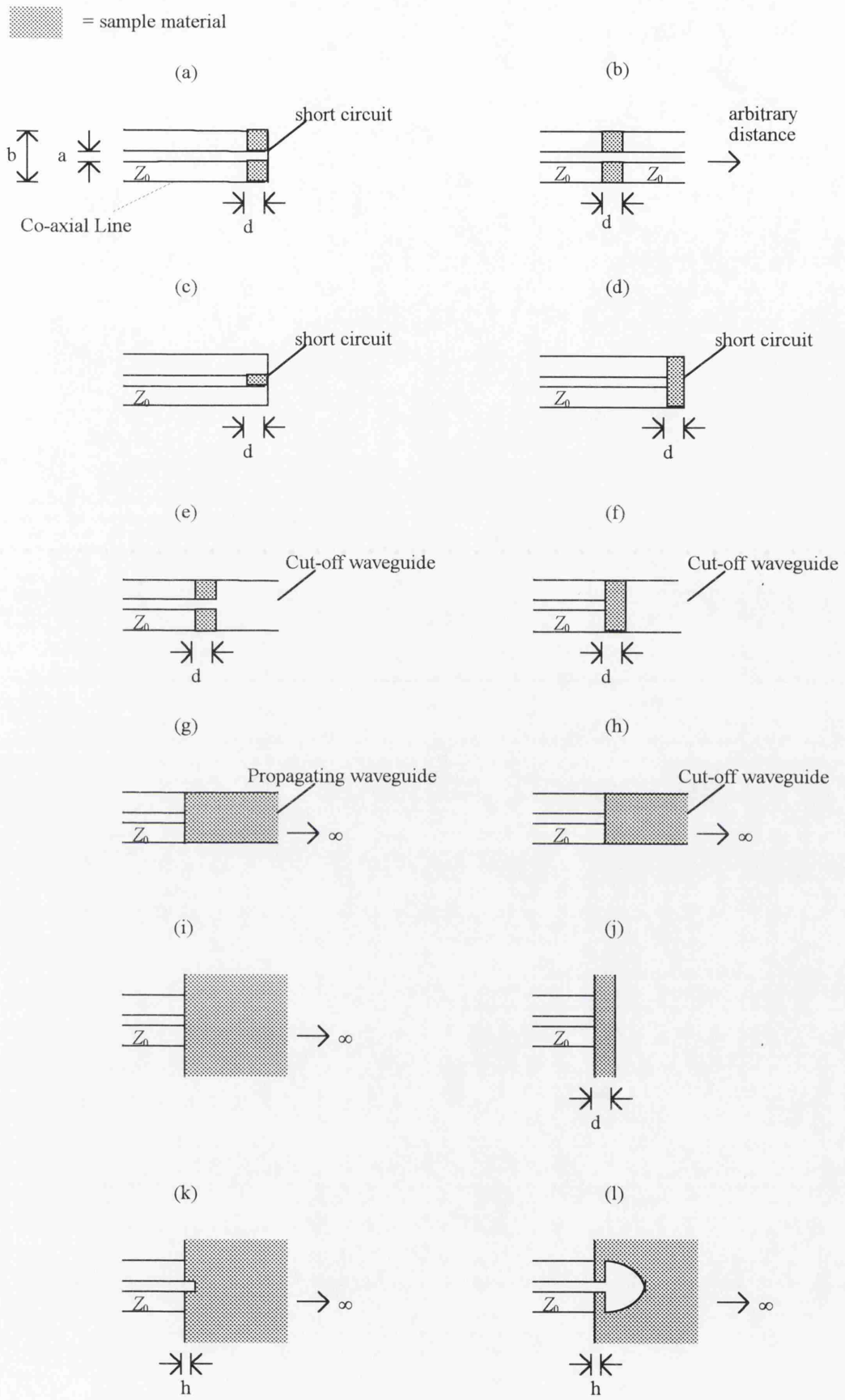

Figure 4.c. Twelve possible configurations for co-axial line permittivity measurements. Methods *i* and *k* place the least restrictions on sample geometry, and are therefore the most suitable for the current study.

most suitable measurement technique for our purposes, as it satisfies all the major criteria outlined in section 4.2.

4.3. Experimental Apparatus.

The apparatus used to measure the permittivity of biological tissue samples in this study is shown in fig. 4.d. A generator provides a 3 GHz microwave signal, and the output frequency is monitored by an electronic frequency counter. The signal is transmitted, via isolating circulators, to a large diameter, precision slotted co-axial transmission line, on which standing wave measurements may be made. This slotted line is connected directly to the experimental probe. All connections between components were made with 50Ω co-axial cable. Low reflection precision connectors and adapters were used to connect the co-axial permittivity probe to the slotted line.
An astable, separately generated 1kHz square-wave signal amplitude modulates the 3 GHz microwave signal after the first isolator, using a PIN diode switch. Amplitude modulation of the original signal allows the use of simple standing wave voltage detection equipment, and increases the detection sensitivity. The modulation component was measured by an amplifying a.c. microvoltmeter, the readings from which were recorded manually.

The isolating circulators fulfil an important purpose. To measure accurately the reflection co-efficient from the terminating medium at the open end of the measurement probe, it is vital that only the original signal incident upon the open end, and that signal reflected from the open end, contribute to the standing wave pattern in the slotted line. Discontinuities in the transmitting system, such as co-axial connectors, may give rise to unintended *secondary reflection* of signals, which affects the shape of the standing wave pattern. Secondary reflection of the signal returning along the slotted line from the open end is minimised by the circulator at the input terminal of the slotted line. This dissipates any signal travelling back towards the signal generator. Another isolator is connected between the microwave signal generator and the amplitude modulation diode in order to remove reflected signals from the switch. This ensures that the generator is not frequency modulated by the PIN switch operation.

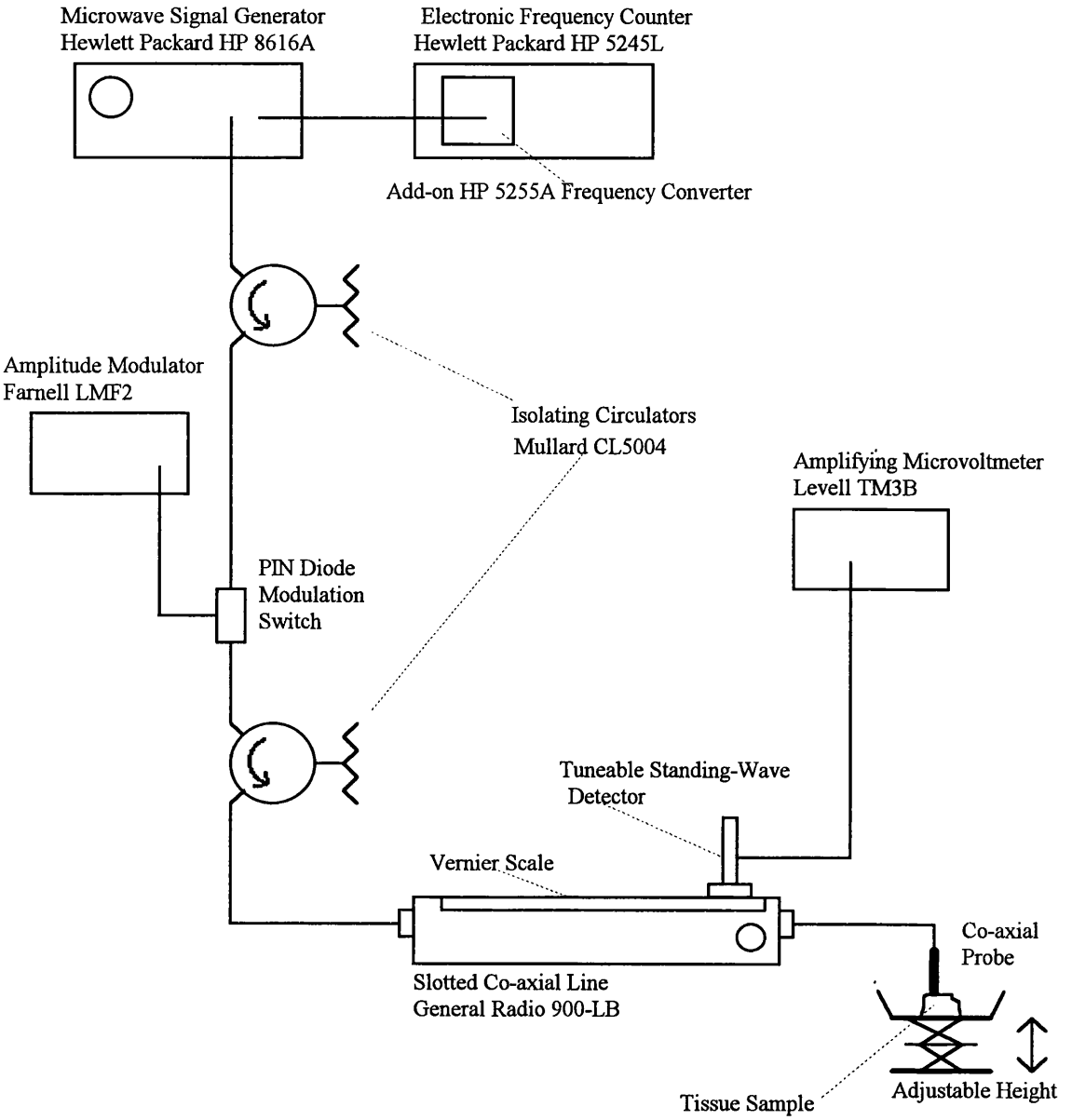

Figure 4.d. Schematic diagram of the apparatus used to make the permittivity measurements in this study.

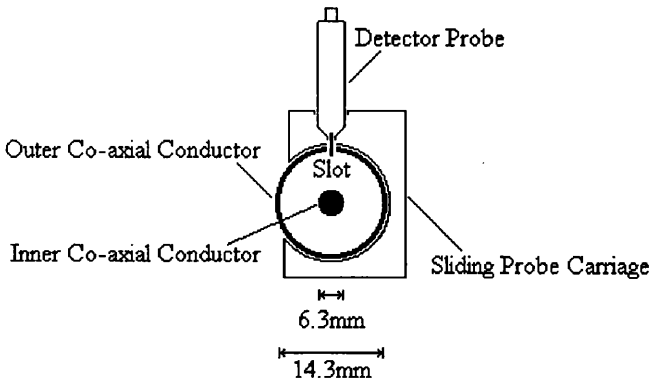

Figure 4.e. Cross-sectional view of General Radio 900-LB Slotted Line used for permittivity measurements.

The adapters and connectors chosen produce reflections with characteristic VSWR ranging from <1.02 to around 1.05 at 3 GHz. Source VSWR with the isolators was probably in the range <1.2 to 1.5.

Mounted on the slotted line is a sliding, tuneable probe detector, travelling on a Vernier scale. To a very close approximation, the detector probe signal, as displayed on the microvoltmeter, is proportional to the square of the electric field at that point on the slotted line, $V_{dis} \propto |\underline{E}|^2$

Measuring the maximum and minimum standing wave signals, by moving the detector probe along the line, gives the magnitude, $|r|$, of the reflection co-efficient from the open ended probe. The phase, θ, of the reflection co-efficient is obtained from the position of the standing wave minima, relative to the position of the standing wave minimum when the open ended probe is short circuited, by measurement on the Vernier scale.

$$|r| = \sqrt{\frac{V_{dis(\max)}}{V_{dis(\min)}}} \qquad \text{and} \qquad \theta = \pi\left[1 - \frac{4(l_{short} - l_{sample})}{\lambda}\right] \qquad (4.3.1)$$

where l_{short} is the position of the standing wave minimum for short circuit, l_{sample} is the position of the standing wave minimum for the sample material, and λ is the wavelength of the radiation in the slotted line.

Under ideal circumstances the standing wave pattern in the slotted line is the result of interference between two propagating microwave signals: an incident wave from the generator, and a wave reflected from the end of the permittivity probe. However, secondary reflections will slightly perturb the pattern. A permittivity evaluation procedure was used which inherently compensates, at least partially, for these residual standing wave effects.

4.4. Equipment Specifications.

4.4.1. Microwave Signal Generator.

Microwave signals in the range 1.8 to 4.5 GHz were supplied by an Hewlett Packard 8616A signal generator. Although this generator is capable of supplying a stable and accurately maintained signal, the frequency control is of a coarse, analog operation, and therefore an accurate frequency counter is required to monitor the output. As measured

by the frequency counter, the output signal frequency of the generator was constant, over a short time, to within ± 5 kHz of the chosen mean frequency. Left unchecked, the signal frequency was found to decrease gradually with time, but over the period required for standing wave measurements on a sample material, was constant to within ± 10 kHz, or 3×10^{-4} % of the mean.

4.4.2. Frequency Counter.

When making frequency measurements with the Hewlett Packard 5245L electronic counter, the basic counter accuracy is determined by two factors. One factor is the ageing rate of the 1MHz crystal standard in the time base, which is less than 2 parts in 10^8 per week. For the particular counter used, this corresponds to an error of approximately 1 part in 10^5. A second factor is the inherent error of ± 1 count present in all counters of this type. This error is due to phasing between the timing pulse that operates the electronic gate, and the pulses that pass through the gate to the counters. At the frequency and counter settings used, the manufacturer's data suggest that this error is less than 1 part in 10^6.

With careful adjustment of the frequency generator, the measured frequency could be maintained to within ± 10 kHz. When added to the crystal ageing error of 1 part in 10^5, the overall uncertainty in the frequency counter measurement is ± 40 kHz. This corresponds to a wavelength uncertainty of approximately ± 0.001mm, which is of the order of ten times smaller than the standing wave position measurement error, and is therefore a negligible effect.

4.4.3. Slotted Co-axial Line.

Standing wave measurements are made on a General Radio 900-LB precision slotted air-dielectric co-axial line. This line has an inner conductor of outer diameter, b, equal to 6.228 ± 0.003mm, and an outer conductor of inner diameter, a, equal to 14.344 ± 0.005mm (see fig. 4.e). The characteristic impedance of a co-axial line is given by $Z_c = \frac{\ln(b/a)}{2\pi}\sqrt{\frac{\mu_0}{\varepsilon_0 \varepsilon_r}}$. In laboratory conditions, the relative permittivity of air is 1.0007,

and so the line impedance is precisely 50Ω. Manufacturers data quotes the impedance of the line to be accurate to ± 0.1%. The deviation from a perfect cylinder, caused by the 3mm width slot in the outer conductor, causes a minute change in line impedance and capacity per unit length, which is compensated by a small increase in the diameter of the inner conductor under the slotted region.

The manufacturers of the slotted line rate the amplitude attenuation in the line as less than 0.0009dB/cm. Over the length of line used for permittivity measurements (~20cm), this generally causes an error of less than 0.1% in reflection co-efficient measurements. This is far less than the effects of electrical noise and measurement accuracy in the line, and is therefore sufficiently small as to be negligible, in the context of permittivity calculations. The effects of attenuative loss elsewhere in the system are compensated for in the probe calibration procedure discussed in chapter 5.

4.4.3. Detector Probe.

The adjustable detector probe-tuner assembly (see fig. 4.f) is an air-dielectric co-axial device, terminating in a sliding short circuit, that forms a tuned structure to maximise the power transfer to the detector display. Detector output is greatly enhanced by the tuneable line section, which can be adjusted to resonate the diode-probe assembly at the frequency of operation. A signal proportional to the square of the detected electric field is available for measurement from the low-noise microwave detector diode in contact with the probe chuck. Once tuned, the penetration of the probe tip into the slot must be adjusted, so that the output of the diode is less than ~5mV, to ensure its operation in the square-law region. Fields whose strength varies periodically along the line are sampled by the probe tip, which introduces reflections in the line proportional to the probe penetration into the slot. As the incident signal in the line is of fairly large amplitude, only a minimal probe penetration of less than 1.5mm is required to give an output of the desired magnitude. According to the manufacturers details, such a probe penetration perturbs the reflection co-efficient in the line by less than 0.1%. A detailed discussion of the detection of microwave power in slotted lines by crystal diodes can be found in Ginzton (1957).

Although the detector probe output is expected to be approximately 'square-law,' it is necessary to check regularly the calibration of the probe, by terminating the line with a

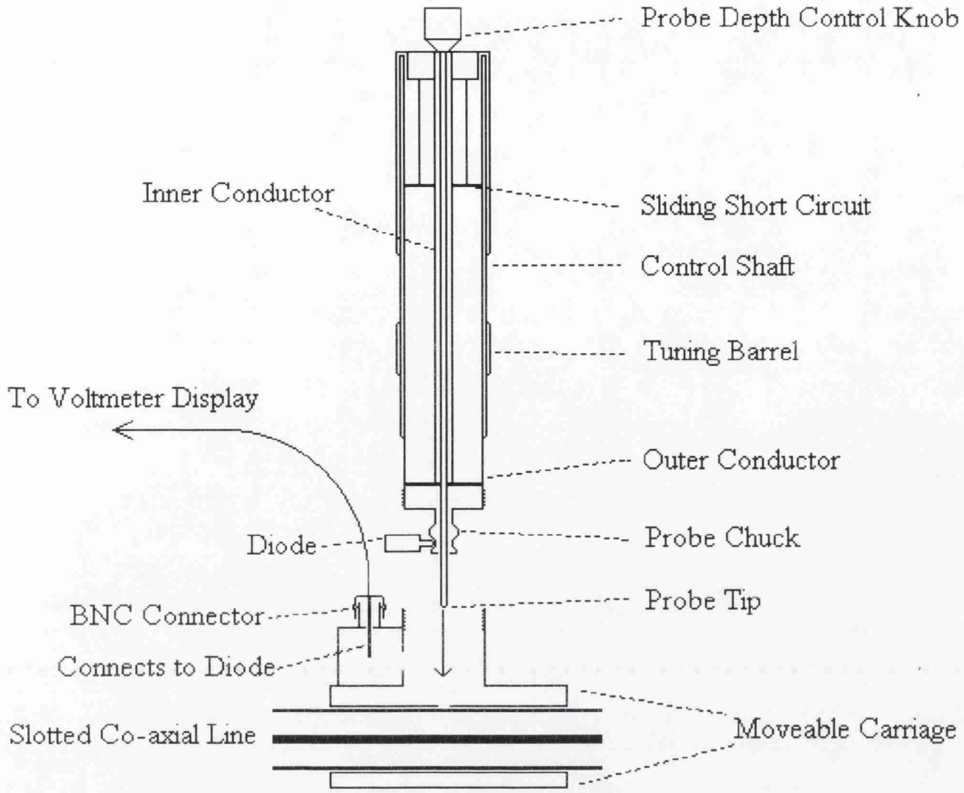

Figure 4.f. Schematic cross-sectional diagram showing detector probe and slotted line geometry.

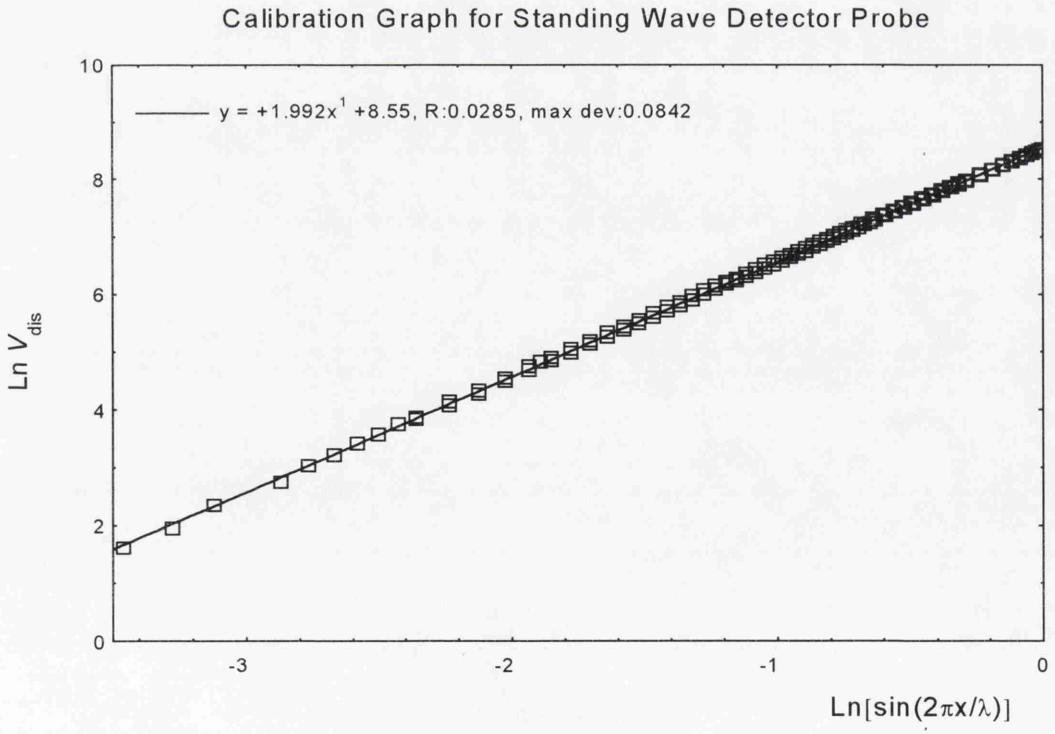

Figure 4.g. Typical detector probe calibration graph, with gradient equal to the detector probe response power n. Correlation co-efficient of fit = 0.9998.

short circuit, and measuring the output voltage displayed on the meter as a function of position. Defining the position of a standing wave null as $x = 0$, the displayed voltage V_{dis}, is expected to vary with position in the form $V_{dis} \propto \sin^n\left(\frac{2\pi x}{\lambda}\right)$, where x is the position of the detector probe on the slotted line. Figure 4.g shows a plot of $\ln V_{dis}$ against $\ln\left[\sin\left(\frac{2\pi x}{\lambda}\right)\right]$. The gradient of the best-fit straight line to these data corresponds to the detector response power n. In this case the value of n was found to be given by $n = 1.992 \pm 0.003$. Calculations in section 5.5 evaluate the error incurred in reflection co-efficient data by assuming this value to be exactly equal to 2.

4.4.5. Co-axial Permittivity Probe.

The transmission system was terminated by the open ended co-axial probe, which is discussed in more detail in the following section. Including connectors, the total line length of the probe assembly beyond the slotted line section was approximately 17cm. For rigidity, the final experimental probe was mounted vertically, with a protective plastic sleeve around the delicate soldered connections. Calibration materials and tissue samples were brought into contact with the end of the probe by manual height adjustment of a small laboratory jack.

4.5. Probe Design.

Preliminary investigations into probe calibration and the measured permittivity of tissue samples were made with a 6.3mm diameter, flat open-ended copper co-axial probe. These highlighted three main experimental problem areas.

- When immersing the probe in calibration liquids, it was very important to ensure that the depth of immersion into each liquid was identical, as inconsistent calibration data would otherwise be obtained. This is because surface currents can travel back up the exterior of the outer co-axial conductor through the calibration liquid, thus changing the effective terminating impedance and affecting the measured reflection co-efficient from the open end.

As long as the immersion depth into the calibration liquids of known permittivity was accurately standardised, it was found that the probe could be calibrated to a sufficient degree of accuracy for tissue measurements. Therefore, the probe could be used only as long as the calibration liquids, and the materials to be measured, could be considered to be semi-infinite media extending from some fixed plane along the length of the probe.

- Another related problem arose from the irregularity of the surface of tissue samples. When probing tissue samples, especially small human tissue samples obtained after surgery, it was difficult to ensure uniform electrical contact between the probe and sample over the whole area of the open end of the probe. By pressing the probe gently into the tissue, to improve the uniformity of contact, samples may be deformed or stretched asymmetrically around the probe (see fig. 4.h). This could give unreliable reflection co-efficient readings, as the consistency of penetration of the probe into the sample can not be guaranteed.

- Finally, the extent of the field distribution from the open end was sufficiently great, that a depth of at least 6mm of the terminating material had to be maintained in front of the area of the open end, before the effects of non-infinite sample size could be regarded as negligible. In practice, this necessitated that samples had minimum volume and geometry restrictions that were thought to be unlikely to be satisfied by small surgery tissue samples.

The dependence of the reflection co-efficient on the immersion depth of the probe can be reduced by fitting a wide ground plane on to the end of the outer conductor of the probe. This tends to isolate that volume of the probed medium lying beyond the open end of the probe, by reducing the surface currents that travel up the outside of the outer co-axial conductor. There may still be some surface currents on and around the edge of the ground plane disk.

If a ground plane disk wide enough to be regarded as infinite in extent is attached to the open end, the resulting simplification of the fields at the end of the probe makes the modelling approximations, on which the probe calibration is based, more rigorously applicable (see section 5.2). For dielectric measurements of large volumes of liquids, this is the optimal probe design. However, in the present case, this solution exacerbates the difficulty in ensuring uniform contact between probe and tissue sample, by increasing the

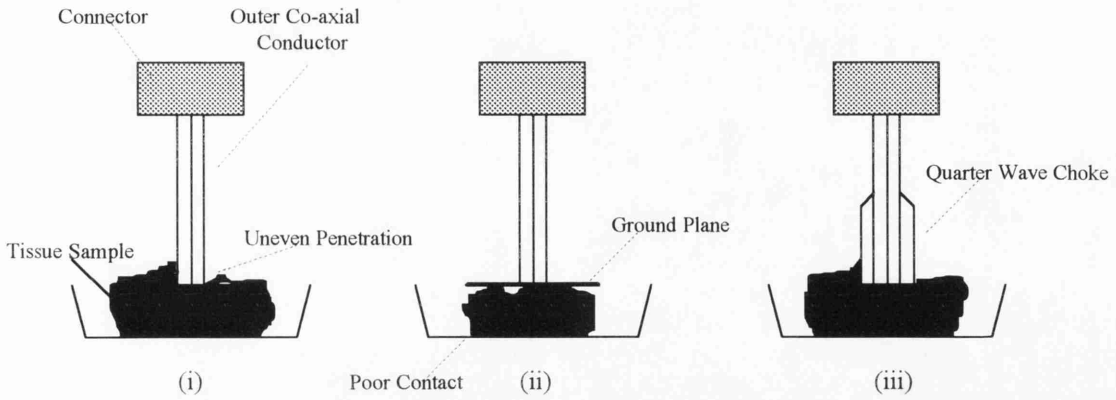

Figure 4.h. Diagram showing problems inherent in the open-ended co-axial probe technique when measuring irregular samples. (i) Uneven penetration creates non-uniform surface currents on outer surface of probe, affecting the validity of the probe calibration. (ii) Large conducting ground plane reduces the effect of surface currents, but is unwieldy and may conceal poor electrical contacts with sample. (iii) Quarter-wave choke at open-end is compact method of reducing surface currents while still allowing good sample contact.

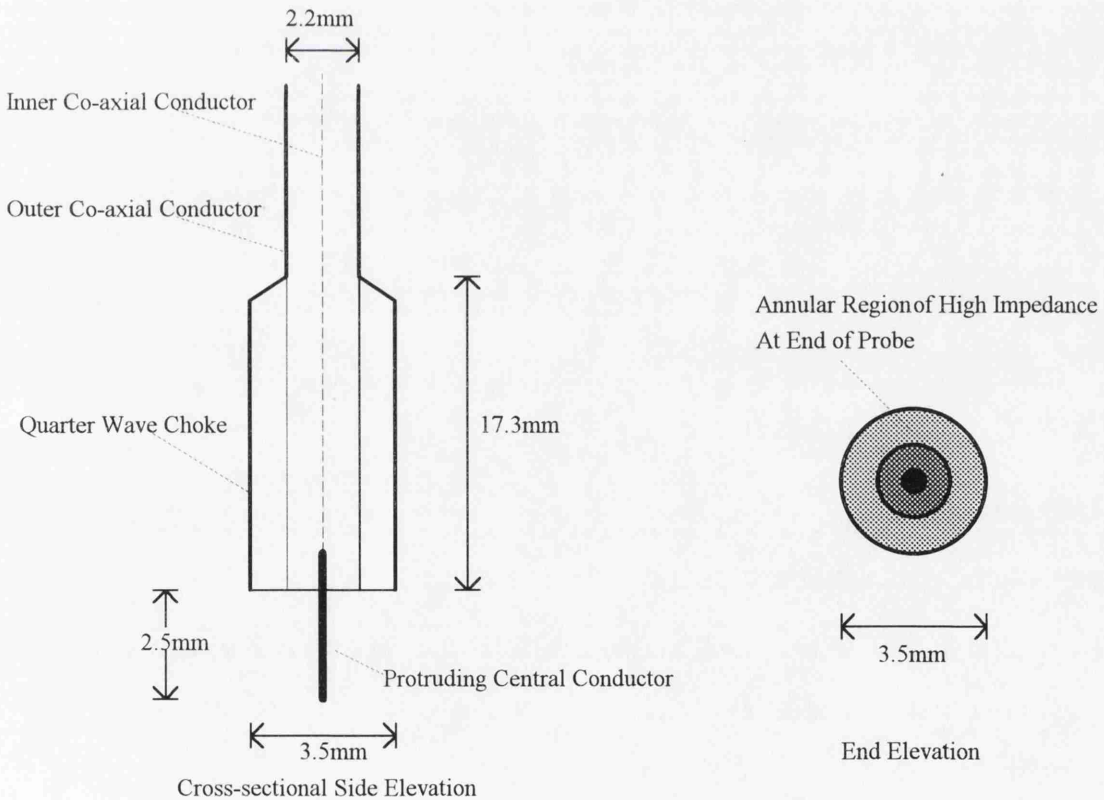

Figure 4.i. Diagrams showing the construction of the experimental co-axial probe with quarter-wave choke used for permittivity measurement. (Not to scale)

likelihood that unseen air pockets may be trapped below the open end. The unwieldiness of a ground plane therefore makes its use practically unsuitable for probing irregular media.

4.5.1. Co-axial Quarter-wave Probe.

All the above problems can be alleviated by reducing the co-axial probe diameter, and fitting around the end of the probe, a quarter-wave choke. A quarter-wave choke is a third concentric cylindrical conducting sleeve short circuited onto the outer co-axial conductor, at a distance from the open end equivalent to one quarter of the operating wavelength of the probe. The original co-axial line and the quarter-wave choke were in this case filled with PTFE dielectric, which has a relative permittivity of approximately 2.1 at all frequencies. Thus the required length of the quarter-wave choke was equal to $2.5/\sqrt{\varepsilon_{PTFE}} = 2.5/\sqrt{2.1}$ cm, or 1.73 cm.

At the short circuit, any current travelling between the outer co-axial conductor and the quarter-wave choke encounters zero impedance. But over the annular area between these two conductors at the open end of the probe, there is a very high (ideally infinite) impedance as a result of the short circuit one quarter of a wavelength back up the line. Thus virtually no stray current can travel up the outside of the outer co-axial conductor, and the fields from the open end of the probe are restricted to the region lying in front of the open end.

As uniform contact had to be seen to be achieved over the entire end of the probe, it was thought beneficial if the overall area of the open end, including the quarter-wave choke, could be kept fairly small. It was therefore preferable to reduce the original co-axial probe diameter from 6.3mm, as fitting a choke on to this cable would have resulted in an overall probe diameter of around 10mm. This is far greater than the distance over which surgery tissue sample homogeneity was expected. For short monopole probes whose central conductor approaches zero length, such as the current probe, there is little radiated field at the open end, but the probe's fringing field is present. In this case the minimum sample volume required is primarily dependent on the distance between the centre and outer conductors.

The experimental probe was constructed from 50Ω impedance RG 405 co-axial cable which has an inner conductor diameter of 0.505mm, outer conductor diameter of 2.17mm, and is loaded with PTFE dielectric. A PTFE loaded quarter-wave choke of outer diameter 3.5mm, was soldered onto the outer conductor. This gives an overall probe diameter which is a consistent size with surgery tissue homogeneity. Rather than having a planar open end, the central conductor of the co-axial cable was extended by approximately 2.5mm. This was found to improve the reliability of the probe-sample contact. As the probe was moved towards contact with a sample, the central conductor pierced the tissue, and located the part of the sample to be investigated relative to the rest of the probe, before full contact was made.
This probe geometry places the field region into the sample material volume, reducing surface effects, and, usefully for the context of this study, measures over a comparable tissue volume as the thermal probe used concurrently to make thermal conductivity measurements. Figure 4.i shows two cross-sectional views of the experimental probe.

Because of the reduction in probe size, any tissue sample large enough to cover the area of the end of the probe to a depth equal to or greater than the length of the extended central conductor could be considered to be infinite in extent, and the effects of fields beyond the sample boundaries may be neglected. In theory, tissue samples with volumes of the order of $50mm^3$ could now be measured, although in practice, samples had to be considerably larger for ease of handling and reliability of probe contact. With constant use, the length of the extended central conductor was gradually reduced to under 1mm, resulting in an even smaller minimum tissue volume restriction.

4.5.2. Measurement Repeatability Improvement With Co-axial Choke.

Tables 4.a and 4.b illustrate the reduction in dependence of the reflection co-efficient on the depth of immersion into the terminating medium that is affected by the addition of a quarter wave choke to a co-axial probe. Reflection co-efficient data were taken for a variety of terminating liquid materials using two different co-axial line probes, immersed to several depths in the liquid. The data in table 4.b were taken using the experimental probe with a quarter wave choke, and the data in table 4.a were taken using an otherwise identical probe, but without a quarter wave choke.

Material	Reflection Co-efficient Magnitude at various Immersion Depths			Relative Phase of Reflection Co-efficient at various Immersion Depths		
	12mm	1.5mm	meniscus	12mm	1.5mm	meniscus
Mercury (short circuit)	>0.95	>0.95	>0.95	π	3.145	3.157
Deionised Water (19°C)	0.679	0.778	0.741	-2.608	-2.454	-2.190
0.15**M** Saline (19°C)	0.642	0.714	0.669	-2.604	-2.472	-2.180
Glycol (19°C)	0.383	0.450	0.507	-0.829	-0.707	-0.575
Methanol (19°C)	0.353	0.421	0.451	-1.345	-1.200	-0.958
30% Sucrose Solution	0.625	0.684	0.629	-2.507	-2.406	-1.938
80/20 Water/Dioxane	0.677	0.736	0.661	-2.535	-2.428	-1.995
60/40 Water/Dioxane	0.635	0.678	0.615	-2.209	-2.102	-1.734
40/60 Water/Dioxane	0.544	0.617	0.587	-1.483	-1.420	-1.178
20/80 Water/Dioxane	0.698	0.752	0.778	-0.751	-0.691	-0.622

Table 4.a. Reflection co-efficient magnitude and phase for chokeless co-axial probe at various immersion depths.

Material	Reflection Co-efficient Magnitude at various Immersion Depths			Relative Phase of Reflection Co-efficient at various Immersion Depths		
	12mm	1.5mm	meniscus	12mm	1.5mm	meniscus
Mercury (short circuit)	>0.95	>0.95	>0.95	π	π	3.148
Deionised Water (19°C)	0.795	0.797	0.794	-2.347	-2.343	-2.325
0.15**M** Saline (19°C)	0.704	0.708	0.708	-2.265	-2.262	-2.246
Glycol (19°C)	0.478	0.481	0.483	-0.701	-0.691	-0.675
Methanol (19°C)	0.464	0.469	0.471	-1.048	-1.034	-1.037
30% Sucrose Solution	0.659	0.664	0.664	-2.017	-2.023	-2.004
80/20 Water/Dioxane	0.732	0.741	0.733	-2.067	-2.048	-2.042
60/40 Water/Dioxane	0.688	0.696	0.688	-1.667	-1.652	-1.649
40/60 Water/Dioxane	0.675	0.682	0.676	-1.078	-1.068	-1.062
20/80 Water/Dioxane	0.793	0.805	0.801	-0.559	-0.543	-0.540

Table 4.b. Reflection co-efficient magnitude and phase for co-axial probe with choke at various immersion depths.

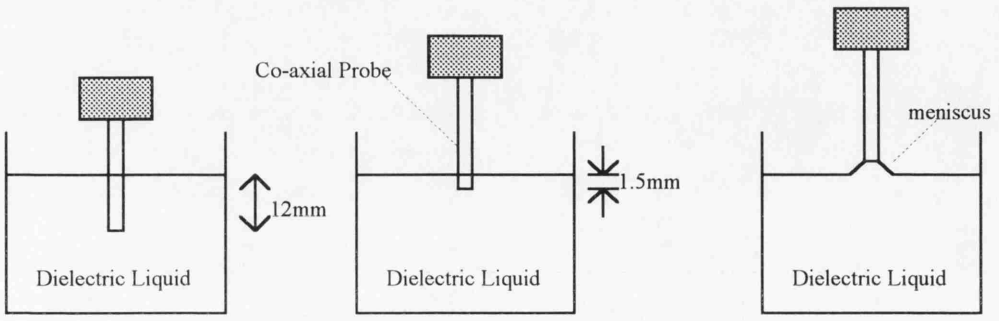

Figure 4.j. Diagram showing the three immersion depths for which permittivity measurements were made on known liquids, to compare the reflection co-efficient of the open-ended co-axial probe with and without a quarter-wave choke. Results of these measurements are listed in tables 4.a and 4.b.

Three immersion depths were considered, as shown in fig. 4.j. It was anticipated that the effective probe immersion encountered when probing solid tissue samples would correspond to an immersion value in between the meniscus and 1.5mm immersion situations. For reference, data from a large immersion depth of 12mm, such as might only be used when calibrating the probes with standard liquids, are also presented. Phase measurements are quoted relative to the short circuit standing wave minimum position at 12mm immersion, which is defined to be equal to π.

It is clear that both the magnitude and phase of the reflection co-efficient are highly sensitive to immersion depth when using the chokeless probe. Between 1.5mm and meniscus immersion, the magnitude is seen to vary by up to 10%, and the phase by up to 20% for some liquids. This corresponds to a shift in the measured position of the standing wave minimum of up to 2mm. Actual magnitude measurements are accurate to approximately $\pm$ 0.5%, and position measurements are accurate to approximately $\pm$ 0.5%. In terms of permittivity, the difference between 1.5mm and meniscus immersion can represent an uncertainty of up to 50% of the true dielectric constant and loss factor. Therefore, unless the immersion depth can be controlled to a far higher degree of accuracy than is feasible during calibration and during sample measurements, sample permittivity measurements using such a probe will be subject to an almost invalidating uncertainty.

With the addition of a quarter wave choke, both magnitude and phase variation are generally reduced to ~1% over the whole immersion range. This represents a great improvement over a chokeless co-axial probe.

It was found that by carefully maintaining the immersion of the probe during calibration to approximately mimic the relative positions of sample and probe during tissue measurement, variation in the reflection co-efficient magnitude and phase could be virtually eliminated.

4.6. Calibration Procedure.

Prior to making permittivity measurements on biological samples, it is necessary to calibrate the open ended probe in order to be able to relate measured reflection co-efficients to sample permittivities. A mathematical model is used to describe the admittance of the open end of the probe, when terminated by materials of relative

permittivity ε_r (see chapter 5). The probe is terminated successively by four calibration liquids of known permittivity, and the parameters of the mathematical model are then determined by the measured reflection co-efficients and known permittivity values of the calibration liquids. Unknown sample material permittivities may then be evaluated using the measured reflection co-efficient of the sample with the parameterised admittance model. Due to the arithmetical intensity of the calibration procedure, it is convenient to perform both calibration and permittivity evaluation calculations using a simple computer program.

By using a suitable admittance model for the probe, and with proper choice of calibration standards, the unknown complex permittivity of materials with a wide range of permittivity can be determined. Calibration standards are chosen that span the whole range of permittivity values expected of biological tissues.

4.7. Calibration Materials.

The permittivity of the tissue samples to be examined was expected to be determined largely by the percentage water content. Water is present in tissue in a form approximately represented by 0.9% (0.15**M**) saline solution. This saline solution not only comprises around 75% of the mass of most soft tissues, but also has a far higher permittivity than the other major components of tissue, such as fats. Thus the high permittivity of water dominates the effects of lower permittivity materials in tissue, even in cases where water is not the majority substance in the tissue. Hence the range of values expected for the permittivity of tissues can be roughly bounded by the permittivities of tissue comprising no saline (fat tissue), and tissue composed almost entirely of saline (intestinal tissue, grey brain matter). At a measurement frequency of 3 GHz this gives the following limits on the real and imaginary parts of permittivity:

$1 < \varepsilon' < 80$ and $0 < \varepsilon'' < 25$.

For reliable calibration it is necessary to use standard calibration materials with permittivities spanning the whole range of expected tissue values. It is convenient to use liquids as the standard materials, as a good electrical contact with the probe open-end can be guaranteed.

Table 4.c shows the range of standard liquids that was selected for calibrating the probe, and the publications from which the reference permittivities were taken. Although only

Material	Reference
Mercury (short circuit)	Not applicable
De-ionised Water	Land, Averaging procedure on collected data.
0.15M Aqueous NaCl Solution	Land , Averaging procedure on collected data.
30% Aqueous Sucrose Solution	Land, 1993 (and unpublished measurements)
Ethylene Glycol $CH_2OH \cdot CH_2OH$	Jordan et al, 1978
Methanol CH_3OH	Jordan et al, 1978
Glycerol $CH_2OH \cdot CHOH \cdot CH_2OH$	Misra and Staebell, 1990
Air	Not applicable
20% / 80% 40% / 60% 60% / 40% 80% / 20% Water / Dioxane Solutions Dioxane = $CH_2 \cdot CH_2 \cdot O \cdot CH_2 \cdot CH_2 \cdot O$	Misra et al, 1990

Table 4.c. List of materials used for probe calibration, with permittivity value references.

Temperature (°C)	ε'	ε''
15	78.5	16.2
20	77.7	13.5
25	76.5	11.5
30	75.2	9.9
35	73.7	8.7
40	72.2	7.7

Table 4.d. Permittivity of water at room to body temperatures as calculated by simple Debye equation parameters given in section 4.7.2.

Temperature (°C)	ε_s	$\pm\Delta\varepsilon_s$	ε_∞	$\pm\Delta\varepsilon_\infty$	$\tau(ps)$	$\pm\Delta$	α	$\pm\Delta\alpha$
10	37.0	0.6	4.7	0.7	70	3	0.035	0.030
20	34.8	0.5	4.5	0.7	56	2	0.044	0.027
30	32.6	0.4	4.4	0.6	44	2	0.040	0.025
40	30.4	0.4	4.0	0.6	35	2	0.026	0.029

Table 4.e. Cole-Cole equation dispersion parameters for methanol as given by Jordan et al, 1978.

four of these liquids are needed for each calibration, the other materials which were not specifically used for the calibration, were used to test its accuracy across the permittivity range.

In subsequent subsections, the parameters quoted by the reference papers for each calibration liquid are presented. For each material, the dispersion parameters and their errors are used to calculate the 3 GHz relative permittivity at room temperature (15 to 25°C), which is the value used in probe calibration.

4.7.1. Mercury.

Liquid mercury was always used as one of the four standard probe calibration liquids. An almost perfect short circuit is formed at the open end of the probe when immersed in a small volume of clean mercury, as the resistance between the inner and outer co-axial conductors becomes virtually zero. Because the admittance of the open end therefore tends to infinity when short circuited with mercury, the calibration equations presented in section 5.2 are greatly simplified, and the calibration accuracy improved.

4.7.2. Deionised Water.

The permittivity of liquid water was discussed in detail in section 3.7. It was shown that to the degree of precision necessary in this work, the microwave dispersion behaviour of water, over the temperature range of interest, could be approximated by a Debye equation of the form

$$\varepsilon_r = \varepsilon_\infty + \frac{\varepsilon_s - \varepsilon_\infty}{1 + j\omega(f/f_c)} \qquad (4.7.1)$$

A simple data averaging procedure was used by the Glasgow group to estimate the behaviour of the dispersion parameters with temperature, from a selection of collected microwave data. Approximate equations (eqns. 3.7.4) for these Debye dispersion parameters were presented in section 3.7. Above 15°C, these equations can be simplified still further, without any significant loss of accuracy, by the lower order expressions given below.

$$\begin{aligned} \varepsilon_s &= 87.7 - 0.387T + 5.52 \times 10^{-4} T^2 \\ \varepsilon_\infty &= 4.3 \\ f_c(GHz) &= 6.1 + 0.511T \end{aligned} \qquad (4.7.2)$$

where T is the temperature in degrees Celsius.

Values of the relative permittivity of water, used to calibrate the co-axial probe, were calculated using the equations 4.7.2. These equations yield values for the complex permittivity of water at temperatures from 15 to 40°C as shown in table 4.d Comparison between the data in this table, and that in table 3.g, shows that almost identical permittivity values are obtained to those given by the higher order approximations for the Debye dispersion parameters, eqns. 3.7.4.

The uncertainty in these permittivity values is estimated to be equal to the uncertainty in the measured values of which these are an approximation. Therefore the error on the dielectric constant is approximately ± 2%, and on the loss factor, approximately ± 3%. At a normal room temperature of 20°C, these figures give the estimated dielectric constant of deionised water as 77.7 ± 1.5, and the loss factor as 13.5 ± 0.4.

4.7.3. Saline Solutions.

A brief discussion of the microwave permittivity of low concentration NaCl solutions was presented in section 3.8. Deviation between published results for the permittivity parameters of saline solutions was found to be considerably greater than that observed between data on the permittivity of pure water. This may have been partially due to disagreement between researchers concerning the magnitude of the extra loss contribution caused by ionic conductivity in the solution. In addition, any calculated values for the permittivity of 0.15**M** saline had to be based on interpolation, as the majority of reported measurements were made on solutions of far higher concentration. More recent measurements (Land, 1993) made specifically on 0.15**M** saline at a frequency of 3 GHz have indicated that the dielectric constant is approximately 75 ± 1.5, and the loss factor approximately 22.0 ± 0.6 at 20°C. The real part is in agreement with interpolated values, but the loss factor is rather higher than was evaluated from the data of most other researchers at this concentration, excepting Saxton (1957). It is, however, in agreement with the value obtained by combining the Debye resonance loss of water with the ionic conductivity loss as given by the CRC Handbook (1974). Temperature variation of the ionic conductivity is given by the equation $\sigma_i(T,0.15) = 0.806 + 0.0317T$, and that of the Debye component was assumed to follow

the dependence displayed by pure water. These values are quite satisfactory for the degree of precision required here.

4.7.4. Sucrose Solutions.

Aqueous sucrose solutions have been used for some time by the Glasgow group as liquid phantoms with dielectric properties similar to those of high water content tissues. Repeated measurements of the permittivity of sucrose solutions at, and near, 3 GHz, have yielded data which enable approximate equations relating the real and imaginary parts of the permittivity to the percentage sucrose (w/w) in the solution. The results are not sufficiently complete to determine the temperature dependence of the permittivity, but at 20°C, the grouping of results suggests that the 3 GHz relative permittivity of an aqueous solution containing 30% w/w sucrose is approximately $57.5 - j19.0$. Uncertainty in the dielectric constant is estimated to be $\pm$ 1.5, and in the loss factor $\pm$ 1. Previous measurements, using a cavity resonator technique, of the permittivity of sucrose solutions at 20°C have been presented by Land (1993) as curves relating the dielectric constant and loss factor to the sucrose concentration. These were taken at a frequency of 3.185 GHz, and are in fairly close agreement with the dielectric constant as measured by the co-axial probe, but have a consistently higher loss factor. By measuring the permittivity of sucrose solutions from 2 to 4 GHz, it was found that over this range, the permittivity of sucrose solutions follows the form of the permittivity of pure water, and so the loss factor is very sensitive to changes in frequency in this region. In this respect the behaviour of the permittivity of sucrose solutions is unlike that of saline solutions, whose loss factor is roughly constant over this range. As biological tissues are composed mainly of an electrolytic solution similar to 0.15M saline, the permittivity of 30% sucrose solution therefore also behaves rather differently from that of biological tissues.

The loss factor of 0.15M saline does not vary considerably over the frequency range 2 to 4 GHz, due to reduction of the contribution of ionic conductivity being compensated for by an increase in absorptive loss. But because the loss factor of 30% sucrose solution was found to rise in a similar fashion to that of water from 2 to 4 GHz, it seems that absorptive loss is the dominant loss process in 30% sucrose solution at around 3 GHz. The permittivity of 30% sucrose was found to vary from approximately $61 - j14$ at 2

GHz, through 57 - j19 at 3 GHz, to 53 - j21 at 4 GHz. Between these same frequencies, the permittivity of some very high water content tissues is roughly constant at around 55 - j18. Therefore, only at frequencies very near 3 GHz is the permittivity of 30% sucrose solution similar to that of comparable high water content biological tissues. Care must be exercised to ensure that the correct frequency range is being used when using sucrose solutions as tissue phantoms.

As there is clearly a danger in using as a calibration reference standard, a permittivity value measured only by the probe to be calibrated, sucrose solutions were only used to check the consistency of successive calibrations in the permittivity range corresponding to high water content tissue.

4.7.5. Methanol.

Data taken from Jordan et al (1978) suggests that the best representation of the dielectric permittivity of methanol in the microwave region is a Cole-Cole equation.

$$\varepsilon_r = \varepsilon_\infty + \frac{\varepsilon_s - \varepsilon_\infty}{1+(j\omega\tau)^{(1-\alpha)}} \qquad (4.7.3)$$

Parameters given by Jordan for the Cole-Cole relaxation equation for methanol, with errors corresponding to 95% confidence limits are presented in table 4.e.

It is necessary to interpolate the dispersion parameters between the given temperatures, so that the permittivity of methanol could be calculated at the measured room temperature.

Interpolated values for the permittivity of methanol at all temperatures over the 10 to 40°C range were estimated from the following approximate functions for the temperature dependence of the dispersion parameters, deduced from the Jordan data.

$$\varepsilon_s = -0.22T + 39.2 \qquad \text{Good straight line} \qquad (4.7.4)$$

$$\varepsilon_\infty = -0.022T + 4.95 \qquad \text{Poor straight line overall, but good around 20°C}$$

$$\tau(ps) = 0.0125T^2 - 1.79T + 86.7 \qquad \text{Good quadratic}$$

$$\alpha = -5.75\times10^{-5}T^2 + 2.56\times10^{-3}T + 0.0153 \qquad \text{Good quadratic}$$

where T is the temperature in degrees Celsius.

At the average room temperature of 20°C, the quoted values of dispersion parameters, and their confidence limits, give the relative permittivity of methanol as 18.7 - j14.2, with an error of ± 1 in both the real and imaginary parts.

4.7.6. Ethylene Glycol.

In the same 1978 publication, Jordan et al present dielectric dispersion parameters for ethylene glycol, commonly called glycol. Their original data were found to fit well to a two-component Debye dispersion equation of the form

$$\varepsilon_r = \varepsilon_\infty + \frac{\varepsilon_s - \varepsilon_H}{1 + j\omega\tau_1} + \frac{\varepsilon_H - \varepsilon_\infty}{1 + j\omega\tau_2} \qquad (4.7.5)$$

This suggests that there are two independent Debye relaxation processes present in the dielectric behaviour of glycol. The parameters for this dispersion equation for glycol, as measured by Jordan et al, and their 95% confidence limits, are presented in table 4.f.

Again, at temperatures other than those quoted, the permittivity of glycol must be estimated by interpolation. The approximate formulae used in this study to obtain the dispersion parameters at intermediate temperatures are given below.

$$\begin{aligned}
&\varepsilon_s = -0.242T + 47.8 && \text{Good straight line} \\
&\varepsilon_H = 7.55 \\
&\varepsilon_\infty = 3.95 && \qquad (4.7.6) \\
&\tau_1(ps) = 0.133T^2 - 11.8T + 332 && \text{Satisfactory quadratic} \\
&\tau_2(ps) = 0.0175T^2 - 1.31T + 32.3 && \text{Poor quadratic}
\end{aligned}$$

where T is the temperature in degrees Celsius.

At 20°C, the quoted dispersion parameter values, and their confidence limits, give a 3GHz relative permittivity of 11.4 - j12.1, with errors of ± 0.8 in the real part, and ± 0.6 in the loss factor.

4.7.7. Water-Dioxane Solutions.

A Cole-Cole relaxation equation (see eqn. 4.7.3) was used to describe the complex permittivity of water-dioxane mixtures. The values of the dielectric dispersion

Temperature (°C)	ε_s	$\pm\Delta\varepsilon_s$	ε_H	$\pm\Delta\varepsilon_H$	ε_∞	$\pm\Delta\varepsilon_\infty$	$\tau_1(ps)$	$\pm\Delta\tau_1$	$\tau_2(ps)$	$\pm\Delta\tau_2$
10	45.5	0.5	7.8	0.8	4.1	0.6	228	9	22	11
20	42.8	0.3	7.3	0.5	3.8	0.5	145	5	10	4
30	40.5	0.3	7.8	2.0	4.1	0.8	100	3	12	14
40	38.2	0.2	7.3	0.7	3.8	0.5	70	2	7	3

Table 4.f. Two-component Debye equation dispersion parameters for ethylene glycol as given by Jordan et al, 1978.

Substance	ε_∞	ε_s	τ (ps)	α
80% water / 20% dioxane	3.75	61.9	11	0
60% water / 40% dioxane	3.35	44.5	15	0.1
40% water / 60% dioxane	3.1	27.2	17	0.1
20% water / 80% dioxane	3.75	11.9	23	0.1
Pure dioxane	2.2	2.2	-	-

Table 4.g. Cole-Cole equation dispersion parameters for water / dioxane solutions as given by Misra et al, 1990.

parameters $\varepsilon_s, \varepsilon_\infty, \tau$ and α at a temperature of 25°C were taken from Misra et al (1990), and are shown in table 4.g. The parameter ε_s was originally obtained from Critchfield et al (1953), and the remaining parameters were estimated by interpolation from Hasted et al (1951).

At a frequency of 3GHz , these parameters give the following complex permittivities for each of the mixtures used.

80% water / 20% dioxane: 59.5-j11.6
60% water / 40% dioxane: 39.3-j10.8
40% water / 60% dioxane: 23.6 - j6.9 (4.7.7)
20% water / 80% dioxane: 10.1 - j2.8

The error on these permittivity values is not clear from the original references. However, the degree of precision quoted on the dispersion parameters suggests that the error in the permittivity factors of the 80% dioxane solution is approximately ± 0.5, rising to ± 1.5 for the 80% water solution.

Because of this uncertainty concerning the validity of these values, and the additional error involved in measuring the volumes of the liquids to be mixed, water-dioxane mixtures were mainly used in this study for checking the probe calibration over the permittivity range, rather than in actual calibration data. Pure dioxane has, however, a permittivity similar to that of pure animal fat, as measured on dehydrated fat samples in this study, and may therefore be useful as a component in low permittivity tissue simulating solutions.

4.7.8. Glycerol.

But for its high viscosity, which makes thorough cleaning of the probe after immersion rather awkward, glycerol is a useful calibration liquid. It has been used as a calibration check by Misra and Staebell (1990) in previous co-axial probe studies, and its dielectric dispersion parameters are well tabulated (Buckley and Maryott 1958). The permittivity of glycerol is broadly similar to that of fatty biological tissues, and so is a worthwhile calibration check in that permittivity range for this study.

Davidson and Cole (1950) first investigated high frequency dielectric relaxation in glycerol, fitting its dielectric dispersion to a Cole-Davidson equation of the form,

$$\varepsilon_r = \varepsilon_\infty + \frac{\varepsilon_s - \varepsilon_\infty}{(1 + j\omega\tau)^{1-\alpha}} \qquad (4.7.8)$$

a form which corresponds to an asymmetrical distribution of relaxation times.
Taking data from several sources, Misra uses the following values for the dispersion parameters of glycerol at room temperature.

$$\varepsilon_s = 42.5 \qquad \varepsilon_\infty = 4.2 \qquad \tau = 2.49 \times 10^{-9} s \qquad \alpha = 0.4 \qquad (4.7.9)$$

These give the room temperature relative permittivity as 6.4 - *j*3.1 at 3 GHz.

4.7.9. Air.

Air provides an accurate and reproducible calibration standard for the low permittivity region of the probe calibration. Pure dioxane was also used to serve this purpose, and comparison of the reflection co-efficients from these two materials showed great consistency. Calibrations using air as one of the standard materials gave very accurate values for the permittivity of dioxane from measured data, and vice-versa. The relative permittivity of air at Standard Temperature and Pressure is 1.0007. Air is a preferable material in which to immerse the co-axial probe to dioxane, as dioxane has a mild dissolving action on the plastic of the co-axial line.

Chapter 5. Calibration of the Open-ended Co-axial Probe.

5.1. Introduction.

There are published several methods for calculating the load permittivity of an open-ended co-axial probe, which lead to slightly differing calibrations. In each case, the measured permittivity of a sample is calculated using its measured impedance at the end of the probe, and a set of calibration data from materials of known permittivity.
In this chapter, the formulation of each expression is used to show how calculations and measurements were made to determine which expression was most suitable for calibrating our probe. Comparison of the methods showed strong similarity between the forms of the relationships between measured impedance and permittivity. This similarity is investigated and its causes explained.
Finally the possible sources of measurement uncertainty and their effects on the overall accuracy of measured permittivity data are evaluated.

5.2. Aperture Modelling.

Modelling the electromagnetic fields at the aperture of an open-ended waveguide by modal analysis has been briefly discussed in section 1.8. A similar modal representation may be used to calculate the reflection co-efficient of an incident TEM wave at the open-end of a co-axial probe (Mosig et al, 1981). An ideal co-axial probe, with infinite conducting ground plane is shown in fig. 5.a. The dimensions of the co-axial line are selected so as to only allow the dominant TEM mode to propagate at the desired operating frequency.
At the probe aperture, the electromagnetic fields excited are those of an ideal TEM waveguide, with additional fringing field components. The discontinuity at $z = 0$ excites a reflected TEM wave and a set of higher order evanescent modes which decay quickly along the line. Fields are radiated into the sample material as a result of the TEM mode and the higher order modes in the aperture plane. As the co-axial line has axial symmetry, and the field variation of the incident TEM mode is independent of azimuthal angle ϕ, only the TM_{0n} higher order modes are generated.

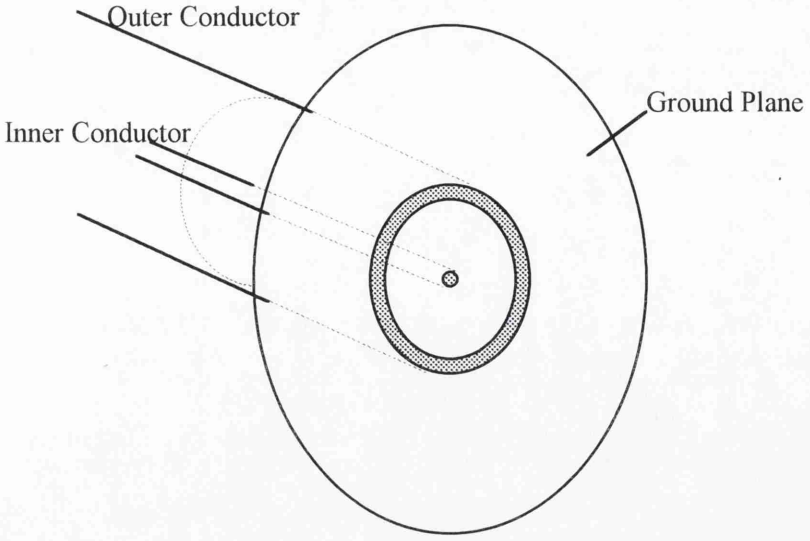

Figure 5.a. Ideal open-ended co-axial probe with large conducting ground plane

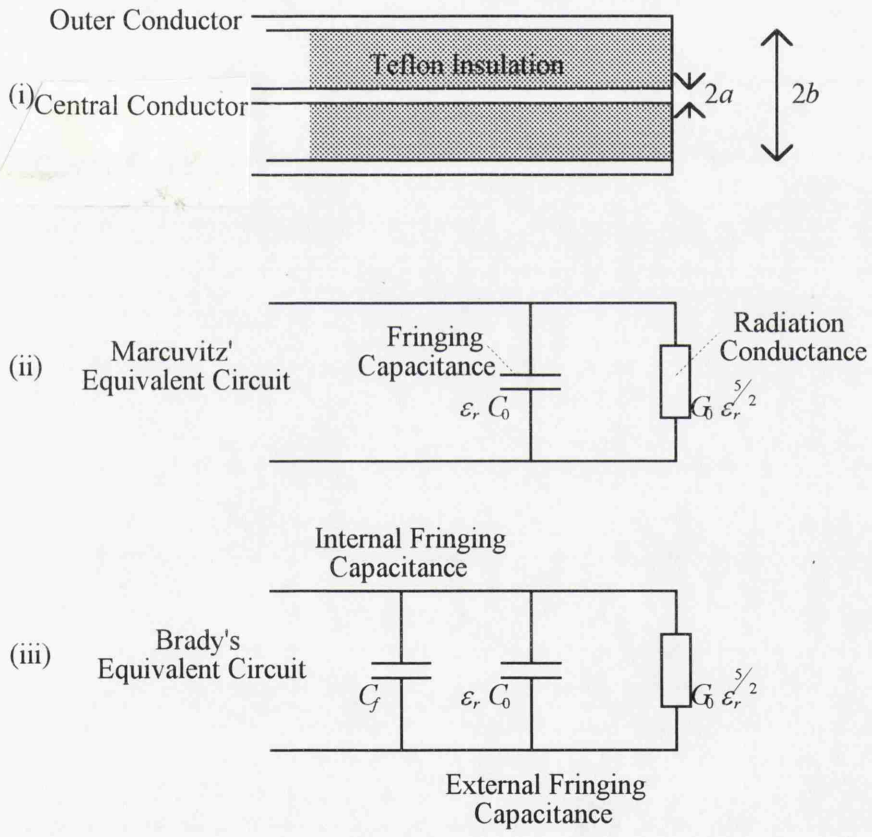

Figure 5.b. (i) Real experimental open-ended co-axial probe for permittivity measurements. (ii) Simple equivalent circuit model for open-ended probe. (iii) Improved equivalent circuit model with capacitance decomposed into two parts; C_f represents the fringing field inside the Teflon dielectric of the cable, and a parallel capacitance $\varepsilon_r C_0$ represents the fringing field in the external dielectric.

Using an integral expression for the $\phi-$ symmetrical magnetic fields, Mosig et al presented a set of nomograms for SR7 type co-axial cable at various frequencies, relating the sample permittivity to the measured reflection co-efficient. The mathematical analysis required to yield these results is rather involved, and the expression for the field does not permit straightforward calculation of the terminating permittivity from measured reflection co-efficient data.

5.2.1. Marcuvitz' Equivalent Circuit Formulation.

An alternative approach used by most researchers is to use an approximate equivalent circuit model for the open-end. The aperture is modelled by lumped circuit elements comprising a capacitance and a conductance, located at the end of an ideal open-circuited line, as shown in fig. 5.b.

An analytic expression for the equivalent circuit admittance of a probe radiating into free space is given by Marcuvitz (1951). Where the probe dimensions are small compared with the wavelength, the admittance of a co-axial aperture can be written

$$Y(\omega,\varepsilon_0) = G\omega^4 + jB\omega \tag{5.2.1}$$

where G and B are functions of probe geometry only. These parameters can be given by

$$G = \frac{Y_0}{\ln\left(\frac{b}{a}\right)}\int_0^{\frac{\pi}{2}} \frac{d\theta}{\sin\theta}\left[J_0(kb\sin\theta) - J_0(ka\sin\theta)\right]^2$$

$$\Rightarrow G \approx \frac{2Y_0}{3\ln\left(\frac{b}{a}\right)}\left[\frac{\pi^2(a^2-b^2)}{\lambda^2}\right]^2 \tag{5.2.2}$$

$$B \approx \frac{8Y_0(a+b)}{\lambda\ln\left(\frac{b}{a}\right)}\left[E\left(\frac{2\sqrt{ab}}{a+b}\right) - 1\right] \tag{5.2.3}$$

where b and a are the outer and inner radii of the co-axial cable respectively ($b,a<<\lambda$), Y_0 is the admittance of the cable, J_0 is the Bessel function, and $E(x)$ is the elliptic integral of the second kind.

For measuring the permittivity of sample materials it is necessary to find the admittance of the probe when radiating into a medium with relative permittivity ε_r rather than just free space.

Deschamps (1962) proposed a modelling theorem which applies to any probe geometry where the medium surrounding the probe is infinite in extent. For a non-magnetic surrounding medium (i.e. $\mu_r = 1$), the measured admittance of the probe, Y, is related to the admittance when radiating into free space by the equation,

$$Y(\omega, \varepsilon_r \varepsilon_0) = \sqrt{\varepsilon_r} Y(\omega\sqrt{\varepsilon_r}, \varepsilon_0) \qquad (5.2.4)$$

Applying eqn. 5.2.4. to eqn. 5.2.1 gives:

$$Y(\omega, \varepsilon_r \varepsilon_0) = G_0(\omega)\varepsilon_r^{\frac{5}{2}} + j\omega C_0 \varepsilon_r \qquad (5.2.5)$$

where $G_0(\omega)$ can be identified as the free space radiation conductance, predicted to vary as ω^4, and C_0 is the fringing field capacitance.

In practical situations, where the dimensions of the line are small compared to the wavelength, the radiation conductance term for a purely open-ended probe is often found to be very small ($G_0 << \omega C_0$). This is especially so at low frequency, and so the radiation term was often ignored by early workers (e.g. Burdette et al, 1980), leaving a purely reactive impedance of the open-end. Stuchly et al (1982a) demonstrated that this simplification can lead to significant errors at high frequency, and when measuring high permittivity materials, for which the radiation term becomes more important, because of the exponent to which the permittivity is raised in this term.

Strictly speaking, the antenna used for the majority of measurements in this work was a very short monopole antenna, rather than a purely open-ended co-axial antenna, having a slightly protruding centre conductor. However, the open-ended line model is still appropriate, as the equivalent circuits for a pure open-end and a very short monopole antenna contain the same two components; a capacitance and a conductance. The presence of the radiation conductance term in eqn. 5.2.5 means that the Marcuvitz model for a co-axial opening can allow for any radiation effect from the protruding conductor, and as the extended length of the centre conductor, h, satisfies the condition $h/\lambda_0 << 1$, the monopole is also sufficiently small as to be regarded as infinitesimal. Hence this treatment is consistent in approach to the limiting case of the admittance of a short monopole antenna with $h < \lambda_0/10$ according to Tai, 1961. A direct comparison of the open-ended and short monopole antenna models is discussed more fully in section 5.4.

5.2.2. Inherent Approximations in the Marcuvitz Formulation.

Equation 5.2.5 for the admittance of an open-ended co-axial line is only approximate, for the following reasons (Marsland & Evans, 1987).

- Since the field at the aperture is not purely TEM, there is no unique admittance, and so the Deschamps theorem cannot strictly be applied.
- Similarly, Marcuvitz' derivation of the admittance also assumes a purely TEM aperture field and ignores the presence of higher order field terms.
- In addition, Marcuvitz' derivation supposes the aperture opens onto an infinite, conducting ground plane. The current open-ended probe possesses a very small ground plane, having only the thickness of the outer conductor.

The problems relating to the absence of a ground plane were addressed by Bahl et al (1979), who considered the effect of ground plane radius on a set of monopole antennae of varying length / wavelength ratios with $h/\lambda_0 << 1$. It was shown that for the extended central conductor length of the current experimental probe ($h = 0.0025\lambda_0$), the change in the input impedance of the co-axial line caused by the absence of an infinite ground plane is negligible. Thus the input impedance of the experimental probe can always be taken as being equal to 50Ω.

To address the remaining problems, Brady et al (1981) split the capacitative term in the equivalent circuit representation into two separate parallel capacitances:- One capacitance, C_f, to represent the fringing field inside the insulating teflon dielectric of the co-axial cable, and another parallel capacitance $\varepsilon_r C_0$ to represent the fringing field in the external sample material. Thus the normalised admittance of the probe is given by

$$y(\omega,\varepsilon_r) = j\omega Z_0(\varepsilon_r C_0 + C_f) + G_0 Z_0 \varepsilon_r^{\frac{5}{2}} \qquad (5.2.6)$$

where Z_0 is the characteristic impedance of the probe. Equation 5.2.6 may be expressed in the form:

$$y(\omega,\varepsilon_r) = K_1 + K_2\varepsilon_r + K_3\varepsilon_r^{\frac{5}{2}} \qquad (5.2.7)$$

where K_1, K_2 and K_3 are constants, generally complex. At this stage Brady et al (1981) used two conceptually equivalent approaches to evaluating the three constants. Firstly, by keeping the sample permittivity constant, the lumped element parameters C_f, C_o and G_0 of eqn. 5.2.6 can be measured by varying the frequency over the range to be used for permittivity measurement. Alternatively, measuring the normalised

admittance of the probe when immersed in three separate samples of known dielectric permittivty allows direct evaluation of K_1, K_2 and K_3. Dielectric liquids with permittivities across a range matching that of the samples to be finally investigated are suitable materials for this calibration method.

Both of these methods require the calculation of the admittance of the probe by measuring the magnitude and phase of the reflection co-efficient of the probe in a variety of environments, either manually, or by use of an automatic network analyser. Inherent in any real measurement system are a number of imperfections. Discontinuities in the test set, cabling and connectors affect the measured reflection co-efficient. In order to account for these, it is common to consider an equivalent two-port network connected between the measuring equipment and the co-axial opening, with a second order scattering matrix $\underline{\mathbf{E}}$, with components E_{11}, E_{12}, E_{21} and E_{22}. The scattering co-efficient E_{11} is the input reflection co-efficient with output matched; E_{22} is the output reflection co-efficient with input matched; $E_{21}E_{12}$ refers to the transmission co-efficient between matched source and matched load. The elements of $\underline{\mathbf{E}}$ can be determined by attachment of three known terminations, short circuit, open circuit and matched load to the open end. It is possible to create a short circuit at the end of the probe by immersion in liquid mercury. An open circuit can be (very) approximately realised by leaving the probe open into air. However, the provision of a matched load is extremely difficult, requiring expensive and time-consuming design and manufacture.

To measure the admittance accurately, the true reflection co-efficient Γ_m may be evaluated from the measured reflection co-efficient ρ_m using the bilinear transform

$$\Gamma_m = \frac{\rho_m - E_{11}}{\rho_m E_{22} - (E_{11}E_{22} - E_{21}E_{12})} \tag{5.2.8}$$

Marsland and Evans (1987) show how this step, and the difficult process of determining the elements of the matrix $\underline{\mathbf{E}}$, may be avoided altogether, by the use of bilinear transformations. There is then no need for a matched load termination.

5.2.3. Bilinear Transformations.

It is often useful, in certain more complicated problems involving complex variables, to associate with a complex number $z = x + jy$, another complex number $w = u + jv$,

defined by a relation $w = f(z)$, where f is a known function. A region in the z-plane may be transformed into a different shaped region in the w-plane via a one-to-one mapping function, f. Thus it is often simpler, when dealing with the variation of some quantity over an awkward region of the z-plane, to make a transformation to a w-plane, such that the region concerned becomes a shape more easy to deal with.

One particular type of complex transformation, known as the *bilinear transformation,* preserves the form of certain functions between the z and w planes. i.e. straight lines in the z-plane transform to straight lines in the w-plane. The bilinear transformation is defined by;

$$w = \frac{az+b}{cz+d} \tag{5.2.9}$$

where a, b, c and d are complex constants such that $ad \neq bc$, and takes its name from the form of the expressions in both the numerator and denominator of the overall function.

An important property of bilinear transforms is *cross-ratio invariance.* Consider the four finite numbers z_1, z_2, z_3, z_4 with finite images under the bilinear transformation (eqn. 5.2.9) given by w_1, w_2, w_3, w_4.

Then
$$(w_i - w_k) = \frac{(ad-bc)(z_i - z_k)}{(cz_i + d)(cz_k + d)} \qquad (i,k = 1,2,3,4) \tag{5.2.10}$$

So,
$$(w_1 - w_2)(w_3 - w_4) = A(z_1 - z_2)(z_3 - z_4) \tag{5.2.11}$$

where A is the abbreviation:
$$A = \frac{(ad-bc)^2}{(cz_1 + d)(cz_2 + d)(cz_3 + d)(cz_4 + d)} \tag{5.2.12}$$

Since A is symmetric in z_1, z_2, z_3, z_4, we also have:

$$(w_1 - w_3)(w_2 - w_4) = A(z_1 - z_3)(z_2 - z_4) \tag{5.2.13}$$

Dividing eqn. 5.2.11 by eqn. 5.2.13 yields:

$$\frac{(w_1 - w_2)(w_3 - w_4)}{(w_1 - w_3)(w_2 - w_4)} = \frac{(z_1 - z_2)(z_3 - z_4)}{(z_1 - z_3)(z_2 - z_4)} \tag{5.2.14}$$

The right hand side of eqn. 5.2.14 is the *cross-ratio* of the four numbers z_1, z_2, z_3, z_4, denoted by (z_1, z_2, z_3, z_4). Thus the cross-ratio of four numbers is invariant under a bilinear transform.
$$(w_1, w_2, w_3, w_4) = (z_1, z_2, z_3, z_4) \tag{5.2.15}$$

5.2.4. Application of Bilinear Transformations to the Equivalent Circuit Model.

The above result was used by Marsland and Evans (1987) to calculate permittivities from

measured reflection co-efficients without first evaluating the scattering matrix $\underline{\mathbf{E}}$. Their method is as follows.

Let y_1, y_2, y_3 and y_m be the true admittances of the probe when terminated by the materials 1,2, 3 and m respectively. Materials 1,2 and 3 are of known permittivity, and the permittivity of the sample material, m, is to be calculated.

The true normalised admittance of the open-end, y_i, when terminated by any material i, is related to the true reflection co-efficient, Γ_i, by the expression $y_i = \dfrac{(1-\Gamma_i)}{(1+\Gamma_i)}$.

Comparison with eqn. 5.2.9 shows that y is a bilinear transform of Γ. From equation 5.2.8 it can also be seen that Γ is a bilinear transform of the measured reflection co-efficient ρ. Thus by cross-ratio invariance, the true admittances are related to the measured reflection co-efficients by:

$$\frac{(y_m - y_1)(y_3 - y_2)}{(y_m - y_2)(y_1 - y_3)} = \frac{(\rho_m - \rho_1)(\rho_3 - \rho_2)}{(\rho_m - \rho_2)(\rho_1 - \rho_3)} = \frac{\delta_{m1}\delta_{32}}{\delta_{m2}\delta_{13}} \tag{5.2.16}$$

where $\delta_{ij} = (\rho_i - \rho_j)$.

The cross-ratio invariance property implies that any arbitrary bilinear transformation can be applied to the admittance without altering the validity of eqn. 5.2.16. Applying the linear transformation

$$y'(\omega, \varepsilon_r) = \left(\frac{1}{j\omega C_0 Z_0}\right) \cdot y(\omega, \varepsilon_r) - \left(\frac{C_f}{C_0}\right) \tag{5.2.17}$$

to the admittance $y(\omega, \varepsilon_r)$ as given in eqn. 5.2.6 yields

$$y'(\omega, \varepsilon_r) = \varepsilon_r + G_n \varepsilon_r^{\frac{5}{2}} \tag{5.2.18}$$

where $G_n = \dfrac{G_0}{j\omega C_0}$. This transformed admittance satisfies $\dfrac{(y'_m - y'_1)(y'_3 - y'_2)}{(y'_m - y'_2)(y'_1 - y'_3)} = \dfrac{\delta_{m1}\delta_{32}}{\delta_{m2}\delta_{13}}$.

In terms of the measured sample permittivity ε_m, this expression may be rewritten

$$G_n \varepsilon_m^{\frac{5}{2}} + \varepsilon_m + \left(\frac{\delta_{m1}\delta_{32} y'_3 y'_2 + \delta_{m2}\delta_{13} y'_1 y'_3 + \delta_{m3}\delta_{21} y'_2 y'_1}{\delta_{m1}\delta_{32} y'_1 + \delta_{m2}\delta_{13} y'_2 + \delta_{m3}\delta_{21} y'_3} \right) = 0 \tag{5.2.19}$$

Thus to solve for the measured sample permittivity it is necessary only to know the reflection co-efficients and permittivities $(\rho_1, \rho_2, \rho_3, \varepsilon_1, \varepsilon_2, \varepsilon_3)$ of the three reference materials, the reflection co-efficient of the sample material ρ_m, and also the normalised radiation conductance G_n. To determine G_n, the value of ρ_m is measured for a fourth known dielectric with permittivity ε_4, giving ρ_4. Then, substituting ρ_4 and ε_4 for ρ_m and ε_m in eqn. 5.2.19, the resulting quadratic in G_n may be solved.

It is convenient to use a short circuit termination as one of the three 'known' dielectrics in the calibration. Firstly, it is easy to make a reliable and effective short circuit for an open-ended line: in this study the open-end was simply immersed in mercury. Also, since a short circuit has infinite admittance, the form of eqn. 5.2.19 is made simpler.

Setting material 3 as the short circuit, $y_3' \to \infty$, and eqn. 5.2.19 becomes

$$G_n \varepsilon_m^{\frac{5}{2}} + \varepsilon_m + \left(\frac{\delta_{m1}\delta_{32} y_2' + \delta_{m2}\delta_{13} y_1'}{\delta_{m3}\delta_{21}} \right) = 0 \qquad (5.2.20)$$

$$\Rightarrow (G_n \varepsilon_m^{\frac{5}{2}} + \varepsilon_m) \left(\frac{\delta_{m3}\delta_{21}}{\delta_{m2}\delta_{13}} \right) = -\left(y_1' + \left(\frac{\delta_{m1}\delta_{32}}{\delta_{m2}\delta_{13}} \right) y_2' \right)$$

If the parameter Δ is defined such that $\Delta = \dfrac{\delta_{m1}\delta_{32}}{\delta_{m2}\delta_{13}}$ then, by arithmetic manipulation, it can be shown that $\left(\dfrac{\delta_{m3}\delta_{21}}{\delta_{m2}\delta_{13}} \right) = -(1+\Delta)$, hence the transformed admittance may be expressed as

$$G_n \varepsilon_m^{\frac{5}{2}} + \varepsilon_m = \left(\frac{y_1' + \Delta y_2'}{1+\Delta} \right) \qquad (5.2.21)$$

The short circuit also facilitates the determination of G_n. Using eqn. 5.2.21, a fourth measurement ρ_4 on a known permittivity ε_4 yields a direct expression for G_n

$$G_n = \frac{(1+\Delta')\varepsilon_4 - \varepsilon_1 - \Delta'\varepsilon_2}{\varepsilon_1^{\frac{5}{2}} + \Delta'\varepsilon_2^{\frac{5}{2}} - (1+\Delta')\varepsilon_4^{\frac{5}{2}}} \qquad (5.2.22)$$

where Δ' is the value of Δ for the specific case where the four materials are the standard calibration materials, and material number 3 is a short circuit termination.

Thus the method used in this study to find the permittivity of sample materials has been outlined. This method was tested using a wide variety of calibration liquids, and was found to give reliable and accurate permittivity measurements across the range of permittivity values expected from body tissues. A suite of computer programs was written firstly to evaluate G_n, using calibration data from three known dielectrics and a short circuit termination, and then to use this value to calculate sample permittivities from reflection co-efficient data, using the Newton-Raphson technique. It will be noted that the values of G_0, C_0 and C_f in the absolute admittance equation 5.2.6, and also the sets of true admittances, y_i, and reflection co-efficients, Γ_i, are not found at any stage in this process. Although the final expressions are simple in form, the two-port system error correction method is still embodied within the formulation.

5.2.5. Practical Application of the Admittance Formula

A selection of eight standard liquids of known permittivity was used to calibrate and check the probe regularly. Three liquids were used in each calibration, and the calculated permittivities from the reflection co-efficients of the remaining five liquids were used to check the consistency of the calibration across the permittivity range. It was found that using this method, a consistent calibration set could give a set of permittivity readings of all the other liquids that differed from their quoted values by a maximum of around ± 1, or 5%, in either their real or imaginary parts. As expected, the term $G_n\varepsilon_r^{\frac{5}{2}}$ contributed only a small fraction of the total transformed admittance $y' = \varepsilon_r + G_n\varepsilon_r^{\frac{5}{2}}$. At low permittivities this contribution was less than 1%, rising to ~8% for the 0.15 **M** saline, the highest permittivity material tested.

However, it was found that the transform factor G_n was subject to considerable variation between different calibration sets, and always contained a real component in addition to its imaginary part. As G_n is equal to $\frac{G_0}{j\omega C_0}$, where G_0 and C_0 are real, G_n should be purely imaginary if the model is a true representation of the probe admittance. This suggests that the radiation conductance and capacitance, G_0 and C_0, may not fully describe the probe admittance.

To investigate this further, the simple approach of solving a set of simultaneous equations in the untransformed admittance, to yield the parameters C_f, C_0 and G_0 was used. This is equivalent to the calibration method used by Brady et al (1981), as has been discussed previously. It was recognised that this would not give a precise calibration, as the systematic two-port error correction is not incorporated. From the measured calibration data, the factors G_0 and C_0 were themselves found to have a small imaginary part in addition to their majority real parts. Brady et al also encountered this phenomenon when calibrating a co-axial probe.

This does not necessarily mean that the transformed calibration results are invalidated, merely that there is perhaps some other factor whose presence has been overlooked in the admittance model.

5.2.6. Misra's Admittance Formula

It has been suggested by Misra (1987), that Marcuvitz' model is restricted at high frequencies by an inadequate circuit model for the probe. Considering the same problem of an open-ended co-axial line terminated by a semi-infinite medium on a ground plane, Misra formulated a stationary relation for the aperture admittance. Under a quasi-static approximation, this relation reduces to

$$Y \approx j\frac{2\omega I_1}{\left(\ln(\frac{b}{a})\right)^2}\varepsilon_r - j\frac{\omega^3\mu_0 I_2}{\left(\ln(\frac{b}{a})\right)^2}\varepsilon_r^2 + \frac{\pi\omega^4\mu_0^{\frac{3}{2}}}{12}\left[\frac{b^2-a^2}{\ln(\frac{b}{a})}\right]^2\varepsilon_r^{\frac{5}{2}} \qquad (5.2.23)$$

where a and b are the inner and outer radii of the co-axial aperture respectively, and I_1 and I_2 are two triple integrals dependent on the radii, but otherwise constant and real. The first and third terms of eqn. 5.2.23 are familiar from the Marcuvitz formulation: the first term represents a capacitance, and the third term is a radiation conductance. This capacitance can be separated into two components to allow for internal and external fringing fields as before. However, the second term represents a new frequency dependent capacitance, which is claimed to account for the high frequency restrictions reported in the work by Marsland and Evans (1987). As the co-efficient of the permittivity in the second term is imaginary, the presence of such a term would yield a real component when the admittance is subjected to the bilinear transform

$$y'(\omega,\varepsilon_r) = \left(\frac{1}{j\omega C_0 Z_0}\right)\cdot y(\omega,\varepsilon_r) - \frac{C_f}{C_0}$$

as was used in the original formulation. It was thought that it is perhaps the presence of this term which was causing the transform parameter G_n to have a real component in the initial calibration.

The applicability of Misra's admittance formula to the experimental probe was considered. Misra suggests that the frequency dependent capacitance may even dominate the radiation conductance at lower microwave frequencies. By neglecting the radiation from the aperture, a bilinear transform can be applied to eqn. 5.2.23 yielding,

$$y' \approx \varepsilon_r + \xi\varepsilon_r^2 \qquad (5.2.24)$$

where the transform factor ξ should be purely real, and is given by

$$\xi = \frac{(1+\Delta')\varepsilon_4 - \varepsilon_1 - \Delta'\varepsilon_2}{\varepsilon_1^2 + \Delta'\varepsilon_2^2 - (1+\Delta')\varepsilon_4^2} \tag{5.2.25}$$

where $$\Delta' = \frac{(\rho_4 - \rho_1)(\rho_3 - \rho_2)}{(\rho_4 - \rho_2)(\rho_1 - \rho_3)} \tag{5.2.26}$$

Equations 5.2.24 and 5.2.25 are direct analogues of equations 5.2.18 and 5.2.22 as used when applying a bilinear transform to the Marcuvitz model. The subscripts 1,2,3 and 4 referring to the four calibration materials, of which material number 3 is a short circuit.

A calibration program was adjusted to give calibration factors from the measured reflection co-efficient data according to this model, rather than the model used by Marsland and Evans. The consistency of each calibration set remained similar to that achieved with the previous model, but the transformed calibration factor ξ was still prone to large variation between calibration sets, and always contained both real and imaginary parts. As when using the lumped parameter model, the term $\xi\varepsilon_r^2$ only contributes several percent of the total value of transformed admittance.

It was found that when the open-ended probe was calibrated using either the equivalent circuit approximation or Misra's formula, combined with the bilinear transform error correction routine, measured reflection co-efficient data accurately predicted the permittivity of known liquids with permittivities ranging from 1 to at least 77 - *j*23, to within the error on the known value.

Figures 5.c and 5.d show curves relating the measured load impedance to the dielectric constant and loss factor of the terminating medium for both calibration formulae, calculated using the same reflection co-efficient data. It can be seen that both methods yield very similar permittivity values for a given measured impedance. Neither model appeared to show a clear advantage over the other as far as measuring sample permittivity was concerned.

The reason that it was felt that Marsland and Evans' formulation (eqn. 5.2.18) better represented the probe admittance was as follows. By using their method, the transform factor G_n was found to be mainly imaginary, as expected, but with a small real component. However, by using Misra's method (eqn. 5.2.24), the transform factor ξ was found to be still mainly imaginary, but with a small real component. Under the bilinear transform, it is to be expected that ξ should be mainly real if eqn. 5.2.24 is a good representation of the admittance. As this was not the case, the physical

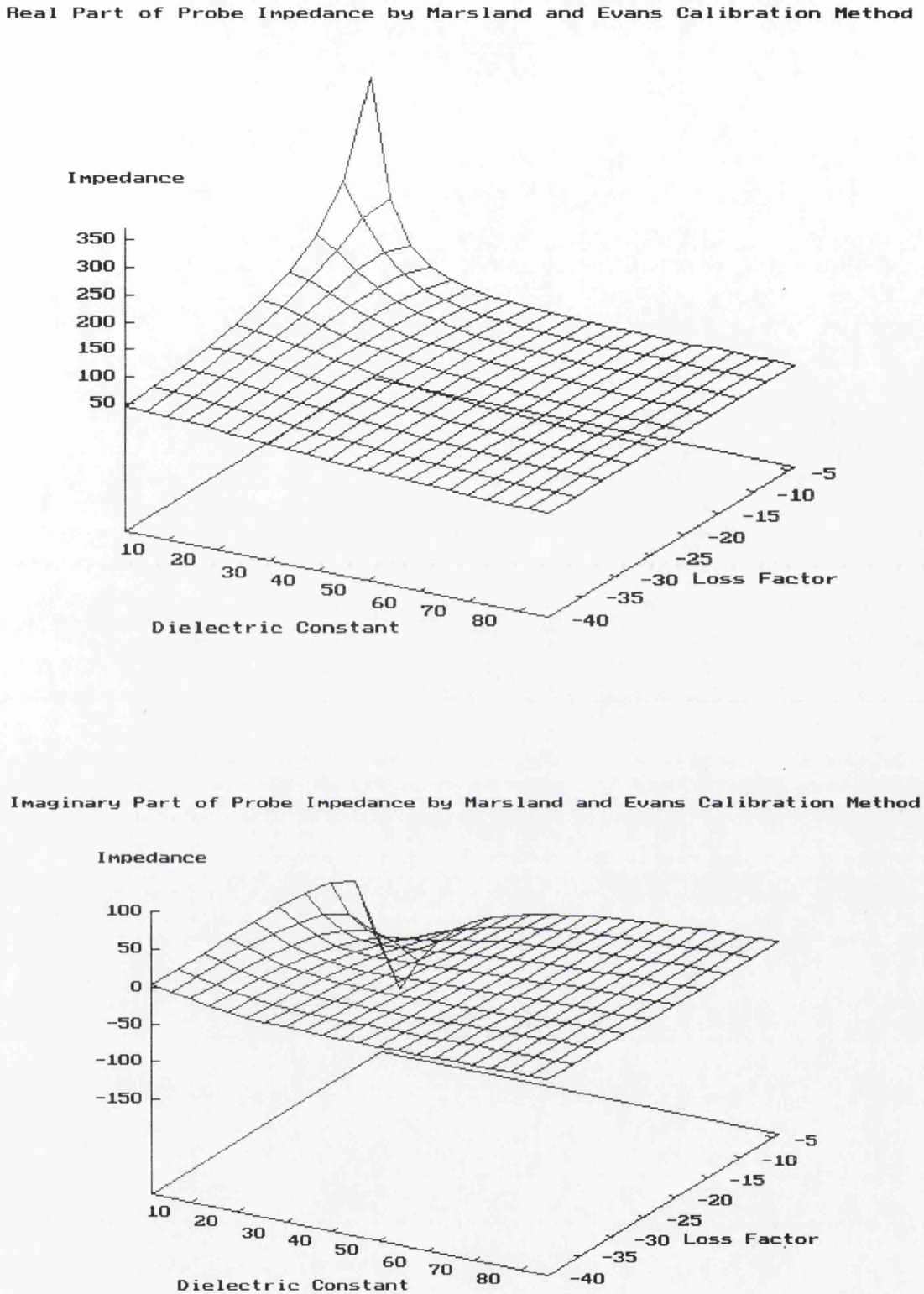

Figure 5.c. Impedance curves for experimental co-axial probe calculated using Marcuvitz' equivalent circuit method, as used by Marsland and Evans (eqn. 5.2.6). Taking reflection co-efficient data from materials of known permittivity, these impedance calibration curves are calculated using the untransformed circuit model for permittivity values in the range expected from biological tissues.

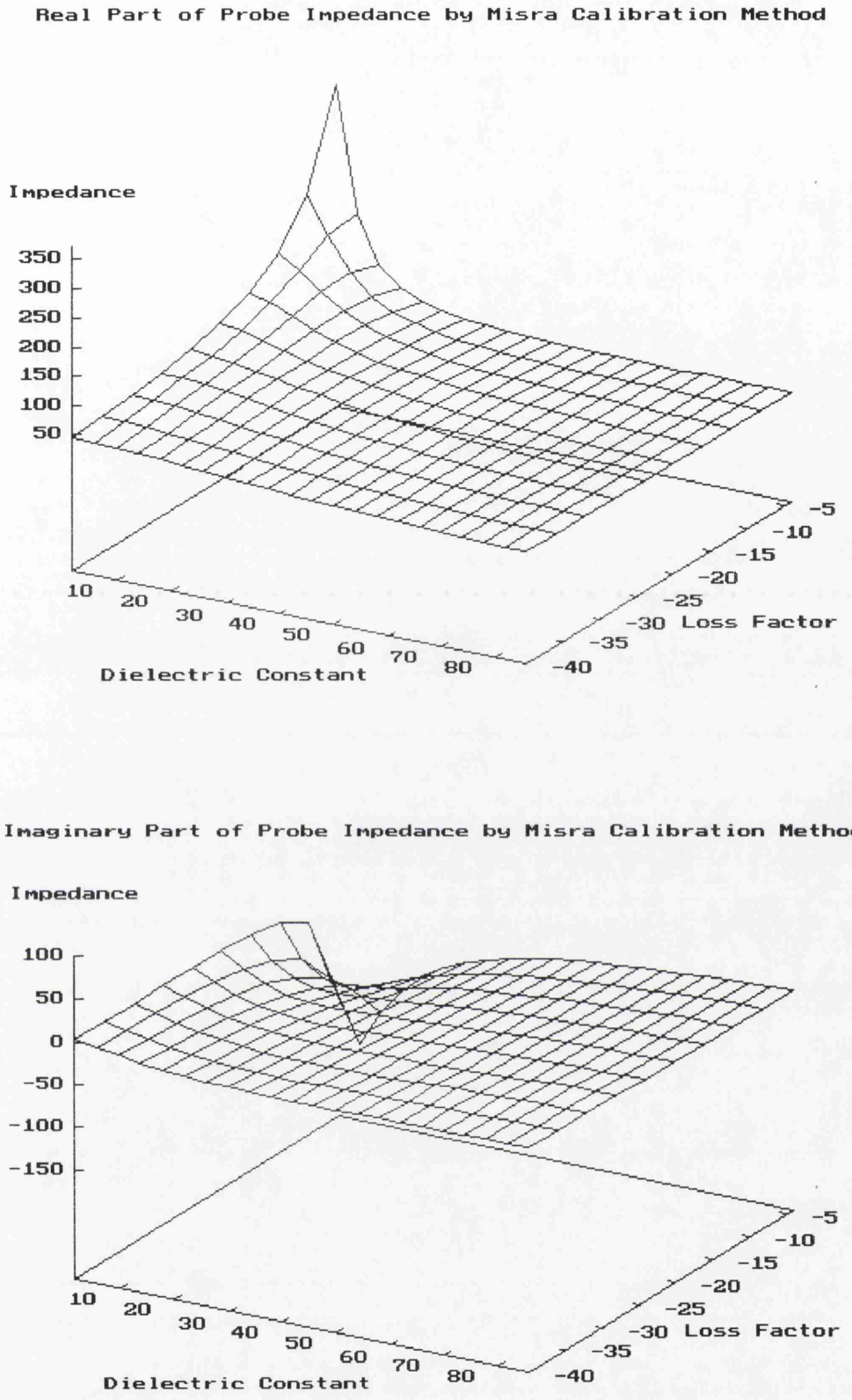

Figure 5.d. Impedance curves for experimental co-axial probe calculated using the calibration method of Misra (eqn. 5.2.23). Note the close similarity between these curves and those of figure 5.c. The difference between calibrations using the two methods is less than the calibration error due to uncertainty in the known permittivity in the calibration liquids.

interpretation was that Marsland and Evans' formulation was a more meaningful description of the co-axial probe in these circumstances.

Therefore it was finally decided to use Marsland and Evans' model for the admittance of the open-ended co-axial probe. This model is based on the equivalent circuit formulation of Marcuvitz, which has been used extensively and successfully by many workers in the field of biological tissue and tissue phantom permittivity measurement. Direct compatibility between these results and those of other researchers is therefore ensured.

5.3. Behaviour of the Factor Δ.

Both the Marsland & Evans lumped parameter model, and the Misra quasi-static analysis model for calculating sample permittivities from measured admittance data, used a bilinear transform approach, to avoid the time consuming and error-prone evaluation of the scattering matrix which describes the imperfections in the measurement system. The parameter Δ was defined by $\Delta = \frac{\delta_{m1}\delta_{32}}{\delta_{m2}\delta_{13}}$, where $\delta_{ij} = (\rho_i - \rho_j)$, the difference between the reflection co-efficients of the materials i and j. This parameter is used in eqns. 5.2.21 and 5.2.24 to simplify the expressions for the transformed admittance of the sample material from which the permittivity is found. A specific calibration value of Δ is also used in eqns. 5.2.22 and 5.2.25, the expressions for the transformed radiation conductance and its mathematical equivalent in the Misra model.

It was shown in section 5.2 that a formula for the transformed admittance of a sample material could be resolved, if the probe was calibrated by measuring the reflection co-efficients of four materials of known permittivity. From a practical point of view, it is convenient to use a short circuit termination as one of those four materials. There may be circumstances where the use of a short circuit is not practical. This would, at first sight, appear to render the entire formulation useless, as, even if a short circuit is not one of the four calibration standards, it is still necessary to find the short circuit null position, l_{short}, to calculate the reflection co-efficients of the calibration materials. However, this is not the case.

The reflection co-efficients ρ_i in the expression for Δ are dependent on the short circuit null position, l_{short}, as measured on the experimental slotted line.

$$\rho_i = r_i e^{i\theta_i} \quad \text{and} \quad \theta_i = \pi\left[1 - \frac{4(l_{short} - l_i)}{\lambda}\right] \tag{5.3.1}$$

where $r_i = |\rho_i|$, $\theta_i = \tan^{-1}\left(\frac{\text{Im.}(\rho_i)}{\text{Re.}(\rho_i)}\right)$, and l_i is the null position for material *i*.

Consider the value of Δ when materials 1,2,3 and 4 are any arbitrary calibration materials. The normalised transformed radiation conductance, G_n, (or its equivalent parameter) may be found by solving a quadratic in G_n, whose co-efficients are combinations of the permittivities of the standard materials, and the calibration value of Δ, called Δ'.

Now $\Delta' = \frac{(\rho_4 - \rho_1)(\rho_3 - \rho_2)}{(\rho_4 - \rho_2)(\rho_1 - \rho_3)}$ where the $\rho_i = r_i \cos\theta_i + jr_i \sin\theta_i$. Thus Δ' can be expanded, and expressed by $\Delta' = \frac{a + jb}{c + jd}$ where

$$a = [r_4 r_3 \cos(\theta_4 + \theta_3) - r_4 r_2 \cos(\theta_4 + \theta_2) - r_1 r_3 \cos(\theta_1 + \theta_3) + r_1 r_2 \cos(\theta_1 + \theta_2)] \tag{5.3.2a}$$

$$b = [r_4 r_3 \sin(\theta_4 + \theta_3) - r_4 r_2 \sin(\theta_4 + \theta_2) - r_1 r_3 \sin(\theta_1 + \theta_3) + r_1 r_2 \sin(\theta_1 + \theta_2)] \tag{5.3.2b}$$

$$c = [r_4 r_1 \cos(\theta_4 + \theta_1) - r_4 r_3 \cos(\theta_4 + \theta_3) - r_1 r_2 \cos(\theta_1 + \theta_2) + r_2 r_3 \cos(\theta_2 + \theta_3)] \tag{5.3.2c}$$

$$d = [r_4 r_1 \sin(\theta_4 + \theta_1) - r_4 r_3 \sin(\theta_4 + \theta_3) - r_1 r_2 \sin(\theta_1 + \theta_2) + r_2 r_3 \sin(\theta_2 + \theta_3)] \tag{5.3.2d}$$

We now prepare to differentiate Δ' with respect to l_{short}.

From eqn. 5.3.1 it is evident that $$(\theta_i + \theta_j) = 2\pi - 4\pi\left[\frac{(2l_{short} - l_i - l_j)}{\lambda}\right] \tag{5.3.3}$$

Therefore $$\cos(\theta_i + \theta_j) = \cos\left(-4\pi\left[\frac{2l_{short} - l_i - l_j}{\lambda}\right]\right). \tag{5.3.4}$$

So $$\frac{\partial \cos(\theta_i + \theta_j)}{\partial l_{short}} = -\sin(\theta_i + \theta_j)\left(\frac{-8\pi}{\lambda}\right) \tag{5.3.5}$$

and, in a similar fashion $$\frac{\partial \sin(\theta_i + \theta_j)}{\partial l_{short}} = \cos(\theta_i + \theta_j)\left(\frac{-8\pi}{\lambda}\right) \tag{5.3.6}$$

Differentiating, we find $$\frac{\partial a}{\partial l_{short}} = \left(\frac{-8\pi}{\lambda}\right)(-b), \quad \frac{\partial b}{\partial l_{short}} = \left(\frac{-8\pi}{\lambda}\right)(a) \tag{5.3.7a}$$

and $$\frac{\partial c}{\partial l_{short}} = \left(\frac{-8\pi}{\lambda}\right)(-d), \quad \frac{\partial d}{\partial l_{short}} = \left(\frac{-8\pi}{\lambda}\right)(c) \tag{5.3.7b}$$

So the differential of Δ' is given by

$$\frac{\partial \Delta'}{\partial l_{short}} = \left[\frac{(c+jd)(-b+ja)-(a+jb)(-d+jc)}{(c+jd)^2}\right]\left[\frac{-8\pi}{\lambda}\right] \tag{5.3.8}$$

$$\Rightarrow \frac{\partial \Delta'}{\partial l_{short}} = 0 \tag{5.3.9}$$

Thus it has been shown that the value of Δ' is independent of l_{short}, when any four known dielectric materials are used for calibration. To calibrate and make subsequent measurements using the probe, it is sufficient only to know the positions of the standing wave nulls of each of the terminations relative to each other, and the VSWR of each pattern. The value of l_{short} may be ignored, and computations made in *relative phase*, should a short circuit termination be unavailable.

Although the calibrations used in this work *are* based on one of the calibration standards being a short circuit, there is a possible advantage to using four other dielectric calibration liquids. The calibration factor Δ' is more sensitive to differences in the measured standing wave null positions when the relative positions of the calibration material nulls are very close. If any error in the known permittivity values, and in measurement of the null positions, could be avoided, then a more precise calibration over the permittivity range of interest could be achieved by using four dielectric standards. Dielectric liquids have permittivities, in the microwave region, of the form $\varepsilon_r = \varepsilon' - j\varepsilon''$, where $\varepsilon' \geq 1$ and $\varepsilon'' \geq 0$, and so present a resistive and capacitative impedance at the end of the probe. Therefore the reactances created by these materials when terminating the co-axial probe, X_i, (where $X_i = \frac{2r_i \sin\theta_i}{1+r_i^2-2r_i\cos\theta_i}$) are negative. To satisfy this, θ_i must conform to $-\pi \leq \theta_i \leq 0$, and subsequently, from eqn. 5.3.1: $\lambda/4 \leq (l_{short} - l_i) \leq \lambda/2$. In the case of all four calibration materials being dielectric liquids, all the standing wave nulls lie in a narrow band between 0.25 and 0.5 wavelengths away from the short circuit null. But when the short circuit is used as a calibration material, with three reference liquids, there are three closely grouped nulls, and one (the short circuit null) at a large distance from the other three. A large error in the position of the short circuit null is only a few percent of the difference between the position of that null and the nulls of

other materials, and so does not seriously affect the value of Δ'; whereas a similar error in one of the other null positions causes a far greater error. Thus a degree of the precision, associated with the short circuit null position, is lost.

However, in practice, there are compensating factors which reduce the advantageous effects of not using the short circuit termination. Firstly, since the reflection co-efficient of a short circuit has a magnitude of 1, the position of the short circuit null may be positioned more precisely than that of any other material. Additionally, using the short circuit termination simplifies the expression for the transformed admittance of sample materials, by reducing the number of terms. This reduces the overall error, as each term is subject to a combination of measurement and systematic error. There are also errors associated with the 'known' values of the permittivities of the calibration dielectric materials, so using an extra dielectric material introduces an extra error.

5.4. Comparison of Monopole and Open-ended Probe Admittance Models.

The experimental probe was constructed with a protruding centre conductor. In addition to using the lumped parameter model, the probe was also calibrated using the admittance model for a short monopole probe according to Tai (1961). It was thought that this might improve the calibration if the lumped parameter model could not account for effects caused by the centre conductor. Initial investigations were made in the untransformed plane (i.e. the admittance formulae in the models were taken as presented, without the error correction of the scattering matrix $\underline{\mathbf{E}}$). Admittance curves for both the Marcuvitz open-ended model and the monopole model, when plotted, were found to be almost exactly co-incident (see figs. 5.c and 5.e), suggesting strong similarity between the two approaches. This can be explained as follows.

According to Tai (1961), the terminal admittance of a short monopole probe, of length less than $\lambda/10$, in free space is given by:

$$Z_m(\omega, \varepsilon_0) = A\omega^2 + \frac{1}{j\omega C} \qquad (5.4.1)$$

where A and C are constants determined by the physical dimensions of the antenna, the constant C representing the capacitance of the antenna. Deschamps' antenna modelling theorem (eqn. 5.2.4) is now applied to this equation. Note that, as when applied to the lumped parameter model (section 5.2), the application of Deschamps' theorem to this equation is not strictly valid, for similar reasons as before.

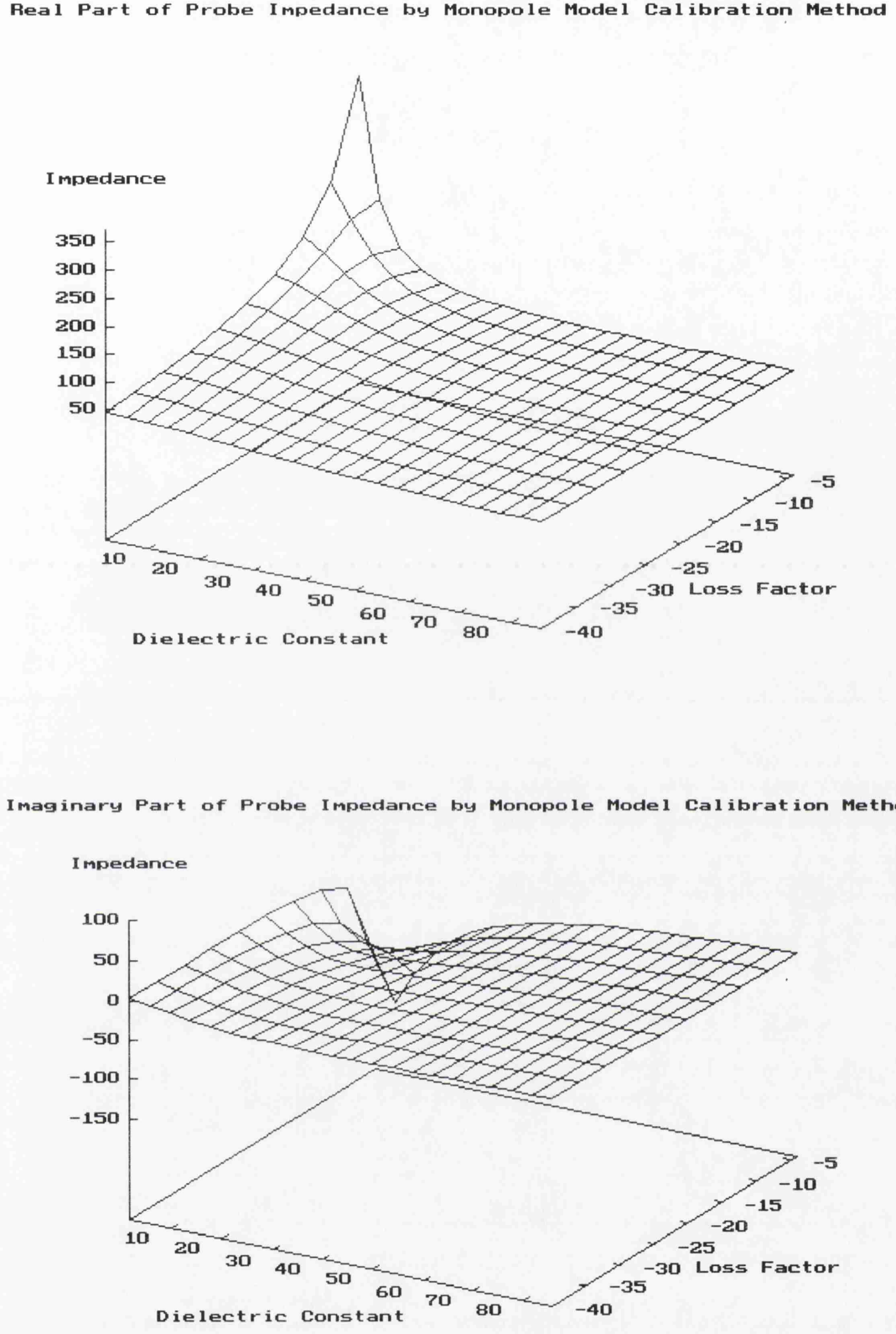

Figure 5.e. Impedance curves for experimental co-axial probe calculated using the monopole model calibration method (eqn. 5.4.4). This method is almost indistinguishable from the Marsland and Evans method, shown in fig. 5.c.

Deschamps' theorem in impedance form is: $Z(\omega,\varepsilon_r\varepsilon_0)=\sqrt{\frac{1}{\varepsilon_r}}Z\left(\omega\sqrt{\varepsilon_r},\varepsilon_0\right)$ (5.4.2)

Applying eqn. 5.4.2 to 5.4.1 gives: $Z_m(\omega,\varepsilon_r\varepsilon_0)=A\omega^2\sqrt{\varepsilon_r}+\frac{1}{j\omega C\varepsilon_r}$ (5.4.3)

Therefore, the admittance is given by: $Y_m(\omega,\varepsilon_r\varepsilon_0)=\frac{j\omega C\varepsilon_r}{j\omega AC\varepsilon_r^{\frac{3}{2}}+1}$ (5.4.4)

The lumped parameter model admittance is $Y_{lp}(\omega,\varepsilon_r\varepsilon_0)=G_0(\omega)\varepsilon_r^{\frac{5}{2}}+j\omega C_0\varepsilon_r$ (5.4.5)

By expanding the expression for the monopole admittance as a polynomial series in $\varepsilon_r^{\frac{1}{2}}$, the similarity between the two models will be shown. However, as the admittance is a function of the complex variable ε_r, it must be shown that the admittance expression $Y_m(\omega,\varepsilon_0\varepsilon_r)$ satisfies the Cauchy-Riemann conditions before it can be differentiated to find the terms of the series expansion.

Consider a function $f(z)$ of the complex variable $z=x+jy$. To differentiate $f(z)$, it is necessary to find $f'(z_0)=\lim_{\Delta z\to 0}\left\{\frac{f(z_0+\Delta z)-f(z_0)}{\Delta z}\right\}$ (5.4.6)

But z may approach z_0 along any direction in the z-plane, so for the derivative to exist, eqn. 5.4.6 must have the same value whatever path is chosen.

Suppose z approaches z_0 along a line through z_0 parallel to the real (x) axis. Then, since $\Delta z=\Delta x+j\Delta y$, it follows that $\Delta z=\Delta x$ for this path. Using $f(x,y)=u(x,y)+jv(x,y)$ in eqn. 5.4.6, yields for this path

$$f'(z_0)=\lim_{\Delta x\to 0}\left\{\frac{u(x_0+\Delta x,y_0)-u(x_0,y_0)}{\Delta x}\right\}+j\lim_{\Delta x\to 0}\left\{\frac{v(x_0+\Delta x,y_0)-v(x_0,y_0)}{\Delta x}\right\}$$

$$\Rightarrow f'(z_0)=\left(\frac{\partial u}{dx}\right)_{x=x_0}+j\left(\frac{\partial v}{\partial x}\right)_{x=x_0} \quad (5.4.7)$$

If z approaches z_0 along a second path through z_0, parallel to the imaginary (y) axis, then in this instance $\Delta z=j\Delta y$. By the same procedure as above, it can be shown that for this path $f'(z_0)=-j\left(\frac{\partial u}{\partial y}\right)_{y=y_0}+\left(\frac{\partial v}{\partial y}\right)_{y=y_0}$ (5.4.8)

As $f'(z_0)$ is to be the same whatever path is chosen the equations 5.4.7 and 5.4.8 must agree. By equating real and imaginary parts, the Cauchy-Riemann equations are found

$$\frac{\partial u}{\partial x}=\frac{\partial v}{\partial y},\ \text{and}\ \frac{\partial u}{\partial y}=-\frac{\partial v}{\partial x} \tag{5.4.9}$$

Any function $f(x,y)=u(x,y)+jv(x,y)$ which does not satisfy these equations is not a differentiable function.

To express the admittance function $Y_m(\omega,\varepsilon_r\varepsilon_0)=\dfrac{j\omega C\varepsilon_r}{j\omega AC\varepsilon_r^{\frac{3}{2}}+1}$ in the form

$Y_m=u(x,y)+jv(x,y)$, it is necessary to write the permittivity as $\varepsilon_r=(x+jy)^2$, so that

$\varepsilon_r^{\frac{3}{2}}=(x+jy)^3$. This gives $Y_m=\dfrac{-2xy\omega C+j\omega C(x^2-y^2)}{1-AC(3x^2y-y^3)+jAC(x^3-3xy^2)}$ (5.4.10)

Then, by multiplying by the conjugate of the denominator

$$u(x,y)=\frac{-2\omega Cxy+\omega^4AC^2(x^5+2x^3y^2+xy^4)}{1-2\omega^3AC(3x^2y-y^3)+\omega^6A^2C^2(3x^4y^2+x^6+y^6+3x^2y^4)} \tag{5.4.11a}$$

and $$v(x,y)=\frac{\omega C(x^2-y^2)-\omega^4AC^2(x^4y+2x^2y^3+y^5)}{1-2\omega^3AC(3x^2y-y^3)+\omega^6A^2C^2(3x^4y^2+x^6+y^6+3x^2y^4)} \tag{5.4.11b}$$

Differentiating $u(x,y)$ and $v(x,y)$, then collecting terms gives equations 5.4.12;

$$\frac{\partial u}{\partial x}=\frac{\partial v}{\partial y}=\frac{(3x^2y^8-3x^8y^2-2x^6y^4+2x^4y^6-x^{10}+y^{10})\omega^{10}A^3C^4+(16x^4y^3-8x^6y+24x^2y^5)\omega^7A^2C^3+(5x^4-6x^2y^2-3y^4)\omega^4AC^2-2Cy}{\left[1-2\omega^3AC(3x^2y-y^3)+\omega^6A^2C^2(3x^4y^2+x^6+y^6+3x^2y^4)\right]^2}$$

and

$$\frac{\partial v}{\partial x}=-\frac{\partial u}{\partial y}=\frac{(8x^3y^7+2x^9y+8x^7y^3+12x^5y^5+2xy^9)\omega^{10}A^3C^4+(12x^5y^2+4x^3y^4-12xy^6-4x^7)\omega^7A^2C^3-(4x^3y+12xy^3)\omega^4AC^2-2Cx}{\left[1-2\omega^3AC(3x^2y-y^3)+\omega^6A^2C^2(3x^4y^2+x^6+y^6+3x^2y^4)\right]^2}$$

Hence the Cauchy-Riemann equations are satisfied by the admittance function and its differential exists.

Expanding the admittance formula eqn. 5.4.4 in the form

$$Y_m(\omega,\varepsilon_r\varepsilon_0)=Y_m(\omega,0)+\varepsilon_r^{\frac{1}{2}}Y_m'(\omega,0)+\frac{\varepsilon_rY_m''(\omega,0)}{2}+\frac{\varepsilon_r^{\frac{3}{2}}Y_m'''(\omega,0)}{6}+\cdots\cdots$$

gives $Y_m(\omega,\varepsilon_r\varepsilon_0)=j\omega C\varepsilon_r+\omega^4AC^2\varepsilon_r^{\frac{5}{2}}-j\omega^7A^2C^3\varepsilon_r^4+O(\varepsilon_r^{\frac{11}{2}})$ (5.4.13)

where $O(\varepsilon_r^{\frac{11}{2}})$ represents terms of in the permittivity of order $\varepsilon_r^{\frac{11}{2}}$ and higher.

It can be immediately seen that the first two terms of this expression are similar to the expression for the admittance according to the lumped parameter model. The series in eqn. 5.4.13 can be represented as a power series in the form $Y_m=\sum_{s=0}^{\infty}a_s\varepsilon_r^{1+\frac{3}{2}s}$, where the co-efficients a_s are given by $a_s=-(-j)^{(s+1)}\omega^{(3s+1)}A^sC^{(s+1)}$. Equation 5.4.13 is valid for

all values of $\varepsilon_r^{\frac{1}{2}}$ such that $\left|\varepsilon_r^{\frac{1}{2}}\right|$ lies within the radius of convergence of the series, R, which is given by

$$R = \lim_{s\to\infty}\left|\frac{a_s}{a_{s+1}}\right| = \lim_{s\to\infty}\left|\frac{-(-j)^{(s+1)}\omega^{(3s+1)}A^sC^{(s+1)}}{-(-j)^{(s+2)}\omega^{(3s+4)}A^{(s+1)}C^{(s+2)}}\right| = \lim_{s\to\infty}\left|\frac{1}{\omega^3 AC}\right| \qquad (5.4.14)$$

Since ω, A and C are all constants, the modular value is independent of the order s. For the equipment used, the value of $\left|\frac{1}{\omega^3 AC}\right|$ was found to be ~10,000. As typical values for the real and imaginary parts of the root, $\varepsilon_r^{\frac{1}{2}}$, of the permittivity of body tissues lie in the ranges $<(\varepsilon_r^{\frac{1}{2}})_{real}<10$, and $0<(\varepsilon_r^{\frac{1}{2}})_{imag}<2$ respectively, it can clearly be seen that the expansion (eqn. 5.4.13) of the monopole admittance formula is valid for all permittivities of real materials. The ratio of successive terms is given by $\omega^3 AC\varepsilon_r^{\frac{3}{2}}$, so the capacitative term of order ε_r is the dominant term in the admittance formula, as is expected. This also means that the third and subsequent terms in the expansion are small in magnitude, and may be neglected.

Comparison of eqn. 5.4.13 with the lumped parameter admittance formula (eqn. 5.4.5) shows that not only can the capacitance C in the monopole model be directly equated with the capacitance term, C_0, in the lumped parameter model, but also that the term $\omega^4 AC^2$ can be equated with the lumped parameter G_0, a radiation conductance. Marcuvitz' original derivation for the lumped parameter model indicates that G_0 should depend on the fourth power of the frequency, as does the term $\omega^4 AC^2$. Thus equations 5.4.5 and 5.4.13 have the same behaviour not only in ε_r, but also in ω.

Therefore it may be said that an equivalent circuit model of an open-ended co-axial probe, with lumped parameters of capacitance and radiation conductance, is capable of describing the admittance of the probe used here for permittivity measurements, despite the protruding central conductor. The dominant term in the impedance of this probe is its capacitance, for which both the monopole and lumped parameter model account directly. Only at very high frequencies, or for a probe with a much longer length / radius ratio than that used, does it become necessary to consider the higher order terms of the short monopole model.

To compare directly the lumped parameter and monopole models numerically, it is necessary to use the untransformed, basic version of the lumped parameter model. This

is because it is impossible to evaluate individually the parameters C_0 and G_0 under the bilinear transform representation.

Using the same reflection co-efficient data from two materials of known permittivity, two sets of simultaneous equations were formed, one set using the lumped parameter model admittance formula, and the other set using the monopole model admittance formula. When each set was solved, it was indeed found that firstly, the capacitative term in each model was equal, with a value of $\sim 3 \times 10^{-14}$ F; and, that a difference of only around 4% was observed between the numerical value of the radiation conductance G_0 of the Marcuvitz model, and the value of $\omega^4 AC^2$ calculated from the calibration factors A and C of the monopole admittance model.

5.5. Sources of Error in Probe Calibration and Permittivity Results.

When measuring a permittivity value, the uncertainty in the value is composed of errors arising from two sources: (i). Error in the calibration of the open-ended permittivity probe, and (ii). Uncertainty in the measurement data for the particular material in question. Because data errors propagate through the permittivity evaluation procedure, it is necessary to evaluate first the measurement data and its uncertainty before the effect of the open-ended probe calibration error may be estimated.

5.5.1. Error in Standing Wave Data.

(i). Reflection Co-efficient.

The information required to characterise the reflection co-efficient of a terminating material consists of the values of the maximum and minimum standing wave voltages, and the position of the standing wave minimum on the slotted line. To ensure measurement consistency, several orders of these parameters on the slotted line were measured for each sample material. This means that the validity of the measurement is checked by ensuring that there is a consistent and regular standing wave pattern in the slotted co-axial line.

Any incompatibility of the measured maximum and minimum voltages, due to temporal drift in the magnitude of the microwave generator signal, can be minimised by grouping together the data in pairs of consecutive maxima and minima to find a series of VSWR

values, which can then be averaged. This is preferable to simply averaging the values of all the maxima and all the minima, then finding one single VSWR.
In fact, the signal output from the microwave generator was sufficiently constant that usually no significant difference could be detected in the values of successive maxima or minima.

The maximum and minimum signals from the detector probe correspond approximately to the squares of the maximum and minimum standing wave voltages on the slotted line respectively. An incident microwave signal was used of sufficient magnitude that, for most sample materials, both the maximum and minimum standing wave detector probe voltages were far larger than the thermal noise signal in the test-set.
Thus, except for pure fat samples, which produce almost 100% signal reflection, the error in the maximum and minimum measured detector probe voltages is equal to the reading error of the meter displaying the voltage. With the meter used, this is approximately 1% of the reading for both maxima and minima.
The VSWR is given by the root of the ratio of the maximum and minimum detector voltages.

$$VSWR = \sqrt{\left(\frac{V_{det}(\text{max.})}{V_{det}(\text{min.})}\right)} = \sqrt{(Ratio)} \qquad (5.5.1)$$

The measurement error, $\delta(Ratio)$, is equal to $\sim\sqrt{2}\%$ of the *Ratio* quantity. Hence the VSWR error is given by

$$\delta(VSWR) = \frac{\delta(Ratio)}{2\sqrt{(Ratio)}} = \frac{VSWR}{100\sqrt{2}} \qquad (5.5.2)$$

which is approximately equal to a 0.7% error. As the magnitude of the reflection coefficient is given by $|r| = \frac{VSWR - 1}{VSWR + 1}$, the error in $|r|$ is related to the error in the *VSWR* by

$$\delta|r| = \frac{2}{(VSWR + 1)^2}\delta(VSWR) \qquad (5.5.3)$$

Thus the error in $|r|$ is maximised when the VSWR is at a minimum. The smallest VSWR measured for any material was greater than 2.5. For this VSWR value, the error in $|r|$ is equal to $\sim 3\times10^{-3}$. This corresponds to a percentage error in the absolute value of $|r|$ of approximately 0.7%. Most tissue sample materials had a VSWR of around 6, which gives a measurement error in $|r|$ of ~0.25%.

For fat samples, the error in the maximum detector voltage signal is still ~1%, but the error in the minimum value is far greater, as the effect of thermal noise must be considered: $\text{True min. signal} = \sqrt{\left[(\text{Total signal})^2 - (\text{Noise signal})^2\right]}$. (5.5.4)

In such cases, there could be a 100% worst-case uncertainty in the value of the true minimum signal when the total signal was close to the noise signal. For a pure fat sample, the uncertainty was such that the reflection co-efficient could typically take a value of 0.94 ± 0.01. Although this represents an uncertainty of over $\pm 2\%$, it can be seen in fig. 5.g that the calibration curve of the open-ended probe in the low permittivity region was quite insensitive to large error in the magnitude of the reflection co-efficient. There is a further source of error in the VSWR value, originating from the uncertainty in the response of the detector probe. It has been assumed throughout, for simplicity, that the detector probe signal is proportional to precisely the square of the true standing wave voltage. However, in section 4.4, a detector probe calibration was shown, with power response given by: $V_{det} \propto (\text{Standing Wave Voltage})^{1.992}$ (5.5.5)

The error in the reflection co-efficient incurred by assuming the power response exponent of the detector probe to be equal to 2, rather than 1.992 may be evaluated thus.

Expressing the VSWR as $VSWR = (Ratio)^{\frac{1}{n}}$

gives $\Rightarrow \delta(VSWR) = -\frac{1}{n^2}\left[\ln(Ratio)\right][Ratio]^{\frac{1}{n}}\delta n$ (5.5.6)

The typical VSWR value for tissue samples was around 6. Thus the error in the VSWR from this source is around 0.04. Using eqn. 5.5.3, it can be seen that this VSWR error value yields an error of 0.25% in the magnitude of the corresponding reflection co-efficient. This error is similar in magnitude to the reading error on the maximum and minimum voltages. It may be noted that the calibration error in the detector probe response contains a contribution arising from attenuation in the slotted line over the range of probe measurement. This confirms that the attenuation error is negligible for reflection co-efficient measurements, as stated in section 4.4.

(ii). Minimum Position.

The error in the measured positions of standing wave minima is more difficult to estimate. Firstly, there is possible error in the judgement of the measurer, as to where on

the slotted line the actual minimum displayed voltage is located. Then, there is the reading error from the Vernier scale which gives the value of the chosen position of the detector probe.

Conventionally, the reading error of the Vernier scale is quoted as being ±half the minimum measurement division on the scale. On the slotted line used, the Vernier scale has divisions down to 0.1mm, so the reading error is quoted as ± 0.05mm.

Typically, the error incurred by human judgement in selecting the true minimum position, was estimated to be at least ± 0.1mm. In cases where the minimum standing wave signal was small in magnitude, the minimum position could be estimated best by measuring the position of two points either side of the minimum, which correspond to the same standing wave voltage. The point halfway between these two points was therefore the true minimum position. The overall error in positioning the standing wave minimum was estimated to be at worst equal to ± 0.2mm.

It must be noted that it is not the absolute value of the minimum standing wave position that is used in the permittivity calculations, but the value of the position relative to the adjacent short circuit null position. The phase of the reflection co-efficient θ is given by

$$\theta = \pi\left[1 - \frac{4(l_{short} - l_{sample})}{\lambda}\right] \qquad (5.5.7)$$

where l_{short} and l_{sample} are the positions of the short circuit null and the sample null respectively. Since the reactive impedance of all terminating sample materials is capacitative, the phase angle θ must always lie between $-\pi \rightarrow 0$. This means that the standing wave null position l_{sample}, must always lie in a small distance band between $\lambda/4$ and $\lambda/2$ away from its corresponding short circuit position l_{short}.

It is shown in section 5.3 that the error in $(l_{short} - l_{sample})$ may be taken exclusively as the error in l_{sample}, due to the independence of the value of the calibration factor Δ on any error in l_{short}. Therefore the error in each individual value of $(l_{short} - l_{sample})$ is ± 0.2mm in a 25mm range.

By measuring more than one value of $(l_{short} - l_{sample})$, the expected error in the mean value of $(l_{short} - l_{sample})$ can be reduced from ± 0.2mm. Consider n measurements of a parameter, each with measurement error δ, yielding results with a mean value m. If all the individual result values lie within the range defined by $m \pm \delta$, then the estimated error

in the mean value m is given by $\pm \delta/\sqrt{n}$. When making standing wave measurements on samples, the positions of four different standing wave minima were measured, relative to their respective short circuit positions. If the four values of $(l_{short} - l_{sample})$ did not lie within a $\pm$ 0.2mm range, the measurements were discarded. Thus although the measurement error, δ, on each individual value of $(l_{short} - l_{sample})$ was $\pm$ 0.2mm, the error on the mean was given by $\pm \delta/2$, which is equal to $\pm$ 0.1mm.

(iii). Overall Measurement Error.

From the above subsections, the error in reflection co-efficient magnitude arising from measurement uncertainty is composed of two approximately equal terms, each of ~0.25%. The overall measurement error in this quantity is thus approximately 0.4%. For the standing wave minima, the positional error is estimated to be around 0.1mm.

It is possible to propagate these error values through the permittivity calculation process. There is no simple algorithm to express the effect of measurement uncertainty on the uncertainty in the evaluated permittivity. Instead, for each measurement set, the maximum and minimum possible values of the real and imaginary parts of the permittivity can be evaluated by computer, using the quoted errors in $|r|$ and $(\overline{l_{short} - l_{sample}})$. Take, for example, a tissue measurement set with $|r|$ equal to $0.750 \pm 0.4\%$, and $(\overline{l_{short} - l_{sample}})$ equal to 31.0 ± 0.1mm. The program finds the maximum and minimum values of ε'_m and ε''_m within the ranges defined by $0.747 < |r| < 0.753$ and $30.9\text{mm} < (\overline{l_{short} - l_{sample}}) < 31.1\text{mm}$. Physically, this process can be illustrated by plotting both $|r|$ and $(\overline{l_{short} - l_{sample}})$ individually, as functions of the real and imaginary parts of sample permittivity, on the same graph, and then viewing the graph from directly overhead. i.e. down the direction of the z-axis. Plotting contours which correspond to the maximum and minimum values of $|r|$ and $(\overline{l_{short} - l_{sample}})$ on each surface gives an intersection area, which covers the range of values of ε'_m and ε''_m that are satisfied by the measurement set.

Figure 5.f shows such a plot, for the above measurement data using a typical probe calibration. This gives the measured dielectric constant as $\varepsilon'_m = 44.7 \pm 0.4$ and loss factor as $\varepsilon''_m = 15.3 \pm 0.3$, where the errors are due only to measurement uncertainty.

The effect of large percentage error on the reflection co-efficient magnitude for low permittivity materials is shown in fig. 5.g. Despite a worst-case error of over ± 1% in $|r|$, the calculated permittivity has a real part value of 4.2 ± 0.6 and loss factor of 1.1 ± 0.4. Therefore the absolute error due to measurement inaccuracy, on the overall permittivity value, is similar over the entire permittivity range expected of biological tissues.

5.5.2 Error in Probe Calibration.

The probe calibration allows a relationship to be established between the measured reflection co-efficient and the permittivity of the load material. Uncertainty in the probe calibration may arise from many sources. Firstly it is not certain that any admittance formula used to model the probe open-end is an exact representation of the field behaviour at the aperture. Secondly, the systematic errors in the test set may not be completely accounted for by a bilinear transform of the scattering matrix $\underline{\mathbf{E}}$ (eqn. 5.2.8). Thirdly, there is a degree of uncertainty associated with the 'known' permittivity values of each of the liquids used for calibration, and finally, all the reflection co-efficient measurements used to evaluate G_n in the calibration are subject to the uncertainties described above.

Excluding the unquantifiable systematic errors, there are 14 variables involved in the probe calibration which may be subject to uncertainty. Six variables in the three complex permittivity values of the calibration liquids, and eight variables in the magnitude and phase of the reflection co-efficients of all four calibration materials including the short circuit. It is difficult to estimate the overall error caused by these factors in the calibration of the co-axial probe.

The error on the calibration factor G_n may be written as

$$\delta G_n = \sum_{i=1,2,3,4} \frac{\partial G_n}{\partial \rho_i} \delta \rho_i + \sum_{i=1,2,4} \frac{\partial G_n}{\partial \varepsilon_i} \delta \varepsilon_i \qquad (5.5.8)$$

From eqn. 5.2.22 it may be seen that this expression, when expanded, is algebraically extremely involved. This error, and the measurement error on an unknown material must

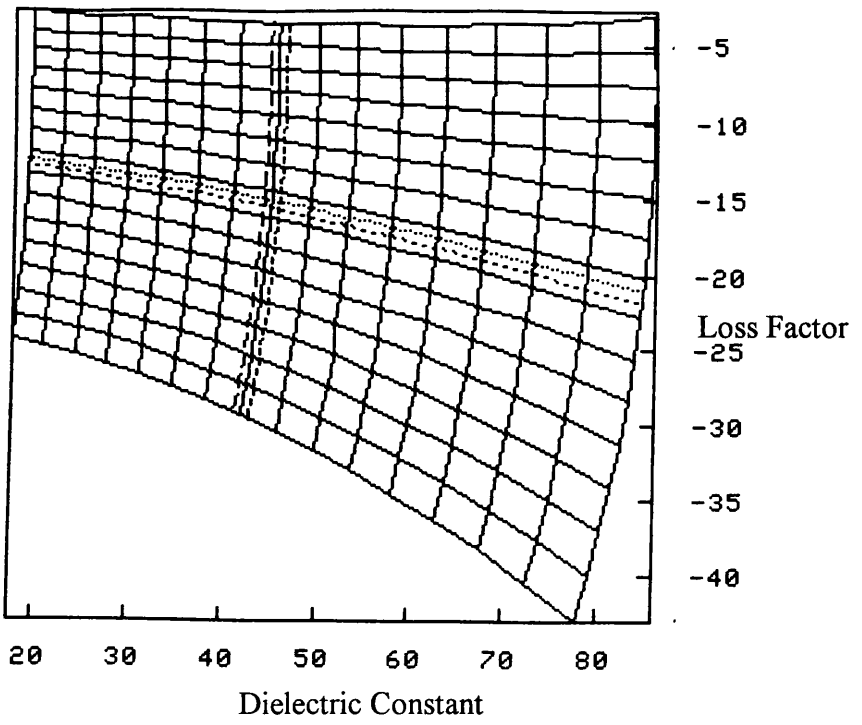

KEY

3-D Calibration Curves (viewed from overhead)

Horizontal Contour for $|r| = 0.753$

Horizontal Contour for $|r| = 0.747$

Vertical Contour for $\overline{(l_{short} - l_{sample})} = 31.1$

Vertical Contour for $\overline{(l_{short} - l_{sample})} = 30.9$

Figure 5.f. Overhead view of three dimensional curves representing the probe reflection co-efficient and standing wave minimum position as functions of load permittivity. Contours representing the maximum and minimum error limits of a typical tissue permittivity measurement give an area of intersection corresponding to the measurement error on the calculated tissue permittivity value.

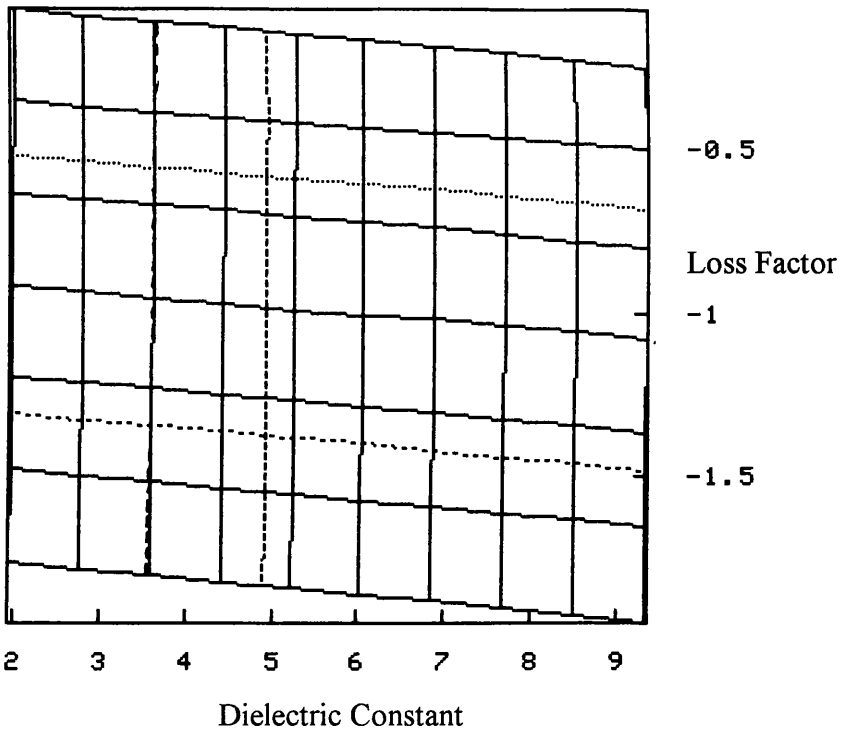

Figure 5.g. Overhead view of three dimensional curves representing the probe reflection co-efficient and standing wave minimum position as functions of load permittivity. Contours representing the maximum and minimum error limits of a tissue permittivity measurement for a typical low water content fat sample give an area of intersection similar to that for a high water content tissue, despite the higher measurement error in reflection co-efficient due to uncertainty in the noise signal.

then be propagated through eqn. 5.2.21 to give the final error on a measured permittivity value. As the initial errors $\delta\rho_i$ and $\delta\varepsilon_i$ are themselves only estimates, it is by no means certain that a meaningful estimate of the overall error will be obtained, even if all the mathematical work is undertaken.

To obtain a more physically meaningful calibration error, an alternative approach was employed. Each time the probe was recalibrated, the reflection co-efficients of all 13 liquids of known permittivity in table 4.c were measured. Four sets of results spanning the whole permittivity range of interest were used to calibrate the probe (usually short circuit, dioxane, methanol and water). Then the measured permittivity for each of the remaining liquids was calculated using the evaluated calibration factor G_n. A good calibration gave a set of measured permittivity values fully consistent with the known permittivity values of these remaining materials. If one or more of the measured permittivity values differed from the known value by significantly more than the estimated uncertainty in the known value, then all the liquids with permittivity similar to the anomalous value were remeasured until a fully consistent set of data were obtained. This way, the calibration is essentially verified for the whole permittivity range, and so the calibration error at a particular permittivity can be approximated as being equal to the error in the known values of materials with similar permittivity. Taking the errors in the known material permittivities presented in section 4.7, it is estimated that for a typical high water content tissue, with a high permittivity of ~ 50 - j18, the calibration error is approximately ± 1.5 in the dielectric constant, and approximately ± 1 in the loss factor. For lower water content tissues (some fats), the estimated calibration error is around ± 1 in the dielectric constant and ± 0.5 in the loss factor. Fats with very low permittivity, similar to that of dioxane, were subject to a calibration error which may have been even smaller than the measurement error, since the permittivity of the dioxane calibration material is very precisely known to be equal to 2.2.

When the calibration error is combined with the measurement uncertainty of around ± 0.5 in both the dielectric constant and loss factor (section 5.5.1), an overall error for a measured permittivity datum can be estimated. The measurement error is similar for all permittivity values, so the maximum expected error on a typical measurement for a high water content tissue is approximately ± 2 in the dielectric constant, and ± 1.5 in the loss factor. For the lowest water content fats, errors of approximately ± 0.75 in the dielectric constant and ± 0.5 in the loss factor are estimated.

Chapter 6. Results of Permittivity Measurements of Animal and Human Tissues.

6.1. Introduction.

In this chapter new permittivity data for human and animal tissues, measured *in vitro*, are presented and discussed. All permittivity measurements were made at a frequency of 3 GHz, using the open-ended co-axial probe technique detailed in the two preceding chapters. The data are presented according to tissue type, using the results from the more numerous domestic animal tissue samples for comparative analysis with the human tissue results. Where necessary, brief comments on the condition and physiology of tissue samples are given. Particular attention is given to fat and skeletal muscle tissue, as these are the most important tissues for thermographic modelling, due to their prevalence in the human body.

To establish consistency, comparison is also made with the permittivity values of similar tissues reported by previous researchers. A wide ranging and comprehensive review of microwave dielectric data on tissue, from which many of the comparisons herein are drawn, was published by Campbell (1990), and includes the collated data of Pethig (1984). As it is not feasible to tabulate all the measured data, most of the data is presented graphically, with tables only of average data values. Standard deviations quoted in the data tables refer only to statistical data spread on measured values. All individual data points are also subject to the experimental and calibration errors discussed in chapter 5. Tables 6.t and 6.u, at the end of this chapter, summarise the mean measured permittivity and water content values for each tissue type.

For the purposes of clarity, the number of *specimens* refers to the number of donors from which tissue of a certain type was obtained. From each tissue specimen, a certain number of *samples* were prepared, and so the number of samples is equal to the number of water content measurements for each tissue. On each sample, one or more permittivity measurements were made.

6.1.1. Tissue Specimen Sources.

All the animal tissues used in this study were obtained from local tradesmen in a state fit for human consumption. After purchase, animal tissues were kept refrigerated in a

sealed container and used within forty eight hours. Specimens of human tissue from surgery and post-mortem subjects were obtained from the pathology and mortuary departments at the Western and Royal Infirmary Hospitals, Glasgow. Most of the breast, uterus and tumour tissues measured in this study were acquired from surgery subjects, whilst post-mortem sources provided all the muscle and other major organ tissues. For hygiene reasons, only otherwise healthy tissue was taken from the post-mortem subjects, who had deceased no more than twenty four hours prior to tissue excision. After excision, human tissue specimens were refrigerated in a sealed container until measurements were made, which was usually within twenty four hours.

6.1.2. Sample Water Content.

After dielectric measurement, each tissue sample was placed in an open glass petri-dish, lined with aluminium foil. The sample was then dehydrated by placing the dish in a drying oven until it reached a stable mass. This usually took around sixteen hours, but could be longer for large samples. Preliminary investigation into the oven drying procedure was made with samples containing computer monitored thermocouples. An oven temperature of 85°C was finally chosen for drying the samples, as it was at about this temperature that most tissue samples showed balance between the energy absorbed through conduction, and that lost by evaporation. The mass of the petri-dish was measured with and without the sample, both before and after drying, to establish the mass fraction of water in the sample. An electronic balance with a resolution of 0.001g was used, giving an uncertainty of $\pm$ <0.3% in the calculated water content of a typical sample with initial mass ~1g.

When relating water content to dielectric measurements, it should be noted that the dielectrically measured tissue volume was far less than the total sample volume used in water content measurement. In order that the measured water content should accurately represent that of the probed volume, samples were sectioned to be as uniform as was possible to judge, and dielectric measurements were always taken on a part of the sample which appeared to be typical of the sample as a whole.

6.1.3. Human Tissue vs. Animal Meat.

There is great physiological similarity between the equivalent tissues of human and common domestic animal species. This is particularly true of porcine tissue; the pig is often used in medical research to test treatments prior to human trials. Several slight differences do exist between human tissue and animal meat that could affect the microwave permittivity.

The tissue of the young animals used for commercial meats typically has a higher water content than that of adults, perhaps of the order of ~2% (Biology Data Book, 1972). However, the tissue of livestock animals may be comparatively more fibrous than that of humans. This would tend to cancel the above effect when comparing human with animal tissue.

Perhaps the difference most important here is the absence of residual blood in animal meat. This may cause a water content difference of several per cent, which can affect the 3 GHz permittivity significantly, and is discussed in more detail where appropriate.

6.2. Fat Tissues.

Present subcutaneously and around internal organs, fat tissue is a low water content connective adipose tissue, mainly composed of lipids and sterols. A lipid is an ester of a fatty acid (long-chain carboxylic acid) and an alcohol, such as glycerol. Sterols are high molecular weight monohydroxy alcohols. As the cells in fat tissue contain very little water, most of the water present is the extracellular type.

Fat tissues have a disperse mesh of delicate fibres, and very low blood supply *in vivo*, as blood is not required for the tissue to fulfil its protective and energy-storing functions ('The Human Body', Brooks and Brooks, 1980). Human and animal fatty tissues contain differing profiles of the various fat molecules, particularly in the relative amounts of saturated and unsaturated fats. Because of these differences, subcutaneous human fatty tissues are typically softer than those of animals. However, as all fats are large molecules, they all have a low 3 GHz permittivity, and so this physiological difference does not affect the microwave tissue permittivity.

Fat tissues have a wide range of water content, so there is no single value for the density of fat tissue. For the purpose of analysis by volume fraction mixture equations therefore, the density of *dehydrated* fat tissue is taken to be 0.86g/ml (Schepps and Foster, 1980).

6.2.1. Animal Fat Tissue.

A total of 74 water content and permittivity measurements were made on porcine fat, originating from cuts of meat from two areas: firstly, from the lumbar area of the lower back, between the pelvis and the ribs, which is commonly referred to as the '*loins*'; and secondly, from the fattened area around the ribs, commonly known as the '*chops*'. Forty three measurements were made on agnine fat; subcutaneous fat from the rib area, and also internal fat from around the heart and kidneys were investigated. The bovine fat, on which 35 measurements were made, originated from the loins, and from around the kidney. Table 6.a shows the average results of this total of 152 permittivity measurements on porcine, bovine and agnine fat, from both external and internal regions. A number of dehydrated internal agnine fat samples from around the kidney and heart were also measured, so as to obtain a permittivity value for *pure fat* to be used in mixture equations.

6.2.2. Overall Results of Animal Fat Measurements.

The ranges of water content and permittivity values measured on all animal fats are shown in the histograms of fig. 6.a, and may be summarised;

- Water Content: Min. value 2.8% Max. value 30.7% Mean value 13.4%
- Dielectric Constant: Min. value 2.1 Max. value 19.3 Mean value 4.43
- Loss Factor: Min. value 0.0 Max. value 6.5 Mean value 0.73

Taking into account all the fat permittivity measurements, an overall mean permittivity value of $4.43 \pm 2.13 - j0.73 \pm 0.78$ was found. The maximum measured values of the dielectric constant and loss factor were exceptional, and do not correspond to the general distribution of values. As can be seen from the histograms, there are only 9 data points out of 152 with a dielectric constant greater than 7, or loss factor greater than 1.5. This indicates that only small regions of fat tissue have a high permittivity and that the

Source of Fat Tissue	No. of Specimens	No. of Samples	No. of Perm. Measurements	Mean Dielectric Constant	Mean Loss Factor	Mean (%) Water Mass Fraction	Mean (%)Water Volume Fraction
Porcine							
Rib	3	23	23	5.46 ± 3.02	1.21 ± 1.04	14.7 ± 5.5	12.9
Lumbar	2	51	51	4.74 ± 0.61	0.74 ± 0.20	14.8 ± 3.8	13.0
Agnine							
Rib	2	7	7	8.63 ± 5.81	2.26 ± 2.33	16.6 ± 6.5	14.6
Heart	1	12	12	4.05 ± 0.37	0.42 ± 0.11	16.8 ± 1.9	14.8
Kidney	1	24	24	2.78 ± 0.42	0.20 ± 0.15	4.7 ± 1.3	4.1
Bovine							
Lumbar	3	18	18	3.67 ± 0.87	0.57 ± 0.29	12.3 ± 3.4	10.8
Kidney *	1	17	17	3.79 ± 0.76	0.56 ± 0.26	16.8 ± 4.7	14.8
Overall Fat	13	152	152	4.43 ± 2.13	0.73 ± 0.78	13.4 ± 5.6	11.7
Dehydrated Agnine Fat							
Heart	1	12	12	3.00 ± 0.31	0.06 ± 0.11	0	0
Kidney	1	20	20	2.30 ± 0.27	0.10 ± 0.11	0	0
* Sample contained blood vessel, therefore unrepresentatively high water content							

Table 6.a. List of mean permittivity and water content values measured on animal fat tissues.

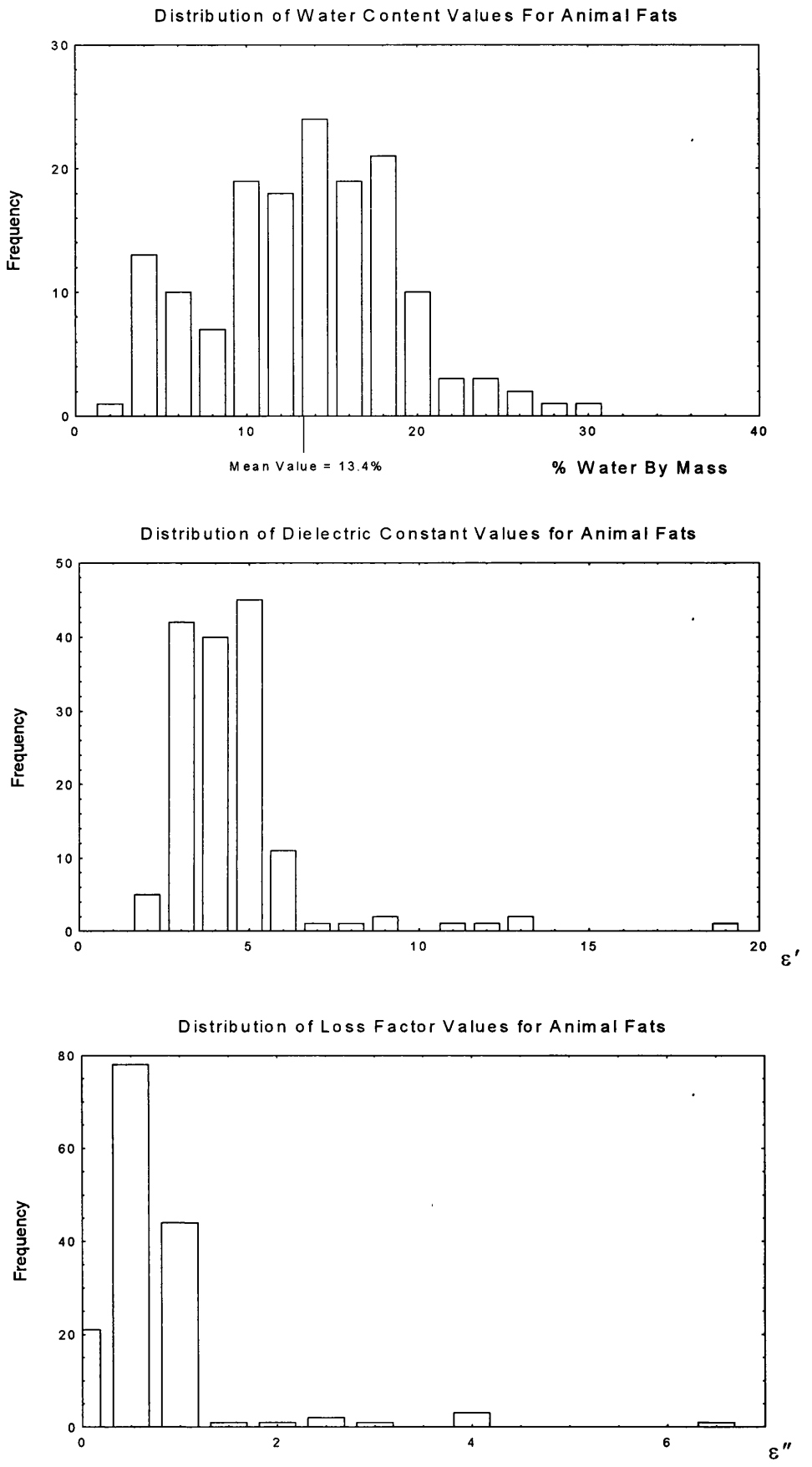

Figures 6.a. Histograms showing distribution of water content and permittivity measurement values for all animal fats.

majority of the volume of the fat tissue is characterised by a low value of permittivity. For all fat from subcutaneous muscular regions, most of the low permittivity values were found in measurements on the larger areas of fat tissue found nearest to the skin surface of each specimen. Higher permittivity values were usually observed in fat tissue located in smaller volumes, away from the skin surface towards the boundary between fat and muscle tissue, as shown in fig. 6.b.

The large volumes of fat located around the agnine kidneys gave the lowest and most consistent permittivity readings and also the lowest water content values. Bovine fat from similar locations gave low permittivity readings, but the specimen measured contained an interior artery, which raised the measured water content by an unknown amount. It is fat from these regions which is used to make suet, so the low water content measured for this fat is likely to be typical in all animals.

Analysis of permittivity data by direct comparison of the dielectric constant with the loss factor of tissue permittivity data has been found to be a revealing technique. Campbell's study on human breast fat permittivity data indicated a well correlated linear relationship between these two factors. That is, each given value of the dielectric constant tends to be uniquely associated with a particular value of the loss factor. Knowledge of the form of this relationship is of great use in tissue dielectric modelling. Permittivity data with higher values of dielectric constant and loss factor are in general indicative of higher local water content in the volume of dielectric measurement.

When plotted in this form (figs. 6.c), the current animal fat data also display linear relations, which can be expressed by:

$\varepsilon'' = 0.353\varepsilon' - 0.836$ corr. co-eff. = 0.966 for all the non-dehydrated data,

$\varepsilon'' = 0.343\varepsilon' - 0.814$ corr. co-eff. = 0.958 for the porcine fat data, and

$\varepsilon'' = 0.374\varepsilon' - 0.930$ corr. co-eff. = 0.985 for the agnine fat data. (6.2.1)

There was insufficient data spread on the bovine fat measurements to fit a meaningful straight line.

Although there are small differences between the straight line fits for porcine and agnine fat data, these may not be significant; over the range of values of the dielectric constant obtained for fat samples, the deviation in loss factor between the two linear approximations for porcine and agnine fat is less than the experimental error in the data

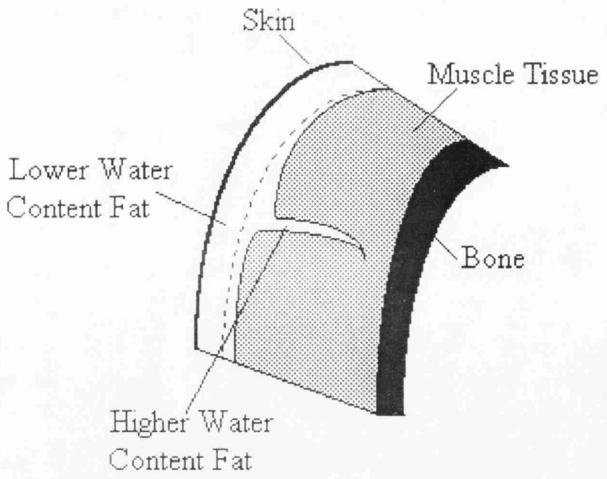

Figure 6.b. Schematic cross-sectional diagram of typical tissue specimen from which fat tissue samples were taken, showing regions where the low and high permittivity fat samples generally originated.

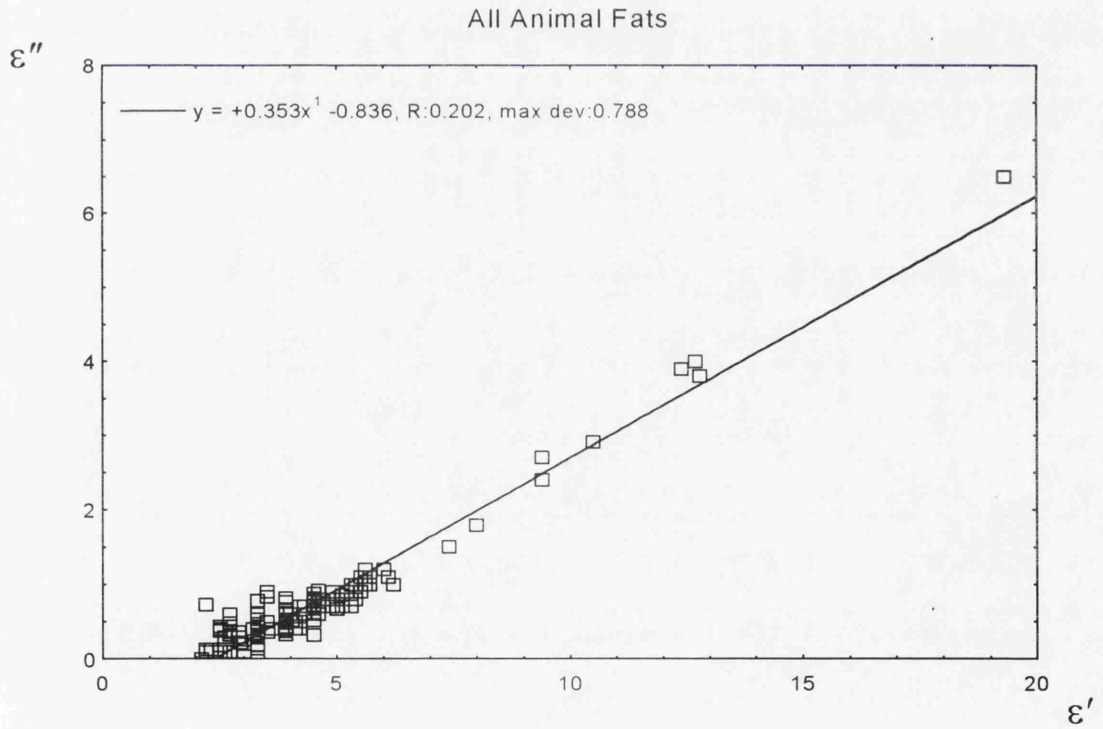

Figure 6.c(i). Measured loss factor vs. dielectric constant for all animal fats. Correlation co-efficient of straight line fit = 0.966

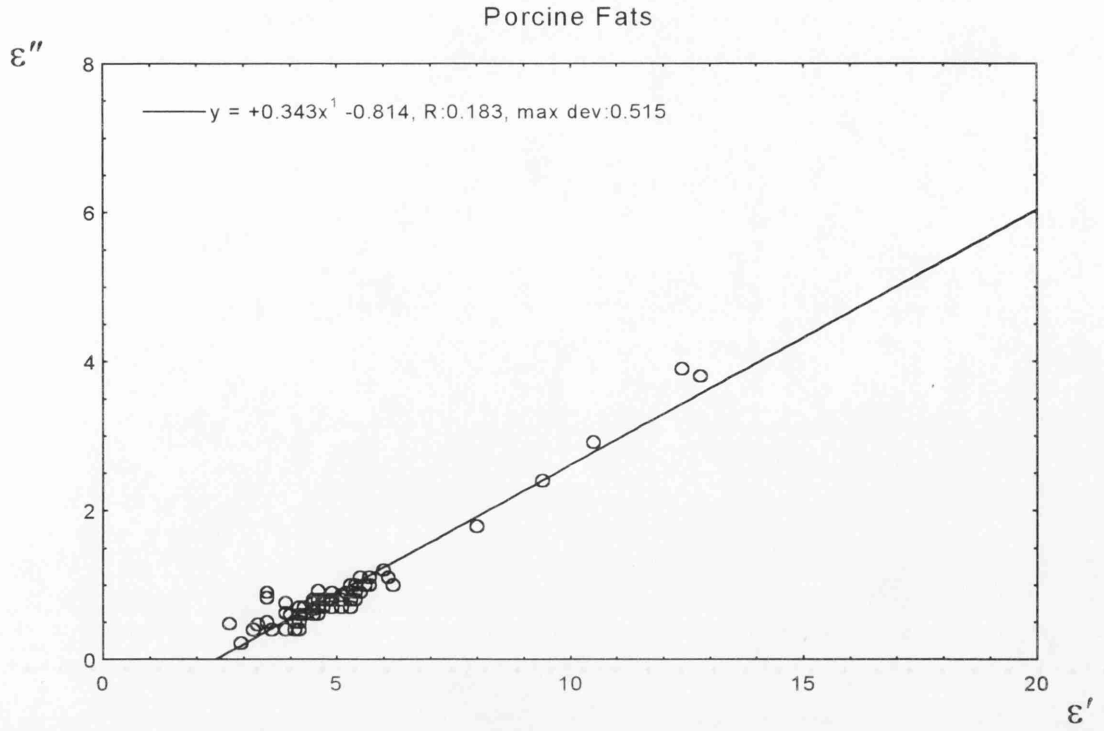

Figure 6.c(ii). Measured loss factor vs. dielectric constant for porcine fats. Correlation co-efficient of straight line fit = 0.958

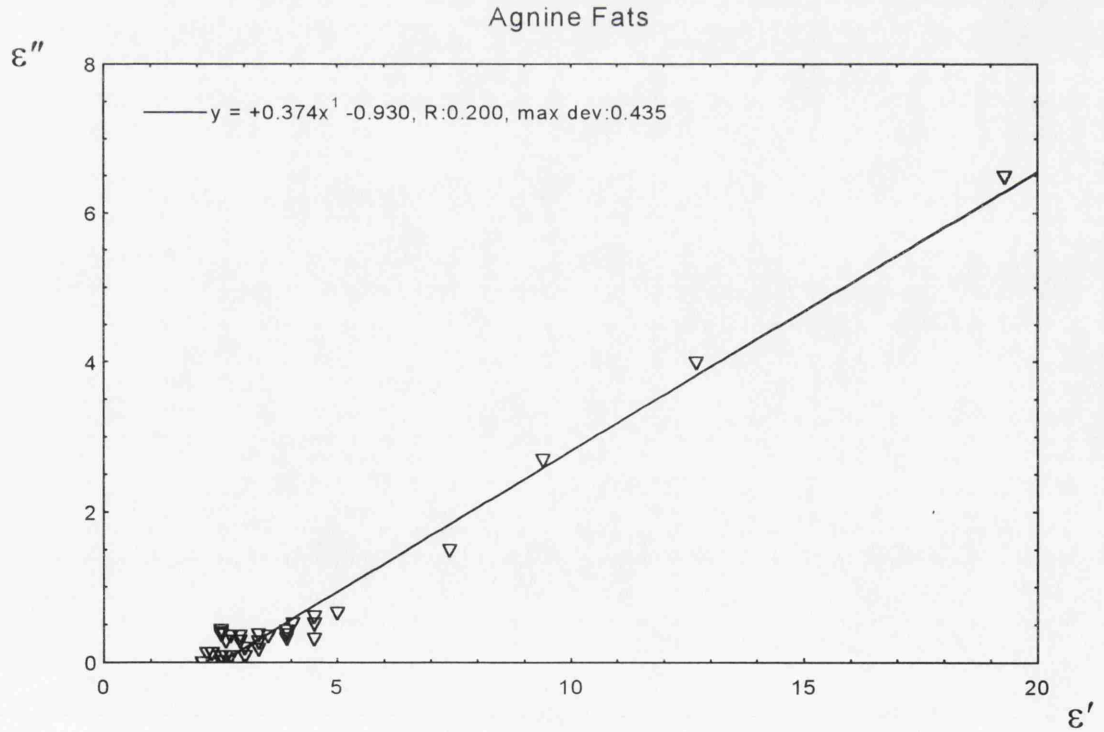

Figure 6.c(iii). Measured loss factor vs. dielectric constant for agnine fats. Correlation co-efficient of straight line fit = 0.985

incurred by the co-axial probe measurement technique. This suggests that the relationship is essentially the same for both types of tissue.

Because the majority of measurements on fat yielded low values of dielectric constant, loss factor and water content, the linear approximations are biased towards these low results, which have greater proportional spread. By considering only those results which yielded permittivity data with a dielectric constant greater than 7, the relationship between dielectric constant and loss factor for higher water content regions of fat tissue can be more closely investigated.

Figure 6.d shows the linear variation for only those high permittivity fat data, from both porcine and agnine samples. Removal of the cluster of data at the lowest values of dielectric constant shows that the relationship between dielectric constant and loss factor at higher values of dielectric constant tends to be characterised by a rather steeper gradient. The relationship is now given by

$$\varepsilon'' = 0.418\varepsilon' - 1.45 \qquad \text{corr. co-eff.} = 0.996 \qquad (6.2.2)$$

As the correlation co-efficient for this line is considerably higher than those of the overall data fit lines, it seems that this expression better represents the behaviour of fat tissues with higher than average permittivities, and that the linear relationship is slightly less pronounced at low permittivities.

The high correlation co-efficient, and the fact that the maximum deviation from the overall data fit line is less than the experimental error, suggest that this relationship is a good approximation for the dielectric behaviour of fat tissues in this permittivity range for either of these animals.

6.2.3. Dehydrated Animal Fat Measurements.

Thirty two permittivity measurements were made on internal agnine fat samples, from the heart and kidney areas, which had had their water content removed by oven dehydration. These dehydrated measurements are of particular use when analysing the normal animal fat data by the use of mixture equations. Unfortunately, fewer dehydrated fat samples were measured than was desired; firstly, many of the samples, when dehydrated, were not of a suitable consistency for dielectric measurement by the co-axial probe, and secondly, contamination of the co-axial probe by pure fat was found to be very hard to remove without necessitating lengthy recalibration.

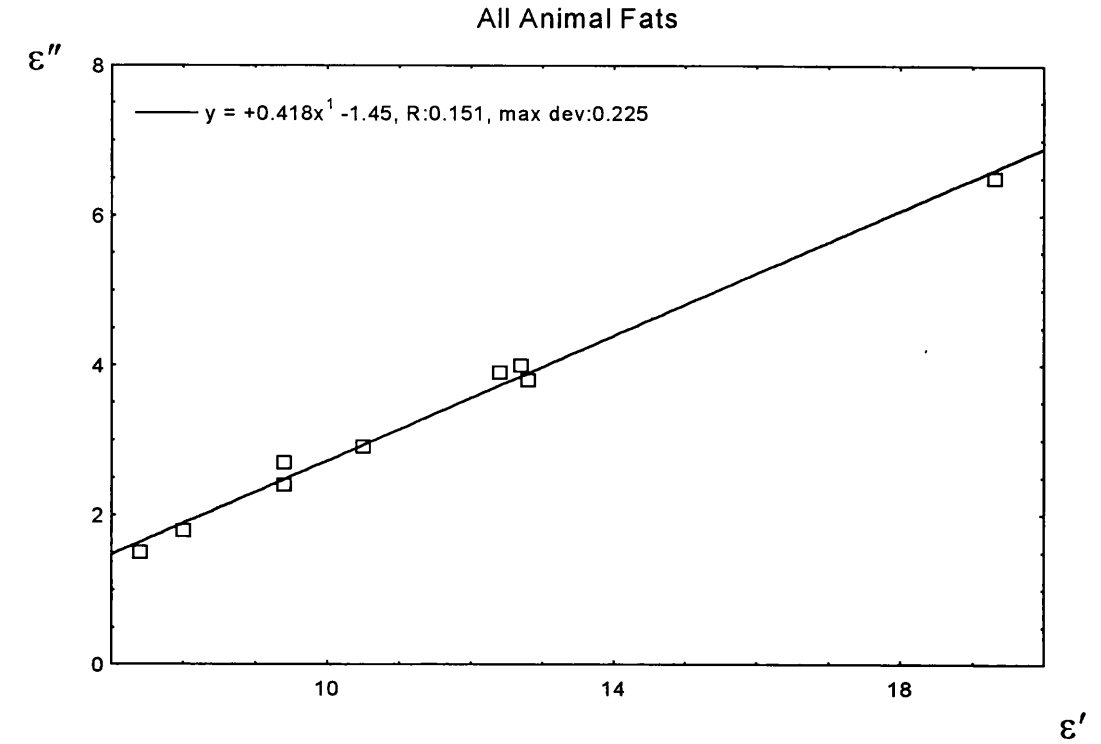

Figure 6.d. Loss factor vs. dielectric constant for all animal fat data with $\varepsilon' > 7$. Correlation co-efficient of straight line fit = 0.996

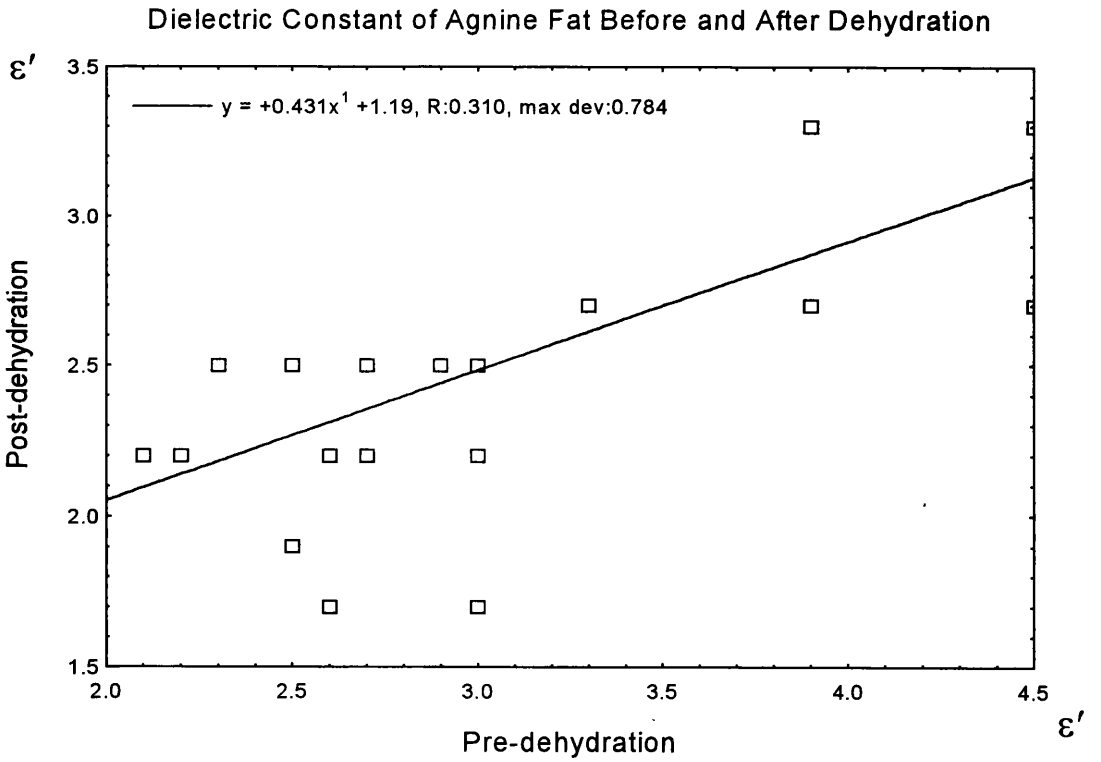

Figure 6.e. Post-dehydration vs. Pre-dehydration dielectric constant for agnine fats. Correlation co-efficient of straight line fit = 0.533

Values of the dielectric constant of pure fat were found to range from 1.7 to 3.3, with a mean of 2.6, and the loss factor ranged from 0 to 0.24, with a mean of 0.09. These values are in close agreement with data presented by Campbell (1990), which gave an average value of $2.7 - j0.2$ for the complex permittivity of dehydrated human breast fat tissue.

As is shown in fig. 6.e, and by the data in table 6.a, the fat tissue samples with the higher initial (pre-dehydration) permittivity generally yielded higher permittivities when dehydrated, although the correlation co-efficient has a value of only 0.533, which is rather poor. This was found to be true even for a variety of samples from the same tissue specimen. It is therefore possible that those non-dehydrated fat tissues with higher or lower than average permittivities may have a pure fat component with a higher or lower permittivity than the average for pure fat.

All of the straight line approximations for non-dehydrated animal fat data intercept with the dielectric constant axis at a value between 2.4 and 3.5. This is approximately the same value as the average measured dielectric constant of pure fat, 2.6 ± 0.4, evaluated by the measurements made on dehydrated samples.

6.2.4. Mixture Equation Analysis of Animal Fat Permittivity Results.

For mixture equation analysis, all of the individual animal fat permittivity data are displayed in figs. 6.f, together with the Hashin-Shtrikman limits on a mixture of two substances with permittivities $75 - j22$ and $2.5 - j0.2$. These two permittivity values have been chosen to represent the permittivity of extracellular electrolyte and pure fat respectively, and have been verified by the measurements on aqueous solutions discussed in section 3.9, and by the measurements on pure fat detailed above.

It can be seen that the large majority of data lie near the Hashin-Shtrikman lower limit, which suggests strongly that fat tissues may be closely modelled by a Maxwell-type mixture equation for a suspension of small particles of extracellular water in a continuum medium of pure fat.

As a range of values for the permittivity of pure fat was measured, the true Hashin-Shtrikman limits relating to each individual datum may vary, according to the varying permittivity of the pure fat component. Figure 6.g shows all the measured dielectric

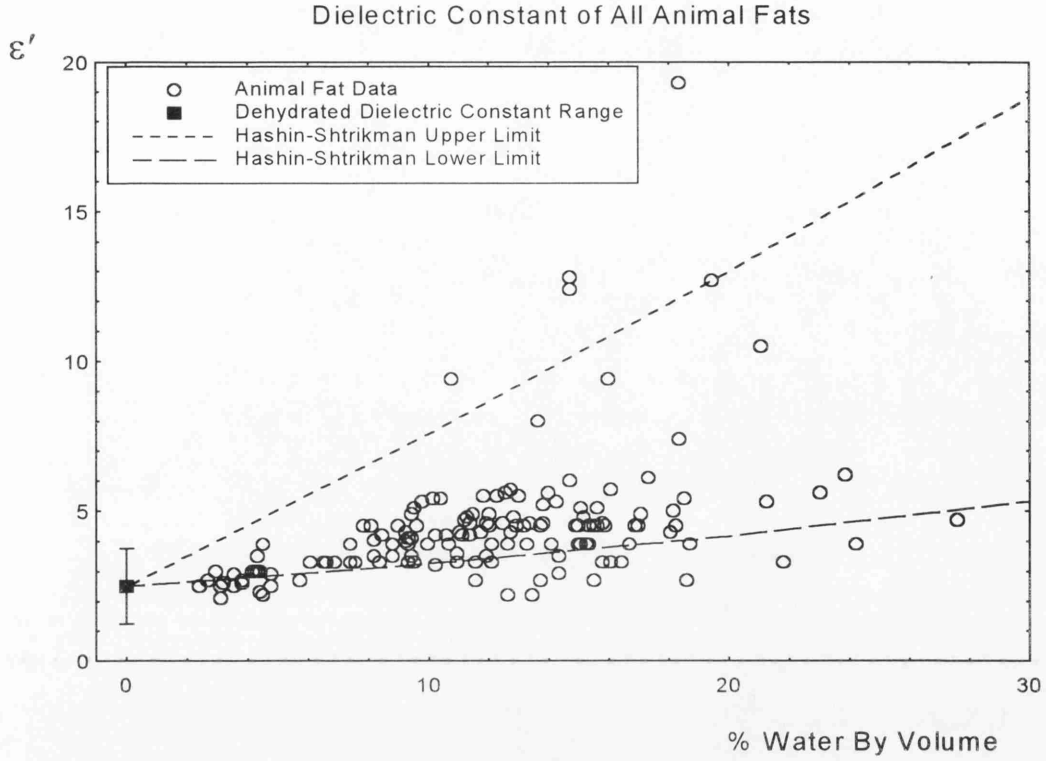

Figure 6.f(i). Measured dielectric constant vs. volume water content for all animal fats. Hashin-Shtrikman mixture equation predictions and range of dielectric constant measured on dehydrated animal fat also shown.

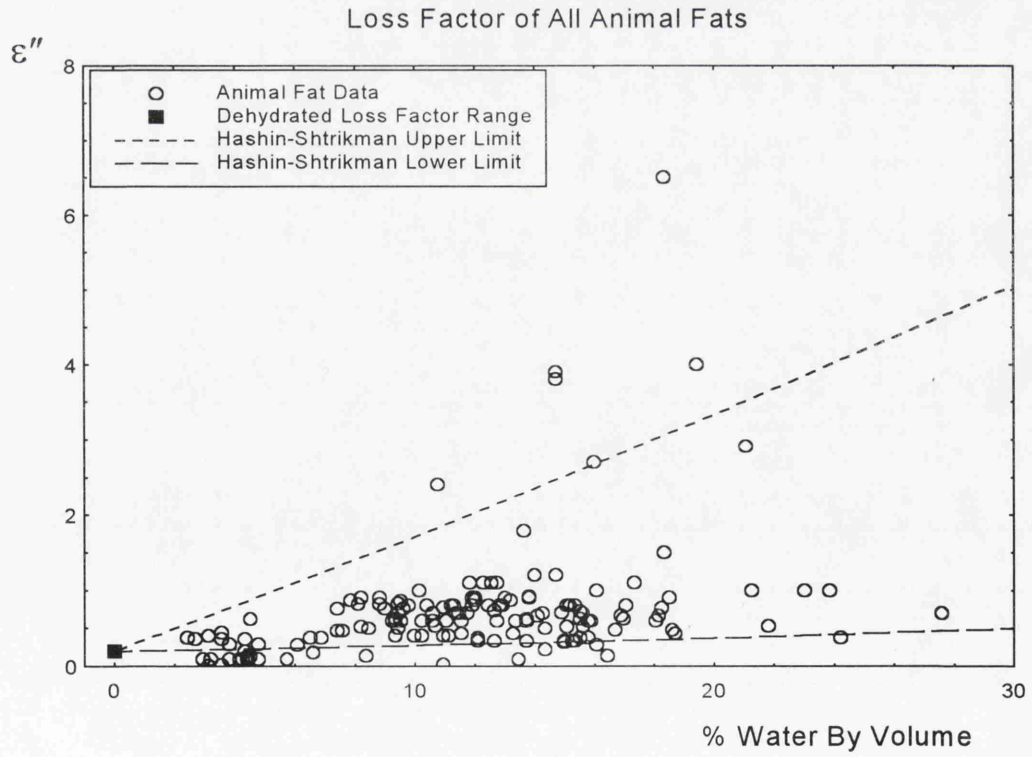

Figure 6.f(ii). Measured loss factor vs. volume water content for all animal fats.

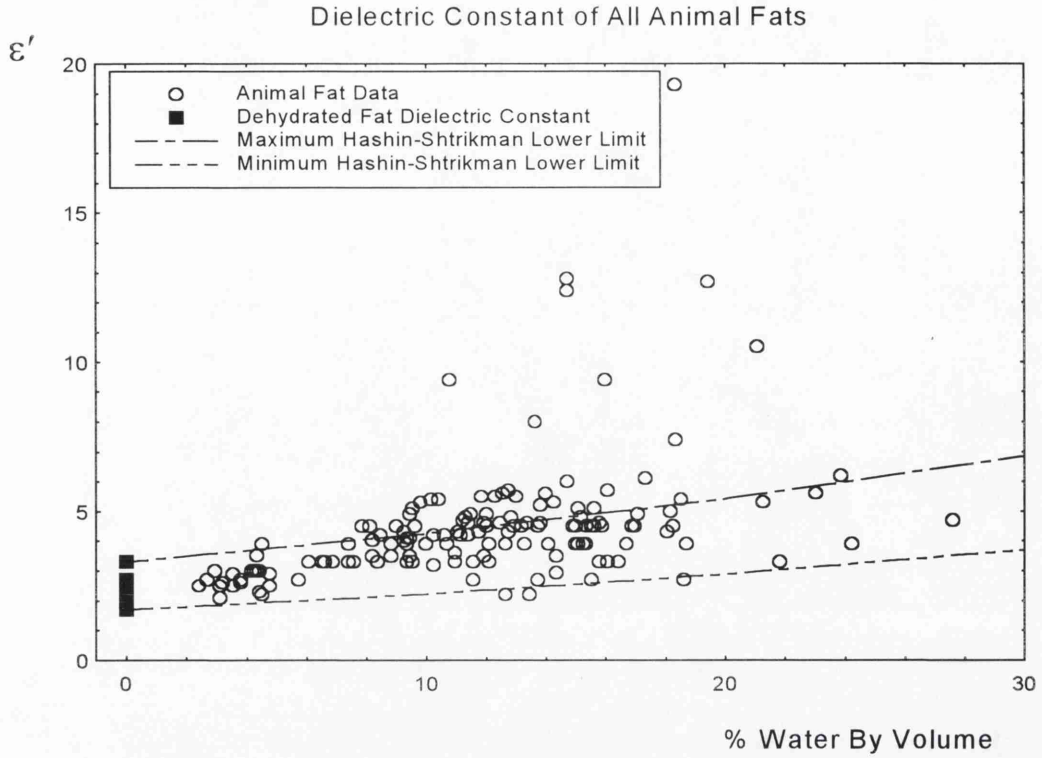

Figure 6.g. Dielectric constant of all animal fats compared with two Hashin-Shtrikman lower limit predictions based on extreme values of the dielectric constant of dehydrated fats. Range of dielectric constant of dehydrated animal fat also shown.

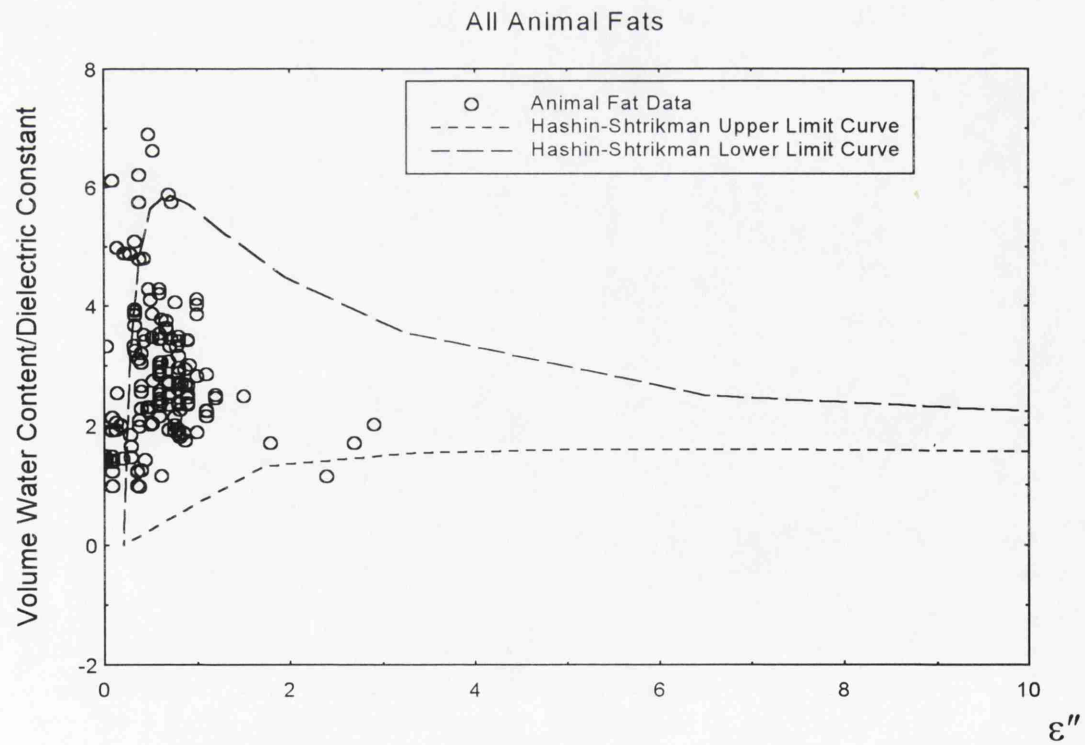

Figure 6.h. Graph of water content/dielectric constant vs. loss factor for all animal fats, showing closer agreement with the Hashin-Shtrikman lower limit.

constant values, plotted with *two* Hashin-Shtrikman lower limits, respectively calculated using the two limiting values of 3.3 - *j*0.24 and 1.7 - *j*0 for the measured permittivity range of pure fat. Approximately seventy five percent of the measured data lie in the region delineated within these lower limits. Of those points lying outwith these limits, most are distant by an amount less than the experimental error on their value. The few still remaining unaccounted for may be the results of measurements on samples with an unrepresentative measured water content, or may have been samples not entirely composed of fat tissue.

The correlation between the measured animal fat permittivity data and the Hashin-Shtrikman lower permittivity limit is further accentuated in fig. 6.h, which directly relates the water content with both the real and imaginary parts of the permittivity of each datum individually.

6.2.5. Summary of Animal Fat Results.

In conclusion, the range of values of dielectric constant and loss factor obtained by these measurements on animal fat tissues, indicates the degree of variability of fat tissue that may be expected, even in a localised volume of tissue from one specimen. The dielectric constant of the tissue may range from 2 to 20, the loss factor from close to 0 to 6, and the water content, by weight, from 4% to 25%, although apparently fatty local tissue volumes may have even higher proportions of water.
Most porcine, bovine and agnine fat tissue has a dielectric constant of between 3 and 5 (see fig. 6.a), and can be modelled by the Maxwell mixture equation for a suspension of electrolytic water in pure fat. The mean loss factor of fat is around 0.75, and generally follows the Maxwell equation prediction, but less closely than the dielectric constant. At such low values of loss, however, this is not necessarily an important deviation. As the water content of fat tissue increases, there is a trend towards an increase in the dielectric constant and loss factor, with a very clear linear relationship between these two parameters. The gradient of this relationship, and the extrapolated zero water content limiting values of the dielectric constant, are in close agreement with the measured permittivity values of pure dehydrated fat, and display the same behaviour as the observations made by Campbell on human breast fat tissue.

There is very little published data on animal fats with which to compare the current results. Smith and Foster (1985) made room temperature measurements on eighteen canine and equine fat samples at frequencies up to 1 GHz. Extrapolating their results to 3 GHz gives a permittivity value of around 12 - $j2$, for tissue with a water content of around 20%. This is in general agreement with the data presented here, although the ratio of loss factor to dielectric constant is rather lower. Significantly, they also found that there was a twofold range in measured permittivity values and a variety of water contents, from 8% to 26%, even for tissue samples ostensibly with the same provenance. For mixture equation analysis these investigators used a value of 2.5 - $j0$ for the permittivity of pure fat, based on measurements of oleic acid, used as a lipid phantom. This value is in accordance with the measurements on dehydrated fat presented here.

6.3. Human Fat Tissue.

A large majority of the human fat permittivity measurements presented here were made on tissue from the female human breast. This is one of the regions currently of greatest interest to the practical applications of microwave thermography. Fatty tissue from the breast is composed of lobules of fat partitioned by fibrous connective tissue, and interspersed with glandular tissue and lactiferous ducts. Breast tissue specimens were obtained from surgery and post-mortem sources. Each donor is believed to have been a post-menopausal woman.

One hundred permittivity measurements were made on fatty female breast tissue which was obtained from eight individual donors. The results of permittivity measurements on human fat samples are listed in table 6.b. Samples of fat from around the colon, heart and pancreas were obtained from one donor for each tissue type respectively. A total of 21 measurements were made on these tissues.

It was intended to measure the thermal conductivity in addition to the dielectric permittivity on as many samples as possible, and as tissue specimens were limited in number, many permittivity measurements were made on each sample. These measurements were made in such a way as to investigate all local areas of each sample. By visual inspection it was possible to select areas of each sample which were composed mainly of fat, or mainly of fibrous tissue. Those measurements known to be taken on solely fibrous breast tissue are presented in section 6.5. However, due to the

Source of Human Fat Tissue	No. of Specimens	No. of Samples	No. of Perm. Measurements	Mean Dielectric Constant	Mean Loss Factor	Mean (%) Water Mass Fraction	Mean (%)Water Volume Fraction
Colon	1	1	3	17.0 ± 6.2	4.57 ± 1.90	38.9	35.4
Heart	1	4	4	13.3 ± 5.3	2.88 ± 1.68	28.6 ± 3.6	25.6
Pancreas	1	2	14	13.4 ± 5.6	3.91 ± 2.23	30.5 ± 3.1	27.4
Breast	8	32	100	6.47 ± 3.49	1.02 ± 1.14	16.2 ± 4.5	14.3
Overall	11	39	121	7.76 ± 4.80	1.51 ± 1.71	18.8 ± 7.5	16.6

Table 6.b. List of mean permittivity and water content values measured on human fat tissues.

inhomogeneity of breast tissue, many of the data in this current section may be the results of permittivity measurements on tissue volumes composed of a combination of tissue types. This is useful in providing data with a wide range of permittivity values, from which the overall dielectric behaviour of breast tissue may be estimated, but has the unfortunate consequence that a considerable range of permittivity values is associated with each water content datum. Detailed analysis of the results by mixture equations is therefore not possible.

6.3.1. Overall Results of Human Breast Fat Measurements.

The histograms of fig. 6.i show the distribution of individual permittivity data and water contents for fatty breast tissue, which can be summarised;

- Water Content: Min. value 10.8% Max. value 32.1% Mean value 18.8%
- Dielectric Constant: Min. value 3.3 Max. value 22.5 Mean value 6.5
- Loss Factor: Min. value 0.05 Max. value 6.6 Mean value 1.02

The short-range inhomogeneity of breast fat was illustrated by the fact that the ranges of permittivity measured on each sample (of mass ~4g) were found to be essentially independent of the net water content of the sample. Even samples with net water contents that differ by a factor of two of more had local areas with similarly high and low permittivity limits.

It can be seen that most data lie in the low permittivity region, with 67% of data giving a dielectric constant of less than six, and 68% percent of data giving a loss factor of less than one. Campbell's (1990) permittivity measurements, made on samples identified as being composed entirely of fat tissue gave a mean dielectric constant of 4.85 ± 1.10 and a mean loss factor of 0.87 ± 0.33. These values correspond to the histogram peaks of the current data, which suggests that the majority of true pure fat tissue in the female breast has a permittivity in this range. The distribution of measured sample water contents also shows a distinct bias towards the lower water content region, with the difference between the minimum value and the mean being only one quarter of the difference between the minimum and maximum values. It will be noted that both of these sets of human fat permittivity data give a slightly higher average permittivity than that value observed on animal fat.

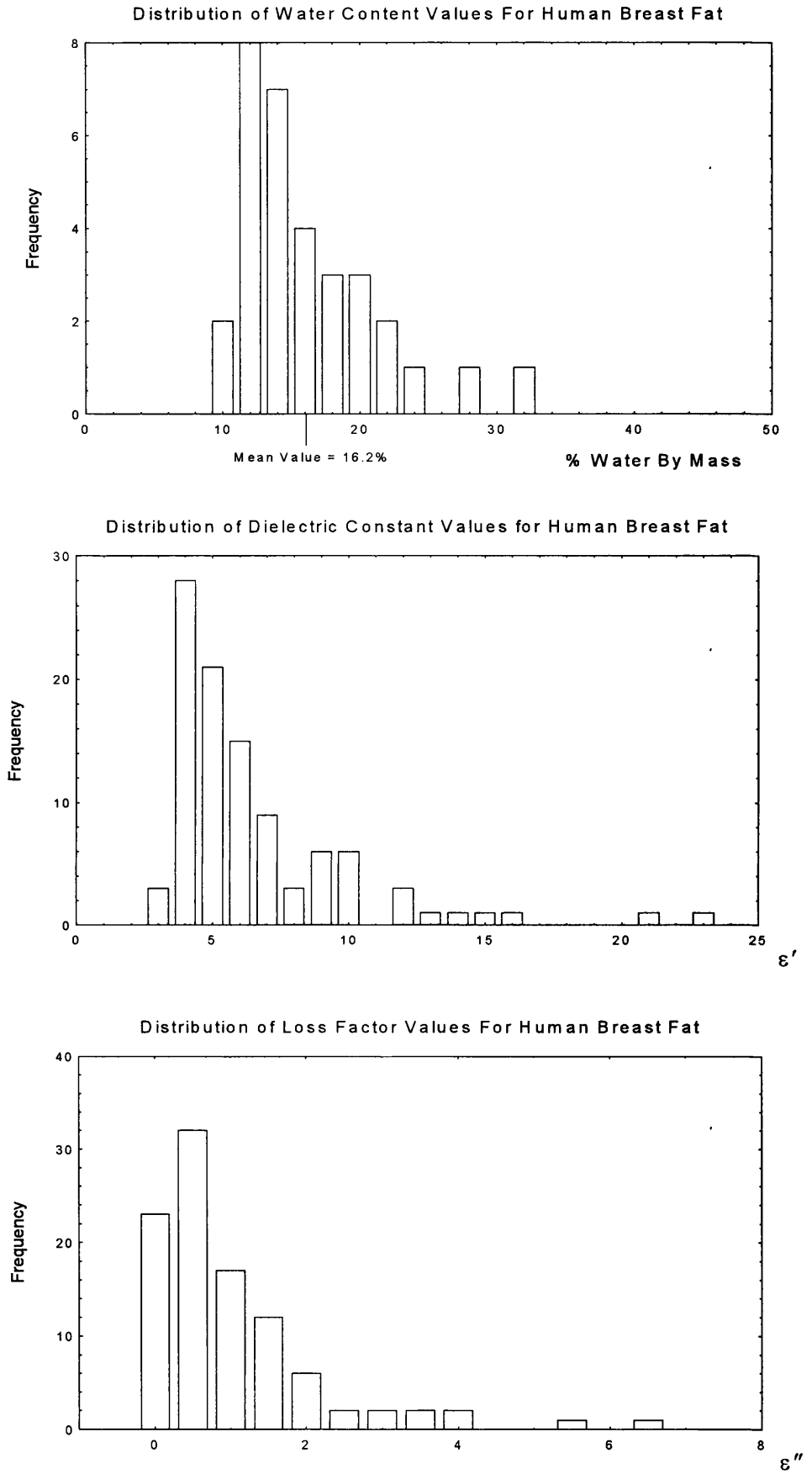

Figures 6.i. Histograms showing distribution of water content and permittivity measurement values for human breast fat.

From the current data it is possible to conclude that dielectrically, the human breast of post-menopausal women may be mainly composed of fat tissue with a permittivity of around 5 - j0.85 and water content of around 12%, interspersed with inhomogeneous and irregular regions with much higher water content and permittivity. As with the animal fat, a linear relationship, shown in fig. 6.j, is observed between the loss factor and dielectric constant in breast fat tissue, and which is expressed by

$$\varepsilon'' = 0.323\varepsilon' - 1.07 \qquad \text{corr. co-eff.} = 0.986 \qquad (6.3.1)$$

There is some deviation between this line and those best-fit lines calculated for animal fats. Although the intercept values are similar, the gradient of the fit for human breast fat data is rather lower. At values of dielectric constant above approximately 15, the expected loss factors of animal fat and human breast fat differ by a greater amount than the combined measurement error.

6.3.2. Human Fat from Non-Breast Regions.

Figure 6.k shows the permittivity data from the colonic, heart and pancreatic regions. As far as can be deduced from the limited data available, the linear relationship displayed by breast fat is also displayed by fat from around the heart and colon.

The pancreatic fat appears to conform to a relationship more similar to that of animal fat, with greater gradient than the other human fat tissues, and which can be expressed by

$$\varepsilon'' = 0.398\varepsilon' - 1.42 \qquad \text{corr. co-eff.} = 0.996 \qquad (6.3.2)$$

The reasons for the discrepancy between pancreatic and other human fats are not clear, but is was noted that the pancreatic fat was similar to animal fats in that it was more rigid than the breast, colon and heart fats, and could be prepared as regularly shaped free-standing samples. Permittivity measurement of many specimens of each of these fat tissues is however required before a definite and consistent difference between fat tissues can be established.

6.3.3. Comparison with Previous Permittivity Measurements.

An interesting comparison can be made between the current results and those presented by Campbell, which are displayed in fig. 6.l. In the previous study, the maximum

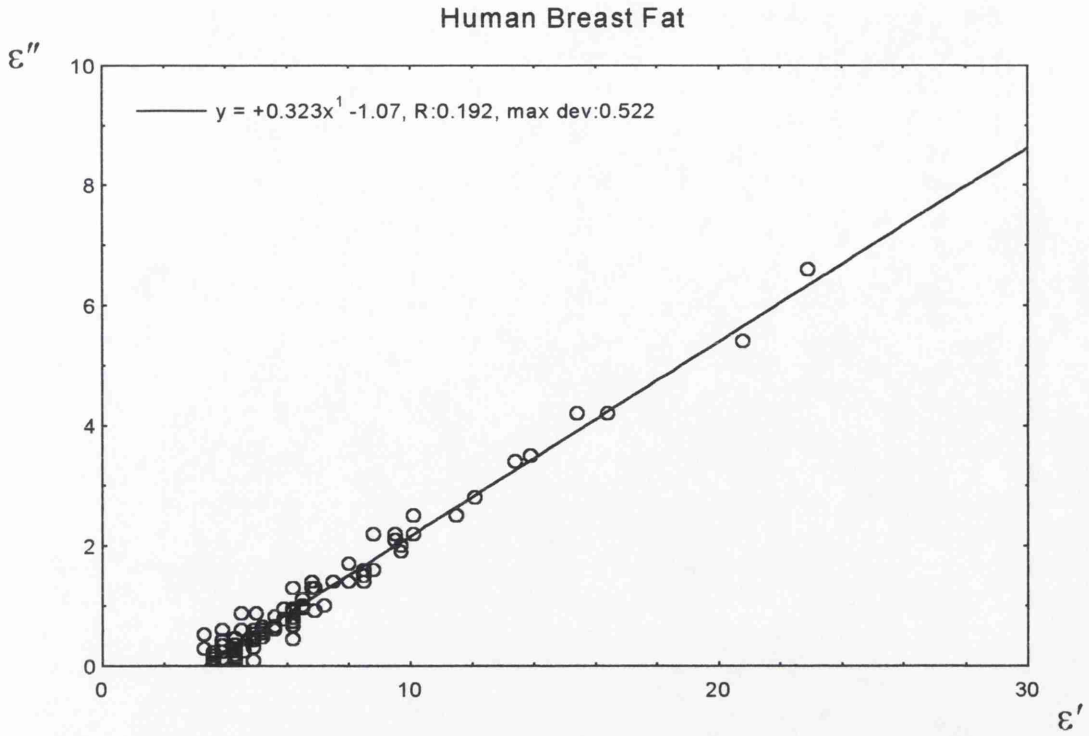

Figure 6.j. Measured loss factor vs. dielectric constant for human breast fat. Correlation co-efficient of straight line fit = 0.986

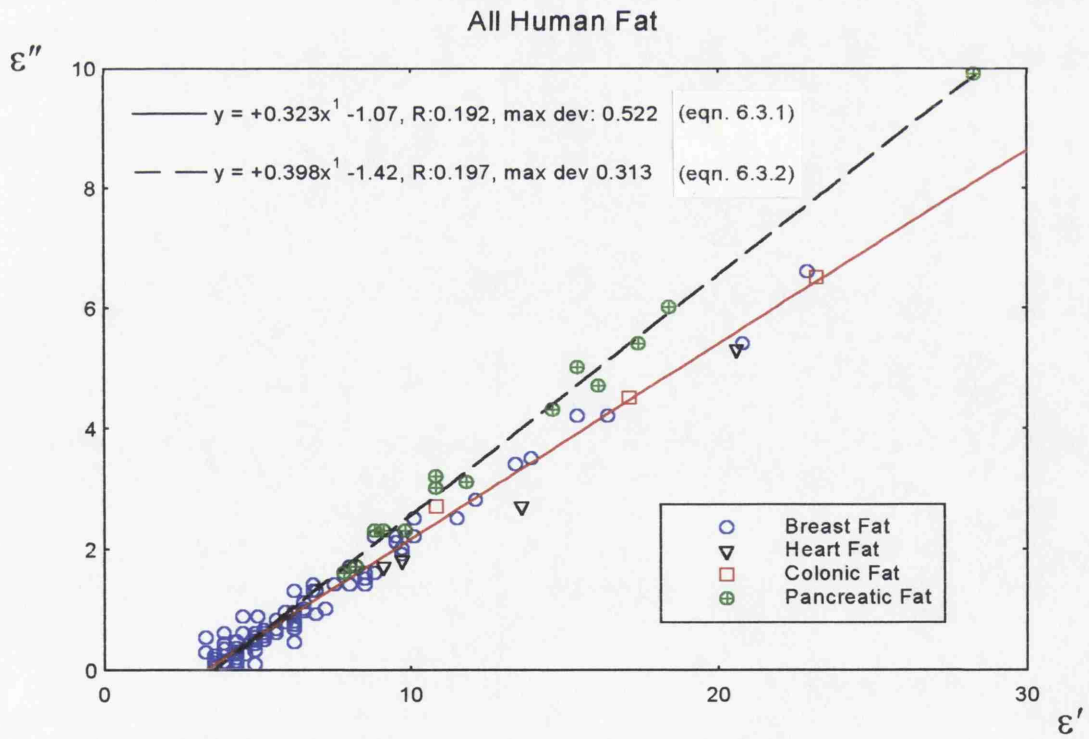

Figure 6.k. Measured loss factor vs. dielectric constant for all human fat data. Correlation co-efficient of dashed straight line fit = 0.996

measured dielectric constant of human breast fat had a value of approximately 8. A straight line fit to these data has equation

$$\varepsilon'' = 0.292\varepsilon' - 0.544 \qquad \text{corr. co-eff.} = 0.965 \qquad (6.3.3)$$

Taking only those data with a dielectric constant less than 8 from the current study, the low permittivity behaviour of both data sets can be compared. Figure 6.m shows that the current data can be represented by a straight line with equation

$$\varepsilon'' = 0.287\varepsilon' - 0.887 \qquad \text{corr. co-eff.} = 0.880 \qquad (6.3.4)$$

The above equations have very similar gradients, and lie well within experimental error of one and other. This illustrates that at very low permittivity values, the gradient of the relationship between loss factor and dielectric constant for fatty breast tissue is reduced in comparison with its mean value. Campbell's data had a lower scatter, but this may be a result of sample selection.

Measurements comparable with the current data are few, but Cook (1951) presented the results of *in vitro* permittivity measurements at 2.98 GHz on five varied fat specimens. These measurements were made at 37°C, but with so little water in the tissues, there will be little difference between these results, and the permittivity at 20°C. Fatty breast tissue gave the extreme upper and lower permittivity values, from 3.9 - j0.9, to 14.7 - j4.0. Abdominal fats, and a specimen from the foot gave intermediate values. A linear approximation of loss factor against dielectric constant for the breast fat results of Cook gives a gradient of 0.286, although little meaning can be inferred from this, as the data are so few.

Herrick et al (1950) gives permittivity values ranging from 3.9 -j0.65 to 7.2 - j1.4 for human fat at 37°C, and at a frequency of 3 GHz. The data of Campbell, Cook and Herrick are all therefore similar to the current values, although it is perhaps significant that all these data sets tend to give a slightly higher loss factor than was observed here, for tissues with very low values of dielectric constant. The difference is smaller than the measurement error, being less than 0.5 relative dielectric units, but is a large proportion of the total loss factor for tissues with a dielectric constant of around 4.

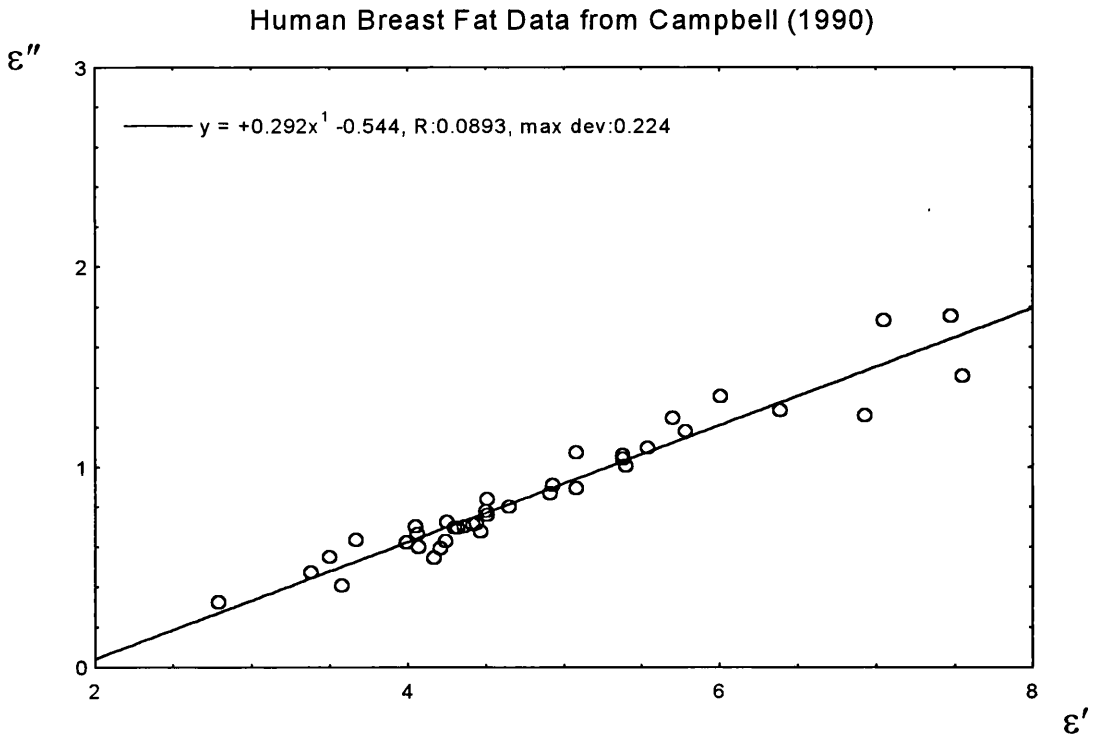

Figure 6.l. Campbell's (1990) human breast fat data. Loss factor vs. dielectric constant. Correlation Co-efficient of straight line fit = 0.965

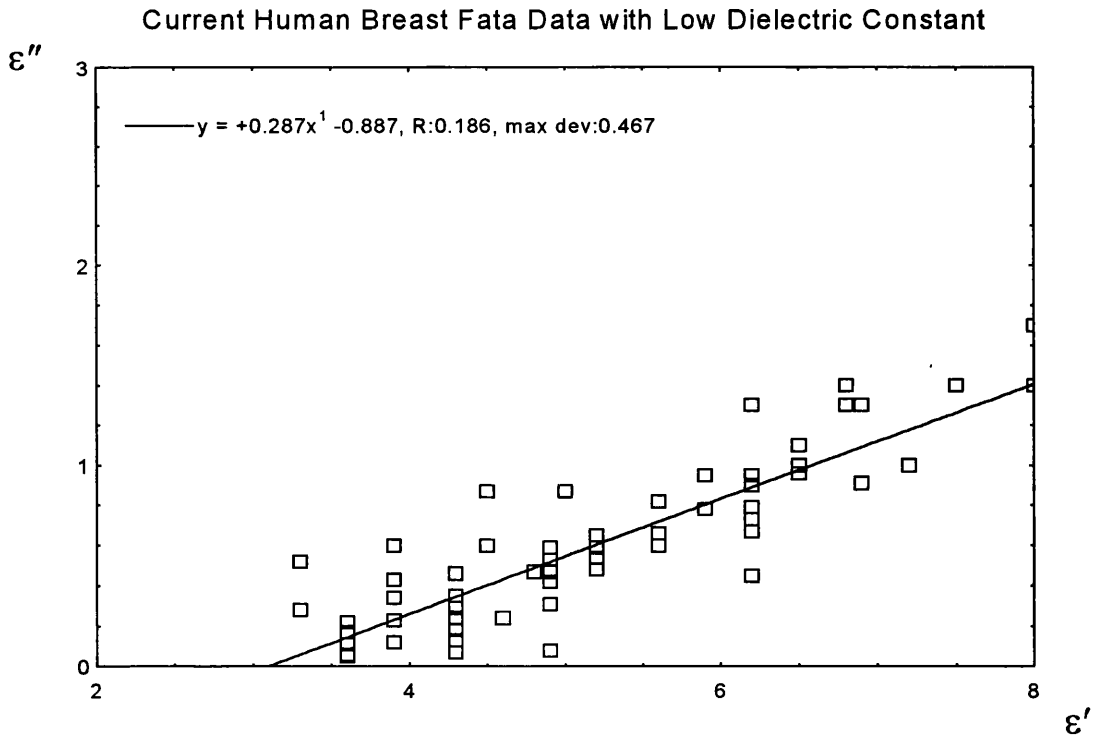

Figure 6.m. Current human breast fat data with $\varepsilon' \leq 8$. Loss factor vs. dielectric constant. Correlation Co-efficient of straight line fit = 0.880

6.3.4. Conclusion.

Fatty human breast tissue, and other similar internal fats, therefore display dielectric properties similar, although not identical, to commercial animal fat. The linear variation of loss factor with dielectric constant is well defined, but with a noticeably lower gradient than is observed for animal fat. For tissue regions with low permittivity, and, by association, low local water content, the gradient of this relationship is further lowered, in a manner also observed on animal fat tissues. Some internal fats in the human body may display a relationship between loss factor and dielectric constant which is very similar to that of animal fat. This may be due to a slight difference in the structure of some internal fat tissues. Animal fats can be used as a good approximation for human fats in tissue phantom experiments, although it should be noted the degree of local variability appears to be greater on human fat than on commercial animal fat. This may be a reflection of the limited range of human fat samples investigated.

6.4. Permittivity Measurements on High Water Content Tissues.

Most of the soft tissue in the body has a water content, by mass, in the region of 75% to 85%. Table 6.c shows a list, compiled from the Biology Data Book (1972), of the water contents of most of the major tissue types that have been dielectrically measured in this study. The permittivity measurements made on soft tissue are reviewed in the following sub-sections according to tissue type. Comparison is drawn between the permittivity of different tissue types, and between the current results and those of previous researchers. Mixture equation analysis of high water content tissue is presented in chapter 7.

6.5. Non-Fat Human Breast Tissue.

As has been mentioned in section 6.3, the specimens of human breast obtained for measurement contained the whole range of tissue types found in the breast. In the previous section, only those measurements on samples, or regions of samples of breast tissue, which appeared to be *mainly* fat tissue were presented. Here, those remaining measurements, which were made on regions of *mainly* fibrous and muscular tissue in the breast are discussed. Due to the heterogeneous nature of this tissue, there may be some

Tissue Type	Water Mass Fraction (%)
Whole Blood	78.5
Muscle	70 - 80
Skin	60 - 76
Fat	5 - 20
Liver	71 - 77
Spleen	77 - 81
Kidney	78 - 84
Heart	71 - 80
Uterus	80
Pancreas	75
Whole Brain	75 - 78
Grey Brain Matter	82 - 85
White Brain Matter	68 -73

Table 6.c. Water contents by mass of the most of the soft tissues investigated in this chapter. Taken from Biology Data Book, 1972.

Breast Tissue Type	No. of Samples	No. of Perm. Measurements	Mean Dielectric Constant	Mean Loss Factor	Mean (%) Water Mass Fraction
White Connective	1	5	41.9 ± 2.0	14.4 ± 0.8	76.3
White Connective	1	10	42.2 ± 6.3	14.0 ± 1.4	70.3
Irregular * Connective	1	6	48.8 ± 3.9	14.5 ± 0.9	82.1
* Could not ensure uniform probe contact during measurement, due to sample irregularity.					

Table 6.d. List of mean permittivity and water content values measured on connective tissue from the human breast.

overlap between the high permittivity values presented in the previous section, and the low permittivity values of this current data.

It can be assumed, from the range of permittivity values obtained, that the volume of tissue investigated in each permittivity measurement may have been composed of a combination of tissue types, with widely varying proportions of each tissue from measurement to measurement. It is not, therefore, strictly true to regard this non-fat breast tissue as being a single, specific tissue type itself. However, such transitional intermediate tissue regions occur in many places on the body, and so it is of interest, in microwave thermography, to investigate the permittivity changes in these regions. The measured volumes of tissue will have local water contents ranging from that of fat, to that of ordinary soft tissues, although again, unfortunately, as many measurements were made on each sample, there is no known water content value which is truly representative for each permittivity datum. As there is no single soft tissue with a water content between 30% and 65% by mass, there would be a large gap in the permittivity data without these intermediate breast tissue measurements.

6.5.1. Overall Results of Non-fat Human Breast Tissue Measurements.

The data presented in fig. 6.n were all taken on intermediate breast tissue samples from one single specimen. A very clearly defined linear relationship between loss factor and dielectric constant is observed, which can be expressed by the equation

$$\varepsilon'' = 0.382\varepsilon' - 2.04 \qquad \text{corr. co-eff.} = 0.995 \qquad (6.5.1)$$

It may be noted that the gradient of this relationship is again rather higher than was observed for the fatty breast samples. This continues the trend pointed out in the previous section, of slowly increasing values of the gradient and intercept with the ε' axis, with increasing dielectric constant.

An overall best-fit for all the breast data so far considered is shown in fig. 6.o, and has equation

$$\varepsilon'' = 0.360\varepsilon' - 1.34 \qquad \text{corr. co-eff.} = 0.997 \qquad (6.5.2)$$

It can be seen that this line significantly deviates from the intermediate breast tissue linear fit only at values of the dielectric constant below 15 and above 55. Within this range, the deviation of the overall fit from the intermediate breast tissue fit is less than the experimental error.

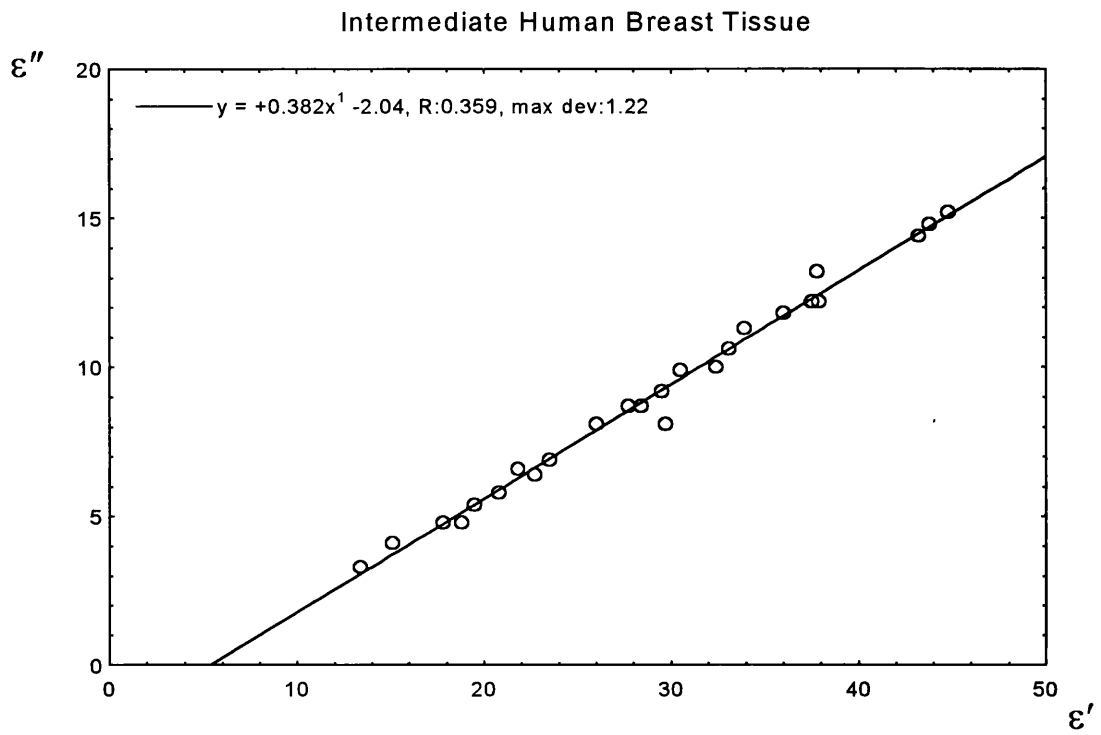

Figure 6.n. Measured loss factor vs. dielectric constant for intermediate breast tissue. Correlation co-efficient of straight line fit = 0.995

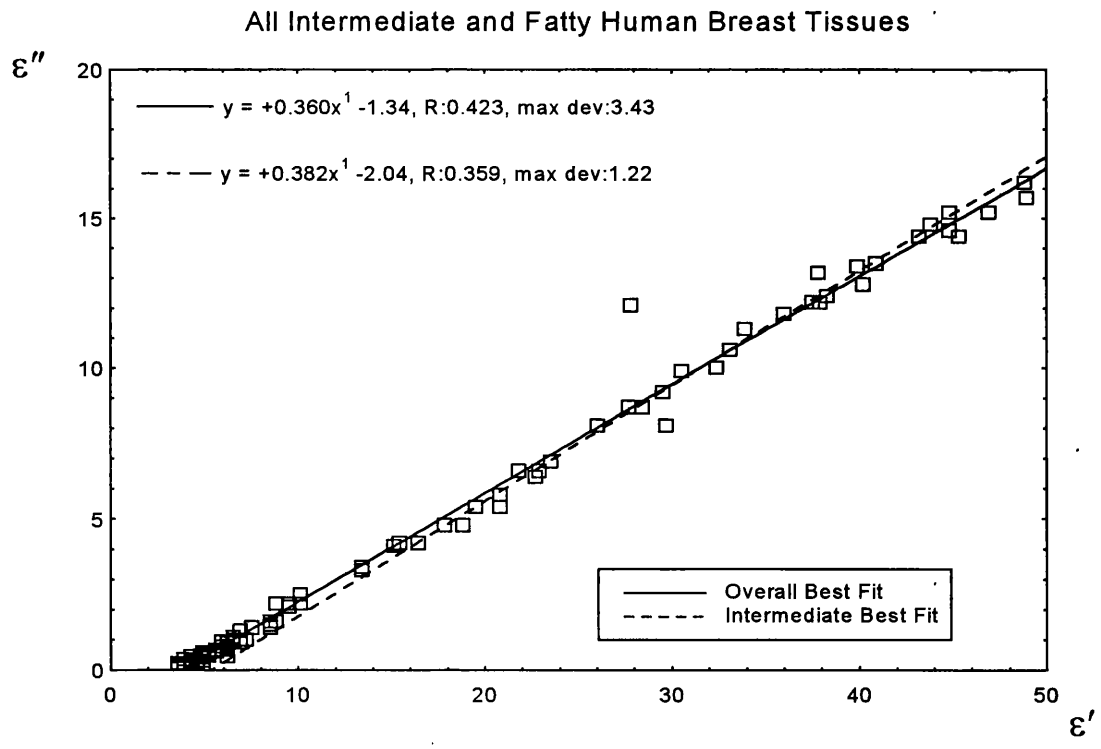

Figure 6.o. Comparison between all intermediate and fatty breast tissues, showing linear relationship between loss factor and dielectric constant.
Correlation co-efficient of overall straight line fit = 0.997

6.5.2. Connective Tissue From the Human Breast.

Three tissue specimens were obtained which originated exclusively from the connective tissue located near the pectoral muscle, deep in the breast. One sample was prepared from each specimen. The results from these samples are displayed in table 6.d. These samples yielded the highest permittivity results of all measured tissue from the breast, and also gave water contents which were truly representative of the permittivity measurement tissue volumes.

Although the available data is limited, fig. 6.p shows that the two samples of white connective tissue gave data which is in broad agreement with the general trend of linear increase in loss factor with dielectric constant, whilst the measurements on the final irregular gristly sample display some deviation from the expected loss factor. There was, however, some difficulty encountered in ensuring a uniform probe contact with this sample. This may have affected the permittivity measurements, so no conclusions will be drawn at this stage.

A linear trend of increasing loss factor with dielectric constant has now been demonstrated for breast tissues with water contents up to those of most high water content soft tissues. In the subsequent sub-sections, the dielectric behaviour of a wide variety of high water content tissues is compared with this established linear relationship.

6.6. Muscle Tissue.

Muscle tissue is by far the prevalent tissue in the human body, and is characterised by its ability to contract. There are three types of muscle tissue; skeletal, smooth and cardiac. Skeletal muscle is the muscle tissue which is attached to the bones and is under voluntary control. By virtue of the fact that skeletal muscle constitutes two thirds of the body weight, knowledge of its dielectric permittivity is of particular importance for microwave thermographical modelling of the body. All the data presented in this section are the results of permittivity measurements on skeletal muscle.

Smooth muscle is the muscle of the digestive system, so named on account of its cellular structure, rather than its variable appearance. Cardiac muscle is the muscle of the heart, characterised by its automatism. Measurements on these latter muscle types are

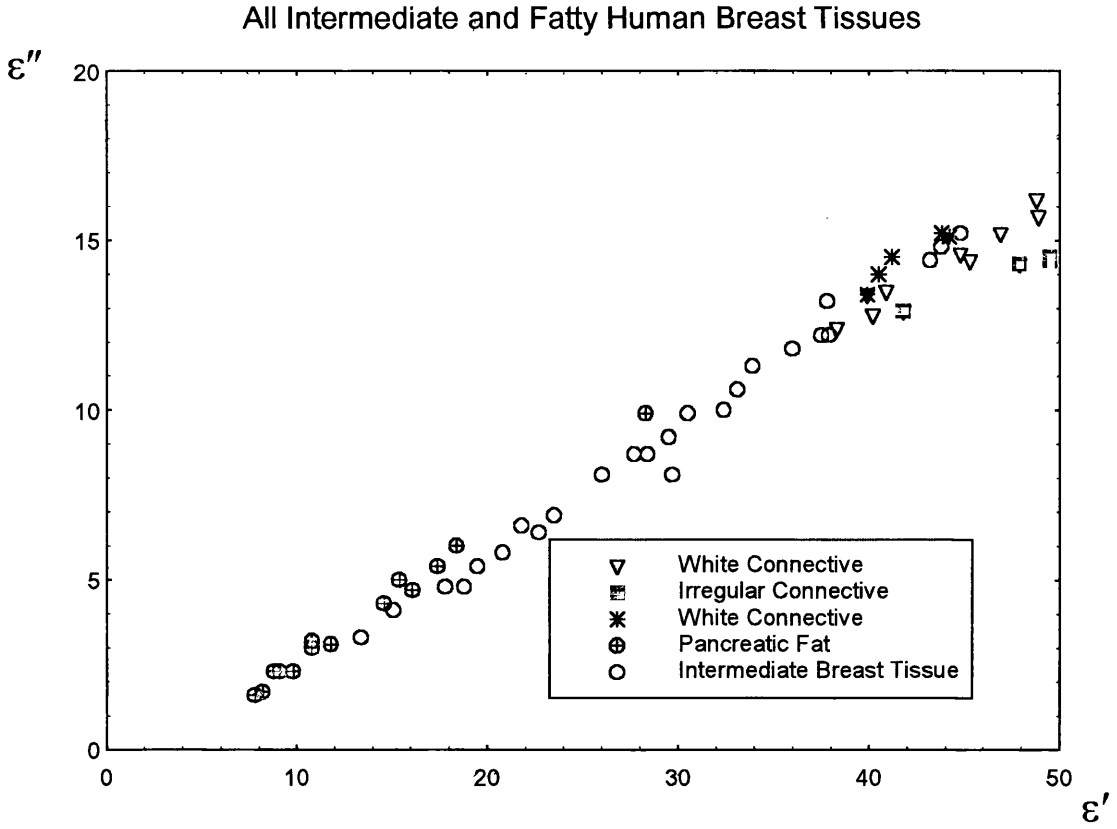

Figure 6.p. Comparison between intermediate breast tissue, connective breast tissue, and pancreatic fat.

presented in later sections. It is usually maintained that human muscle tissue is physiologically almost indistinguishable from porcine, bovine and agnine muscle tissue.

6.6.1. Tissue Quality.

At this stage it is useful to define the terms *high quality* and *low quality*, which are used throughout the remainder of this chapter to describe commercially obtained tissue specimens. Those tissue specimens referred to as being of *high quality* were characterised by a uniformity of tissue over a relatively large distance, of the order of several centimetres. These specimens were composed overwhelmingly of just one tissue type, for instance skeletal muscle. The tissue of *low quality* specimens was characterised by intrusions of unwanted tissue types, usually connective or fatty tissues. These intrusions can affect the water content and permittivity of local sample volumes on a specimen, giving a wider scatter of results, and in the case of fatty intrusions, lower the average values of the water content and permittivity. In commercial tissues, a strong correlation was found between the qualitative *quality* of tissues, and their quantitative *price*. Most human tissue samples were found to be less uniform than their animal equivalents, and so were regarded as being of *low quality*. However, any financial correlation could not be investigated in this case.

6.6.2. Animal Skeletal Muscle.

Table 6.e shows the average water content and permittivity values obtained from a total of 378 measurements on porcine, bovine and agnine skeletal muscle. The number of measurements on each species was well distributed; 138 porcine, 96 bovine and 144 agnine permittivity measurements were made. Nine specimens of lean porcine muscle from the lumbar and rib areas were investigated, as well as 2 other lower price specimens, also from these regions. Five specimens of bovine muscle from the lumbar area, and one from the upper foreleg were also studied. Agnine muscle tissue for permittivity measurements was obtained from 4 specimens from the rib area, and one lower quality specimen of unknown provenance, which was frozen prior to purchase. For comparison, additional data resulting from 71 permittivity measurements on skeletal muscle from poultry are also shown in table 6.e.

Type of Muscle Tissue	No. of Specimens	No. of Samples	No. of Perm. Measurements	Mean Dielectric Constant	Mean Loss Factor	Mean (%) Water Mass Fraction
Porcine						
overall	11	138	138	45.0 ± 3.9	16.2 ± 1.9	74.0 ± 2.2
chop	7	57	57	46.0 ± 3.9	16.5 ± 1.5	73.8 ± 1.5
loin steak	2	52	52	47.0 ± 1.5	17.5 ± 0.7	74.4 ± 2.6
other cuts	2	29	29	39.0 ± 2.3	13.3 ± 0.8	73.6 ± 2.4
Agnine						
overall	5	144	144	46.5 ± 2.5	15.6 ± 1.1	72.8 ± 3.7
chop	4	38	38	47.0 ± 1.7	16.4 ± 0.6	74.9 ± 1.5
diced (pre-frozen)	1	106	106	46.3 ± 2.6	15.3 ± 1.1	72.2 ± 3.5
Bovine						
overall	6	96	96	45.4 ± 2.2	16.1 ± 0.9	73.9 ± 1.6
foreleg	1	30	30	43.5 ± 2.7	15.3 ± 1.1	74.6 ± 1.0
loins steak	5	66	66	46.2 ± 1.1	16.4 ± 0.6	73.6 ± 1.7
Poultry						
Chicken Breast	1	12	12	48.8 ± 0.7	18.3 ± 0.3	74.1 ± 0.4
Turkey Breast	2	59	59	48.1 ± 1.4	19.0 ± 0.7	73.2 ± 1.3

Table 6.e. List of mean permittivity and water content values measured on animal skeletal muscle tissues. Also shown are limited results taken from poultry skeletal muscle.

6.6.3. Overall Results of Animal Skeletal Muscle Measurements.

The distributions of results of water content, dielectric constant and loss factor measurements for each animal are shown in figs. 6.q, 6.r and 6.s. Each of these properties will be considered in turn. The ranges of measured water content can be summarised as follows;

- Porcine Muscle: Min. value 65.6% Max. value 78.1% Mean value 74.0%.
- Bovine Muscle: Min. value 68.6% Max. value 76.5% Mean value 73.9%
- Agnine Muscle: Min. value 60.8% Max. value 77.5% Mean value 72.8%

The porcine water content histogram shows two major peaks, corresponding to the loins and rib muscle specimens respectively, and one minor low water content peak caused by samples from the lower quality tissue specimens. For agnine muscle it can be seen from the histogram that the most common water content is around 75% but that the distribution is skewed towards lower water content due to the majority of measurements being made on poor quality tissue.

The ranges of measured dielectric constant for these tissues are summarised;

- Porcine Muscle: Min. value 34.3 Max. value 53.0 Mean value 45.0.
- Bovine Muscle: Min. value 36.4 Max. value 49.0 Mean value 45.4
- Agnine Muscle: Min. value 36.1 Max. value 50.4 Mean value 46.5

It should be noted that the upper and lower limits for these tissues, are uncommon, extreme values. The porcine dielectric constant histogram shows two clear peaks; one at around 46, due to measurements on the majority of high quality tissue, and a smaller peak caused by measurements on lower quality samples, containing fatty intrusions. The distribution of values of the dielectric constant of agnine muscle is also skewed, for the same reasons as described above for the water content.

Histograms representing the measured loss factor on tissues from each animal display distribution profiles similar to those for the dielectric constant. Measured loss factor values ranged from

- Porcine Muscle: Min. value 11.3 Max. value 19.7 Mean value 16.2
- Bovine Muscle: Min. value 13.1 Max. value 17.7 Mean value 16.1

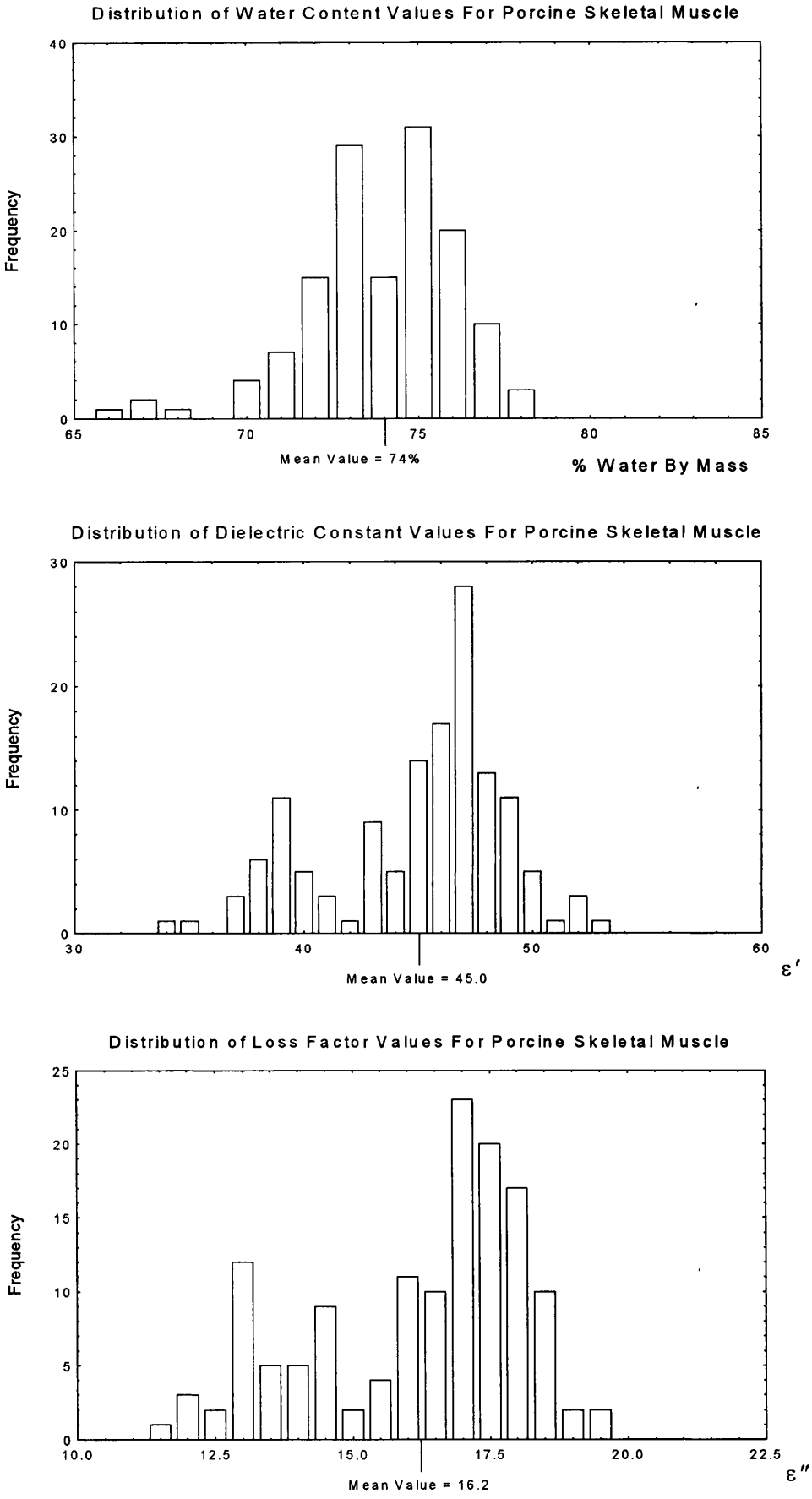

Figures 6.q. Histograms showing distribution of water content and permittivity measurement values for porcine skeletal muscle.

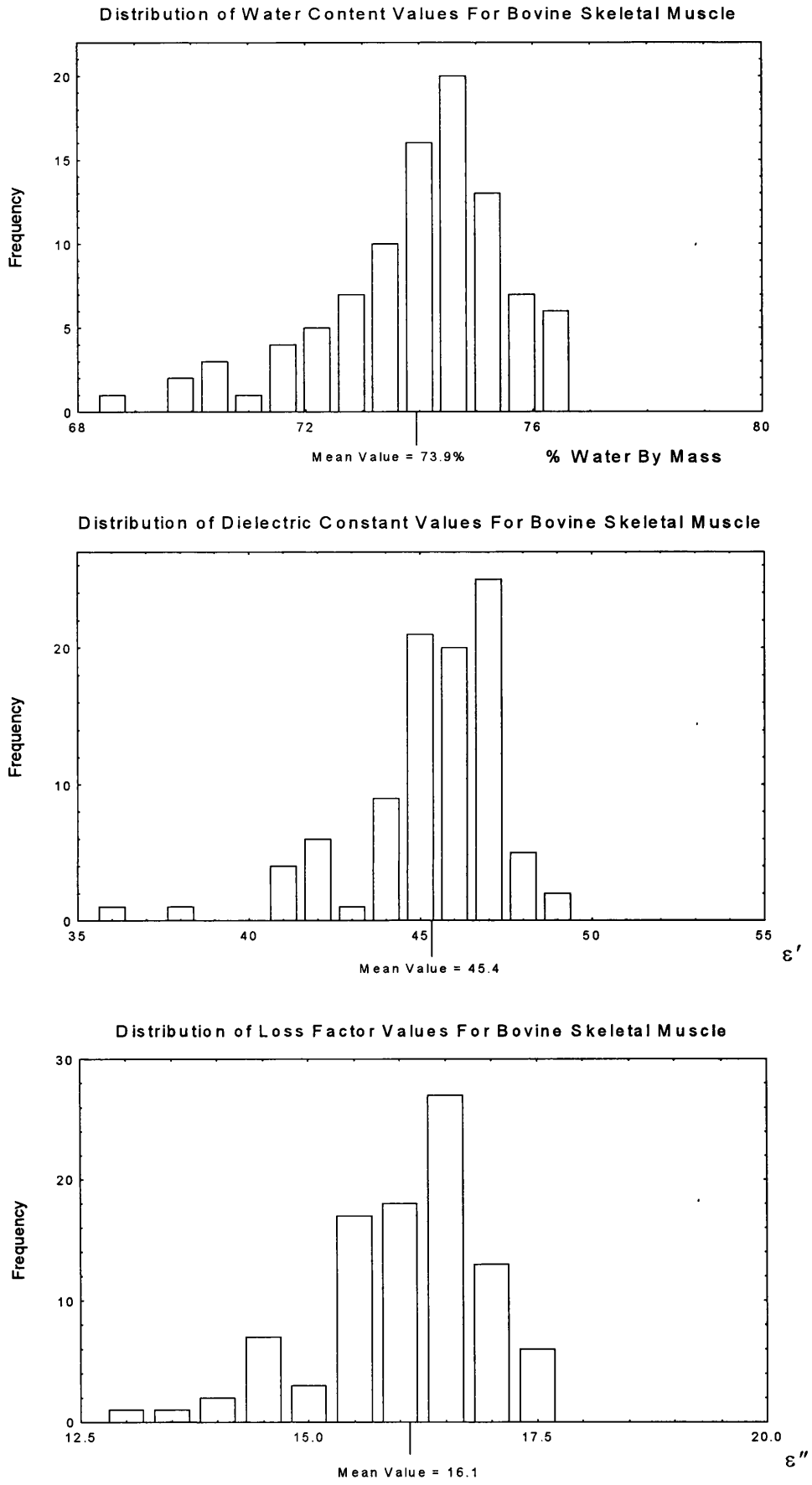

Figures 6.r. Histograms showing distribution of water content and permittivity measurement values for bovine skeletal muscle.

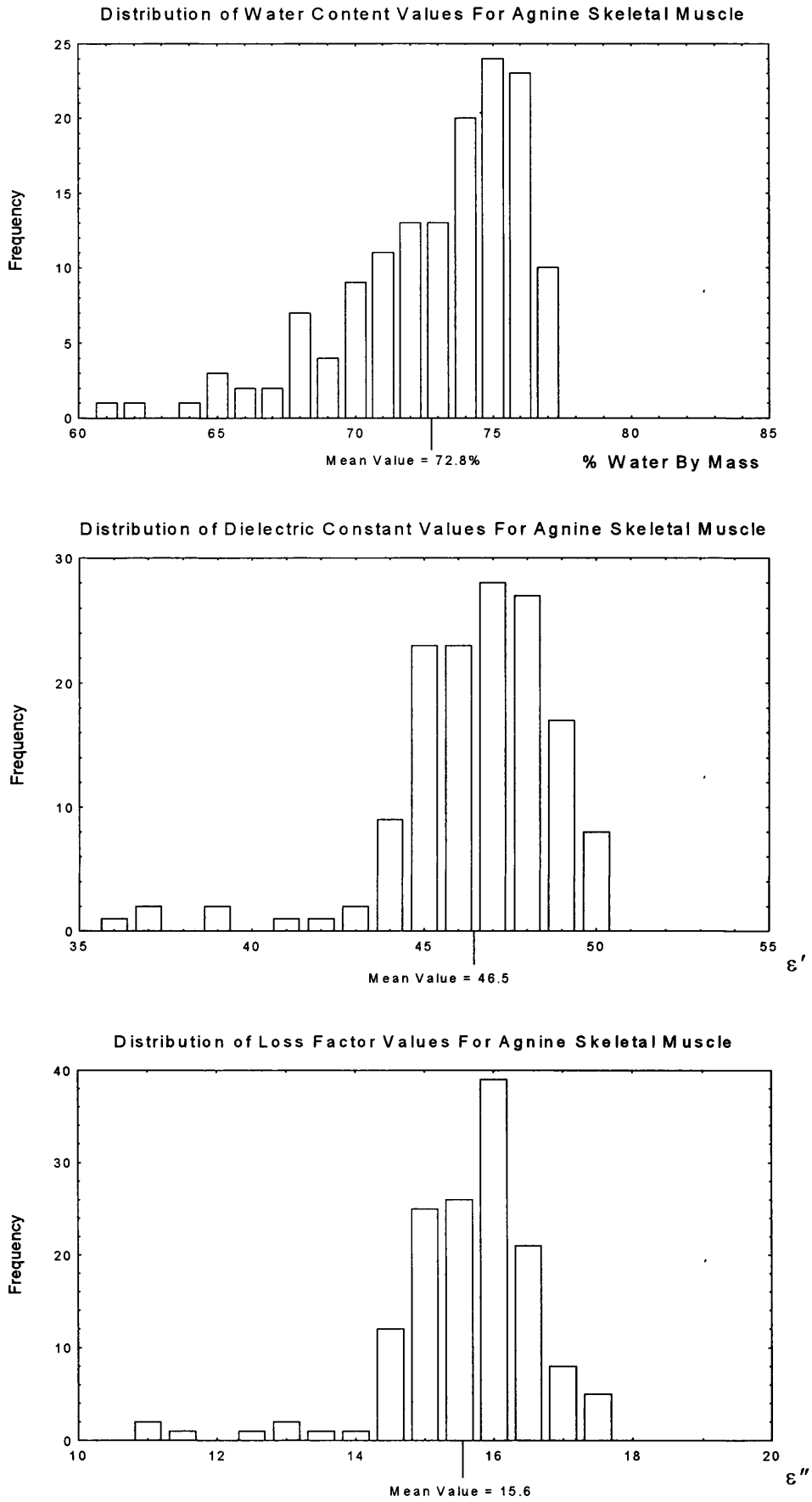

Figures 6.s. Histograms showing distribution of water content and permittivity measurement values for agnine skeletal muscle.

- Agnine Muscle: Min. value 10.8 Max. value 17.4 Mean value 15.6

Higher quality tissues regularly displayed higher loss factors than other muscle tissues with a similar dielectric constant.

It can be seen from the close grouping of mean water contents, dielectric constants and loss factors, that skeletal muscle from these three animals displays very similar dielectric properties. For tissue samples of each individual species, the most common water content, to the nearest integer, is 75%, and the most common value of dielectric constant is 47. The most common loss factor is 17, although for agnine tissue, a modal integer value of 16 is observed.

Although the mean loss factors of porcine, bovine and agnine tissue are close, it can be seen in the histograms that there are very few bovine and agnine data with loss factor greater than 17.5, whereas there are many porcine loss factor data in that region. This difference is again considered after presentation of the bovine and agnine results, in section 6.6.9.

6.6.4. Porcine Skeletal Muscle.

The behaviour of loss factor with dielectric constant for porcine muscle is shown in fig. 6.t. A well correlated linear relationship is once again observed, with equation

$$\varepsilon'' = 0.466\varepsilon' - 4.72 \qquad \text{corr. co-eff.} = 0.951 \qquad (6.6.1)$$

This expression has a slightly higher gradient than was observed on lower permittivity tissues. However, as is displayed in fig. 6.u, the behaviour of the lower permittivity region of animal muscle data is continuous from the higher permittivity region of human breast tissue data. If tissue physiology is similar between species, this suggests that there is no sudden jump in permittivity in the transition from fatty, through connective, to muscle tissue.

Figure 6.v displays the same porcine muscle data as fig. 6.t, but broken down into sets referring to the cuts of meat on which data were taken. This shows clearly that the highest quality tissues have higher dielectric constant and loss factor values than the lower quality cuts, but that all porcine muscle tissue fits the same general trend. It can also be seen that the specimens from the lumbar region are mainly responsible for the high loss factor values observed from the histograms.

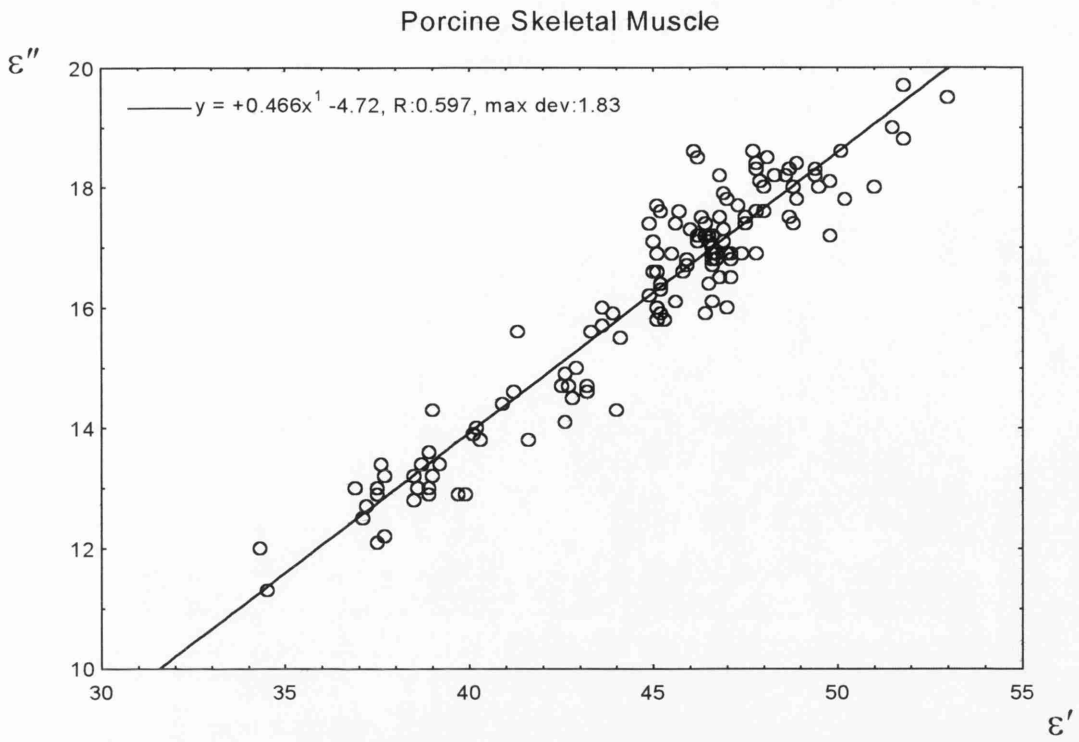

Figure 6.t. Measured loss factor vs. dielectric constant for all porcine skeletal muscle tissue. Correlation co-efficient of straight line fit = 0.951

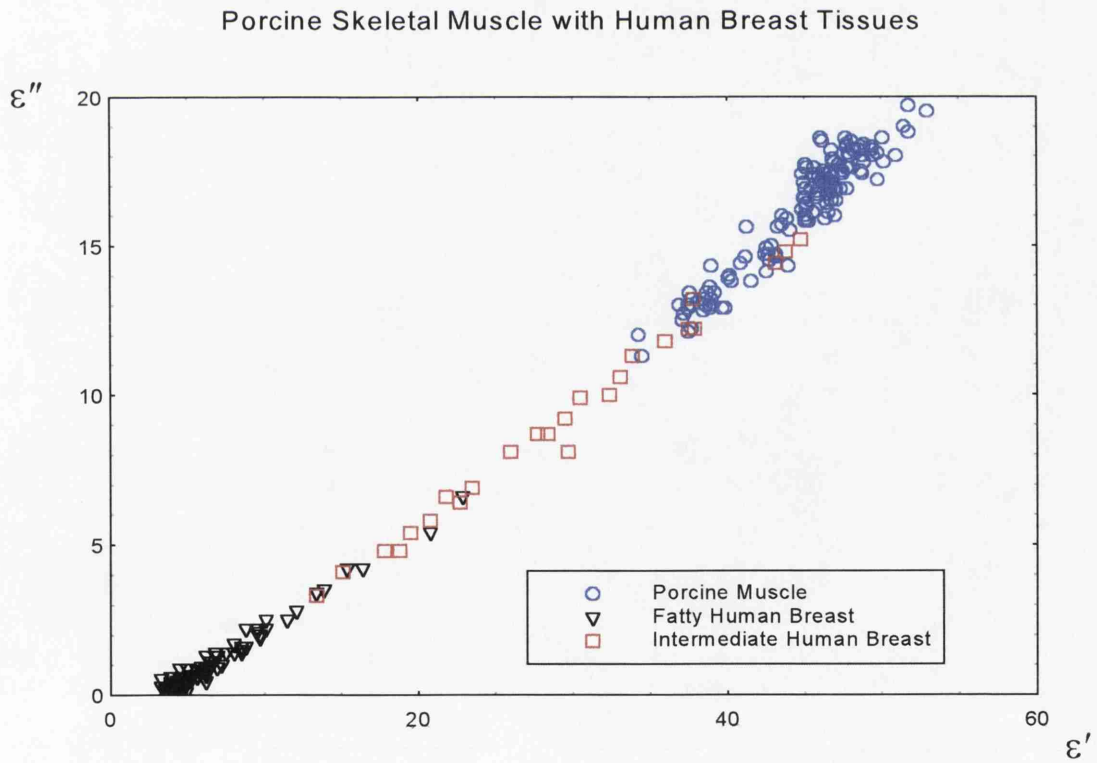

Figure 6.u. Comparison between measured loss factor vs. dielectric constant for porcine skeletal muscle with intermediate and fatty human breast tissues.

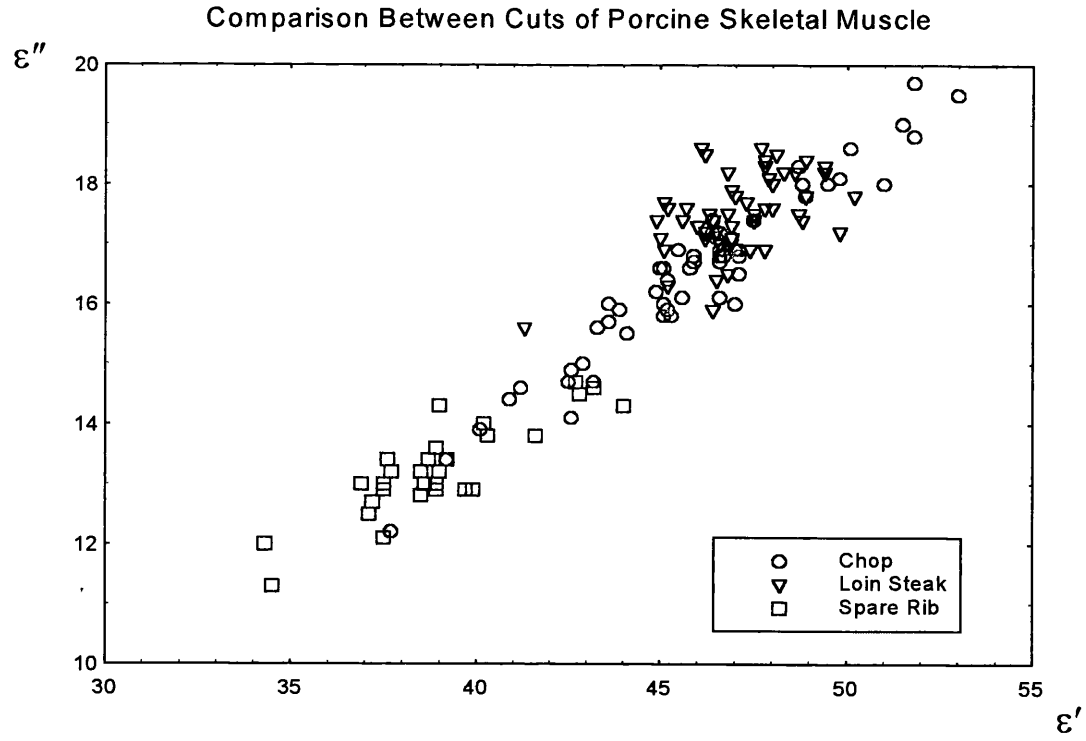

Figure 6.v. Comparison between different cuts of porcine skeletal muscle, showing that higher permittivity values are typical of higher quality tissues.

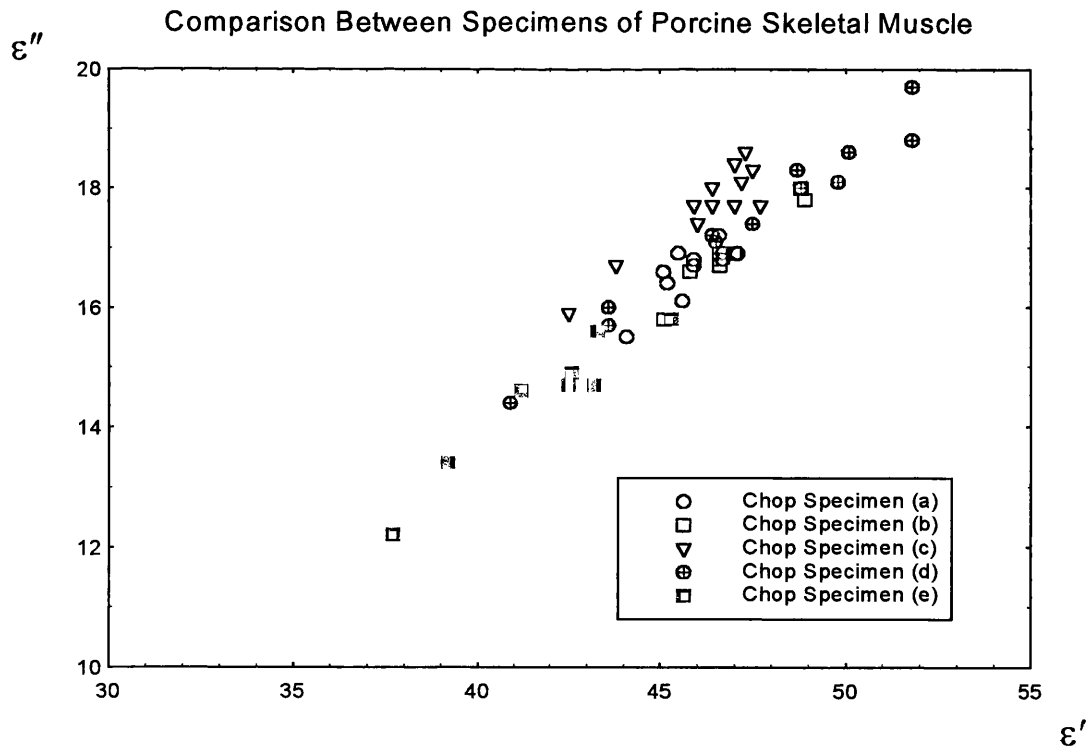

Figure 6.w. Comparison between different specimens of porcine muscle from the rib area.

It will be noted that there is a considerable degree of data scatter displayed in figs. 6.t and 6.v. This is at least partially due to the number and variety of different tissue specimens investigated. Results from measurements on selected individual pork specimens are displayed in fig. 6.w and table 6.f. It can be seen that the results from each individual specimen are grouped more closely than the overall data scatter. Varying tissue quality from specimen to specimen is probably responsible for this.
The standard deviation data in table 6.f show that the range of data scatter on individual specimens is similar in magnitude to the experimental error on the mean permittivity value.
Comparison between the data in tables 6.e and 6.f shows that there is a greater deviation between the average permittivity values of individual specimens from only the porcine sources, than there is between the average values for tissue from all animal species. It is therefore unlikely that there is significant inter-species differentiation of dielectric properties for skeletal muscle.

6.6.5. Correlation between Permittivity and Water Content.

Within the porcine muscle tissue data, there was very little observed correlation between either the dielectric constant or the loss factor, and the water content (see fig. 6.x). This observation was found to be true when only considering one of any of the individual tissue types investigated. That is not to say that there is no correlation within a particular tissue type, only that the current experimental technique was not sufficiently precise to detect it. As was mentioned in section 6.1.2, because of the local variability in water content, even within single samples, it was felt that measured water contents could be regarded as only broadly representative of the water content of the volume of tissue on which a permittivity measurement was made. This, and the additional permittivity and water content measurement errors, meant that water content comparison was only useful when comparing average values of permittivity from differing tissue types.

6.6.6. Bovine Skeletal Muscle.

Permittivity data obtained from measurements on bovine skeletal muscle is compared to those from porcine muscle in fig. 6.y. Most points lie fairly well distributed amongst the

Type of Tissue	No. of Samples	No. of Perm. Measurements	Mean Dielectric Constant	Mean Loss Factor	Mean (%) Water Mass Fraction
Chop (a)	11	11	45.9 ± 1.3	16.6 ± 0.5	73.1 ± 0.5
Chop (b)	8	8	45.9 ± 0.9	16.9 ± 0.7	74.3 ± 1.7
Chop (c)	13	13	46.3 ± 1.5	17.7 ± 0.7	74.2 ± 0.7
Chop (d)	12	12	47.5 ± 3.4	17.4 ± 1.5	73.8 ± 1.6
Chop (e)	8	8	41.9 ± 2.4	14.5 ± 1.2	72.8 ± 1.1

Table 6.f. List of mean permittivity and water content values measured on selected porcine skeletal muscle specimens.

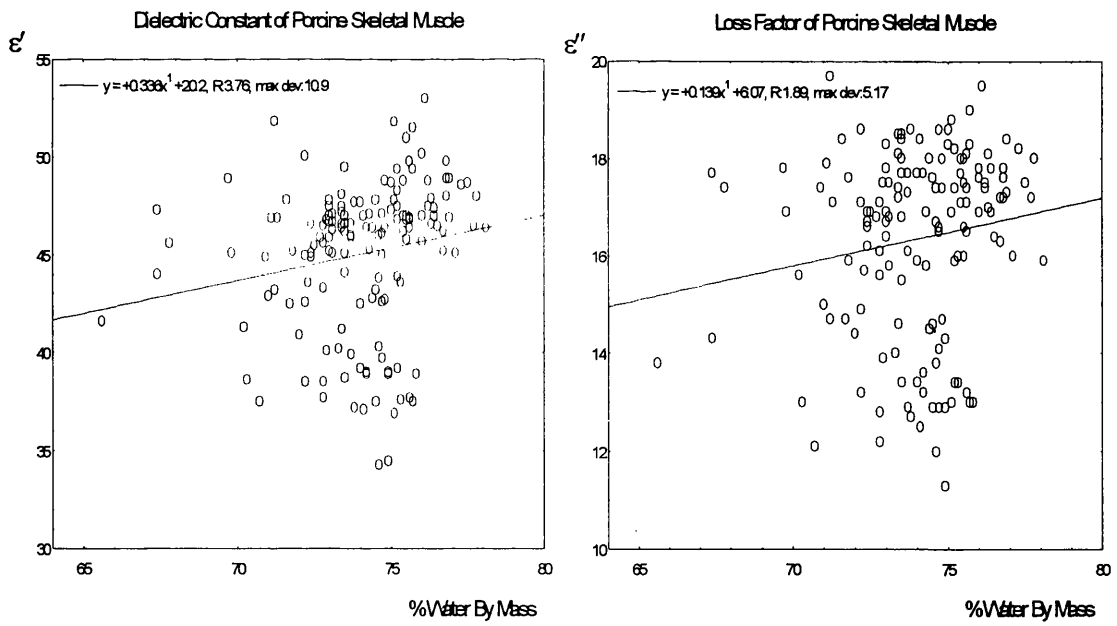

Figure 6.x. Measured dielectric constant and loss factor vs. water content for porcine muscle samples, showing the lack of correlation between these factors and water content within samples, due to local water content variability. Correlation co-efficient of dielectric constant straight line fit = 0.184. Correlation co-efficient of loss factor straight line fit = 0.152.

porcine data, although, as was noted from the histograms in section 6.6.3, there tend to be fewer data with high loss factors. Towards the region of lower dielectric constant, the bovine points are more evenly distributed amongst the porcine data. Also notable from fig. 6.y, and from the data in table 6.e, is a reduction in data scatter when compared with porcine permittivity data. This may be due to the fact that bovine specimens of only two types and from only a narrow quality (price) range were studied.

A linear relationship between loss factor and dielectric constant is observed, with a correlation co-efficient rather lower than that for the porcine permittivity data.

$$\varepsilon'' = 0.374\varepsilon' - 0.926 \qquad \text{corr. co-eff. } 0.909 \qquad (6.6.2)$$

The gradient is close to those of the straight lines fitted to animal fat permittivity data, and is even more similar to the linear approximations for human breast tissue than is the porcine muscle linear best-fit.

Breaking the data down into samples from the different cuts of meat (fig. 6.z) again shows that the lower permittivity measurements tended to be made on lower quality meat, as was noted for porcine tissue.

There is therefore little to distinguish bovine skeletal muscle tissue from porcine muscle tissue in water content and dielectric permittivity. It is possible, however, as has been stated, that porcine tissue with a comparatively high dielectric constant has a rather higher average loss factor than bovine tissue with the same dielectric constant. The maximum difference seems to be of the order of one relative dielectric unit, or 6%.

6.6.7. Agnine Skeletal Muscle.

The permittivity measurements taken on agnine tissue were the least satisfactory of the animal skeletal muscle results. This is thought to be because one of the specimens from which many results were taken had been frozen prior to purchase. Figure 6.aa shows that despite still displaying a linear relationship between loss factor and dielectric constant, the data is divisible into two distinct sets, one characterised by a slightly higher loss factor than the other. The equation of the best linear fit is

$$\varepsilon'' = 0.391\varepsilon' - 2.64 \qquad \text{corr. co-eff. } = 0.889 \qquad (6.6.3)$$

The correlation co-efficient is the lowest observed in any of the animals investigated, but the relation is still very similar to those observed on animal fat and human breast tissues.

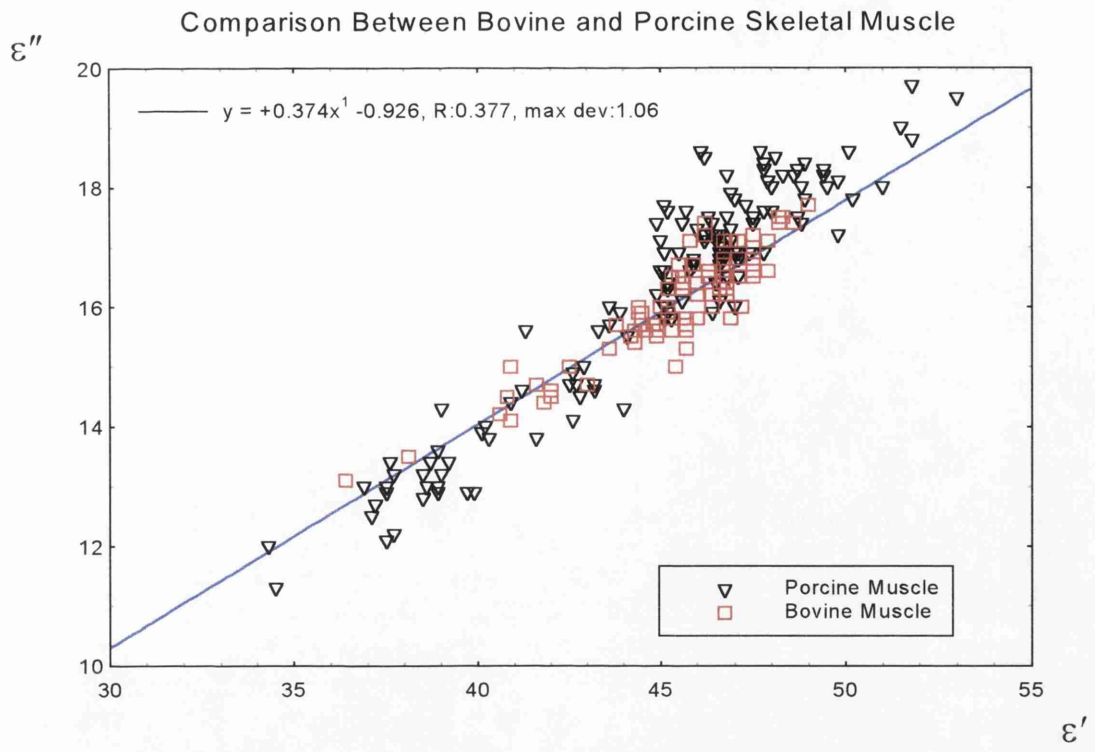

Figure 6.y. Comparison between measured loss factor vs. dielectric constant for porcine and bovine skeletal muscle.
Correlation co-efficient for bovine straight line fit = 0.909

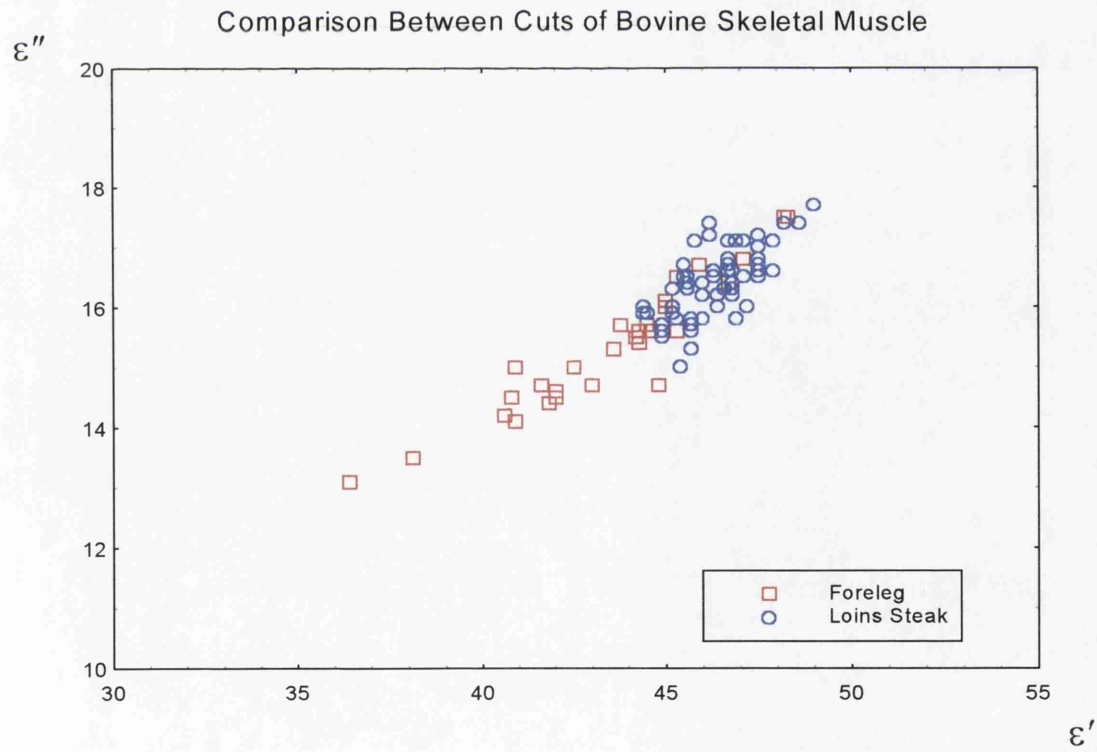

Figure 6.z. Comparison between different cuts of bovine skeletal muscle, showing again that higher permittivity values are typical of higher quality tissues.

Separation of the overall data into those taken on high quality tissue from the rib area, and those taken on the deep-frozen specimen of unknown provenance (fig. 6.bb), shows that the clear distinction between data sets is specimen dependent. No further investigation was made on whether this difference is due to the poor quality of the deep-frozen specimen, or the action of deep-freezing on the tissue.

6.6.8. Comparison with Previous Permittivity Measurements.

A fair body of research has been published on the microwave permittivity of skeletal animal muscle *in vitro*, although most measurements have been of feline, canine and rat tissues, which seem to have larger dielectric constants at 3 GHz than those tissue considered here.

Many researchers have made their permittivity measurements at body temperature, 37°C, rather than room temperature of around 20°C. Human tissue is mainly composed of an electrolytic solution similar to 0.15M saline. At 37°C, the permittivity of 0.15M saline is approximately 71 - j20. At 20°C, the value is approximately 75 - j22. Thus the difference in dielectric constant is ~5%, and in loss factor is ~9%. When comparing data taken at 37°C with the current values, it is therefore expected that the 37°C results should probably show a slightly lower values of both dielectric constant and, especially, the loss factor. However, as the water in tissue electrolyte is in various unknown states of binding, and constitutes only around 75% of the total tissue mass, it is difficult to quantify the exact expected differences.

Typical 3 GHz permittivity values are 53 - j15 for feline muscle (Stuchly et al, 1982b), 53 - j17 for rat tissue (Kraszewski et al, 1982), and 50 - j19 for canine muscle (Schwan et al, 1980). Of the species currently of interest, Brady et al (1981) give the permittivity of bovine muscle tissue as 47 - j15, at a temperature of 37°C.

This shows a similar dielectric constant, but slightly lower loss factor than the current measurements. Thus good agreement is shown with the current data when the reduction in the loss factor of water with increasing temperature is considered. Measurements on many commercially prepared animal tissues, taken at room temperature, using a frequency of 2.8 GHz, have been presented by Bengtsson and Risman (1971). The permittivity of raw pork meat (no further description) is quoted as ranging from 43 - j15 to 52 - j17, and that of raw beef ranges from 43 - j14 to 50 - j 17. Buffler and Stanford

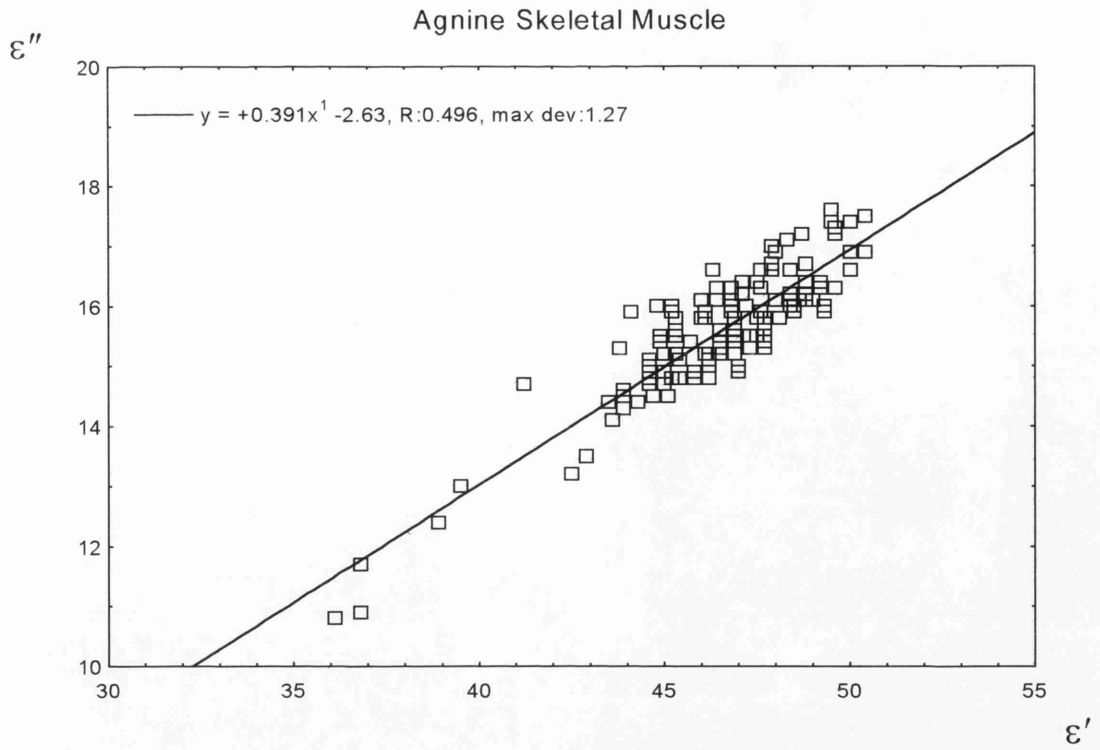

Figure 6.aa. Measured loss factor vs. dielectric constant for agnine skeletal muscle. Correlation co-efficient of straight line fit = 0.889.

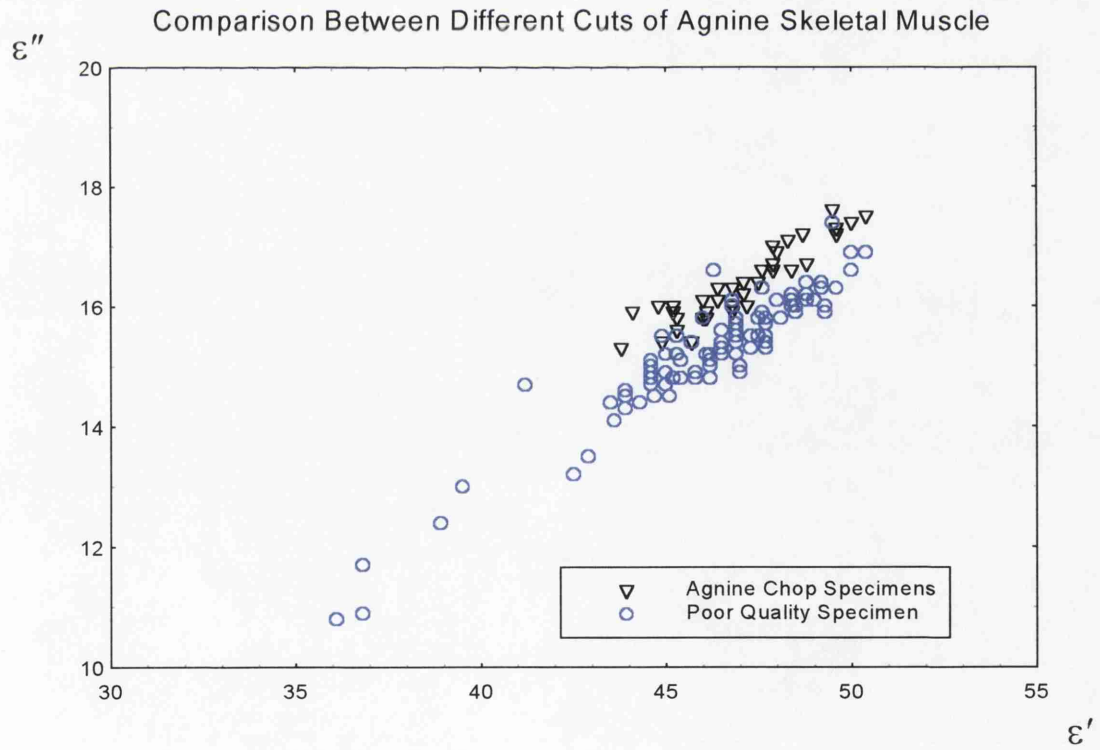

Figure 6.bb. Comparison between different cuts of agnine muscle, contrasting the rib specimens with the pre-frozen specimen of unknown provenance.

(1991) give the permittivity of raw beef and pork at 2.45 GHz as 52 - j17, for measurements at room temperature. The current data are consistent with these observations, as little difference, other than perhaps a slight drop in dielectric constant due to the water component, is expected in the permittivity over the frequency range between 2 - 3 GHz. (Variation in tissue permittivity over this range is discussed in more detail in section 7.7). No comparative data on agnine muscle tissue could be located.

6.6.9. Summary of Animal Skeletal Muscle Results.

In conclusion, the dielectric permittivity at 3 GHz of skeletal muscle tissue from each of the animals investigated is very similar, both in the range of measured values, and their averages. Mean permittivity and water content values for each species differed by less than the estimated experimental error. The modal integer permittivity value for each species of animal muscle tissue was 47 - j17, which is in good agreement with the values measured by many other researchers.

Tissues from each species also display a linear relationship between loss factor and dielectric constant, with a gradient close, but slightly higher, to that fitted to animal fat permittivity measurements. Figure 6.cc shows all animal fat and muscle permittivity data, together with a best-fit straight line.

There generally appears to be no significant difference between the dielectric properties of skeletal muscle tissue from any of these animals. However, the loss factor of some porcine specimens with high dielectric constant can be comparatively larger than the loss factor of bovine and agnine specimens with similar dielectric constant, despite the fact that tissue from each animal has a very similar average water content of around 74 - 75%. It can be seen from the mean data in table 6.e that this effect was particularly noticeable for porcine tissues from the lumbar region. The increase in average loss factor observed in the porcine lumbar specimens compared to porcine chop specimens, and most bovine and agnine muscle tissues, is of the order of 1 relative dielectric unit, or ~6%. The difference in dielectric constant is only ~ 2%. It is possible that the difference in loss factor is partially caused by slight variation in the ionic mobility or water binding of tissue electrolyte between differing regions of the body, or between different individual creatures. As many more porcine specimens were measured than bovine or agnine specimens, not only were more individual animals investigated, but it is also

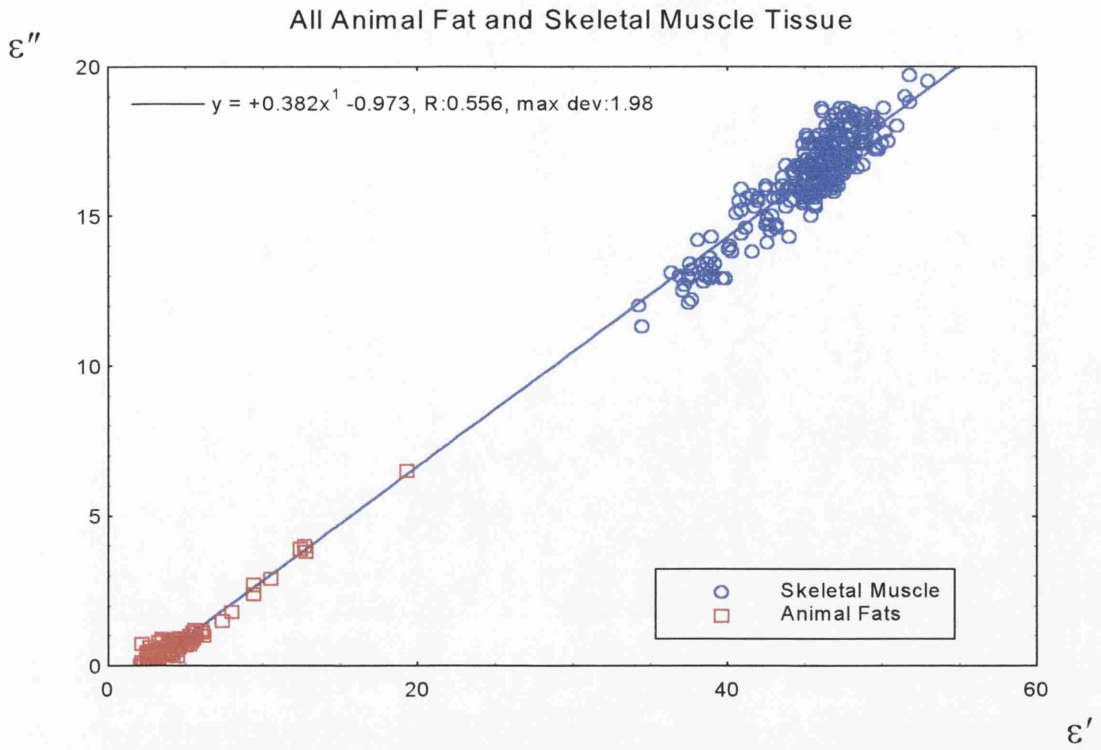

Figure 6.cc. Overall best fit of loss factor vs. dielectric constant for animal muscle and fat tissues. Correlation co-efficient of overall straight line fit = 0.997

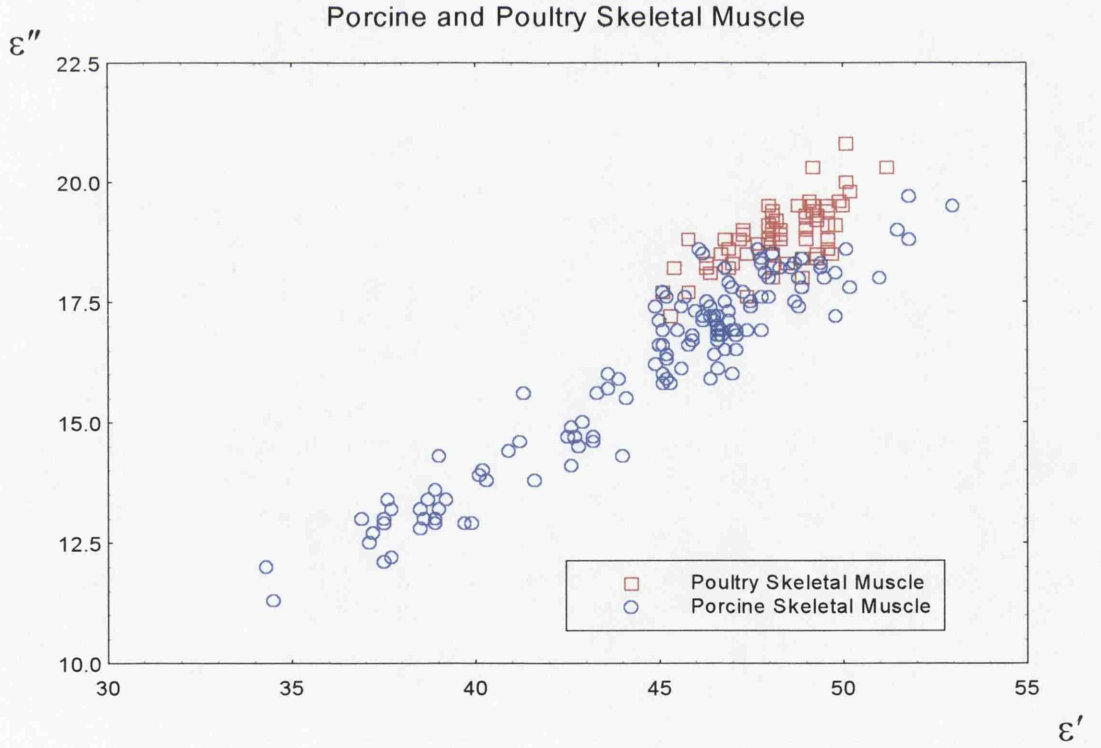

Figure 6.dd. Comparison between porcine and poultry skeletal muscle, showing that poultry muscle has a loss factor similar to the highest loss factors observed in porcine muscle.

possible that porcine tissues originating from a greater number of local body regions were measured.

6.6.10. Poultry Measurements.

Finally, although listed in table 6.e for comparison, the 71 measurements on poultry muscle have not been discussed in detail, as no other tissues from these animal species were investigated, and additionally, these tissues are less physiologically similar to human tissue. The poultry specimens, however, gave both permittivity and water content measurements with very low scatter, indicating a much lower degree of local tissue variability. It may be noted that both the dielectric constant, and, particularly, the loss factor, of these tissue specimens are higher than those of porcine, bovine and agnine tissues, despite having essentially the same water content. As is shown in fig. 6.dd, the poultry results tended to overlap with those porcine tissue specimens with higher than average loss factor.

6.7. Human Skeletal Muscle.

Permittivity measurements were made on human skeletal muscle from four individual donors. The results are summarised in table 6.g. A total of 287 readings were obtained from the four specimens; one from the thigh (quadricep), two from the lower leg (gastrocnemius and soleus), and one abdominal muscle, the provenance of which was not precisely known. The gastrocnemius specimen will be referred to hereon as *calf* muscle.

6.7.1. Overall Results of Human Skeletal Muscle Measurements.

The ranges of measured values for all human skeletal muscle are summarised by;

- Water Content: Min. value 69.3% Max. value 81.5% Mean value 77.0%
- Dielectric Constant: Min. value 45.5 Max. value 54.0 Mean value 49.3
- Loss Factor: Min. value 14.5 Max. value 18.5 Mean value 16.7

Histograms illustrating the overall distributions of these parameters in human muscle are shown in fig. 6.ee.

Type of Tissue	No. of Specimens	No. of Samples	No. of Perm. Measurements	Mean Dielectric Constant	Mean Loss Factor	Mean (%) Water Mass Fraction
Human Muscle overall	4	61	287	49.3 ± 1.4	16.7 ± 0.7	77.0 ± 2.6
Abdominal muscle	1	12	77	48.2 ± 1.2	16.6 ± 0.4	74.6 ± 1.8
Soleus muscle	1	16	87	49.6 ± 1.7	17.0 ± 0.7	76.2 ± 2.7
Calf muscle	1	8	36	49.5 ± 1.7	16.0 ± 0.6	79.1 ± 1.2
Quadricep muscle	1	25	87	49.9 ± 1.7	16.7 ± 0.6	77.9 ± 2.1
Connective Tissue in Quadricep	1	3	39	40.8 ± 2.3	14.8 ± 0.8	72.0 ± 3.3

Table 6.g. List of mean permittivity and water content values measured on human skeletal muscle tissues.

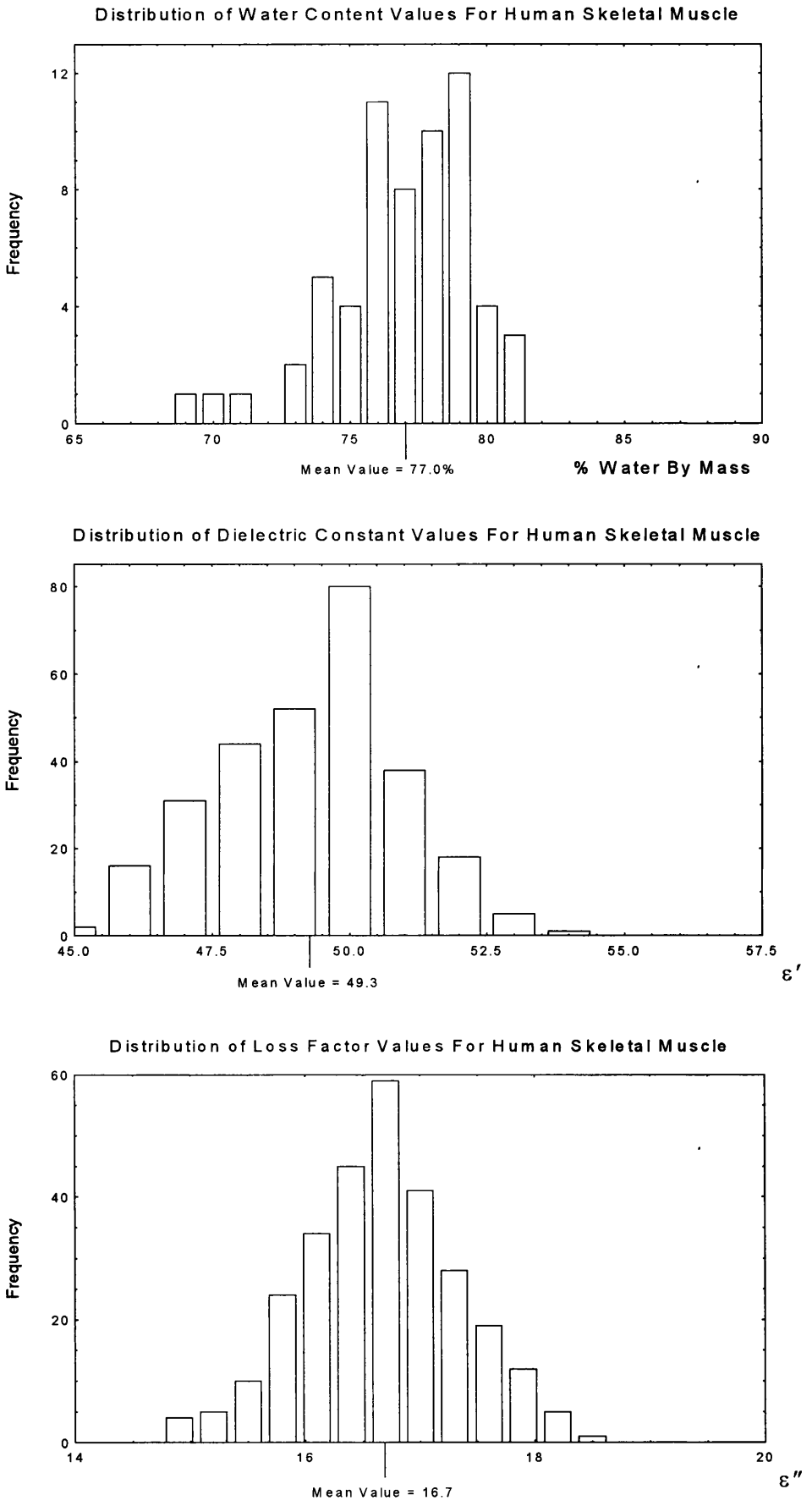

Figures 6.ee. Histograms showing distribution of water content and permittivity measurement values for human skeletal muscle.

The permittivity results from each individual specimen showed linear trends between loss factor and dielectric constant, shown in fig. 6.ff, and given below by eqns. (6.7.1)

$\varepsilon'' = 0.316\varepsilon' + 0.363$ corr. co-eff. = 0.905 for the calf muscle,

$\varepsilon'' = 0.278\varepsilon' + 3.17$ corr. co-eff. = 0.803 for the abdominal muscle,

$\varepsilon'' = 0.341\varepsilon' - 0.379$ corr. co-eff. = 0.890 for the quadricep muscle,

and $\varepsilon'' = 0.368\varepsilon' - 1.25$ corr. co-eff. = 0.903 for the soleus muscle.

These equations have similar gradients to the best-fit line already calculated for human breast fat and intermediate breast tissues (eqns. 6.3.1 and 6.5.1), although the gradient for abdominal muscle is rather lower than usual. General conclusions must not be drawn from these linear fits, as each fit refers only to one tissue specimen (c.f. 12 porcine muscle specimens). The overall best-fit is given by

$$\varepsilon'' = 0.297\varepsilon' + 2.03 \qquad \text{corr. co-eff.} = 0.753 \qquad (6.7.2)$$

and is plotted in fig. 6.gg. This fit is of rather lower gradient than the average of each of the individual specimens, and also lower than the gradient of the fits for all types of breast tissues. The low gradient may however be due to an uneven distribution of the number of measurements on each specimen rendering the overall best-fit straight line slightly unrepresentative of the true overall behaviour. From fig. 6.gg, which shows the results separated by specimen, it is clear that the smaller number of results for calf tissue could give a bias to the computed best-fit.

However, from figs. 6.gg and 6.hh, which compares human skeletal muscle with breast tissues, it is apparent that the human muscle results closely continue the approximate linear trend of loss factor with dielectric constant that have already been observed on breast tissues.

Figure 6.gg also shows that, as observed with animal tissues, the data grouping within a set of results from one specimen is tighter than the overall spread. Again, a qualitative association may be drawn between the mean permittivity values for a specimen, and its subjective tissue *quality*, which depends on the quantity of fatty intrusions into the muscle tissue. Of the four specimens, the calf muscle was judged to contain the lowest quality tissue, and was found to give a lower mean loss factor than the other specimens. The abdominal and soleus specimens were considered to be the best quality specimens, and gave most of the results with comparatively higher loss factor. These are similar

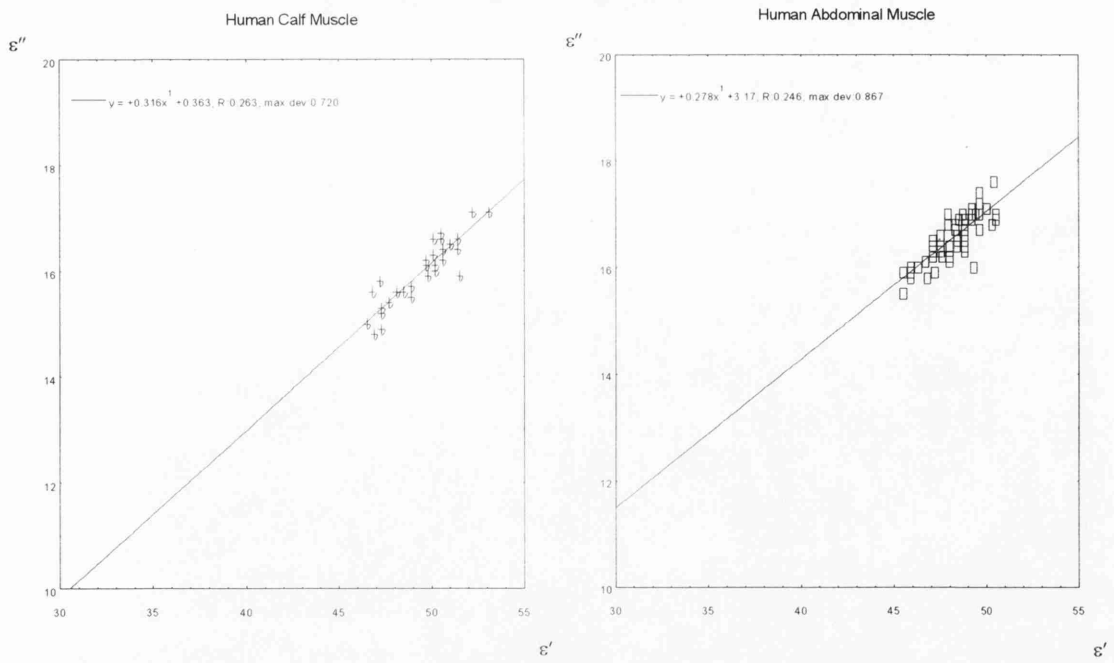

Figure 6.ff(i). Measured loss factor vs. dielectric constant for human skeletal muscle.
Correlation co-efficient of straight line fit for calf muscle = 0.905
Correlation co-efficient of straight line fit for abdominal muscle = 0.803

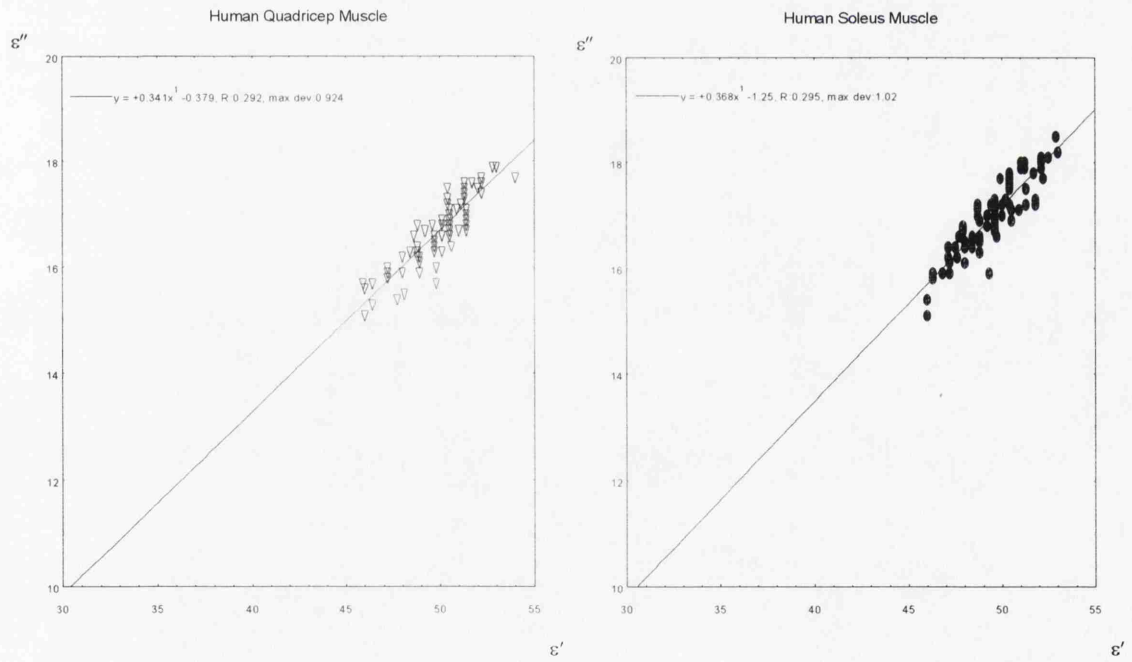

Figure 6.ff(ii). Measured loss factor vs. dielectric constant for human skeletal muscle.
Correlation co-efficient of straight line fit for quadricep muscle = 0.890
Correlation co-efficient of straight line fit for soleus muscle = 0.903

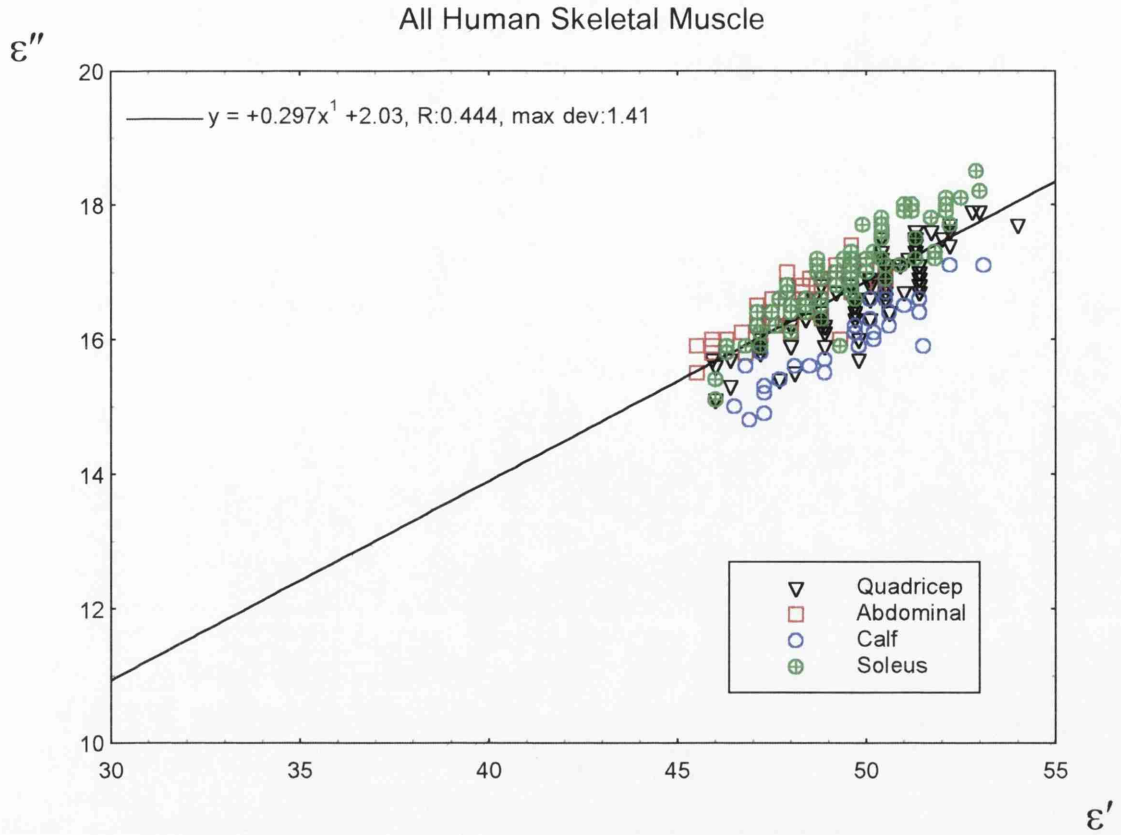

Figure 6.gg. Comparison of loss factor vs. dielectric constant for all human skeletal muscle, showing that the uneven distribution of data appears to give a misrepresentative best-fit straight line, with more shallow gradient than may be suggested by the data.
Correlation co-efficient of calculated line = 0.753

observations to those made on variable quality porcine and agnine tissues in the previous section.

6.7.2. Comparison between Human and Animal Skeletal Muscle Tissues.

The most noticeable difference between the human and animal muscle specimens is that the water content of the human muscles took an average value of 77% by mass, approximately 4% higher than the animal muscle average. This difference may be caused by the presence of residual blood fluid in the human tissue. Blood is an aqueous solution containing dissolved ions and many cells, with a permittivity of approximately $57 - j18$. Preparation of commercial animal tissue involves the drainage of excess blood fluid immediately after slaughter, lowering the water content in comparison with human tissues. Residual blood was visibly present in all human tissue specimens, not just skeletal muscle specimens, and could be made to seep from the tissues by gentle compression. Human muscle was also less rigid than its animal counterpart, presumably due to the increased water content, and also possibly because the human muscle tissue was of lower quality than the animal tissue.

It is to be expected that tissues with a higher electrolytic water content should have higher dielectric constant, and indeed, the effect of the extra blood in the human tissues gave a mean dielectric constant of around 49, compared to around 46 for animal muscle tissues. However, because the loss factor of blood is only a little higher than that of muscle tissue, the loss factor of human tissues was found to be broadly similar to that of animal tissue, at a value of 16 - 17 relative dielectric units. It is possible that the slight extra loss caused by the residual blood was roughly compensated for by the fact that the actual human tissue was generally that poorer quality tissue which is characterised by a rather lower loss factor than that of animal tissues. The human tissue itself may also have lower ionic conductivity than the animal tissues, due to differing ionic mobility in tissue electrolyte. Figure 6.ii compares human with animal muscle tissues, and shows that the human tissue overlap with, and lie in line with the animal data which were taken on poor animal tissue specimens.

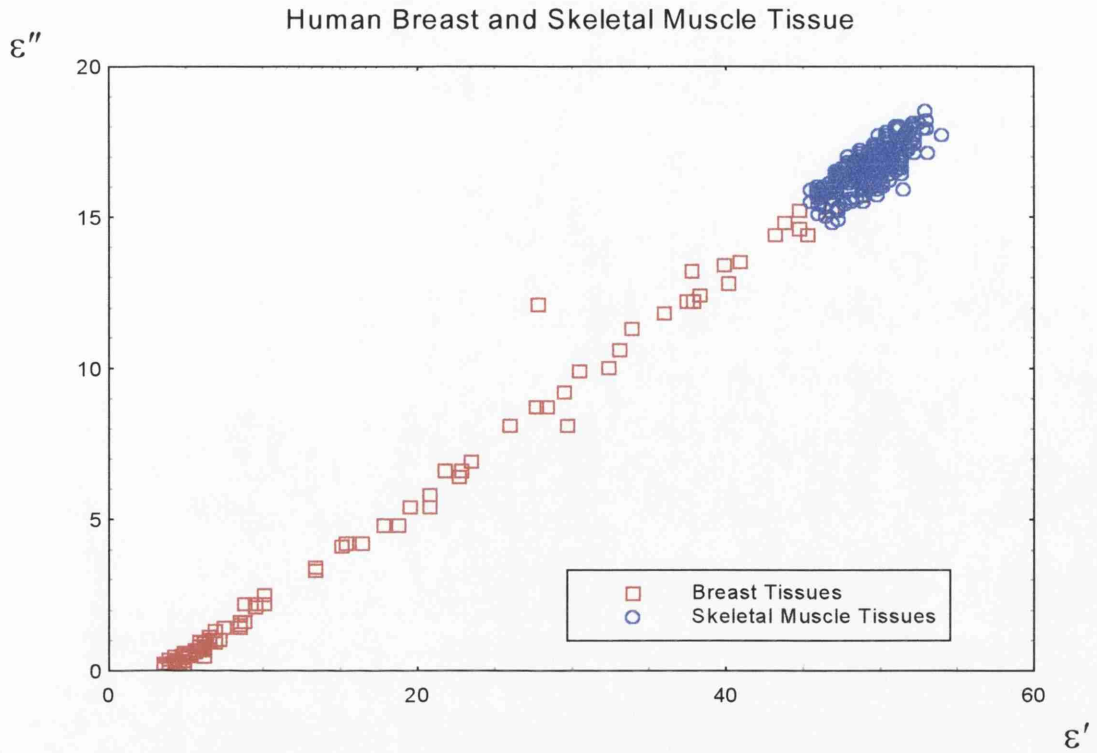

Figure 6.hh. Comparison between human breast and skeletal muscle, showing continuation of the linear relationship between loss factor and dielectric constant observed in the low water content tissues.

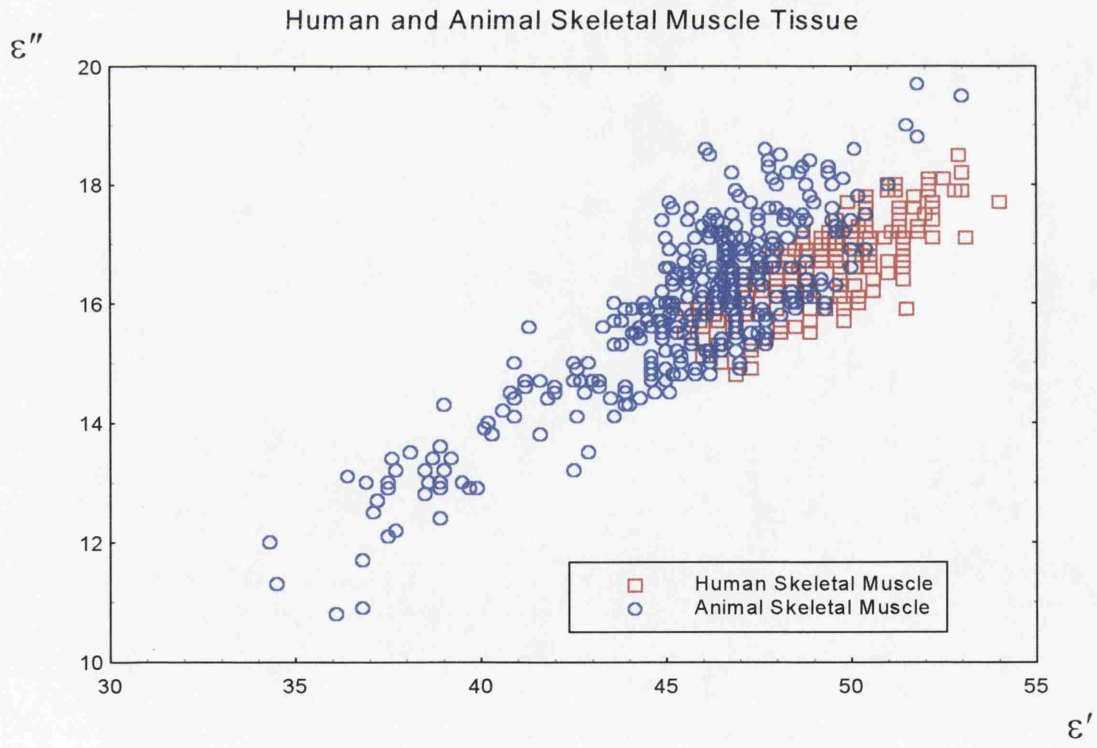

Figure 6.ii. Comparison between human and animal skeletal muscle, showing that the average loss factor values for human muscle generally lie in the lower region of animal loss factor values.

6.7.3. Comparison with Previous Permittivity Measurements.

Cook (1951) made permittivity measurements at 2.98 GHz on three human skeletal muscle specimens, one of soleus muscle, and two of pectoral muscle. Values of the dielectric constant at 37°C ranged from 51 to 52, and the loss factor ranged from 17 to 19. These measurements correspond to the upper permittivity region of the current data. Herrick et al (1950) gives average values of 45 to 48 for the dielectric constant, and 13.5 for the loss factor of skeletal muscle at 37°C, both of which values are rather lower than the average of the data presented here, but are still in fair agreement when the effects of higher measurement temperature are considered.

6.7.4. Connective Tissues from Within Human Skeletal Muscle Specimens.

The quadricep muscle specimen contained considerable amounts of fibrous white connective tissue, in the form of muscle sheath and tendon. This material was removed from muscle samples before permittivity and water content measurement, and was sufficiently extensive to be dielectrically investigated itself. As this tissue exists mainly in thin sheets, it was necessary to separate a large sheet and repeatedly fold the tissue to obtain sufficient thickness for dielectric measurement. The folded sample had then to be compressed rather more tightly than was usual during measurement, to ensure no air was included in the measured volume. Three such samples were prepared, and the average results are listed in table 6.g. Figure 6.jj shows that this tissue displays a linear relationship between loss factor and dielectric constant that is characterised by a higher loss factor than is displayed by other tissue of similar dielectric constant. Comparison between the data in tables 6.d and 6.g shows that the white connective tissue of the breast gave permittivity values close to that of the quadricep connective tissue, but with a slightly lower loss factor / dielectric constant ratio.

6.7.5. Summary of Human Skeletal Muscle Results.

In conclusion, human skeletal muscle was found to have an average permittivity of approximately $49.5 - j16.5$. Residual blood in the tissue was thought to be responsible for raising the water content considerably above that of animal muscle, and for giving a

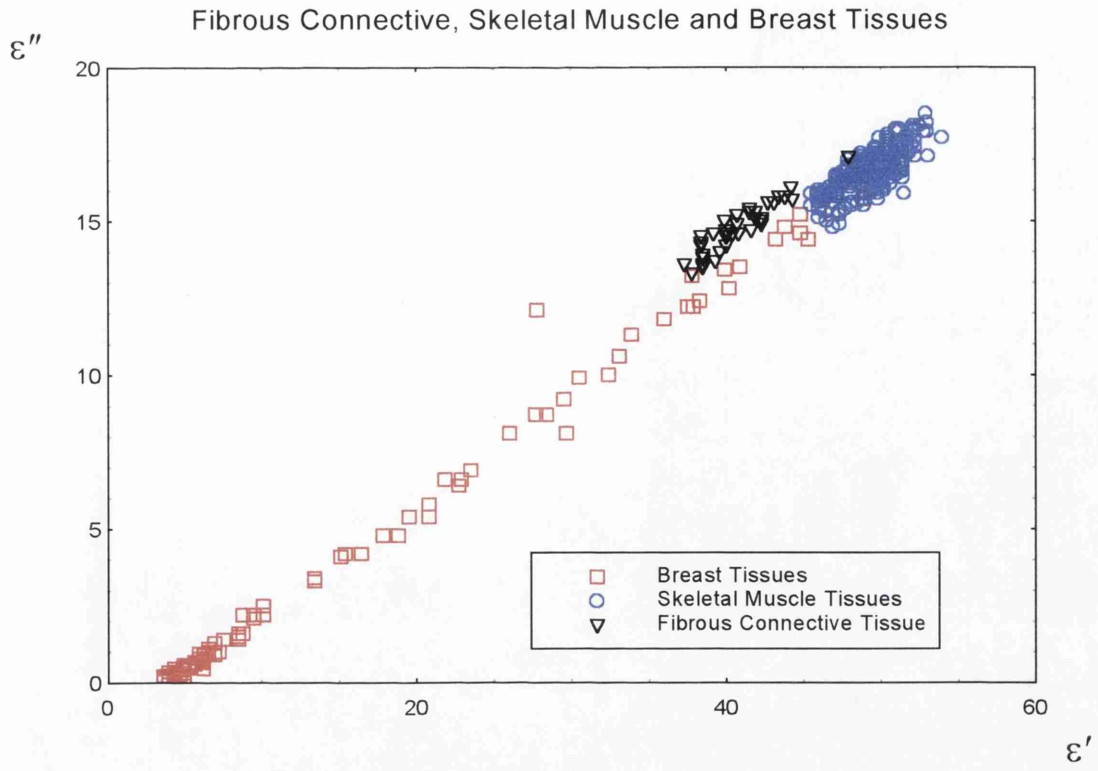

Figure 6.jj. Comparison between fibrous white connective tissue, skeletal muscle and breast tissues. The linear relationship between loss factor and dielectric constant for this connective tissue has similar gradient, but is offset from the other tissues by virtue of its proportionally higher loss factor.

dielectric constant around 3 relative units (approximately 6%) higher than that of animal muscle. A combination of effects were thought to have been responsible for the loss factor remaining approximately the same as that of animal tissue. These are the raising of loss factor due to the residual blood, but from a lower initial value due to the poor tissue quality or lower ionic loss of the tissue electrolyte.
Skeletal human muscle continues the linear trend of loss factor with dielectric constant observed in fatty and transitional tissues. The presence of residual blood probably renders these *in vitro* measurements more representative of the *in vivo* permittivity than are the measured animal tissue values. This likelihood is enhanced by the short time (generally less than 24 hours) between the demise of the tissue donor and permittivity measurement.

6.8. Liver Tissue.

Situated beneath the diaphragm, the liver is the largest organ in the human body, weighing several kilograms in the adult. Because of its size, the microwave dielectric properties of liver are of importance in thermographic modelling of the abdomen.
Four or five specimens each of porcine, bovine and agnine liver were investigated, with a total or around 60 permittivity and water content measurements being made on each type. Two large specimens of human liver were obtained, from which 210 permittivity measurements were made on 49 samples. Limited measurements were also made on one specimen of duck liver. Table 6.h lists the results of all of these measurements.

6.8.1. Overall Results of Animal Liver Measurements.

The water content of each type of animal liver was very similar;

- Porcine Liver: Min. value 65.1% Max. value 70.7% Mean value 68.0%
- Bovine Liver: Min. value 65.8% Max. value 70.0% Mean value 68.1%
- Agnine Liver: Min. value 65.4% Max. value 68.7% Mean value 66.8%.

Measured dielectric constant values were also close;

- Porcine Liver: Min. value 35.8 Max. value 43.4 Mean value 39.4
- Bovine Liver: Min. value 36.0 Max. value 42.0 Mean value 39.7

Type of Tissue	No. of Specimens	No. of Samples	No. of Perm. Measurements	Mean Dielectric Constant	Mean Loss Factor	Mean (%) Water Mass Fraction
Porcine liver	4	65	65	39.4 ± 1.6	13.5 ± 0.5	68.0 ± 1.2
Bovine liver	5	56	56	39.7 ± 1.3	13.6 ± 0.8	68.1 ± 1.0
Agnine liver	4	56	56	38.7 ± 1.4	13.2 ± 1.0	66.8 ± 0.8
Human liver (all)	2	49	210	41.7 ± 1.2	13.5 ± 0.4	74.8 ± 0.8
specimen *a*	1	11	61	41.3 ± 1.4	13.5 ± 0.5	74.9 ± 0.3
specimen *b*	1	38	149	41.8 ± 1.1	13.5 ± 0.4	74.7 ± 0.9
Pre-frozen human liver	1	10	62	41.8 ± 1.7	13.4 ± 0.7	73.2 ± 1.0
Duck liver	1	14	14	41.6 ± 1.1	14.7 ± 0.6	73.6 ± 0.8

Table 6.h. List of mean permittivity and water content values measured on animal and human liver tissues.

Type	Dielectric Constant	Loss Factor	Notes
Human	42.5	12	Herrick (1950) 37°C
Bovine	43	13	Brady et al (1981) 37°C
	38	17	Buffler et al (1991) 20°C
Feline	44	12	Stuchly et al (1982) (in vivo)
Canine	49	14	Xu et al (1987) 20°C
Rat	46	12.5	Kraszewski et al (1982) (in vivo)

Table 6.i. Results of liver tissue measurements at 3 GHz by previous researchers.

- Agnine Liver: Min. value 35.5 Max. value 42.6 Mean value 38.7

Finally, the range of loss factor from each animal species was;

- Porcine Liver: Min. value 12.5 Max. value 14.4 Mean value 13.5
- Bovine Liver: Min. value 12.4 Max. value 15.6 Mean value 13.6
- Agnine Liver: Min. value 10.8 Max. value 15.2 Mean value 13.2

The range of loss factor for agnine tissue is larger due to a few unusually low measurements on a region of one particular specimen. Figure 6.kk shows the overall distribution of water content and permittivity results for all animal liver specimens.
As can be seen from fig. 6.ll and table 6.h, the results from each type of liver all lie fairly evenly distributed amongst the data from the other types (excepting the 5 unusually low measurements from one specimen). The overall scatter is similar to the scatter measured on each individual type of liver, and the calculated standard deviation of permittivity values is approximately the same as the measurement error on each datum. This strongly indicates that all these types of liver display essentially the same dielectric behaviour.
Liver tissue was found to give amongst the most reliable and repeatable permittivity and water content results of any tissue type. The texture of the surface of liver samples ensured that good electrical contact with the open-ended measurement probe was easy to obtain, and the low standard deviation of the measured water contents of liver tissues indicates that there was less variability between specimens than was observed in some muscle tissues.
A best-fit straight line to all the porcine, bovine and agnine liver permittivity results is given by the equation $\varepsilon'' = 0.368\varepsilon' - 1.05$ corr. co-eff. = 0.717 (6.8.1)
This line is of a form similar to those of muscle and fat tissue, and, as can be seen from fig. 6.mm, the liver results continue the general trend of behaviour already observed in animal muscle and fat tissues. The liver data overlap the lower permittivity results from poor quality muscle tissue with fatty inclusions, and more variable local water content.

6.8.2. Correlation between Permittivity and Water Content.

It is noticeable that although the mean water contents of each of these types of liver are close, the rank order for the measured dielectric constant and loss factor of the three

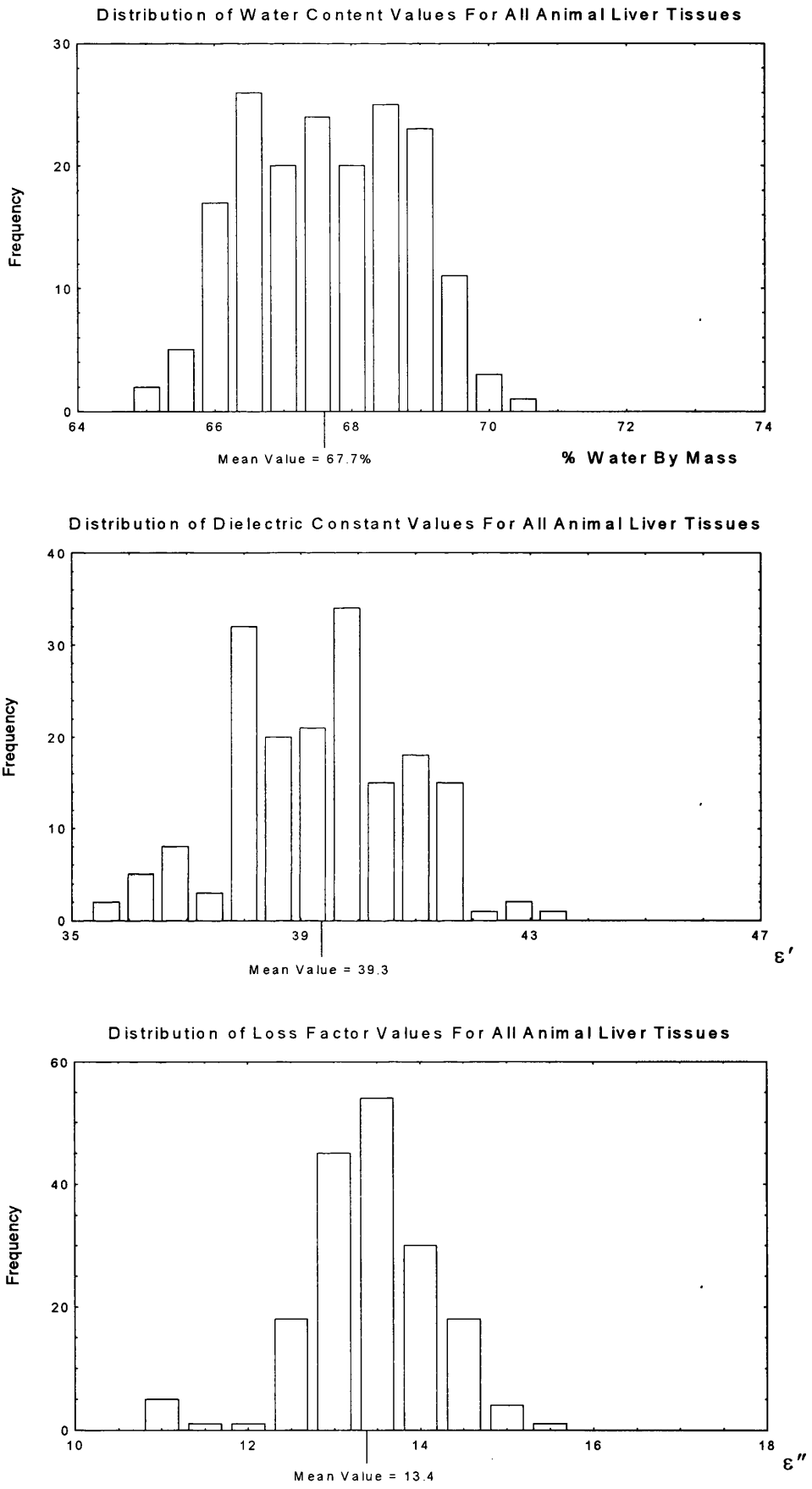

Figures 6.kk. Histograms showing distribution of water content and permittivity measurement values for all animal liver tissues.

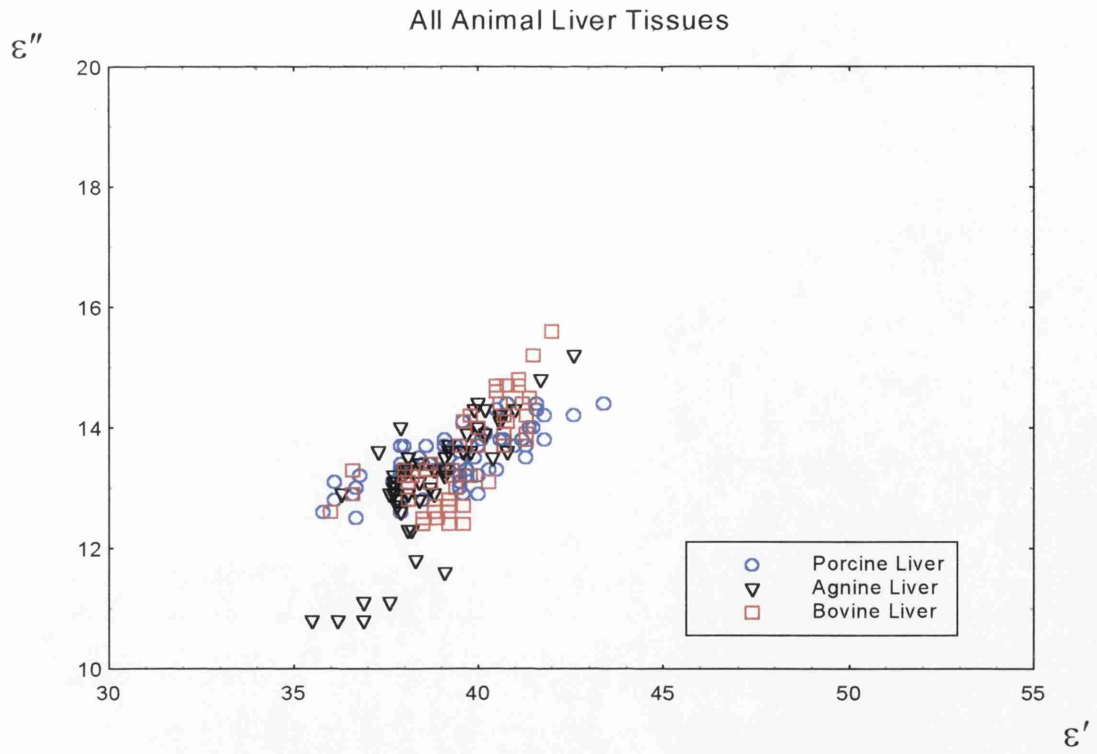

Figure 6.ll. Measured loss factor vs. dielectric constant for porcine, bovine and agnine liver tissues.

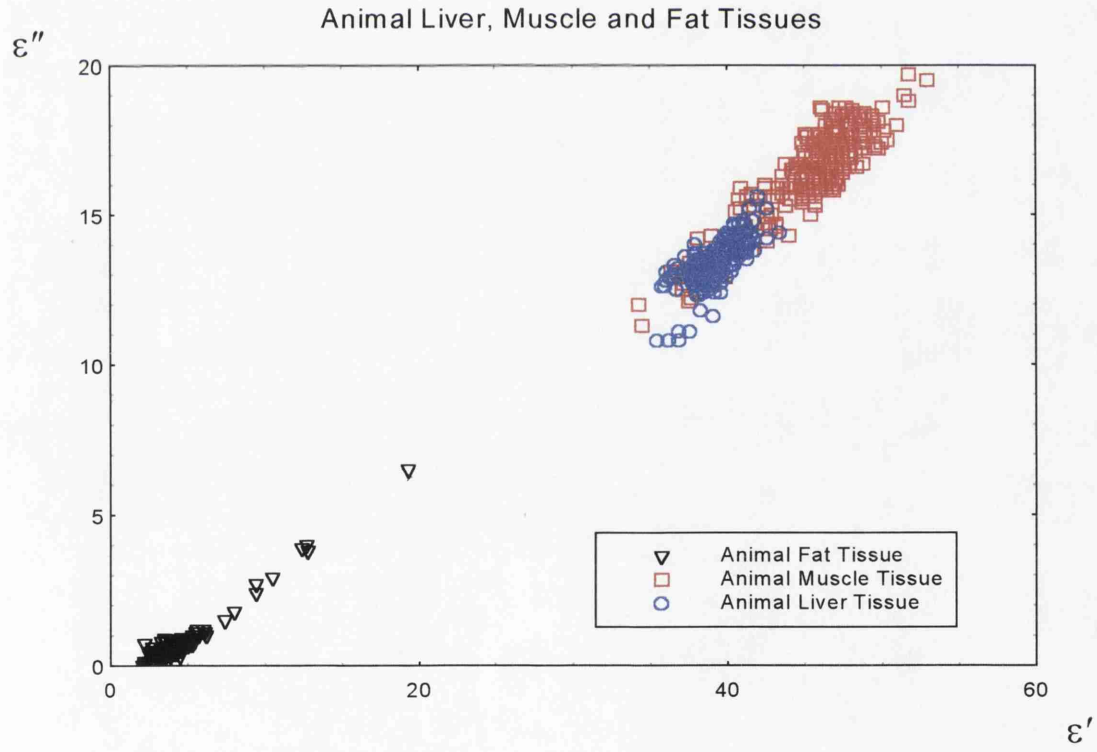

Figure 6.mm. Comparison between animal liver, skeletal muscle and fat tissues showing continued conformance to an approximate linear relationship between loss factor and dielectric constant.

individual types is the same as the rank order for water content. That is to say, for example, bovine liver, which has the highest mean water content, also has the highest dielectric constant and loss factor of these liver types. Porcine and agnine liver result are also ranked accordingly. As with the muscle tissue measurements, however, there is no correlation between the dielectric constant or loss factor and the water content of individual samples. Nevertheless, this ranking of the overall mean values may illustrate the uniformity of water distribution throughout liver tissue specimens, and the dominant effect of aqueous electrolyte content on tissue permittivity.

6.8.3. Human Liver Tissue.

The average results of dielectric measurements on human liver are listed in table 6.h, and the distributions of individual data are shown in fig. 6.nn. Measured ranges of water content and permittivity of human liver samples were;

- Water Content: Min. value 73.3% Max. value 76.8% Mean value 74.8%
- Dielectric Constant: Min. value 39.0 Max. value 44.0 Mean value 41.7
- Loss Factor: Min. value 12.4 Max. value 14.5 Mean value 13.5

In common with animal liver, human liver tissue also gave results with a very low scatter, as can be seen from the small values of the standard deviation on the average water content and permittivity values.
Results from each of the two specimens are fairly evenly distributed, as shown in fig. 6.oo. The mean water content and permittivity for the two specimens were also very similar, indicating that there is less dielectric variability between human liver specimens than between the various muscle tissues.

6.8.4. Comparison between Human and Animal Liver Tissues.

Comparison between human and animal liver data yields the same pattern of behaviour as was observed between human and animal muscle results. Human liver contained significantly more water by mass than did animal liver, giving an average dielectric constant noticeably higher than animal liver, but an almost identical loss factor. Presumably, the same reasons postulated in the previous section could apply equally well

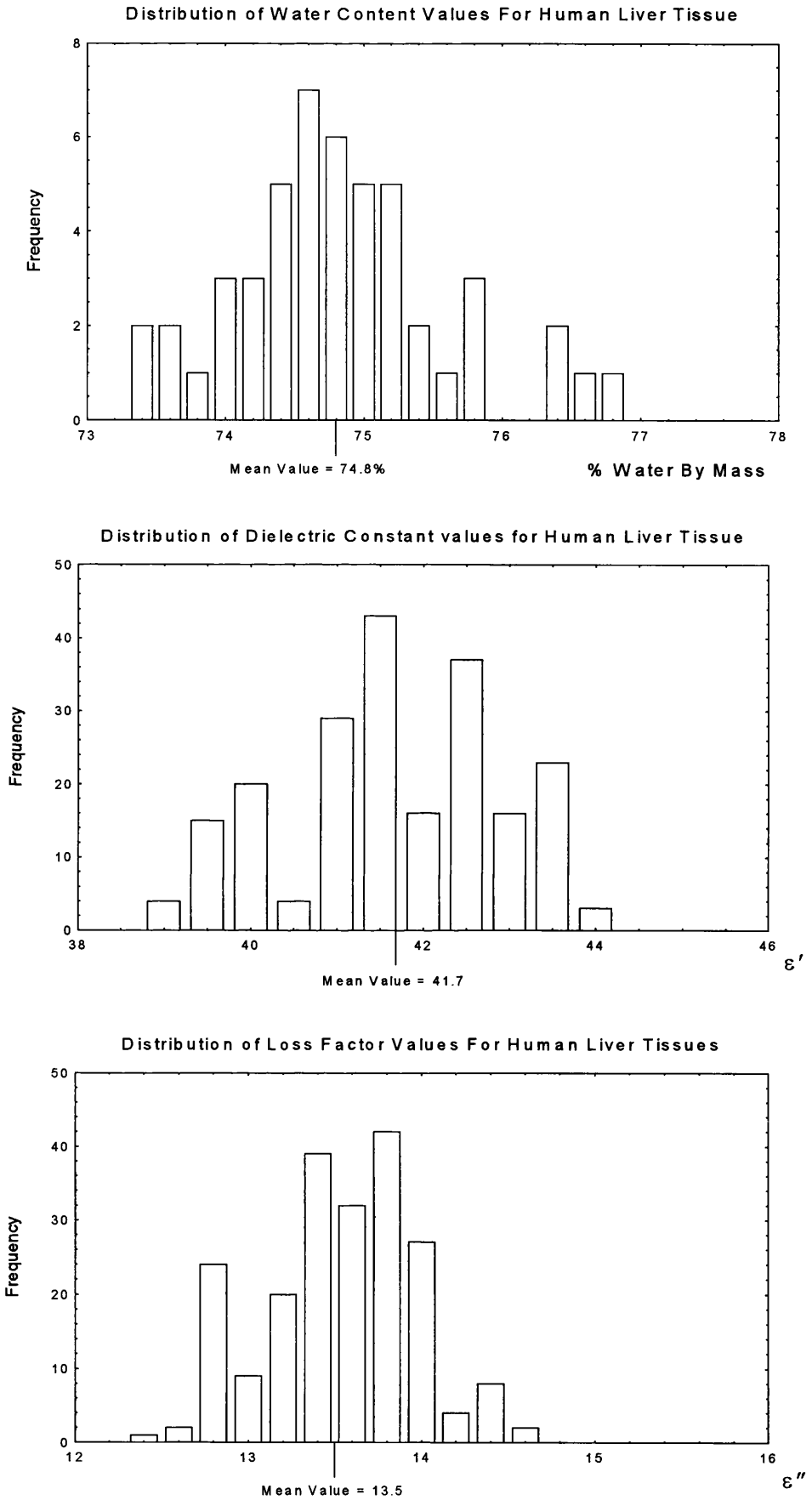

Figures 6.nn. Histograms showing distribution of water content and permittivity measurement values for human liver tissue.

here; excess blood fluid in the human tissue raises the dielectric constant, but any increase in loss factor is compensated by the loss factor of the actual tissue being rather lower than that of animal liver, as shown by poorer tissue quality and rigidity in human tissue. It is certain that there was considerable residual blood present in the human liver specimens, as the pressure of excess handling of the tissue caused droplets to collect on the surface of samples.

Interesting comparison may be drawn between the human liver results, and those taken on a specimen of duck's liver. The duck's liver also contained a large amount of blood, which could easily be made to seep from the tissue by gentle compression, and had a water content of 73.6%, much closer to that of human liver than other animal liver specimens. The dielectric constant of duck's liver was almost identical to that of human liver, considerably higher than other animal specimens. However, the loss factor was also higher than that of the animal liver, by an amount roughly in proportion to the increase in dielectric constant. This would tend to suggest that the duck liver was a specimen with very similar properties to porcine, bovine or agnine liver, but containing extra electrolytic water in the form of residual blood, whereas the actual human liver tissue has a characteristically lower loss factor than other animals.

6.8.5. Comparison with other Human Tissues.

The dielectric data from human liver continue the trend of linear variation of loss factor with dielectric constant observed in muscle tissue measurements, as is shown in fig. 6.pp. Figure 6.pp also highlights the difference between the dielectric behaviour of the white connective tissue and other soft tissues. White connective has similar water content and dielectric constant to those of liver, but has a loss factor larger by 1 to 1.5 relative units. Possible reasons for this behaviour include relative differences in ionic profile and amounts of bound water between liver and white connective tissue. This will be discussed in greater detail in chapter 7.

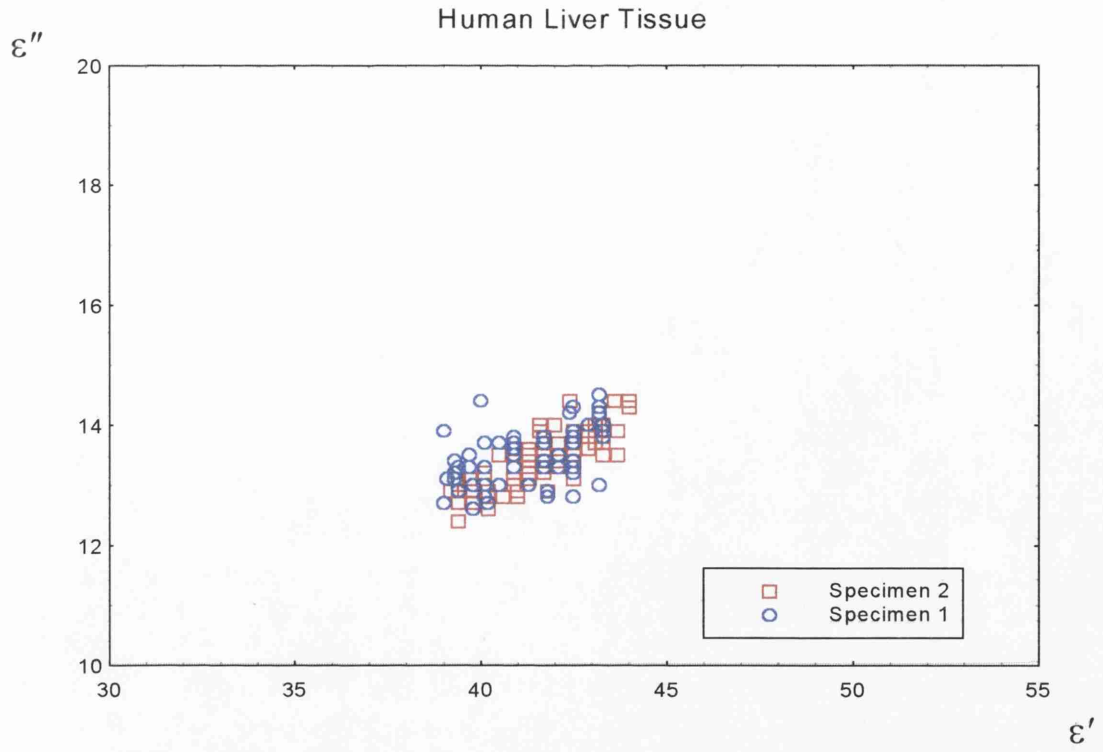

Figure 6.oo. Measured loss factor vs. dielectric constant for both investigated specimens of human liver tissue. Specimen 1: mean dielectric constant = 41.3 ± 1.4, mean loss factor = 13.5 ± 0.5. Specimen 2: mean dielectric constant = 41.8 ± 1.1, mean loss factor = 13.5 ± 0.5

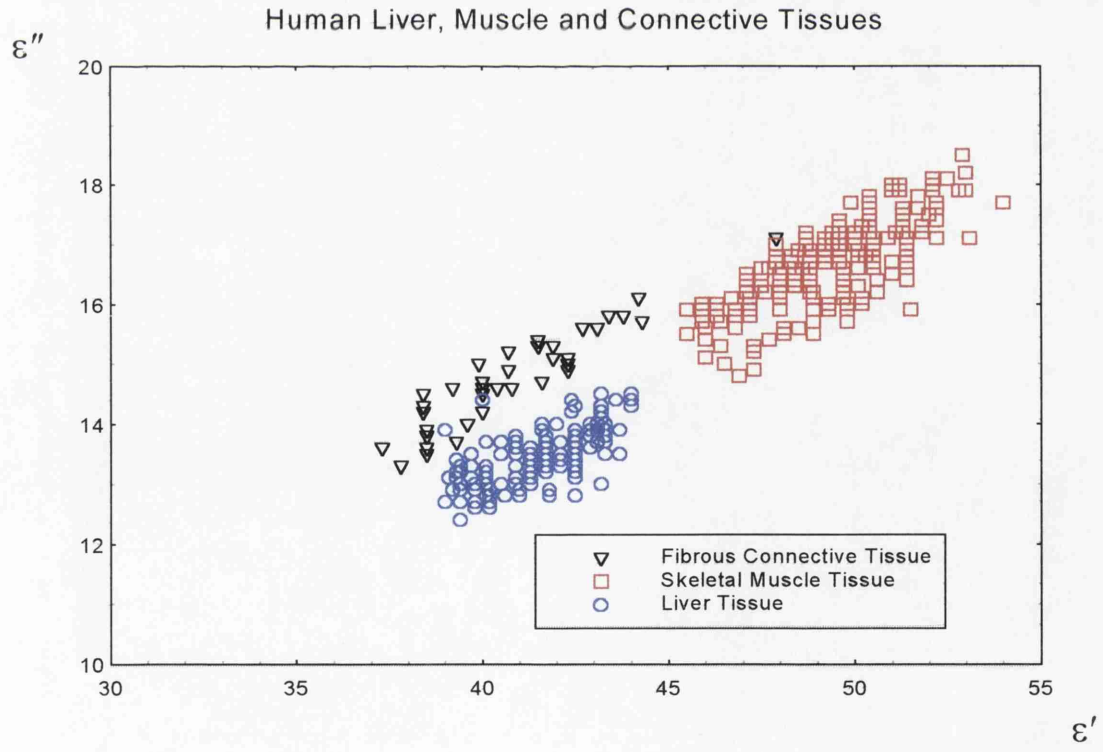

Figure 6.pp. Comparison between human liver, skeletal muscle and muscle connective tissues, illustrating the similar dielectric constant of liver and fibrous connective tissues, but differing loss factor.

6.8.6. Comparison with Previous Permittivity Measurements.

Table 6.i lists data collated from several sources, giving the results of measurements of the permittivity at 3 GHz of liver tissue from a variety of animals.
Herrick et al (1950) give a dielectric constant for human liver which lies well within the experimental error of the current mean value given in table 6.h. His loss factor is lower by around 1.5 dielectric units, slightly greater than the experimental error. The current values for the dielectric constant and loss factor of bovine liver lie between those given by Brady et al and Buffler et al. In particular, the loss factor according to Buffler is almost certainly overestimated.
The dielectric constant values reported for canine and rat liver are significantly higher than those of human and bovine liver. This was also the case when comparing feline, canine and rat muscle with the measurements presented on human and bovine muscle. Since the values for liver are quoted from the same researchers as the corresponding values for muscle, it may be either that there is significant difference between feline, canine and rat tissues and those of other animals, or it may be that these results are systematically high.

6.8.7. Frozen Human Liver Specimen.

A small section of one human liver specimen was measured after being frozen at -18°C in a domestic two-star freezer for one week. As is shown by the data in table 6.h, this had little effect on the average permittivity values, but did increase the range of individual results, and reduced the water content by mass by 1.5%. This reduction in water content was probably due to seepage of the residual blood from some regions of the specimen on de-frosting.

6.9. Kidney Tissue.

The kidneys are bean-shaped organs, weighing around 200g, and are embedded in the posterior abdominal wall. Although not currently of widespread thermographic interest, a preliminary study is under way in the Glasgow thermography group, investigating

whether slight increases in kidney temperature, symptoms characteristic of some disorders, can be detected by microwave thermographic scanning.
A cross-section of the kidney (see fig. 6.qq) shows that the tissue is broadly divisible into two types; an outer *cortex* region, which comprises the majority of the tissue volume, and a smaller inner *medulla*. Cup-shaped *calyces* carry the kidney's waste products into the ureter. The bovine kidney differs from human, porcine and agnine kidney, being composed of many lobes, each consisting of cortex, medulla and calyces.

6.9.1. Animal Kidney Tissue

Porcine, bovine and agnine kidney were again investigated prior to making measurements on human kidney tissue. Around 60 permittivity and water content measurements were made on cortex tissue from each of these animals. A total of twenty measurements were made on medulla tissue from agnine and bovine specimens. Average results from these measurements are listed in table 6.j. Medulla tissue was found to have a significantly higher water content than cortex tissue, but, as the transition between tissues is gradual, there may be some overlap in permittivity and water content results of tissue samples of each type.

6.9.2. Overall Results of Animal Kidney Cortex Measurements.

The distributions of water content and permittivity data values for all animal cortex measurements are shown in fig. 6.ss. Kidney cortex gave water contents in the range;

- Porcine Cortex: Min. value 73.7% Max. value 82.5% Mean value 79.0%
- Bovine Cortex: Min. value 71.5% Max. value 81.1% Mean value 76.0%
- Agnine Cortex: Min. value 74.6% Max. value 81.4% Mean value 78.2%

The measured dielectric constant of kidney cortex ranged from;

- Porcine Cortex: Min. value 46.9 Max. value 52.1 Mean value 49.7
- Bovine Cortex: Min. value 45.3 Max. value 50.8 Mean value 48.3
- Agnine Cortex: Min. value 46.9 Max. value 51.5 Mean value 49.3

Loss factor values ranged from;

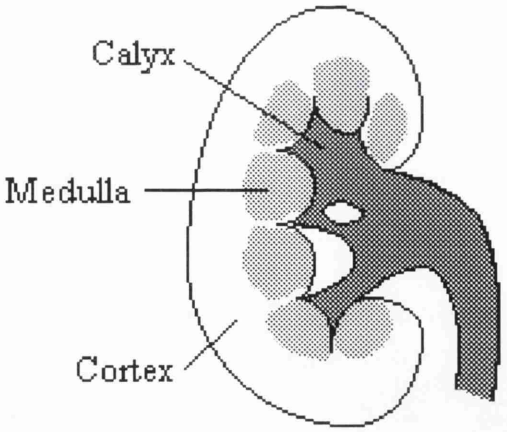

Figure 6.qq. Schematic cross-sectional diagram of the human kidney. Porcine and agnine kidneys follow the same pattern, whilst bovine kidney is similar, but is formed from many individual lobes of cortex and medulla tissue.

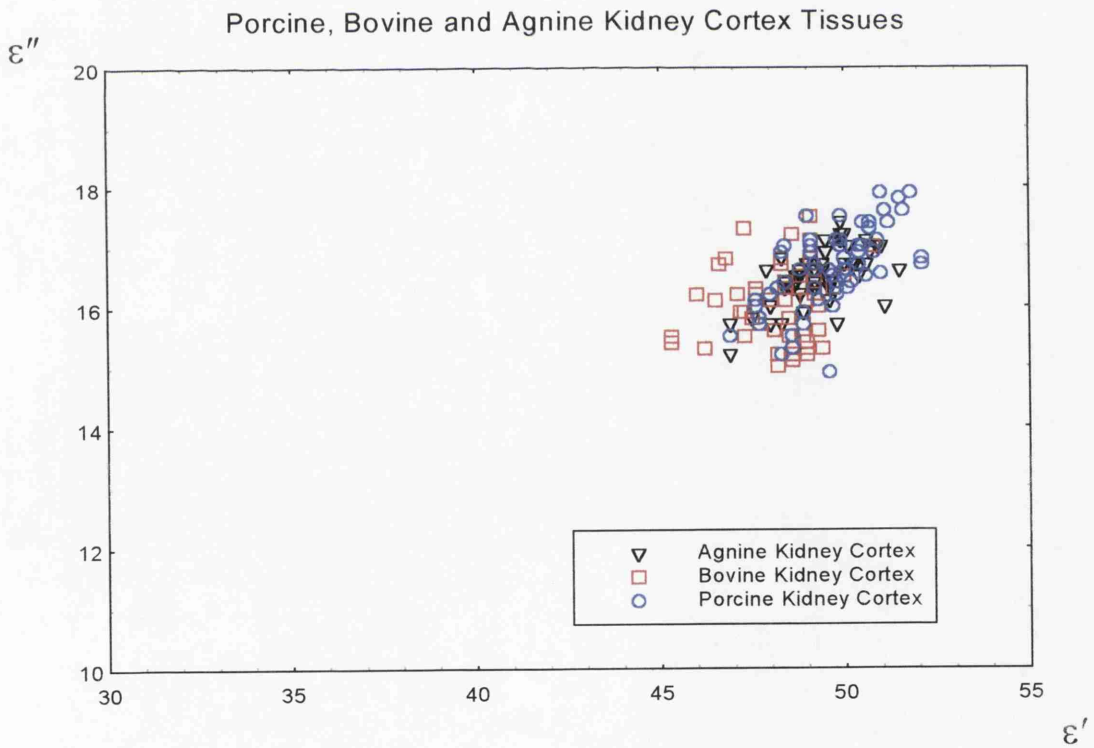

Figure 6.rr. Measured loss factor vs. dielectric constant for porcine, bovine and agnine kidney cortex tissues. A larger scatter is observed in bovine data than the others.

Source of Tissue	No. of Specimens	No. of Samples	No. of Perm. Measurements	Mean Dielectric Constant	Mean Loss Factor	Mean (%) Water Mass Fraction
Porcine						
kidney (c)	5	66	66	49.7 ± 1.2	16.6 ± 0.7	79.0 ± 2.2
Bovine						
kidney (c)	3	62	62	48.3 ± 1.1	16.1 ± 0.7	76.0 ± 2.7
(m)	3	17	17	53.8 ± 1.4	18.6 ± 0.5	82.7 ± 2.0
Agnine						
kidney (c)	4	54	54	49.3 ± 1.4	16.5 ± 0.4	78.2 ± 2.0
(m)	2	3	3	53.7 ± 1.2	19.8 ± 0.7	83.9 ± 0.7
Overall						
(P,B,A)(c)	12	182	182	49.1 ± 1.3	16.4 ± 0.7	77.7 ± 2.5
(m)	5	20	20	53.8 ± 1.4	18.8 ± 0.7	82.9 ± 1.9
Human						
kidney (c)	2	35	174	49.7 ± 1.2	17.3 ± 0.6	78.8 ± 1.3
(m)	2	-	4	53.9 ± 1.9	18.8 ± 1.0	-
c =cortex m= medulla						

Table 6.j. List of mean permittivity and water content values measured on animal and human kidney tissues.

Animal	Dielectric Constant	Loss Factor	Notes
Bovine	48	16	Brady et al (1981) 37°C
Canine	49	18	Stuchly and Stuchly (1980) 37°C
	47	16	Burdette et al (1980) (cortex)
Feline	47	13	Kraszewski et al (1982) (cortex) 36°C
Rat	51	14	Kraszewski et al (1982) (cortex) 36°C

Table 6.k. Results of kidney tissue measurements at 3 GHz by previous researchers.

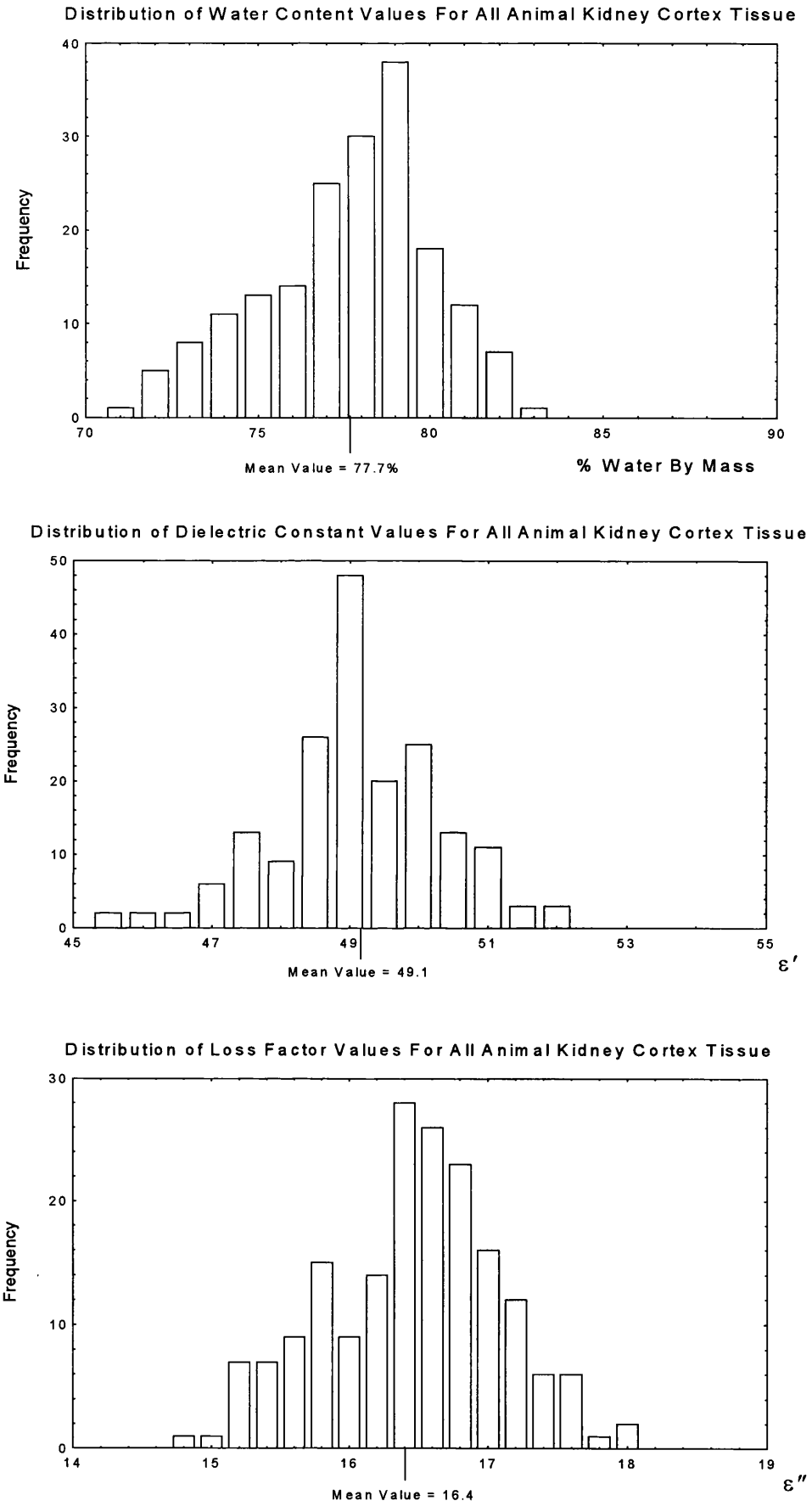

Figures 6.ss. Histograms showing distribution of water content and permittivity measurement values for all animal kidney cortex tissue.

- Porcine Cortex: Min. value 14.9 Max. value 17.9 Mean value 16.6
- Bovine Cortex: Min. value 15.0 Max. value 17.5 Mean value 16.1
- Agnine Cortex: Min. value 15.2 Max. value 17.4 Mean value 16.5

Very little difference between specimens was noticed for porcine and agnine measurements, with the data scatter of each specimen approximately equal to the overall scatter. There was more grouping of results from different bovine specimens. Figure 6.rr shows the distribution of permittivity values for kidney cortex from each of the animal species. The scatter of the bovine data is visibly greater than the scatter on porcine or agnine data. It is also noticeable from fig. 6.rr and the data in table 6.j, that a match between the rank order of the average water content and permittivity values from each species is once again observed, suggesting low variability in water content in cortex tissue between specimens. This helps to confirm that electrolytic water content is the major influence on tissue permittivity, as there is little other physiological difference between the kidneys of these animals.

Linear approximation of the variation in loss factor with dielectric constant gives, for the overall animal cortex data, a poorly correlated straight line with equation

$$\varepsilon'' = 0.282\varepsilon' + 2.54 \qquad \text{corr. co-eff.} = 0.544 \qquad (6.9.1)$$

However, removal of the badly scattered bovine cortex results gives a relation

$$\varepsilon'' = 0.332\varepsilon' + 0.143 \qquad \text{corr. co-eff.} = 0.631 \qquad (6.9.2)$$

This is shown in fig. 6.tt, and is of similar form to the behaviour observed for other tissues.

6.9.3. Kidney Medulla Tissue.

Figure 6.uu shows the cortex results, the results of measurements on tissue of the medulla, which contained around 5% more water by mass than the cortex, and the results of permittivity measurements on skeletal muscle. It can be seen that the form of the linear behaviour of loss factor with dielectric constant for cortex tissue is approximately continued by the medulla. The increased water content of medulla tissue gives a proportional increase in both dielectric constant and loss factor. Although typical values of the water content and dielectric constant of kidney cortex tissue are around 4 - 6%

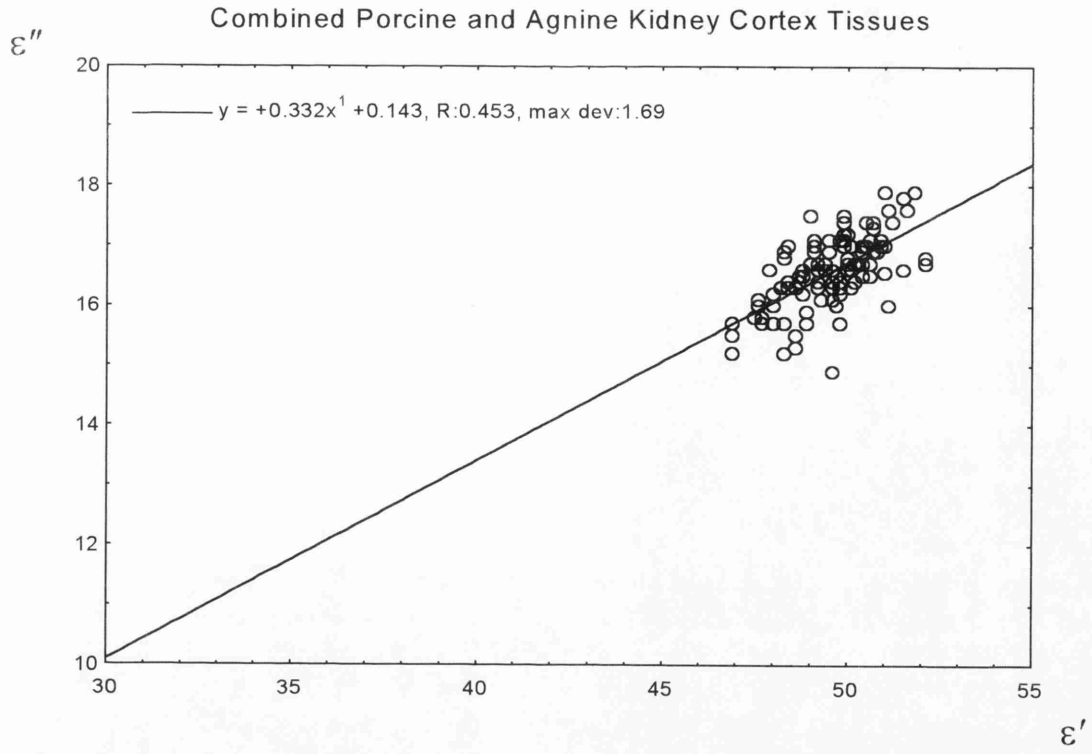

Figure 6.tt. Measured loss factor vs. dielectric constant for porcine and agnine kidney cortex tissues. Correlation co-efficient of straight line fit = 0.631

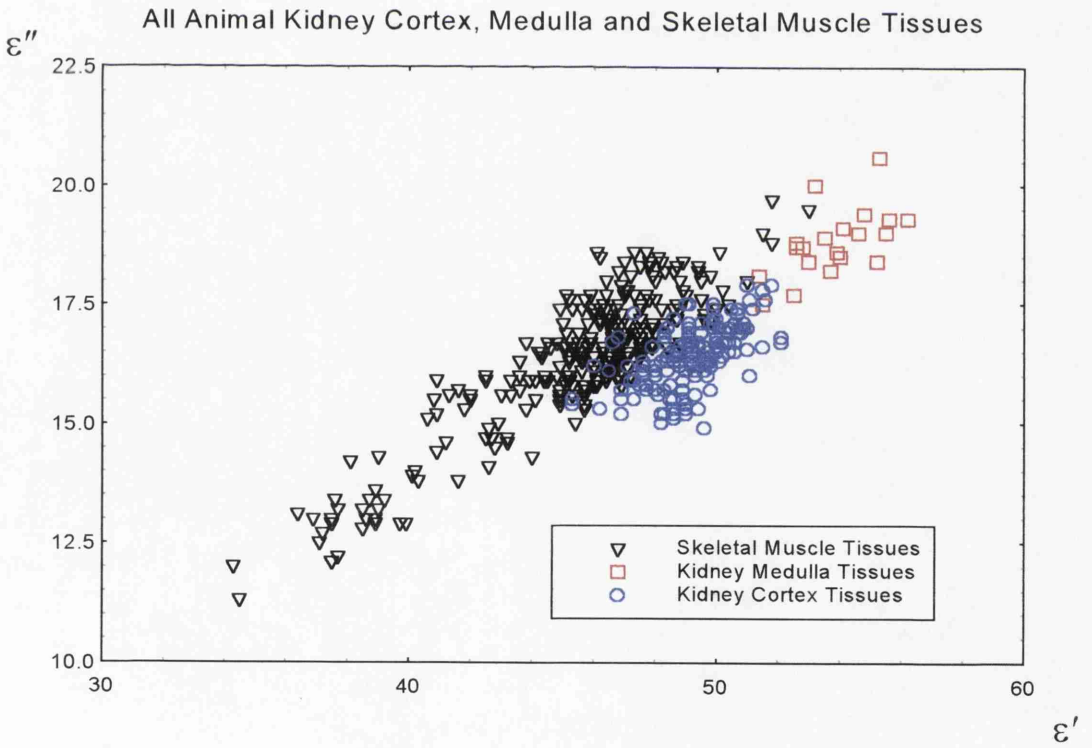

Figure 6.uu. Comparison between animal kidney cortex, medulla, and skeletal muscle, showing that the kidney medulla tissue follows a similar linear trend of loss factor with dielectric constant to that observed in cortex tissue.

higher than those of skeletal muscle, the typical loss factor is of approximately the same magnitude. This suggests that either the ionic profile and/or mobility of the electrolytic water in kidney tissue differs from those of muscle tissue, or that the states and distribution of water molecule binding in kidney tissue are different. It is possible that a combination of both these effects is responsible for the reduced loss factor of the water in kidney tissue.

6.9.4. Human Kidney Tissue.

Two specimens of human kidney were obtained for dielectric investigation. Water content measurements were made on 35 samples, and a total of 178 permittivity measurements made. Four of the permittivity readings (but no water content readings) were made on medulla tissue. The average results of these sets of readings are displayed in table 6.j, and the overall distributions of cortex results are shown in fig. 6.vv.

6.9.5. Overall Results of Human Kidney Measurements.

Results taken on each of the two specimens lay evenly distributed amongst each other. A summary of the ranges and mean values of the measured quantities for cortex gives;

- Water Content: Min. value 75.7% Max. value 81.1% Mean value 78.8%
- Dielectric Constant: Min. value 47.1 Max. value 53.0 Mean value 49.7
- Loss Factor: Min. value 15.9 Max. value 18.5 Mean value 17.3

For medulla tissue, the dielectric constant ranged from 52.1 to 56.4, and the loss factor ranged from 17.9 to 19.8 for medulla tissue.

There is great similarity between the results for human and animal kidney tissues. The mean water content of cortex tissue lies well within the range of measurement error of the water content of both porcine and agnine cortex, and the mean dielectric constant of both human cortex and medulla also lie within the range of experimental error of the results for each animal species, especially porcine cortex, for which the mean values are identical. A noticeable difference is only observed in the loss factor, which, for human kidney cortex, is higher than those measured on animal cortex by around 1 relative unit, or ~6%.

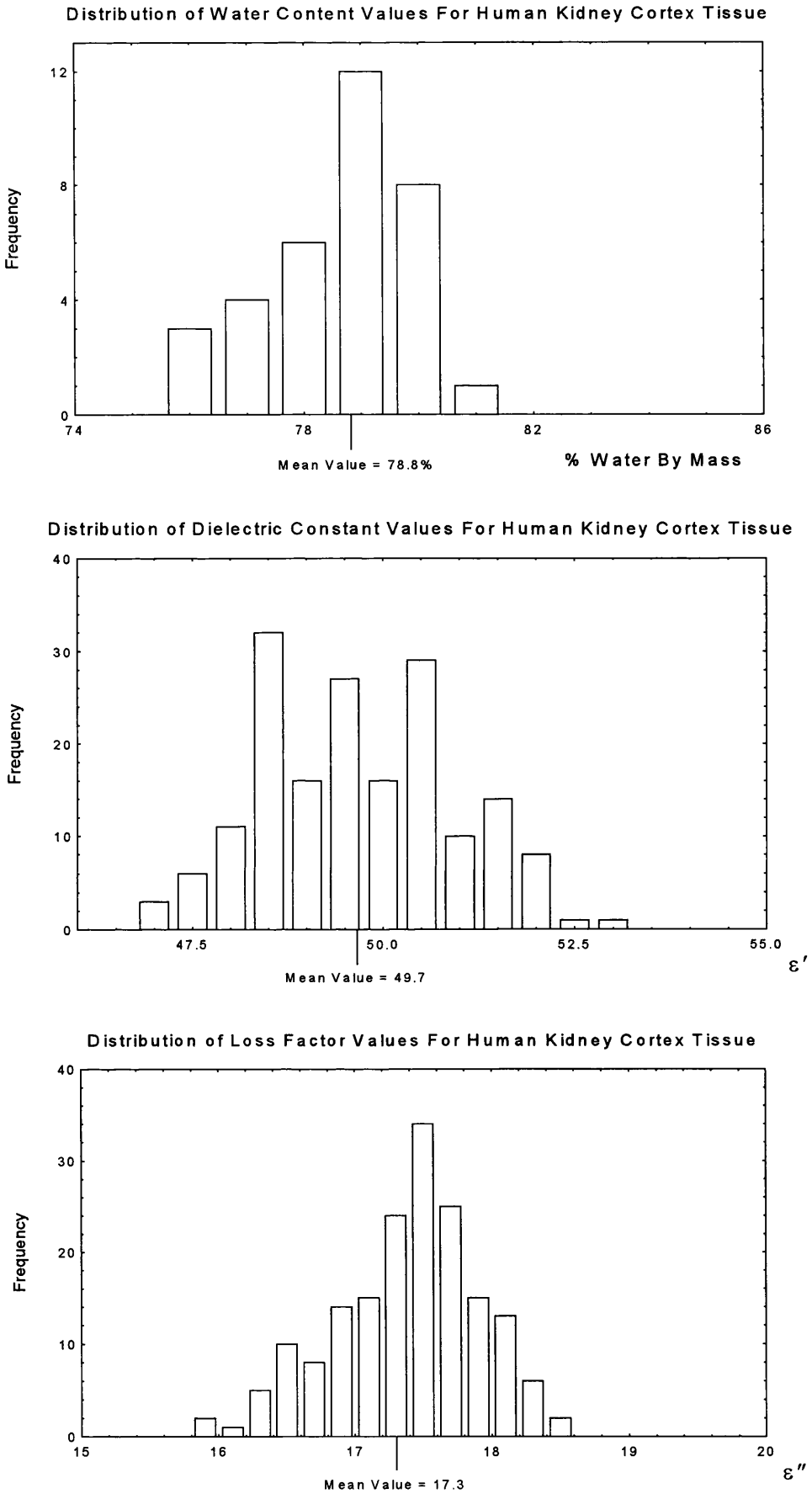

Figures 6.vv. Histograms showing distribution of water content and permittivity measurement values for human kidney cortex tissue.

No obvious explanation could be found for this; although the presence of extra residual blood was suggested by the darker colour of the human kidney tissue specimens, less was visible on kidney sample surfaces than on liver samples, and the respective water contents of human and animal kidney were found to be approximately the same. However, as blood has a slightly higher loss factor (around 18), this still seems the most likely reason for the higher loss factor of the human kidney samples.

The loss factor of human kidney displayed a rather poorly correlated linear relationship with dielectric constant, shown in fig. 6.ww, and given by the equation

$$\varepsilon'' = 0.277\varepsilon' + 3.58 \qquad \text{corr. co-eff.} = 0.713 \qquad (6.9.3)$$

This has similar gradient to the corresponding equations for other human tissues. Because of the comparatively low loss factor of human skeletal muscle, the human kidney permittivity data, in contrast to the animal kidney results, generally lie above the human muscle data, on a graph of loss factor against dielectric constant (fig. 6.xx). Table 6.k lists collated data from a variety of previous permittivity measurements on kidney tissue at 3 GHz. It is not clear from some articles which type of kidney tissue is measured, but it seems certain that the results for bovine and canine kidney, of around 48 - j16, refer to cortex tissue. Hence the results here are similar to those obtained by Brady et al, and Stuchly and Stuchly.

6.10. Heart Muscle Tissue.

The heart is a fist-sized organ, composed mainly of cardiac muscle tissue, located behind the sternum. Cardiac muscle is broadly similar to skeletal muscle, but has a different cellular construction. At the present moment, the heart has not been of interest in any practical microwave thermography study, and so the data in this section will be considered only briefly. However, the permittivity of cardiac muscle may be of some interest in aspects of hyperthermia treatment.

6.10.1 Animal Heart Tissue.

Three specimens of agnine heart muscle were subjected to a total of 42 permittivity and water content measurements. Table 6.l lists the average results of these measurements,

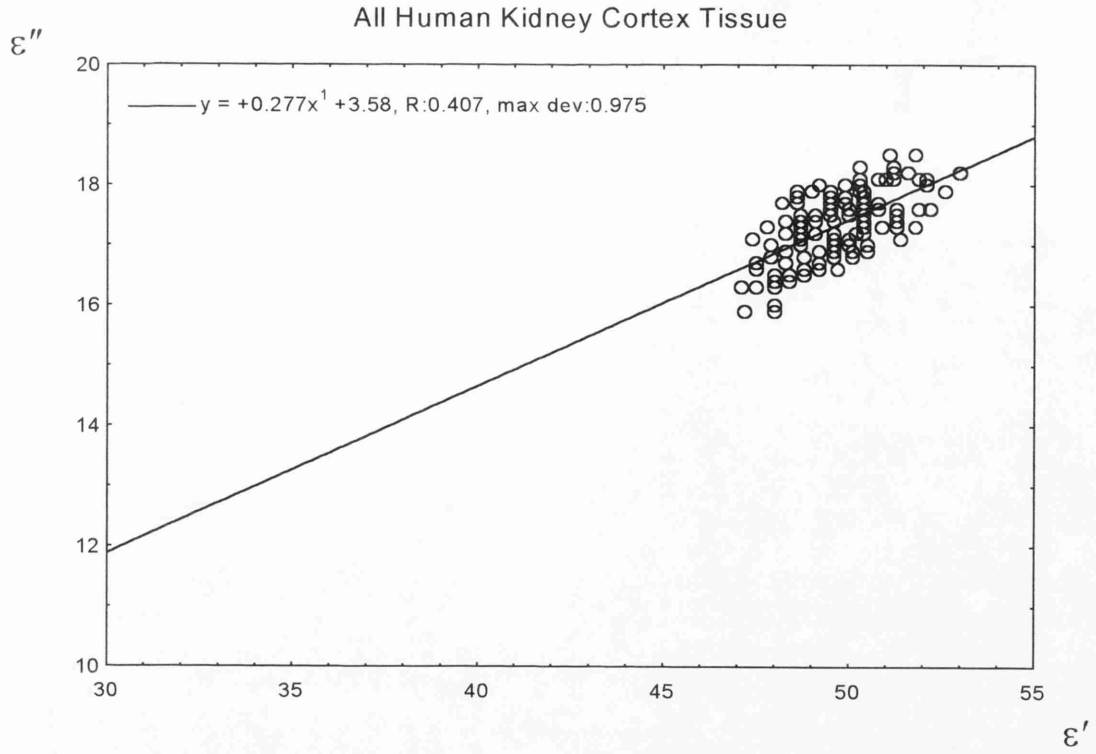

Figure 6.ww. Measured loss factor vs. dielectric constant for all human kidney cortex tissues. Correlation co-efficient of straight line fit = 0.713

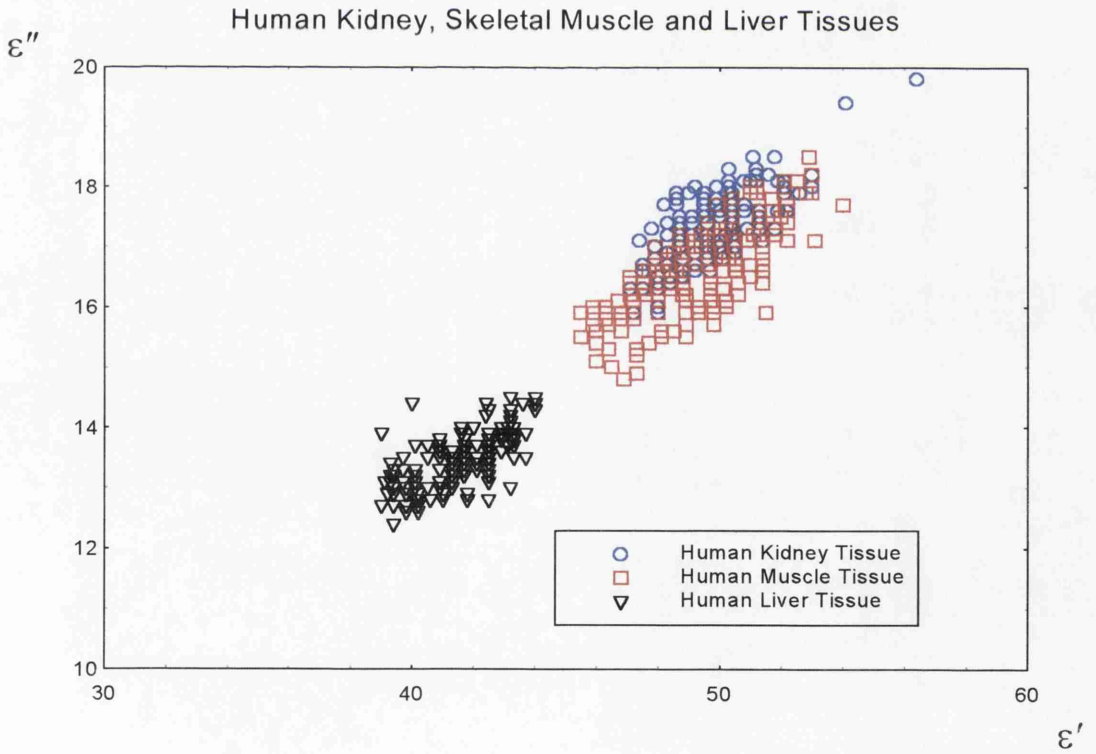

Figure 6.xx. Comparison between human kidney (cortex and medulla), skeletal muscle and liver tissues.

and fig. 6.zz shows the distribution of permittivity and water content values. Measured water content and permittivity values are summarised;

- Water Content: Min. value 70.6% Max. value 78.9% Mean value 76.0%
- Dielectric Constant: Min. value 43.2 Max. value 47.8 Mean value 46.0
- Loss Factor: Min. value 13.8 Max. value 15.6 Mean value 14.7

The mean water content, by mass, of 76.0%, is a value lying between the water contents of skeletal muscle and kidney tissue respectively. By virtue of this, a dielectric constant also lying between those of the latter tissues might be expected. An average of 46.0 was found for the dielectric constant of heart tissue, which is similar to that of skeletal muscle, but not higher.

However, it was found that heart muscle is dielectrically distinguished from skeletal muscle by the lower loss factor of heart muscle. An average value of 14.7 was found for the loss factor of agnine heart muscle, compared to 16.4 for the reliable agnine skeletal muscle. This difference is considerably greater than the experimental error, and indicates either that the water in cardiac muscle is subject to states of molecular binding which differ from those in skeletal muscle, or that the contribution to the loss factor from dissolved ions in the tissue electrolyte is less. Only accurate permittivity measurements over a wide frequency range can resolve this uncertainty.

As with other tissues, a linear increase in loss factor with dielectric constant over the cardiac tissue permittivity results was observed. The best-fit straight line had equation

$$\varepsilon'' = 0.307\varepsilon' + 0.570 \qquad \text{corr. co-eff.} = 0.724 \qquad (6.10.1)$$

and is shown in fig. 6.yy.

Limited measurements on the heart of a duck gave similar results. The mean water content was 76.7% by mass, approximately 3% higher than the mean value for animal skeletal muscle; the dielectric constant was 45.5, almost the same as skeletal muscle; and the average loss factor of duck heart was 13.9, again much lower than that of skeletal muscle. The only 3 GHz permittivity value for heart tissue which could be found from literature is the value of $52 - j13$ quoted by Xu et al (1987), for canine heart at 20°C.

Type of Tissue	No. of Specimens	No. of Samples	No. of Perm. Measurements	Mean Dielectric Constant	Mean Loss Factor	Mean (%) Water Mass Fraction
Agnine heart	3	42	42	46.0 ± 1.0	14.7 ± 0.4	76.0 ± 1.8
Human heart						
specimen a	1	1	5	49.8 ± 1.0	14.8 ± 0.4	80.8
specimen b	1	29	99	51.3 ± 1.2	14.3 ± 0.4	82.4 ± 1.0
Duck heart	1	6	6	45.5 ± 2.0	13.9 ± 0.6	76.7 ± 1.5

Table 6.I. List of mean permittivity and water content values measured on agnine and human heart muscle tissues.

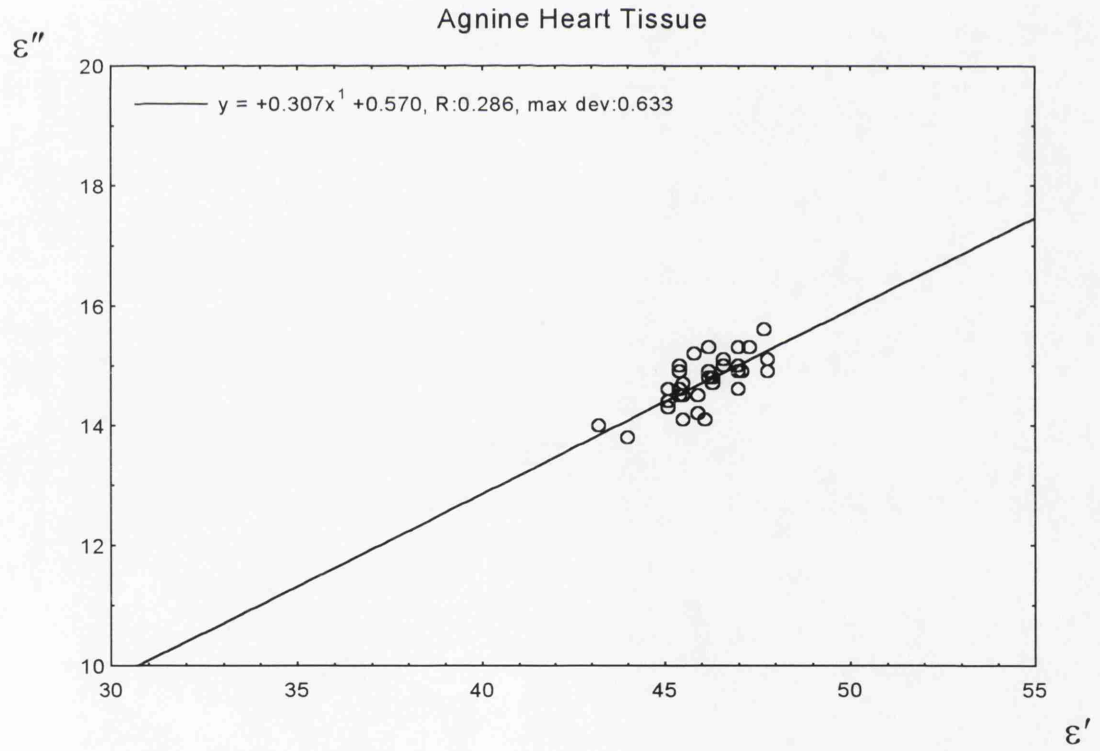

Figure 6.yy. Measured loss factor vs. dielectric constant for agnine heart tissue. Correlation co-efficient of straight line fit = 0.724.

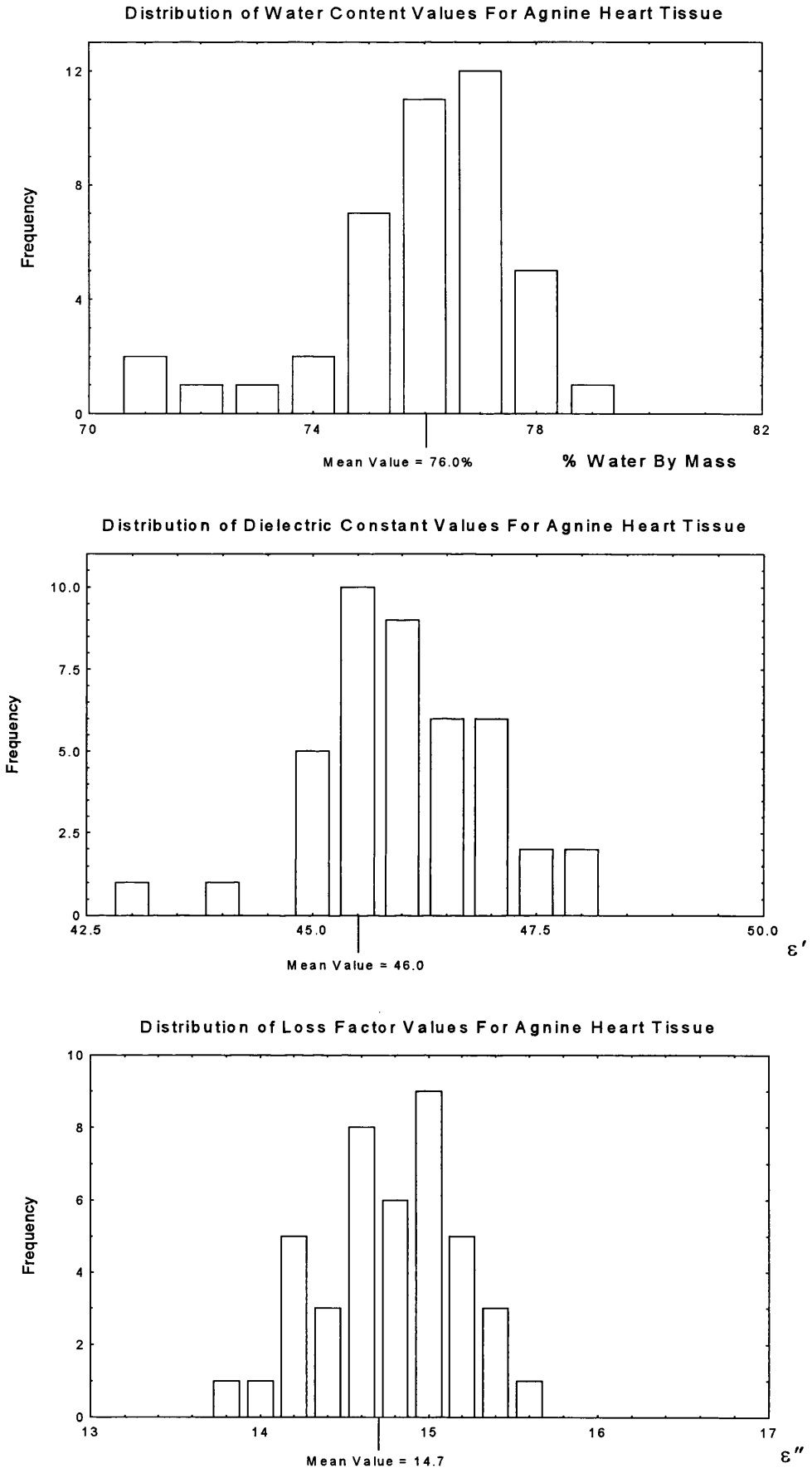

Figures 6.zz. Histograms showing distribution of water content and permittivity measurement values for agnine heart tissue.

6.10.2. Human Heart Tissue.

Two specimens of human heart tissue were investigated. However, the larger of these specimens (specimen *b*) had been immersed in water for over 48 hrs. to preserve the tissue, and gave clearly anomalous results. Only 5 permittivity measurements could be made on the smaller specimen (specimen *a*), but these are far more reliable. The average results taken on both specimens are listed in table 6.1.

As with most human tissues, the water content of specimen *a* was higher than that of the corresponding animal tissue by around 4%, presumably due to the presence of residual blood. This had the effect of raising the average dielectric constant to 49.8, 3.8 relative units higher than that of agnine heart, but maintaining the loss factor at 14.8. It can be seen that this behaviour is similar to that observed when comparing the permittivities of skeletal muscle and liver from both human and animal specimens. The water content of the human tissue is higher, giving a corresponding increase in dielectric constant, but the loss factor is not significantly affected.

With only five data points, each separated by little more than the experimental error, a linear approximation for the variation in loss factor with dielectric constant cannot be regarded as definitive, but the calculated best-fit for this specimen *a* is

$$\varepsilon'' = 0.280\varepsilon' + 0.890 \qquad \text{corr. co-eff. } 0.759 \qquad (6.10.2)$$

This conforms approximately to the usual behaviour observed in other tissue.

Although not strictly representative of heart tissue, the measurements on the larger (anomalous) specimen *b* illustrate the effect of adding water to a tissue. The mean water content of specimen *b* was 82.4%. This extremely high value must be due to the tissue absorbing some of the water in which it was immersed. As water has a dielectric constant of 78 at room temperature, the dielectric constant of the heart tissue is also raised, with an average value of 51.3. In comparison to agnine heart tissue, specimen *a* had 4.8% more water, and a dielectric constant 3.8 units higher. Specimen *b* had 6.4% more water, and a dielectric constant 5.3 units higher. Thus the relative increases in dielectric constant are both roughly proportional to the excess water content. The loss factor of specimen *b* was still only 14.3, slightly lower than that of the agnine tissue. This is because the excess water itself has a loss factor of approximately 14, the same as the heart tissue, and so absorption of water has little effect on the overall loss factor.

Initial ionic imbalance between the tissue electrolyte and the storage water may result in leaching of ions from the tissue, thus reducing its conductivity, as was observed.
A plot of loss factor against dielectric constant for specimen *b* (fig. 6.aaa) also shows that, because of the absorption of water, any correlation between loss factor and dielectric constant in the tissue is removed.

6.11. Human Tumour Tissues.

One of the main areas of interest to microwave radiometry is thermographic scanning of the female human breast. It is thought that the presence of breast cancer is characterised by an increase in temperature around the tumour, due to inflammation of the local tissues. Tumours also typically have a high water content, especially compared to the fatty breast tissue in which they are often situated. It is therefore of interest to know typical values of the microwave permittivity of tumours, and whether they differ dielectrically from other high water content tissues. The results presented here may be a useful addition to the current body of data on tumour permittivity.
Five human tumour specimens were obtained from five individual donors. Four were breast tumours from post-menopausal women, and one was a bowel tumour from a male donor. All of the specimens were believed to be malignant tumours, although the precise pathology of each tumour is not known.
The results from each of the specimens are listed individually in table 6.m. Two to four permittivity measurements were made on each tumour specimen. Due to the small size, rigidity, and irregular shape of these tumours, it was more difficult than usual to ensure reliable probe contact during co-axial probe permittivity measurements. One of the breast tumours was not easily separable from the surrounding fat tissue, and so gave an unusually low water content and permittivity values, which were excluded from the calculations of mean values.
In general, the high water content of breast tumours was confirmed; values from 80.3% to 83.8% water by mass were recorded, with 84.5% for the bowel tumour. The mean water content of 82.7% is similar to that of kidney medulla and spleen tissue, and only grey brain matter had a water content that was significantly higher. As a range of dielectric constant values from 49.4 to 57.2, with a mean of 52.6, was measured, it seems that the dielectric constant of tumours is similar to that of the other tissues with

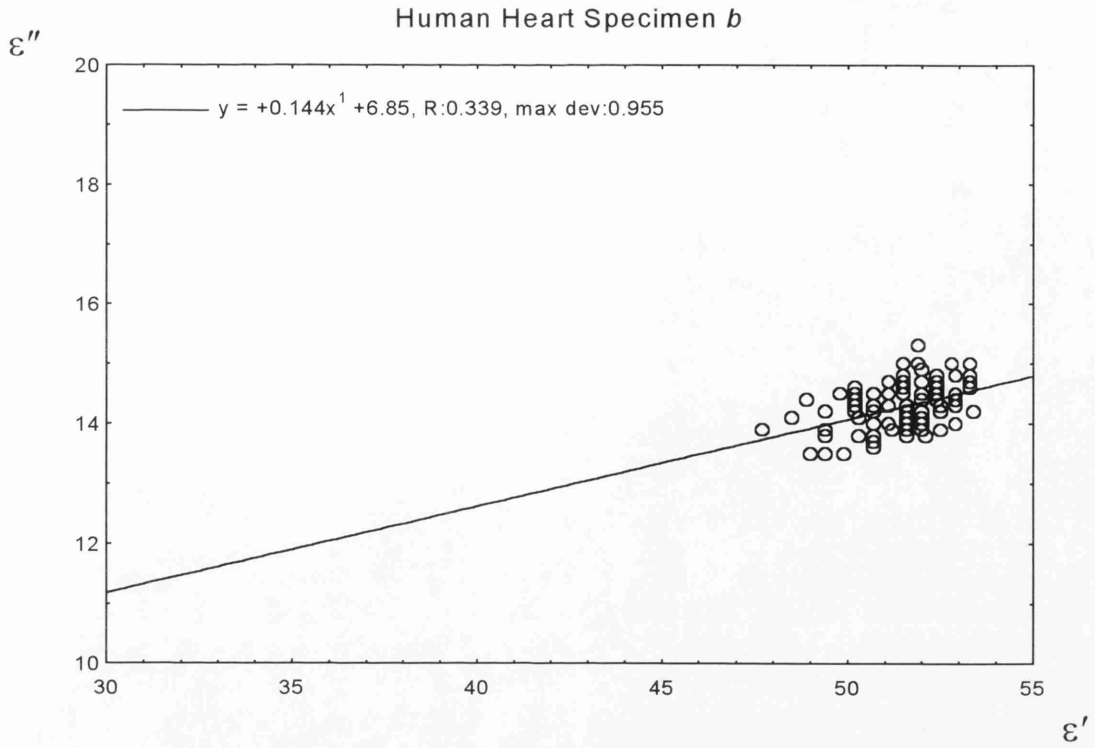

Figure 6.aaa. Measured loss factor vs. dielectric constant for human heart tissue specimen *b*, which had been immersed in water prior to measurement. Correlation co-efficient of straight line fit = 0.353.

Type of Tumour	No. of Specimens	No. of Samples	No. of Perm. Measurements	Mean Dielectric Constant	Mean Loss Factor	Mean (%) Water Mass Fraction
Breast (1)	1	1	2	50.3 ± 1.2	15.5 ± 0.4	80.3
Breast (2)	1	1	2	53.2 ± 1.4	15.7 ± 0.0	83.8
Breast (3)	1	1	3	53.8 ± 0.8	16.6 ± 0.3	82.3
Breast (4) *	1	1	3	45.1 ± 2.7	14.7 ± 0.6	45.8
Bowel **	1	1	4	53.2 ± 2.9	15.9 ± 1.3	84.5
Overall	4	4	11	52.8 ± 2.2	15.9 ± 0.8	82.7 ± 1.6
* Fatty tissue attached ** Difficult to ensure reliable probe contact						

Table 6.m. List of mean permittivity and water content values measured on human tumour tissues.

similar water content. Although the number of measurements may not make this study of great statistical significance, it appears that the loss factor of tumour tissues is rather lower than those of other human tissues with similar water content. A mean value for the loss factor of 15.9 was found, compared to 18.8 for kidney medulla, and 17.2 for spleen. From the limited data, no distinction can be made between breast and bowel tumour.

For comparison, England (1950) reported values of 62 - j15 and 57 - j18 for breast carcinomae at 37°C, although the water contents of these specimens was not reported. What seems certain is that the permittivity of breast tumours differs considerably from that of the surrounding tissue, which is usually rather fatty material. It is hoped that these results will aid dielectric modelling of the human breast for cancer screening.

6.12. Miscellaneous Human Tissues.

This section contains the results of measurements which were taken on human tissue types for which no animal equivalent tissue was measured for comparison. Of minimal thermographic interest, the data help to reveal the role of water in determining the dielectric properties of tissues, and the dielectric similarity between different tissues of the same water content.

6.12.1. Uterus Tissue.

The uterus is a hollow reproductive organ in the female, and is composed of smooth muscle tissue. Uterine tissue is unique in this study in that all the specimens obtained were removed from their respective donors during surgery, rather than at post-mortem. Thirty nine permittivity measurements were made on 11 specimens of smooth uterine muscle tissue. Table 6.n lists the average results of these measurements, the ranges of which are summarised;

- Water Content: Min. value 76.2% Max. value 82.0% Mean value 79.6%
- Dielectric Constant: Min. value 45.9 Max. value 51.8 Mean value 49.1
- Loss Factor: Min. value 14.4 Max. value 16.9 Mean value 15.8

Type of Tissue	No. of Specimens	No. of Samples	No. of Perm. Measurements	Mean Dielectric Constant	Mean Loss Factor	Mean (%) Water Mass Fraction
Human Pancreas *	1	21	72	49.2 ± 1.1	16.6 ± 0.6	67.8 ± 3.1
Spleen **	1	8	70	55.4 ± 1.5	17.2 ± 0.4	83.3 ± 1.0
Uterus						
normal	11	11	39	49.1 ± 1.5	15.8 ± 0.5	79.6 ± 1.8
fibroid	3	3	7	48.8 ± 3.6	15.8 ± 1.2	78.6 ± 1.3
Cervix						
normal	1	1	3	48.2 ± 1.0	15.6 ± 0.2	74.6
fibroid	1	1	3	49.3 ± 1.0	15.6 ± 0.2	79.9

* Lots of fat around samples, so unrepresentatively low water content

** Contained a large amount of blood

Table 6.n. List of mean permittivity and water content values measured on human pancreas, spleen, uterus and cervix tissues.

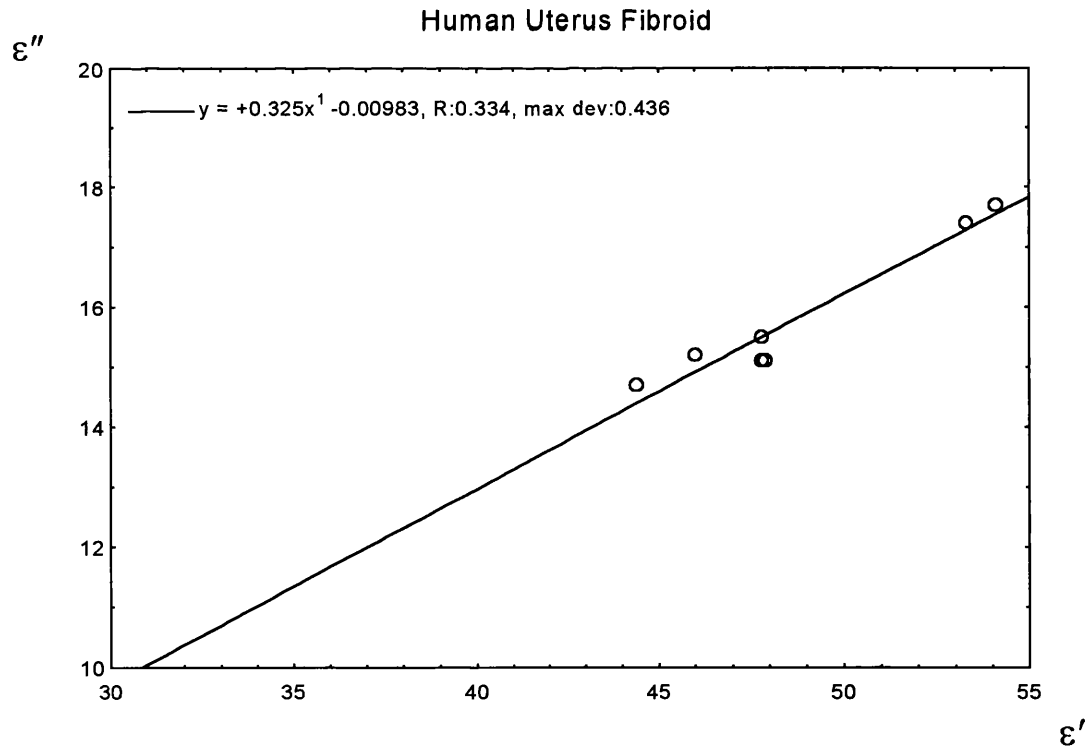

Figure 6.bbb. Measured loss factor vs. dielectric constant for human uterus fibroid tissue. Correlation co-efficient of straight line fit = 0.968.

The mean value and the spread of water content for uterus tissue are similar to those of human kidney cortex and heart tissues (specimen *a*). This gives a dielectric constant also with a similar mean and spread to those of kidney and heart tissue. The mean loss factor of 15.8 lies midway between those of kidney cortex and heart muscle.

In addition to the smooth uterine muscle specimens, three specimens of fibroid tissue from around the uterus were investigated, the average results for which are listed in table 6.n. Overall, these specimens gave a mean water content, dielectric constant, and loss factor very similar to those of uterine muscle tissue. However, the range of permittivity values calculated was considerably larger, spreading from 44.4 to 54.1 for the dielectric constant, and from 14.7 to 17.7 for the loss factor. This is probably due to the local tissue variability exhibited by such tissues with coarse fibrous structure, in which local regions of high and low water content exist within the tissue.
Although the number of measurements on fibroid tissue was few, the comparatively wide range of values gave a well correlated linear relationship between loss factor and dielectric constant, shown in fig. 6.bbb. The linear relation of best-fit is

$$\varepsilon'' = 0.325\varepsilon' - 0.010 \qquad \text{corr. co-eff.} = 0.968 \qquad (6.12.1)$$

Dielectric measurements were also made on two small specimens of tissue from the cervix, one of smooth muscle tissue, and the other of fibroid tissue. The results show that these specimens displayed almost identical dielectric permittivity values to the major uterine specimens, and also had very similar water content.

Hence all of these uterine tissues display dielectric behaviour similar to that of other tissues, in which the dielectric constant is strongly dependent on the water content, but the loss factor is also dependent on the tissue type as well as the water content.

6.12.2. Spleen Tissue.

The spleen is an ovoid organ situated on the left-hand side of the body, directly below the diaphragm. This organ serves as a reservoir for blood, destroying micro-organisms and worn-out blood cells, and replacing many chemicals in the circulatory system. As a consequence of this, the spleen tissue specimen investigated in this study contained a considerable amount of residual blood. A mean water content of 83.3% was measured

on this specimen, whereas the commonly accepted value for spleen tissue is 79%. The measurements on this specimen may not therefore be strictly representative of the actual tissue of the spleen, but may instead better represent the *in vivo* permittivity of heavily perfused tissue.

Mean values of the 8 water content and 70 permittivity measurements on spleen tissue are listed in table 6.n, and may be summarised;

Water Content:	Min. value 82.2%	Max. value 84.6%	Mean value 83.3%
Dielectric Constant:	Min. value 50.9	Max. value 58.6	Mean value 55.4
Loss Factor:	Min. value 16.2	Max. value 18.2	Mean value 17.2

It is reasonable to assume that the lowest values of these parameters correspond more closely to the true permittivity of spleen tissue, as they suggest the presence of less blood in the volume of permittivity measurement.

By comparison, Kraszewski et al (1982) reported a value of 52 - *j*15 for feline and rat spleen tissue at 32 to 36°C. The slightly lower loss factor and dielectric constant may be due to the higher measurement temperature. However, feline and rat tissues may not be so close to human tissues as are the animals considered here. Stuchly et al (1982b) also give a value of 52 - *j*15 for feline spleen at 35°C *in vivo*.

As with the human heart specimen that had been immersed in water (specimen *b*), it can be seen from fig. 6.ccc, that the presence of this excess blood in the spleen tissue had the effect of reducing the correlation between loss factor and dielectric constant of the permittivity measurements. This is because the material measured was not a single tissue type which displayed the well correlated behaviour, but a combination of tissue and residual blood.

6.12.3. Pancreas Tissue.

The pancreas is a long narrow gland running horizontally behind the stomach, and touching the spleen at one end. Its function is to produce and release digestive enzymes and sodium bicarbonate to neutralise stomach acid.

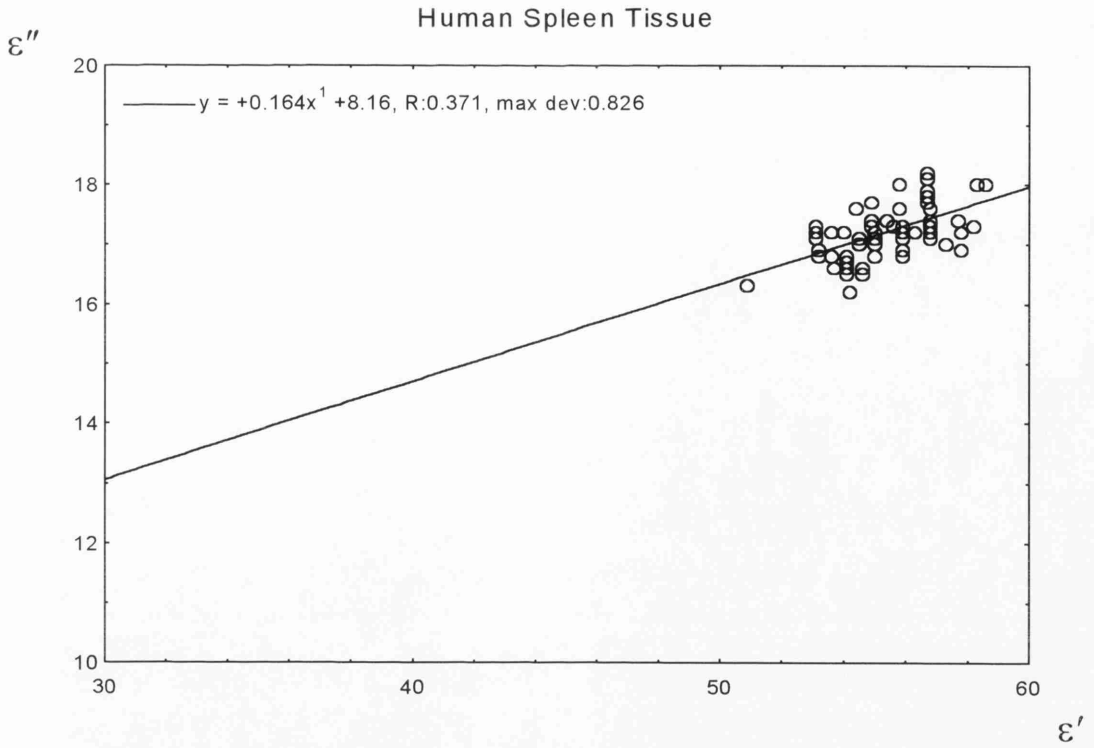

Figure 6.ccc. Measured loss factor vs. dielectric constant for human spleen tissue. Linear fit has low correlation , probably due to presence of residual blood. Correlation co-efficient of straight line fit = 0.550.

Type of Tissue	No. of Specimens	No. of Samples	No. of Perm. Measurements	Mean Dielectric Constant	Mean Loss Factor	Mean (%) Water Mass Fraction
Grey Matter	1	8	81	54.9 ± 1.7	12.5 ± 0.5	86.0 ± 1.7
White Matter	1	5	51	31.8 ± 3.0	7.3 ± 0.6	75.2 ± 1.2
Intermediate Samples	1	3	11	39.3 ± 3.2	8.7 ± 1.0	79.0 ± 2.6
Overall						80.7 ± 1.6

Table 6.o. List of mean permittivity and water content values measured on human brain tissues.

A total of 72 permittivity measurements were made on 21 samples of pancreas tissue, and the average results are listed in table 6.n. Measured values of the dielectric constant ranged from 46.7 to 51.4, and the loss factor ranged from 15.2 to 18.5. These values suggest a water content of around 80% by mass, as they are broadly similar to those measured on kidney and uterine tissues, which had this water content. The commonly accepted value for the water content of pancreas is around 75% (Biology Data Book, 1972).

The pancreas specimen was surrounded by fatty tissue with no distinct boundary between the pancreas tissue and the fatty tissue. Consequently, it was difficult to prepare samples of pure pancreas tissue, and so the measured water contents were rather lower than the literature value of 75%.

6.12.4. Brain Tissue.

The brain is a 1.5kg mass of nervous tissue consisting of both grey and white nervous matter. Grey nervous matter is found predominantly around the outside of the brain, and is composed of neuron cell bodies and nerve fibres, which carry impulses in the brain. White matter consists of nerve fibres which are surrounded by a white fatty material called myelin. Nervous tissue has a far less rigid structure than the other soft tissues considered in this study, and, because of the fat content, also has a density of only ~1.033g/ml (Rose and Goldberg, 1979), lower than the 1.05g/ml typical of other soft tissues. As the water content of the whole brain is ~78% by mass, the non-water fraction of brain tissue therefore has a density of ~1.17g/ml, rather than the value of around 1.3g/ml for the dry protein in other soft tissues.

One specimen of brain tissue was obtained, taken from the upper cerebrum. A total of 81 permittivity measurements were made on samples prepared entirely of grey matter, and 51 permittivity measurements were made on samples composed entirely of white matter. A small number of measurements were also made on samples containing both types of nervous tissue, but for these measurements it was impossible to tell what proportion of the measured volume was composed of each tissue type, except by estimation from the final calculated permittivity value. Mean values of these sets of results are presented in table 6.o.

Brain tissue is of a delicate nature, being scarcely able to support its own weight when once removed from the cranium, and is also prone to rapid degradation. To preserve the specimen, it was immersed in water until dielectric investigation. This is not ideal preparation for dielectric and water content measurements, as it is possible that water ingress into the tissue may have occurred, perturbing the true permittivity and water content. Also, ionic imbalance between the electrolytic water in the brain and the water in which the sample was stored may have leached some ions from the tissue electrolyte, reducing the conductivity of the brain tissue. By taking permittivity measurements only on the interior surfaces of samples, any possible effect on the permittivity values caused by the immersion in water was hoped to be minimised. However, it can be seen from the lists of measured data values that the mean measured water content of each tissue type was certainly rather higher than the accepted average values of 70% for white tissue and 84% grey tissue (Biology Data Book 1972).

The range of water content and permittivity values found from white matter were;

- Water Content: Min. value 74.3% Max. value 77.2% Mean value 75.2%
- Dielectric Constant: Min. value 27.5 Max. value 38.2 Mean value 31.8
- Loss Factor: Min. value 6.3 Max. value 9.0 Mean value 7.3

For grey matter, the range of measured values were;

- Water Content: Min. value 83.1% Max. value 88.8% Mean value 86.0%
- Dielectric Constant: Min. value 49.4 Max. value 59.2 Mean value 54.9
- Loss Factor: Min. value 11.7 Max. value 14.5 Mean value 12.5

Measurements on samples containing both tissue types gave an average permittivity value of $39 - j9$.

Brain tissue also showed a linear increase of loss factor with dielectric constant, although characterised by a noticeably lower gradient than for other tissue types, as the data in fig. 6.ddd shows. A well correlated linear relationship was observed, with best-fit equation

$$\varepsilon'' = 0.226\varepsilon' + 0.0475 \qquad \text{corr. co-eff.} = 0.984 \qquad (6.12.2)$$

The same linear fit expresses the behaviour of both white and grey brain tissues, and applies over a wide range of dielectric constant values, from around 30 to 60 relative dielectric units.

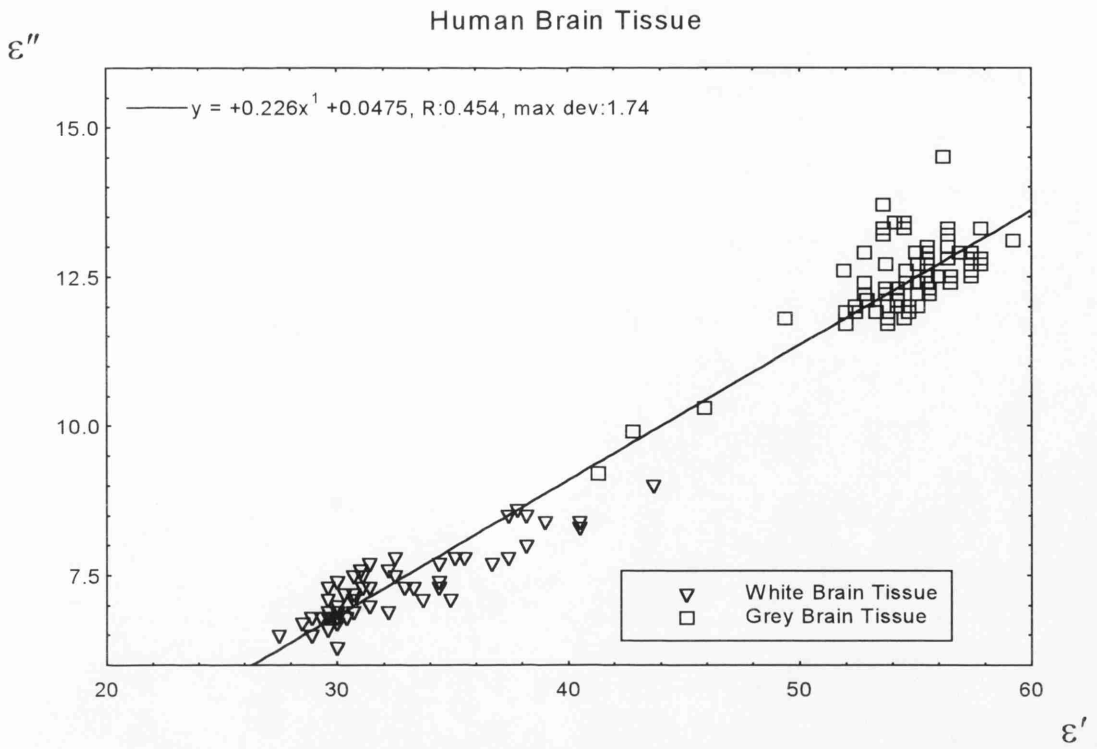

Figure 6.ddd. Measured loss factor vs. dielectric constant for human brain tissues. Correlation co-efficient of straight line fit = 0.984

Tissue Type	Dielectric Constant	Loss Factor	Notes
Mouse			
whole brain	41	11	Nightingale et al (1980)
whole brain	38	11	Nightingale et al (1983)
grey 86% water	59	16	
80% water	46	13	Thurai et al (1984)
77% water	43	11	
Rabbit (20°C)			
grey	50	13	Steel and Sheppard (1985)
white	37	9	(Noted no difference between
macerated	42	11	rabbit and mouse brain)
Cat (in vivo) grey	52	13	Stuchly et al (1982b)
Human macerated	34	15	
Combined macerated			Lin (1975)
data from many species	35	11	

Table 6.p. Results of brain tissue measurements at 3 GHz by previous researchers.

Table 6.p shows permittivity values at 3 GHz estimated from the data of several previous researchers, all of which were taken at 37°C, unless stated otherwise.

In general, the collated data for grey matter are similar to the values observed in this study. When compared to the current results and collated data from other soft tissues, it can be seen that the loss factor of both brain tissues is considerably lower than is observed in other tissues of similar water content. In section 7.2, it will be shown that this is partially due to the very low conductivity contribution from ionic and other low frequency conductivity sources. Kidney medulla tissue has a mean dielectric constant value of 53.9, and a mean water content of 83%. This suggests that the mean dielectric constant of grey brain tissue, which is 54.9, is consistent with a water content of around 84%, the accepted water content value of grey matter. This is rather lower than the water content value obtained here. It is probable that water ingress into the outermost regions of the tissue increased the overall water content of the measured samples, but did not alter significantly the local water content deep within the samples, where permittivity measurements were made. It may be that when analysing the results using mixture equations in the next chapter, it will be more appropriate to use the accepted biology data book water content values to represent the local sample water content than the mean values measured here.

The current mean permittivity values for white matter are significantly lower than those reported by Steel and Sheppard (1985). Perturbation of the measured values by water ingress would presumably have had the effect of raising the dielectric constant above its true value, whereas the opposite effect is found. The dielectric constant of macerated brain tissue reported by Lin (1975) is much lower than that of Steel and Sheppard, and therefore suggests that the dielectric constant of white matter is also much lower, probably in the region of 30 relative dielectric units. Comparison between these two data sets with other results does indicate that the measurements of Steel and Sheppard are more consistent with those of other researchers than are those of Lin.

Nevertheless, the current data, and those of previous researchers, all indicate that the 3 GHz dielectric constant of white brain tissue is considerably lower than those of other soft tissues with similar water content. This is thought to be due to there being a larger proportion of water which is bound in white brain tissue, and not contributing significantly to the dielectric constant at this frequency.

6.13. Miscellaneous Animal Tissues.

This section contains the results of measurements on animal tissues for which no equivalent human tissues were investigated.

6.13.1. Blood.

Although a liquid, blood is regarded as a type of connective tissue, characterised by a fluid matrix. Blood perfuses all the soft tissue regions of the body, there being an average of 70ml/kg body weight in the normal adult human. It is therefore useful to be aware of the microwave permittivity of blood for thermographic purposes.
Permittivity and water content measurements were made on two specimens of fresh animal blood, less than one hour after letting. One specimen was of female porcine origin, and had not been treated with anti-coagulant, and the other was male bovine blood, which had been treated with an unknown amount of the anti-coagulating agent Phosphorous-B.
Very consistent and uniform results were obtained, listed in table 6.q, with an average measured permittivity of $53.6 - j22.1$, and water content of 79.1% by mass for the bovine blood, and an average permittivity of $57.2 - j18.2$, with water content of 81.5% for the porcine blood.
There is a marked difference between male and female blood, as male blood contains approximately 15% more protein in red cells than female blood. This may partially explain the lower water content and dielectric constant of the male bovine blood.
Previous researchers have obtained very similar results. Cook (1952) quoted a value $58.5 - j18.5$ for male human blood at 20°C, Jenkins et al (1989) obtained $56 - j16$ at 25°C, and England (1950) obtained a value of $53 - j15$ at 37°C. The measurements made here on porcine blood are therefore in fairly good agreement with previous results, but the bovine blood has a significantly higher loss factor. This may be due to the anti-coagulant in the bovine blood affecting the blood conductivity, and so this result is probably anomalous.
It may be noted that blood has a dielectric constant significantly higher than those of soft tissues with similar water content. The dielectric behaviour of blood is discussed in more detail in section 7.6, where the high value of dielectric constant is found to be probably

Type of Tissue	No. of Specimens	No. of Samples	No. of Perm. Measurements	Mean Dielectric Constant	Mean Loss Factor	Mean (%) Water Mass Fraction
Bovine Tripe						
outer layers	2	36	136	60.6 ± 2.2	13.5 ± 0.9	88.7 ± 2.7
mucosa	2	20	49	72.9 ± 1.8	15.8 ± 0.9	94.9 ± 1.4
overall	2	117	18	66.5 ± 4.1	15.3 ± 0.5	91.4 ± 1.2
Human Bowel						
Specimen (a)	1	1	7	52.7 ± 2.2	14.9 ± 0.5	85.5
Specimen (b)	1	1	3	53.2 ± 1.4	14.1 ± 0.7	80.2
Porcine Blood	1	1	7	57.2 ± 0.8	18.2 ± 0.4	81.4 ± 0.2
Bovine Blood	1	1	5	53.6 ± 1.0	22.1 ± 0.5	79.1 ± 0.2
Porcine Skin						
outer surface	1	1	6	29.4 ± 2.1	11.6 ± 0.8	55.3 ± 1.3
inner surface	1	1	6	39.3 ± 0.8	14.1 ± 0.2	58.0 ± 0.8

Table 6.q. List of mean permittivity and water content values measured on miscellaneous animal tissues.

Source of Skin Tissue	Dielectric Constant	Loss Factor	Notes
Hand	38	12.5	Tanabe and Joines (1976) (in-vivo)
Faecal Fistula	51	15	
Breast	40	12.5	Cook (1950) (2.98 GHz) 37°C
Foot	42	13	
Breast and Leg	43.5	16.5	England (1950) (average value)
Canine Skin	39	11	Xu et al (1987) 20°C

Table 6.r. Results of skin tissue measurements at 3 GHz by previous researchers.

due to the relatively small amount of bound water in blood which does not contribute to the overall dielectric constant.

6.13.2. Skin.

Twelve permittivity measurements were made on the same number of samples of porcine skin, all taken from one tissue specimen originating from the area over the ribs. Porcine skin from this area is very much thicker than human skin, and so it is easier to obtain more reliable dielectric measurements than would be possible from human skin specimens.

Prior to measurement, the skin samples were trimmed from the subcutaneous fat in as precise a fashion as possible, so as not to leave excess fat to perturb the measured water content or permittivity. Six permittivity measurements were made on the outer surface of the skin, and six on the inner surface. Mean permittivity and water content results are listed in table 6.q. By mass, the water content of the skin samples varied from 53.3 % to 59.1%, although this may be an unrepresentatively low value due to the presence of fat on the samples. On the outer surface, the mean permittivity value was $39.3 - j14.1$, and on the inner surface, a mean value of $29.4 - j11.6$ was measured. The lower value on the inner surface was presumably due to the presence of remaining fat tissue, which could not be fully removed from the skin.

Table 6.r lists permittivity values of skin tissue from previous studies at 3 GHz frequency. All these measurements were made on the outer skin surface of human samples, unless stated otherwise. It can be seen that most of the listed values are in reasonable agreement with the current measured averages. Only the measurement by England, and one of the measurements by Cook, show significant deviation.

Comparison between the permittivity results for skin and other soft tissues suggests that if the same dielectric behaviour is displayed, the water content of skin should be around 65-70%. Depending on the origin of the skin, a great variation in water contents can be found. The Biology Data Book (1972) lists water content values from 60 to 76% by mass for human skin. This could explain the high permittivity results reported by some researchers.

The mean permittivity of the outer skin surface is similar in dielectric constant and loss factor to that of liver, and therefore seems to follow the usual linear relationship between

loss factor and dielectric constant, as shown in fig. 6.eee. Measurements on the inner surface displayed a slightly higher ratio of loss factor over dielectric constant than is usually observed in single tissue types, although there are complications associated with this surface that have already been mentioned.

6.13.3. Tissue of the Digestive Tract.

The digestive tract, from the oesophagus to the rectum, is composed of tissue with a layered structure, as shown in fig. 6.fff. On the inner surface, there is a delicate jelly-like layer of connective tissue called the *mucosa*, which is covered by finger-like projections, or *villi*, whose purpose is to maximise the surface area for digestion and absorption. Towards the outside are two layers of smooth muscle, sandwiched between two layers of stronger connective tissue, called the *submucosa* and the *serosa.*

Although the digestive tract is currently not an area of great thermographic interest, it was thought that its tissues, especially the mucosa, may have very high water contents, and therefore be worthy of investigation. Table 6.s contains typical water content values, which refer to all layers, taken from the Biology Data Book (1972).

Unfortunately, due to its *in-vivo* environment, tissue from animal digestive tracts, usually called *tripe*, is only available in a pre-cooked form, having been boiled prior to sale to kill bacteria. Thus the water content and ionic profile of tripe cannot necessarily be regarded as indicative of the *in-vivo* tissue.

However, a number of measurements were made on the inner and outer layers of bovine tripe. The average permittivity and water content values are listed in table 6.q, and the variation of loss factor with dielectric constant is shown in fig. 6.ggg. Measured water contents ranged from 86.8% for the outer layers, to 96.0% for the mucosa. The overall mean value of 91.4% is around 8% higher than the data book values, indicating that the tissue may be considerably affected by boiling. Dielectric constant values ranged from 55.7 for outer layers, to 76.6 for the mucosa, and the corresponding loss factor values ranged from 11.1 to 18.6.

In comparison with other tissues, the gradient of the best-fit linear relation between loss factor and dielectric constant is low, and similar to that observed for human brain tissue. The dielectric constant continues the trend of increasing towards that of water as the water content increases, but the loss factor is far lower than those of other tissues with

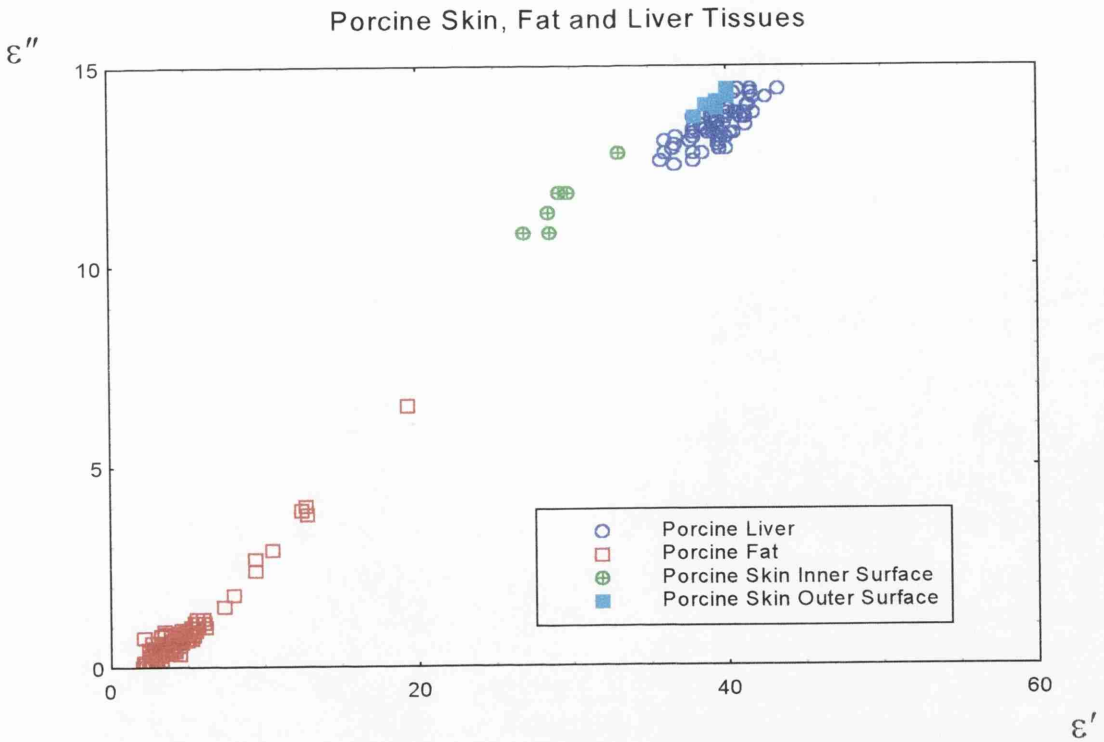

Figure 6.eee. Comparison between measured loss factor vs. dielectric constant for several porcine tissues, showing the permittivity of porcine skin in relation to those of porcine liver and fat.

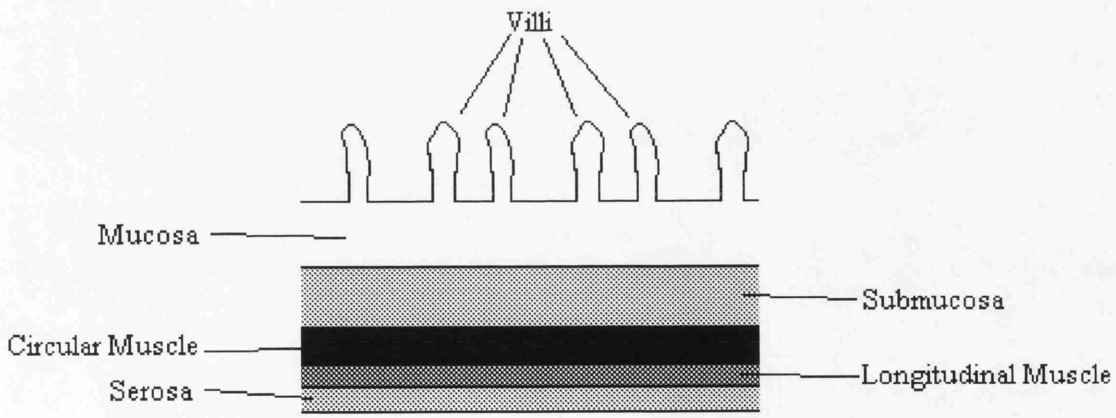

Figure 6.fff. Schematic cross-sectional diagram of the tissue of the intestinal tract, showing the characteristic layering of tissue types.

Tissue Type (Rat and Rabbit)	Water Mass Fraction (%)
Stomach	77 - 80
Small Intestine	80.6
Duodenum	80.0
Ileum	82.0
Cecum	83.3
Large Intestine	77.1
Colon	74.8

Table 6.s. List of intestinal tissue water contents, from Biology Data Book, 1972.

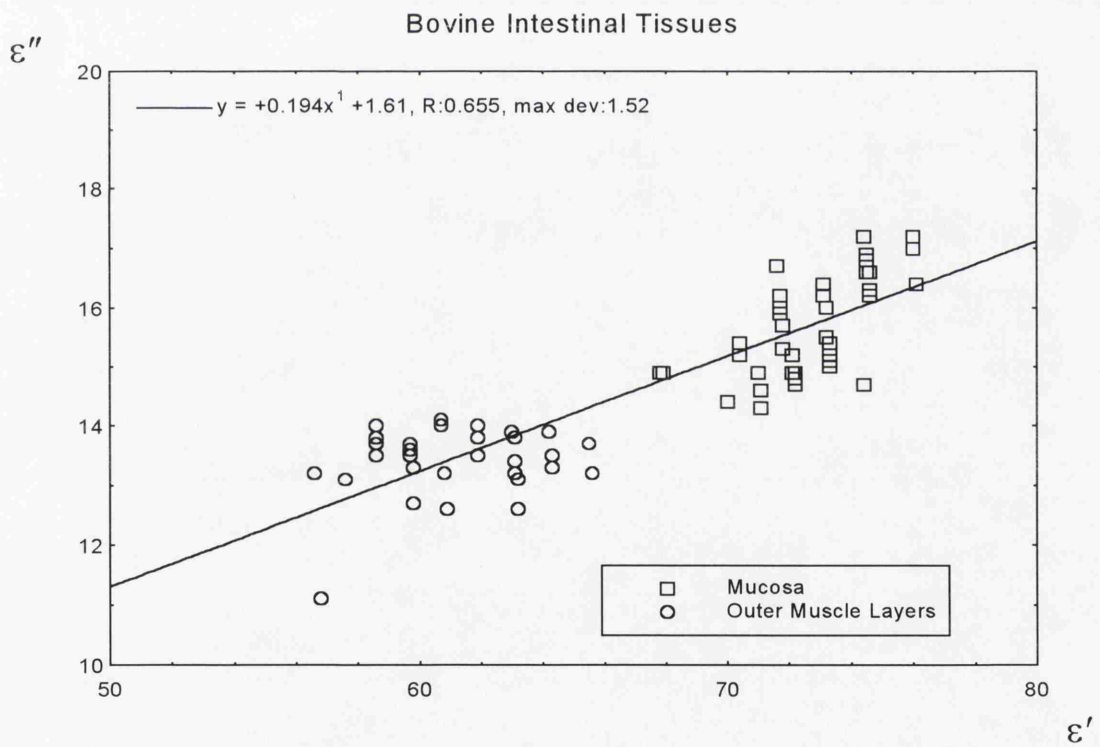

Figure 6.ggg. Measured loss factor vs. dielectric constant for bovine intestinal tissue. Correlation co-efficient for straight line fit = 0.875

similar dielectric constant; this could be due to leeching of ions and liberation of bound water during the boiling process, and may also be indicative of intestinal tissue having a low ionic conductivity. There are however, no other dielectric data on intestinal tissues available from which either of these hypotheses may be investigated.

Two specimens of human bowel tissue were obtained, from which the mean results are listed in table 6.q. On these specimens, the layering of tissues was too fine to distinguish between layers for permittivity measurements. The water contents of these specimens were lower than that of bovine tripe, which helps confirm the supposition that the bovine samples were affected by boiling. The average dielectric constant value of around 53 is typical for tissues of 80 - 85% water content; the average loss factor of 14.5 is considerably lower than those of tissues of similar water content, such as kidney medulla. It is therefore possible, as suggested above, that this is due to the electrolytic water of intestinal tissue having a low frequency ionic conductivity which differs from the normal values for other tissues.

6.14. Summary Tables of Tissue Permittivity Data.

Tables 6.t and 6.u display the mean permittivity and water content values for domestic animal and human tissues. Tissue data from all the animal species studied are used, but it must be noted that for some tissues, such as heart, data were obtained from only one species.

Animal Tissue Type	Mean Dielectric Constant	Mean Loss Factor	Mean (%age) Water Content by Mass
Skeletal Muscle	49.3 ± 1.4	16.7 ± 0.7	77.0 ± 2.6
Liver	39.3 ± 1.5	13.4 ± 0.8	67.6 ± 1.2
Kidney Cortex	49.5 ± 1.1	16.5 ± 0.6	78.5 ± 2.0
Kidney Medulla	53.8 ± 1.4	18.8 ± 0.7	82.9 ± 1.9
Heart	46.0 ± 1.0	14.7 ± 0.4	76.0 ± 1.8
Fats	4.4 ± 2.1	0.7 ± 0.7	13.4 ± 5.6
Blood (porcine)	52.7 ± 0.8	18.2 ± 0.4	81.4 ± 0.2
Skin (porcine)	29 - 39	11 - 14	56.5
Intestine Mucosa **	72.9 ± 1.8	15.8 ± 0.9	94.9 ± 1.4
Intestine Outer Layers **	60.6 ± 2.2	13.5 ± 0.9	88.7 ± 2.7
* Estimated ** After boiling process			

Table 6.t. Summary of measured permittivity and water content values for animal tissues.

Human Tissue Type	Mean Dielectric Constant	Mean Loss Factor	Mean (%age) Water Content by Mass
Skeletal Muscle	49.3 ± 1.4	16.7 ± 0.7	77.0 ± 2.6
Liver	41.7 ± 1.2	13.5 ± 0.4	74.8 ± 0.8
Kidney Cortex	49.7 ± 1.2	17.3 ± 0.6	78.8 ± 1.3
Kidney Medulla	53.9 ± 1.9	18.8 ± 1.0	--
Heart	49.8 ± 1.0	14.8 ± 0.4	80.8
White Connective	40.8 ± 2.3	14.8 ± 0.4	72.0 ± 3.3
Uterus	49.1 ± 1.5	15.8 ± 0.5	79.6 ± 1.8
Spleen	55.4 ± 1.5	17.2 ± 0.4	83.3 ± 1.0
Pancreas	49.2 ± 1.1	16.6 ± 0.6	75*
Brain Grey Matter	54.9 ± 1.7	12.5 ± 0.5	86.0 ± 1.7
Brain White Matter	31.8 ± 3.0	7.3 ± 0.6	75.2 ± 1.2
Breast Fat	6.5 ± 3.5	1.0 ± 1.1	16.2 ± 4.5
Other Fats	14.6	3.8	32.7
Intermediate Breast Tissue	13 - 45	3 - 15	--
Tumour	52.8 ± 2.2	15.9 ± 0.8	82.7 ± 1.6
* Estimated			

Table 6.u. Summary of measured permittivity and water content values for human tissues.

Chapter 7. Analysis of Tissue Permittivity Data.

7.1. Introduction.

For the purposes of dielectric modelling, high water content biological tissue can be considered to be approximated by a two-phase medium; the suspending majority phase consists of electrolytic water; and the minority, suspended non-water matrix consists usually of protein, lipid or a combination of these two materials. The tissue water contains many dissolved ions, which when simulated, has a 3 GHz permittivity of approximately 75 - j22 at room temperature. Measurements by Campbell (1990) have shown that at 3 GHz, the permittivities of pure protein and pure lipid from human body tissues are approximately equal, with values of around 2.5 - j0.2.

The following analysis is based on the Maxwell and Bruggeman mixture equations, which relate the permittivity of a two-phase dielectric material with the permittivities of each individual phase.

Maxwell's mixture equation is

$$\frac{\varepsilon_{mix} - \varepsilon_2}{\varepsilon_{mix} + 2\varepsilon_2} = \frac{\varepsilon_1 - \varepsilon_2}{\varepsilon_1 + 2\varepsilon_2} v_1 \qquad (7.1.1)$$

and Bruggeman's mixture equation is

$$\left(\frac{\varepsilon_2}{\varepsilon_{mix}}\right)^{\frac{1}{3}} \left(\frac{\varepsilon_1 - \varepsilon_{mix}}{\varepsilon_1 - \varepsilon_2}\right) = (1 - v_1) \qquad (7.1.2)$$

where ε_1 and ε_2 are the permittivities of the matrix and electrolyte respectively, ε_{mix} is the permittivity of the mixture, and v_1 is the volume fraction of the suspended medium. When $\varepsilon_2 >> \varepsilon_1$, and v_1 is low, as is the case in biological tissue, then ε_{mix} is fairly insensitive to uncertainty in the value of ε_1. Even if the estimated tissue non-water fraction permittivity of 2.5 - j0.2 differs from the true permittivity of the non-water fraction of a particular tissue by 100%, the error in the permittivity of the mixture, as calculated by Maxwell or Bruggeman's equations, is only around 1.5%. Thus, at room temperature of around 20°C, the permittivities of the two separate components of biological tissue will usually be taken as being equal to 2.5 - j0.2, and 75 - j22.

When the protein and electrolyte are combined in biological tissues, *molecular binding* alters the permittivity of the water fraction, and ionic conductivity can be impeded. Mixture equations do not intrinsically allow for binding effects, but, as was discussed in section 3.12, can generally be a useful tool when analysing the dielectric constant of

partially bound aqueous systems. They are, however, less successful when considering the loss factor of these systems, which at 3 GHz may be very susceptible to slight changes in the relaxation frequency of the water component, and are affected by any restriction in ionic conductivity. Based on the measured values of tissue dielectric constant, mixture equations will be used to calculated what fraction of the water molecules are bound to the protein molecules in biological tissues. The resulting loss factor will then be considered in relation to bound water loss, and low frequency ionic conductivity.

First considered are the major high water content soft tissues which conform to approximately the same dielectric behaviour. These are skeletal muscle, liver, kidney and heart tissues. Brain tissue has a differing dielectric behaviour with a lower loss factor, and which appears to suggest the presence of more bound water than is present in other tissues. This tissue will be considered separately. Finally, the dielectric behaviour of blood is investigated. This tissue is unique in that the conductivity of its separate components has been previously reported, which allows for complete explanation of its 3 GHz permittivity.

7.2. Mixture Equation Analysis of Animal Tissue Permittivity Data.

To utilise mixture equations, it is necessary to know the volume fraction of each component in the mixture, which can be calculated from the known mass fraction of each component and the overall density of the tissue. Oven dehydration measurements on tissue samples gave the water mass fraction, but no tissue density measurements were made.

The density of high water content soft tissues has been calculated in previous studies (e.g. Campbell, 1990) by assuming that the entire non-water fraction of the tissue has a density equal to average density of dry protein, which is given as 1.3g/ml by Schepps and Foster (1980). Alternatively, tables of density values for common tissue types can be found in many texts on ultrasonic imaging, for which tissue density is an important parameter in establishing the sonic propagation velocity. The density values for human tissue used in this study are taken from Rose and Goldberg (1979). Animal tissue has been assumed to have the same density as the corresponding human tissue. It must be noted that density values are only approximate, and there may be some variation not only

from individual to individual, but also between tissues taken from different areas from one donor. This unfortunately introduces yet another modest uncertainty into the data for mixture equation analysis.

Table 7.a lists the average permittivity values for the major animal tissues investigated (muscle, liver, kidney and heart), together with the average water volume fraction evaluated from the measured mass fraction. When compared with the Maxwell equation predictions, as shown in fig. 7.a, it can be seen that the dielectric constant of the tissues lie systematically below the values predicted. However, the loss factor values of the tissues all lie close to the Maxwell equation predicted values.

The overall dielectric constant of tissues is composed of contributions originating only from the water and protein in the tissues. Ions in the tissue electrolyte do not significantly affect the tissue dielectric constant, but do affect the tissue loss factor. The magnitudes of the individual contributions to tissue loss factor at 3 GHz are considered in detail in sections 7.2.4 and 7.4.1.

7.2.1. Non-contributing Bound Water.

To try to gain an insight into the binding process present, the following popular method as used by Foster et al (1979) is employed. The total tissue water content is supposed to be divisible into two sets; that essentially free water which contributes to the tissue dielectric constant at 3 GHz, and that bound water, which does not contribute significantly, as its relaxation frequency is greatly reduced. Using the measured tissue dielectric constant values, and assuming that the dielectric constant is well expressed by the mixture equations, the effective volume fraction of the tissue which does not contribute significantly to the dielectric constant can be evaluated. This effective volume fraction therefore consists of the non-water component of the tissue, together with the bound water. Here the dielectric constant of the non-contributing fraction is taken as 2.5. In fact, the minimum dielectric constant of the bound water is ε_∞, which is equal to approximately 4.5; when combined with the protein, the overall dielectric constant of the 'non-contributing' fraction will therefore be slightly greater than 2.5. However, as was stated in the introduction to this chapter, a large proportional error in the estimated value of the low permittivity component makes little difference to estimated volume fraction, so the non-contributing fraction can be assumed to have a dielectric constant of

Animal Tissue Type	Dielectric Constant	Loss Factor	% age Water Content by Mass	Density (g/ml)	Water Volume Fraction
Skeletal Muscle	46.5	16.5	74.0	1.08	0.799
Liver	39.3	13.4	67.6	1.06	0.717
Kidney Cortex	49.3	16.5	78.5	1.04	0.816
Kidney Medulla	53.8	19.0	83.0	1.04	0.863
Heart	46.0	14.7	76.0	1.05	0.798

Table 7.a. List of mean measured permittivity and mass water content values for major animal tissues, with water volume content calculated from tissue density values taken from Rose and Goldberg, 1979.

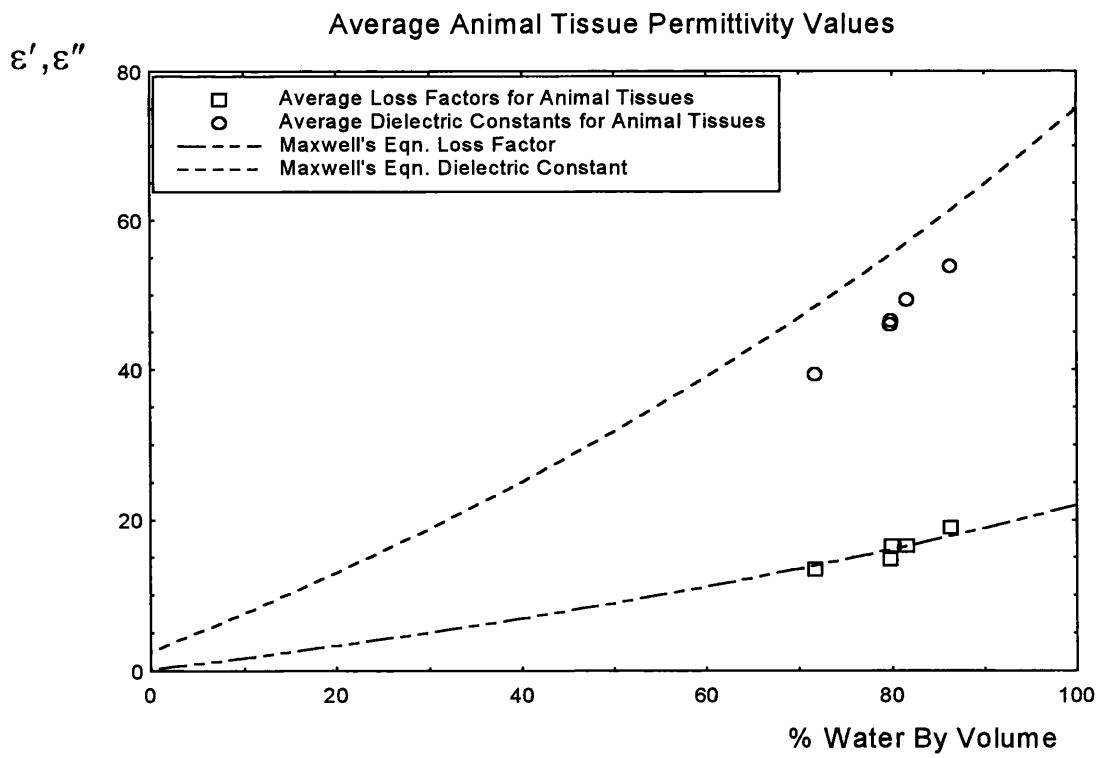

Figure 7.a. Average measured dielectric constant and loss factor vs. water content for animal muscle, kidney, liver and heart tissues. Maxwell mixture equation predictions also shown.

2.5 without incurring significant error. The dielectric constant of the unbound water fraction is taken as 75, which is approximately the dielectric constant of 0.15**M** saline solution.

Table 7.b shows the effective non-contributing volume fractions of the animal tissues as calculated using the measured values of tissue dielectric constant, by Maxwell and Bruggeman's equations. From these, the mass of non-contributing water (i.e. bound water) per mass of non-water material (i.e. protein) in each tissue can be calculated, as is also shown in table 7.b.

It is concluded that, on average, around 0.4grams water per gram protein in each of these animal tissues does not contribute significantly to the tissue dielectric constant at 3 GHz. This value is in agreement with the amounts of bound water previously reported on biological tissues by Schepps (1981), on various protein polymer solutions by Cooke and Kuntz (1974), and by the other researchers whose results are discussed in section 3.11.

These amounts of bound water have been evaluated using only the measured dielectric constant data, and so are not affected by any uncertainty in the relative magnitude of the water and ionic components of the tissue loss factor. However, the assumption made that the bound water does not contribute to the dielectric constant can give rise to a potential anomaly when the observed loss factor is considered.

7.2.2. Low Frequency Conductivity of Tissues.

To analyse the loss factor of animal tissues in terms of the bound water fraction, it is first necessary to subtract the effects of conductivity processes other than the dipolar relaxation of water from the measured loss factor values. These processes include the ionic conductivity of the ions in tissue electrolyte, dipolar relaxation of large protein molecules, and counterion diffusion. The contribution of these processes to tissue conductivity losses is discussed in chapter 3. Since the data here are only from one frequency, the overall effects of the unwanted conductivity processes will have to be deduced from the measurements of other researchers.

As was noted in section 3.3, most biological tissues display two major characteristic dispersions, the α and β dispersions, at frequencies well below 3 GHz. With each of these dispersions is associated a conductivity increase. The data required therefore, refer

Animal Tissue Type	Measured Dielectric Constant	Water Mass Fraction	Non-Water Volume Fraction	Non-contributing Volume Fraction (Maxwell's eqn.)	Bound Water Volume Fraction	Mass Bound Water per Mass Protein (g/g)
Skeletal Muscle	46.5	0.740	0.201	0.305	0.104	0.37
Liver	39.3	0.676	0.283	0.397	0.114	0.33
Kidney Cortex	49.3	0.785	0.184	0.271	0.087	0.39
Kidney Medulla	53.8	0.830	0.137	0.219	0.082	0.46
Heart	46.0	0.760	0.202	0.311	0.109	0.43
* Estimated						

Table 7.b. List of non-contributing volume fraction and amount of bound water for major animal tissues as evaluated by Maxwell's equation.

Tissue Type	Averaged Residual Conductivity at 0.1 GHz	Effective Residual Loss Factor at 3 GHz
Skeletal Muscle	0.7 S/m	4.2
Liver	0.55 S/m	3.3
Kidney	0.7 S/m	4.2
Heart	0.5 S/m	3.0
Spleen	0.75 S/m	4.5
Brain (Grey matter)	0.6 S/m	3.6
Brain (White matter)	0.35 S/m	2.1

Table 7.c. Collated residual conductivity results for major tissue types at a frequency well below the dipolar dispersion of water.

Animal Tissue Type	Water Volume Fraction	Corrected Permittivity	Corrected Effective Permittivity of Water Fraction (Maxwell eqn.)	Corrected Effective Permittivity of Water Fraction (Bruggeman eqn.)
Skeletal Muscle	0.799	46.5 - j12.3	62.8 - j16.8	63.6 - j17.0
Liver	0.717	39.3 - j10.1	60.6 - j15.9	62.4 - j16.4
Kidney Cortex	0.816	49.3 - j12.3	64.8 - j16.4	65.6 - j16.6
Kidney Medulla	0.863	53.8 - j14.0*	65.8 - j17.3	66.2 - j17.4
Heart	0.798	46.0 - j11.7	62.2 - j16.0	63.1 - j16.3
* Estimated				

Table 7.d. List of mean measured permittivity values for animal tissues, with the estimated contribution to the loss factor from ionic and other low frequency conductivity effects removed.

to tissue conductivity at frequencies above the β dispersion, but well below the γ dispersion. When this conductivity is subtracted from the current data, only the dipolar conductive effects of tissue water will remain.

Unfortunately, because many tissues also display the small δ dispersion over the frequency range between the β and γ dispersions, it is not completely clear at which frequency the magnitude of the unwanted effects should be evaluated. Campbell (1990) and Stoy et al (1982) have presented extensive tables of collated data listing the conductivity and dielectric constant of various biological tissues at frequencies from 0.1 MHz to 10 GHz. By examining the data in these tables, a general region of tissue conductivity invariance was noted at a frequency of around 100 MHz. This lies well below the typical relaxation frequencies for pure and bound water, and so measured conductivity values at this frequency will refer mainly to those unwanted processes.

At 100 MHz, the scatter in collated tissue conductivity data is far greater than was observed for tissues at 3 GHz. In chapter 6, when comparing the new permittivity data with that already published, general agreement in values to within around 10% was noted. However, the data collated from many individual tissues at 100 MHz in Campbell (1990) deviate by as much as a factor of 2. By considering from the two above publications only those data taken *in-vitro* at room temperature (the same conditions as were used here), a list of residual conductivity values for each tissue type was drawn up, and is shown in table 7.c. By necessity, data from a variety of different animal species had to be considered to deduce many of the individual conductivity values, but it may be noted that the final estimated values are not dissimilar to those measured on macerated human tissues in the thorough study by Schwan, 1957.

From these conductivity values, a residual loss factor at 3 GHz due to unwanted effects can be evaluated (from $\varepsilon''_{res} = {}^{\sigma_{res}}\!/_{\omega\varepsilon_0}$). This is also listed in table 7.c.

7.2.3. Applying Mixture Equations to Corrected Tissue Permittivity Values.

Table 7.d shows the average animal tissue permittivity data, but with the appropriate residual loss factor subtracted from the measured loss factor values. This then gives the values of tissue dielectric constant and loss factor arising only from the dipolar relaxation of water.

If, in addition to the respective volume fractions of the components of a mixture, the permittivities of both the mixture and one of the pure components are known, Maxwell and Bruggeman's mixture equations can be solved to find the permittivity of the other pure component. By using the corrected permittivity data and measured water volume fractions for the animal tissues, together with the 'known' permittivity value of 2.5 - j0.2 for the permittivity of pure protein and/or lipid, the *effective* permittivity of the water fraction was calculated for each tissue.

It can be seen that whilst the effective dielectric constants of tissues decrease with decreasing water volume fraction, the effective loss factor remains approximately the same, at a value of around 16 relative dielectric loss units. The effective dielectric constant decreases because a greater proportion of the overall water fraction is bound in the tissues which contain a larger proportion of protein.

7.2.4. Proposed Reason for Uniform Overall Loss Factor of Tissue Water.

The measured loss factor values, when corrected to remove the residual tissue conductivity, suggested that the effective loss factor of the water fraction of all the tissues was around 16 relative units. If the bound water is bound in such a way as to have a relaxation frequency very much lower than microwave frequencies, then the bound water will have a dielectric constant of around 4.5, and a loss factor of approximately zero at 3 GHz. When combined with the estimated loss factor of the protein at 3 GHz (permittivity = 2.5 - j0.2), the magnitude of the loss factor of the overall non-contributing fraction will be approximately equal to 0.2. This is very close to the loss factor of protein alone which was employed in evaluating the effective non-contributing volume fraction of the tissues. However, the corrected effective loss factor of the total tissue water fraction was calculated to be around 16. This value is higher even than the loss factor of the unbound water, and cannot be achieved by a mixture of substances with permittivities 2.5 - j0.2 and 75 - j13.5 respectively.
This anomaly is likely to be caused by the unrealistic assumption that the bound water has a relaxation frequency very much lower than microwave frequencies. In fact, previous estimates of the relaxation frequency of bound water in tissues vary from 0.1 to 5 GHz (Campbell, 1990).

It is unlikely that the relaxation frequency of bound water in these tissues is near 5 GHz, because the bound water would have a very high loss factor (~35) at 3 GHz if this were the case. By examining the dielectric constant, it has been estimated that 0.4 grams / gram protein is bound. This corresponds to approximately 10% of the tissue water, so such a relaxation frequency would be manifest by a noticeably higher tissue loss factor than was observed. The dielectric constant of this bound water would be around 50, and so would also contribute significantly to the overall tissue dielectric constant.
But if the bound water had a relaxation frequency of, say, 0.6 GHz, and ε_s and ε_∞ were unchanged from their unbound values, then the dielectric constant of the bound water at 3 GHz would be around 7. This dielectric constant is less than 10% of the dielectric constant of the free water. Therefore, when evaluating the effective non-contributing volume fraction, little error would be incurred in neglecting its contribution over and above the dielectric constant of 2.5 for protein, which constitutes the majority of the 'non-contributing' fraction. However, the loss factor of this bound water at 3 GHz would be around 14. Thus the loss factor of all the water in the tissue would be around 14, which is close to the predicted overall loss factor of 16. The small remaining difference could be due to slight underestimation of the low frequency conductivity values, a minor binding effect acting on some of the 'free' water in the tissue raising its loss factor, or just the combination of estimates and assumptions which have been employed in evaluating the approximate bound water properties.

Small binding effects acting on the bulk 'free' water in biological tissues have already been reported. Foster et al (1979) deduced that the relaxation time if the 'free' water in brain tissue was up to 15% higher than the relaxation time of true 'free' water. An increase of 15% in relaxation time increases the loss factor of water at 3 GHz by approximately 2 relative dielectric units. Thus, the value of around 16 for the effective loss factor of all tissue water would be, qualitatively at least, explained by the combination of these two effects.

7.3. Partial Evaporation Permittivity Measurements.

The current analysis of the permittivity of bound water is dependent on the use of mixture equations to evaluate the effective volume fraction of tissues which does not

contribute significantly to the overall tissue dielectric constant. Soft tissues with volume water contents from around 70 to 90% have been investigated. It would be useful to measure the permittivity of tissues with water content between those of fats and soft tissues, so as to investigate further the dielectric behaviour of tissue water.

In an attempt to fill-in the water content gap, permittivity measurements were made on animal tissue samples which had been subjected to *partial evaporation* prior to dielectric investigation. This process involved placing a tissue sample in a drying oven at a low heat (~50-70°C) for up to several hours, to remove a component of the water content by partial evaporation. The sample was then allowed to cool, then the hardened outer layer removed, before making permittivity measurements in the usual way. Then the approximate volume of investigation was removed from the overall sample, and fully dehydrated to give a water content value.

In practice, this process was found to give rather unreliable permittivity and water content results. Partially dehydrated samples were prone to large fluctuations in local water content, so evaluation of a water content representative of the investigated tissue volume was subject to large uncertainty.

Measurements were made on partially dehydrated skeletal muscle, kidney and liver tissues. Kidney tissue gave the least satisfactory results, with a large overall scatter. This was due to large local water content fluctuations caused by the small size of kidney samples, and the high initial water content of kidney. Liver tissue gave the best results, due to the large scale homogeneity of the tissue, and also, because it has the lowest initial water content of all the tissues, a greater range of low water contents could be achieved by the partial evaporation process.

Figure 7.b shows the permittivity results of partial evaporation experiments on bovine liver and muscle tissues as a function of water content, in comparison with the average permittivity values for undried tissues. Similar results were also obtained for porcine and agnine liver and muscle tissues. Because the density of the partially evaporated tissues could not be measured, the protein volume fractions were calculated by assuming that the non-water fraction of tissues has a density of 1.3 g/ml (Schepps and Foster, 1980).

Two interesting points were noted from these results. Firstly, the quantities of bound water in the partially dehydrated tissues were evaluated, by using Maxwell's equation to calculate the effective volume fraction of the samples which does not contribute to the dielectric constant. Values of the amount of bound water ranged from 0.2 to 0.5 grams

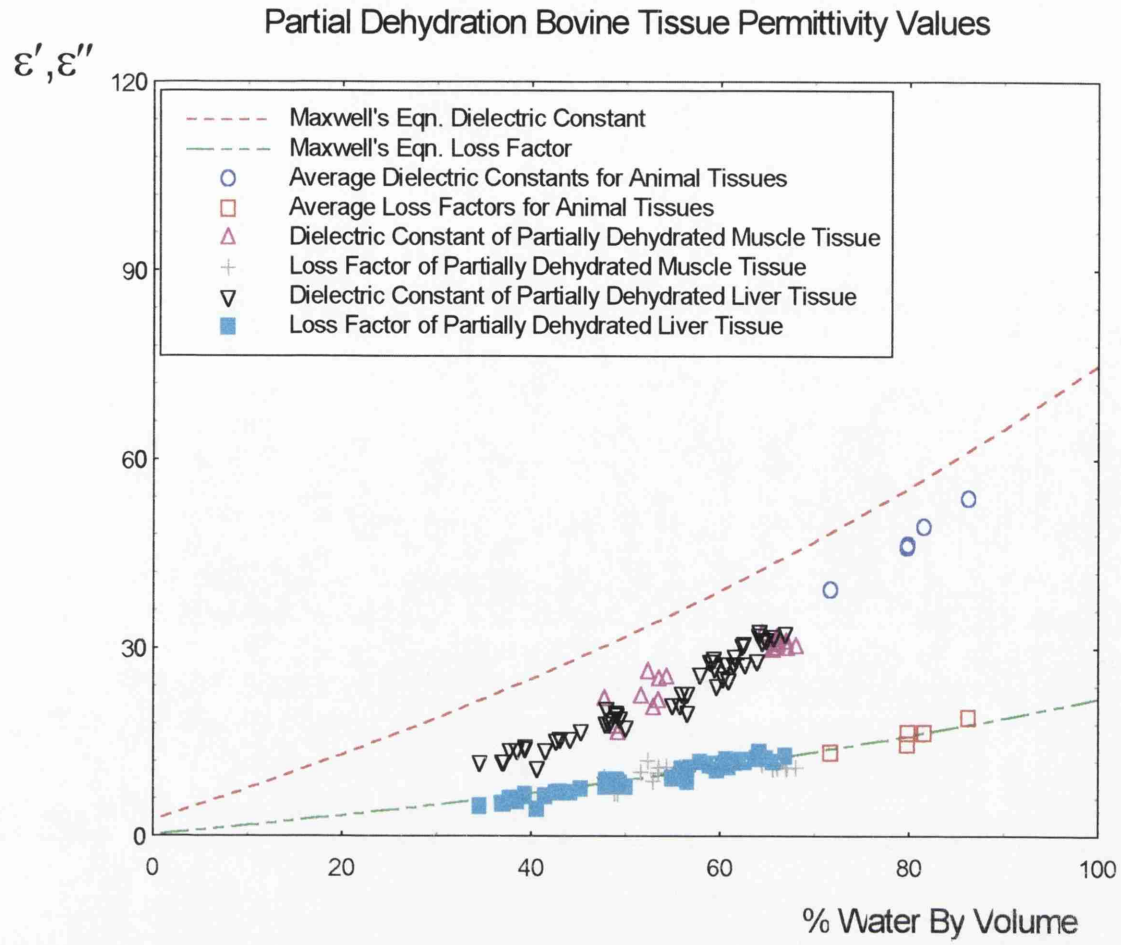

Figure 7.b. Measured dielectric constant and loss factor vs. water content for partially dehydrated bovine tissues. Also shown are the mean undried tissue values and the Maxwell equation prediction values. It may be noted that the partially dehydrated samples continue the behaviour observed on real tissues.

per gram protein, with an average of 0.35g/g protein. Tissue samples which had only a small fraction of their water content removed by dehydration gave bound water values of around 0.4 g/g protein, the same as for undried tissues. This suggests that the water which is first removed from the tissue by dehydration is unbound water, as would be expected. This water is probably extracellular water. Unlike intracellular water, extracellular water is not protected from evaporation by the cell membrane, and is also less likely to be bound to other non-water molecules.

As the protein volume fraction approached the maximum attained (around 70% protein by volume), the amount of bound water tended to decrease to around 0.25g/g protein. This presumably coincided with cell membrane breakdown in the tissue allowing the bound water to evaporate as well. When only a small amount of water had been evaporated from the tissue, the dielectric constant of the partially dehydrated samples drops steeply, up to the point where around 50% of the tissue volume is water. subsequently, the removal of more water has a reduced effect of the overall dielectric constant. This also suggests that the initial water removed is mainly 'free' unbound water, with a high dielectric constant, and that the water removed later consists more of bound water, with a lower dielectric constant.

The second point refers to the loss factor of the partially dehydrated tissue samples. It can be seen from fig. 7.b that the loss factors of the partially dehydrated samples all lie close to the loss factor predicted by Maxwell's equation for a mixture of substances with permittivities $2.5 - j0.2$ and $75 - j22$. Close agreement is observed even when the water volume fraction is reduced to below 40%. This therefore continues the behaviour of the undried tissues shown in fig. 7.a, in which the tissue loss factor values all lie close to the same predicted line. The data in table 7.a show that the effective loss factor of the tissue electrolyte is approximately the same for all tissue types. When once the effects of low frequency conductivity were subtracted from the animal tissue loss factors, the effective loss factor of all the tissue water, without ionic contributions, was still approximately the same for all tissues (see data in table 7.d). Figure 7.c shows the variation of the effective loss factor of the electrolytic water fraction of partially dehydrated bovine liver samples as a function of protein volume fraction. It is not possible to quantify the ionic conductivity contribution to the loss factor for these measurements, so the values presented include ionic effects. It can be seen that initial removal of water has little effect; the effective loss factor of the tissue electrolyte remains constant at a value of

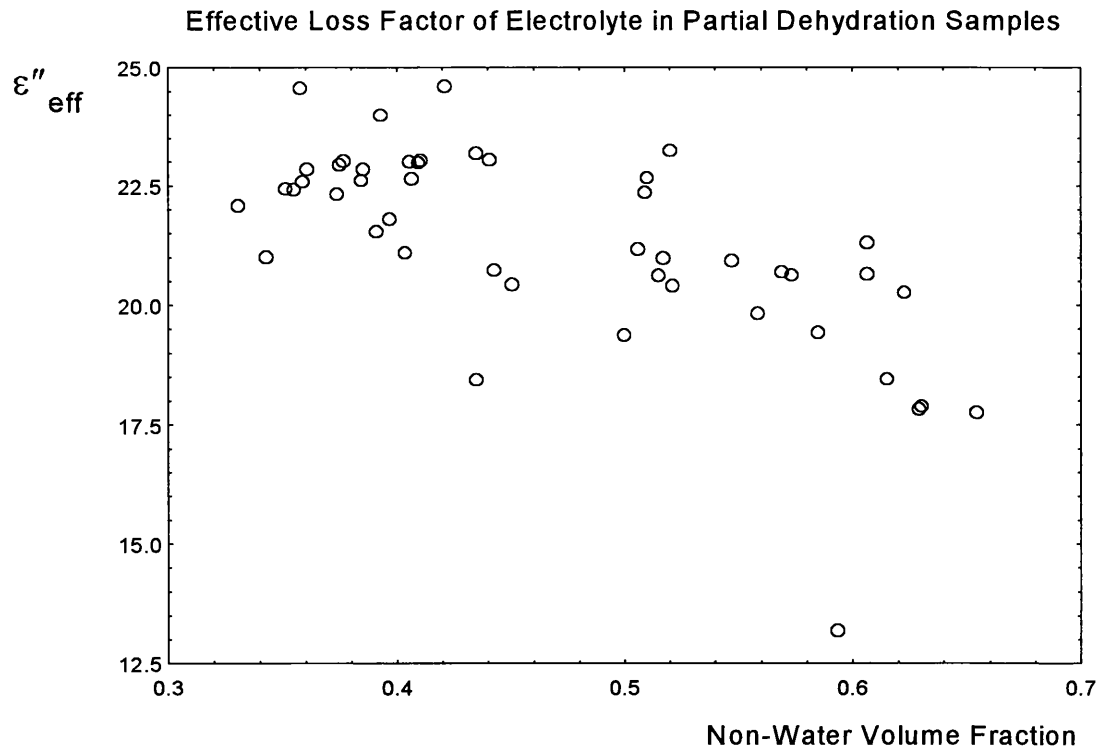

Figure 7.c. Effective loss factor of partially dehydrated bovine liver samples as a function of protein volume fraction. Gradual decline is observed beyond a protein volume fraction above around 0.4.

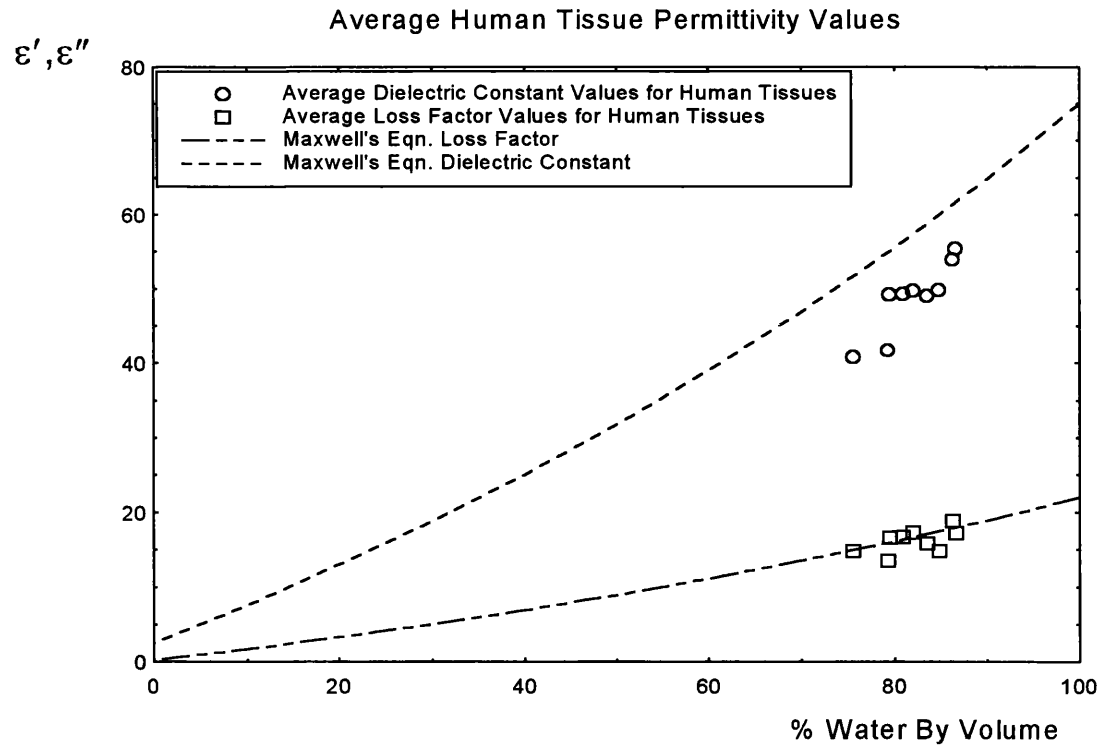

Figure 7.d. Average measured dielectric constant and loss factor vs. water content for major human tissues. Maxwell mixture equation predictions also shown. Brain tissue results shown separately in fig. 7.e

around 22.5, the value which was calculated for undried tissues. Even when the protein volume fraction is above 0.6, which corresponds to over two thirds of the initial tissue water having been evaporated, the effective loss factor of the remaining tissue electrolyte is around 18, and so has fallen by only 20%. Much of this fall could be due to greater restriction of ionic conductivity in the electrolyte as the water volume fraction decreases. Although the residual low frequency conductivity of the partially dehydrated samples could not be evaluated, the fact that the effective loss factor of tissue water does not appear to be affected by evaporation of unbound water does tend to support the theory that the bound water and unbound water have similar loss factors.
At very high values of protein volume fraction, the Maxwell equation becomes a less appropriate equation with which to model and predict the mixture permittivity. Some deviation from this predicted behaviour may therefore be expected at low water volume fraction.

The partial evaporation data admittedly are, at best, qualitative estimates of the permittivity of a theoretical low water content soft tissue, with similar structure to that of real tissues. They do, however, further illustrate that the dielectric constant of biological tissues can be accounted for by assuming that ~0.4grams per gram protein of the tissue water is bound with a low relaxation frequency, such that the dielectric constant of the bound water is low, but the bound water loss factor is still significant.

7.4. Mixture Equation Analysis of Human Tissue Results.

Table 7.e lists the average measured permittivity and water content values for each major human tissue type investigated, and the estimated water content by volume, based on the tissue density values given in Rose and Goldberg (1979). Brain tissue will be discussed separately in the following section. The measured average permittivity values are plotted as a function of volume water content in fig. 7.d. By comparison with fig. 7.a, it can be seen that although both the dielectric constant and loss factor of the human tissues lie in the same area as those of animal tissues, the clearly defined decreasing trend of tissue dielectric constant and loss factor with decreasing water content shown by animal tissues, is not reproduced here. This is presumably due to a combination of factors; firstly, the human tissue contained excess blood, which perturbed the permittivity

Human Tissue Type	Dielectric Constant	Loss Factor	% age Water Content by Mass	Density (g/ml)	Non-water Volume Fraction
Skeletal Muscle	49.3	16.7	77.0	1.05	0.809
Liver	41.7	13.5	74.8	1.06	0.793
Kidney Cortex	49.7	17.3	78.8	1.04	0.820
Kidney Medulla	53.9	18.8	83.0	1.04	0.863
Heart	49.8	14.8	80.8	1.05	0.848
White Connective	40.8	14.8	72.0	1.05	0.756
Uterus (incl. Fibroid)	49.0	15.8	79.5	1.05	0.835
Spleen	55.4	17.2	83.3	1.04	0.866
Pancreas	49.2	16.6	75 *	1.06	0.795
* Estimated					

Table 7.e. List of mean measured permittivity and water content values, with water volume content calculated using tissue density values taken from Rose and Goldberg, 1979.

Human Tissue Type	Measured Dielectric Constant	Non-water Volume Fraction	Non-contributing Volume Fraction (Maxwell's eqn.)	Bound Water Volume Fraction	Mass Bound Water per Mass Protein (g/g)
Skeletal Muscle	49.3	0.191	0.271	0.080	0.33
Liver	41.7	0.207	0.365	0.158	0.59
Kidney Cortex	49.7	0.180	0.266	0.086	0.39
Kidney Medulla	53.9	0.137	0.218	0.081	0.46
Heart	49.8	0.152	0.265	0.113	0.56
White Connective	40.8	0.244	0.377	0.133	0.45
Uterus (incl. Fibroid)	49.0	0.165	0.275	0.110	0.51
Spleen	55.4	0.134	0.201	0.067	0.38
Pancreas	49.2	0.205*	0.272	0.067	0.25
* Estimated					

Table 7.f. List on non-contributing volume fraction and amount of bound water for major human tissues as evaluated using Maxwell's equation.

measurements relative to the animal tissue measurements, and secondly, the presence of this blood affected the water content by mass and density of the tissues, which led to poor estimation of the volume water content of the tissues.

There is however, an overall trend of decreasing permittivity values with decreasing volume water content, which appears to follow a course relative to the Maxwell equation prediction that is similar to the trend observed in animal tissues. It is therefore reasonable to assume that bound water in most human tissue has dielectric behaviour similar to that observed in animal tissues.

By again supposing that the bound water fraction does not contribute significantly to the tissue dielectric constant, the effective non-contributing volume fraction was calculated for each tissue type, and from this, the amount of bound water per unit mass of protein in the tissues was evaluated. The results of these calculations are listed in table 7.f. It must be noted that the densities of some of these tissues are only estimates, and may therefore give unrepresentative non-water volume fractions.

The estimated amounts of bound water for tissues other than brain tissue vary from 0.25 to 0.59 g per gram protein, with an average value of 0.44g per gram protein. This value is 10% higher than the average value evaluated for animal tissues. There is a greater variation in bound water values in human tissues than in animal tissues, but this may partially be due to the difficulty in correctly estimating the tissue density, and the presence of residual blood in the human tissues. Considering the unquantifiable uncertainty in estimating the bound water fractions, the values of 0.4 g/g protein for animal tissues and 0.44g/g protein for human tissues suggest that there is little difference between the average amounts of bound water in human and animal tissue. Although the average amounts of bound water are similar between human and animal tissues, the calculated amounts for the individual tissue types show greater variation between species. The notable exceptions to this general observation are the kidney cortex and medulla tissues. Measured water content and permittivity results for kidney tissues gave the most consistent results between human and animal species of all the tissue types (see section 6.9), as can be seen from the mean data in tables 7.a and 7.e. Therefore the calculated amounts of bound water in kidney cortex and medulla tissues are almost exactly the same.

7.4.1. Dependence of Microwave Tissue Loss Factor on Low Frequency Conductivity.

The average volume water content and permittivity data listed in tables 7.a and 7.e, and shown in figs. 7.a and 7.d, indicate that the dielectric constant of tissues displays a well defined systematic decrease with decreasing volume water content. This is particularly apparent for animal tissues, for which the water content was uniform, and unaffected by residual blood. Average measured loss factor values for tissues, on the other hand, do not display such well defined behaviour with volume water content.

Consider animal heart and skeletal muscle tissues. Each was found to have a volume water content very close to 80%. The average dielectric constant of muscle was 46.5, and that of heart, 46.0, a difference of ~1%. However, the average loss factor of muscle was 16.5, whilst that of heart was 14.7, a difference of ~10%. Because of the similarity in volume water content and dielectric constant, the amount of bound water in these tissues was estimated to be approximately the same. Other tissues with similar dielectric constant, but significantly differing loss factor include human liver and white connective tissues.

There are three factors which may contribute to the considerable difference in 3 GHz loss factor between muscle and heart tissues. (i). The bound water fractions in the two tissues have differing net relaxation times, which can significantly alter the loss factor of the bound water in each tissue at 3 GHz. (ii). The essentially 'free' water fractions in the two tissues are subject to a slight difference in loss factor, due to differing levels of interaction with proteins and other materials in the electrolyte of each tissue. (iii). The residual low frequency conductivity of the two tissues differ, due to their differing cell structure and differing ionic conductivity of the electrolyte in each tissue.

It is likely that the observed difference in loss factor between tissues of similar water content is due to a combination of each of these effects, but at this stage, the difference in low frequency conductivity of tissues is worthy of consideration as a major factor in determining tissue microwave loss factor.

In section 7.2.2, average conductivity values from collated dielectric measurements at 0.1 GHz were estimated for many tissue types. Table 7.c showed the results. It was thought that at this frequency, the conductivity effects would be due to processes other than dipolar relaxation of water. The average conductivity of skeletal muscle was ~0.7

S/m, and that of heart tissue was ~0.5 S/m. At 3 GHz, these values correspond to a residual loss factor of 4.2 for muscle and 3.0 for heart tissues, a difference of 1.2 relative dielectric units. Thus, by considering only the low frequency conductivity, a significant proportion of the overall difference of 1.8 relative units between the 3 GHz loss factors of muscle and heart tissues has been accounted for.

Unfortunately, this method may be susceptible to the frequency chosen at which to estimate the non-water conducting effects. Average room temperature conductivity values for various tissue types were therefore also drawn up for frequencies of 10 MHz and 0.5 GHz, using the collated data in Stoy et al (1982) and Campbell (1990) respectively. The estimated average conductivity values are listed in table 7.g. These two frequencies lie above and below the original chosen frequency of 0.1 GHz. As for the 0.1 GHz results, data from a wide variety of animals by necessity had to be included to obtain the average conductivity values, although the averaged values at 10 MHz are once again similar to the measurements made on macerated human tissues by Schwan (1957).

Between 10 MHz and 0.5 GHz, the conductivity of the tissues varies quite considerably, in some cases by as much as a factor of two. This illustrates the degree of uncertainty in estimating the magnitude of the conductivity effects which should be subtracted from the overall measured 3 GHz tissue loss factors, to leave only the dipolar loss from tissue water. However, the general rank order of tissue conductivity is preserved over all this frequency range. Spleen has consistently the highest conductivity, followed by skeletal muscle, with liver the lowest of the abdominal tissues, and white brain matter the overall lowest. Whichever frequency is chosen, the relative conductivity corrections made to the microwave loss factor will remain approximately the same, and will account for a large proportion of the loss factor difference between muscle and heart tissues, and the other tissues with similar dielectric constant but differing loss factor. This variation of low frequency conductivity may therefore be regarded as one of the major factors affecting the microwave frequency loss factors of tissue.

7.5. Bound Water in Human Brain Tissue.

The average results of permittivity measurements made on human brain tissue were presented in section 6.12.4. Because the tissue specimen had been temporarily stored in

Tissue Type	Averaged Residual Conductivity at 10 MHz	Averaged Residual Conductivity at 0.1 GHz	Averaged Residual Conductivity at 0.5 GHz
Skeletal Muscle	0.6 S/m	0.7 S/m	1.0 S/m
Liver	0.4 S/m	0.55 S/m	0.65 S/m
Kidney	0.6 S/m	0.7 S/m	0.85 S/m
Heart	-	0.5 S/m	0.8 S/m
Spleen	0.65 S/m	0.75 S/m	1.0 S/m
Brain (Grey matter)	0.3 S/m	0.6 S/m	0.85 S/m
Brain (White matter)	0.2 S/m	0.35 S/m	0.4 S/m

Table 7.g. Collated residual conductivity results for major tissue types at frequencies well below the dipolar dispersion of free water.

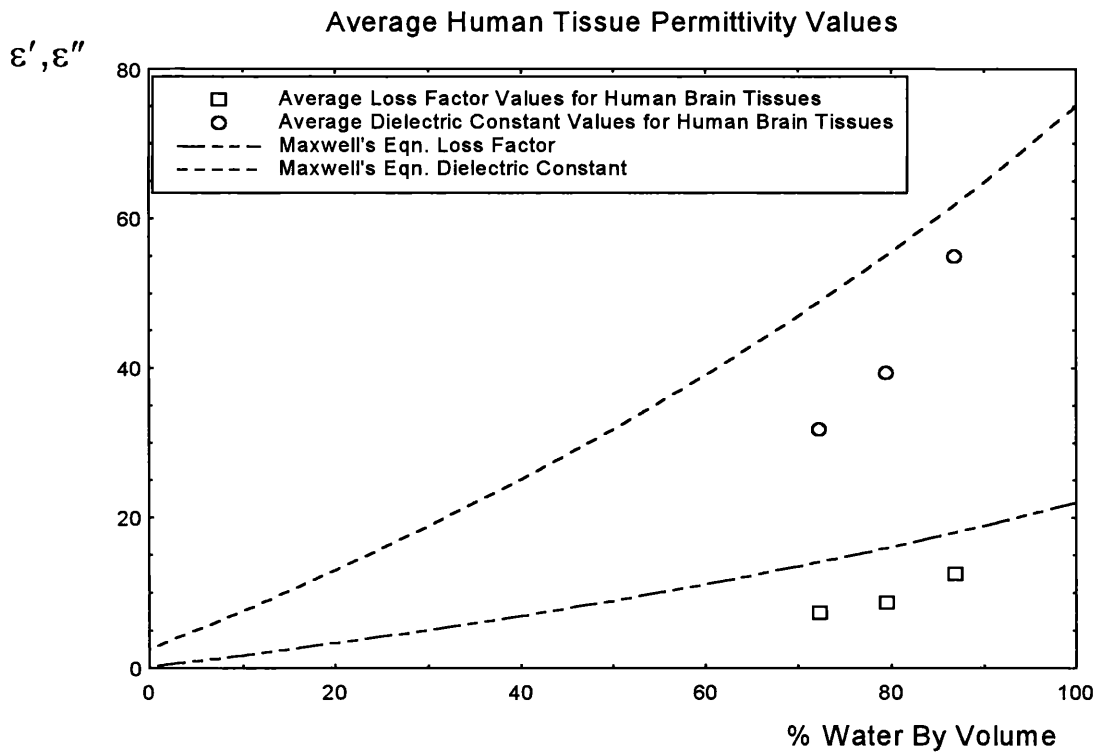

Figure 7.e. Average measured dielectric constant and loss factor vs. water content for human brain tissues. The data represent, in order of increasing water content, white matter, intermediate measurements, and grey matter. Maxwell mixture equation predictions also shown.

water, it was thought that the overall measured water content values may have been raised above the true water content deep within the specimen, where the permittivity measurements were made. It was therefore decided that the water content of brain tissues should be taken from the Biology Data Book (1972), rather than using the values measured here. The above publication gives the water content by mass of grey brain matter to be 84%, that of white matter, 70%, and the overall water content mean as 77%. Figure 7.e shows the mean measured values of dielectric constant and loss factor of brain tissues as a function of volume water content. The non-water fraction of brain tissue contains a large amount of the fat myelin, and so the density of the non-water fraction in this tissue is lower than for the other high water content soft tissues. Rose and Goldberg (1979) give a value of 1.033g/ml for the density of brain tissues, and it is this value which is used to evaluate the non-water volume fraction of brain tissues in this section. Table 7.h lists the results of calculations to find the bound water fraction of brain tissues.

A value of 0.45 grams bound water per gram non-water material was found for grey brain matter. This is close to the average amount of 0.44g bound water per gram dry weight found in other high water content tissues. Good agreement is observed between this, and the findings of Foster et al (1979), made on canine brain, and the findings of Steel and Sheppard (1985), made on rabbit, mouse and rat brain.

However, a much larger proportion of 0.72 grams bound water per gram non-water was found for white brain matter. Foster et al (1979) and Steel and Sheppard (1985) found that the proportion of bound water was approximately the same for grey and white matter from the specimens they investigated. Here, the proportion of bound water in white matter is far greater than in grey matter, and also far greater than was found in all the other high water content soft tissues.

7.5.1. Loss Factor of Brain Tissues.

Brain tissues were found to have a significantly lower loss factor at 3 GHz than other soft tissues of comparable water content. This is partially due to the low residual conductivity of brain tissues. Table 7.g lists average conductivity values for several tissue types at frequencies of 10 MHz, 0.1 GHz and 0.5 GHz, estimated from collated data. The low frequency conductivity of white matter has a consistently small

Brain Tissue Type	Measured Dielectric Constant	Water Mass Fraction	Non-water Volume Fraction	Non-contributing Volume Fraction (Maxwell's eqn.)	Bound Water Volume Fraction	Mass Bound Water per Mass Protein (g/g)
Grey Matter	54.9	0.84*	0.132	0.206	0.074	0.45
White Matter	31.8	0.70*	0.277	0.500	0.223	0.72
* Estimated						

Table 7.h. List of non-contributing volume fraction and amount of bound water for human brain tissue, as evaluated by Maxwell's equation.

Brain Tissue Type	Water Volume Fraction	Corrected Permittivity	Corrected Effective Permittivity of Water Fraction (Maxwell eqn.)	Corrected Effective Permittivity of Water Fraction (Bruggeman eqn.)
Grey Matter	0.868	$54.9 - j8.9$	$66.6 - j10.9$	$67.0 - j10.9$
White Matter	0.723	$31.8 - j5.2$	$48.2 - j8.0$	$49.5 - j8.3$

Table 7.i. List of effective permittivity values for the water fraction of human brain tissues, as calculated by mixture equations.

Blood Type	Measured Dielectric Constant	Water Mass Fraction	Non-water Volume Fraction	Non-contributing Volume Fraction (Maxwell's eqn.)	Bound Water Volume Fraction	Mass Bound Water per Mass Protein (g/g)
Porcine Blood	57.2	0.814	0.141	0.182	0.041	0.22
Bovine Blood	53.6	0.791	0.165	0.221	0.056	0.27

Table 7.j. List of non-contributing volume fraction and amount of bound water for porcine and bovine blood as evaluated by Maxwell's equation.

magnitude, and at 0.1 GHz, well below the dipolar relaxation frequency of 'free' water, takes a value of around 0.35 S/m. Grey matter displays rather more variation in conductivity over this frequency range, but at 0.1 GHz has a conductivity of around 0.6 S/m.

At 3 GHz, these conductivity values give rise to a residual loss factor due to non-water effects of 2.1 relative units for white matter, and 3.6 relative units for grey matter. These residual amounts can be subtracted from the measured loss factors, to leave only the contributions arising from water, and the result extrapolated using a mixture equation to find the effective loss factor of all the tissue water. The results of these calculations are listed in table 7.i.

It can be seen that there is a notable difference between the effective loss factor of all the water in brain tissue, and that of all the water in other tissues. For other tissues, the effective loss factor was always around 16 units, which suggested that the bound water contributed significantly to the loss, or that the essentially 'free' water was subject to a slight overall increase in relaxation time. For brain tissues, the effective loss factor is much lower, and decreases as the volume of 'free' water decreases, suggesting that the bound water does not contribute significantly to the overall loss factor.

7.6. The Dielectric Behaviour of Blood.

Blood is composed of cell bodies suspended in plasma, an electrolytic solution containing many solutes, including inorganic salts, proteins, lipids and glucose. Plasma constitutes approximately 55 to 58% of the volume of whole blood, with cellular elements comprising around 42 to 45%. Red blood cells are the prevalent blood cell, out numbering all other blood cells by about 20 to 1. The red blood cell is a biconcave disk, about 8μm in diameter, without a nucleus, containing the protein haemoglobin, which makes up around one third of the cell, most of the remainder being intracellular water. Thus there are about 15 grams of red cells in 100ml of blood. The concentration varies between sexes; in the adult male there are about 5 million red cells per millilitre of blood, whilst in the female, there are about 4.5 million red cells per millilitre.

Blood is perhaps dielectrically the best understood biological tissue, as it conforms very well to the standard two-phase mixture equation model of a dilute suspension of regularly shaped objects in a continuum medium. In addition, the two components of

this suspension, plasma and red blood cells, can be separated from each other by centrifuging, and studied independently.

7.6.1. Conductivity of Blood.

The ionic profile of plasma electrolyte can be closely approximated by 0.15**M** saline solution (see chapter 3). At 20°C therefore, a low frequency conductivity of around 1.44 S/m is expected. Pauly and Schwan (1966) found that the true conductivity of blood plasma was lower, at around 1.25 S/m. This reduction of ionic conductivity is thought to be due to the presence of large polymer molecules in the plasma, which can restrict ionic mobility.

Considerable reduction of the ionic conductivity of the intracellular water of red blood cells is also observed. Intracellular water comprises two thirds of the red blood cell volume, and also has an ionic profile which suggests its conductivity may be around 1.44 S/m at room temperature. At low frequencies, the lipid membrane of red blood cells provides a barrier to electrical conduction, but at higher frequencies the red blood cells can conduct. At between 70 to 100 MHz (well below the dipolar relaxation frequency of water) red blood cells have been found to exhibit a conductivity plateau of magnitude ~ 0.5 S/m (Pauly and Schwan, 1966). This is less than is expected from a mixture of one third non-conducting protein and two thirds electrolyte, with conductivity 1.44 S/m, and so it is concluded that the ionic conductivity of the intracellular water in red blood cells is restricted by the protein molecules.

Using these values, the residual conductivity of whole blood can be estimated. When the red cells do not conduct, the blood mixture can be approximated as non-conducting oblate spheroids suspended in a conducting medium. Taking the red blood cell axial ratio to be 1/4.25, Fricke (1924) used his own mixture formulation (eqn. 2.8.1) to accurately predict the low frequency conductivity of blood which had been diluted or concentrated to various extents by the removal or addition of plasma. At 100 MHz, the conductivity of the plasma is ~1.25 S/m and that of the red cells is ~0.5 S/m. From equations 2.8.2 to 2.8.4, the Fricke form factor is 1.51. If the red cell volume fraction is 45%, the Fricke mixture equation then gives the residual conductivity of whole blood as just less than 0.9 S/m. This figure will vary according to the red cell concentration, which differs between sexes, but only by 5%. Schwan's (1953) measurement of the

conductivity of whole blood gave an estimated value of just under 1.0 S/m at this frequency. Therefore, the residual conductivity of blood is quite well known, and can be taken as being around 1.0 S/m at 100 MHz, a frequency at which all conductivity effects are present, except the dipolar relaxation of the tissue water.

7.6.2. Dielectric Constant of Blood at 3 GHz.

The permittivity measurements on porcine and bovine blood presented in section 6.13.1 gave mean permittivity values of 57.2 - *j*18.2 and 53.6 - *j*22.1 respectively. The lower dielectric constant of the bovine blood is probably due to the slightly higher red blood cell concentration of this blood, which was from a male animal, as compared with that of the porcine blood, which was from a female animal. The non-water fraction of the bovine blood was also several percent higher, which supports this supposition. However, as the bovine blood had been treated with an unknown amount of anti-coagulant which may have affected the conductivity, the porcine blood was considered to give the more reliable results. Good agreement with the results of Jenkins (1989), Cook (1951), and England (1949) was obtained.

The low frequency limiting dielectric constant of red blood cells has been suggested to range from 42 (Cook, 1952) to 51 (Pauly and Schwan, 1966). As the red blood cells are two thirds water, Maxwell's equation can be used to show that these values suggest that the dielectric constant of the water fraction in red cells is around 80, similar to that of the plasma water fraction. By treating the whole blood as a mixture of electrolytic water with a dielectric constant at 3 GHz of 75, with the remaining fraction being protein, with a dielectric constant of 2.5, Maxwell's equation can be used to estimate the total non-contributing volume fraction. For calculations involving the dielectric constant, the form factor is taken to be equal to two. The results of these calculations are shown in table 7.j. It can be seen that the non-contributing volume fraction in porcine blood is only a little greater than the non-water fraction, and that there is only about 0.22 grams bound water per gram protein in the blood. This is around half the amount of bound water as was found in other soft tissues, and is in reasonable agreement with the estimates of Grant (1984), which suggested that about 2% of water in blood is bound. The dielectric constant of the bovine blood also gives a low bound water fraction of 0.27g per gram

protein. This is probably a reasonable estimate, as the anti-coagulant in the bovine blood probably does not seriously affect the dielectric constant.

7.6.3. Loss Factor of Blood at 3 GHz.

At 3 GHz, the residual conductivity of 1.0 S/m gives rise to a residual loss factor of 6 relative dielectric units. When subtracted from the measured loss factor of porcine blood, the corrected permittivity is $57.2 - j12.2$. Maxwell and Bruggeman's equations can be used to extrapolate the effective permittivity of the water in blood. By Maxwell's equation, the effective water permittivity was found to be $70.4 - j15.1$, and by Bruggeman's equation, was $70.9 - j15.2$. The effective loss factor was again similar to the loss factor of free water, suggesting that the free and bound water behave in a similar manner to the water in soft tissues, described above.

In conclusion, the observed 3 GHz permittivity of blood can be quite well explained by subtraction of a residual conductivity of 1.0 S/m at frequencies well below the dipolar relaxation of water, and by assuming that approximately 0.22 grams water is bound to proteins and does not contribute significantly to the dielectric constant. As with other soft tissues, the overall effective blood water loss factor is slightly higher than that of free water. This may be because the bound water may have a relaxation frequency of around 0.5 GHz, and therefore contribute significantly to the overall loss factor, or it may be due to slight binding effects on the essentially 'free' water.

7.7. Frequency Behaviour of Tissue Permittivity Between 2 to 4 GHz.

Using the same open-ended co-axial probe and measurement equipment described in chapter 4, the permittivity of some tissue samples was measured at frequencies ranging from 2 to 4 GHz. Not only was this range the maximum available from the signal generator, but it also completely spans the range of operating frequency of the Glasgow radiometer system, and the systems of many other medical radiometry researchers. Limited measurements were made, to check for any notable anomalies in tissue dielectric behaviour in this frequency range, and to further investigate the permittivity of tissue water.

At frequencies other than 3 GHz, the quarter-wave choke on the co-axial probe is not a quarter of a wavelength long, and so does not present such a high impedance at the open end. Therefore, the performance of the probe was not expected to be so reliable, as the reflection co-efficient became more susceptible to depth of penetration into tissue samples, and calibration liquids. The scope for error was larger for these measurements than for those at 3 GHz.

Approximately 12 measurements were taken at each frequency per tissue type. Table 7.k lists the mean results, with the permittivity values of water and 0.15M saline, calculated from the equations presented in chapter 4. The values of the dielectric constants of water and 0.15M saline both display a slight fall of around 3 to 5% between 2 and 4 GHz. Over this frequency range, the loss factor of free water displays a considerable increase, whereas the loss factor of 0.15M saline is almost constant. This is due to the reduction in ionic loss approximately compensating the increase in the dipolar loss of water. In biological tissues, the ionic conductivity of tissue electrolyte is reduced from the ionic conductivity of a true free solution of the same electrolyte. It is to be expected therefore, that the increase in dipolar loss of water from 2 to 4 GHz will not be so fully compensated by the decrease in ionic loss, and so the loss factor of the unbound tissue electrolyte will show a slight increase between 2 to 4 GHz.

Any water in the tissues which is bound, has a decreased relaxation frequency compared with free water. If the relaxation frequency of the bound water is below 2 GHz, as it appears to be, then both the dielectric constant and loss factor of the bound water will fall over the 2 to 4 GHz range. This will at least partially compensate for the increase in loss factor of the free electrolyte. However, as the relaxation frequency of the bound water is not known, this cannot be quantified.

If, as suggested by the models of Cooke and Kuntz (1974), and Spiridonov (1982), discussed in section 3.11, the bound water has a wide range of relaxation frequencies, then the dielectric behaviour over this narrow frequency range will be even more complex. The overall dielectric constant must still fall, but the overall loss factor may be very difficult to predict.

From the data in table 7.k for muscle, heart and liver tissues, it can be seen that the permittivity values remain fairly constant over the frequency range; the loss factor values for these tissues in particular stay constant to within the experimental error. The

Tissue Type	Mean Permittivity at Various Frequencies				
	2.0 GHz	2.5 GHz	3.0 GHz	3.5 GHz	4.0 GHz
Porcine Muscle	49.8 - *j*16.7	48.3 - *j*16.5	46.5 - *j*16.5	46.1 - *j*15.8	45.0 - *j*16.8
Agnine Heart	48.4 - *j*14.8	46.6 - *j*13.9	46.0 - *j*14.7	47.0 - *j*14.1	45.2 - *j*14.9
Porcine Liver	41.6 - *j*13.1	40.1 - *j*13.2	39.3 - *j*13.4	39.8 - *j*13.1	40.3 - *j*13.2
Bovine Intestine					
Smooth Muscle	63.0 - *j*10.2	64.4 - *j*11.3	60.6 - *j*13.5	62.6 - *j*13.5	62.0 - *j*15.2
Mucosa	73.0 - *j*10.4	72.6 - *j*12.3	72.9 - *j*15.8	70.8 - *j*15.2	68.7 - *j*16.7
Water	79.1 - *j*9.2	78.5 - *j*11.4	77.7 - *j*13.5	76.9 - *j*15.6	75.9 - *j*17.5
0.15**M** Saline	76 - 22	75.5 - *j*22	75 - *j*22	74 - *j*23	73.5 - *j*24
Unbound Tissue Electrolyte	79.1 - *j*15.5	78.5 - *j*16.5	77.7 - *j*17.5	79.6 - *j*19	75.9 - *j*20.5

Table 7.k. Results of permittivity measurements on major animal tissues from 2 to 4 GHz.

Tissue Type		Permittivity at 2 GHz	Permittivity at 3 GHz	Permittivity at 4 GHz	Notes
Liver	Canine	52 - *j*13.5	49 - *j*14	46 - *j*12	Xu (1987) 20°C
	Feline	50 - *j*13.5	49 - *j*14	47 - *j*11	Kraszewski (1982) 36°C
	Feline	50 - *j*13	46 - *j*12	45 - *j*11	Stuchly (1982b) 35°C
	Rat	47 - *j*12	46 - *j*12.5	45 - *j*12	Kraszewski (1982) 32°C
	Bovine	44 - *j*13	43 - *j*13	42 - *j*12	Brady (1981) 37°C
Kidney	Canine	54 - *j*15	53 - *j*14	49 - *j*11	Xu (1987) 20°C
	Canine	47 - *j*13.5	--	44 - *j*12	Burdette (1986) 37°C
	Feline	41 - *j*10.5	47 - *j*13	38 - *j*8.5	Kraszewski (1982) 36°C
	Rat	51 - *j*13	51 - *j*14	50 - *j*12.5	Kraszewski (1982) 32°C
	Bovine	51 - *j*14.5	48 - *j*15.5	44 - *j*12.5	Brady (1981) 37°C
Muscle	Canine	54 - *j*15	53 - *j*15	49 - *j*12.5	Xu (1987) 20°C
	Canine	46 - *j*17.5	--	44 - *j*17	Schepps (1981) 37°C
	Feline	55 - *j*14.5	53 - *j*15	49 - *j*13	Stuchly (1982b) 34°C
	Feline	54 - *j*14.5	53 - *j*17	50 - *j*13	Kraszewski (1982) 36°C
	Rat	60 - *j*17	58 - *j*18	55 - *j*15	Burdette (1980) 31°C
	Bovine	47 - *j*15	47 - *j*15	46 - *j*13	Brady (1981) 37°C
	Human	51 - *j*18.5	51 - *j*18	47 - *j*19	Cook (1951) 37°C
	Human	48 - *j*14.5	46 - *j*13.5	44 - *j*15.5	Stuchly (1980b) 37°C

Table 7.l. Collated permittivity data for major tissues from 2 to 4 GHz.

dielectric constant values show a possible slight drop over the frequency range, especially for muscle and heart tissue. The magnitude of this drop is around 3 to 10%. Since water, saline and bound water also show a decline in dielectric constant from 2 to 4 GHz, it is to be expected that the dielectric constant of tissue should fall over this range.

In section 7.4.1, the conductivity of animal tissues at frequencies much lower than the dipolar relaxation frequency of water were estimated from examination of collated dielectric data. The results are listed in table 7.g. At 0.1 GHz, the residual conductivity of most animal tissues was estimated to be between one third and one half of that of a free solution of 0.15M saline, which has a conductivity of around 1.44 S/m. The residual conductivity of skeletal muscle, for example, was estimated to be around 0.7 S/m. If this is assumed to be the 'ionic' contribution to the tissue conductivity, then the residual loss factor caused by this ionic conductivity can be added to the loss factor of water, to give a rough approximation of the variation in the loss factor of a material which mimics unbound 'tissue electrolyte'. These values are listed in the final row of table 7.k. It can be seen that the loss factor for this theoretical solution rises only by a factor of around one third over the frequency range 2 to 4 GHz, whereas that of free water rises by a factor of around two.
It was found that around 0.4g water per gram protein is bound in each animal tissue. For muscle tissue, which has a water mass fraction of approximately 74%, it is concluded that around 14% of tissue water is bound. This fraction of the water will have a decreasing loss factor over the frequency range 2 to 4 GHz, and so will partially compensate for the probable rise in loss factor of the unbound water.

It may be noted that the loss factor of bovine intestinal tissues displayed very similar behaviour to that predicted above for unbound tissue water. When the results from these tissues are extrapolated by mixture equation to give the effective dielectric constant of the tissue water fraction, a value very close to that of free water is obtained at each frequency. This is especially true for mucosa tissue, and suggests that there is almost no bound water in this tissue. The boiling process applied to intestinal tissue prior to purchase may be at least partially responsible for this lack of bound water.

The results from 2 to 4 GHz were compared with those of previous researchers over this range. Campbell (1990) lists 5 collated sets of previous research on liver and kidney tissues, and 8 sets on muscle tissues from 2 to 4 GHz. The findings of these studies are listed in table 7.1. Mostly, these previous measurements have been taken on canine, feline and rat tissues, but are the only comparable data available.

It is noticeable that for each tissue type, every researcher reported a gradual decrease in dielectric constant of between 2 to 10% as the frequency rose from 2 to 4 GHz. Equally notable is the fact that the loss factor for each tissue measured by each researcher shows no consistent variation at all over this frequency range. Many report an almost constant tissue loss factor from 2 to 4 GHz; some report a slight, but not significant fall; some report a slight, but again insignificant, rise with frequency. Taking these results as a whole, it seems that the loss factor of biological tissues such as muscle, liver, kidney and heart varies very little over the frequency range 2 to 4 GHz. Certainly larger variation in loss factor was observed between individual muscle specimens, than was observed in either the current or reported loss factor data from 2 to 4 GHz.

As little difference was observed between the permittivity of porcine and agnine tissues and their equivalent human tissues at 3 GHz, it can reasonably be expected that from 2 to 4 GHz there is also little difference in the permittivity of human tissues. Thus the dielectric constant of human tissue is expected to fall by around 5%, whilst the loss factor remains approximately constant between 2 to 4 GHz. It seems likely that these effects are the result of the water in tissues being in many differing states of binding, with a wide distribution of relaxation times.

Chapter 8. An Extrapolation Technique for Investigating the Permittivity of the Water Fraction in Gelatine Solutions and Animal Tissues.

8.1. Introduction.

In this chapter the effects of molecular binding and ionic conductivity reduction are investigated in gelatine solution, which is thought to be useful as a tissue phantom material at microwave frequencies. As a gelatine solution is a simplified water / protein mixture not unlike biological tissues, it is thought that the study of gelatine solutions may help the understanding of water behaviour in tissues.

The results of permittivity and low frequency conductivity measurements are presented, and the state of bound water in the solutions is examined using Maxwell and Bruggeman's mixture equations. It is found that the permittivity of gelatine solutions at 3 GHz could not be accounted for by assuming that the water was in large 'contributing' and small 'non-contributing' fractions. The loss factor of gelatine solutions suggests that the bound water in gelatine solutions has a net relaxation frequency of around 5 GHz, and so makes considerable contribution to the dielectric constant, and especially, to the loss factor of the overall solution.

A new technique for predicting the approximate dielectric constant, loss factor, and relaxation frequency of bound water using mixture equations is introduced. The method involves calculation of the *effective* permittivity of the water fraction of the solution as a function of water content using mixture equations. To estimate the permittivity of bound water in the solution, these effective values can be extrapolated down to a water content approaching zero. This method gives quite consistent loss factor and dielectric constant predictions for gelatine solutions, even with permittivity data from only one measurement frequency. It is suggested that with permittivity data from a range of frequencies, this method could help parameterise a Cole-Cole dispersion relation for the bound water in gelatine solutions.

For biological tissues, encouraging results were also obtained. If the permittivity results from only undehydrated biological samples were considered, the method did not give consistent predictions for the permittivity of bound water in biological tissues, which appears to be better explained by division of the tissue water into 'contributing' and 'non-contributing' fractions, as described in the previous chapter. But by considering the

partial evaporation tissue measurements, an estimated bound water permittivity which is broadly consistent with all the observed permittivity values for biological tissues was obtained. However, great variation in the states of bound water in tissues, and large uncertainty in the residual conductivity of tissues renders the estimated bound water permittivity values for biological tissue subject to a very considerable error.

8.2. Gelatine.

Gelatine is an animal protein product, derived from the hides of cattle. It is commercially readily available in the form of an hydrous crystalline powder, which is composed not of a pure molecular species, but rather as a combination of different amino-acid based protein molecules, of various polymer chain lengths.
When gelatine powder is dissolved in hot water and allowed to cool, a semi-solid gel is formed, as the protein molecules form hydrogen bonds with the water, binding the solution together. A material is obtained which has microwave dielectric properties similar to those of biological tissue; the water may exist in many states, bound and unbound to protein molecules. By adding sodium chloride to the water prior to dissolving the gelatine, the effect of the protein on the ions in the tissue phantom may be investigated.

8.2.1. Gelatine Solutions.

The gelatine powder used in this study was "Supercook" brand. Its manufacturer, Brandway Ltd., claims that the powder consists, by mass, of 88% protein, 11% water, and 1% non-protein animal based materials. A check on the water fraction by oven drying of a sample of the powder concurred with the declared value of 11% by mass. Dielectric measurements were made on solid and semi-solid gelatine solutions, made both with pure water, and with 0.15 **M** sodium chloride. Solutions with gelatine concentration ranging from 2% to 50% by mass were made. It was found practically not to be possible to make homogenous gelatine solutions with a gelatine mass fraction greater than 50%. To find the water volume fraction of each solution, it was necessary also to calculate the density of the gelatine when once dissolved in water, whilst allowing for the 11% water fraction of the gelatine powder itself. A formula for the effective

density, $\rho_{gelatine}$, of the gelatine in solution was calculated as a function of true water mass fraction, x, giving $\rho_{gelatine} = 1.438 - 3.037 \times 10^{-5} \exp(x / 0.1044)$ (8.2.1)

This relation is shown in fig. 8.a.

Measurements were made of the permittivity of gelatine solutions at 3 GHz as a function of water content, using the co-axial probe technique described in chapter 5. The temperature of the gelatine samples was measured with a thermocouple to be between 17 and 20°C during measurement. At 18°C, the permittivity of pure water is approximately 78 - j14.5, so this is the value used in mixture equation analysis on solutions made with pure water. In analysis on gelatine solutions made with saline, the permittivity of 0.15**M** saline is taken as being equal to 75 - j22.

Average results of the permittivity measurements are listed in tables 8.a and 8.b. Figures 8.b and 8.h show the values of the measured dielectric constant and loss factor of the gelatine solutions, as a function of water volume fraction, compared to the expected values as predicted by the Maxwell mixture equation. It can be seen that the dielectric constant lies systematically below that predicted by mixture equations, whereas the loss factor lies consistently well above the theoretical value. This is due to the partial binding of water to the protein molecules in the gelatine, which increases the effective relaxation time of the bound water molecules (see below).

8.3. Gelatine Solutions with Pure Water.

The solutions made from gelatine and pure water are considered first. By using the same technique as was utilised for biological tissues, the amount of bound water in the gelatine solutions can be estimated. The water is supposed to be divisible into two sets; that which is essentially unaffected by binding and has the dielectric properties of free water at 3 GHz; and that which is bound and does not contribute significantly to the dielectric constant of the solution. The dielectric constant of the entire 'non-contributing' fraction is taken to be equal to 2.5, which is the approximate dielectric constant of protein, and the dielectric constant of free water is taken as 78. Using the measured values of the dielectric constant of the gelatine solutions, the effective volume which does not contribute significantly to the overall dielectric constant can be calculated by Maxwell's equation.

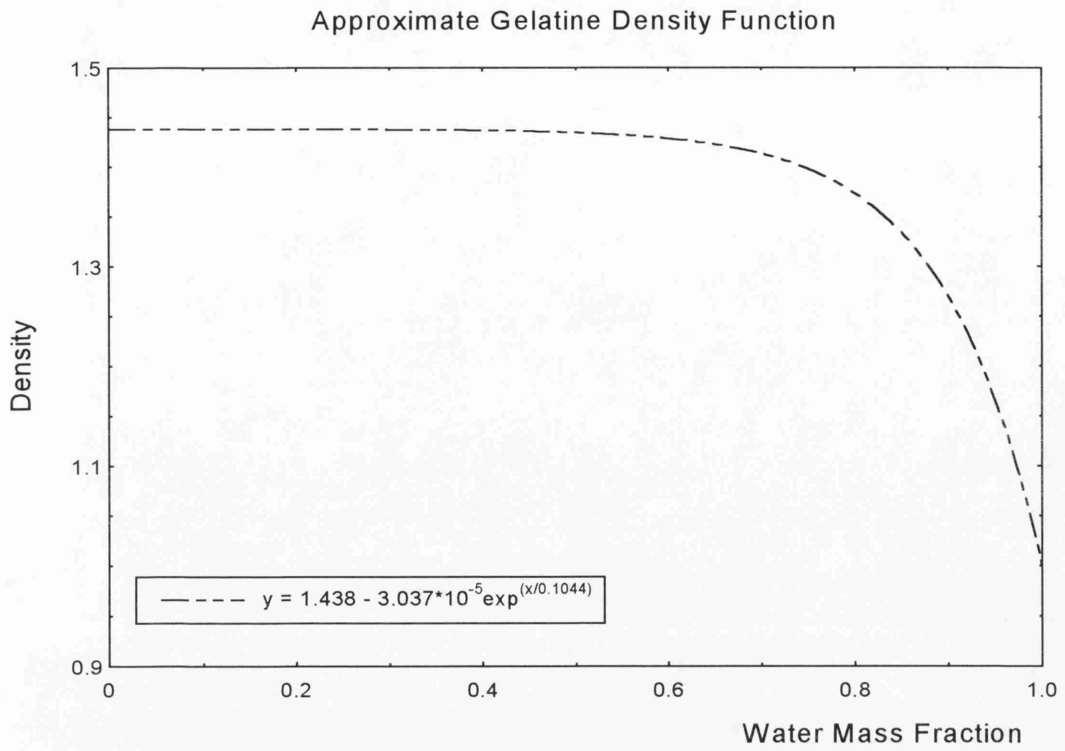

Figure 8.a. Approximate function for the density of gelatine in aqueous solution, evaluated from mass/volume measurements.

Volume Fraction of Water in Gelatine Solution (Pure Water)	Dielectric Constant of Gelatine Solution	Loss Factor of Gelatine Solution	Effective Permittivity of Water Fraction (Maxwell eqn.)	Effective Permittivity of Water Fraction (Bruggeman's eqn.)
1.000	77.5	14.5	77.5 - *j*14.5	77.5 - *j*14.5
0.983	75.4	15.1	77.2 - *j*15.5	77.2 - *j*15.5
0.968	72.8	15.4	76.2 - *j*16.1	76.2 - *j*16.1
0.947	67.4	15.5	72.7 - *j*16.8	72.8 - *j*16.8
0.928	64.2	16.0	71.3 - *j*17.8	71.4 - *j*17.9
0.863	56.7	17.9	69.4 - *j*22.1	69.9 - *j*22.3
0.828	52.0	16.5	67.0 - *j*21.5	67.7 - *j*21.8
0.794	48.2	18.3	65.7 - *j*25.3	66.6 - *j*25.7
0.720	42.2	15.8	64.9 - *j*24.8	66.7 - *j*25.6
0.641	33.5	14.5	59.0 - *j*26.4	61.8 - *j*27.9

Table 8.a. List of mean measured permittivity values for gelatine solutions made with pure water. Also listed are the results of calculations of the *effective* permittivity of the water fraction of each solution, using mixture equations.

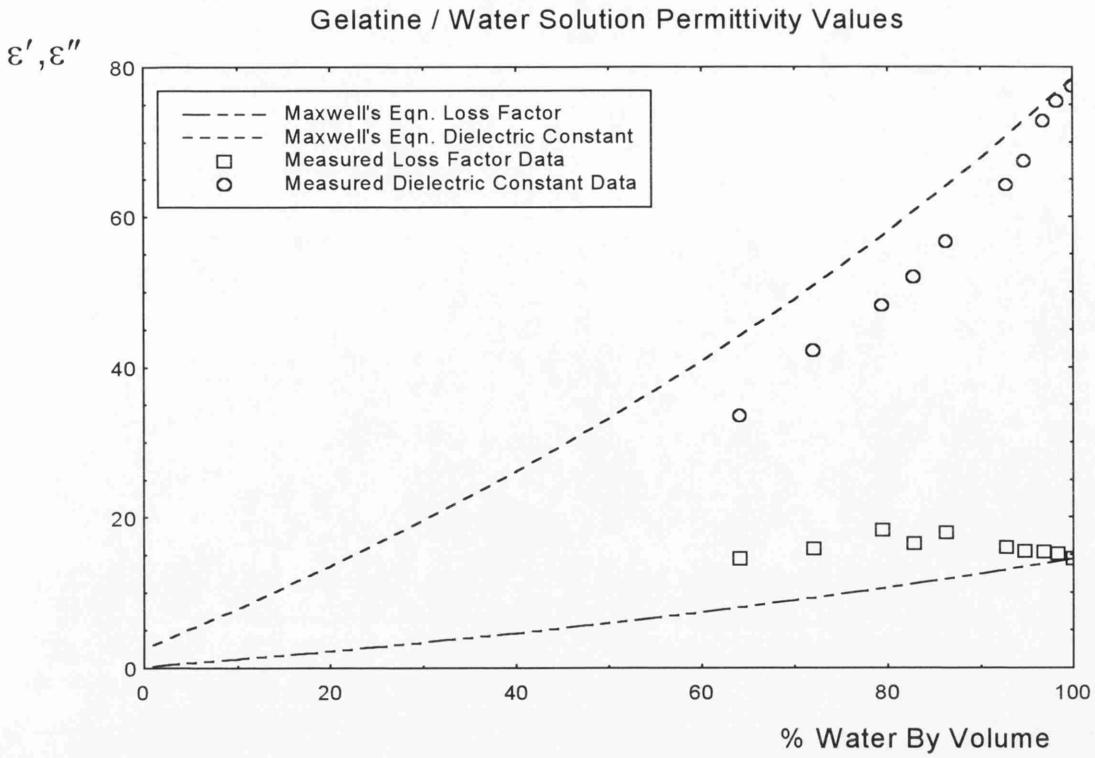

Figure 8.b. Measured dielectric constant and loss factor vs. water content for gelatine solutions made with pure water. Maxwell mixture equation predictions also shown.

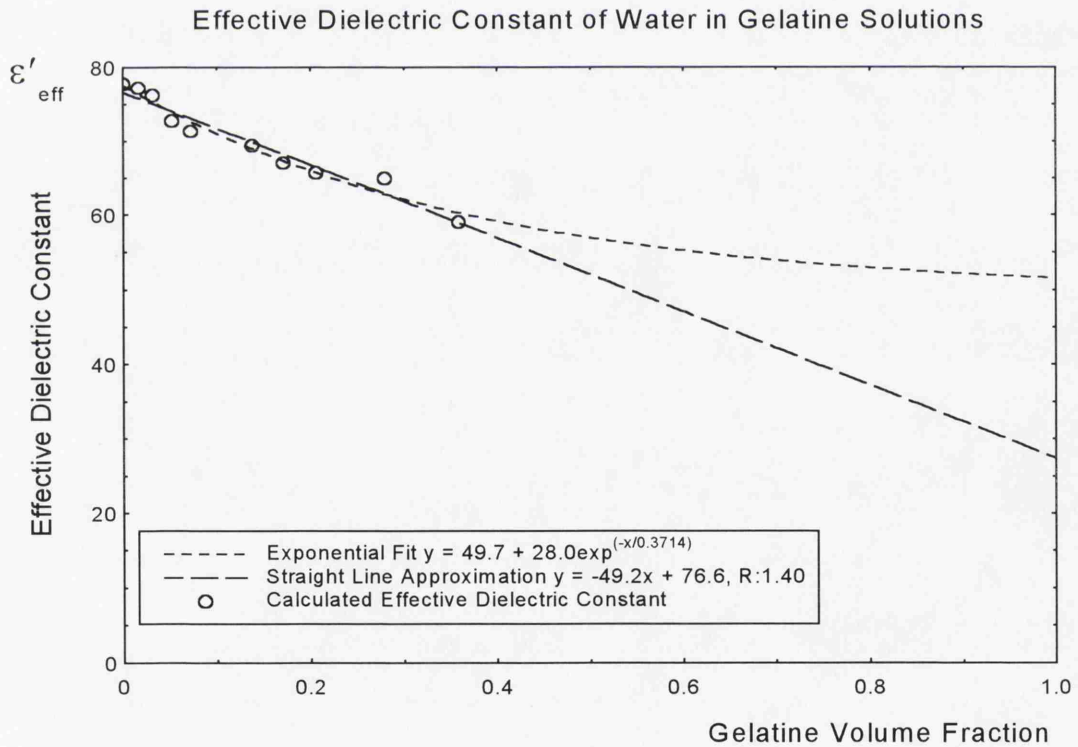

Figure 8.c. Effective dielectric constant of water in gelatine / water solutions calculated by Maxwell's equation, as a function of gelatine concentration. Best-fit linear and exponential functions also shown.

The calculated amount of bound water was found to range from 0.25 to 0.74 grams per gram protein, with an average of 0.43 g/g. This is close to the value found for biological tissues; as the values of dielectric constant for gelatine solutions of given water volume fraction are close to the dielectric constants of tissues with similar water fraction, this similarity in the estimated amount of bound water is not surprising. However, this approach gives rise to a considerable anomaly when considering the loss factor of the gelatine solutions.

8.3.1. Loss Factor of Gelatine Solutions with Pure Water.

When considering the bound water in biological tissues, it was found that the loss factor of the tissues due only to tissue water was a little higher than was expected if the bound water were not contributing significantly to the loss (section 7.2.4). From this it was postulated that perhaps the bound water was contributing to the loss, by having a relaxation frequency in the 0.1 to 1 GHz range, or that the 'free' water was affected by binding in such a way as to have a slightly lower relaxation frequency than true free water. Underestimation of the residual ionic conductivity of the tissues could also have caused the apparently high loss factor of tissue water.

For gelatine solutions, however, the overall loss factor lies very considerably above the predicted value. The data in table 8.a and fig 8.b show that, for example, the overall loss factor of a gelatine solution with water volume fraction 0.72 was around 16, whereas the value expected from Maxwell's equation was around 9 relative dielectric units.

This may be due to residual conductivity of the protein molecules in solution. To investigate this possibility, low frequency (1 kHz) conductivity measurements were made on gelatine solutions of various concentrations. As there is no cellular structure to the protein solutions, unlike biological tissues, all the volume of the gelatine solution could contribute to low frequency conductivity. The low frequency conductivity of gelatine solutions was found to be always below 0.075 S/m, which means that any ionic contribution to the loss factor at 3 GHz was below 0.5 relative dielectric units. Some other process must be responsible for the large difference between expected and observed loss factor.

8.3.2. Effective Permittivity of Water Fraction in Gelatine Solutions.

Again using mixture equations, a different approach was investigated to try to explain the observed permittivity values. From the measured permittivity and volume water fraction of the solution, and assuming that the protein fraction has a permittivity of 2.5 - j0.2, the *effective* permittivity of the water fraction in the solution alone was calculated. The results of these calculations for each concentration of gelatine are presented in table 8.a. It can be seen that as the gelatine concentration increases, the effective dielectric constant of the water shows a gradual decrease, but the effective loss factor shows a gradual increase.

8.3.3. Dielectric Constant of Gelatine-Bound Water

Figure 8.c shows the variation of the *effective* dielectric constant of water in gelatine solutions, as calculated by Maxwell's equation. As the concentration, c, of gelatine increases, the number density of available hydrogen bonding sites on the protein molecules increases, more water becomes located in bound states with lower dielectric constant than free water, and so the effective dielectric constant of the water with which the gelatine is mixed is reduced. If the bound water were to have a relaxation frequency of the order of 3 GHz, then loss factor of the bound water would be very high at the measurement frequency of 3 GHz, and this would explain the high effective loss factor values calculated for the water fraction.
Were it possible to make a homogeneous gelatine solution with a gelatine concentration approaching unity, all the water molecules in this solution would be in bound states, and so the effective dielectric constant of the water would be equal to the average dielectric constant of gelatine-bound water.

This value can be estimated by extrapolating the best-fit lines in fig. 8.c up to a gelatine volume fraction of 1. Both straight line and exponential curve fits are shown. Unfortunately, the scatter on the data is such that no particular curve fit is immediately suggested. The straight line approximation, however, is probably unrepresentative of the theoretical variation at high gelatine concentrations; the effective dielectric constant of the added water must be fairly constant until all the bond sites have one associated water

molecule, so the extrapolated line is expected to level off at high gelatine concentration. Therefore, the exponential curve seems a more realistic approximation. Modest evidence for this is that the mean square deviation of the data from the exponential fit is 1.05, whilst the mean square deviation from the linear fit is 1.25.

The two approximate fits for the data are

$$\varepsilon'_{eff} = -49.2c + 76.6 \qquad \text{(linear)}$$

and

$$\varepsilon'_{eff} = 49.68 + 27.95\exp(-c/0.3711) \qquad \text{(exponential)} \qquad (8.3.1)$$

These functions intersect with the line c=1 at values of 27.4 and 51.6 respectively, which are therefore approximate values for the dielectric constant of water bound to protein molecules in gelatine solutions.

Pure water displays a microwave dispersion which is closely approximated by a Debye equation

$$\varepsilon = \varepsilon_\infty + \frac{\varepsilon_s - \varepsilon_\infty}{1 + j\omega\tau} \qquad (8.3.2)$$

As was discussed in chapter 3, water molecule binding appears to significantly affect only the relaxation time, τ, and not the limiting high and low frequency permittivity values ε_∞ and ε_s. Therefore, if it is assumed that all the bound water has the same relaxation frequency, then the permittivity of the bound water can also be expressed by a Debye equation. The exponential fit intersect value of 51.6 can then be inserted into the Debye equation for the dielectric constant, and the effective relaxation time for bound water found. The Debye equation gives

$$\varepsilon'_{eff} = \varepsilon_\infty + \frac{\varepsilon_s - \varepsilon_\infty}{1 + (\omega\tau_{eff})^2} \qquad (8.3.3)$$

where, for water at ~20°C, ε_∞=4.3, ε_s=80.4 and ω=3 GHz.

This gives a value of τ_{eff} = 41.4ps for the relaxation time of bound water, which corresponds to a relaxation frequency of 3.84 GHz. At 20°C, free water has a relaxation frequency of approximately 17 GHz. The linear fit intersect value, 27.4, gives a relaxation frequency of 1.98 GHz, so there is a factor of approximately two in the uncertainty of the bound water relaxation frequency as estimated by this method.

8.3.4. Loss Factor of Gelatine-bound Water.

The loss factor of pure water / gelatine solutions is shown in fig. 8.d. At zero water concentration, the loss factor has the value 0.2, that of pure unhydrated protein. A

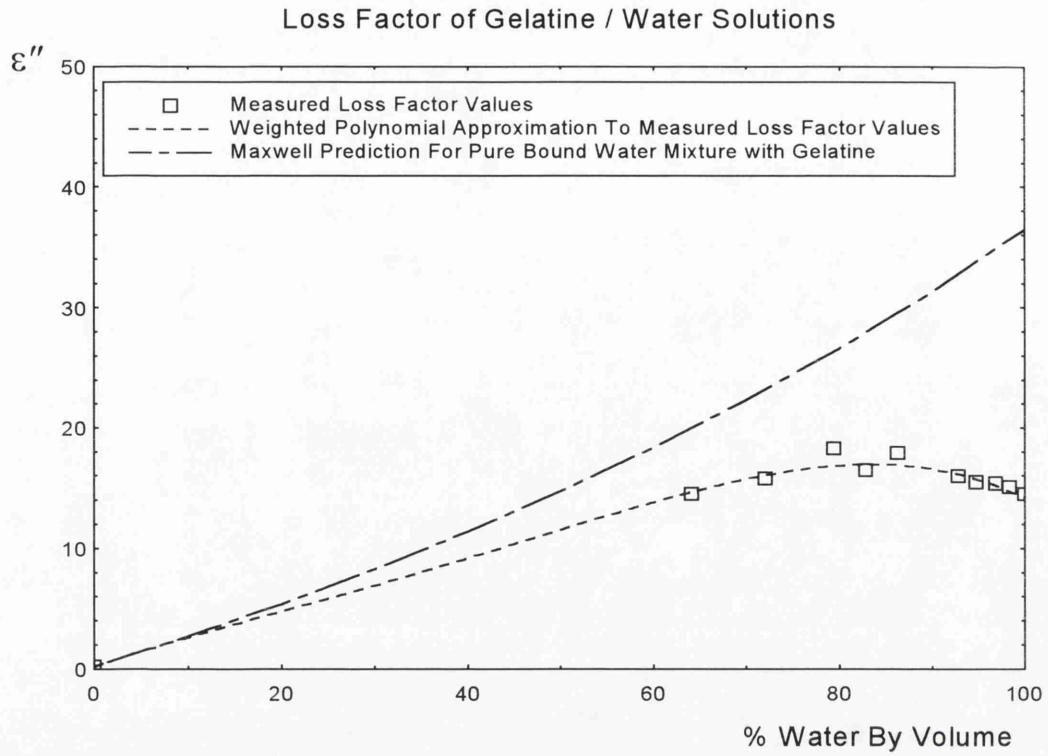

Figure 8.d. Comparison between measured loss factor values and those predicted by Maxwell's equation for a mixture of pure bound water in gelatine. Close agreement at low water concentration is desired.

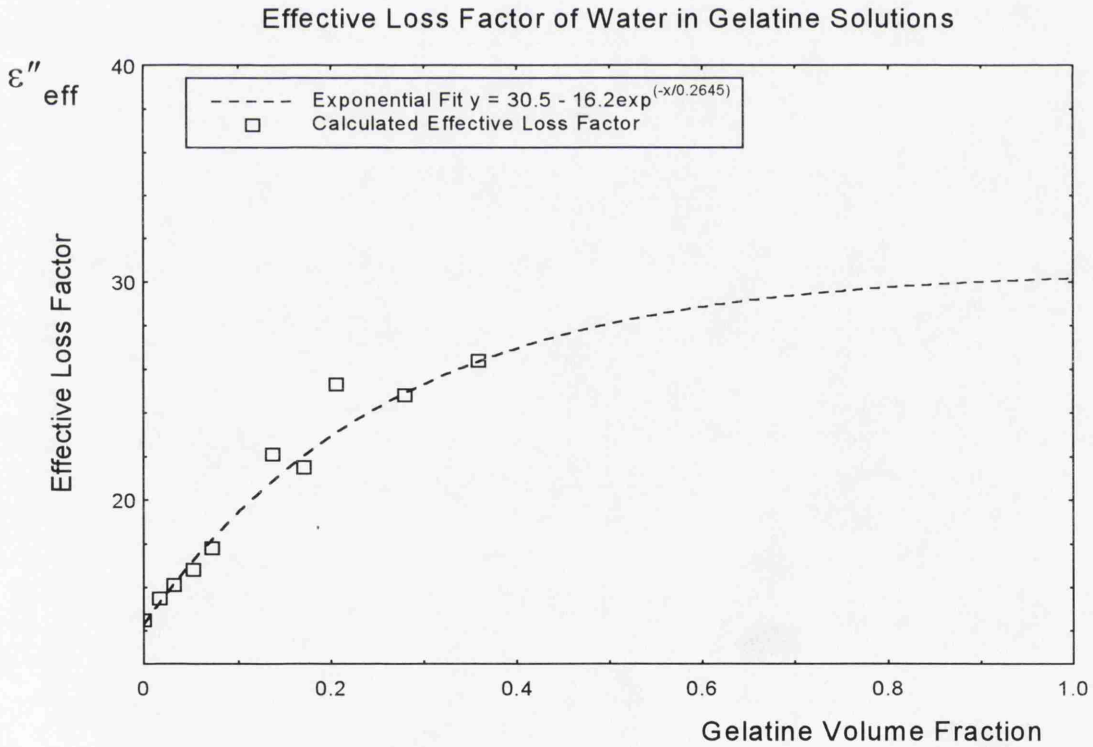

Figure 8.e. Effective loss factor of water in gelatine / water solutions calculated by Maxwell's equation. Best fit exponential has a value of 30.2 for ~100% gelatine. This is slightly lower than the value calculated from extrapolation of the effective dielectric constant.

polynomial best fit, heavily weighted to pass through the point (0, 0.2), shows the approximate behaviour expected of the loss factor for the range of unobtainable low water concentration values.

For theoretical solutions of low water concentration in which all the water molecules are bound, the loss factor of the solution must tend to a value dependent on the loss factors of pure gelatine and pure bound water. By taking the value of the relaxation time for pure bound water, obtained above by considering the dielectric constant, the Debye equation can be used to evaluate the loss factor of pure bound water. This again assumes that all the bound water has the same relaxation frequency.

From the Debye equation $$\varepsilon'' = \frac{(\varepsilon_s - \varepsilon_\infty)\omega\tau_{eff}}{1+(\omega\tau_{eff})^2} \qquad (8.3.4)$$

Taking ε_∞=4.3, ε_s=80.4 and a value of τ_{eff} =41.4ps for the relaxation time of bound water, this gives a value for the loss factor of bound water of $\varepsilon'' = 36.9$. Therefore the estimated permittivity of bound water at ~20°C is 51.6 - j36.9, and the relaxation frequency is 3.84 GHz.

Figure 8.d shows the loss factor data for pure water / gelatine solutions, and the values of the loss factor predicted by Maxwell's equation for a mixture of gelatine with a substance with relative permittivity 51.6 - j36.9, in other words, pure bound water. It can be seen that at low water concentrations, the polynomial approximation for the measured loss factor data closely approaches the Maxwell equation prediction for a mixture of gelatine with pure bound water, as calculated from values of the effective dielectric constant of water in gelatine solutions.

It is possible to estimate the average loss factor of the bound water by initial extrapolation of the loss factor of the gelatine solutions, rather than by using the estimated dielectric constant in a Debye dispersion equation. This is probably a preferable technique, as it does not assume that all the bound water has a single relaxation time.

For comparison with the loss factor for bound water predicted by analysis of the dielectric constant, fig. 8.e shows the effective loss factor values calculated by Maxwell's equation as a function of gelatine concentration. From this, the exponentially extrapolated loss factor of bound water was found to be 30.6. This is rather lower than the value of ~37 predicted by the Debye equation from the extrapolated dielectric

constant, but is satisfactory considering the degree of uncertainty in both of the extrapolated values.

It must be noted, however, that this extrapolated loss factor value of ~31 is equally consistent with either the linear or exponential estimate for the limiting dielectric constant in eqn. 8.3.1. If the limiting dielectric constant is taken to be equal to the linear estimate of 27, the loss factor predicted by the Debye equation is 35. Therefore the apparent agreement between the predicted and extrapolated bound water loss factor values can not be regarded as convincing evidence that the method is valid.

It is preferable to extrapolate both the dielectric constant and loss factor of bound water independently, rather than using the Debye dispersion equation, as the Debye equation is not strictly applicable, due to the expected large spread of relaxation times in bound water.

8.3.5. Analysis Using Bruggeman's Equation.

Also shown in table 8.a are the effective permittivity values of the water fraction for gelatine solutions of all concentrations calculated using Bruggeman's equation. Bruggeman's equation is an integral form of Maxwell's equation, and is thought to better represent the permittivities of mixtures with larger suspended volume fraction. Plotting the effective dielectric constant as a function of gelatine concentration again allows a linear or exponential best-fit to be calculated, giving the dielectric constant of pure bound water at high values of gelatine concentration. This is shown for pure water gelatine solutions in fig. 8.f. For the exponential best-fit, the limiting value of the effective dielectric constant is 59.6. Substituting this value into the Debye dispersion equation (eqn. 8.3.3) gives the average relaxation time of bound water as 32.5*ps*, and therefore a relaxation frequency of 4.89 GHz. From these values, the limiting loss factor of the bound water at 3 GHz can be calculated as 33.9, using eqn. 8.3.4.

By plotting the effective loss factor of the water as calculated using Bruggeman's equation as a function of gelatine concentration, as shown in fig 8.g, the limiting bound water loss factor can be extrapolated at high gelatine concentrations. The exponential best-fit for the loss factor gives a limiting value of 33.9. Although this is exactly equal to the value predicted by using the extrapolated dielectric constant in the Debye equation, this close agreement is probably only a coincidence, as the uncertainty in each of these

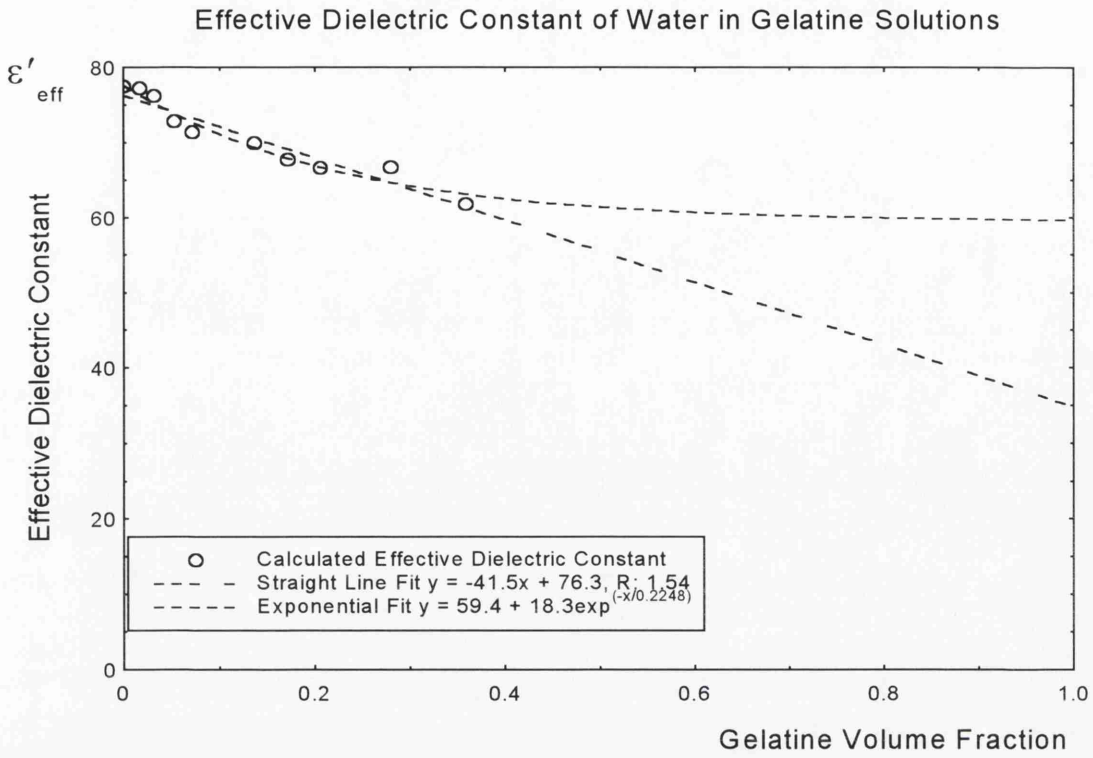

Figure 8.f. Effective dielectric constant of water in gelatine / water solutions calculated by Bruggeman's equation, as a function of gelatine concentration. Best fit linear and exponential functions also shown.

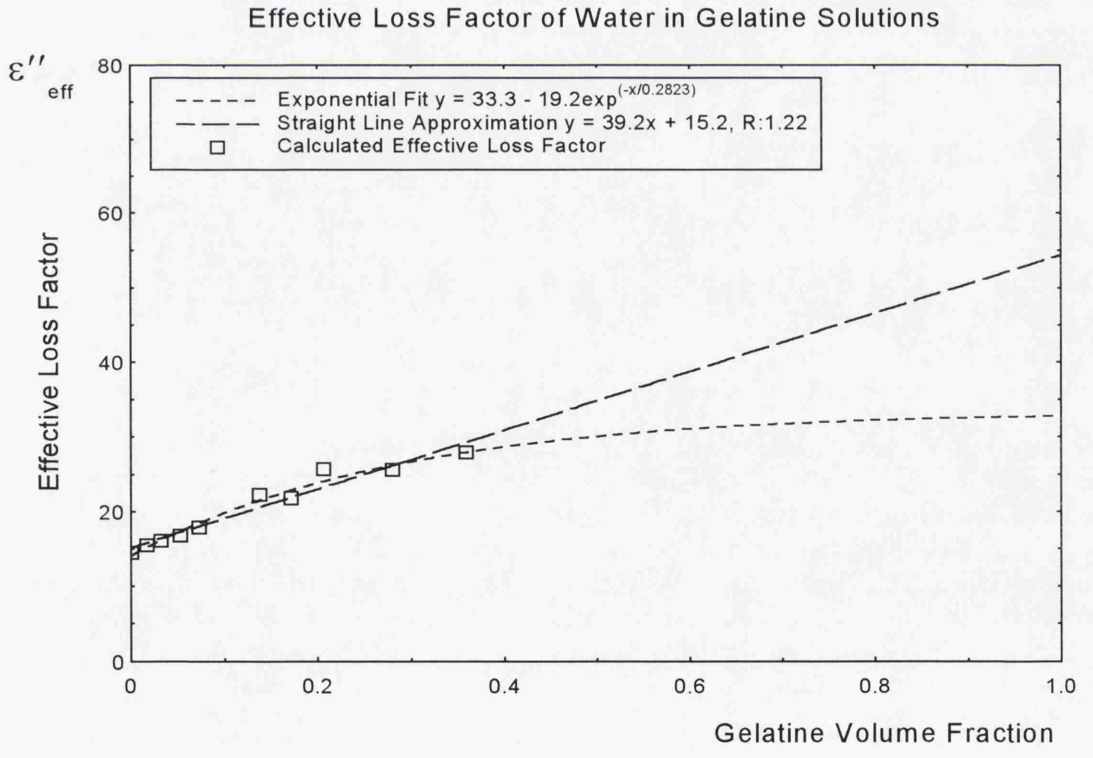

Figure 8.g. Effective loss factor of water in gelatine / water solutions calculated by Bruggeman's equation, as a function of gelatine concentration. Best fit linear and exponential functions also shown.

values is so great. However, this does suggest that the variation of the effective dielectric constant and loss factor with gelatine concentration is quite well described by this method using an exponential best-fit. It can be seen from fig 8.g that the linear approximation for the variation of loss factor with gelatine concentration is probably unrealistic. The limiting loss factor value for bound water as given by the linear fit is 54.4. Since the maximum possible loss factor for a material in a dispersion region is equal to $(\varepsilon_s - \varepsilon_\infty)/2$, the limiting value of 54.4 from the linear approximation is greater than the maximum possible loss factor of water at microwave frequencies, which is equal to $(80.4-4.5)/2 \approx 38$.

8.3.6. Applicability of the Debye Equation to Bound Water.

Using permittivity data from one measurement frequency, 3 GHz, from gelatine solutions of various concentrations, the overall permittivity of water which is bound to the protein molecules has been estimated. The bound water dielectric constant value of 52 obtained using Maxwell's equation, and the value of 60 obtained using Bruggeman's equation, are subject to a very large error indeed, as the limiting permittivity values extrapolated from graphs such as fig. 8.c, have very large uncertainty.

In the real gelatine solutions, which have fairly high water concentrations, there are more water molecules than there are bonding sites on the proteins, so some of the water molecules are free, and some exist in various states of binding. As there is probably a wide distribution of water binding states in the solutions, the estimated dielectric constant value does not represent the dielectric constant of a pure molecular species, but rather a *net* value for a combination of bound states. In this case one particular value of the net dielectric constant of bound water cannot be uniquely associated with one single loss factor value implied via the Debye equation. Therefore, the Debye equation cannot strictly be applied to the bound water dielectric constant value to give a bound water loss factor value; it is likely that a more accurate estimate of the bound water loss factor can be obtained by extrapolation of the effective loss factor values, rather than by using Debye's equation.

This does not mean that the extrapolated estimates for the dielectric constant and loss factor of the bound water are necessarily 'incorrect.' It means that the estimated bound

water dielectric constant and loss factor values are *net* values for water in all bound states, and should therefore really be evaluated individually.
With accurate permittivity measurement over a wide frequency range, preferably 2 decades of frequency, it would be possible to estimate the spread of bound relaxation frequencies and the proportions of water molecules in each state. Then a more appropriate dispersion equation such as a Cole-Cole equation, which allows for a distribution of relaxation times, could be used to parameterise the permittivity data. This could improve the accuracy of the current permittivity estimates for bound water, and would permit direct implication of the bound water loss factor value from calculated values of the bound water dielectric constant.

8.3.7. Summary.

In summary of these data, the minimum estimated net dielectric constant of bound water in gelatine solution was 27, found by linear extrapolation of the overall effective dielectric constant of all the water in solution, as calculated by Maxwell's equation. The maximum estimated net dielectric constant was 60, found by exponential extrapolation of the effective dielectric constants as calculated by Bruggeman's equation. Debye's equation was then used to estimate the net bound water relaxation frequency, with values from 2 to 5 GHz suggested by the above values of bound water dielectric constant.
The range of estimated net bound water loss factor values lay between 30 and 37. This range suggests a net bound water relaxation frequency of between 1.5 to 6 GHz. Thus the independently predicted net bound water loss factor values are roughly consistent with the predicted dielectric constant values, in that each suggests a similar range of net relaxation frequency.

8.3.8. Gelatine Solutions as Biological Tissue Phantoms.

From the permittivity data in table 8.a it can be seen that a gelatine solution, made from pure water, with a water volume fraction of around 80%, has dielectric properties at 3 GHz similar to those of typical high water content soft biological tissues. Therefore, such a solution may be useful as a tissue phantom for use in thermographic research. It must however be noted that the loss factor in this gelatine solution is entirely due to

dielectric relaxation of water, in various states of binding. In biological tissue it is expected that at least part of the loss is due to ionic conductivity, which is not present in pure water / gelatine solutions.

8.4. Gelatine Solutions with Saline.

The results of permittivity measurements on gelatine solutions made with 0.15**M** saline rather than pure water are listed in table 8.b. It was thought that the introduction of ions to the solutions would make the dielectric behaviour closer to that of biological tissues, the electrolytic water in which is similar to 0.15**M** saline. Figure 8.h compares the experimental data to the values predicted by Maxwell's equation for a mixture of two materials with relative permittivities 2.5 - *j*0.2 and 75 - *j*22.

As with the pure water solutions, the dielectric constant lies consistently below the prediction, and the loss factor lies consistently above. This is again due to binding of the water molecules to the proteins of the gelatine. However, it may be noted that the loss factor for saline solutions reaches a peak value at higher water concentration than the loss factor for pure water solutions. It was found that this was due to restriction of the ionic conductivity of the electrolyte by the gelatine.

8.4.1. Restriction of Ionic Conductivity in Gelatine Solutions.

Pure 0.15**M** saline has a d.c. or low frequency conductivity of 1.44 S/m. The contribution of ionic conductivity to the loss factor of 0.15**M** saline is given by $\varepsilon''_{ionic} = \frac{\sigma_{low\,freq.}}{\omega\varepsilon_0}$. By making low frequency (1 kHz) conductivity measurements on gelatine solutions made with saline, it was possible to investigate the variation of the ionic conductivity with increasing gelatine concentration. Figure 8.i shows the low frequency conductivity as a function of water volume fraction. The measured data can be approximated by a straight line of equation

$$\sigma_{low\,freq.} = 0.0388x - 2.40 \qquad (\sigma_{low\,freq.} \text{ in S/m}) \qquad (8.4.1)$$

where x is the gelatine percentage concentration. Of course, the minimum possible value of the conductivity is zero, so at concentrations below the intercept of this line with the ordinate axis, a value for the conductivity of zero theoretically should be taken. In fact,

Volume Fraction of Water in Gelatine Solution (0.15**M** Saline)	Dielectric Constant of Gelatine Solution	Loss Factor of Gelatine Solution	Effective Permittivity of Water Fraction (Maxwell's eqn.)	Effective Permittivity of Water Fraction (Bruggeman's eqn.)
1.000	75.0	22.0	75.0 - *j*22.0	75.0 - *j*22.0
0.983	71.2	22.6	72.9 - *j*23.2	72.9 - *j*23.2
0.968	69.5	22.8	72.7 - *j*23.9	72.8 - *j*23.9
0.947	64.6	22.5	69.7 - *j*24.3	69.7 - *j*24.4
0.928	61.3	22.4	68.1 - *j*25.0	68.2 - *j*25.0
0.863	54.6	20.8	66.8 - *j*25.7	67.2 - *j*25.9
0.828	49.6	20.3	63.9 - *j*26.5	64.5 - *j*26.8
0.794	47.9	20.0	65.2 - *j*27.7	66.2 - *j*28.1
0.758	44.4	19.0	64.1 - *j*28.0	65.4 - *j*28.6
0.720	39.5	17.9	60.6 - *j*28.2	62.3 - *j*29.1
0.641	33.2	16.0	58.5 - *j*29.2	61.2 - *j*30.9

Table 8.b. List of mean measured permittivity values for gelatine solutions made with saline. Also listed are the results of calculations of the *effective* permittivity of the water fraction of each solution, using mixture equations.

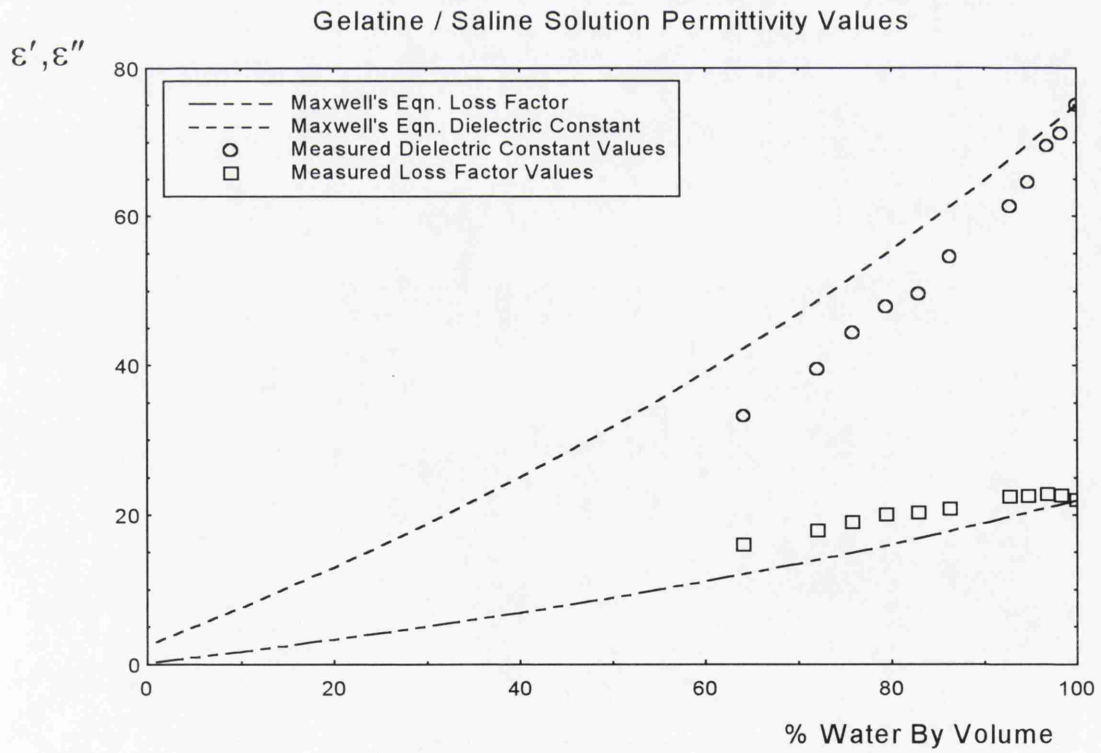

Figure 8.h. Measured dielectric constant and loss factor vs. water content for gelatine solutions made with saline. Maxwell mixture equation predictions also shown.

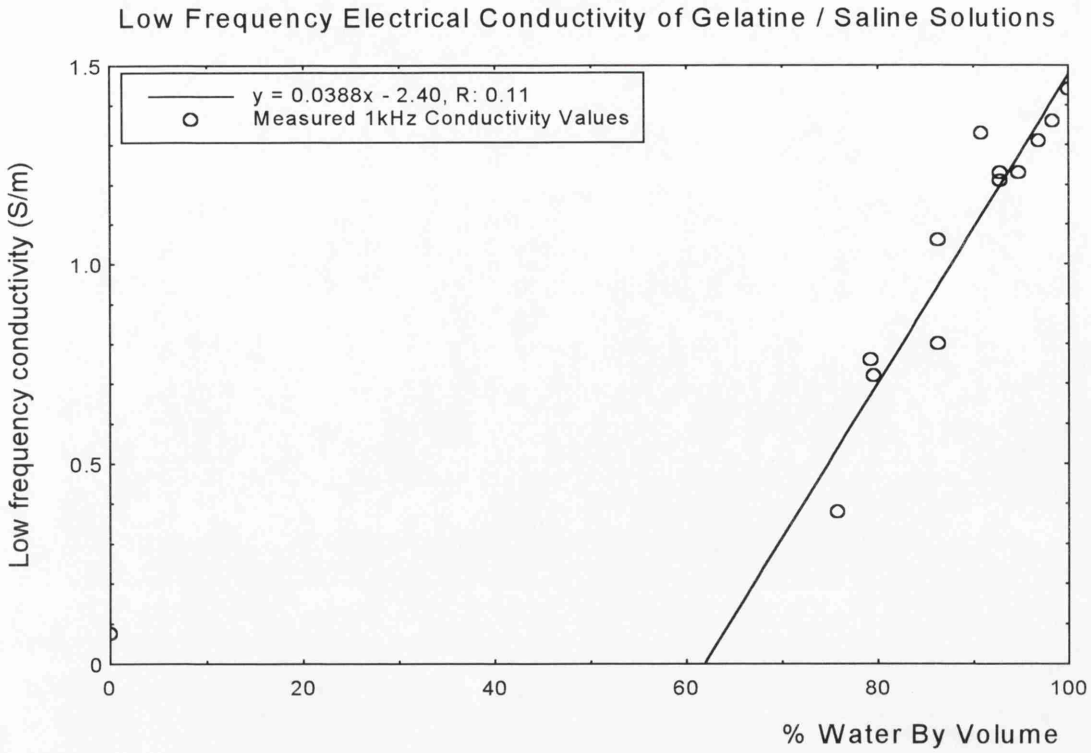

Figure 8.i. Measured values of the low frequency conductivity of gelatine / saline solutions at room temperature. Straight line fit valid for region of high water concentration.

Water Volume Fraction (Gelatine with 0.15**M** saline)	Measured Dielectric Constant	Corrected Loss Factor	Corrected Effective Permittivity of Water Fraction (Maxwell's eqn.)	Corrected Effective Permittivity of Water Fraction (Bruggeman's eqn.)
1.000	75.0	13.1	75.0 - *j*13.1	75.0 - *j*13.1
0.983	71.2	14.1	72.9 - *j*14.5	72.9 - *j*14.5
0.968	69.5	14.7	72.7 - *j*15.4	72.8 - *j*15.4
0.947	64.6	14.9	69.7 - *j*16.2	69.7 - *j*16.2
0.928	61.3	15.2	68.1 - *j*17.0	68.2 - *j*17.0
0.863	54.6	15.1	66.8 - *j*18.8	67.3 - *j*18.8
0.828	49.6	15.4	63.9 - *j*20.1	64.5 - *j*20.3
0.794	47.9	15.9	65.2 - *j*22.0	66.2 - *j*22.4
0.758	44.4	15.8	64.1 - *j*23.2	65.4 - *j*23.7
0.720	39.5	15.5	60.6 - *j*24.4	62.3 - *j*25.2
0.641	33.2	14.5	58.5 - *j*26.5	61.2 - *j*27.9

Table 8.c. List of mean measured permittivity values for gelatine solutions made with saline, with the contribution to the loss factor due to ionic conductivity removed. Also listed are the *effective* permittivity values of the water fraction in each solution.

measurements of the low frequency conductivity of gelatine solutions made with pure water indicated that the gelatine itself has a residual ionic conductivity of approximately 0.075 S/m, so this is the minimum limiting conductivity value.

This restriction of ionic electrolyte conductivity has also been observed by other researchers investigating the conductivity of protein solutions. Bull and Breese (1969) measured the conductivity at 1 kHz of a variety of low concentration protein solutions of several electrolytes, and found that the conductivity displayed a linear variation with concentration, approximately given by

$$\sigma_{solution} = \sigma_{electrolyte}(1 - 2.06c) \qquad (8.4.2)$$

where c is the protein concentration. Thus the conductivity of the electrolyte in which the protein is suspended drops to zero at a water fraction of 52%. Schepps and Foster (1980) reported that the 1 kHz conductivity of electrolytes falls linearly with increasing protein concentration in the electrolyte, and tends to zero at a water volume fraction of around 0.6. The behaviour has also been noted on electrolytic solutions of polymers other than proteins. Foster et al (1984) showed that the conductivity of polyethylene oxide in solution with 0.1**M** saline drops rapidly with increasing polymer concentration, initially in a linear fashion before levelling off at very high polymer concentration.

8.4.2. Ionic Conductivity Correction to Measured Loss Factor.

Using the low frequency conductivity correction equation (eqn. 8.4.1), the effect of ionic conductivity in the gelatine solutions with saline electrolyte can be subtracted from the measured loss factor data values, leaving only the dipolar relaxation contribution from the water. The results of this are shown in table 8.c and in fig. 8.j. Having subtracted the ionic conductivity effects, the loss factor now displays a variation with concentration of similar form to that of gelatine solutions made with pure water, as shown in figs 8.a and 8.d. The corrected loss factor peak now occurs at a water volume fraction of around 0.8, and as the water volume fraction decreases, the corrected and uncorrected loss factors tend to the same value, as the ionic conductivity effect becomes less.

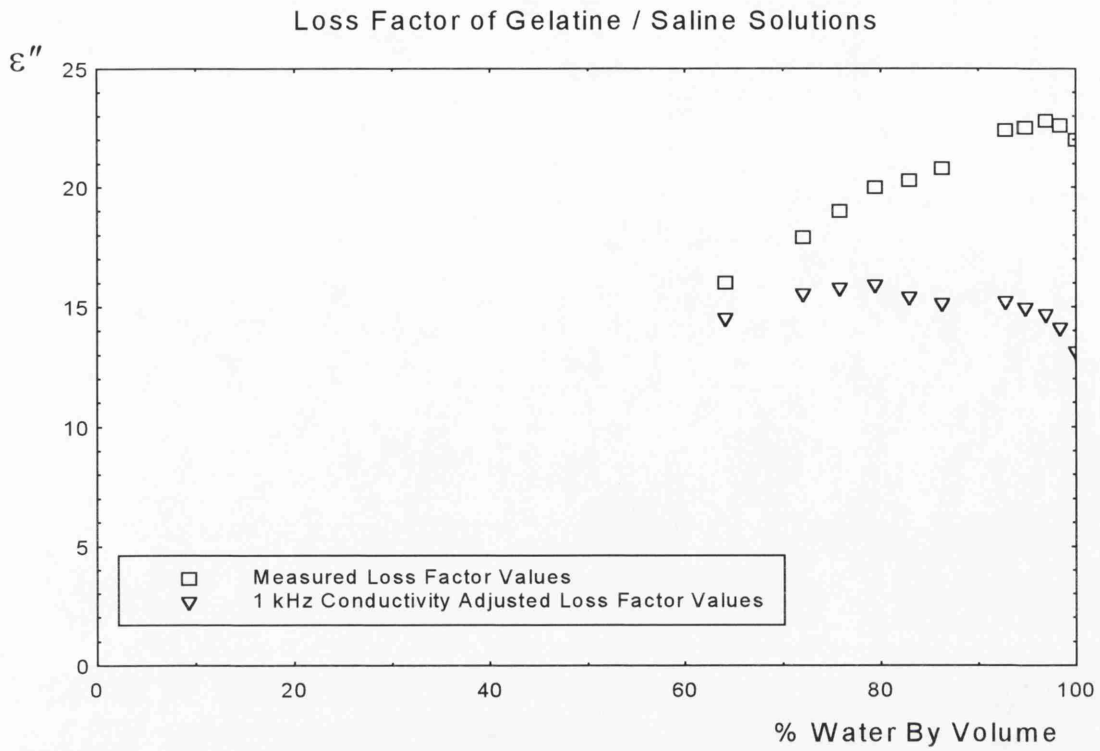

Figure 8.j. Measured loss factor of gelatine / saline solutions compared with adjusted loss factor values with ionic conductivity contribution subtracted.

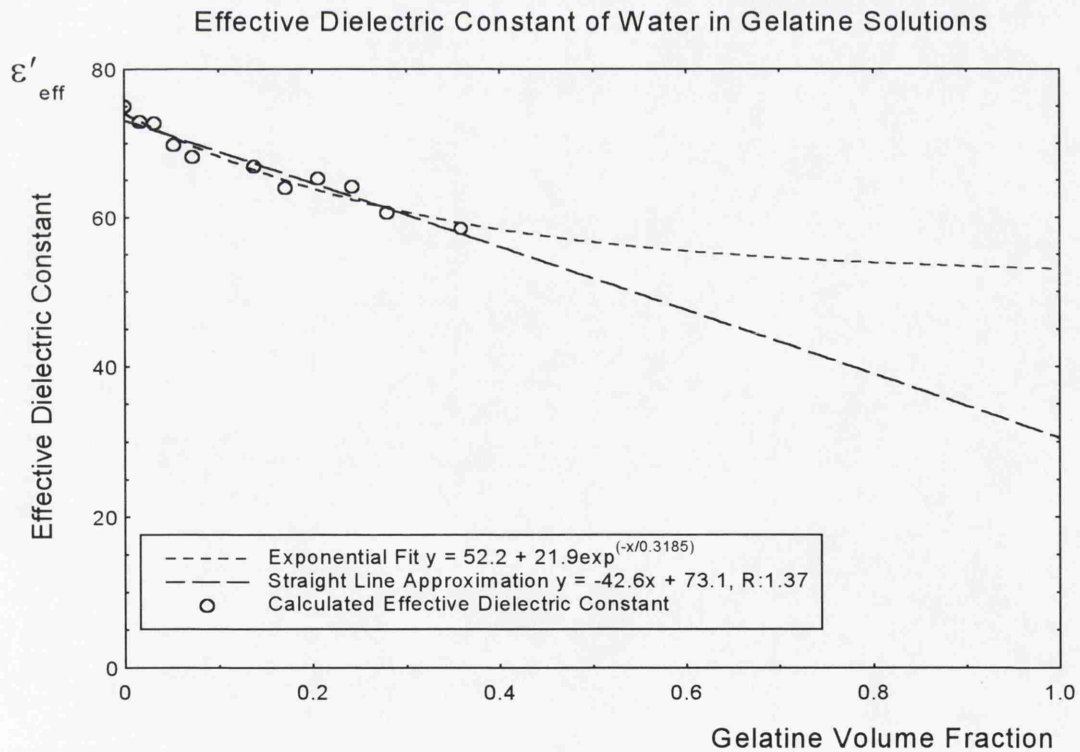

Figure 8.k. Effective dielectric constant of water in gelatine / saline solutions calculated by Maxwell's equation, as a function of gelatine concentration. Best fit functions also shown.

8.4.3. Bound Water in Gelatine Solutions with Saline.

The procedure for evaluating an approximate value for the dielectric constant of the bound water in electrolytic gelatine solutions is the same as for the solutions made with pure water. Maxwell's equation is used with the corrected permittivity values to calculate the *effective* permittivity of the water fraction in each gelatine solution. The results of these calculations are displayed in table 8.c. Then the effective dielectric constant of the water fraction is plotted as a function of gelatine concentration, as is shown in fig. 8.k. Again a linear and exponential best-fit are calculated, with the exponential fit expected to be the most realistic, because of the necessity for the dielectric constant to level off to a constant value when the gelatine concentration is high. The equations of the best-fit lines are

$$\varepsilon'_{eff} = -42.6c + 73. \qquad \text{(linear)}$$

and

$$\varepsilon'_{eff} = 52.15 + 21.95\exp(-c/0.3185) \qquad \text{(exponential)} \qquad (8.4.3)$$

These two functions intercept the line c=1 at values of 30.5 and 53.1 respectively. Both values are similar to the approximate extrapolated values for the dielectric constant of bound water calculated in the previous section for non-electrolytic gelatine solutions. As was discussed in chapter 3, dissolving ions in water slightly changes its microwave dielectric properties. For water in 0.15**M** saline solution, the high frequency permittivity limit ε_∞ is unchanged from the limiting value of ~4.3 for pure water, but the low frequency limit, ε_s, is reduced to approximately 77. Here it will be assumed that these parameters are not affected either by the bonding process, or the restriction of ion mobility. Inserting the (more likely) value of 53.1 for the dielectric constant of bound water calculated above into the Debye equation (eqn. 8.3.3), gives a net value for the relaxation time of bound water of τ = 37.1ps, corresponding to a relaxation frequency of 4.29 GHz. This again requires the assumption that all the bound water can be characterised by a single Debye equation.

Using this relaxation time in the Debye equation for the loss factor (eqn. 8.3.4), gives a loss factor of 34.1. Thus it is concluded that the approximate permittivity of water bound to protein molecules in an electrolytic 0.15**M** saline solution is 53 - *j*34, very similar to the value evaluated for non-electrolytic gelatine solutions. Again, the

uncertainty in this value is large, due to the error in estimating the limiting value of the dielectric constant of bound water from the experimental data.

Figure 8.l shows the *corrected* (i.e. with ionic contribution removed) effective loss factor values as calculated by Maxwell's equation as a function of gelatine concentration. An exponential best-fit gives a limiting value of 39.0 for the loss factor of high concentration solutions. Considering the error in estimating the form of the best-fit, and the added error incurred in the approximate correction for ionic loss, this is in quite good agreement with the value calculated using the dielectric constant.

When the same permittivity data for gelatine solutions with saline are analysed in this way by Bruggeman's equation, the estimated dielectric constant of bound water is 60.4, and the estimated bound water loss factor is 30.5. This is shown in fig 8.m, and again is similar to the permittivity value evaluated for bound water from pure water / gelatine solutions.

8.4.4. Predictions of Other Mixture Equations.

The Bruggeman and Maxwell mixture equations have been shown to give estimations of the dielectric constant and loss factor of gelatine solutions that are fairly consistent with each other. It seems therefore, that these equations can be of use in analysing the permittivity of biological tissue and tissue phantoms. The other common mixture equations, which were criticised in chapter 2, give less consistent estimations. Figure 8.n shows the gelatine permittivity results plotted in comparison to the permittivity predictions of Looyenga's mixture equation, based on the limiting permittivities of 2.5 - j0.2 and 78 - j14.5, which is approximately that of pure water. It can be seen that the dielectric constant of the gelatine solutions lies very close to the Looyenga prediction. This would suggest that no effect other than the homogeneous mixing of two materials is taking place, and that perturbation of the permittivity of water by binding is not occurring. Therefore the great deviation between the experimental and predicted loss factor values would be completely unexplained by Looyenga's equation. The Lichteneker mixture equation is even less realistic, suggesting considerable enhancement of both dielectric constant and loss factor above the predicted values.

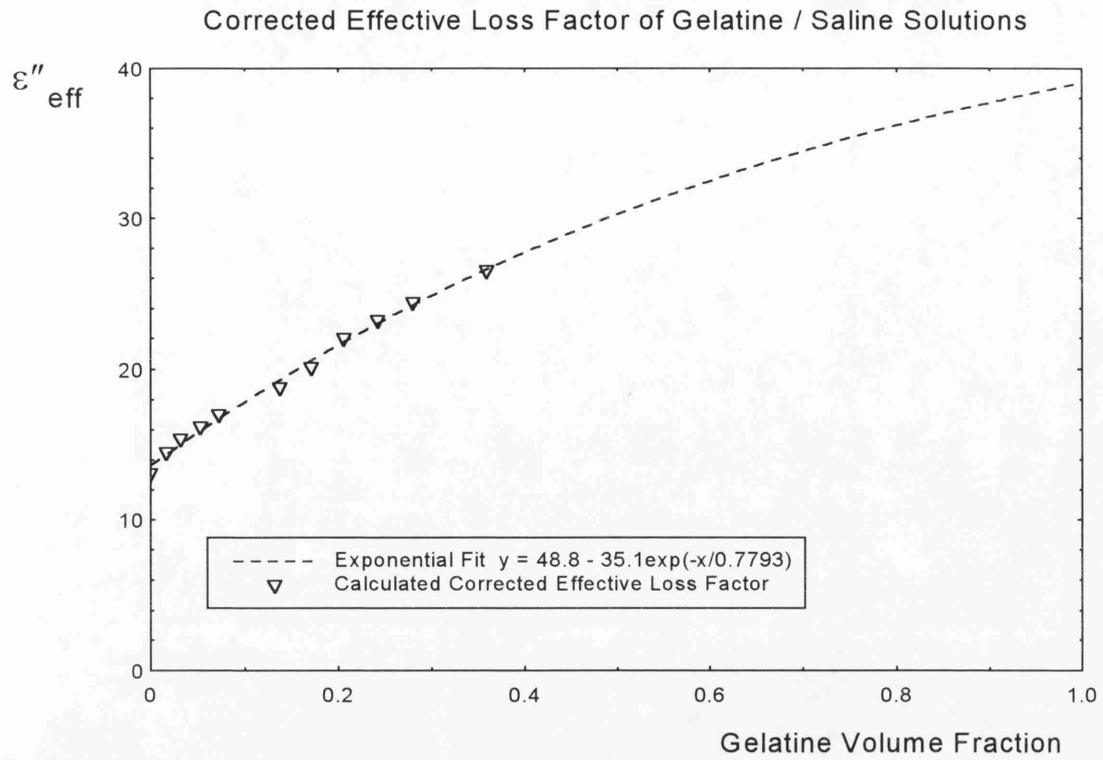

Figure 8.l. Corrected effective loss factor of water in gelatine / saline solutions as calculated by Maxwell's equation. Best-fit exponential has value of ~39 for 100% gelatine.

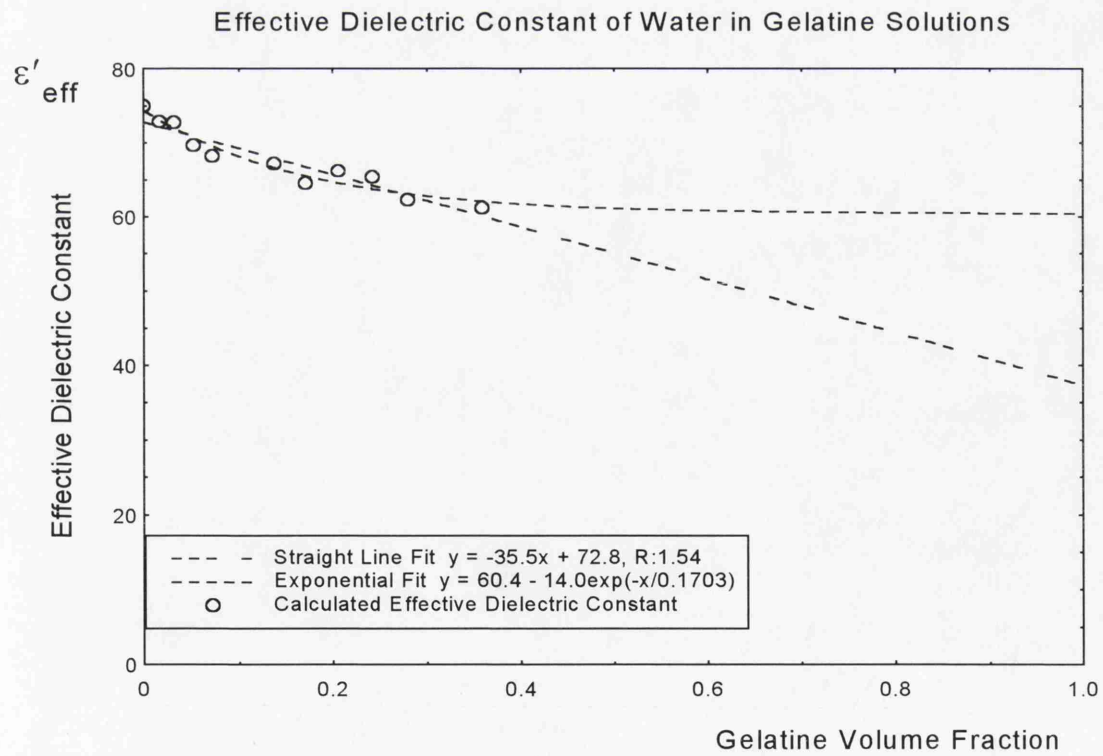

Figure 8.m. Effective dielectric constant of water in gelatine / saline solutions as calculated by Bruggeman's equation.

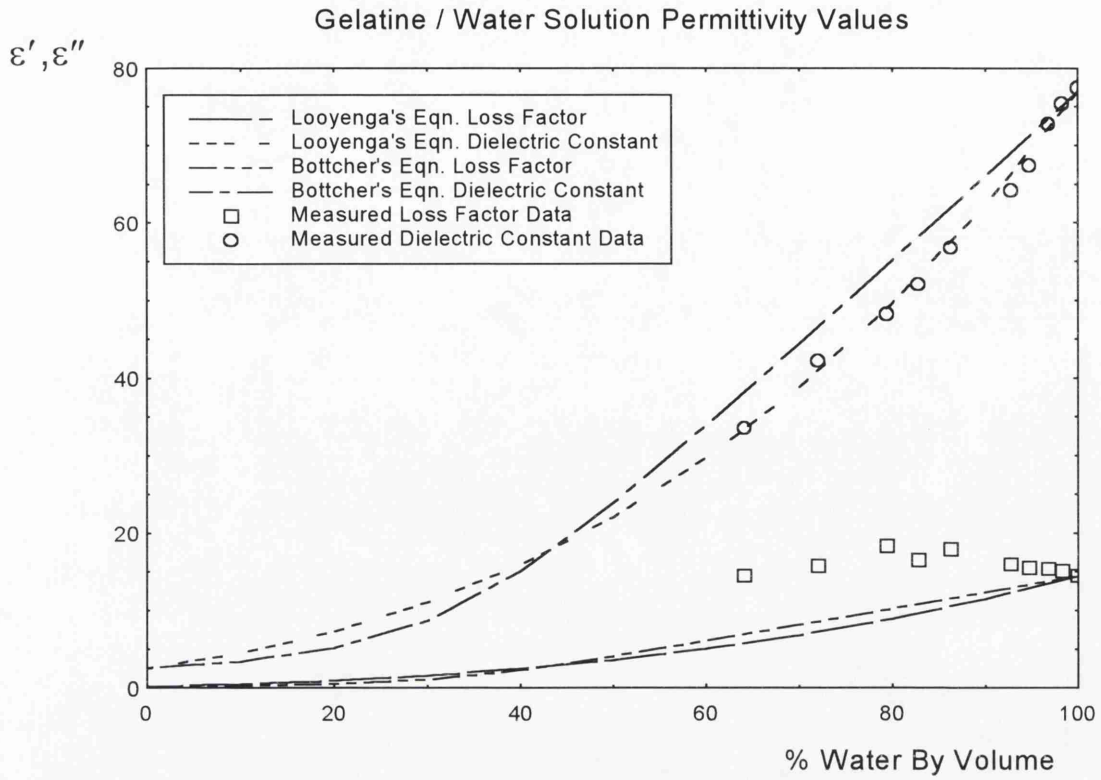

Figure 8.n. Measured dielectric constant and loss factor vs. water content, compared to the predictions of Bottcher and Looyenga's equations. The dielectric constant data lie particularly close to Looyenga's equation, but this therefore cannot account for the deviation in loss factor, and so it is an unsuitable model.

Animal Tissue Type	Water Volume Fraction	Corrected Permittivity	Corrected Effective Permittivity of Water Fraction (Maxwell eqn.)	Corrected Effective Permittivity of Water Fraction (Bruggeman eqn.)
Skeletal Muscle	0.799	46.5 - j12.3	62.8 - j16.8	63.6 - j17.0
Liver	0.717	39.3 - j10.1	60.6 - j15.9	62.4 - j16.4
Kidney Cortex	0.816	49.3 - j12.3	64.8 - j16.4	65.6 - j16.6
Kidney Medulla	0.863	53.8 - j14.0*	65.8 - j17.3	66.2 - j17.4
Heart	0.798	46.0 - j11.7	62.2 - j16.0	63.1 - j16.3
* Estimated				

Table 8.d. List of mean measured permittivity values for animal tissues, with the estimated contribution to the loss factor from ionic and other low frequency conductivity effects removed.

8.5. Extrapolation Technique Applied to Biological Tissues.

Tables 8.d and 8.a list the calculated values for the effective permittivity of the water fraction in animal tissues and gelatine solutions respectively. For gelatine solutions, the decrease in effective dielectric constant is accompanied by an increase in effective loss factor. In the limit of low water content, both the effective dielectric constant and loss factor of water in gelatine solutions tended to values roughly compatible with a large amount of the water in solution being affected by binding, with an average bound water relaxation frequency of around 4 GHz. For animal tissues, extrapolation of the effective dielectric constant and loss factor of the water fraction by an exponential fit to the effective tissue water dielectric constant values does not give such consistent results. The effective dielectric constant of the water in animal tissues is first considered. Because each tissue type has a different composition, it is not strictly legitimate to extrapolate the variation of the effective dielectric constant of tissue water down to zero water content to find the dielectric constant of bound water, as was done for gelatine solutions. However, when this process is carried out, as is shown in figure 8.o, an indication of the limiting permittivity of the bound tissue water may be obtained. The effective dielectric constant values calculated by Maxwell's equation have best-fit curves given by

$$\varepsilon'_{eff} = -52.5c + 74.0 \qquad \text{(linear)}$$

and

$$\varepsilon'_{eff} = 52.5 + 22.6\exp(-c/0.2669) \qquad \text{(exponential)} \qquad (8.5.1)$$

where c is the non-water fraction of the tissue. The exponential relation gives a value of 53.0 for the net dielectric constant of bound water for a theoretical tissue with water content nearing zero. Assuming the bound water can be characterised by a single net relaxation frequency, Debye's dispersion equation predicts the net relaxation frequency of the bound water to be 4.27 GHz. The linear extrapolation gives a net dielectric constant of 21.5 for bound water, and consequently, a net relaxation frequency of 1.67 GHz.

Extrapolation of the predictions of Bruggeman's equation is shown in fig 8.p. By the exponential relation, these give a net dielectric constant of 58.4 for the bound water, and thus a net relaxation frequency of 5.11 GHz, and a net dielectric constant of 27.4, with net relaxation frequency 2.04 GHz, by the linear relation.

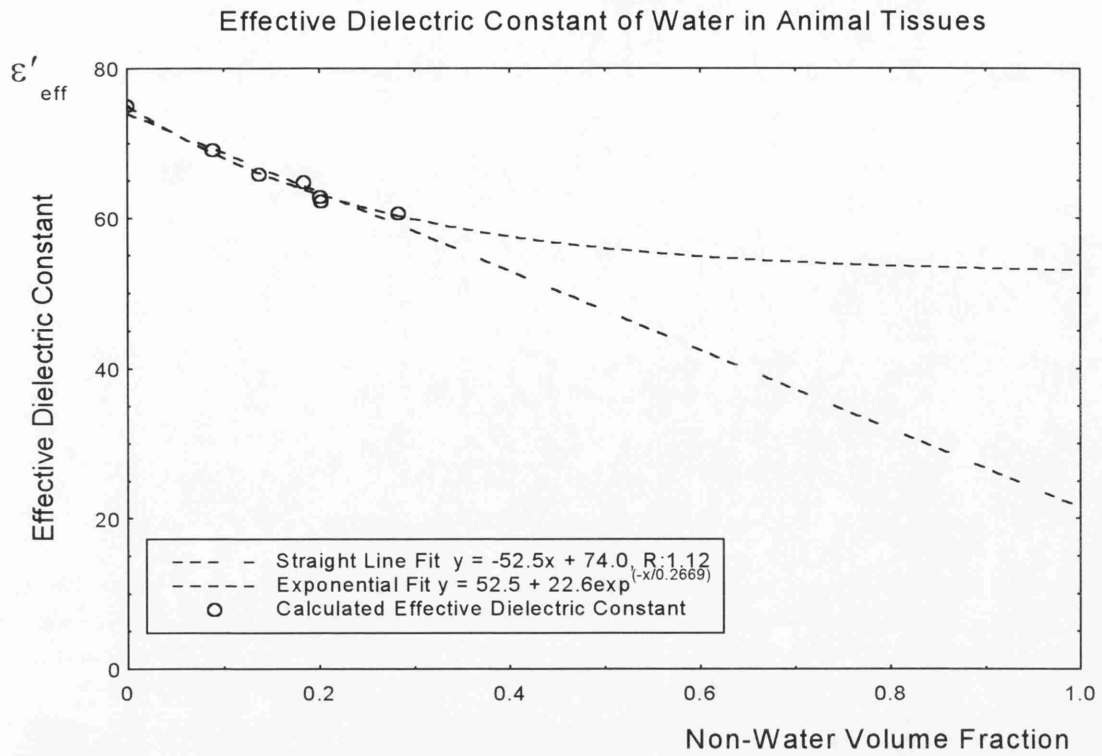

Figure 8.o. Effective dielectric constant of water in animal tissues calculated by Maxwell's equation, as a function of non-water volume fraction. Best fit exponential function also shown.

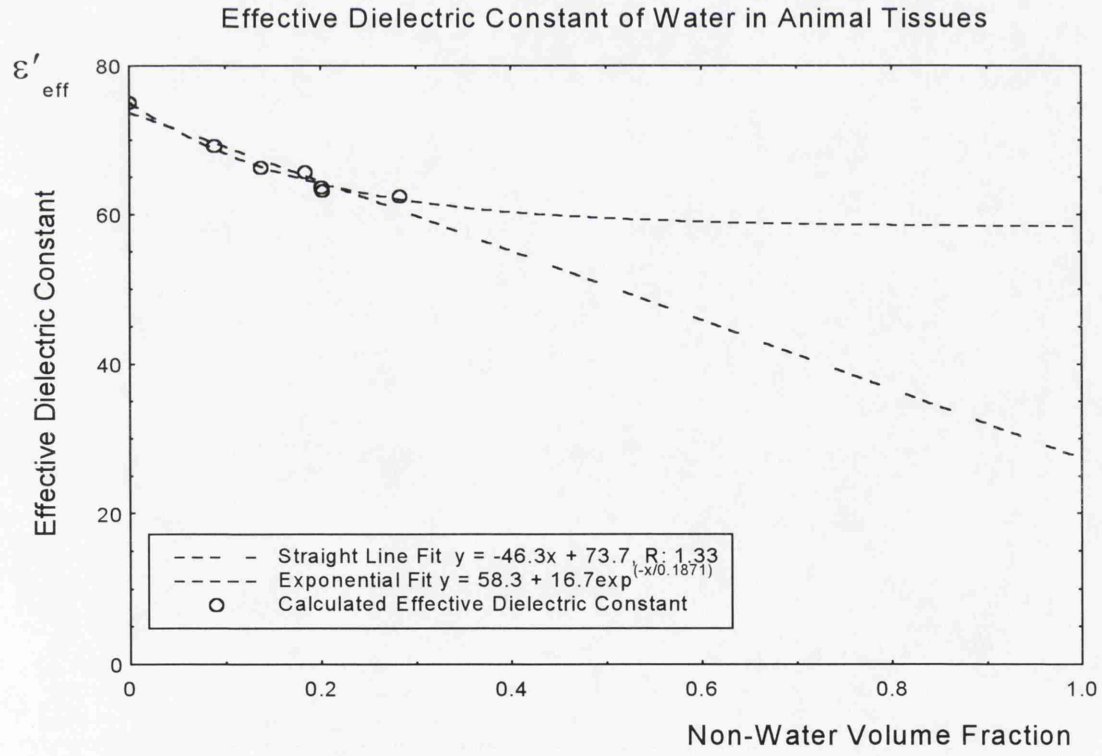

Figure 8.p. Effective dielectric constant of water in animal tissues calculated by Bruggeman's equation, as a function of non-water volume fraction. Best-fit exponential function also shown.

All of these predicted values for the dielectric constant of bound water suggest that the loss factor of the bound water should be around 30 to 38, if the water is fairly well described by a single relaxation frequency. This should be approximately the value obtained if the effective loss factor values were extrapolated up to high non-water fraction concentration.

However, the value of the effective loss factor for the water in all of the tissues is around 16, and there is no systematic variation in the value with increasing non-water fraction concentration. Therefore there is no meaningful extrapolated loss factor value for a theoretical high non-water volume fraction tissue other than 16. In addition, the partial evaporation measurements of section 7.3 continue this trend of consistency in the effective tissue water loss factor, even up to high non-water fraction concentrations. Of course, the values of the effective loss factor of the water in the tissues are dependent on the correct estimation of the residual conductivity to be subtracted from the overall measured loss factor values. Poor estimation of the residual conductivity of each tissue type could mask any systematic variation of the effective loss factor of the tissue water that is, in fact, present.

There are therefore seeming inconsistencies between the prediction of the extrapolated effective dielectric constant and the actual observed loss factors for biological tissues.

These may be partially due to the extrapolation process to find the dielectric constant of bound water being unrealistic. With so few mean tissue data points, covering such a limited range of water content, the extrapolation of the effective dielectric constant of the tissue water down to 100% non-water fraction will be prone to error. To extend the range of water content, the partial evaporation results presented in section 7.3 can again be used.

Figure 8.q shows the effective tissue water dielectric constant values calculated using Maxwell's equation for undried tissues, together with values for the same parameter in partially dehydrated bovine liver samples. These data have non-water volume fraction as high as 0.6, and so indicate the form of the effective tissue water dielectric constant when more of the tissue water is bound.

It can be seen that the values calculated from partially dehydrated samples suggest that the effective tissue water dielectric constant falls in a roughly linear fashion with increasing non-water volume fraction. The exponential fit which was assumed to be

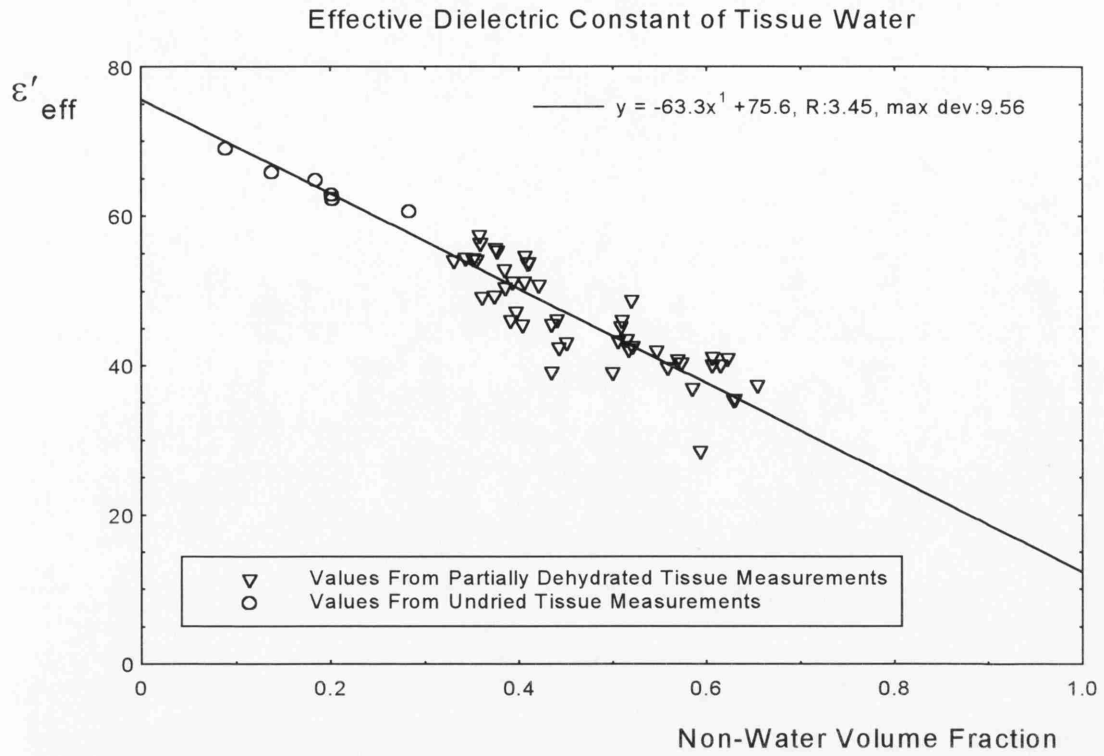

Figure 8.q. Effective dielectric constant of the water fraction of undried tissues and partially dehydrated bovine liver samples. The effective dielectric constant varies with the non-water volume fraction in an approximately linear manner, not the approximately exponential manner previously expected.

more realistic, and which gave consistent results for gelatine solutions, appears to be unrepresentative of the behaviour of the effective dielectric constant of tissue water. A linear fit of the effective dielectric constants from the partially dehydrated samples has equation

$$\varepsilon'_{eff} = -63.3c + 75.6 \qquad (8.5.2)$$

where c is the non-water volume fraction of the tissue. When c approaches unity, the effective dielectric constant of the tissue water, which is thus the net dielectric constant of bound water in the tissue, is therefore estimated to be around 12 relative units.
If the bound water can be approximately characterised by a single relaxation frequency, and has the same values of ε_s and ε_∞ as free water, then the value of 12 for the dielectric constant at 3 GHz suggests a relaxation frequency of 1.03 GHz, and a loss factor at 3 GHz of around 22.

The predictions of this method for investigating the bound water in tissues are now fairly consistent with the method of considering water fractions which are either 'contributing' or 'non-contributing' to the overall dielectric constant. When calculating the amount of bound water in tissues in chapter 7, it was assumed that the relaxation frequency of the bound water was sufficiently low that it did not contribute significantly to the overall dielectric constant. But it was found that the effective loss factor of the tissue water was sufficiently high that it seemed likely that the bound water *was* contributing to the loss factor. The new extrapolated value of 12 for the dielectric constant of bound water helps confirm this hypothesis. In comparison with the dielectric constant of the 'free' tissue electrolyte, the dielectric constant of 12 for bound water gives only a small, although not entirely negligible, contribution to the overall dielectric constant. However, the implied loss factor of around 22 for the bound water *is* considerable, and may help explain how the effective loss factor of the whole tissue water fraction was consistently found to be around 16 relative units.
However, the failure of the initial extrapolation based on undried tissue measurements indicates that this method of estimation of the net relaxation time of bound water, from extrapolation of the effective permittivity values of the water fraction of a composite material, may be prone to considerable error. The limited range of water content gives rise to large uncertainties in the expected behaviour of the effective tissue water dielectric constant at high non-water concentrations. This is especially true when the

state of the water in the composite material is not well understood, and several conductivity effects which are hard to quantify individually are present.

8.6. Summary of Gelatine Results.

In conclusion then, permittivity measurements on gelatine solutions made with pure water have been used to estimate the overall permittivity of water that is affected by hydrogen bonding to proteins. The analysis has assumed that any deviation between the measured permittivity of a solution and the permittivity predicted by a mixture equation is *entirely due to the binding of water molecules.*

By using values of the effective permittivity of the whole water fraction in a solution, calculated using Maxwell or Bruggeman's equations, a limiting value for dielectric constant and loss factor at high gelatine concentration can be estimated. These values are thought to correspond to the overall permittivity of bound water. Because of the scatter in the original data, and the small range of gelatine concentrations which can be investigated, there is a large uncertainty in the estimated limiting permittivity, possibly as large as a factor of two.

Analysis using Maxwell's equation gives the overall dielectric constant of bound water in gelatine solutions as 52 at a frequency of 3 GHz. If it is assumed that all the bound water has the same relaxation frequency, then this dielectric constant value of 52 corresponds to a relaxation frequency of 3.8 GHz, and implies a loss factor of 37 at 3 GHz. Using Bruggeman's equation, a value of 60 is estimated, corresponding to a relaxation frequency of 4.9 GHz, and implies a loss factor of 34 at 3 GHz. Minimum estimates for the dielectric constant give a relaxation frequency of ~2 GHz. The limiting loss factors found by independent extrapolation were 31 by Maxwell's equation, and 34 by Bruggeman's equation. Thus good agreement is observed, particularly with Bruggeman's equation, between the bound water loss factor as estimated, using the Debye equation, from dielectric constant data, and that deduced from independent extrapolation. Therefore, it can be stated that the average relaxation frequency of bound water in gelatine solutions probably lies between 2 and 5 GHz. Similar values were obtained from permittivity values measured on gelatine solutions made with 0.15**M** saline.

The conductivity of ions dissolved in gelatine solutions was found to be reduced, presumably by the solidification of the solution restricting ionic movement through the protein matrix. A linear reduction in low frequency conductivity with concentration was observed, in a similar fashion to that previously noted for protein solutions by Bull and Breese.

In real biological tissues, the initial extrapolation of effective dielectric constant down to a low tissue water content was found to give a value for the dielectric constant of tissue bound water of 53, which was inconsistent with the observed loss factor of the tissues. This may indicate that exponential extrapolation of the effective dielectric constant down to low water content is not a reliable method for estimation of the dielectric constant of bound water in a particular tissue type. However, by using dielectric constant values from partially dehydrated tissue samples, the form of the behaviour of the effective dielectric constant of tissue water could be predicted at high non-water volume fractions. An extrapolation based on partially dehydrated samples gave a value for the permittivity of bound water of 12. This is broadly consistent with the observations made on real tissue samples, and helps account for the seemingly high loss factor of tissue water reported in chapter 7.

The failure of the initial extrapolation based on effective tissue water dielectric constant values from several tissue types is presumably partially due to the fact that each tissue type has a different structure. Different tissues may not therefore be regarded simply as solutions of the same two-phase material with differing concentrations of the two components, as is the case for gelatine solutions.

For gelatine solutions, the extrapolation technique appears to be quite successful, even with measured permittivity values from only one frequency. The structure of gelatine solutions is far more simple than that of biological tissues, with no cellular construction, and only two major types of molecular species present.

In gelatine solutions, the protein molecules are uniformly distributed in the water, giving the maximum possible number of water bonding sites. The cellular structure of biological tissue is such that many of the protein molecules in biological tissue are ordered in a complex fashion. Intermolecular binding between proteins, between proteins and other biological macromolecules, and interactions between water and all the

other components of biological tissues is likely to alter the effect on the permittivity of bound water in real tissues.

With measurements on gelatine solutions from several different frequencies, the extrapolated dielectric constant values for bound water could be fitted to a Cole-Cole equation, and even better comparison between this and the extrapolated loss factor values could be made. This would also identify any small water fraction which is so strongly bound as to be removed from the microwave dispersion altogether.

Conclusion.

There is a need for comprehensive microwave permittivity data for human and animal tissues in many branches of biomedical physics. Current research for which such data may be useful includes microwave thermography, hyperthermia and tomography, and evaluation of the exposure hazard from personal mobile telecommunications.
Permittivity values for animal meats may also be of use in the industrial preparation of meat based foodstuffs. The specific aim of this work was to provide permittivity values for all major body tissue types at 3 GHz, in the operating frequency range of many biomedical radiometer systems, and then to interpret the observed values in terms of the permittivity of the component materials of the tissue.
To this end, permittivity measurements were made with an open-ended co-axial probe, precision calibrated with known dielectrics, using the equivalent circuit approximation of Marcuvitz, and the bilinear transform method of Marsland and Evans to correct for equipment imperfections in the measurement set. A novel co-axial probe design was developed, with a third concentric outer conductor on the probe forming a quarter-wave choke. This provided an annular high impedance region around the open end of the outer co-axial conductor, limiting surface currents, and rendering the probe reflection co-efficient far less susceptible to variation in the physical depth of probe penetration into the measured medium. The probe had a diameter of around 3mm, with a protruding central conductor of approximately the same length. In practice, tissue samples as small as $300\,\mathrm{mm}^3$ could be measured, although the volume investigated by the probe's field could be lower than $50\,\mathrm{mm}^3$.
This new probe was found to be very successful, allowing quick and accurate measurements of permittivity to be made on a large number of tissue and tissue phantom samples. The technique was used to make *in vitro* measurements on animal meat tissues and fresh human tissues of many types, after which the samples were fully dehydrated to find their water content. In general, the tissue permittivities measured were consistent with those found by other authors.
Probe calibration materials were chosen to span the range of tissue permittivity, with dielectric constant from 1 to 78 and loss factor from 0 to 23 relative units. For typical high water content tissue ($\varepsilon_r \approx 50 - j17$), the estimated error in the measured dielectric constant was ± 2, and in the loss factor, ± 1.5 relative units. For lower water content

fatty tissue ($\varepsilon_r \approx 5 - j1$) errors of ≤ 0.5 relative units were expected in both parameters. These errors were quite small enough for the investigation undertaken.

The permittivity of tissue at 3 GHz is strongly dependent on water content. However, the tissue water molecules are thought to exist in many states from a free liquid state to states tightly bound to protein molecules, with relaxation frequency shown to be considerably lower than that of liquid water (~17 GHz at 20°C). By considering the water to be separable into free and bound components, the simple Maxwell-Fricke and Bruggeman mixture equations were applied successfully to the measured data to estimate the proportions of free and bound water in tissues.

Low water content fat tissues from human and animal sources gave permittivities consistent with the predictions of mixture equations for a dilute suspension of free water in a majority fat matrix. For high water content tissues, the water contents and physiology of prepared animal meats could differ slightly from those of the corresponding fresh human tissue. However, it was found that the dielectric constants of most soft tissue types, both human and animal (excepting blood and brain tissues), approximately conformed to a single predictable relationship with water content. Mixture equation analysis suggested that for every gram of protein solids in these tissue types, there could be associated approximately 0.4 grams of bound water which did not contribute significantly to the tissue dielectric constant.

For analysis of the tissue water loss factor, the effects of other loss mechanisms in the tissue, particularly ionic conductivity loss, had to be subtracted from the overall loss factor. The low frequency loss for each tissue type was estimated from the measurements of other authors, at a frequency at which there were assumed to be no loss contributions from tissue water. Since there is great variation between different authors in the quoted low frequency loss for each tissue type, and also since the frequency chosen was only estimated, this process introduced a considerable and unquantifiable error into the calculations for this particular part of the investigation.

Having corrected the measured tissue loss factors to allow for these loss mechanisms, mixture equations were used to estimate the effective loss factor of the whole tissue water fraction. This quantity was similar for each tissue type, with a value of around 16.5 relative units, and did not show any predictable variation with water content. If the bound water were contributing significantly neither to the tissue dielectric constant nor loss factor, the effective loss factor of the tissue water would be expected to be lower

than that of liquid water, and to decrease with decreasing tissue water content. These observations suggest that the bound water does contribute to the loss factor, and so imply that the bound water has a relaxation frequency below 1 GHz, perhaps in the 0.5 GHz range. At 3 GHz, the dielectric constant of this bound water would be less than 10, and so be very nearly insignificant compared to the value of 78 for free water. The loss factor would be around 14, which is similar to that of free water, and so significant. By this mechanism, the effective loss factor of tissue water would be high, and almost invariant with tissue water content.

To further investigate the properties of bound and free water in protein solutions, the permittivity of gelatine / water solutions from 0 to 50% gelatine mass fraction was measured. It was thought that the water in these solutions may quite closely mimic the water in biological tissues. The dielectric constant of these solutions was once again found to vary predictable with water content, and lie systematically below the values predicted by mixture equations (figs. 8.b and 8.h), in a manner similar to that observed for tissues (figs. 7.a and 7.d). By assuming that the bound water did not contribute significantly to the overall dielectric constant, it was estimated that 0.43g water was bound for each gram of gelatine solid. This is similar to the estimate from tissue measurements.

However, the loss factor of the gelatine solutions was always considerably higher than the mixture equation predicted value, indicating that the bound water loss factor in these solutions was very high. This could have meant that the net relaxation frequency of the bound water was higher than that estimated for biological tissues, rendering incorrect the assumption that the bound water dielectric constant was insignificant at 3 GHz. To explain this, a novel technique for estimating the permittivity of bound water using mixture equations has been presented. The effective dielectric constants and loss factors of the whole water fraction of the gelatine solutions were calculated as a function of water content, yielding encouragingly predictable behaviour. Then the variation of these parameters was extrapolated down to a water content approaching zero. For such a theoretical solution, all the water would be bound, so the extrapolated permittivity values could be related to the permittivity of gelatine-bound water.

It was estimated by this method that the dielectric constant of the bound water at 3 GHz was between 27 and 60, and the loss factor was between 30 and 37. These values are

consistent with the net relaxation frequency of the bound water being between 2 and 6 GHz, although there probably exists a broad distribution of relaxation times.

Gelatine solutions made with saline were also investigated. The dielectric constant of these solutions followed approximately the same pattern as for solutions made with pure water. For low gelatine concentrations, the ionic conductivity contribution to the overall loss factor was found to follow a linear function of concentration. When once this effect was subtracted from the overall loss factor, approximately the same behaviour was observed for the resultant relaxation-only loss factor as was observed for solutions made with pure water. Extrapolation of the effective dielectric constant and loss factor of the water fraction suggested that the net relaxation frequency of the gelatine-bound water was again of the order of 4 GHz.

Application of the effective permittivity extrapolation technique to high water content biological tissues was slightly less satisfactory, as may be expected, since each different tissue type has a different cellular structure, and the range of water content available is very limited. To help alleviate these problems, measurements were made on partially dehydrated tissue samples of several tissue types. This gave effective tissue water dielectric constant values for much lower water content theoretical tissues.

Extrapolation of the effective dielectric constant of tissue water down to zero water content gave an estimated value of around 12 relative units for the dielectric constant of tissue bound water. This value suggests a net bound water relaxation frequency in the 0.5 GHz range. This is consistent with the previous observations on tissue water, and shows that the extrapolation technique can be a useful method for analysing bound water in complex systems.

In future it may be instructive to measure accurately the permittivity of gelatine solutions and a single tissue type over a wide frequency range from ~0.1 to ~20 GHz using a co-axial probe with adjustable quarter-wave choke. With additional partial dehydration tissue measurements, it may then be possible to verify the estimated tissue and gelatine bound water relaxation frequencies, and also to estimate the spread of bound molecule relaxation times.

References.

Abdul-Razzak, M.M., et al, "Microwave thermography for medical applications," *IEE Proc.*, Vol. 134, No. 2, (1987), pp. 171 - 174.

Bahl, I.J. and Stuchly, S.S., "Effect of finite size of ground plane on the impedance of a monopole immersed in a lossy medium," *Electron. Lett.*, Vol. 15, No. 22, (1979), pp. 728 - 729.

Bardati, F. et al, "Multispectral microwave radiometry for thermal imaging," *J. Photographic Sci.*, Vol. 37, (1989), pp. 154 - 156.

Bardati, F. and Tognolatti, P., "Multifrequency microwave radiometry imaging," *Proc. IEEE/URSI /93 Conf.*, Rome, Oct. 11 - 14, (1993), pp. 217 - 220.

Barrett, A.H., Myers, P.C. and Sadowsky, N.L., "Microwave thermography in the detection of breast cancer," *Amer. J. Roent.*, Vol. 134, (1980), pp. 365 - 368.

Bergman, D.J., "The dielectric constant of a composite material - a problem in classical physics," *Physics Reports*, Vol. 43, No. 9, (1978), pp. 378 - 407.

Bengtsson, N.E. and Risman, P.O., "Dielectric properties of food at 3 GHz as determined by a cavity perturbation technique. Part 2: Measurements on food materials," *J. Microwave Pow.*, Vol. 6, (1971), pp. 107 - 123.

Biology Data Book, Vol. 1, ed. Altman P.L. and Dittmer, D.S., *Fed. Amer. Socs. for Expt. Biol.*, (1972).

Bleaney, B.I. and Bleaney, B., "Electricity and Magnetism," 3rd. ed., Oxford University Press, (1976).

Bocquet, B. et al, "Visibilty of local thermal structures and temperature retrieval by microwave radiometry," *Electron. Lett.*, Vol. 22, No. 3, (1986), pp. 120 - 122.

Bocquet, B. et al, "An example of thermometry in volume by microwave radiometry," *IEEE Trans. Biomed. Eng.*, Vol. 40, No. 9, (1993a), pp. 990 - 992.

Bocquet, B., Ait-Abdelmalek, R. and Leroy, Y., "Deconvolution and Weiner filtering of short-range radiometric images," *Electron. Lett.*, Vol. 29, No. 18, (1993b), pp. 1628 - 1629.

Bocquet, B. et al, "Influence of the permittivity of breast tissues on the robustness of microwave radiometric imaging," *IEE Colloquim "Applications of Microwaves in Medicine" digest 1995/041*, (1995), sect. 6.

Boned, C. and Peyrelasse, J., "Some comments on the complex permittivity of ellipsoids dispersed in continuum media," *J. Phys. D: Appl. Phys.*, Vol. 16, (1983) pp. 1777 - 1784.

Bottcher, C.J.F., "The dielectric constant of crystalline powders," *Rec. Trav. Chim.*, Vol. 64, (1945), pp. 47.

Brady, M.M., Symons, S.A. and Stuchly, S.S., "Dielectric behaviour of selected animal tissues *in-vitro* at frequencies from 2 to 4 GHz," *IEEE Trans. Biomed. Eng.*, Vol. 28, No. 3, (1981), pp. 305 - 307.

Brooks, S.M. and Brooks, N.P., "The Human Body," 2nd ed., C.V. Mosby, (1980).

Broquetas, A. et al, "Active microwave computed tomography cylindrical scanner for biomedical applications," *J. Photographic Sci.*, Vol. 37, (1989).

Brown, V.J., "Development of computer modelling techniques for microwave thermography," PhD Thesis, University of Glasgow, (1989).

Bruggeman, D.A.G., "Berechnung verschneidener physkalischer Konstanten von heterogenen Substanzen," *Annalen. Physik.*, Vol. 24, (1935), pp. 637 - 679.

Buckley, F. and Maryott, A.A., "Tables of dielectric dispersion data for pure liquids and dilute solutions," *Nat. Bureau Standards Circular 598.*, (1958).

Buffler, C.R. and Stanford, M.A., "Effects of dielectric and thermal properties on the microwave heating of foods," *Microwave World.*, Vol. 12, No. 4, (1991), pp. 15 - 23.

Bull, H.B. and Breese, K., "Electrical conductance of protein solutions," *J. Colloid. Interface. Sci.*, Vol. 29, (1969), pp. 492.

Burdette, E.C., Cain, F.L. and Seals, J., "*In-vivo* probe measurement technique for determining dielectric properties at VHF through microwave frequencies," *IEEE Trans. Microwave Theory Tech.*, Vol. 28, No. 4, (1980), pp. 414 - 427.

Burdette, E.C., Cain, F.L. and Seals, J., "*In-situ* tissue permittivity at microwave frequencies: perspective, techniques, results," in *Medical applications of microwave imaging*, eds. Larsen, E.L., and Jacobi, J.H., IEEE, New York, (1986).

Campbell, A.M., "Measurements and analysis of the microwave dielectric properties of tissues," PhD Thesis, University of Glasgow, (1990).

Caorsi, S. and Gragnani, G.L., "Thermal distribution simulation by using a multifrequency digital radiometer," *Proc. IEEE/URSI /93 Conf.*, Rome, Oct. 11 - 14, (1993), pp. 229 - 232.

Chandrasekhar, S., "Study of stellar structure," Dover Publications, (1939).

Chandrasekhar, S., "Radiative transfer," Oxford, (1950).

Cheever, E., Leonard, J.B. and Foster, K.R., "Depth of penetration of fields from rectangular apertures into lossy media," *IEEE Trans. Microwave Theory Tech.*, Vol. 35, No. 9, (1987), pp. 865 - 867.

Chive, M. et al, "Modelling of different types of applicators used for microwave hyperthermia based on FDTD method," *IEE Colloquim "Applications of Microwaves in Medicine" digest 1995/041*, (1995), sect. 5.

Clausse, M., "Dielectric properties of emulsions and related systems," in *Encyclopaedia of Emulsion Technology*, ed. Becher, P., Marcel-Dekker, New York, (1983).

Clegg, J.S. et al, "Microwave dielectric measurements (0.8 - 70 GHz) on Artemia cysts at variable water content," *Phys. Med. Biol.*, Vol. 29, (1984), pp. 1409.

Collie, C.H., Hasted, J.B. and Ritson, D.M., "The dielectric properties of water and heavy water," *Proc. Phys. Soc. Lond.*, Vol. 60, (1948), pp. 145 - 160.

Cook, H.F., "The dielectric behaviour of some types of human tissues at microwave frequencies," *Brit. J. Appl. Phys.*, Vol. 2, (1951), pp. 295 - 300.

Cook, H.F., "A comparison of the dielectric behavior of pure water and human blood at microwave frequencies," *Brit. J. Appl. Phys.*, Vol. 3, (1952), pp. 249 - 255.

Cooke, R. and Kuntz, I.D., "The properties of water in biological systems," *Ann. Rev. Biophys. Bioeng.*, Vol. 3, (1974), pp. 95.

CRC Handbook of chemistry and physics, CRC Press , 54th ed., (1974).

Critchfield, F.E., Gibson, J.A. and Hall, J.L., "Dielectric constant of the dioxane-water system," *J. Amer. Chem. Soc.*, Vol. 75, (1953), pp. 1991 - 1992.

Davidson, D.W. and Cole, R.H., "Dielectric relaxation in glycerine," *J. Chem. Phys.*, Vol. 18, (1950), pp. 1417.

Debye, P., "Polar Molecules," Chemical Catalogue Co., New York, (1929).

Decreton, M.C. and Gardiol, F.E., "Simple nondestructive method for the meaurement of complex permittivity," *IEEE Trans. Instrum. Meas.*, Vol. 23, No. 4, (1974), pp. 434 - 438.

Deschamps, G.A., "Impedance of an antenna in an conducting medium," *Trans. IRE.*, (1962), pp. 648 - 650.

Duhkin, S.S., "Dielectric properties of disperse systems," *Sur. Coll. Sci.*, Vol. 3, (1971), pp. 83 - 165.

Eagland, D., "Nucleic acids, peptides and proteins," in *Water: A comprehensive treatise*, ed. Franks, F., Plenum, New York, Vol. 4, Ch. 5, (1972).

Enel, L. et al, "Improved recognition of thermal structures by microwave radiometry," *Electron. Lett.*, Vol. 20, (1984), pp. 293 - 294.

England, T.S., "Dielectric properties of the human body for wavelengths in the 1 - 10 cm range," *Nature*, Vol. 166, (1950), pp. 480.

Epstein, B.R., Foster, K.R. and MacKay, R.A., "Microwave dielectric properties of ionic and non-ionic microemulsions," *J. Colloid. Interface. Sci.*, Vol. 95, (1983), pp. 218 - 227.

Foster, K.R. et al, "Dielectric properties of brain tissue between 0.01 and 10 GHz," *Phys. Med. Biol.*, Vol. 24, (1979), pp. 1177.

Foster, K.R. et al, "Transport properties of polymer solutions," *Biophys. J.*, Vol. 45, (1984), pp. 975 - 984.

Foster, K.R., Schepps, J.L. and Schwan, H.P., "Microwave dielectric relaxation in muscle. A second look," *Biophys. J.*, Vol. 29, (1980), pp. 271.

Foster, K.R. and Schwan, H.P., "Dielectric properties of tissues and biological materials: a critical review," *Crit. Rev. Biomed. Eng.*, Vol. 17, (1989), pp. 25 - 104.

Franks, F., "The solvent properties of water," in *Water:A comprehensive treatise*, ed. Franks, F., Plenum, New York, Vol. 2, Ch. 1, (1972).

Fraser, S.M., Land, D.V. and Sturrock, R.D., "Microwave thermography - an index of inflammatory disease," *Brit. J. Rheumatology*, Vol. 26, (1987), pp. 37 - 39.

Fricke, H., "A mathematical treatment of the dielectric conductivity and capacity of disperse systems," *Phys. Rev.*, Vol. 24, (1924), pp. 575 - 587.

Fricke, H., "An experimental study of the electrical conductivity of disperse systems. Part 1: cream," *Phys. Rev.*, Vol. 26, (1925a), pp. 361 - 367.

Fricke, H., "The electrical capacity of suspensions of red corpuscles of a dog," *Phys. Rev.*, Vol. 26, (1925a), pp. 682 - 687.

Fricke, H., "The complex conductivity of a suspension of stratified particles of spherical or cylindrical form," *J. Phys. Chem.*, Vol. 59, (1955), pp. 168.

Giese, A.C., "Cell physiology," 4th ed., W. B. Saunders, (1973).

Ginzton, E.L., "Microwave measurements," McGraw-Hill, New York, (1957).

Grant, E.H., Buchanan, T. and Cook, H.F., "Dielectric behaviour of water at microwave frequencies," *J. Chem. Phys.*, Vol. 26, (1957), pp. 156 - 161.

Grant, J.P., "Measurement, medical significance and applications of the dielectric properties of biological materials," PhD Thesis, University of Surrey, (1984).

Green, H.D., "Circulatory system: physical principles," In *Medical Physics II*, ed. Glasser, O., Chicago, Year Book Publishers, (1950), pp. 228 - 251.

Haggis, G., Hasted, J.B. and Buchanan, T., "The dielectric properties of water in solutions," *J. Phys. Chem.*, Vol. 20, (1952), pp. 1452 - 1465.

Hale, D.K., "The physical properties of composite materials," *J. Mat. Sci.*, Vol. 11, (1976), pp. 2105 - 2141.

Hamilton, G., PhD Thesis, University of Glasgow, *to be published*, (1996).

Hanai, T., "Electrical properties of emulsions," in *Emulsion Science*, ed. Sherman, P., Academic Press, London, (1968).

Hanai, T. and Koizumi, N., "Dielectric relaxation of W/O emulsions in particular reference to theories of interfacial polarisation," *Bull Inst. Chem. Res., Kyoto Univ.*, Vol. 53, (1975), pp. 153 - 160.

Harness, P.C. and Land, D.V., "Finite element analysis of microwave thermographic images," *Thermologie Österreic , Oct. 1994, Conf. "The Thermal Image,"* (1994), pp. 162.

Hashin, Z. and Shtrikman, S., "Note on the effective constants of composite materials," *J. Franklin Inst.*, Vol. 271, (1961), pp. 423 - 426.

Hasted, J.B., "Liquid water: dielectric properties," in *Water: A comprehensive treatise*, ed. Franks, F., Plenum, New York, Vol. 1, Ch. 7, (1972).

Hasted, J.B., "Aqueous Dielectrics", Chapman and Hall, London, (1973).

Hasted, J.B. and el-Sabeh, S., "The dielectric properties of water in solutions," *Trans. Faraday Soc.*, Vol. 49, (1953), pp. 1003 - 1011.

Hasted, J.B., Haggis, G.H. and Hutton, P., "Dielectric dispersion of water-dioxane mixtures," *Trans. Faraday Soc.*, Vol. 47, (1951), pp. 577 - 580.

Hasted, J.B., Ritson, D.M. and Collie, C.H., "Dielectric properties of aqueous ionic solutions," *J. Chem. Phys.*, Vol. 16, (1948), pp. 1 - 11.

Hatfield, H.S., "Measurement of the thermal conductivity of animal tissue," *J. Physiol.*, Vol. 120, (1953), pp. 35 - 36.

Herrick, J.F., Jelatis, D.G. and Lee, M., "Dielectric properties of tissues important in microwave diathermy," *Fed. Proc.*, Vol. 9, (1950), pp. 60.

Hill, N.E., "Interpretation of the dielectric properties of water," *Trans. Faraday Soc.*, Vol. 59, Part 1, (1963), pp. 344 - 346.

Homburger, F. and Fishman, W.H., "The physiopathology of cancer, " Hoeber-Harper, New York, (1953).

Jenkins, S. et al, "Dielectric measurements on human tissues between 100 MHz and 3 GHz," *Advances in medical and microwave imaging* conf., University of Lille, France, (1989).

Johnson, R.H., Preece, A.W. and Green, J.L., "Capabilities and limitations of electromagnetic hyperthermia applicators," *IEE Colloquim "Applications of Microwaves in Medicine" digest 1995/041*, (1995), sect. 12.

Jordan, B.P., Sheppard, R.J. and Szwarnowski, S., "The dielectric properties of formamide, ethanediol and methanol," *J. Phys. D: Appl. Phys.*, Vol. 11, (1979), pp. 695 - 701.

Kaatze, U. et al, "Dielectric relaxation in aqueous solutions of some oxygen-containing linear hydrocarbon polymers," *J. Phys. Chem.*, Vol. 82, (1978a), pp. 112 - 120.

Kaatze, U., "Dielectric relaxation in aqueous solutions of polymers," *Prog. Colloid. Polym. Sci.*, Vol. 65, (1978b), pp. 214 - 224.

Kelso, M.B., "A study of the use of combined thermal and microwave modelling of body regions for microwave thermography," PhD Thesis, University of Glasgow, (1995).

Kirkland, R.W., "In-vivo thermal conductivity values for bovine and caprine osseus tissue," *Proc. Ann. Conf. Eng. in Med. & Biol., Boston, Mass.*, (1967), pp. 204.

Kraszewski, A. et al "*In-vivo* and *in-vitro* dielectric properties of animal tissues at radio frequencies," *Bioelectromagnetics*, Vol. 3, (1982), pp. 421.

Kuntz, I.D., "Hydration of macromolecules. Part 3: Hydration of polypeptides," *J. Amer. Chem. Soc.*, Vol. 93, Part 1, (1971), pp. 514 - 516.

Land, D.V., "Radiometer receivers for microwave thermography," *Microwave. J.*, Technical Feature, May (1983), pp. 196 - 201.

Land, D.V., "Measurement of radio-frequency and microwave fields by nonresonant perturbation," *Proc. IEE.*, Vol. 131, (1984), pp.1 - 8.

Land, D.V., "A clinical microwave thermography system," *Proc. IEE.*, Vol. 134, No. 2, (1987), pp.193 - 200.

Land, D.V., "Application of the nonresonant perturbation technique to the measurement of high-frequency fields in biological phantom materials," *Electron. Lett.*, Vol. 24, (1988), pp. 70 - 72.

Land, D.V., "Simplified nonresonant perturbation method of measuring aspects of performance of UHF and microwave antennas for biomedical applications," *Electron. Lett.*, Vol. 28, (1992), pp. 1190 - 1192.

Land, D.V., "Recent measurements of microwave dielectric properties of tissues and tissue simulating materials," *Proc. IEEE/URSI /93 Conf.*, Rome, Oct. 11-14, (1993), pp. 259 - 262.

Land, D.V., "Investigations of the behaviour of microwave thermography antennas when coupled to layered tissue regions," *IEE Colloquim "Applications of Microwaves in Medicine" digest 1995/041*, (1995), sect. 7.

Lau, R.W. and Sheppard, R.J, "The modelling of biological systems in three dimensions using the time domain finite difference method: 1. The implementation of the model," *Phys. Med. Biol.*, Vol. 31, No.11 (1986), pp. 1247 - 1256.

Lewin, L., "The electrical constants of a material loaded with spherical particles," *J. Inst. Elec. Eng.*, Vol. 94, Part 3, (1947), pp. 65 - 68.

Lichteneker, K., "Mischkopertheorie als Wahrscheinlichkeitsproblem," *Physik. Zeitschr.*, Vol. 30, (1929), pp. 805 - 809.

Lin, J.C., "Microwave properties of fresh mammalian brain tissue at body temperature," *IEEE Trans. Biomed. Eng.*, Vol. 22, (1975), pp. 74 - 76.

Link, G.L. and Herrmann, D.B., "Properties of dielectrics," in *American Institute of Physics Handbook*, ed. Gray, D.E., McGraw-Hill, (1972).

Lipkin, M. and Hardy, J.D., "Measurement of some thermal properties of human tissues," *J. Appl. Physiol.*, Vol. 7, (1954), pp. 212 - 217.

Livesay, D.E. and Chen, K.M., "Electromagnetic fields induced inside arbitrarily shaped biological bodies," *IEEE Trans. Microwave Theory Tech.*, Vol. 22, (1974), pp. 1273 - 1280.

Looyenga, H., "Dielectric constants of heterogeneous mixtures," *Physica*, Vol. 31, pp. 401 - 406.

Lowry, O.H., "Electrolytes in the cytoplasm," *Biol. Symp.*, Vol. 10, (1943), pp. 233 - 245.

Ludeke, K.M., Schiek, B. and Kohler, J., "Radiation balance microwave thermograph for industrial and medical applications," *Electron. Lett.*, Vol. 14, No. 6, (1978), pp. 194 - 195.

Lynch, D.R., Paulsen, K.D. and Strohbehn, J.W., "Finite element solution of Maxwell's equations for hyperthermia treatment planning," *J. Comp. Phys.*, Vol. 58, (1985), pp. 246 - 269.

Malmberg, C.G. and Maryott, A.A., "Dielectric constant of water from 0 to 100°C," *J. Reasearch of Nat. Bur. Standards.*, Vol. 56, No.1, (1956), pp. 1 - 8.

Mamouni, A. et al, "Introduction to correlation microwave thermography," *J. Mic. Pow.*, Vol. 18, No. 3, (1983), pp. 285 - 293.

Mamouni, A., "Radiometrie microonde en champ proche," PhD Thesis, University of Science and Technology de Lille, (1988).

Mamouni, A. et al, "Computation of near-field microwave radiometric signals: definition and experimental verification," *IEEE Trans. Microwave Theory Tech.*, Vol. 39, No. 1, (1991), pp. 124 - 132.

Marcuvitz, N., "Waveguide handbook," McGraw-Hill, New York, (1951).

Marsland, T.P. and Evans, S., "Dielectric measurements with an open-ended co-axial probe," *IEE Proc. H*, Vol. 134, No. 4, (1987), pp. 341 - 349.

Maxwell, J.C., "A treatise on electricity and magnetism," Clarendon Press, London, (1881).

Mimi, M., "An investigation of radiometer and antenna properties for microwave thermography," PhD. Thesis, University of Glasgow, (1990).

Misra, D.K., "A quasi-static analysis of open-ended co-axial lines," *IEEE Trans. Microwave Theory Tech.*, Vol. 35, No. 10, (1987), pp. 925 - 928.

Misra, D.K. and Staebell, K.F., "An experimental technique for *in-vivo* permittivity measurements of material at microwave frequencies," *IEEE Trans. Microwave Theory Tech.*, Vol. 38, No. 3, (1990), pp. 337 - 340.

Misra, D.K. et al, "Noninvasive electrical characterisation of materials at microwave frequencies using an open-ended co-axial line: Test of an improved calibration technique," *IEEE Trans. Microwave Theory Tech.*, Vol. 38, No. 1, (1990), pp. 8 - 14.

Mosig, J.R., "Reflection of an open-ended co-axial line and application to nondestructive measurement of materials," *IEEE Trans. Instrum. Meas.*, Vol. 30, (1981), pp. 46 - 51.

Newton, R., "Non-invasive thermometry by correlation and multi-frequency microwave thermometry," PhD Thesis, University of Aberdeen, (1986).

Ni, C. et al, "Non-invasive *in vivo* measurement of tissue permittivity," *Proc. IEEE/URSI /93 Conf.*, Rome, Oct. 11-14, (1993), pp. 251 - 254.

Nightingale, N.R.V. et al, "The use of time domain spectroscopy to measure the dielectric properties of mouse brain at radiowave and microwave frequencies," *Phys. Med. Biol.*, Vol. 25, No. 6, (1980), pp. 1161 - 1165.

Nightingale, N.R.V. et al, "The dielectric properties of the cerebellum, cerebrum and brain stem of mouse brain at radiowave and microwave frequencies," *Phys. Med. Biol.*, Vol. 28, No. 8, (1983), pp. 897 - 903.

Pauly, H. and Schwan, H.P., "Uber die Impedanz einer Suspension von kugelformingen Teilchen mit einer Schale," *Z. Naturforsch.*, Vol. 14B, (1959), pp. 125.

Pauly, H. and Schwan, H.P., "Dielectric properties and ion mobility in erythrocytes," *Biophys.J.*, Vol. 6, (1966), pp. 621 - 631.

Pennes, H.H., "Analysis of tissue and arterial blood temperatures in the resting human forearm," *J. Appl. Physiol.*, Vol. 1, (1948), pp. 93 - 122.

Pethig, R., "Dielectric properties of biological materials: biophysical mechanisms and medical applications," *IEEE Trans. Elec. Ins.*, Vol. 19, (1984), pp. 453 - 474.

Polder, D. and Van Santen, J.H., "The effective permieability of mixtures of solids," *Physica*, Vol. 12, No. 5, (1946), pp. 257 - 271.

Ramo, S., et al, "Fields and waves in communication electronics," 3rd. ed., Wiley, New York, (1994).

Reif, F., "Fundamentals of statistical and thermal physics," McGraw-Hill, (1965).

Risman, P.O., "Microwave properties of water in the temperature range +3 to +140°C," *Electromagn. Energy Rev.*, Vol. 1, (1988), pp. 3 - 5.

Rose, J.L. and Goldberg, B.B., "Basic physics in diagnostic ultrasound," Wiley, New York, (1979).

Saxton, J.A., "Dielectric dispersion in pure polar liquids at very high radio-frequencies. Part 2: Relation of experimental results to theory," *Proc. Roy. Soc. A.*, Vol. 213, (1952), pp. 473 - 491.

Saxton, J.A., "Electrical properties of water," *Wireless Eng.*, Vol. 26, (1949), pp.288.

Saxton, J.A. and Lane, J.A., "Dielectric dispersion in pure polar liquids at very high radio-frequencies. Part 3: The effect of electrolytes in solution," *Proc. Roy. Soc. A.*, Vol. 213, (1952a), pp. 531 - 545.

Saxton, J.A. and Lane, J.A., "Electrical properties of sea water-reflection and attenuation characteristics at V.H.F.," *Wireless Eng.*, Vol. 29, (1952b), pp. 269 - 275.

Schepps, J.L., "The measurement and analysis of the dielectric properties of normal and tumour tissues at UHF and microwave frequencies," PhD Thesis, University of Pennsylvania, (1981).

Schepps, J.L. and Foster, K.R., "The UHF and microwave dielectric properties of normal and tumour tissues: variation in dielectric properties with tissue water content," *Phys. Med. Biol.*, Vol. 25, (1980), pp. 1149.

Schwan, H.P., "Electrical properties of tissue and cell suspensions," *Adv. Biol. Med. Phys.*, Vol. 5, (1957), pp. 147 - 209.

Schwan, H.P., "Electrical properties of bound water," *Ann. N.Y. Acad. Sci.*, Vol. 125, (1965), pp. 344 - 354.

Schwan, H.P. and Foster, K.R., "RF-field interactions with biological systems: electrical properties and biophysical mechanisms," *Proc. IEEE*, Vol. 68, (1980), pp. 104.

Slater, J.C., "Microwave transmission," McGraw-Hill, (1942).

Smith, S.R. and Foster, K.R., "Dielectric properties of low water content tissues," *Phys. Med. Biol.*, Vol. 30, (1985), pp. 965.

Smith, G.S. and Scott, W.R., "The use of emulsions to represent dielectric materials in electromagnetic scale models," *IEEE Trans. Microwave Theory Tech.*, Vol. 38, (1990), pp. 323 - 334.

Spiridonov, V.I., "A relaxation model for the dielectric properties of water in heterogeneous mixtures," *Meas. Tech.*, Vol. 25, (1982), pp. 448 - 452.

Steel, M.C. and Sheppard, R.J., "Dielectric properties of mammalian brain tissue between 1 and 18 GHz," *Phys. Med. Biol.*, Vol. 30, (1985), pp. 621.

Stogryn, A., "Equations for calculating the dielectric constant of saline water," *IEEE Trans. Microwave Theory Tech.*, Vol. 19, (1971), pp. 733 - 736.

Stoy, R.D., Foster, K.R. and Schwan, H.P., "Dielectric properties of mammalian tissues from 0.1 to 100 MHz: a summary of recent data," *Phys. Med. Biol.*, Vol. 27, No.4 (1982), pp. 501 - 513.

Stuchly, M.A. and Stuchly, S.S., "Co-axial line reflection methods for measuring dielectric properties of biological substances at radio and microwave frequencies - a review," *IEEE Trans. Instrum. Meas.*, Vol. 29, No. 3, (1980a), pp. 176 - 183.

Stuchly, M.A. and Stuchly, S.S., "Dielectric properties of biological substances - tabulated," *J. Mic. Pow.*, Vol. 15, (1980b), pp. 19.

Stuchly, M.A. et al, "Equivalent circuit of an open-ended co-axial line in a lossy dielectric," *IEEE Trans. Instrum. Meas.*, Vol. 31, No. 2, (1982a), pp. 116 - 119.

Stuchly, M.A. et al, "Dielectric properties of animal tissue *in-vivo* at radio and microwave frequencies: comparison between species," *Phys. Med. Biol.*, Vol. 27, (1982b), pp. 927.

Tai, C.T., "Characteristics of linear antenna elements," in *Antenna engineering handbook*, ed. Jasik, H., McGraw-Hill, New York (1961), Ch. 3.

Tanabe, E. and Joines, W.T., "A non-destructive method for meauring the complex permittivity of dielectric materials at microwave frequencies using an open-ended transmission line resonator," *IEEE Trans. Instrum. Meas.*, Vol. 25, No. 3, (1976), pp. 222 - 226.

Taylor, H.C., Hand, J.W. and Lau, R.W., "FDTD modelling for microwave dosimetry and thermography," *IEE Colloquim "Applications of Microwaves in Medicine" digest 1995/041*, (1995), sect. 11.

Thurai, M. et al, "Variation with age of the dielectric properties of mouse brain cerebrum," *Phys. Med. Biol.*, Vol. 29, No. 9, (1984), pp. 1133 - 1136.

Touloukian, Y.S., Liley, P.E. and Saxena, S.C., in *Thermophysical Properties of Matter, The TPRC Data Series*, IFI/Plenum, New York, (1970), Vol. 3, pp. 120 - 209; Vol. 10, pp. 290 - 589.

Valvano, J.W., Cochran, J.R. and Diller, K.R., "Thermal conductivity and diffusivity of biomaterials measured with self-heated thermistors," *Int. J. Thermophys.*, Vol. 6, (1985), pp. 301 - 311.

Van Beek, C.K.H., "Dielectric behaviour of heterogeneous systems," *Progress in Dielectrics*, Vol. 7, (1965), pp. 69 - 114.

Velick, S. and Gorin, M., "The electrical conductance of suspensions of ellipsoids and its relation to the study of avian erythrocytes," *J. Gen. Physiol.*, Vol. 23, (1940), pp. 753 - 771.

Von Hippel, A.R., "Dielectrics and Waves," Wiley, New York, (1954).

Wagner, K.W., "Erklarung der dielektrischen Nachwirkungsvorgange auf Grund Maxwellscher Vorstellungen," *Archiv Electrotechnik*, Vol. 2, (1914), pp. 371.

Weinbaum, S., Jiji, L.M. and Lemons, D.E., "Theory and experiment for the effect of vascular microstructure on surface tissue heat transfer - part 1: Anatomical foundation and model conceptualization," *J. Biomech. Eng.*, Vol. 106, (1984a), pp. 321 - 330.

Weinbaum, S., Jiji, L.M. and Lemons, D.E., "Theory and experiment for the effect of vascular microstructure on surface tissue heat transfer - part 2: Model formulation and solution," *J. Biomech. Eng.*, Vol. 106, (1984b), pp. 331 - 341.

Weinbaum, S., Jiji, L.M. and Lemons, D.E., "A new simplified bioheat equation for the effect of blood flow on local average tissue temperature," *J. Biomech. Eng.*, Vol. 107, (1985), pp. 131 - 139.

Weiner, O., "Herkunft und Stellung der Aufgabe," *Abh. Sachs. Akad. Wiss.*, Math-Phys. K1., Vol. 32, (1912), pp. 509.

Wilheit, T.T., "Radiative transfer in a plane stratified dielectric," *IEEE Trans. Geosci. Elec.*, Vol. 16, (1978), pp. 138 - 143.

Wissler, E.H., "Comments on the new bioheat equation proposed by Weinbaum and Jiji," *J. Biomech. Eng.*, Vol. 109, (1987), pp. 226 - 233.

Wyman, J. and Ingalls, E.N., "The dielectric constant of deuterium oxide," *J. Amer. Chem. Soc.*, Vol. 60, Part 1, (1938), pp. 1182 - 1184.

Xu, D., Liping, L. and Zhiyan, J., "Measurement of the dielectric properties of biological substances using an improved open-ended co-axial line resonator method," *IEEE Trans. Microwave Theory Tech.*, Vol. 35, No. 12, (1987), pp. 1424 - 1428.

Yee, K.S., "Numerical solution of initial boundary value problems involving Maxwell's equations in isotropic media," *IEEE Trans. Ant. and Prop.*, Vol. 14, No. 3, (1966), pp. 302 - 307.

GLASGOW UNIVERSITY LIBRARY